

**INSTITUTE OF ORGANIC CHEMISTRY POLISH
ACADEMY OF SCIENCES**



Institute of Organic Chemistry
Polish Academy of Sciences

DISSERTATION

in the form of a coherent thematic series of articles published
in scientific journals

**Synthesis and photophysical properties of
novel merocyanine dyes**

Kateryna Vygranenko, M.Sc.

Supervisor: prof. dr hab. Daniel Tomasz Gryko

Warsaw 2023

**INSTYTUT CHEMII ORGANICZNEJ POLSKIEJ
AKADEMII NAUK**



**Instytut Chemii Organicznej
Polskiej Akademii Nauk**

ROZPRAWA DOKTORSKA

w formie spójnego tematycznie cyklu artykułów opublikowanych
w czasopismach naukowych

**Synteza i właściwości fotofizyczne nowych
barwników merocyjaninowych**

Kateryna Vygranenko, M.Sc.

Promotor: Prof. dr hab. Daniel Tomasz Gryko

Warszawa 2023

Praca doktorska wykonana w ramach projektu:



**INNOWACYJNA
GOSPODARKA**
NARODOWA STRATEGIA SPÓJNOŚCI



Fundacja na rzecz Nauki Polskiej

UNIA EUROPEJSKA
EUROPEJSKI FUNDUSZ
ROZWOJU REGIONALNEGO



*“New generation of fluorescent probes for stimulated emission depletion
microscopy”*

Realizowanego w ramach programu TEAM

Fundacji na rzecz Nauki Polskiej

Numer grantu: POIR.04.04.00-00-3CF4/16-00-TEAM/2016-3/22

Acknowledgements:

To start with, I would like to express my gratitude to my supervisor Prof. Daniel T. Gryko, who gave me an opportunity to be a PhD student in his group. Prof. Gryko possesses the most important skills of team leader – excellent time-management and effective organisation of team cooperation. His contribution to my success is hard to overestimate. Again, I thank him for his guidance, encouragement, support and patience throughout the years.

Secondly, I am very grateful to all current and past group members for their support during hard times, encouragement in moments of complete disappointment, sharing their knowledge and experience, cosy working environment and feeling that you are not alone among your problems. Special thanks to Dr. Yevgen Poronik for teaching me to pay a lot of attention to details, Dr. Olena Vakuliuk, who took care of me like mother, Dr. Mariusz Tasiar and Dr. Beata Koszarna for their optimism and support regardless the situation, Jaqueline Stella Araujo Badaro, Dr. David Young, and Dr. Dinesh Kumar for their contribution to my English practice and support. In particular, I would like to thank Olena Vakuliuk and Yevgen Poronik once more for their friendship, guidance and company in the lab for over the years.

Again, I would like to give special thanks to Dr. David Young for the proofreadings.

I also thank all my collaborators, especially Dr. Antoni Wrzosek and Prof. Adam Szewczyk for great support and guidance in bio-imaging studies, Prof. Denis Jacquemin and Manon H. E. Bousquet for theoretical calculations, Dr. Łukasz Dobrzycki for X-Ray diffraction measurements, Brunella Bardi, Prof. Francesca Terenziani and Prof. Anna Painelli for spectroscopic characterization and theoretical calculations.

Additionally, I would like to thank the FNP-TEAM for funding my PhD.

Finally, I want to thank the whole Poland for being the first country to help in the darkest times, for compassion and empathy, for being always ready to help and share their home and resources with refugees.

I dedicate this thesis to my parents and my husband, whose encouragement, support and love made it possible to finish my research.

TABLE OF CONTENTS

1. LIST OF PUBLICATIONS INCLUDED IN THE DOCTORAL THESIS	- 10 -
2. LIST OF PUBLICATIONS NOT INCLUDED IN THE DOCTORAL THESIS	- 11 -
3. PARTICIPATION IN CONFERENCES AND SEMINARS.....	- 12 -
4. ABSTRACT IN ENGLISH	- 13 -
5. ABSTRACT IN POLISH / STRESZCZENIE W JĘZYKU POLSKIM.....	- 14 -
6.1 Purpose of the work	- 15 -
6.2 The current state of knowledge in a given field of chemistry.....	- 17 -
6.2.1 Synthesis of classic rhodols.....	- 19 -
6.2.2 Synthesis of π -expanded rhodols and ‘rhodol-type merocyanines’	- 26 -
6.2.3 Synthesis of rhodols with an endocyclic heteroatom.....	- 28 -
6.3 Results and discussions	- 33 -
6.3.1 Red emissive sulfone-rhodols as mitochondrial imaging agents.....	- 33 -
6.3.2 Direct transformation of coumarins into orange-red emitting rhodols	- 36 -
6.3.3 One-step transformation of aminophenols and coumarins into rhodols and ‘rhodol-like’ merocyanines.....	- 40 -
6.4 Summary and conclusions.....	- 45 -
7. BIBLIOGRAPHY	- 47 -
8. ORIGINAL PUBLICATIONS.....	- 53 -
9. DECLARATIONS OF THE AUTHORS OF PUBLICATIONS	- 265 -

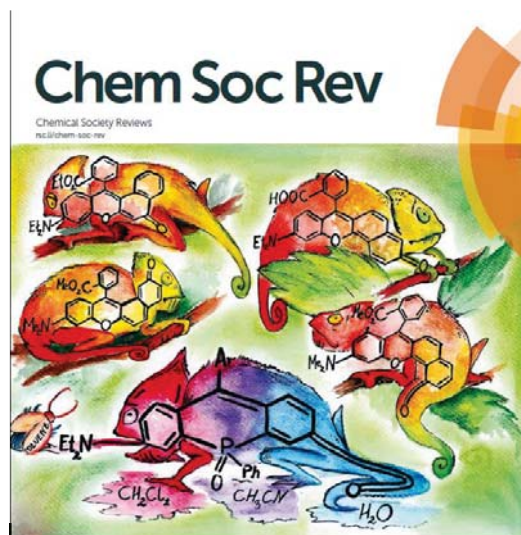
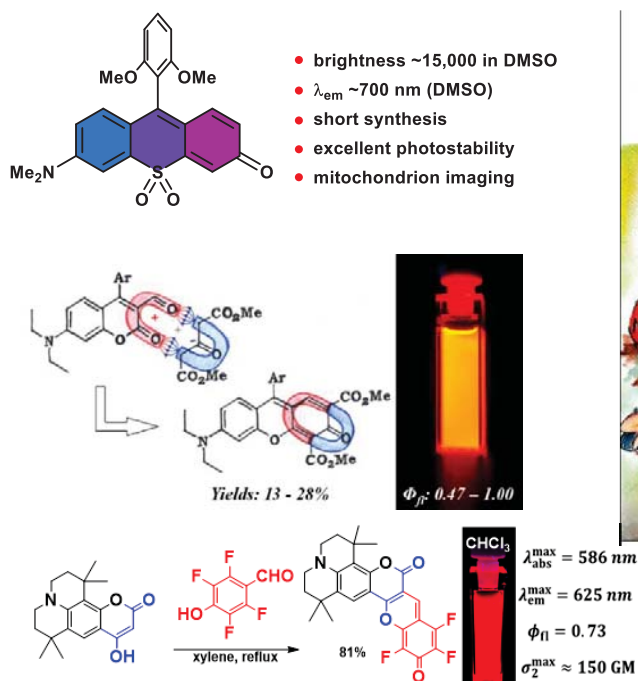
1. LIST OF PUBLICATIONS INCLUDED IN THE DOCTORAL THESIS

1. Yevgen M. Poronik, **Kateryna V. Vygranenko**, Dorota Gryko and Daniel T. Gryko, *Chem. Soc. Rev.*, 2019, 48, 5242-5265. 'Rhodols – synthesis, photophysical properties and applications as fluorescent probes'. IF₂₀₂₃ = 60.615.

2. **Kateryna V. Vygranenko**, Yevgen M. Poronik, Antoni Wrzosek, Adam Szewczyk and Daniel T. Gryko, *Chem. Comm.*, 2021, 57, 7782-7785. 'Red emissive sulfone-rhodols as mitochondrial imaging agents'. IF₂₀₂₃ = 6.065.

3. **Kateryna V. Vygranenko**, Yevgen M. Poronik, Manon H. E. Bousquet, Olena Vakuliuk, Denis Jacquemin and Daniel T. Gryko, *Chem. Comm.*, 2022, 58, 1542-1545. 'Direct transformation of coumarins into orange-red emitting rhodols'. IF₂₀₂₃ = 6.065.

4. Brunella Bardi, **Kateryna V. Vygranenko**, Beata Koszarna, Olena Vakuliuk, Łukasz Dobrzycki, Daniel T. Gryko, Francesca Terenziani and Anna Painelli, *Chem. - A Eur. J.*, 2023 - doi.org/10.1002/chem.202300979. 'A novel method for the synthesis of merocyanines: new photophysical possibilities for a well-known class of fluorophores'. IF₂₀₂₃ = 5.02.



2. LIST OF PUBLICATIONS NOT INCLUDED IN THE DOCTORAL THESIS

1. Olena Vakuliuk, Yong Woong Jun, **Kateryna Vygranenko**, Guillaume Clermont, Ye Jin Reo, Mireille Blanchard-Desce, Kyo Han Ahn, Daniel T. Gryko, *Chem. Eur. J.*, 2019, 25, 13354–13362. ‘Modified isoindole-1-one derivatives as bright fluorescent probes for cell and tissue imaging’ IF₂₀₂₃ = 5.02.
2. Łukasz Kielesiński, Irena Deperasińska, Olaf Morawski, **Kateryna V. Vygranenko**, Erik T. Ouellette and Daniel T. Gryko, *J. Org. Chem.*, 2022, 87, 5961–5975. ‘Polarized, V-shaped, and conjoined biscoumarins: from lack of dipole moment alignment to high brightness’. IF₂₀₂₂ = 4.198.

3. PARTICIPATION IN CONFERENCES AND SEMINARS.

1. 2nd CHAOS Training School C-H Activation in Organic Synthesis, Athens, Greece, 10-13.09.2019.
2. The training workshop, Newark, NJ, USA, 30.04.2022. “How to approach computer simulations for molecules and materials: from theory to practice”.
3. The 19th international symposium on novel aromatic compounds (ISNA 2019), Warsaw, Poland, 3-8.07.2022. ‘Direct transformation of coumarins into orange-red emitting rhodols’.

4. ABSTRACT IN ENGLISH

The main objective of my PhD course was to gain deep insight the synthesis and optical properties of rhodols, which might be applied in cell imaging and STED microscopy. I have started with development of the synthesis rhodols possessing endocyclic sulfone fragment. This was achieved via the 3-step synthesis of corresponding rhodamines, followed by the substitution of dimethylamino moiety with the oxygen atom. Having new sulfone-rhodols in hand, I decided to modify one of them by incorporation of hexyl chain with the quaternary phosphonium center at the terminal position to make the dye suitable for cell imaging. These compounds possess intriguing optical properties i.e. high fluorescent quantum yields and high Stokes shifts as well as excellent photostabilities.

The next goal was to develop the synthetic approach towards rhodols from coumarins via Knoevenagel condensation. For this purpose, I have synthesized 4-hydroxycoumarins possessing diethylamino moiety and the coumarin analogue with the annulated nitrogen atom at the position 7 and after additional 3 steps I have obtained 3-formyl-coumarins as the rhodol precursors. This double Knoevenagel condensation of 3-formyl coumarins with dimethyl 1,3-acetonedicarboxylate is absolutely unprecedented, because at the second step the source of carbonyl group is lactone ester, which is typically considered to be inert in this type of reactions. I have performed a huge part of work trying to find the best conditions for this condensation. In this case I tried various Lewis acids, bases, solvents, different temperature and the reaction time. Besides, on the basis of the electronic spectroscopy I have developed a convenient method for screening multiple experiments in the tiny scale to evaluate conversion and yields of reactions without workup and purification. As a matter of fact, the best catalyst revealed to be piperidine. This reaction allowed me to obtain new rhodols possessing two ester groups in 13-28% yield. The obtained rhodols demonstrate excellent quantum yields: 0.47 – 1.00 in DCM and DMSO.

The final of my research was a discovery of an extraordinary straightforward one-step synthesis of rhodols from *m*-aminophenols and tetrafluorohydroxybenzaldehyde. This method is similar to classic Friedel-Crafts condensation with a difference that a molecule of HF forms during the reaction instead of water as in the original method. The reaction successfully proceeds in toluene or xylene at elevated temperatures and does not require any bases or other additives. The product precipitates from the reaction mixture and can be purified via simple recrystallization. This approach is applicable to *m*-aminophenols, 4-hydroxy-7-aminocoumarins and hydroxyaminonaphthalenes, that allowed me to obtain an uncommon π -expanded linear rhodol and π -expanded rhodol analogues. This is the first representative of π -expanded rhodols with the additional benzene ring from amino side possessing the linear chromophore.

5. ABSTRACT IN POLISH / STRESZCZENIE W JĘZYKU POLSKIM

Głównym celem mojej pracy doktorskiej było pogłębienie wiedzy na temat syntezy i właściwości optycznych rodoli, które mogą znaleźć zastosowanie w obrazowaniu komórkowym i mikroskopii STED. W pierwszej fazie opracowałam syntezę rodoli posiadających endocykliczny fragment sulfonowy. Osiągnęłam to poprzez 3-etapową syntezę odpowiednich rodamin, a następnie podstawienie ugrupowania dimetyloaminowego atomem tlenu. Mając w rękę nowe rodole sulfonowe, zdecydowałam się zmodyfikować jeden z nich poprzez włączenie łańcucha heksylowego z czwartorzędowym centrum fosfoniowym w pozycji końcowej, aby barwnik nadawał się do obrazowania mitochondriów w komórkach eukariotycznych. Związki te posiadają intrygujące właściwości optyczne, tj. wysokie wydajności kwantowe fluorescencji i wysokie przesunięcia Stokesa, a także doskonałą fotostabilność.

Kolejnym celem było opracowanie syntetycznego podejścia do rodoli z kumaryn poprzez kondensację Knoevenagela. W tym celu zsyntetyzowałam 4-hydroksykumaryny posiadające ugrupowanie dietyloaminowe i analog kumaryny z pierścieniowym atomem azotu w pozycji 7 i po dodatkowych 3 etapach otrzymałam 3-formylo-kumaryny jako prekursor rodolu. Zastosowana w ostatnim etapie podwójna kondensacja Knoevenagela 3-formylokumaryn z 1,3-acetonodikarboksylianem dimetylu jest absolutnie bezprecedensowa, ponieważ w drugim etapie źródłem grupy karbonylowej jest ester laktonowy, który zwykle uważa się za niereaktywny w tego typu reakcjach. W czasie optymalizacji tej kondensacji, próbowałam różnych kwasów Lewisa, zasad, rozpuszczalników, różnej temperatury i czasu reakcji. Poza tym na podstawie spektroskopii elektronowej opracowałam wygodną metodę „skringu” wielu eksperymentów w małej skali w celu oceny konwersji i wydajności reakcji bez obróbki i oczyszczania. W rzeczywistości najlepszym katalizatorem okazała się być piperodyna. Ta reakcja pozwoliła mi otrzymać nowe rodole posiadające dwie grupy estrowe z wydajnością 13-28%. Otrzymane rodole wykazują doskonałe wydajności kwantowe fluorescencji: 0,47 – 1,00 w DCM i DMSO.

Zwieńczeniem moich badań było odkrycie niezwykle prostej, jednoetapowej syntezy rodoli z *m*-aminofenoli i tetrafluorohydroksybenzaldehydu. Metoda ta opiera się na klasycznej reakcji Friedela-Craftsa po której następuje wewnątrzcząsteczkowe aromatyczne podstawienie nukleofilowe. Reakcja z powodzeniem przebiega w toluenie lub ksylenie w podwyższonej temperaturze i nie wymaga żadnych katalizatorów. Produkt wytrąca się z mieszaniny reakcyjnej i można go oczyścić przez prostą rekrytalizację. Podejście to ma zastosowanie do *m*-aminofenoli, 4-hydroksy-7-aminokumaryn i hydroksyaminonaftalenów, co pozwoliło mi uzyskać rzadki liniowy π -rozszerzony rodol i analogi rodolu o π -rozszerzonym łańcuchu. Jest to pierwszy przedstawiciel π -rozprężonych rodoli z dodatkowym pierścieniem benzenowym od strony aminowej, posiadający liniowy chromofor.

6. GUIDE TO THE DOCTORAL THESIS

6.1 Purpose of the work

The study of biological systems at the cellular and subcellular levels is greatly aided by small molecule fluorophores of which members of the xanthene family, including fluorescein and rhodamine, have proven to be invaluable.¹ Recently, there has been an increased focus on the manipulation of the photophysical properties of these ubiquitous dyes through structural modifications. In particular π -expansion, and replacement of the xanthene oxygen atom bridge with silicon,²⁻⁴ phosphorus,⁵ sulfur,⁶ or carbon⁷⁻⁹ in rhodamine,¹⁰⁻¹³ fluorescein,^{14,15} and rhodol¹⁶ scaffolds have proven to be effective. The dyes from this extended family, despite their structural and functional diversity, share the quintessential characteristics: (a) planar aromatic structures; (b) excellent spectroscopic properties including intense absorption and fluorescence; (c) relatively small Stokes shifts; (d) biocompatibility. These features made them particularly attractive in fluorescence microscopy.

Since the design of commercially available confocal microscopes in 1960s, fluorescence microscopy has been one of the most important cell research methods, indispensable for life sciences. Moreover, as biological material by itself shows weak fluorescence response, the usage of fluorescent markers in microscopy techniques allows selective visualization of the diverse intracellular structures and monitoring different cellular processes.

The main drawback of this technique however was its spatial resolution which does not exceed 200 nm in the object plane (x, y) and 600 nm along the optical axis. The development of optical methods in microscopy has led to the emergence of a large number of modern techniques. In 1994 Stimulated Emission Depletion Microscopy (STED microscopy) was proposed as a new super resolution scanning fluorescence microscopy method.¹⁷ This approach is based on reducing the diameter of dots with an additional STED laser, which suppresses spontaneous emission in the outer region of the fluorescent spot due to the effect of stimulated emission. The beams of the exciting and STED lasers are carefully aligned, and the intensity distribution of the STED laser in focus has the form of a “donut”, with zero intensity in the centre. As a result, at high intensities of the STED laser, only those molecules exhibit fluorescence, which are located close to the region with zero intensity, while in the high-intensity zone is mainly stimulated emission of fluorophores that are rejected in the optical path due to coincidence with the wavelength of the STED laser.¹⁸ Sequential scanning of the entire sample gives a complete picture with super-resolution. In other words, a STED microscope is a laser scanning confocal microscope that reaches resolution beyond the diffraction limit by selective quenching of fluorescence.¹⁹ Therefore, fluorescence microscopy has

proven to be the best method for studying the mechanisms of functioning of organisms at the cellular, subcellular and molecular levels. The first dye used for theoretical description of STED-microscopy was rhodamine B. Nevertheless, the majority of existing fluorescent dyes turned out to be ineligible for super resolution imaging due to low photostability or non-suitable optical properties. Over the last decade, STED microscopy has become a general fluorescent technique, rather than highly specific method. The desire to answer more advanced cell-biological questions has led to the increased need for more advanced dyes, which can fulfil principal requirements: large fluorescence quantum yield in the near-infrared region, large Stokes shift good cell-permeability and most importantly high photostability.

My PhD-Thesis has two goals, which I plan to realize in parallel. Predominantly I challenged myself with developing entirely new synthetic methodologies leading to rhodols, rhodols modified at central bridging atom and 'rhodol-like' merocyanines. The methodologies available in the spring 2018 when I started my research work, although useful had many limitations. Predominantly they did not enable an access to broader range of rhodols possessing additional functionalities and/or an altered chromophore. The parallel goal was to obtain rhodols with the combination of more suitable photophysical properties i.e. bathochromically shifted emission, large fluorescence quantum yield and enhanced photostability.

6.2 The current state of knowledge in a given field of chemistry

The first mention about rhodol appeared in 1889, when it was prepared in a roundabout way starting from the decomposition of fluorescein, and was named by Bayer as ‘neuer Farbstoff’.²⁰ Being a structural hybrid of two dyes already known at that time – rhodamine and fluorescein – the new chromophore was named ‘rhodafluor’ (lately ‘rhodol’) – the one similar to rhodamine and at the same time possessing a ‘phenol component’ of fluorescein.²¹ Rhodols inherited photophysical properties of the parent dyes in terms of large extinction coefficient, large fluorescence quantum yield and solubility in majority of solvents (Fig.1). On the other hand, rhodols are more photostable compared to fluoresceins.¹⁶

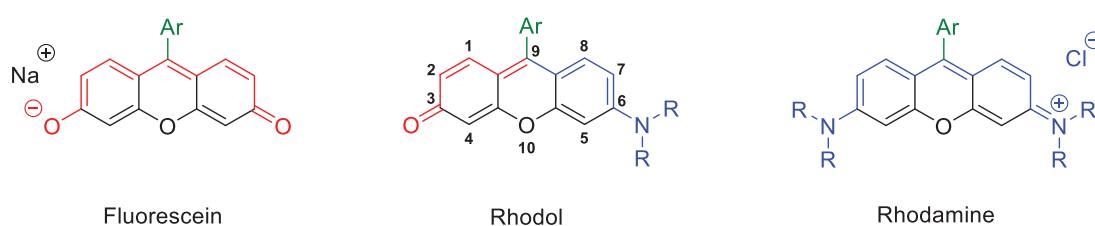


Figure 1. Structures of fluorescein, rhodol and rhodamine scaffolds.

All of the abovementioned dyes refer to polymethine dyes, since they possess a chromophore system, which consists of conjugated double bonds located between two terminal polar moieties. Rhodamine as one of the most distinguished representatives of cyanine dyes possesses a delocalized positive charge along the conjugated system, while fluorescein belongs to the oxonole group of dyes having a delocalized negative charge. In opposition to both parent dyes, rhodol corresponds to the merocyanine family and has an electronically neutral structure, which is illustrated in two limiting forms – neutral and dipolar (Figure 2).²²

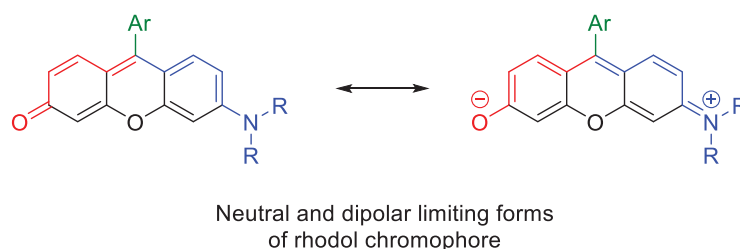


Figure 2. Balance between neutral and dipolar limiting forms of rhodol chromophore.

Comparable to fluoresceins, rhodols illustrate positive solvatochromism possessing red-shifted absorption and emission maxima in polar solvents. In the same way as parent dyes, rhodols can be

modified to influence the conjugation chain and, as a matter of fact, the photophysical properties, which allows to obtain the desired compound suitable for various applications (Figure 3).

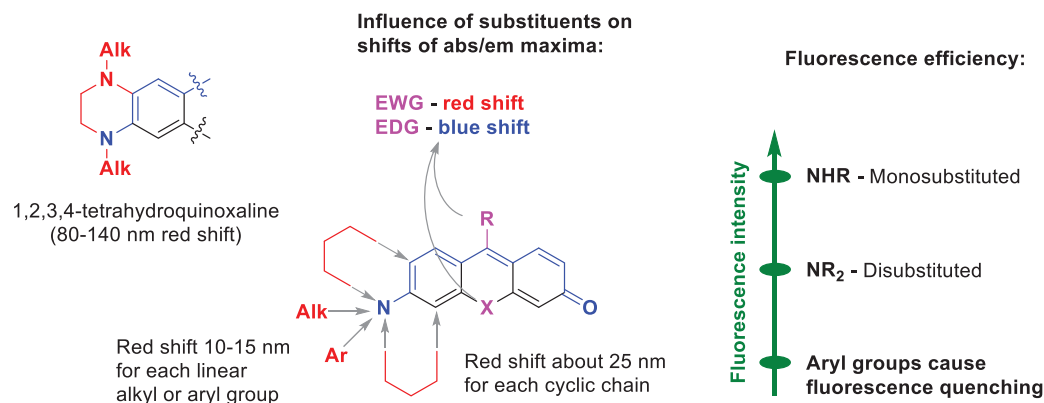


Figure 3. The influence of substituents on optical properties of rhodafluors.

The study of the substituent's nature influence on the absorption and emission spectra is rationalized by the Dewar-Knott rule.^{23,24} It states that incorporation of electron-donating groups into *meso*-position 9 and bridging position 10 results in blue-shift of the absorption maxima, meanwhile the electron-withdrawing groups provoke the opposite effect.

Furthermore, the spectral characteristics of rhodol fluorophores, such as emission maximum and fluorescence quantum yield, are quite dependent on the substitution patterns of the nitrogen atom in a similar manner to rhodamine.^{25,26} Rhodols with unsubstituted amino group exhibit very strong fluorescence at 516 nm. The addition of one alkyl substituent leads to the bathochromic shift of both absorption and emission maxima.²⁷ Meanwhile, rhodols comprising fully annulated terminal C-N bonds (julolidine moiety) exhibit even more red-shifted maxima, due to the restricted rotation of the amino group, though with reduced fluorescence quantum yields. In addition, the introduction of 1,2,3,4-tetrahydroquinoxaline moiety leads to the Stokes shift increase (80-140 nm) due to the presence of second electron-donating amino group in the neighboring position (Figure 3).^{28,29}

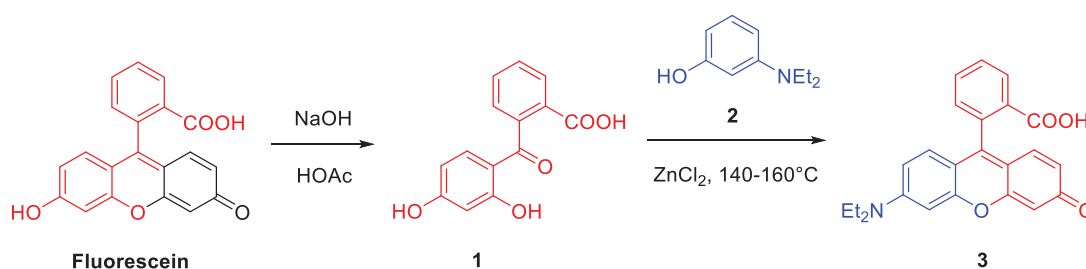
The aryl moiety plays a substantial role in rhodamines, fluoresceins and rhodols, governing some of their chemical and photophysical properties. Although, it is located orthogonally to the xanthenes scaffold and is not a part of the chromophore, it decreases the sensitivity of fluorophore's π -conjugated system to the nucleophiles.³⁰ The presence of the bulky substituent at *ortho*-position of benzene moiety increases the fluorescence efficiency, since it inhibits rotation of the aryl part and in this way minimizes the radiationless deactivation of the excited state.³¹⁻³⁴

Consequently, the analysis of the abovementioned led me to the conclusion that synthesis of new derivatized rhodols may be the perfect starting point to develop a new generation of stable functional dyes possessing range of key properties such as: high photostability, cell permeability, intense fluorescence and susceptibility to external stimuli.

6.2.1 Synthesis of classic rhodols

The first rhodol was synthesized in 1889 by Bayer. Previously he had developed synthesis of fluorescein and rhodamine, which acquired later an industrial value. The further investigations led to the formation of first rhodol and, thus, a new class of the merocyanine dyes. For this purpose Bayer had utilized base-induced hydrolysis of fluorescein followed by the formation of dihydroxybenzoylbenzoic acid and its condensation with *m*-aminophenol (Scheme 1).

Unfortunately, the authors did not provide any information about yields of both reactions.

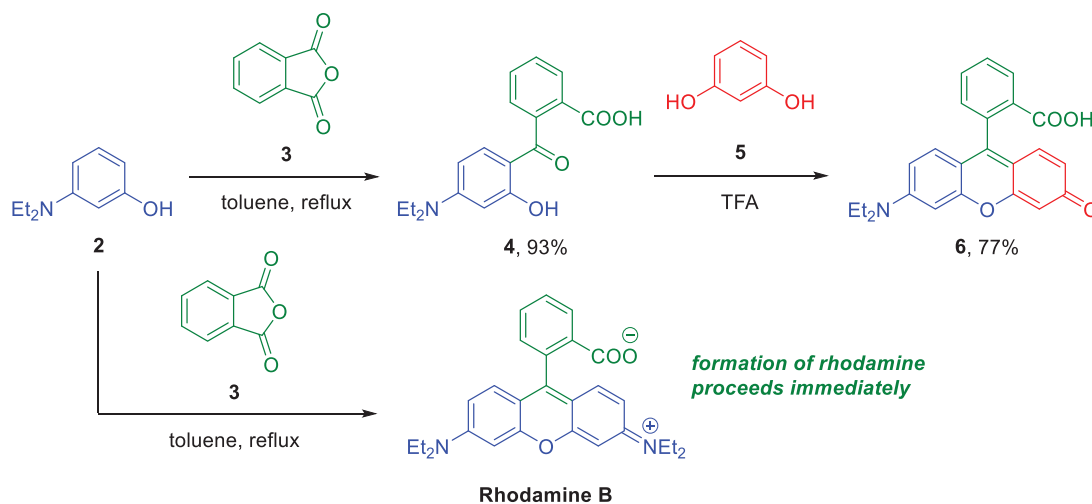


Scheme 1. Original method of rhodol formation based on a reversed substrate model.

Since 19th century this method still remains favored and is employed in many modern publications.^{28,29,43–49,35–42} However, the way of synthesis of benzophenones nowadays is different, since hydrolysis of fluorescein is not very convenient. Another option is condensation of phthalic anhydride with resorcinol derivatives in the presence of Lewis acids. This method of rhodol synthesis is more convenient than ‘classic’ one (Scheme 2) particularly in the case of complex *m*-aminophenols.

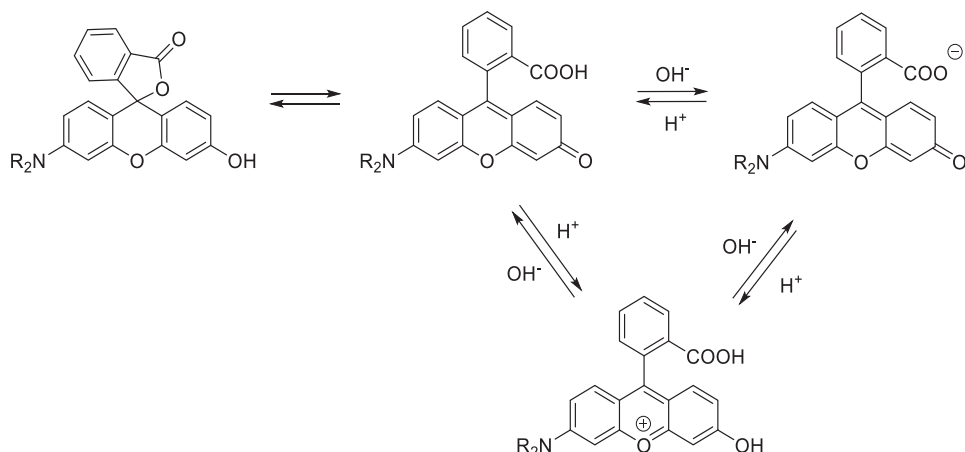
The most common method of preparation of symmetrical rhodamines and fluoresceins is a Friedel-Crafts acylation which involves phthalic anhydride and resorcinol or 3-dialkylaminophenol.^{50,51} However, this one-pot method is not applicable for rhodol attainment due to its asymmetrical structure. For this reason the most straightforward access to the rhodol structure is a two-step condensation of phthalic anhydride **3** with 3-dialkylaminophenol **2** followed by the reaction of the obtained benzophenone **4** with resorcinol **5** (Scheme 1).^{52,53} Even though this is the original and short method leading to the formation of the rhodol, the first step suffers from a significant

disadvantage. The concurring formation of rhodamine B via the addition of second molecule of 3-dialkylaminophenol **2** is preferable and proceeds almost immediately. For this reason it is crucial to use a considerable excess of phthalic anhydride to inhibit the side reaction.



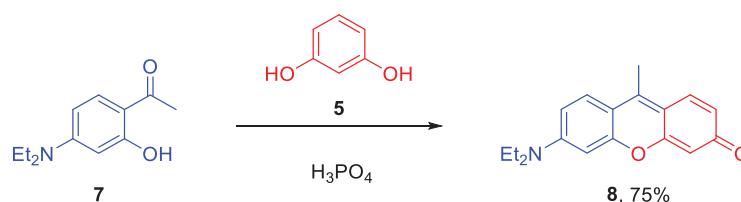
Scheme 2. ‘Classic’ method of rhodol synthesis from phthalic anhydride, 3-aminophenol and resorcinol.

Nevertheless, this simple procedure results in formation a rhodol skeleton possessing COOH group in the aryl moiety making product better soluble in water and more attractive for further modifications. Moreover, the carboxylic group equilibrates between spiro and open dye forms (Scheme 2). Acidic conditions stimulate the formation of the protonated or the spiroform, while in basic media rhodols are in the open dye form, since ring closure is impossible due to the salt formation. Despite all disadvantages, this method still remains one of the most inexpensive, fastest and the most straightforward approaches towards rhodols.^{30,35,61–70,52,71,54–60}



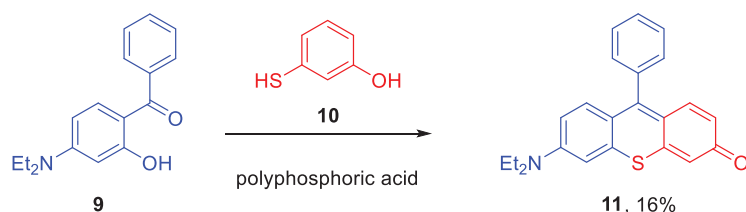
Scheme 3. The equilibrium between the dye open form and spiroform.

The use of acetophenone in the abovementioned method allows to incorporate a methyl group instead of aryl one at the meso-position of rhodol skeleton (Scheme 4).^{50,72,73} The original procedure includes Fries rearrangement of 3-acetoxy-*N,N*-dimethylaniline into acetophenone, which occurs however, in only 16% yield.⁵⁰ On the other hand, the transformation of 7-diethylamino-4-hydroxycoumarin into acetophenone results in 90% yield via ring-opening followed by decarboxylation.⁷³ The condensation of acetophenone **7** with resorcinol **6** occurs in phosphoric acid and leads to the rhodol formation in 75 % yield. Even though this method allows to incorporate different substituents in position 9, the synthetic access to the starting aromatic ketones is quite limited.



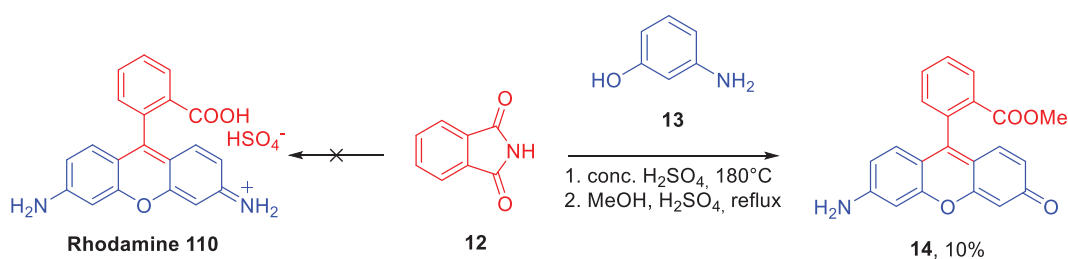
Scheme 4. The synthesis of rhodol **8** from acetophenone **7**.

A modification of the original method, employing monothioresorcinol **10** and benzophenone **9**, gives rhodol analogue **11** possessing the endocyclic sulphur instead of the oxygen atom.⁵⁰ On the other hand, the substitution of polyphosphoric acid with 50% sulfuric acid causes the conversion of monothioresorcinol into resorcinol, thus, resulting in the formation of O-rhodol instead of S-rhodol. By the time I started my investigation this was the only known example of rhodol with endocyclic sulphur atom.



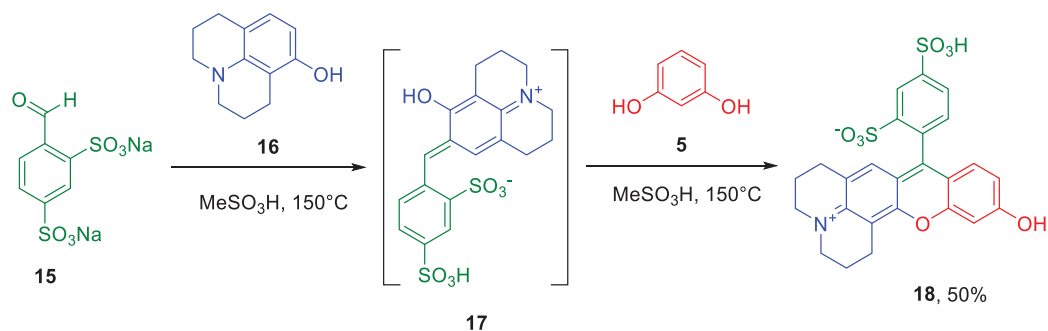
Scheme 5. The synthesis of rhodol with the endocyclic sulphur atom.

One of the most uncommon methods is the condensation of phthalimide with *m*-aminophenols in the presence of sulfuric acid.⁷⁴ The authors apply double excess of aminophenol **13**, that surprisingly do not result in the formation of **Rhodamine 110**, but leads to the cleavage of C-N bond to form rhodol **14**.



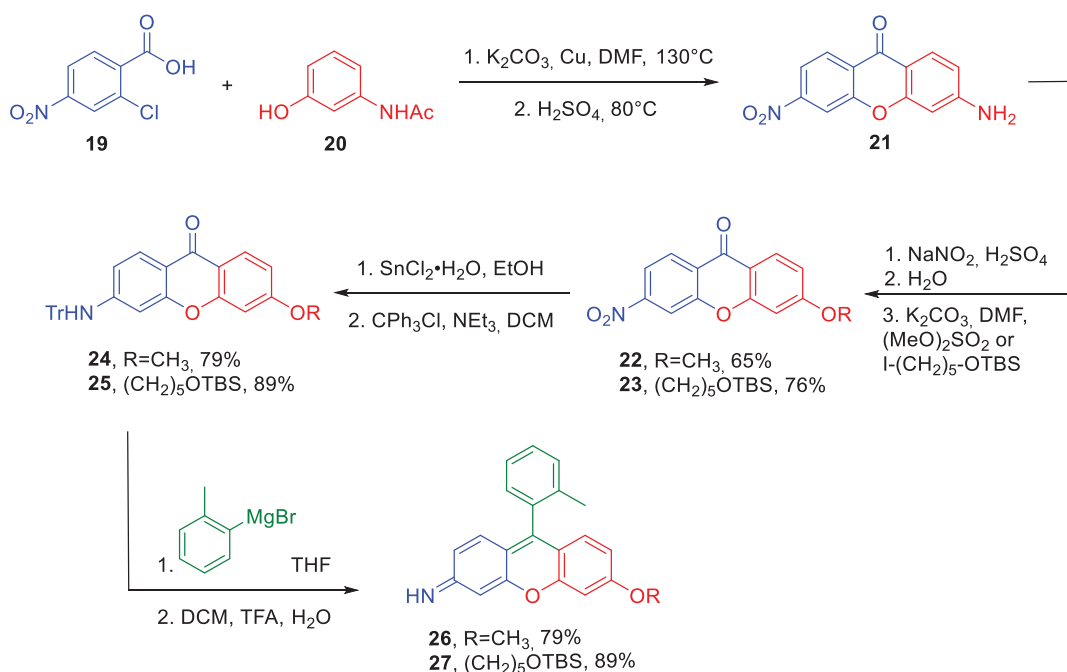
Scheme 6. Rhodol formation from phthalimide.

The use of substituted unsymmetrical phthalic anhydrides for rhodol synthesis via ‘classic’ method results in the formation of the mixture of 5- and 6-substituted derivatives. The separation of these isomers is challenging and in some cases is even impossible. However, Chevalier has offered the solution to this issue.^{75–77} His group has discovered that it is more convenient to use functionalized aldehydes, instead of phthalic anhydride derivatives, together with 8-hydroxyjulolidine. The intermediate **17** formed after the reaction of julolidine **16** with aldehyde **15** next undergoes the reaction with resorcinol affording rhodol **18** (Scheme 7). This type of Friedel-Crafts reaction is more common for synthesis of fluoresceins or rhodamines than for rhodols. Condensation of aldehyde with resorcinol or *m*-aminophenols affords methine intermediate which is more reactive than starting aldehyde, hence, the further reaction with second molecule of the substrate proceeds immediately and results in the formation of symmetric dye (rhodamine or fluorescein). That means that these conditions without any adjustment are not suitable for synthesis of unsymmetrical rhodols. Chevalier’s group has solved this problem utilizing modern techniques, like RP-HPLC for analysis and purification. Furthermore, chromatography fractions need to be lyophilized. This method was applied to various aminophenols affording new rhodols.



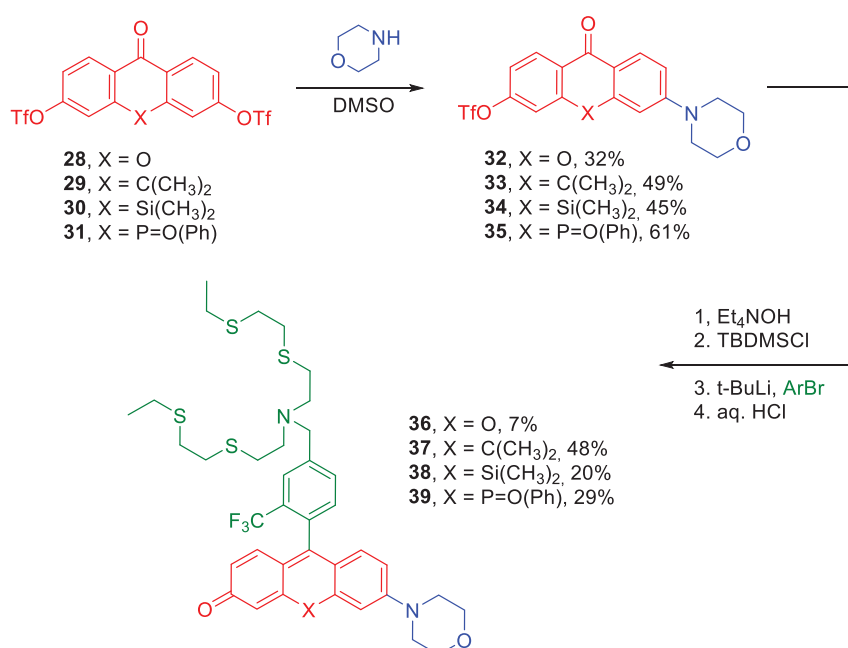
Scheme 7. Rhodol synthesis starting from benzaldehyde and 8-hydroxyjulolidine.

A more advanced synthetic route towards the rhodol chromophore is based on the preparation of the corresponding xanthone followed by the arylation with organo-metallic reagents (Scheme 8). This general strategy was utilized for the synthesis of both rhodamines and rhodols. The most challenging part is the preparation of the suitable xanthone scaffold, which allows for the modification of the main rhodol skeleton that is impossible to perform applying the conventional methods. This approach was used to prepare Singapore Green.⁷⁸ It starts from the condensation of 2-chloro-4-nitrobenzoic acid **19** and 3-acetamidophenol **20**, followed by the substitution of the amino with the alkoxy group. Consecutive reduction and protection afford compounds **24** and **25**. The following arylation and deprotection results in formation of Singapore Green dyes **26** and **27**.



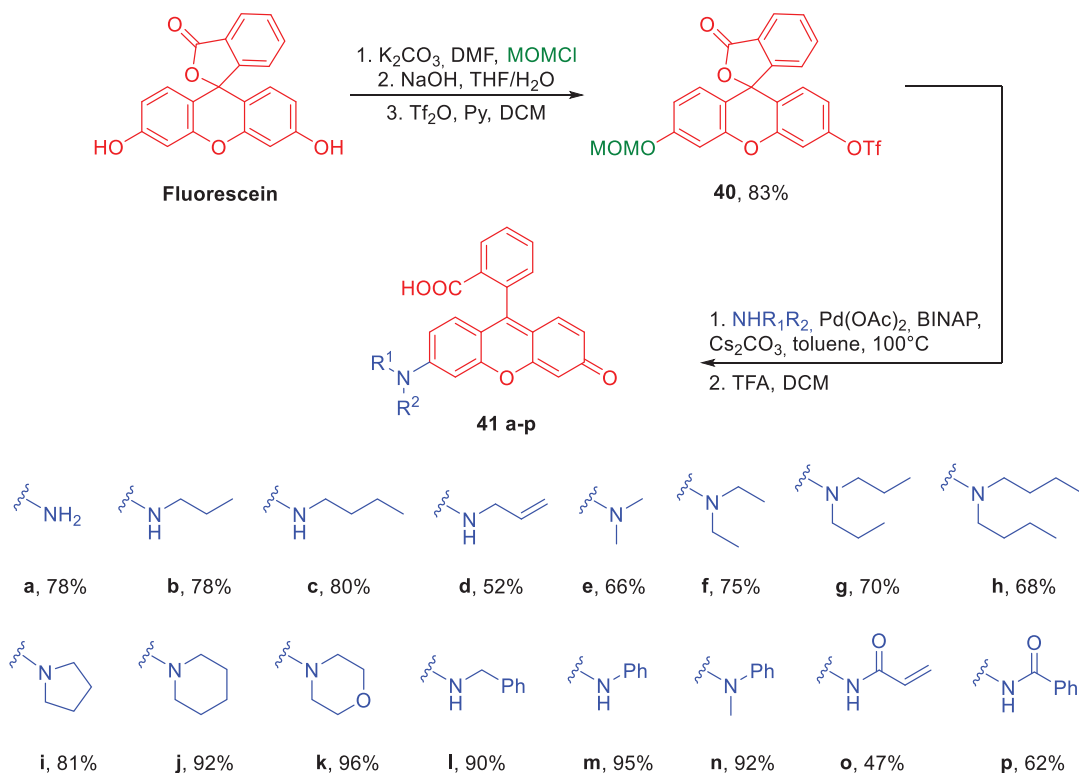
Scheme 8. The synthesis of Singapore Green **26** and **27**.

Alternatively, substitution of *meso*-position of xanthone can be beneficial in combination with a triflation of both hydroxy groups, followed by the amination of one of them (Scheme 9).^{79,80} The subsequent quenching of the remaining triflate group, its further protection with *tert*-butyldimethylsilyloxy group and arylation lead to the formation of the variety of rhodols **36-39**. The method has a great potential to increase the scope of new rhodols by the preparation of the rhodol heteroanalogues on the one hand, and introducing a plethora of secondary and tertiary amines on the other hand.



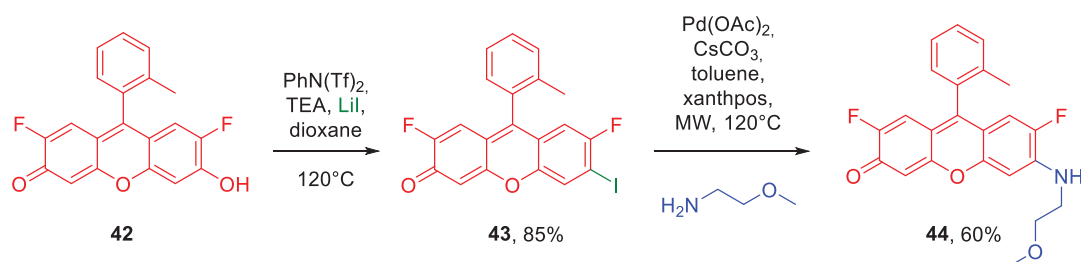
Scheme 9. General synthesis of rhodols from xanthone derivatives.

Another alteration of this procedure starts from fluorescein possessing carboxylic group in lactone form. In the original procedure one hydroxy group undergoes protection with MOMCl, while another one is transformed into triflate yielding compound **40** (Scheme 10).^{81,82} The subsequent amination in the presence of Pd catalyst, followed by deprotection of another OH group results in formation of a range of rhodols **41a-p** possessing different amino groups. This approach with a few slight modifications was successfully applied in the investigations by some other scientific groups.⁸²⁻⁸⁷ The reactivity of the carboxylic groups in the benzene ring at the *meso*-position is quite different so these can be converted independently.⁸⁸



Scheme 10. Synthesis of rhodols possessing various amino substituents via the catalyzed amination of fluorescein.

The following method shows a partial analogy with the amination of triflated fluoresceins. Fluorescein derivatives like Pennsylvania Green (**42**) can undergo the substitution of hydroxy group with the iodine atom, followed by the Buchwald-Hartwig amination reaction with microwave irradiation resulting in the formation of rhodol **44** (Scheme 11).⁸⁹

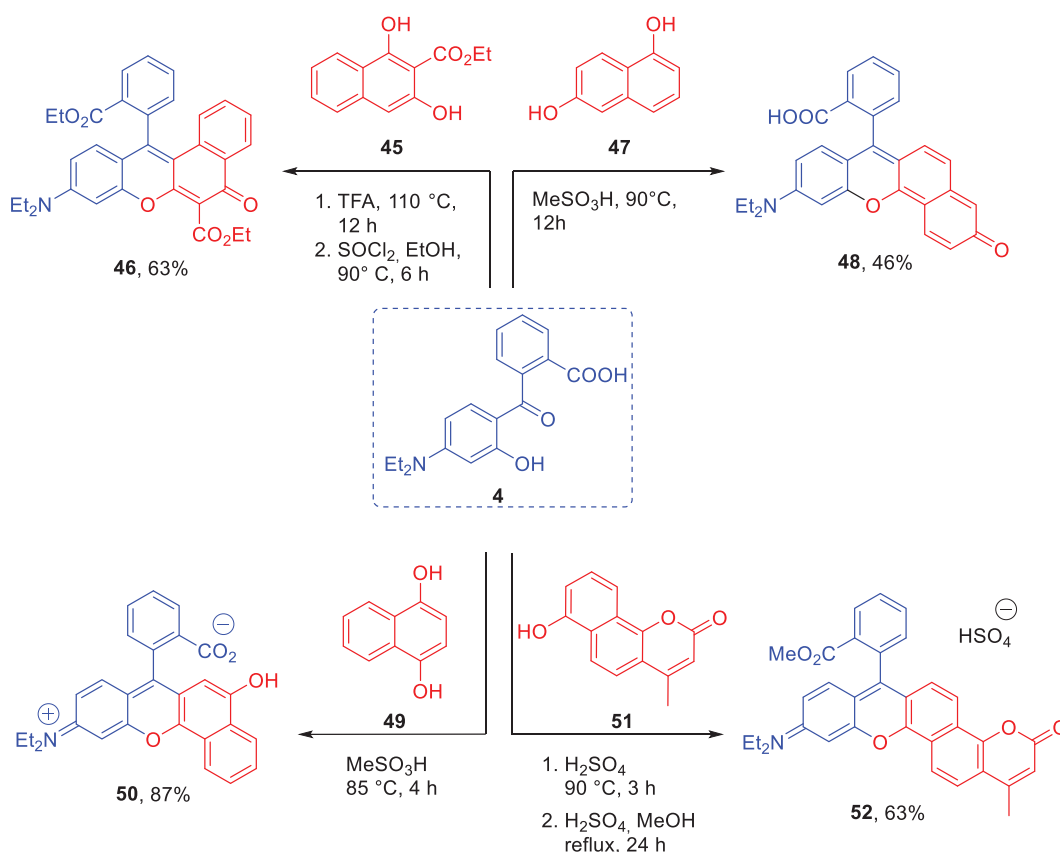


Scheme 11. Rhodol preparation method via iodine derivative of fluorescein.

6.2.2 Synthesis of π -expanded rhodols and 'rhodol-type merocyanines'

Seminaphthorhodafluors or 'SNARFs' are also members of rhodol family. These molecules possess a substituted naphthalene moiety instead of benzene from the side of hydroxy group. Initially, the authors have utilized 1,6-naphthalenediol **47** and 4-diethylamino-2-hydroxybenzophenone derivative **4** in the presence of methanesulfonic acid (Scheme 12).⁵⁶ This is another alteration of the routine rhodol synthesis in which resorcinol is substituted with various naphthalenediols. In some cases carboxylic group at the upper ring undergoes esterification to facilitate the purification process of products.

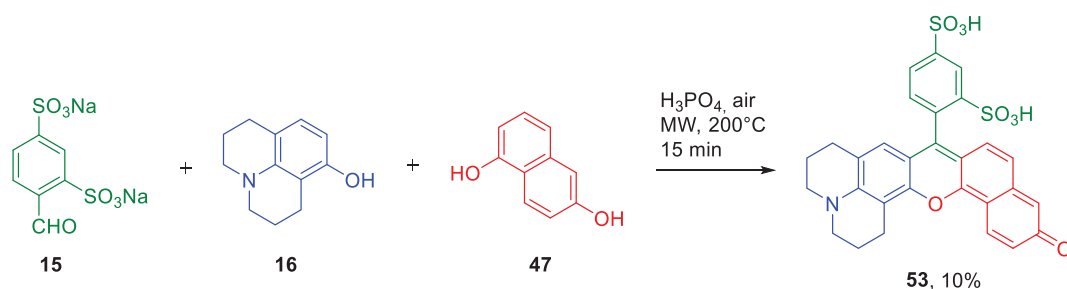
Originally abbreviation 'SNARF' corresponded only to the rhodols obtained in the reaction with 1,6-naphthalenediol by Haugland's group in 1991.⁵⁶ However, in following publications authors have applied this name to fluorophores obtained from another naphthalenediols, including benzocoumarin **51**.^{55,90-96}



Scheme 12. Preparation of seminaphthorhodafluors.

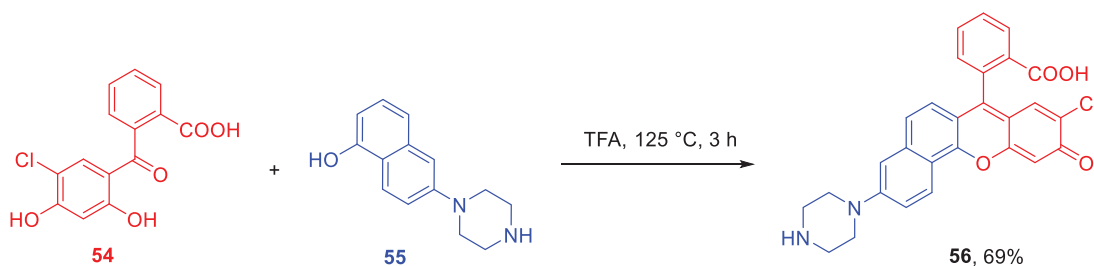
The use of aldehyde **15** and *m*-aminophenol instead of ready benzophenone is the adjustment of the abovementioned method. The one pot reaction of compounds **15** and **16** together with 1,6-

naphthalenediol **47** in the presence of phosphoric acid using microwave irradiation leads to the formation of rhodol **53** (Scheme 13).⁹⁷ This approach suffers from several significant drawbacks: low yield of rhodol (due to the formation of corresponding fluorescein in large amounts) as well as the difficulties with products' separation and purification. Meanwhile, Chevalier's group has managed to receive the same product in 43% yield applying two-step method, which was already mentioned (Scheme 7).⁷⁵



Scheme 13. One-pot three component method for SNARF preparation.

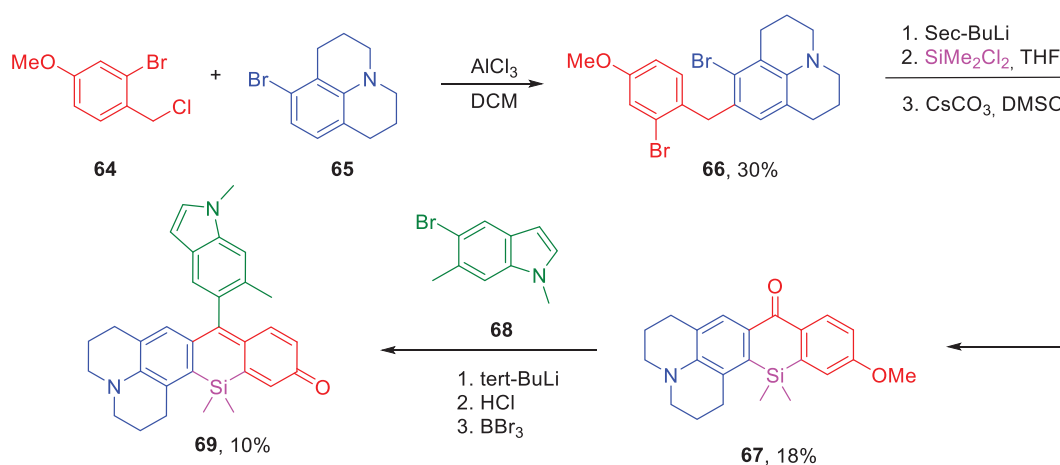
Exceptional representatives of π -expanded rhodols are fluorophores possessing naphthalene fragment from amino side. This can be probably explained by difficulty of synthesis of the corresponding substrates for such reversed ring configuration in comparison to the original pattern. Rhodol **56** was obtained as a result of condensation between 1-hydroxy-6-piperazine-naphthalene (**55**) and benzophenone **54** in the presence of trifluoroacetic acid (Scheme 14).⁴⁴



Scheme 14. Reversed substrate pattern method for synthesis of naphthorhodol.

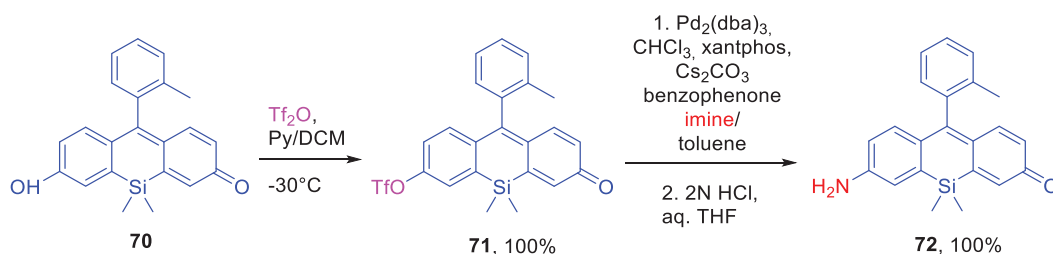
The aryl moiety at position 9 typically does not influence the photophysical properties since it is located orthogonally to the main chromophore scaffold. Linking of the aryl fragment to the xanthene core gives rise to so-called V-shaped dyes.^{98,99} Even though the expansion is not caused by addition of another benzene ring, additional bond between aryl and xanthene moieties introduces π -expansion, so compounds **60-62** can be still formally classified as π -expanded rhodols (Scheme 15).

Similarly to previously reported fluorescein and rhodamines,^{30,31,102,51,53,55,61,64,65,100,101} the substitution of the endocyclic electron-donor oxygen atom in rhodol scaffold with more electron-deficient silica, selenium or phosphorus containing moieties as well as carbon fragment leads to the bathochromic shift of both absorption and emission maxima. Furthermore, rhodols with phosphine oxide moiety exhibit an extraordinary photostability,⁵ compared to that of C-substituted rhodols.⁹ The orbital interaction between the newly incorporated bridging moiety and xanthene scaffold leads to the red-shifted absorption and emission properties. This effect can be enhanced by introduction of more electron-withdrawing moiety.



Scheme 16. Preparation of Si-rhodols.

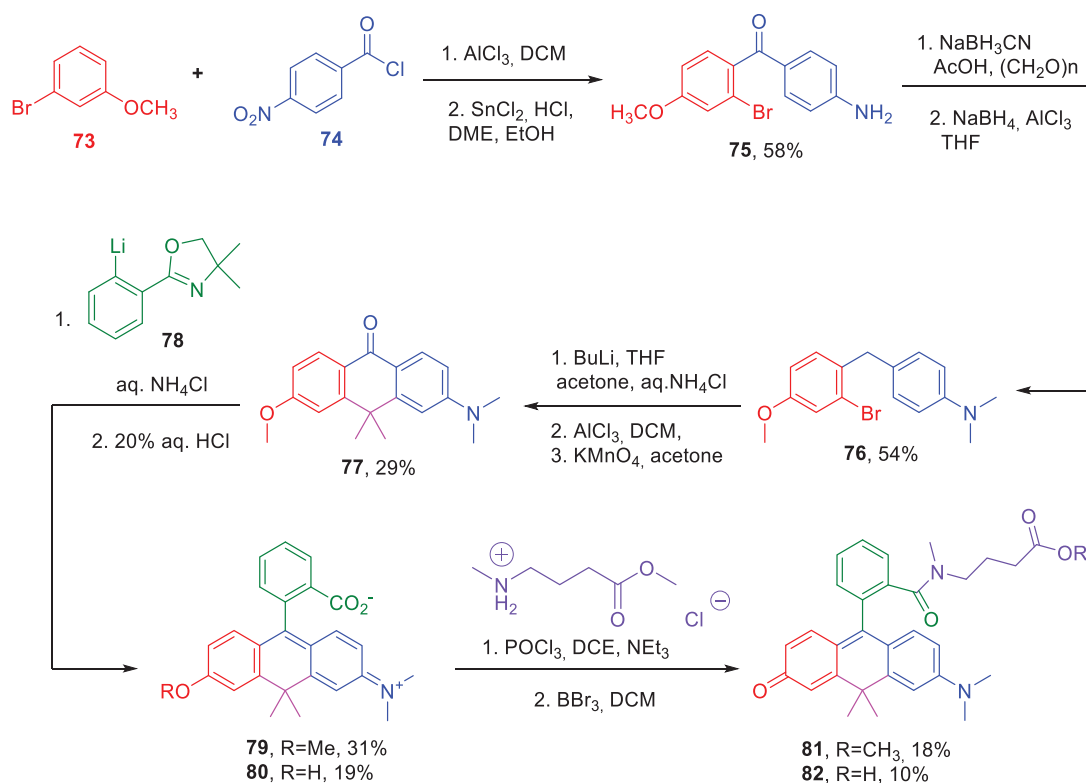
A few approaches towards Si-rhodols were reported. One of them is based on synthesis of the silicon-containing xanthone **67** starting from 8-bromojulolidine **65** and 2-bromo-4-methoxybenzyl chloride **64**, followed by ring closure via silylation and oxidation of methylene fragment (Scheme 16).¹⁰³ The subsequent arylation of xanthone **67** and deprotection of hydroxy group results in formation of Si-rhodol **69**.



Scheme 17. Preparation of Si-rhodols via Pd-catalyzed amination of the corresponding fluorescein.

Another approach towards Si-rhodols starts from the corresponding fluorescein analogue **70**,¹⁰⁴ which is subjected to the triflation of hydroxy group and its following substitution with amino group in the Pd-catalyzed conditions (Scheme 17).¹⁰⁵

The preparation method for the carborhodols is the most complex among other rhodol analogues. The synthetic approach consists of 11 steps and proceeds through the formation of unsymmetric xanthone derivative **77** possessing carbon bridge, followed by the arylation and deprotection of hydroxy group (Scheme 18).¹⁰⁶

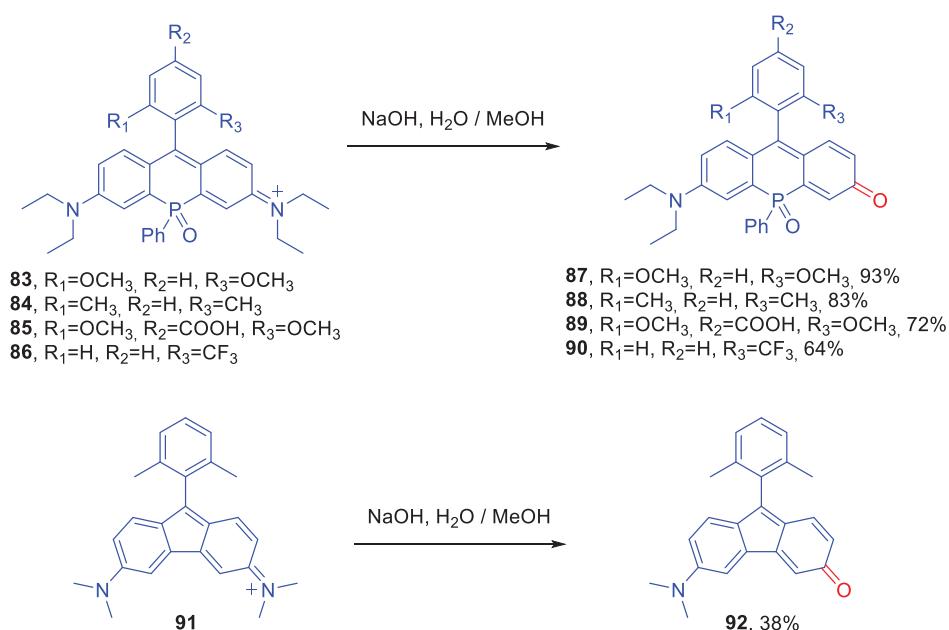


Scheme 18. Preparation of C-rhodols.

The transformation of rhodamines into rhodols via hydrolysis was first reported in the end of 20th century.²⁷ This method seemed to be inefficient with classic oxygen-bridged rhodamines, thus, it was forgotten for many years. However, rhodamines possessing electron-withdrawing endocyclic heteroatom appeared to be more reactive in terms of the hydrolysis to form rhodols. Thus, P=O-bridged rhodamines **84-87** easily undergo substitution of diethylamino moiety with the oxygen atom under basic conditions resulting in formation of P=O-rhodols **88-91** in high yields.¹⁰⁷ The use of highly concentrated solutions of sodium hydroxide leads to the formation of the corresponding fluoresceins. The authors also emphasize that the presence of a bulky substituent at *ortho*-position

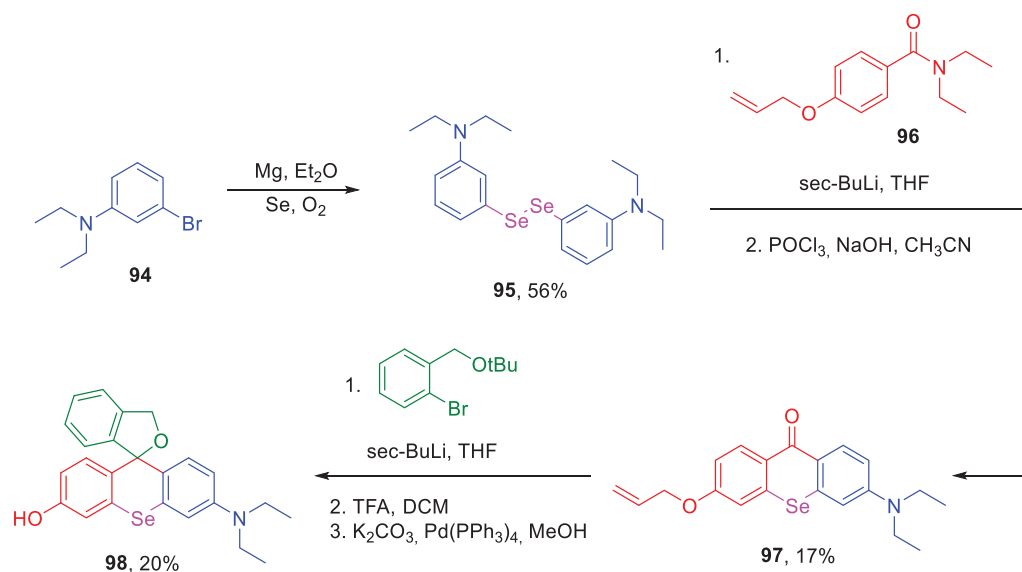
of aryl moiety is crucial to avoid nucleophilic attack of the hydroxyl ion at position 9, that leads to the breaking of chromophore conjugation and, thus, to discoloration.

The same approach was utilized for the synthesis of fluorene analogue of rhodol. Grzybowski et.al. has performed an unprecedented synthesis of rhodamine analogues, which possess central five-membered ring instead of 6-membered heterocycle.¹⁰⁸ Such rhodamine **91** was subjected to the hydrolysis reaction in the presence of NaOH resulting in the formation of rhodol analogue **92** (Scheme 19).



Scheme 19. Formation of the rhodol-type chromophore via the hydrolysis of corresponding rhodamines.

Rhodols bearing endocyclic selenium atom are known as well and can be obtained starting from transformation of 3-bromo-N,N-diethylaniline **94** into diselenide **95**.¹⁰⁹ This method was originally used for synthesis of rhodamines containing endocyclic selenium atom.^{110,111} In this case, to obtain rhodol **98** the authors had to couple diselenide **95** with allyloxybenzamide **96** affording xanthone **97** and then to perform arylation and deprotection of hydroxy group.



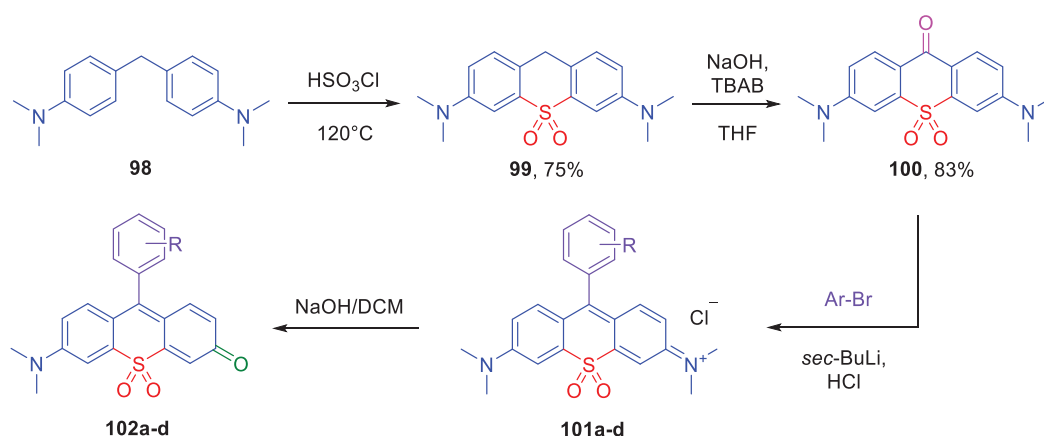
Scheme 20. Preparation of Se-rhodols.

To sum up, all synthetic approaches towards rhodols can be differentiated into 3 general techniques: (a) condensation of aromatic 4-amino-2-hydroxyketones with resorcinols or vice versa – 2,4-dihydroxybenzophenons with *m*-aminophenols, (b) formation of the correspondent xanthenes and their further arylation and (c) catalytic amination of the appropriate fluorescein derivative. Besides, there are some methods for the preparation of individual compounds without the possibility of employing them as a general synthetic approach (e.g. Schemes 5 and 6). Besides, the syntheses of rhodol analogues possessing endocyclic heteroatoms different from oxygen still are not developed enough. Formation of C-rhodols is the most challenging and rhodols possessing sulfur groups were unknown. Another issue is synthesis of π -expanded rhodols. Even though there were several reports about these compounds, still their formation and the usage are challenging due to the unavailability of the substrates, difficulty in their synthesis, low yields due to side reactions or poor solubility of products making them inappropriate for further studies.

6.3 Results and discussions

6.3.1 Red emissive sulfone-rhodols as mitochondrial imaging agents

By the time I started my first project, I had performed literature search and found out that there was only one example of rhodol with endocyclic sulfur atom.⁵⁸ Besides, there was no single report on rhodols containing sulfone or sulfoxide fragment either.¹⁶ Taking into consideration that C-, Si-, Se- and P-rhodols possess red-shifted absorption and emission maxima, higher quantum yields and better photostability in comparison to O-rhodols, I have concluded that considering electron-withdrawing properties of the SO₂ moiety, SO₂-rhodols may exhibit even better photophysical properties than other representatives of this family. Since P=O rhodamines successfully undergo transformation into rhodols due to the presence of electron-withdrawing P=O moiety,¹⁰⁷ I expected that the presence of stronger SO₂ group should accelerate such reaction as well. I have started my work from synthesis of the scope of sulfone-rhodamines using the earlier reported synthetic approach, which starts from crosslinking of 4,4'-methylenebis(N,N-dimethylaniline) **98** with oleum.³¹ At this point I decided to substitute oleum with chlorosulfonic acid, since it is more commercially available and more convenient to work with (Scheme 21). As a matter of fact I have received a product **99** with yield slightly higher than in the original method. The conditions of the subsequent oxidation were altered as well. I have utilized sodium hydroxide in the presence of TBAB instead of iron (III) chloride in hydrochloric acid and obtained xanthone **100** in 83% yield (35.7% in the original approach).



Scheme 21. Synthetic procedure for SO₂-rhodols

Another controversy was the choice of aryl bromides for future rhodamines. It was very important to choose the most fitting substituents in SO₂-rhodols, because even small structural changes can influence the photophysical properties. The attack of nucleophile at C9-position of unhindered rhodols leads to the interruption of the π -conjugation and, thus, to the decoloration.¹⁰¹ Besides, this substituent had to be bulky enough to prevent the addition of nucleophile. For example, P=O-rhodols possessing methyl group in *ortho*-position undergo nucleophilic attack under basic conditions, because CH₃ group is not big enough to shield carbon in *meso*-position, while CF₃ or OMe, manage to prevent disruption of chromophore's π -conjugation system.¹⁰⁷

For this reason, I have chosen anthracene and aryls possessing trifluoromethyl and methoxy group in *o*-position. Despite my expectations, I was not able to obtain pure SO₂-rhodamines **101a-d**. Mass analysis showed that there was always a second rhodamine possessing a monomethylamino moiety due to the cleavage of one methyl group. It was impossible to purify products using column chromatography with any liquid or solid phases. Recrystallization did not help either. I decided to use these rhodamines in next step without any purification. The subsequent hydrolysis cleanly afforded SO₂-rhodols **102a-d** (Figure 4).

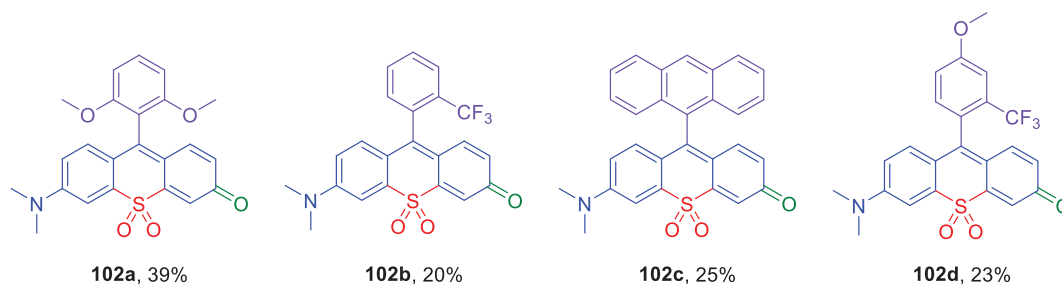
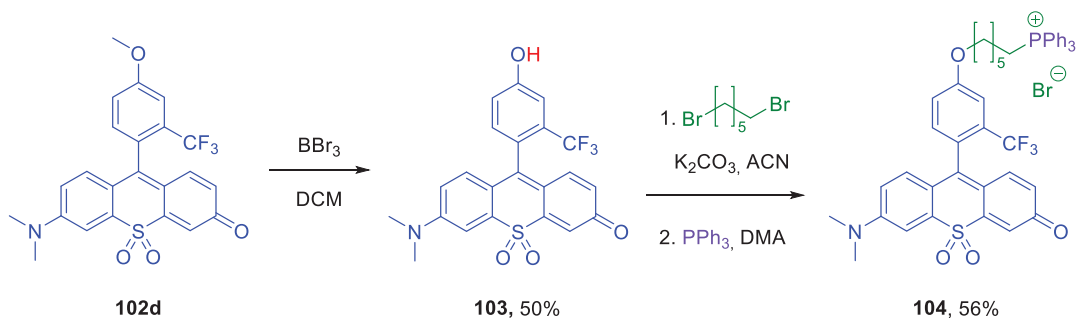


Figure 4. Obtained sulfone-rhodols **102a-d**

The subsequent idea was to modify one of the obtained rhodols by introduction of triphenylphosphonium salt to make it suitable for cell imaging. For this reason, I have performed cleavage of methyl group of rhodol **103d** followed by monoalkylation with 1,6-dibromohexane (Scheme 22).



Scheme 22. Synthesis of rhodol for mitochondria imaging

The further reaction with triphenylphosphine leads to SO₂-rhodol **104**. The last step is very unreliable, since even small changes can influence the conversion, purity and yield. It should be conducted under inert atmosphere, at high temperature with 10 eq. of PPh₃ and short reaction time. Unfortunately, both substrate and product decompose if the reaction time is prolonged. Compound **104** was successfully used for staining mitochondria in cardiac H9C2 cell line.

As I expected, fluorophores **102a-d**, **103** and **104** exhibited red-shifted absorption and emission maxima in comparison to the classic rhodol. Besides, they demonstrated a significant positive solvatochromism: from $\lambda_{\text{abs}} = 543 - 553$ nm in toluene to $\lambda_{\text{abs}} = 667 - 669$ nm in H₂O/DMSO mixture (Figure 5).

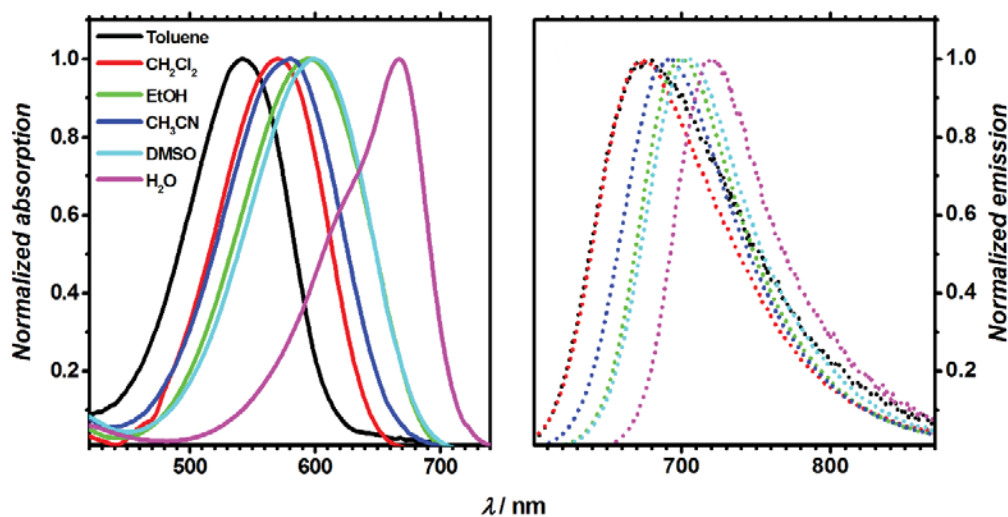


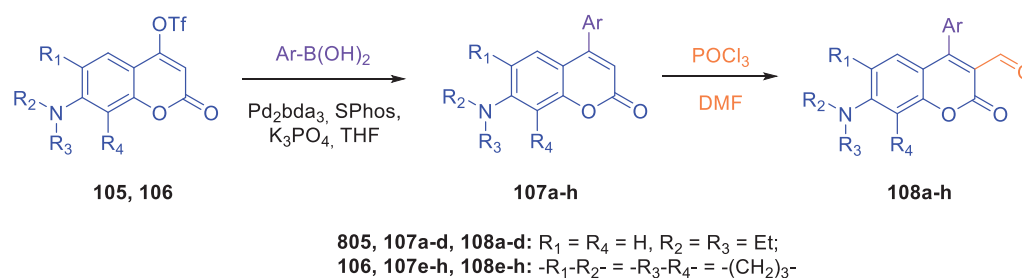
Figure 5. Absorption (solid) and emission (dotted) spectra of rhodol **102a** in different solvents.

These compounds possess high quantum yields in polar solvents – around 0.5 in ethanol, acetonitrile and DMSO with brightness up to $35,000 \times \text{M}^{-1} \times \text{cm}^{-1}$. The only exception is rhodol **102c** – the quantum yield of this compound is low in any solvent (from 0.01 in DMSO to 0.13 in DCM).

Another advantage of these new core-modified rhodols is their photostability. Dyes **102a** and **103** displayed excellent photostability comparable to that of Rhodamine 6G and Cresyl Violet.

6.3.2 Direct transformation of coumarins into orange-red emitting rhodols

Next project was focused on the idea of transformation of coumarins into rhodols. The root of this concept goes back to the work reported by Gandioso et.al, which based on the transformation of coumarin's lactone group into thiolactone (C=S) to make it reactive enough for the condensation with activated CH₂ group.^{112,113} First, I tried to apply this approach to a few bis-coumarins,¹¹⁴ to which I had access, to obtain new V-shaped rhodols. I have managed to obtain bis-thio derivatives, but these compounds revealed to be too capricious and unstable in the reaction mixture. The final second step was very challenging and the product I obtained displayed poor solubility. Then I decided to change the reaction platform to start from compounds which would express similar reactivity. First, I synthesized a scope of 3-formyl coumarins **108a-h** (Scheme 23).



Scheme 23. Synthesis of 3-formyl-4-arylcoumarins.

This approach proceeded through the already known formation of 4-hydroxy coumarins from *m*-aminophenols and ‘magic malonate’ followed by triflation of the hydroxy group.¹¹⁵⁻¹¹⁷ Next I performed Suzuki reaction with various aryl moieties to afford coumarins **107a-h**. The following formylation allowed me obtaining 3-formyl coumarins **108a-h** in reasonable yields (Table 1).

Table 1. Yields of compounds **107a-h** and **108a-h**

<i>Nr</i>	<i>R</i> ₁	<i>R</i> ₂	<i>R</i> ₃	<i>R</i> ₄	<i>Ar</i>	<i>Yield, %</i>
107a	H	Et	Et	H	<i>o</i> -tolyl	97
107b	H	Et	Et	H	2,6-dimethoxyphenyl	76
107c	H	Et	Et	H	2,3-dimethoxyphenyl	92
107d	H	Et	Et	H	pyrenyl	86
107e	-(CH ₂) ₃ -		-(CH ₂) ₃ -		<i>o</i> -tolyl	90

107f	-(CH ₂) ₃ -	-(CH ₂) ₃ -	2,6-dimethoxyphenyl	94
107g	-(CH ₂) ₃ -	-(CH ₂) ₃ -	2,3-dimethoxyphenyl	89
107h	-(CH ₂) ₃ -	-(CH ₂) ₃ -	2,4-dimethoxyphenyl	84
108a	H Et	Et H	<i>o</i> -tolyl	60
108b	H Et	Et H	2,6-dimethoxyphenyl	50
108c	H Et	Et H	2,3-dimethoxyphenyl	28
108d	H Et	Et H	pyrenyl	80
108e	-(CH ₂) ₃ -	-(CH ₂) ₃ -	<i>o</i> -tolyl	84
108f	-(CH ₂) ₃ -	-(CH ₂) ₃ -	2,6-dimethoxyphenyl	87
108g	-(CH ₂) ₃ -	-(CH ₂) ₃ -	2,3-dimethoxyphenyl	86
108h	-(CH ₂) ₃ -	-(CH ₂) ₃ -	2,4-dimethoxyphenyl	32

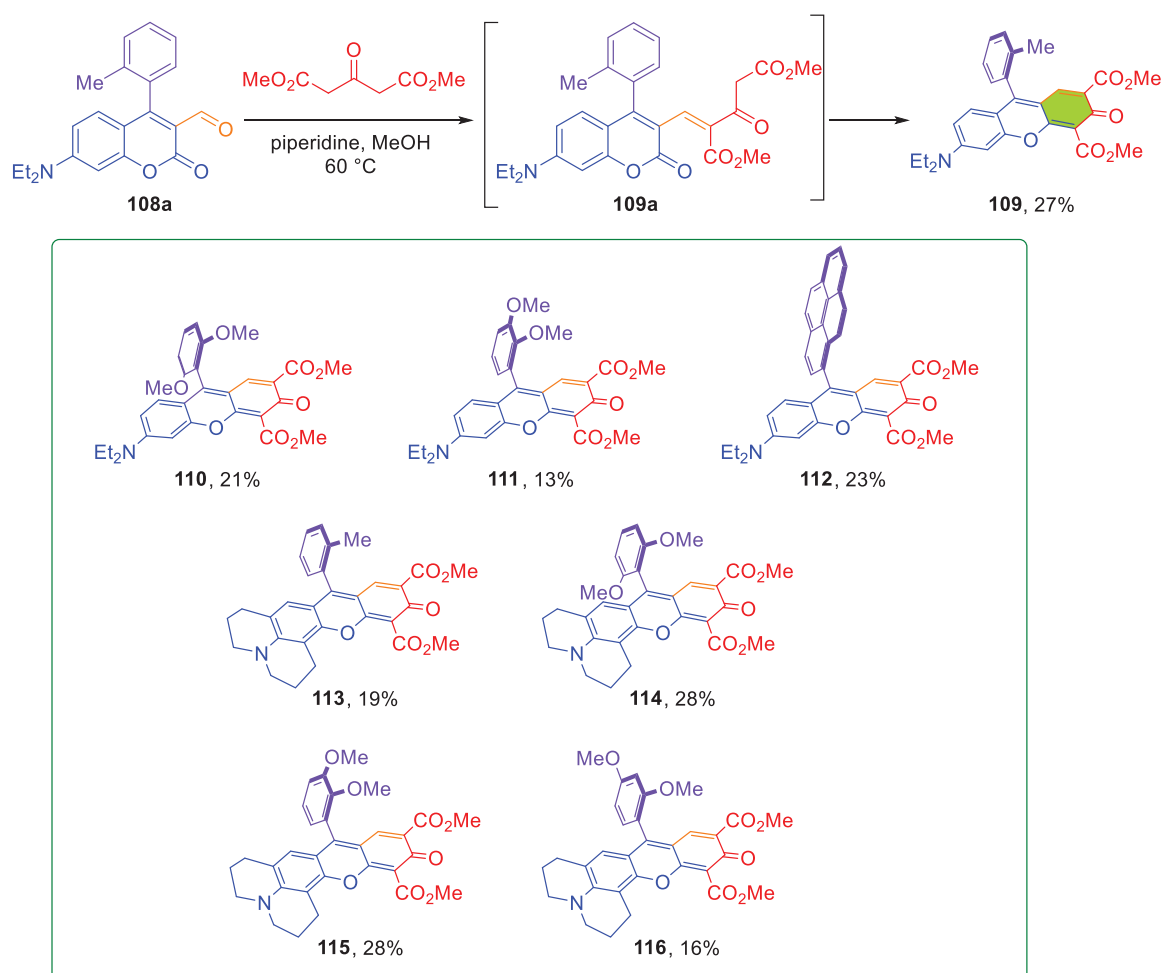
The following step was to perform the reaction between 3-formylcoumarin **108a** and Lawesson's reagent. Unfortunately, I did not manage to obtain the desired product and the use of P₂S₅ did not help either. Meanwhile, I decided to try the direct transformation of 3-formylcoumarins into rhodols without the conversion into the intermediate thione.

My first attempt was performed with 4-tolyl-3-formylcoumarin **108a** and dimethyl 1,3-acetonedicarboxylate in the presence of InCl₃ and acetic acid anhydride. As a matter of fact, I have obtained a mixture of lots of products, in which I have managed to identify and purify the desired rhodol **109**. However, the yield was extremely low and the purification required several chromatographic steps. Thus, I have embarked on the long optimization choosing coumarin **108a** and dimethyl 1,3-acetonedicarboxylate as model substrates. In numerous attempts I have altered acidic and basic catalysts, solvents as well as temperature and the reaction time. Finally, I have found that the best results I observed when 2,6-lutidine was used. The yield of the product **X** was 26%. However, when I tried to perform this reaction with coumarin **108b** I faced another issue: there was no substrate in the mixture, but there was a lot of unreacted intermediate (e.g. **109a**) even after 24h of heating.

At this point I had to start another optimization to find better conditions. Together with Dr. Poronik I have found, that substrate, intermediate and final product have yellow, orange and pink colours respectively that prompted us to the idea, that reactions for optimisation can be performed in very small scales and the conversion can be monitored using spectrophotometer. On the basis of the Lambert-Beer law, I was able to calculate concentrations of the substrate, intermediate and the product to find the reaction conversion and the product yield. Characteristic band of rhodol was 537 nm, while for substrate **108b** and intermediate it was 437 nm and 448 nm respectively. This optimization technique enabled screening multiple reaction conditions in short time. Eventually, I

found that the best catalytic system is a piperidine in methanol. The final step in the optimization was to analyse how the excess of dimethyl 1,3-acetonedicarboxylate influences the reaction kinetics. I have checked the rate of condensation with 2, 5 and 10 eq. of dimethyl 1,3-acetonedicarboxylate and the best results were achieved with 10 eq. of the diester. The main drawback of this method is that acetonedicarboxylate is a highly reactive compound capable to undergo self-condensation along with numerous other undesired processes in the presence of piperidine. These by-products possess characteristic bands in the electronic spectrum which can overlap with the diagnostic peaks, thus making the visualization method less precise.

The double Knoevenagel condensation allows to obtain a range of new rhodols **109 – 116** (Scheme 24).



Scheme 24. Knoevenagel condensation of 3-formylcoumarin with dimethyl 1,3-acetonedicarboxylate and scope of the obtained rhodols

These new dyes absorb light around 535-560 nm and emit at 560-590 nm (Figure 6). They do not possess a significant positive solvatochromism, like the majority of other merocyanine dyes, however, they display large fluorescence quantum yields: 0.47 – 0.68 for rhodols **109-112** and 0.86 – 1.00 for dyes **113-116**.

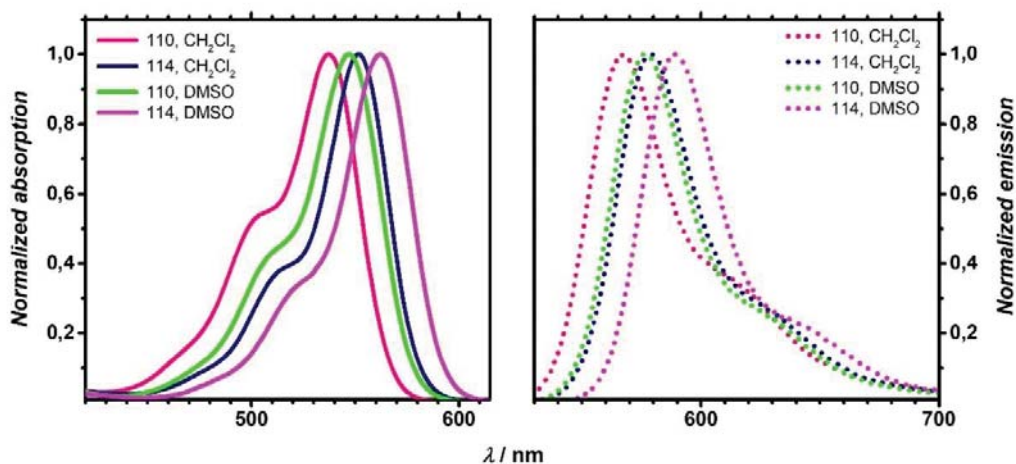
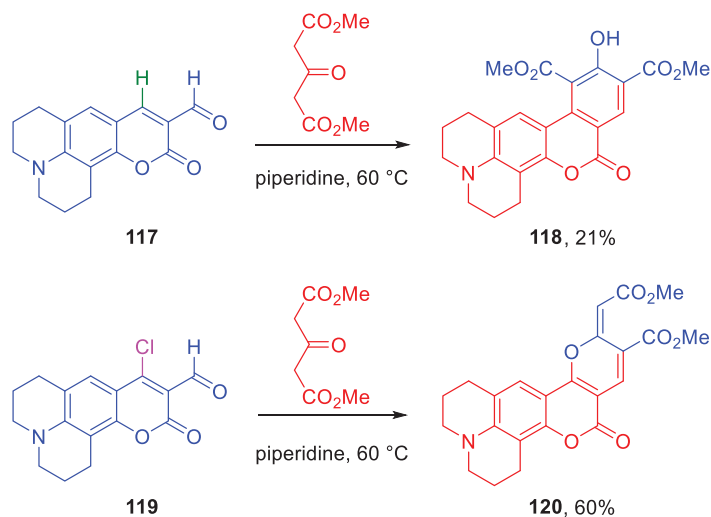


Figure 6. Absorption (solid) and emission (dotted) spectra of rhodols **110** and **114**.



Scheme 25. Condensation of other 3-formylcoumarins with dimethyl 1,3-acetonedicarboxylate

I was curious whether applying this method I would be able to obtain rhodols with unsubstituted position 9 or with chlorine atom at C9, which could be suitable for further modifications. For this

reason, I have utilized the corresponding coumarins **117** and **119**. To my surprise, I did not observe even a trace of expected rhodols (Scheme 25). Instead, I had got yellow and red solids with the identical signals in the MS spectrum. The structures were identified by means of X-ray diffraction analysis.

6.3.3 One-step transformation of aminophenols and coumarins into rhodols and ‘rhodol-like’ merocyanines

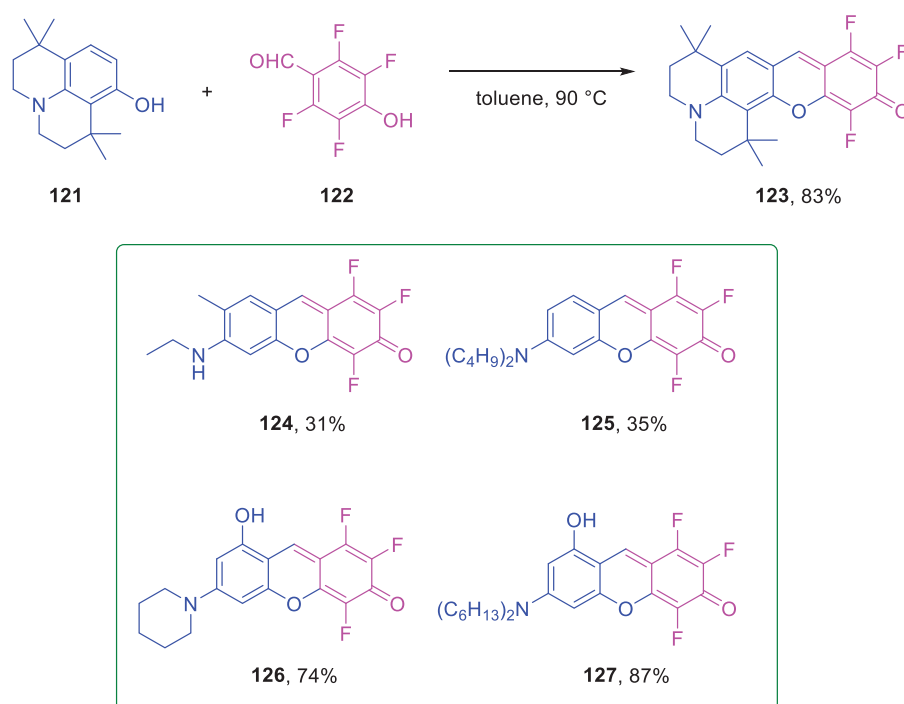
My final project was focused on the one-step preparation of rhodols and ‘rhodol-like’ merocyanines starting from easily available substrates. This idea appeared in reference to the reported earlier procedure of nucleophilic substitution of activated fluoroarenes with phenols.¹¹⁸ Taking into consideration, that *m*-aminophenols easily undergo the condensation with aldehydes, I concluded, that an appropriate arenes possessing a formyl along with the adjacent position prone to the aromatic nucleophilic substitution can be utilized in synthesis of rhodols. At this point I decided that the best compound for this aim should be 4-hydroxy-2,3,5,6-tetrafluorobenzaldehyde **122**. Since it was not easily available in large amounts, I had to introduce a formyl group into 2,3,5,6-tetrafluorophenol using Duff reaction.^{119–121} Next I have employed this compound in the reaction with 1,1,7,7-tetramethyl-8-hydroxyjulolidine **121** in toluene at 60 °C without any additives (Scheme 26). To my satisfaction, I have observed the colour change from white to deep pink and glittering crystals precipitated from the reaction mixture upon cooling. As the yield of rhodols **X** was not acceptable I modified the conditions and found that temperature rise positively affects the reaction outcome resulting in the increase of the reaction yield from 37% to 83%. At the same time other changes i.e. the addition of Lewis acids, bases or the solvent change did not influence the reaction positively (Table 2). I have concluded, that nonpolar solvents and high temperature allow to achieve the highest possible yields without any catalysts or additives.

Table 2. Optimization parameters for reaction of phenol **121** with aldehyde **122**

Entry	solvent	Temp. / °C	catalyst	time / h	yield
1	toluene	60	none	12	37%
2	toluene	90	none	1	83%
3	toluene	90	AlCl ₃	1	68%
4	toluene	90	Sc(OTf) ₃	1	70%
5	toluene	90	2,4,6-tri- <i>tert</i> -butylpyridine	1	78%
6	toluene	90	phosphazene base P ₁ - <i>t</i> -Bu	1	trace amount

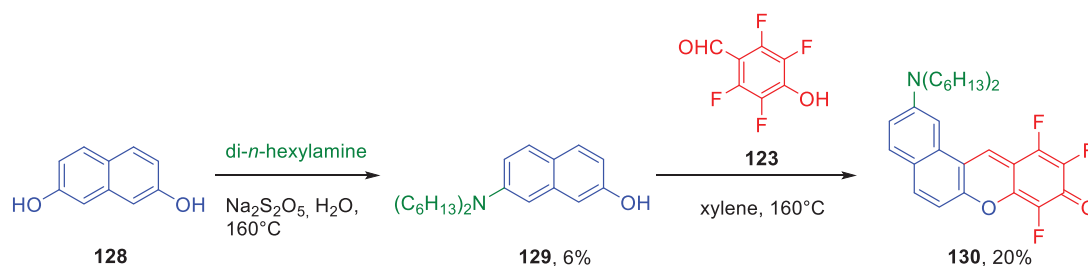
7	HFIP	80	none	1	0%
8	mesitylene	165	none	1	75%
9	xylenes	135	none	1	75%

Having the optimised procedure in hands, I decided to apply it to other already available *m*-aminophenols and obtained several new rhodols **124-127**. My next idea was to expand the reaction scope by the synthesis of π -expanded ‘rhodol-type’ merocyanines.



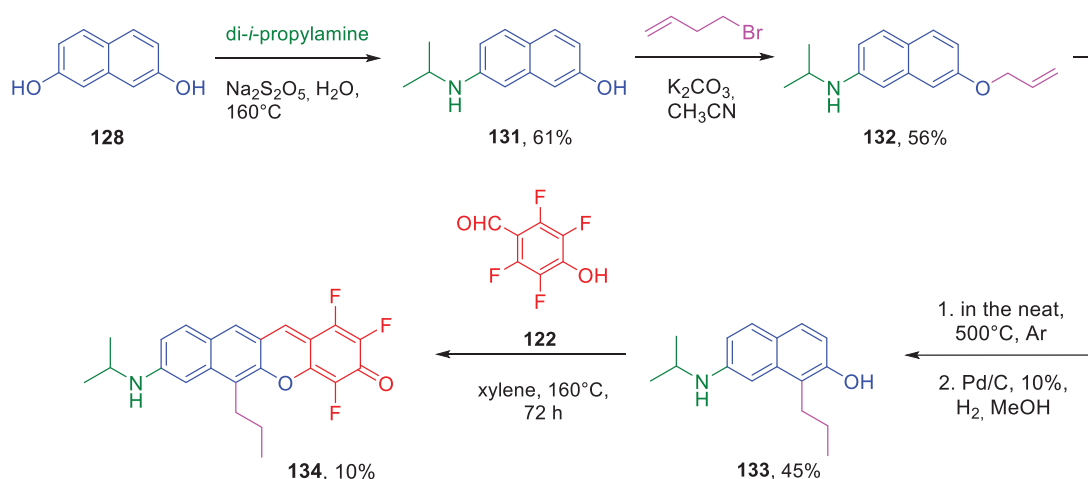
Scheme 26. One-step synthesis of rhodols **123-127** from aminophenols and tetrafluorohydroxybenzaldehyde (**122**)

The 7-(dihexylamino)naphthalen-2-ol (**129**) was obtained from 2,7-dihydroxynaphthalene **128** via Bucherer reaction. Since I expected that merocyanine **130** would be hardly soluble, I had chosen dihexylamino moiety to improve this physicochemical property. Even though, the yield of this reaction was very poor, the product was subjected to the condensation conditions with aldehyde **123** affording ‘rhodol-like’ merocyanine **130** in 20% yield.



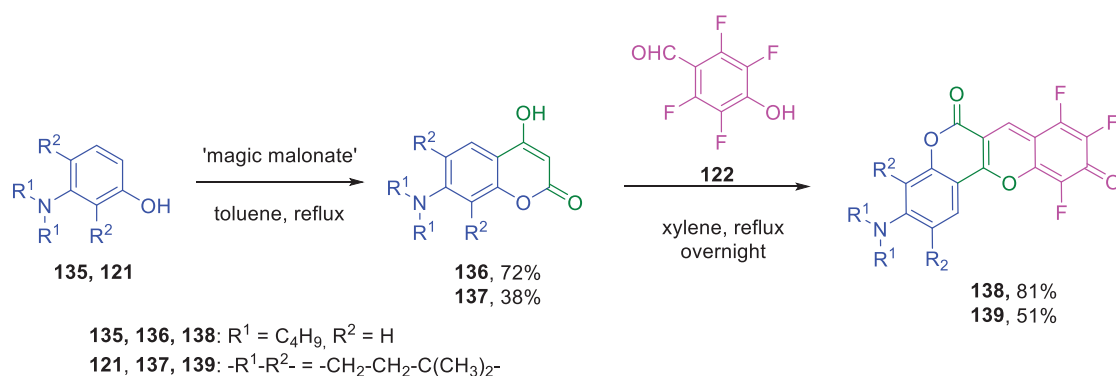
Scheme 27. Preparation of ‘rhodol-like’ merocyanine **130**

At the time when I started my research, I had performed literature search, which indicated clearly that linear π -expanded ‘rhodol-like’ merocyanines were something really uncommon and their synthesis might be challenging. The reason for this is that the position 1 in compound **129** is much more electron-rich than position 3 causing all electrophilic aromatic substitutions to proceed towards dye **130**, and not to its linear isomer. I decided to synthesize the π -expanded rhodol precursor with the occupied position 1 thus to suppress the condensation into the position 3. This time I have performed Bucherer reaction of 2,7-dihydroxynaphthalene (**128**) and di-*i*-propylamine. To my surprise, I have obtained a naphthalene derivative **131** with a mono-substituted amino fragment. The following allylation, rearrangement and reduction of double bond resulted in formation of product **133**. The condensation with benzaldehyde **122** in toluene at 90 °C failed, so I have finally managed to obtain merocyanine **134** after 72 h reaction in xylene at 160 °C.



Scheme 28. Synthetic procedure for linear π -expanded ‘rhodol-like’ merocyanine **134**

The last idea was to investigate if I could apply this procedure for 4-hydroxycoumarins to obtain ‘coumarino-rhodols’. For this aim, I obtained coumarins **136** and **137** from 3-dibutylaminophenol **135** and 1,1,7,7-tetramethyl-8-hydroxyjulolidine **121**. As in previous case, I had to apply solvent with the high boiling point. Finally, I managed to obtain merocyanine dyes **138** and **139** in 81% and 51% yields respectively.



Scheme 27. One-pot synthesis of ‘rhodol-like’ merocyanines **138-139** from 4-hydroxycoumarins **136-137**

The new dyes display gentle positive solvatochromism of both absorption and emission. As it was expected, the substitution of nitrogen with one ethyl moiety (**124**) results in a blue-shift of absorption (491 – 536 nm) and emission (550 – 555 nm). Meanwhile the full substitution with alkyl chains results in bathochromic shift and higher Φ_f (533/547 nm with Φ_f 89% in case of compound **125** versus 527/547 nm with 77% yield for **124** in acetone) (Table 3). The red-shift is even higher in case of fully annulated terminal C-N bond ($\lambda_{abs} = 498 - 554$ nm, $\lambda_{em} = 546 - 576$ nm with quantum yield up to 85 % in acetone). The presence of hydroxy group at position 8 in some rhodols (**126**, **127**) does not have a significant influence on the photophysical properties. The distinction of rhodols **138** and **139** is that they show increased Stokes shifts in comparison to classic rhodols **123** – **127** and their emissions are red-shifted by 50-70 nm.

Table 3. Spectroscopic properties of the obtained merocyanine dyes in chosen solvents - toluene as nonpolar and acetone as a polar one. Full spectroscopic data can be found in the publication.

	<i>Solvent</i>	λ_{abs}^{max} [nm]	λ_{em}^{max} [nm]	Φ_f [%]
123	Toluene	542	558	0.68
	Acetone	546	567	0.85
124	Toluene	491	550	0.43
	Acetone	527	547	0.77

125	Toluene	528	550	0.68
	Acetone	533	557	0.89
126	Acetone	533	555	0.91
127	Toluene	527	550	0.68
	Acetone	534	552	0.90
130	Toluene	519	578	0.10
	Acetone	575	798	0.01
134	Toluene	527	594	0.52
	Acetone	545	685	0.34
138	Toluene	528	586	0.21
	Acetone	566	619	0.71
139	Toluene	575	598	0.51
	Acetone	581	655	0.38

The incorporation of benzene ring into the rhodol scaffold results in the formation of π -expanded rhodols **130** and **134**. These compounds possess large Stokes shifts (up to 4900 cm^{-1} in acetone for **130** and 4400 cm^{-1} in acetonitrile for **134**). Rhodol **130** display a significant positive solvatochromism possessing emission maxima from 578 nm in hexane to 798 nm in acetone yet with low Φ_f , which almost disappear in polar solvents. In contrast, rhodol **134** shows blue-shifted absorption and emission compared to **130** ($\lambda_{\text{abs}} = 527 - 547\text{ nm}$ and $\lambda_{\text{em}} = 594 - 721\text{ nm}$ with somewhat higher quantum yields). Both dyes **130** and **134** possess broad and quite featureless absorption curves (Figure 7).

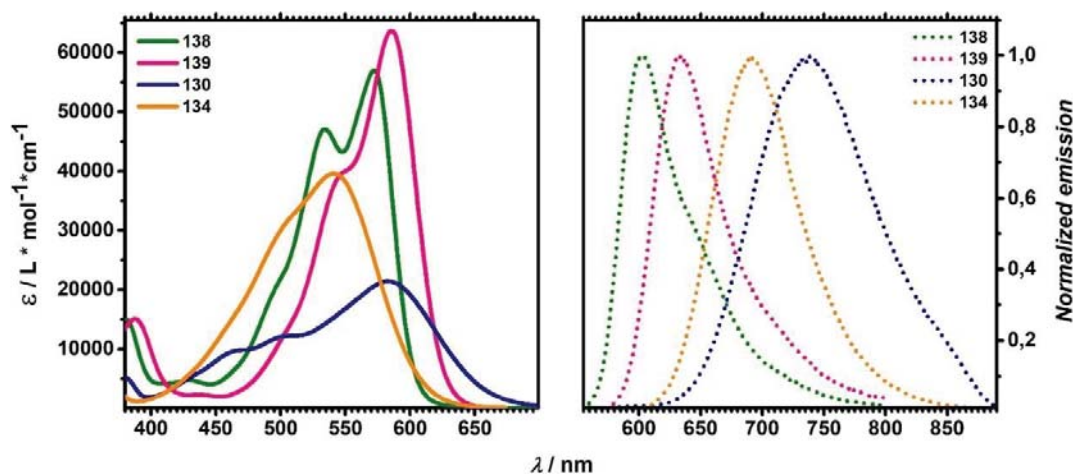


Figure 7. Absorption (solid) and emission (dotted) of ‘rhodol-like’ merocyanines **130**, **134**, **138** and **139** measured in methylene chloride.

6.4 Summary and conclusions

I have developed an unprecedented chromophore which possesses an SO₂ group in the middle of a rhodol skeleton. Moreover it has been achieved in a straightforward manner and the procedure consists of only four steps. Electronic spectra of all these modified rhodols display strong absorption in the range of 500-600 nm, which is almost independent of the nature of the solvent. Red fluorescence is markedly stronger in polar solvents reaching 50% in DMSO. I have found that rhodol analogs with the bridging oxygen atom replaced by an SO₂ group, and equipped with a triphenylphosphonium functionality, selectively accumulates in mitochondria and allows for selective penetration and well-resolved fluorescent imaging at nanomolar concentrations.

I have also developed an unprecedented synthesis of rhodols from coumarins. Moreover it has been achieved in a straightforward manner and the procedure consists of only four steps from easily available, commercial substrates. This approach involves the double Knoevenagel condensation of 3-formylcoumarins via activation of a lactone's C=O. This is the first example of this type reactivity for the ubiquitous lactone group described in the literature. To test the influence of different aryl groups on both the synthesis and the photophysical properties of the resulting dyes, I have prepared an extensive family of rhodols. Their electronic spectra display strong absorption in the range of 500-600 nm, which is almost independent of the nature of the solvent. Orange-red fluorescence is very strong in both non-polar and polar solvents reaching 100% in some cases.

Finally I developed a strikingly simple synthetic strategy to rhodols and 'rhodols-type' merocyanines bearing unprecedented sets of substituents. This approach relies on the tandem reaction of dialkylaminophenols, dialkylaminonaphthols and 4-hydroxycoumarins with tetrafluorohydroxybenzaldehyde, with two-steps occurring one after another, namely a Friedel-Crafts reaction followed by intramolecular nucleophilic aromatic substitution. This constitutes the shortest pathway towards rhodols ever developed. Three heretofore unknown merocyanine-based architectures were prepared using this strategy from dialkylaminonaphthols and 4-hydroxycoumarins. The ability to change the structure of original rhodol chromophore into π -expanded merocyanines translates to a comprehensive method for the modulation of photophysical properties such as shifting the absorption and emission bands across almost the entire visible spectrum, reaching the highest recorded Stokes shift i.e. 4800 cm⁻¹, ca. 80,000 M⁻¹ cm⁻¹ brightness, two-photon absorption cross-section above 150 GM and switching-on/off solvatochromism. Together with collaborating group from Parma found that replacing linear with non-linear

conjugation in rhodols-type architectures leads to profound changes in the photophysics originating from differences in permanent dipole moment changes between ground and the excited states.

Summing up, I realized most of the goals initially stated. In particular I developed three new synthetic methodologies affording rhodols-type fluorophores. Photostability of these rhodols and 'rhodol-like' merocyanines is not better compared to classical rhodols and other photostable dyes. They are not however markedly less stable either. I demonstrated new synthetic routes which allow the fine-tuning of the properties for xanthene dyes. Thanks to the widespread use of this class of fluorophores in multifarious applications, I believe that my results are of paramount importance for a very broad pool of scientists in different fields.

7. BIBLIOGRAPHY

- 1 A. Yamagami, H. Ishimura, A. Katori, K. Kuramochi and K. Tsubaki, *Org. Biomol. Chem.*, 2016, **14**, 10963–10972.
- 2 P. Shieh, V. T. Dien, B. J. Beahm, J. M. Castellano, T. Wyss-Coray and C. R. Bertozzi, *J. Am. Chem. Soc.*, 2015, **137**, 7145–7151.
- 3 G. Lukinavičius, L. Reymond, K. Umezawa, O. Sallin, E. D'Este, F. Göttfert, H. Ta, S. W. Hell, Y. Urano and K. Johnsson, *J. Am. Chem. Soc.*, 2016, **138**, 9365–9368.
- 4 T. Ikeno, T. Nagano and K. Hanaoka, *Chem. - An Asian J.*, 2017, **12**, 1435–1446.
- 5 M. Grzybowski, M. Taki and S. Yamaguchi, *Chem. - A Eur. J.*, 2017, **23**, 13028–13032.
- 6 J. Liu, Y.-Q. Sun, H. Zhang, H. Shi, Y. Shi and W. Guo, *ACS Appl. Mater. Interfaces*, 2016, **8**, 22953–22962.
- 7 A. N. Butkevich, G. Y. Mitronova, S. C. Sidenstein, J. L. Klocke, D. Kamin, D. N. H. Meineke, E. D'Este, P.-T. Kraemer, J. G. Danzl, V. N. Belov and S. W. Hell, *Angew. Chemie Int. Ed.*, 2016, **55**, 3290–3294.
- 8 J. B. Grimm, A. J. Sung, W. R. Legant, P. Hulamm, S. M. Matlosz, E. Betzig and L. D. Lavis, *ACS Chem. Biol.*, 2013, **8**, 1303–1310.
- 9 M. V. Sednev, C. A. Wurm, V. N. Belov and S. W. Hell, *Bioconjug. Chem.*, 2013, **24**, 690–700.
- 10 S. Takahashi, Y. Kagami, K. Hanaoka, T. Terai, T. Komatsu, T. Ueno, M. Uchiyama, I. Koyama-Honda, N. Mizushima, T. Taguchi, H. Arai, T. Nagano and Y. Urano, *J. Am. Chem. Soc.*, 2018, **140**, 5925–5933.
- 11 L. D. Lavis, *Biochemistry*, 2017, **56**, 5165–5170.
- 12 Y. J. Gong, X. B. Zhang, G. J. Mao, L. Su, H. M. Meng, W. Tan, S. Feng and G. Zhang, *Chem. Sci.*, 2016, **7**, 2275–2285.
- 13 J. Chan, S. C. Dodani and C. J. Chang, *Nat. Chem.*, 2012, **4**, 973–984.
- 14 C. Deo, S.-H. Sheu, J. Seo, D. E. Clapham and L. D. Lavis, *J. Am. Chem. Soc.*, 2019, **141**, 13734–13738.
- 15 P. Shieh, M. J. Hangauer and C. R. Bertozzi, *J. Am. Chem. Soc.*, 2012, **134**, 17428–17431.
- 16 Y. M. Poronik, K. V. Vygranenko, D. Gryko and D. T. Gryko, *Chem. Soc. Rev.*, 2019, **48**, 5242–5265.
- 17 S. W. Hell and J. Wichmann, *Opt. Lett.*, 1994, **19**, 782.
- 18 H. Blom and J. Widengren, *Curr. Opin. Chem. Biol.*, 2014, **20**, 127–133.
- 19 K. I. Willig, J. Keller, M. Bossi and S. W. Hell, *New J. Phys.*, 2006, **8**, 1–8.
- 20 Farbenfabriken vorm. Frieds. Bayer & Co. in Elberfeld, *DE54085*, 1889.

- 21 Badische Anilin- und Soda-Fabrik, *DE54684*, 1890.
- 22 V. Z. Shirinian and A. A. Shimkin, in *Heterocyclic Polymethine Dyes*, Springer Berlin Heidelberg, Berlin, Heidelberg, 2008, pp. 75–105.
- 23 M. J. S. Dewar, *J. Chem. Soc.*, 1950, 2329–2334.
- 24 J. Fabian and H. Hartmann, in *Reactivity and Structure Concepts in Organic Chemistry; V. 12*, eds. K. Hafner, C. W. Rees, B. M. Trost, L.-M. Lehn, P. von Rague Schleyer and R. Zahnradnik, Springer-Verlag, Berlin Heidelberg New York, 1980, pp. 162–197.
- 25 Y. M. Poronik, K. V. Vygranenko, D. Gryko and D. T. Gryko, *Chem. Soc. Rev.*, 2019, 48, 5242–5265.
- 26 J. B. Grimm, A. K. Muthusamy, Y. Liang, T. A. Brown, W. C. Lemon, R. Patel, R. Lu, J. J. Macklin, P. J. Keller, N. Ji and L. D. Lavis, *Nat. Methods*, 2017, **14**, 987–994.
- 27 J. E. Whitaker, R. P. Haugland, D. Ryan, P. C. Hewitt, R. P. Haugland and F. G. Prendergast, *Anal. Biochem.*, 1992, **207**, 267–279.
- 28 W. Chen, S. Xu, J. J. Day, D. Wang and M. Xian, *Angew. Chemie - Int. Ed.*, 2017, **56**, 16611–16615.
- 29 T.-B. Ren, W. Xu, W. Zhang, X.-X. Zhang, Z.-Y. Wang, Z. Xiang, L. Yuan and X.-B. Zhang, *J. Am. Chem. Soc.*, 2018, **140**, 7716–7722.
- 30 S. S. Patil, K. G. Thorat, R. Mallah and N. Sekar, *J. Fluoresc.*, 2016, **26**, 2187–2197.
- 31 J. Liu, Y. Q. Sun, H. Zhang, H. Shi, Y. Shi and W. Guo, *ACS Appl. Mater. Interfaces*, 2016, **8**, 22953–22962.
- 32 Y. Koide, Y. Urano, K. Hanaoka, T. Terai and T. Nagano, *ACS Chem. Biol.*, 2011, **6**, 600–608.
- 33 J. Arden-Jacob, J. Frantzeskos, N. U. Kemnitzer, A. Zilles and K. H. Drexhage, in *Spectrochimica Acta - Part A Molecular and Biomolecular Spectroscopy*, 2001, vol. 57, pp. 2271–2283.
- 34 Z. Lei, X. Li, Y. Li, X. Luo, M. Zhou and Y. Yang, *J. Org. Chem.*, 2015, **80**, 11538–11543.
- 35 G. A. Smith, J. C. Metcalfe and S. D. Clarke, *J. Chem. Soc. Perkin Trans. 2*, 1993, 1195.
- 36 W. Xuan, Y. Cao, J. Zhou and W. Wang, *Chem. Commun.*, 2013, **49**, 10474–10476.
- 37 B. C. Dickinson, Y. Tang, Z. Chang and C. J. Chang, *Chem. Biol.*, 2011, **18**, 943–948.
- 38 S. J. Lippard and S. Burdette, *US2003008405A1*, 2003.
- 39 S. J. Lippard and S. Hilderbrand, *US2003068275(A1)*, 2003.
- 40 K. Huang, M. Liu, X. Wang, D. Cao, F. Gao, K. Zhou, W. Wang and W. Zeng, *Tetrahedron Lett.*, 2015, **56**, 3769–3773.
- 41 K. Huang, L. Yu, P. Xu, X. Zhang and W. Zeng, *RSC Adv.*, 2015, **5**, 17797–17801.

- 42 K. Huang, M. Liu, Z. Liu, D. Cao, J. Hou and W. Zeng, *Dyes. Pigments.*, 2015, **118**, 88–94.
- 43 M. A. Clark, K. Duffy, J. Tibrewala and S. J. Lippard, *Org. Lett.*, 2003, **5**, 2051–2054.
- 44 M. A. Clark, S. A. Hilderbrand and S. J. Lippard, *Tetrahedron Lett.*, 2004, **45**, 7129–7131.
- 45 S. C. Burdette and S. J. Lippard, *Inorg. Chem.*, 2002, **41**, 6816–6823.
- 46 S. J. Lippard and C. C. Woodroffe, *US2004224420A1*, 2004.
- 47 X. Zhu, M. Xiong, H. Liu, G. Mao, L. Zhou, J. Zhang, X. Hu, X.-B. Zhang and W. Tan, *Chem. Commun.*, 2016, **52**, 733–736.
- 48 E. Tomat and S. J. Lippard, *Inorg. Chem.*, 2010, **49**, 9113–9115.
- 49 M. Ren, B. Deng, K. Zhou, J. Y. Wang, X. Kong and W. Lin, *J. Mater. Chem. B*, 2017, **5**, 1954–1961.
- 50 R. R. Sauers, S. N. Husain, A. P. Piechowski and G. R. Bird, *Dyes. Pigments.*, 1987, **8**, 35–53.
- 51 B. C. Dickinson, C. Huynh and C. J. Chang, *J. Am. Chem. Soc.*, 2010, **132**, 5906–5915.
- 52 M. Kondo, M. Tanaka, N. Sakamoto and H. Ooyoshi, *EP0511019(A2)*, 1992.
- 53 S. V. Patel, M. P. Patel and R. G. Patel, *J. Serb. Chem. Soc.*, 2005, **70**, 931–936.
- 54 H. Zheng, X. Q. Zhan, Q. N. Bian and X. J. Zhang, *Chem. Commun.*, 2013, **49**, 429–447.
- 55 Y. Zhao, Y. Ren, H. Li, T. Han, H. Chen and W. Guo, *Dyes. Pigments.*, 2016, **132**, 255–261.
- 56 J. E. Whitaker, R. P. Haugland and F. G. Prendergast, *Anal. Biochem.*, 1991, **194**, 330–344.
- 57 K. Tiensomjit, R. Noorat, S. Chomngam, K. Wechakorn, S. Prabpai, P. Kanjanasirirat, Y. Pewkliang, S. Borwornpinyo and P. Kongsaree, *Spectrochim. Acta. A*, 2018, **195**, 136–141.
- 58 M. Taki, K. Akaoka, K. Mitsui and Y. Yamamoto, *Org. Biomol. Chem.*, 2014, **12**, 4999–5005.
- 59 F. Mao, W.-Y. Leung and R. P. Haugland, *US6130101(A)*, 1997.
- 60 J. Han and K. Burgess, *Chem. Rev.*, 2010, **110**, 2709–2728.
- 61 E. A. Halabi, Z. Thiel, N. Trapp, D. Pinotsi and P. Rivera-Fuentes, *J. Am. Chem. Soc.*, 2017, **139**, 13200–13207.
- 62 G. S. Ghotekar, A. C. Shaikh and M. Muthukrishnan, *J. Org. Chem.*, 2019, **84**, 2269–2276.
- 63 K. R. Gee, M. Poot, D. H. Klaubert, W.-C. Sun, R. P. Haugland and F. Mao, *US6162931(A)*, 1996.
- 64 Z. Diwu, J. Liu and K. Gee, *US2004147747(A1)*, 2004.
- 65 Z. Diwu, J. Liu, R. P. Haugland and K. R. Gee, *US2002059684(A1)*, 2002.
- 66 T. Chin, Frederick, J. Klockow, K. Hettie and T. Glass, *WO2016210054(A1)*, 2016.

- 67 R. Alford, H. M. Simpson, J. Duberman, G. C. Hill, M. Ogawa, C. Regino, H. Kobayashi and P. L. Choyke, *Mol. Imaging*, 2009, **8**, 341–354.
- 68 S. Kamino, H. Ichikawa, S. ichi Wada, Y. Horio, Y. Usami, T. Yamaguchi, T. Koda, A. Harada, K. Shimanuki, M. Arimoto, M. Doi and Y. Fujita, *Bioorganic Med. Chem. Lett.*, 2008, **18**, 4380–4384.
- 69 M. Kamiya, D. Asanuma, E. Kuranaga, A. Takeishi and M. Sakabe, *J. Am. Chem. Soc.*, 2011, **133**, 12960–12963.
- 70 X. Jiao, C. Liu, K. Huang, S. Zhang, S. He, L. Zhao and X. Zeng, *Org. Biomol. Chem.*, 2015, **13**, 6647–6653.
- 71 W. Dong, H. Wen, X. F. Yang and H. Li, *Dyes. Pigments.*, 2013, **96**, 653–658.
- 72 E. M. Poronik, M. P. Shandura and Y. P. Kovtun, *Chem. Heterocycl. Compd.*, 2005, **41**, 546–547.
- 73 Y. M. Poronik, M. P. Shandura and Y. P. Kovtun, *Dyes. Pigments.*, 2007, **72**, 199–207.
- 74 X. Lv, J. Liu, Y. Liu, Y. Zhao, M. Chen, P. Wang and W. Guo, *Sensors Actuators, B Chem.*, 2011, **158**, 405–410.
- 75 A. Chevalier, P. Y. Renard and A. Romieu, *Chem. - A Eur. J.*, 2014, **20**, 8330–8337.
- 76 A. Chevalier, K. Renault, F. Boschetti, P. Y. Renard and A. Romieu, *Eur. J. Org. Chem.*, 2015, **2015**, 152–165.
- 77 S. Orega, V. Chalansonnet, A. Chevalier, P.-Y. Renard, A. Romieu and B. Roubinet, *US2016146814A1*, 2016.
- 78 J. Li and S. Q. Yao, *Org. Lett.*, 2009, **11**, 405–408.
- 79 S. C. Dodani, A. Firl, J. Chan, C. I. Nam, A. T. Aron, C. S. Onak, K. M. Ramos-Torres, J. Paek, C. M. Webster, M. B. Feller and C. J. Chang, *Proc. Natl. Acad. Sci.*, 2014, **111**, 16280–16285.
- 80 D. K. Sharma, S. T. Adams, K. L. Liebmann, A. Choi and S. C. Miller, *Org. Lett.*, 2019, **21**, 1641–1644.
- 81 D. Yang and T. Peng, *WO2009121244 (A1)*, 2009.
- 82 R. U. Kulkarni, D. J. Kramer, N. Pourmandi, K. Karbasi, H. S. Bateup and E. W. Miller, *Proc. Natl. Acad. Sci.*, 2017, **114**, 2813–2818.
- 83 T. Peng and D. Yang, *Org. Lett.*, 2010, **12**, 4932–4935.
- 84 A. A. Contractor and E. W. Miller, *Biochemistry*, 2018, **57**, 237–240.
- 85 T. Peng, N. K. Wong, X. Chen, Y. K. Chan, D. H. H. Ho, Z. Sun, J. J. Hu, J. Shen, H. El-Nezami and D. Yang, *J. Am. Chem. Soc.*, 2014, **136**, 11728–11734.
- 86 K. Kawai, N. Ieda, K. Aizawa, T. Suzuki, N. Miyata and H. Nakagawa, *J. Am. Chem. Soc.*, 2013, **135**, 12690–12696.

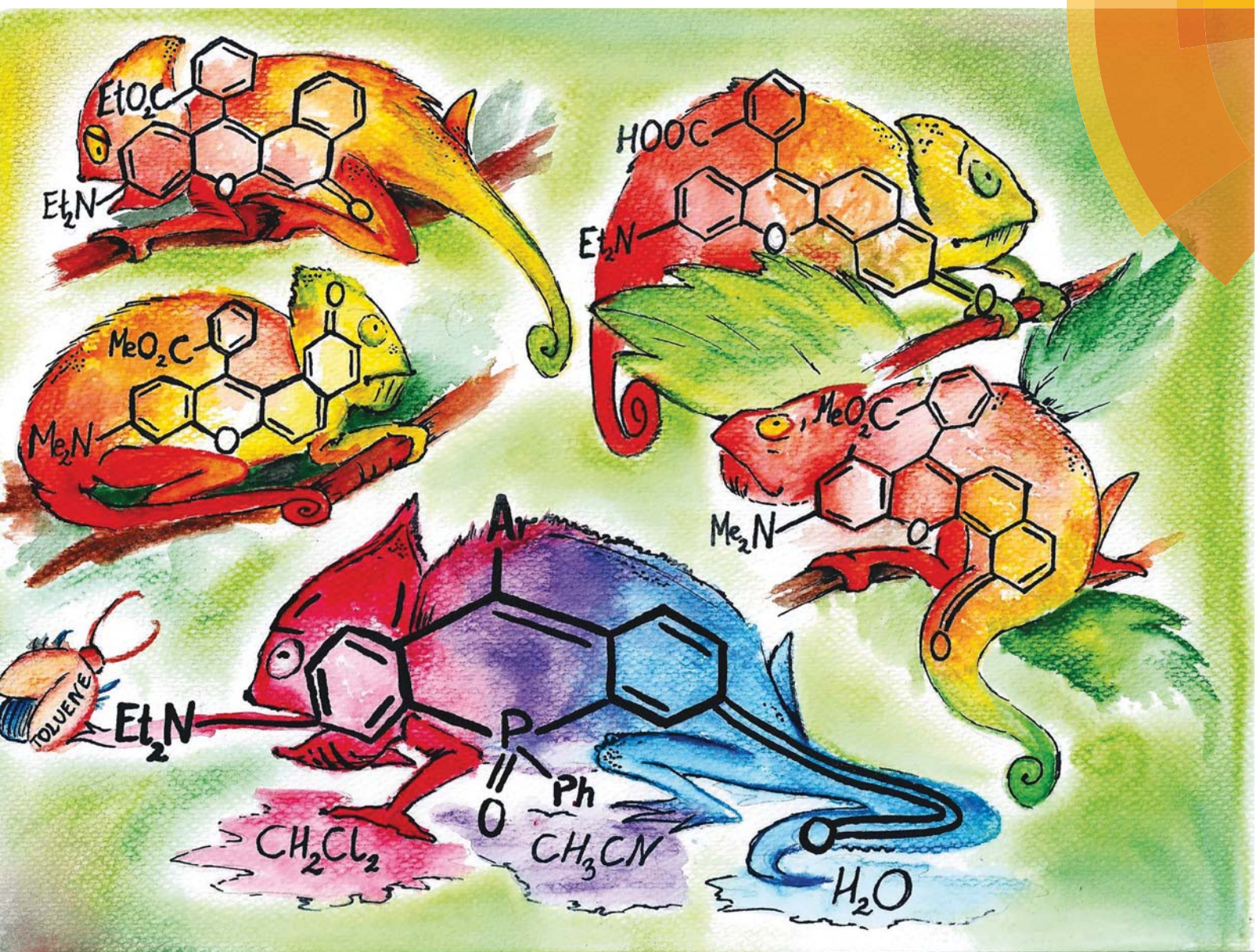
- 87 T. Fiala, E. V. Mosharov, J. Wang, A. M. Mendieta, S. J. Choi, E. Fialova, C. Hwu, D. Sulzer and D. Sames, *ACS Chem. Neurosci.*, 2022, **13**, 1251–1262.
- 88 B. F. Dutter, A. Ender, G. A. Sulikowski, C. David Weaver and C. D. Weaver, *Org. Biomol. Chem.*, 2018, **16**, 5575–5579.
- 89 J. M. Meinig, L. Fu and B. R. Peterson, *Angew. Chemie - Int. Ed.*, 2015, **54**, 9696–9699.
- 90 C. Richter, N. P. Ernsting and R. Mahrwald, *Synth.*, 2016, **48**, 1217–1225.
- 91 E. Nakata, Y. Yukimachi, Y. Nazumi, Y. Uto, H. Maezawa, T. Hashimoto, Y. Okamoto and H. Hori, *Chem. Commun.*, 2010, **46**, 3526.
- 92 Y. Liu, K. Xiang, B. Tian and J. Zhang, *Luminescence*, 2017, **32**, 78–85.
- 93 J. Liu, Z. Diwu and W.-Y. Leung, *Bioorg. Med. Chem. Lett.*, 2001, **11**, 2903–2905.
- 94 Y. Fu, M. M. Collinson and D. A. Higgins, *J. Am. Chem. Soc.*, 2004, **126**, 13838–13844.
- 95 L. G. Wang, I. Munhenzva, M. Sibrian-Vazquez, J. O. Escobedo, C. H. Kitts, F. R. Fronczek and R. M. Strongin, *J. Org. Chem.*, 2019, **84**, 2585–2595.
- 96 L. Wang, C. W. Barth, M. Sibrian-Vazquez, J. O. Escobedo, M. Lowry, J. Muschler, H. Li, S. L. Gibbs and R. M. Strongin, *ACS omega*, 2017, **2**, 154–163.
- 97 S. A. Hilderbrand and R. Weissleder, *Tetrahedron Lett.*, 2007, **48**, 4383–4385.
- 98 A. Yamagami, H. Ishimura, A. Katori, K. Kuramochi and K. Tsubaki, *Org. Biomol. Chem.*, 2016, **14**, 10963–10972.
- 99 A. Yamagami, K. Kawano, S. Futaki, K. Kuramochi and K. Tsubaki, *Tetrahedron*, 2017, **73**, 7061–7066.
- 100 J. B. Grimm, A. J. Sung, W. R. Legant, P. Hulamm, S. M. Matlosz, E. Betzig and L. D. Lavis, *ACS Chem. Biol.*, 2013, **8**, 1303–1310.
- 101 L. Geng, X. F. Yang, Y. Zhong, Z. Li and H. Li, *Dyes. Pigments.*, 2015, **120**, 213–219.
- 102 H. J. Rivera-Jacquez and A. E. Masunov, *Spectrochim. Acta. A*, 2018, **198**, 123–135.
- 103 A. Roth, H. Li, C. Anorma and J. Chan, *J. Am. Chem. Soc.*, 2015, **137**, 10890–10893.
- 104 T. Egawa, Y. Koide, K. Hanaoka, T. Komatsu, T. CoorTeraiper and T. Nagano, *Chem. Commun.*, 2011, **47**, 4162–4164.
- 105 T. Nagano, K. Hanaoka, T. Egawa, Y. Kushida, K. Numasawa, T. Myochin and W. Piao, *EP2942352(A1)*, 2015.
- 106 M. V. Sednev, C. A. Wurm, V. N. Belov and S. W. Hell, *Bioconjug. Chem.*, 2013, **24**, 690–700.
- 107 M. Grzybowski, M. Taki and S. Yamaguchi, *Chem. - A Eur. J.*, 2017, **23**, 13028–13032.
- 108 M. Grzybowski, O. Morawski, K. Nowak and P. Garbacz, *Chem. Commun.*, 2022, **58**, 5455–5458.

- 109 Y. Ichikawa, M. Kamiya, F. Obata, M. Miura, T. Terai, T. Komatsu, T. Ueno, K. Hanaoka, T. Nagano and Y. Urano, *Angew. Chemie - Int. Ed.*, 2014, **53**, 6772–6775.
- 110 D. J. Del Valle, D. J. Donnelly, J. J. Holt and M. R. Detty, *Organometallics*, 2005, **24**, 3807–3810.
- 111 M. R. Detty, P. N. Prasad, D. J. Donnelly, T. Ohulchansky, S. L. Gibson and R. Hilf, *Bioorg. Med. Chem.*, 2004, **12**, 2537–2544.
- 112 A. Gandioso, R. Bresolí-Obach, A. Nin-Hill, M. Bosch, M. Palau, A. Galindo, S. Contreras, A. Rovira, C. Rovira, S. Nonell and V. Marchán, *J. Org. Chem.*, 2018, **83**, 1185–1195.
- 113 A. Gandioso, M. Palau, R. Bresolí-Obach, A. Galindo, A. Rovira, M. Bosch, S. Nonell and V. Marchán, *J. Org. Chem.*, 2018, **83**, 11519–11531.
- 114 Ł. Kielesiński, I. Deperasińska, O. Morawski, K. V. Vygranenko, E. T. Ouellette and D. T. Gryko, *J. Org. Chem.*, 2022, **87**, 5961–5975.
- 115 R. S. Coleman and M. L. Madaras, *J. Org. Chem.*, 1998, **63**, 5700–5703.
- 116 T. Kappe, *Encycl. Reagents Org. Synth.*, , DOI:10.1002/047084289X.RB202.
- 117 L. Schmidt, T. Doroshenko, P. Barbie, A. Grüter, G. Jung and U. Kazmaier, *Synth.*, 2016, **48**, 3077–3086.
- 118 D. T. Gryko, D. Wyrostek, A. Nowak-Król, K. Abramczyk and M. K. Rogacki, *Synth.*, 2008, 4028–4032.
- 119 J. C. Duff and E. H. Bills, *J. Chem. Soc.*, 1932, 1987–1988.
- 120 K. Skonieczny, G. Charalambidis, M. Tasiór, M. Krzeszewski, A. Kalkan-Burat, A. G. Coutsolelos and D. T. Gryko, *Synth.*, 2012, **44**, 3683–3687.
- 121 W. E. Smith, *J. Org. Chem.*, 1972, **37**, 3972–3973.

8. ORIGINAL PUBLICATIONS

Chem Soc Rev

Chemical Society Reviews
rsc.li/chem-soc-rev



ISSN 0306-0012



ROYAL SOCIETY
OF CHEMISTRY

Celebrating
IYPT 2019

REVIEW ARTICLE





Yevgen M. Poronik, Daniel T. Gryko *et al.*

Rhodols – synthesis, photophysical properties and applications as fluorescent probes



Cite this: *Chem. Soc. Rev.*, 2019, **48**, 5242

Rhodols – synthesis, photophysical properties and applications as fluorescent probes†

Yevgen M. Poronik,  Kateryna V. Vygranenko,  Dorota Gryko * and Daniel T. Gryko *

The formal replacement of one dialkylamino group in rhodamines with a hydroxyl group transforms them into rhodols. This apparently minor difference is not as small as one may think; rhodamines belong to the cyanine family whereas rhodols belong to merocyanines. Discovered in the late 19th century, rhodols have only very recently begun to gain momentum in the field of advanced fluorescence imaging. This is in part due to the increased understanding of their photophysical properties, and new methods of synthesis. Rationalization of how the nature and arrangement of polar substituents around the core affect the photophysical properties of rhodols is now possible. The emergence of so-called π -expanded and heteroatom-modified rhodols has also allowed their fluorescence to be bathochromically shifted into regions applicable for biological imaging. This review serves to outline applicable synthetic strategies for the synthesis of rhodols, and to highlight important structure–property relationships. In the first part of this Review, various synthetic methods leading to rhodols are presented, followed by structural considerations and an overview of photophysical properties. The second part of this review is entirely devoted to the applications of rhodols as fluorescent reporters in biological imaging.

Received 28th February 2019

DOI: 10.1039/c9cs00166b

rsc.li/chem-soc-rev

1. Introduction

Rhodols belong to the xanthene dye family and have recently become popular fluorescent scaffolds with many applications connected to fluorescence microscopy. Though these dyes have

been known since the 19th century their appearance in the literature has remained limited, being largely overshadowed by the more popular xanthene chromophores – rhodamine and fluorescein. Since the title chromophore was first indirectly synthesized from fluorescein in 1889,¹ it was named rhodol² highlighting its similarity to rhodamine yet emphasizing the inclusion of a ‘phenol functionality’ (Fig. 1). Until 1990 rhodols remained largely forgotten and only a few reports appeared in the literature,^{3–17} presumably due to the fact that more

Institute of Organic Chemistry, Polish Academy of Sciences, Kasprzaka 44/52, 01-224 Warsaw, Poland. E-mail: dorota.gryko@icho.edu.pl, dtgryko@icho.edu.pl

† Electronic supplementary information (ESI) available. See DOI: 10.1039/c9cs00166b



Yevgen M. Poronik

donor–acceptor chromophoric systems, synthesis and application of functional organic dyes.

Dr Yevgen Poronik received his MSc (2001) from Department of Chemical Technology of Kyiv Technical University and PhD (2006) from Institute of Organic Chemistry, Ukrainian Academy of Sciences, under the supervision of Prof. Yuriy Kovtun. He worked as a post-doctoral researcher at Institute of Organic Chemistry of Polish Academy of Sciences in the group of Prof. Daniel Gryko. He is currently a research assistant in the same group, working on new



Kateryna V. Vygranenko

Kateryna Vygranenko was born in Ukraine in 1992. She obtained her MSc from Taras Shevchenko National University of Kyiv in 2015. She is a PhD student at the Institute of Organic Chemistry Polish Academy of Sciences under the supervision of Prof. Daniel Gryko. Her research interest currently focuses on developing new organic dyes for STED-microscopy.

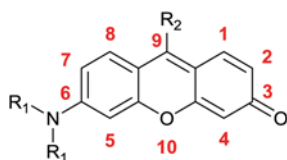


Fig. 1 Position numbering in the rhodol chromophore.

convenient methods for the preparation of both rhodamines and fluoresceins were available.

Nevertheless, since the last decade of the 20th century, the chemistry of rhodol dyes has been experiencing a renaissance due to the development of new fluorescent sensing and imaging techniques requiring specifically designed functional organic dyes. As a consequence, many of the scientific reports detailing the applications of rhodol dyes have a biological or medical focus. Many of these reviews only touch on rhodols (sometimes called rhodafluors),^{18–20} their focus mainly devoted to other research topics and describe rhodol chemistry in a fragmentary manner. This work comprehensively presents chemical advances related to the synthesis, properties, and applications of rhodols and their close analogues.

2. Introduction of rhodol electronic structure

Structural analysis of rhodols, like all xanthen chromophores, reveals their similarity to polymethine dyes. Indeed, xanthen dyes contain a polymethine-like conjugation chain located between polar terminal moieties. As the rhodamine chromophore possesses a positive charge delocalized along the conjugated system it bears a stronger resemblance to typical cyanine chromophores. Fluorescein chromophores, on the other hand, possess a negative charge delocalized along the conjugated system and belong to oxonole family. The rhodol system, in contrast, has an electronic structure

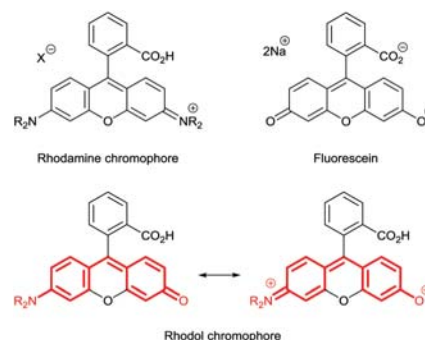


Fig. 2 Resonance structures of rhodol as a hybrid of fluorescein and rhodamine.

represented by two limiting forms (neutral and dipolar) and is analogous to merocyanine chromophores (Fig. 2).²¹

Although the oxygen bridge atom at the central position of the molecule is not a part of the polymethine chromophore it plays a dual role of increasing the rigidity of the chromophore and acting as a polar substituent. Chromophores of the same length without the oxygen bridge have been known since 1950^{22,23} and demonstrate much stronger solvatochromism in comparison to rhodols. In nonpolar solvents unbridged analogues show blue-shifted absorption (<450 nm) but in polar solvents the absorption maxima can occur at longer than 570 nm. According to X-ray diffraction structural analysis the unbridged chromophore adopts a propeller-like shape,²³ the dihedral angle and the charge distribution of which is affected by the nature of the solvent. Conversely, the oxygen bridge leads to more planar and rigid structures²⁴ which show much stronger fluorescence responses and much weaker solvatochromism in both absorption and fluorescence compared with unbridged chromophores (Fig. 3).^{15,22,23}

The aryl substituent at the central position of rhodol (position 9, Fig. 1) is not a part of the xanthen chromophore. Indeed, in the S_0 state the aryl substituents are oriented almost orthogonally (Fig. 3).



Dorota Gryko

Dorota Gryko obtained a PhD from the Institute of Organic Chemistry at the Polish Academy of Sciences in 1997, under the supervision of Prof. J. Jurczak. After a post-doctoral stay with Prof. J. Lindsey in North Carolina State University (1998–2000), she started an independent career in Poland. In 2009 and 2018, she received the prestigious TEAM grants from the Foundation for Polish Science. Her current research interests

are focused on light-induced processes with particular attention being paid to porphyrinoid catalysis as well as on vitamin B₁₂ chemistry.



Daniel T. Gryko

Daniel T. Gryko obtained his PhD from the Institute of Organic Chemistry of the Polish Academy of Sciences in 1997, under the supervision of Prof. J. Jurczak. After a post-doctoral stay with Prof. J. Lindsey at North Carolina State University (1998–2000), he started his independent career in Poland. He became Full Professor in 2008. The same year he received the Society of Porphyrins and Phthalocyanines Young Investigator Award and in

2017 the Foundation for Polish Science Award. His current research interests are focused on the synthesis of various functional dyes as well as on two-photon absorption, solvatochromism, excited-state intramolecular proton transfer and fluorescence probes.

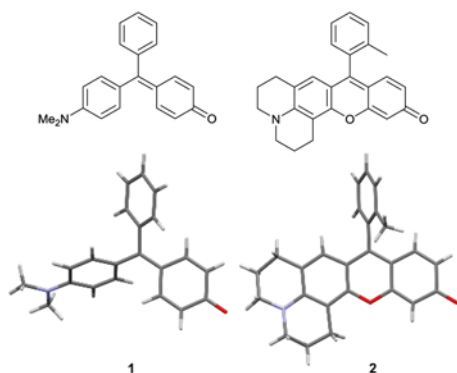


Fig. 3 Single crystal X-ray diffraction structures of compounds **1** (CCDC 1413998) and **2** (CCDC 1564215).[†]

In the S_1 state the dihedral angle between the aryl substituent and the xantheno framework is reduced somewhat, however, the angle is still large enough to prevent *meso*-aromatic substituents from being significantly conjugated with the main chromophore.²⁵

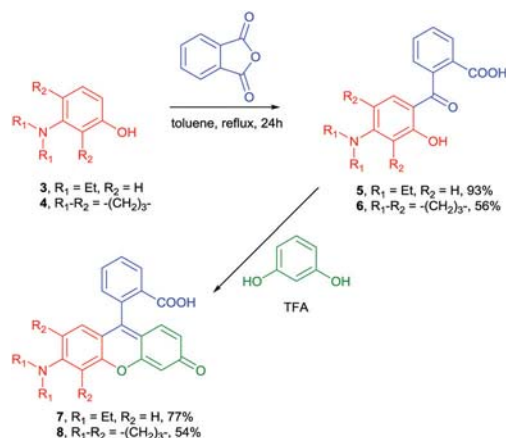
Moreover, the presence of an aryl substituent at the *meso*-position decreases the sensitivity of the rhodol chromophore to nucleophiles, *e.g.* unsubstituted rhodol reacts with the bisulfite anion resulting in the interruption of the conjugation chain.²⁶

Computational studies based on TD-DFT calculations suggest that the HOMO displays a mainly neutral character as a large portion of the electron density localizes on the terminal amino group. Upon excitation, the electron density from the amino group redistributes towards the keto group, thus, the LUMO demonstrates charge transfer character. Indeed, the dipole moment in the S_1 state is higher than that of S_0 , indicating a more polar excited state. Therefore polar solvents stimulate the charge separation thus decreasing an energy gap between HOMO and LUMO of rhodol and related chromophores.^{25,27}

3. Synthesis

3.1. Rhodols

The most common method for the preparation of rhodols, like for other xantheno dyes, is based on the Friedel–Crafts acylation methodology.^{15,28} Typically the symmetry of xantheno dyes enables their synthesis in a one-pot procedure from phthalic anhydride and two equivalents of either a 3-dialkylaminophenol (for rhodamine) or a 1,3-dihydroxybenzene (for fluorescein). This is not the case for rhodols, which due to their asymmetry, must be synthesized in a stepwise manner from phthalic anhydride. The condensation of resorcinol with 4-dialkylamino-2-hydroxybenzophenones **5** and **6**,^{17,29} resulting from the reaction of phthalic anhydride with corresponding 3-aminophenols **3** and **4**, represents the most straightforward synthetic route to rhodols (Scheme 1).^{5–8,17–20,24,25,28–40} In contrast to the simple one-step rhodamine synthesis proceeding easily in approx. 30% yield,⁴¹ the two step rhodol preparation *via* a benzophenone intermediate, requires an excess of phthalic anhydride to suppress the formation of unwanted rhodamine, and leads generally to diminished yields. The application of unsymmetrically substituted phthalic anhydrides



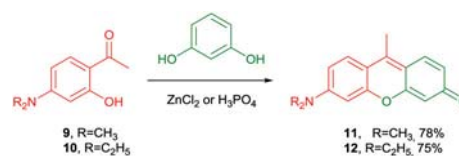
Scheme 1 The classical rhodol synthesis from phthalic anhydride, *m*-aminophenol and resorcinol.

is also impractical for the synthesis of rhodols as the key intermediate forms as a mixture of regioisomers which are difficult to separate, lowering the yield even further.

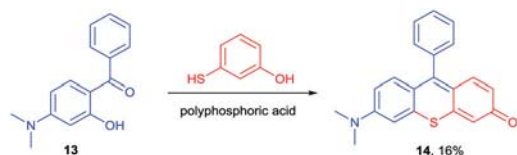
Despite its two-step nature, the readily available starting materials and operationally simple synthetic procedure contribute to this method's popularity. The presence of the COOH group in the product's structure offers an additional advantage since it enables: (1) increased polarity and hence water solubility; (2) the formation of a leuco-lactone structure; (3) conjugation with various molecules. A modification of the above method, employing acetophenones **9**, **10**^{15,42} gives access to rhodols **11**, **12** substituted with the methyl group at the *meso*-position (Scheme 2).⁴³ Acetophenone **9** is synthesized *via* the Fries rearrangement of 3-acetoxy-*N,N*-dimethylaniline in 16% yield.¹⁵ A more convenient synthetic route to acetophenone **10** starts from 7-diethylamino-4-hydroxycoumarin and gives the product in 90% yield *via* ring opening and subsequent decarboxylation after treatment with mineral acid.⁴³ The use of phosphoric acid instead of the commonly applied sulfuric acid for the condensation of acetophenone with resorcinol leads to rhodol **12** in 75% yield. The product can be easily isolated by precipitation of the xanthylium perchlorate salt from an aqueous solution.

This modification enables a better control over the character of the substituent at position 9. At the same time, however, the availability of aromatic ketones with a substitution pattern similar to **9** remains problematic.

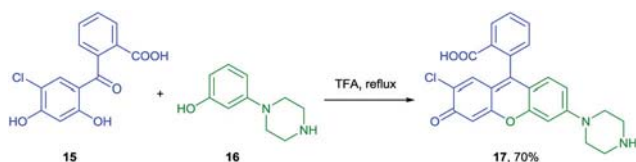
Monothioresorcinol has been reacted with benzophenone **13** in polyphosphoric acid resulting in compound **14** which incorporates a sulfur atom at the bridge position in place of oxygen (Scheme 3).¹⁵ This reaction is the only example of a rhodol analogue with an endocyclic sulfur atom reported.



Scheme 2 The synthesis of 9-methylrhodols **11** and **12**.



Scheme 3 The synthesis of rhodol with sulfur in position 10.



Scheme 4 Rhodol formation from dihydroxybenzophenone and 3-aminophenols.

Curiously, the same reaction in sulfuric acid leads to the unsubstituted rhodol with an endocyclic oxygen atom. This is due to the conversion of thioresorcinol to resorcinol under the reaction conditions.

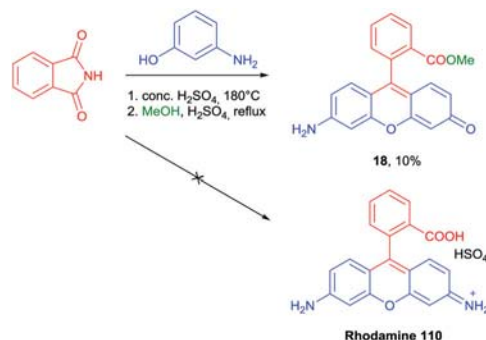
Another classical rhodol preparation method^{6,44–59} is based on a reversed substrate pattern utilizing 2,4-dihydroxybenzophenones⁴⁷ and 3-aminophenol derivatives as substrates (Scheme 4).

The roots of this synthetic protocol date back to the 19th century with Bayer's observation of the formation of rhodol from 2-carboxy-2',4'-dihydroxybenzophenone, which was generated by an alkali-induced decomposition of fluorescein.¹ In the original patent, 3-dimethylamino-, 3-diethylamino-, or 3-(phenylamino)-phenols were condensed with dihydroxybenzoylbenzoic acid, as well as with its bromo- and dibromo-derivatives in the presence of ZnCl₂ at 140–160 °C. This initial strategy was later utilized by Ghatak⁴ and Chen's groups.¹⁶ As an alternative to fluorescein hydrolysis, the benzophenone intermediate can also be generated by the reaction of phthalic anhydride with resorcinol derivatives in the presence of a Lewis acid. Although this 'reverse' methodology does not offer any substantial advantages over the classical one, in cases where the 3-aminophenol is more complex this particular strategy can minimize the use of the more expensive and less available substrate.

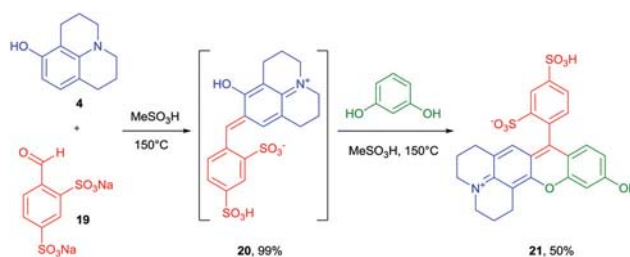
The unusual coupling of phthalimide with 3-aminophenols can afford rhodol derivatives in decent yields.⁶⁰ The original idea behind this strategy was to improve the yield of rhodamine 110 by avoiding side reactions. Nevertheless, the treatment of phthalimide with an excess of 3-aminophenol in sulfuric acid leads to hydrolysis of the C–N bond to form rhodol 18 instead of rhodamine 110 (Scheme 5).

Rhodols containing a highly functionalized 9-aryl group are typically prepared from phthalic anhydride derivatives as an isomeric mixture of 5- and 6-substituted derivatives which are non-trivial to separate. Chevalier and co-workers discovered that functionalized aldehydes, used in place of phthalic anhydride derivatives, give rise to an intermediate possessing a structure similar to monomethine dye 20 which then reacts with resorcinol to afford rhodol 21 in 50% yield (Scheme 6).^{61–63}

Even though this method solves the regioselectivity problem, it appears to be demanding, since RP-HPLC is exploited for



Scheme 5 The synthesis of rhodol from phthalimide and 3-aminophenol.

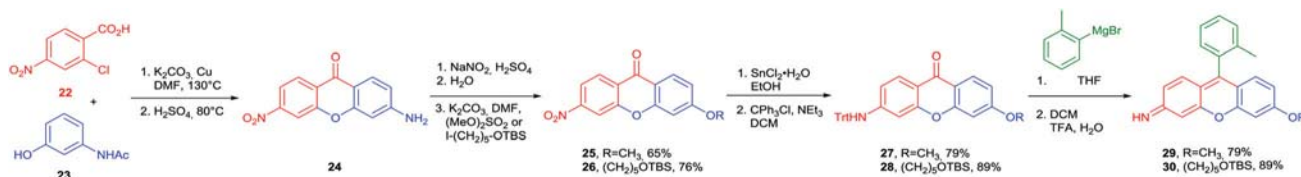


Scheme 6 The synthesis of rhodols from benzaldehydes developed by Chevalier and co-workers.

analysis and purification. The chromatography fractions containing product were lyophilized to give rhodol as a TFA salt. Curiously, the authors did not supply information on the character of the oxidation, which occurs in the last step. The same synthetic protocol was employed with various *m*-aminophenols as phenolic partners to generate a range of unsymmetrical sulforhodamines with similar yields.

The Friedel–Crafts reaction of aldehydes with two equivalents of resorcinol or 3-dialkylaminophenol is much more often used for the synthesis of fluoresceins and rhodamines¹⁰ than it is for rhodols. The simple reason is that in the case of rhodols, the reaction must be somehow stopped upon reaching the methine salt (*i.e.* after first step), which is not easy since this intermediate is typically more reactive than the starting aldehyde.

The synthesis of fluoresceins and rhodamines through the preparation of xanthenes and subsequent addition of organometallic reagents is currently broadly utilized. The same strategy has been employed for the synthesis of Singapore Green, a structural hybrid of rhodamine 110, and Tokyo Green. In attempts to find a fluorophore which can be employed for microarray-based protease substrates a synthetic protocol for the rhodol isomer Singapore Green with an amino-group on one side as a centre of peptide sequence conjugation was developed. The targeted molecule should also possess absorption and emission maxima in the visible range, and phenolic group on the other side providing solid-phase peptide synthesis and microarray immobilization.⁶⁴ The conjugate is sensitive to protease activity, which causes amide bond cleavage, thus releasing the highly fluorescent dye. The synthetic protocol proceeds through the formation of asymmetric xanthenone 24 *via* the Ullmann-type coupling of 3-acetamidophenol (23) with 2-chloro-4-nitrobenzoic acid (22). After introduction of an



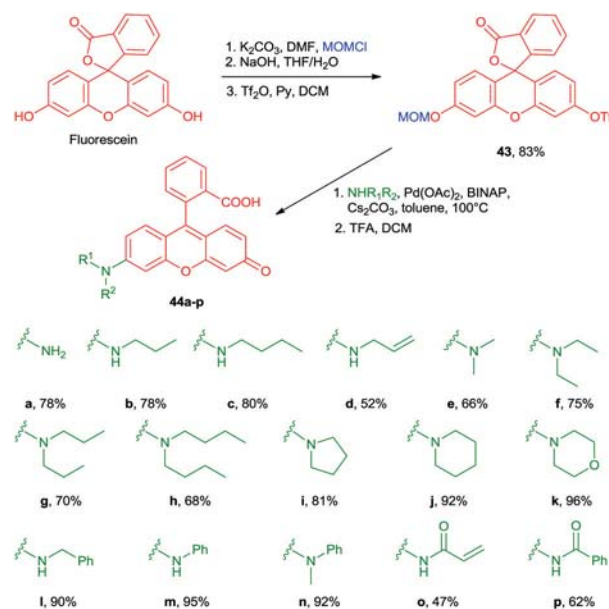
Scheme 7 The synthesis of Singapore Green 29 and 30.

alkoxy substituent in place of the amino group, compound 25 is reduced and protected to give derivative 27. Consecutive arylation and deprotection affords Singapore Green fluorophores 29 and 30 (Scheme 7).

A combination of substitution at the *meso*-position of xanthenes with catalytic amination *via* a trifluoromethylsulfonate derivative is an alternative synthetic approach towards the rhodol skeleton.^{65,66} In bistrifluoromethylsulfonate derivatives, one triflate group is substituted with the amino group in the first step, which after a series of subsequent transformations, *i.e.*, hydrolysis of the trifluoromethylsulfonate group, protection of hydroxyl group with TBDMSCl, arylation and deprotection, leads to O-rhodol 39, C-rhodol 40, Si-rhodol 41 and P-rhodol 42⁶⁷ (Scheme 8).

The Buchwald–Hartwig amination can also be utilized for the synthesis of rhodols starting from fluoresceins. Trying to find an easy combinatorial method for the construction of a rhodol library, an efficient synthetic protocol was developed with a catalytic amination reaction as the key step.^{68,69}

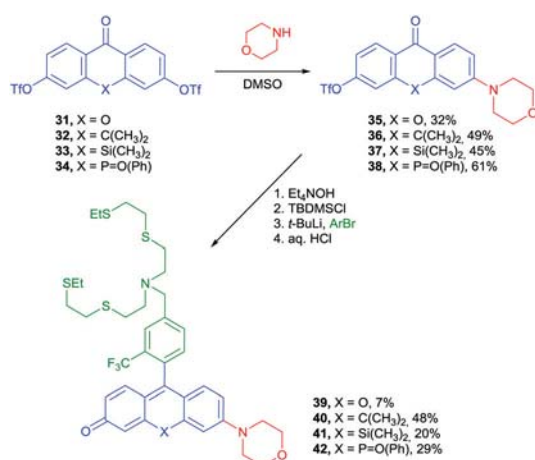
Monoprotected fluorescein^{68,70–74} in the spiroform can be transformed into trifluoromethyl sulfonate 43 which then undergoes catalytic amination and deprotection to yield a large variety of rhodol derivatives 44a–p (Scheme 9). In the original method mono-phenol protection by MOM was employed with subsequent triflation and catalytic amination of the other phenolic group. This procedure works well for fluoresceins in their spiroform, where the carboxyl group is effectively protected. For 5-carboxyfluorescein, the carboxylic group was transformed into a *t*-butyl ester and the phenolic group was protected with



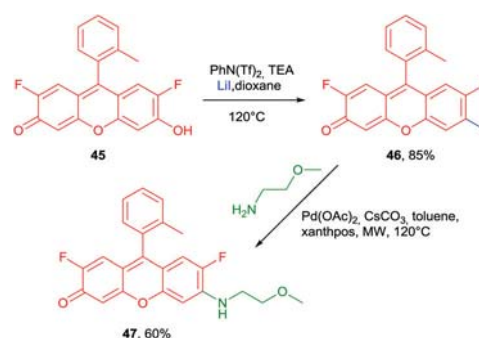
Scheme 9 General method for rhodol preparation via Pd-catalyzed amination starting from fluorescein.

benzyl chloride.⁷⁵ This approach allows for the deprotection of the phenol or carboxylic acid functional groups without affecting each other. Similar to previous approaches used to prepare rhodols from fluoresceins through triflation, conversion of fluoresceins to iodoarenes with subsequent catalytic amination gives rhodols.⁷⁶

The synthesis of rhodol 47 in 2 steps with 51% yield from Pennsylvania Green 45 exemplifies the utility of this methodology (Scheme 10). The synthesized rhodol 47 and its analogues possess fluorine atoms at the 2- and 7-positions for improved



Scheme 8 The general synthetic route to O-, C-, Si- and P-rhodols.

Scheme 10 The method for rhodol preparation from corresponding fluoresceins *via* Pd-catalyzed amination.

photophysical properties, and a hydrophobic methyl substituent instead of a polar carboxyl group for better cellular membranes affinity.

Over the years quite a few synthetic strategies leading to rhodols have been developed. All of these approaches can be roughly divided into two major methodologies: (a) condensation of aromatic 2-hydroxyketones with resorcinol, its derivatives and analogs, and (b) synthesis of xanthenes, followed by addition of organometallic reagents. It seems that the first strategy has been exhausted over the last century and one cannot expect further synthetic developments in this field. At the same time it is at present the most often used as it possesses the two significant advantages of a low number of synthetic steps and large overall yields. Consequently, it can be recommended for newcomers in the field who would like to reach their target without significant time investment. The 'reverse methodology' utilizing 2,4-dihydroxybenzophenones and 3-aminophenols as substrates is surprisingly underdeveloped especially taking into consideration that aromatic 1,3-dihydroxyketones are easier to obtain than analogous compounds bearing an R_2N group. There is some room for optimization and use here.

It seems that the methodology utilizing xanthenes is the most promising in terms of modular approach, generality and the broadest range of potentially available functionalities. At the same time, it is the longest one when considering the number of steps and therefore the poor overall yields. The simplification of this strategy is therefore a viable target for future research. Undoubtedly the most recommended pathway towards rhodols possessing a 2'-carboxyphenyl substituent at position 9, starts from easily available fluorescein with Buchwald–Hartwig amination of the MOM-protected triflate **43** as the key step (Scheme 9). This method contains a reasonable number of steps with the ability to introduce a broad range of amino groups.

Some of the published methodologies such as condensation with monothioresorcinol or reaction of aldehyde with 8-hydroxyjulolidine remained an exotic curiosity, typically due to the combination of low yields, unavailability of the starting materials or narrow scope.

3.2. π -Expanded rhodols

In addition to the aforementioned rhodol representatives, there is a family of functional organic dyes analogous to rhodols with a π -expanded chromophore system. Commonly, π -expanded rhodol-like chromophores are divided into two groups depending on the conjugation type (Fig. 4). Cooperative conjugation defines systems where charge transfer between the donor and acceptor moieties exists in a similar manner to the parent rhodol. Non-cooperative conjugation defines systems where the π -expansion obstructs the transfer in charge due to a change in relative orientation between the amine and carbonyl moieties. Formally, representatives from this second group do not belong to the rhodol family in terms of the electronic structure, though, as these compounds are prepared in similar ways to the former group, they will be considered in this synthetic section.

3.2.1. π -Expanded rhodols (cooperative effect). Undoubtedly the most well-known π -expanded rhodol derivatives are

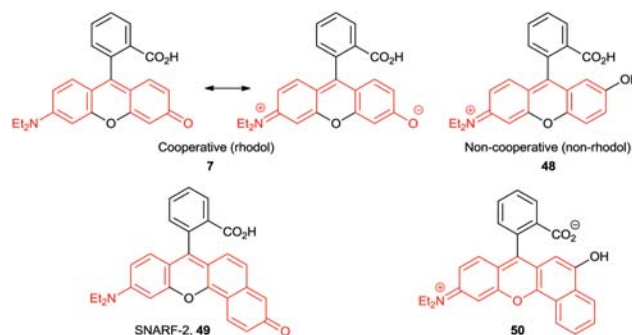


Fig. 4 π -Expanded rhodol-like chromophores.

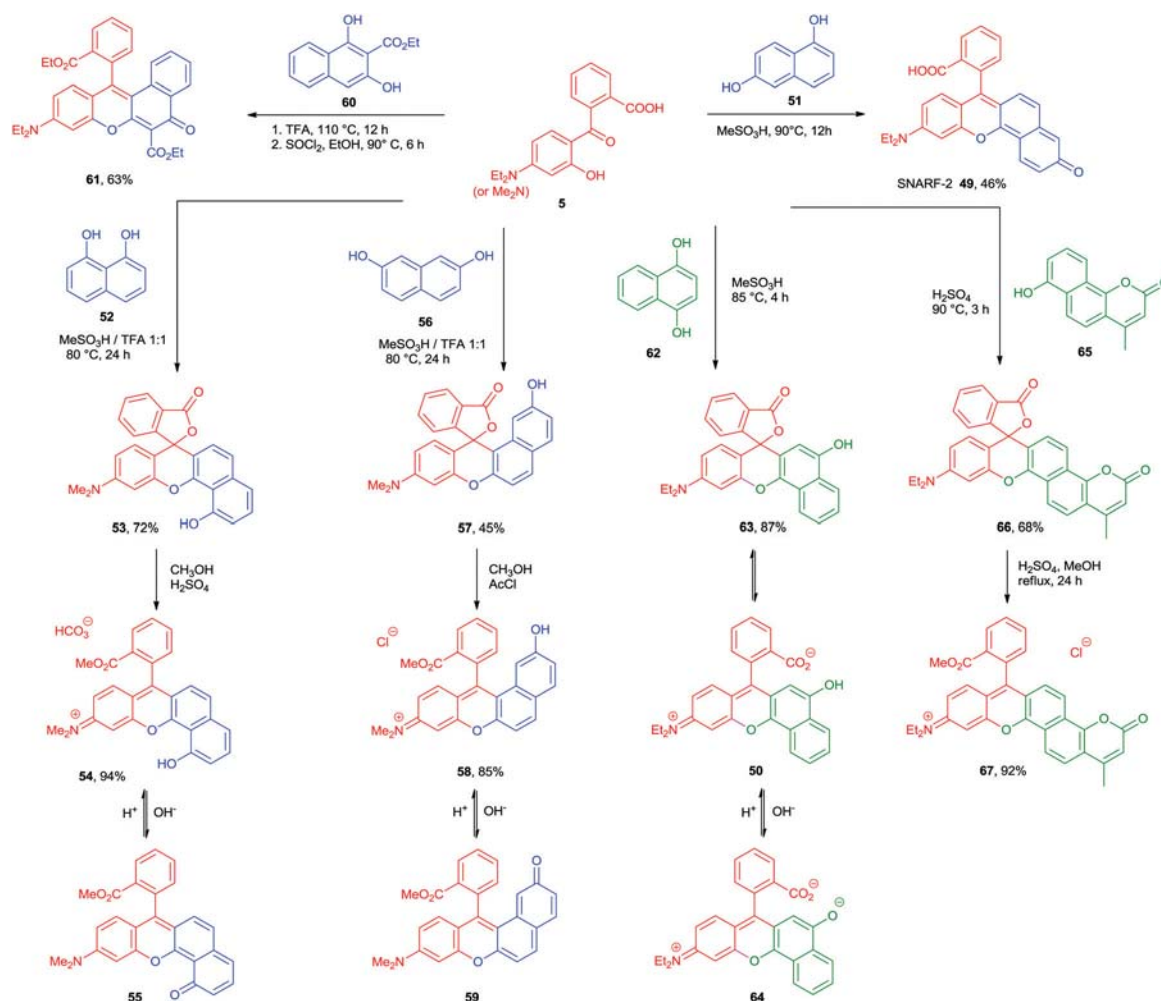
seminaphthorhodafluors (SNARFs), featuring rhodol-like molecules expanded with a naphthalene fragment instead of one phenyl ring. The synthesis of SNARF-2 **49**, presented in Scheme 11, exemplifies the method for seminaphthorhodafluor preparation discovered by Haugland and co-workers in 1991.⁷⁷ 1,6-Naphthalenediol **51** used for SNARF synthesis possesses hydroxyl groups in the correct orientation to reinforce conjugation which is crucial to secure the rhodol-like chromophore. Indeed, any naphthalenediols with an analogous configuration of the substituents tend to form rhodol-like chromophores. Subsequently, the method for the seminaphthorhodafluor preparation has been developed by other groups.^{78,79} Although, the vast majority of known SNARFs⁸⁰ are prepared using an analogous procedures to that of Haugland, another approach, based on a mixed condensation of aldehyde and two phenol derivatives, was reported (Scheme 12).^{61,81} Despite the original chromophore structure and promising properties, classic SNARFs are not common fluorophores due to the complexity of substrates required.^{81–83} Initially, the name seminaphthorhodafluor and the abbreviation SNARF concerned only fluorophores – products of the reaction with naphthalenediol **51**,⁷⁷ nevertheless, in later reports the authors used the same name to refer to analogous π -expanded rhodols derived from other naphthalenediols, though with hydroxyl groups at reinforcing positions.

Researchers from another group found that using a 1:1 mixture of CH_3SO_3H and TFA improved the yield of Haugland's method significantly. Scheme 11 shows the synthesis of the SNARF spiroform **53** from naphthalenediol **52**.⁸⁴ The former underwent ring-opening and the seminaphthorhodafluor **54** was obtained as the ester form. The protonated form of SNARF **54** equilibrates with its rhodol-like form **55**.

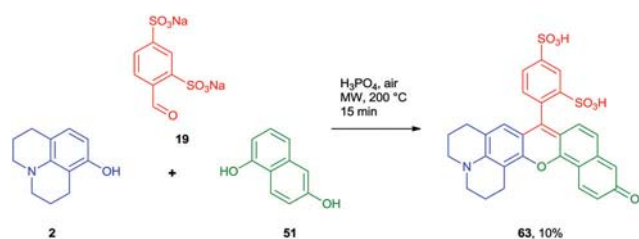
Seminaphthorhodafluors can also be obtained with naphthalenediol **56** to give spiroform **57**, which after esterification is in equilibrium with the rhodol form **59**.^{32,85}

Expansion of the π -system on the amino side of the rhodol as opposed to the hydroxyl is much rarer and leads to seminaphthorhodafluors with the reversed ring configuration.^{51,84} Compound **70** was obtained in 69% yield *via* the condensation of benzophenone **15** with 1-hydroxy-6-piperazyno-naphthalene **69** in neat TFA at 125 °C (Scheme 13).

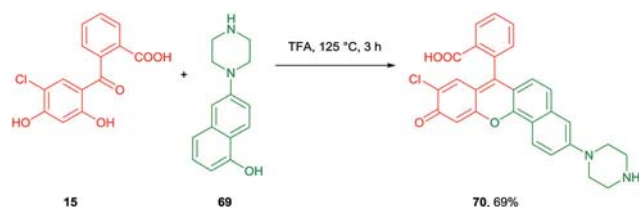
A recent report presents the synthesis of two π -expanded rhodols which cannot be described as seminaphthorhodafluors as the additional benzene or naphthalene moieties are annulated



Scheme 11 The synthesis of seminaphthorhodafluors.



Scheme 12 The mixed method for SNARF preparation.



Scheme 13 The synthesis of naphthorhodol 70.

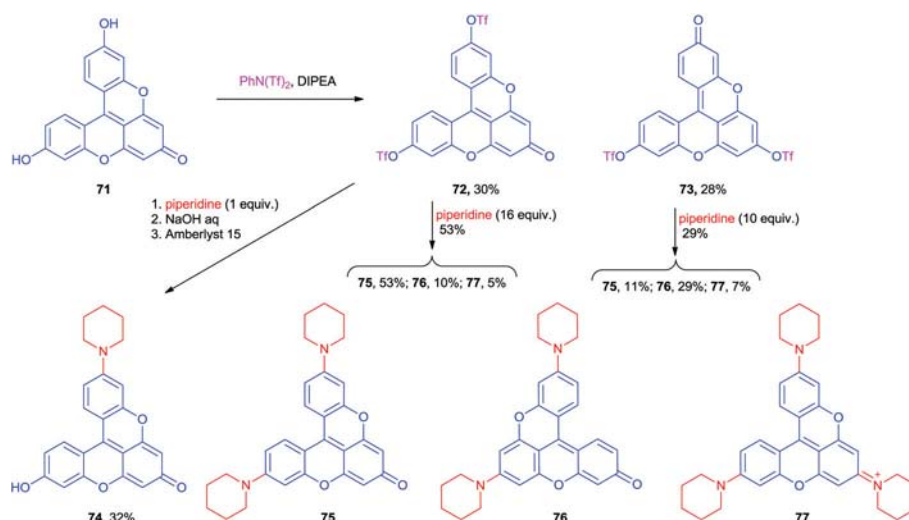
to the rhodol chromophore without its lengthening. The reaction of benzophenone 5 and dihydroxy naphthalene 60 in neat TFA leads to the formation of the carboxylic acid intermediate, which

was then transformed into ester 61 in order to facilitate purification (Scheme 11).³⁴ Given the reasonably good access to the necessary building blocks this approach was also utilized for the synthesis of analogs possessing an additional fused benzene ring.³⁴

3.2.2. π -Expanded chromophores (non-cooperative effect). The situation when benzophenone 5 reacts with 1,4-dihydroxy naphthalene 62 differs from the aforementioned SNARF synthesis as the product 63 does not formally contain the rhodol chromophore as the phenol moiety is not conjugated with the amine (Scheme 11). Although, chromophores with such a configuration are not technically speaking π -expanded rhodols,³⁹ their synthesis is mentioned due to the formal structural similarity.

An extension of this concept is the replacement of the naphthalenediol 62 with the benzocoumarin 65. The resulting product was obtained in reasonable yield in the lactone form 66 and further transformed to its open form 67 *via* esterification.⁸⁶

3.2.3. V-shaped bis-xanthene dyes. Since the aryl moiety at position 9 is orthogonal to the xanthene framework, it hardly influences the photophysical properties of rhodol dye. In order to expand the π -system in this direction, V-shaped xanthene dyes with a quinone moiety mutually shared by two rhodols



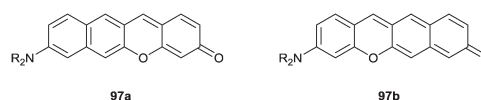
Scheme 14 Synthesis of V-shaped rhodol analogues.

were designed.⁸⁷ Compared to simple fluorescein, the V-shaped dye **71** has significantly red-shifted absorption and emission maxima, but possess poor solubility and a low quantum yield (Scheme 14). In attempts to mitigate these disadvantages, the rhodamine and rhodol like V-shaped fluorophores comprising one to three piperidine moieties were prepared.

The dyes **74–76** can be considered as π -expanded rhodols, although the π -expansion here is not due to the presence of additional fused aromatic rings, but rather the fusing of the benzene ring at position 9 to the core xanthene unit. The synthetic route proceeds through the formation of derivatives **72** and **73**, generated from V-shaped fluorescein **71** (Scheme 14).⁸⁸ In the case of a large excess of piperidine the amination of compound **72** leads to V-shaped rhodol **75** as a major product (53%) along with the regioisomer **76** and overaminated derivative **77** as minor products (10% and 5% respectively). In the neutral form these products exhibit a considerable increase in the fluorescence quantum yield and bathochromically shifted absorption and emission maxima with respect to **71** in DMSO.

The synthesis of both types of π -expanded rhodols mostly relies on the classical approach *i.e.* condensation of aromatic *o*-hydroxyketones with electron-rich dihydroxynaphthalenes. Needless to say this strategy limits the control over the pattern of substituents. Moreover, the number of dihydroxynaphthalenes which are commercially available is rather limited and this substrate pool has been exhausted already. On the other hand the synthesis of both SNARFs and less popular π -expanded rhodols is a straightforward two-step process from commercially available materials, which makes it appealing for researchers aiming at imaging applications. More importantly, certain key scaffolds are not available using the so far developed methodologies. Prominent examples of these are **97a,b** which are shown in Fig. 5. The strategies employing xanthene analogs have not been attempted in this sub-field so far.

Consequently, new, more general methods are waiting to be discovered in order to avoid the drawback of the limited variety of substituents and cores.

Fig. 5 Structures of not yet synthesized π -expanded rhodols.

3.3. Heteroatom substituted rhodols

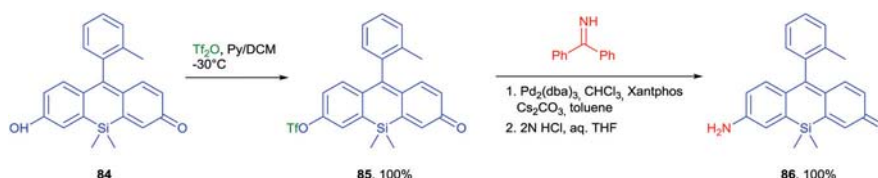
The replacement of the bridging oxygen atom in rhodol with carbon, silicon or phosphorus is an efficient strategy to modify the photophysical properties (Scheme 8). Two methods for the synthesis of silicon analogues from the fluorescein TokyoMagenta⁸⁹ and from the respective xanthone have been described.⁹⁰ The coupling of 2-bromo-4-methoxybenzyl chloride (**78**) with 8-bromo-julolidine (**79**) catalyzed by AlCl_3 followed by silylation with dichlorodimethylsilane and subsequent oxidation provides silaxanthone **81**. Subsequent reaction with lithium derivative of indole **82** and deprotection affords Si-rhodol **83** (Scheme 15). The indolyl moiety was then functionalized to produce a reaction-based fluorescent probe for the detection and imaging of formaldehyde in living cells.

Fluorescein-like derivatives lacking the carboxyl group in the *meso*-aryl moiety do not require MOM protection thus allow a somewhat shortened synthetic route to rhodols.^{69,91,92} Tokyo Magenta dye **84** is transformed into Si-rhodol **86**, *via* the monotriflated intermediate **85**, forming in quantitative yields (Scheme 16).⁸⁹

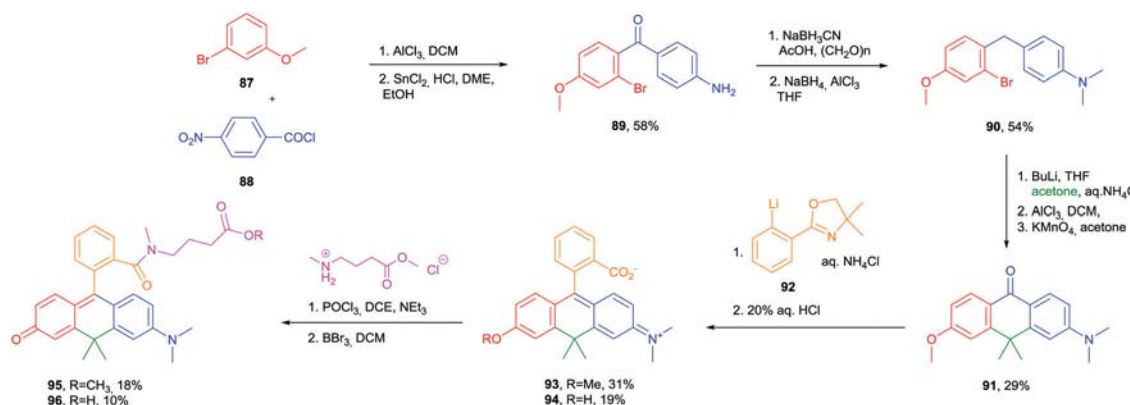
In terms of pure synthetic accessibility, carborhodols represent the class of rhodol analogues that are the most difficult to synthesize. Indeed, their synthesis requires introduction of a carbon bridge to the asymmetrically substituted substrate. An eleven-step synthetic route to carborhodols starts from the coupling of 3-bromoanisole and 4-nitrobenzoyl chloride in the presence of a Lewis acid and subsequent reduction of the nitro group affording ketone **89**.⁹³ Since ketal protection proved challenging, the keto-group was fully reduced after methylation of the amino group. Subsequently the six-step process of ring-closure and arylation produces the methylated rhodol



Scheme 15 The synthesis of Si-rhodols.



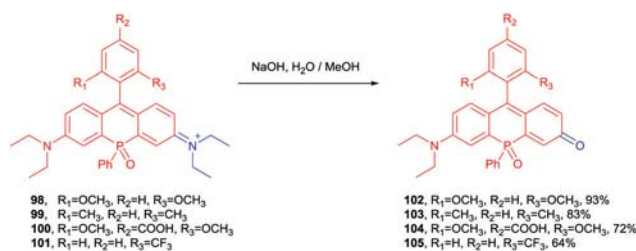
Scheme 16 The method for Si-rhodol preparation via Pd-catalyzed amination.



Scheme 17 The synthesis for C-rhodols.

molecule which, after amidation followed by demethylation, gives rise to carborhodol **96** with an overall yield of 1.6% (Scheme 17).

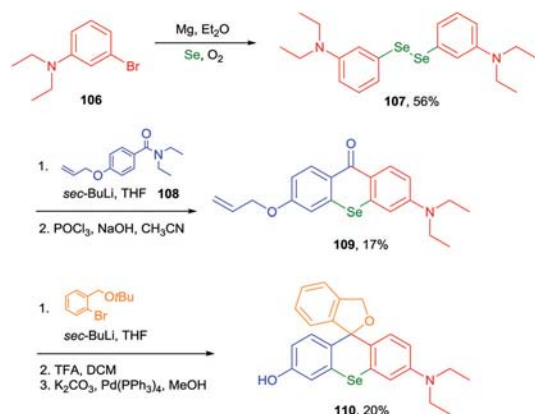
The method of rhodol preparation through rhodamine hydrolysis^{5,91} is now generally considered obsolete and fallen from usage since it requires long reaction times and yields low conversion. However, the replacement of the bridge fragment with more electron-withdrawing moieties facilitates the hydrolysis of an amino group in rhodamine-like chromophores thus increases the potential utility of this method. Hydrolysis of P=O-bridged rhodamines **98–101** occurs much faster than in conventional rhodamines and provides rhodols **102–105** in good yields (Scheme 18).⁹⁴ Steric hindrance of the 9-position is crucial since it prevents nucleophilic attack of the hydroxyl ion at this position leading to discoloration under exposure to basic conditions. This is exemplified by the fact that the 2-tolyl-substituted P=O-bridged rhodamine does not yield the corresponding P=O-bridged rhodol, whereas the 2,6-dimethoxyphenyl derivative **98** efficiently provides to P=O-bridged rhodol **102**. The hydrolysis of these P=O-bridged rhodamines to P=O-bridged



Scheme 18 The synthesis of P-rhodols via the rhodamine hydrolysis.

rhodols proceeds selectively, because rhodols precipitate from the reaction mixture preventing further hydrolysis. Full conversion to P=O-bridged fluoresceins is much slower demanding more concentrated alkali solutions and prolonged reaction times. An exception to this is rhodol **104** formed as a water soluble sodium salt, which undergoes further hydrolysis easily.

The synthesis of rhodols with an endocyclic selenium atom⁹⁵ using an earlier developed methodology for Se-rhodamines has been reported.^{1,96,97} 3-Bromo-*N,N*-diethylaniline (**106**) was transformed into



Scheme 19 The synthesis of Se-rhodols.

the diselenium bridged intermediate **107**, followed by the condensation with allyloxybenzamide **108** to form selenoxanthone **109** (Scheme 19). Subsequent arylation and cleavage of the allylic moiety afforded the spiroform of Se-bridged rhodol **110** in 20% yield.

While the photophysical properties of core-modified rhodols are in most cases better compared with their parent chromophore, their synthesis is more complex. All developed synthetic routes are long and low-yielding. There is strong motivation to find shorter and more efficient strategies, especially to Si-rhodols and C-rhodols, but the problem is challenging and requires an inventive approach.

Since the first review detailing the synthesis of rhodols in 1922,³ new approaches based on modern organic and organometallic chemistry for the synthesis of these dyes have been developed and thoroughly investigated. Over the last 10 years, seen by an increased number of publications, rhodols have been attracting much more attention due to their application in bio-imaging. Still, the number of synthetic routes to the rhodol skeleton is very limited and warrants further study. Moreover, many potentially interesting scaffolds are yet to be synthesized using any methodology. No single heterocyclic analogue of rhodol exists possessing any carbon atom replaced by nitrogen, or a benzene unit with a five-membered heterocyclic ring for example.

4. Photophysical properties

4.1. Linear optical properties

The solvent polarity governs the contribution of the two limiting forms of merocyanines, which affects the position of the absorption maxima (Fig. 2). In the case of equal contribution of the nonpolar and dipolar limiting forms the chromophore approaches an ideal state with no bond alternation⁹⁸ and the excited state geometry closely resembles the Franck–Condon geometry. The absorption spectrum of the chromophore with ideal conjugation shows a narrow band with minimal or without a vibronic mode.⁹⁹ Rhodol molecules, as with the majority of merocyanine dyes, show positive solvatochromism where an increase in solvent polarity leads to a red-shift of the absorption maxima.¹⁰⁰ DFT calculations confirm that in nonpolar media

model rhodol **111** has an electronic structure with low charge separation, while in the polar media it exhibits a polarized structure close to the ideally conjugated state (Fig. 6).^{14,15,94,100} The effect of solvent polarity on the absorption spectrum can be clearly seen for **112** in Fig. 7.

The majority of rhodol derivatives obtained from the two-step condensation method with phthalic anhydride¹⁵ contain the carboxyl group at the 2'-position of the *meso*-aryl substituent necessitating an intrinsic equilibrium between spiro (A) and open dye (B) forms (Scheme 20).

Fig. 8 shows that the spiro form of rhodamine in dioxane readily makes the dye form with the minimal addition of water.

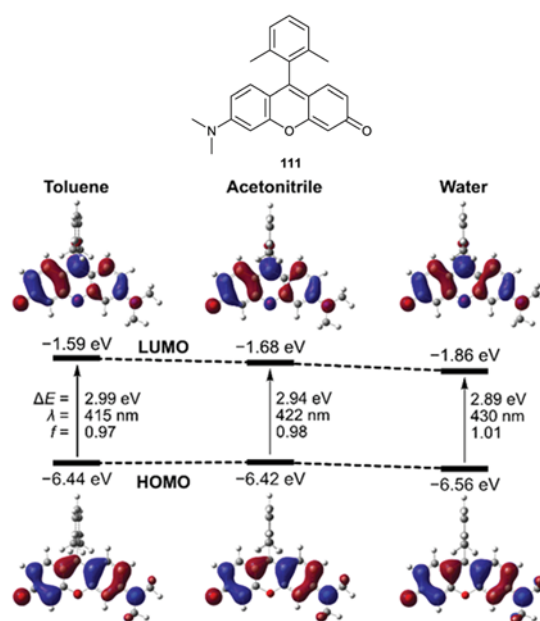


Fig. 6 TD DFT calculation data of model rhodol **111** for toluene, acetonitrile and water. Reprinted with permission from *Chem. – Eur. J.*, 2017, 23, 13028–13032. Copyright © 2017, John Wiley and Sons.

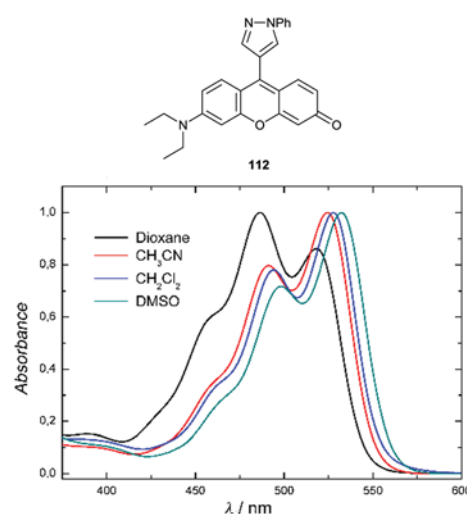
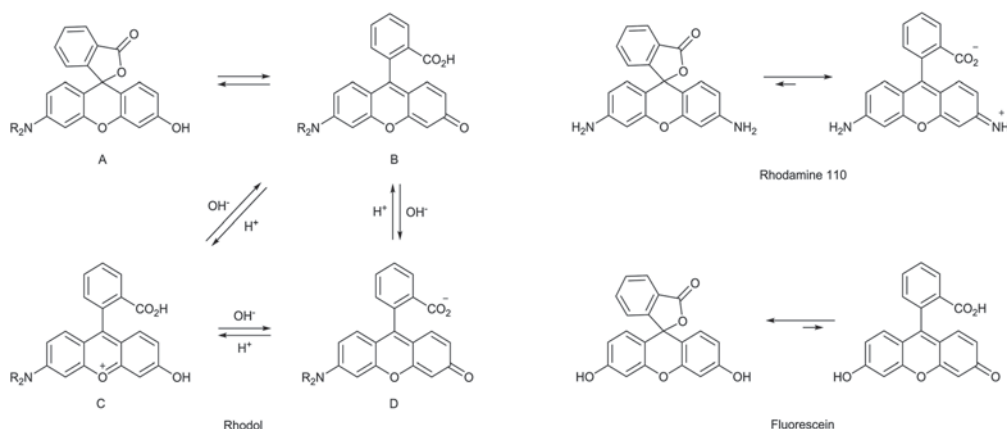


Fig. 7 The absorption spectra of rhodol **112** in solvents of different polarity. Reprinted with permission from *J. Org. Chem.*, 2013, 78, 11721–11732. Copyright © 2013, American Chemical Society.



Scheme 20 The equilibrium between the dye and the spiroforms for rhodol, rhodamine 110 and fluorescein.

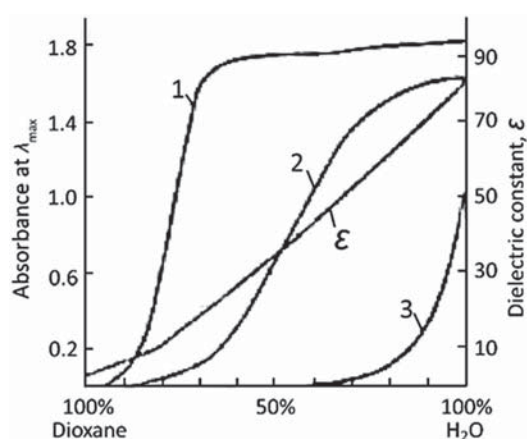


Fig. 8 The dependence of equilibrium between spiro and open forms for rhodamine 110 (1, R = H), rhodol (2, R = H) and fluorescein (3) in dioxane–water mixtures. Reprinted from *Zh. Org. Khim.*, 1965, **1**, 343–346.

For rhodol, the equilibrium becomes significant in a 1:1 dioxane–water mixture. On the other hand, fluorescein mainly exists in the spiro form even in pure water.¹¹

In basic conditions rhodols exist in the dye form (D) as the formation of the rhodol salt prevents ring closure, while in acidic conditions depending on the substituents the equilibrium shifts to either isomeric spiroform (A) or protonated form (C) (Scheme 20).^{11,25,37}

Fig. 9 shows how polar substituents affect the optical properties of rhodol dyes with regard to both their nature and position. Moreover the photophysical data of selected rhodol dyes are summarized in Table S1 (ESI[†]).

Unsubstituted rhodol (**44a**) exhibits an absorption maximum at 493 nm in water with a strong fluorescence response (Scheme 9). The addition of one alkyl substituent at the nitrogen atom (**44b**) increases the electron-donor strength of the amino group and leads to a small red-shift (10–15 nm) in both absorption and fluorescence maxima. In the case of an analogue of **44b** fused with one cyclohexane ring (**113a**) the bathochromic effect is somewhat stronger (about 25 nm) due to restricted rotation of the amino group (Fig. 10).

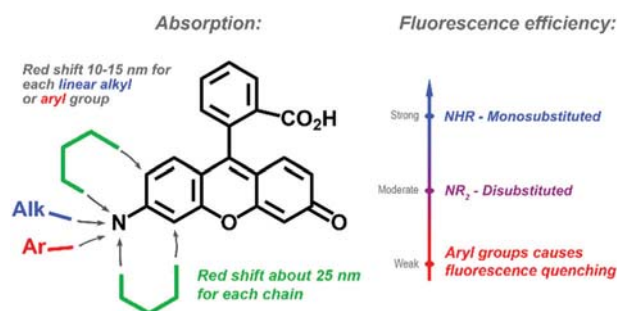


Fig. 9 The influence of polar substituents on optical properties of rhodol dyes.

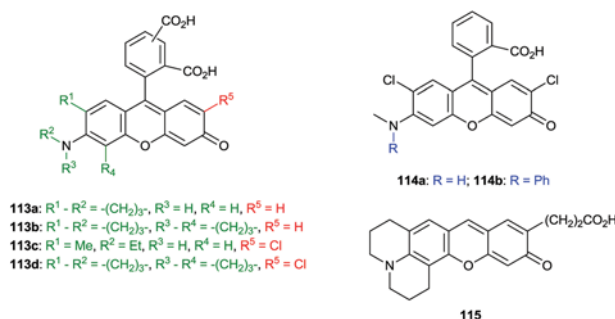


Fig. 10 Substituted rhodols.

The presence of second alkyl group (**44e**) leads to an additional bathochromic shift in both absorption and fluorescence maxima by another 10–15 nm. What is more, the position of the absorption and the fluorescence maxima for the iso-electronic analogues of rhodol **44e** with cyclic alkyl substituents on the nitrogen atom (**44i,j**) hardly differ from that of **44e** (Scheme 9).

On the other hand, the introduction of two fused cyclohexane rings (**113b**) gives rise to an additional bathochromic shift of the absorption maximum (about 50 nm compared with **44a**) as the fused alkyl chains increase the rigidity of the chromophore and make polar conjugation more efficient. In the context of fluorescence efficiency, rhodols substituted with one alkyl

group at the nitrogen atom (**44b**, **113a**) demonstrate the strongest fluorescence response, which is comparable with that of unsubstituted rhodol **44a**, while dialkyl amino derivatives, either linear (**44e**), cyclic (**44i,j**) or fused (**113b**) exhibit much weakened fluorescence efficiency. In contrast to *N*-alkyl rhodols, all *N*-arylated derivatives exhibit very low fluorescence signals (**44m,n**).

Introducing an electron-withdrawing group at the nitrogen atom leads to a reversed effect compared with mono and dialkyl substitution. The acylation of the nitrogen atom weakens the electron donating properties of the amino group resulting in a blue-shift of the absorption and emission (**44p**).

There is a number of known rhodol molecules substituted at the position adjacent to the carbonyl group. This sort of substitution weakly affects the rhodol chromophore and leads to a small bathochromic shift (about 5 nm) on both absorption and fluorescence (**113c,d**, **114a,b**).

The optical properties of rhodols unsubstituted at the *meso*-position (**115**) fit this trend and its photophysical properties resemble that of its analogue **113b**. Nevertheless, dye **115** is more sensitive toward nucleophiles, which hinders the measurement of its fluorescence quantum yield.

Annulation of the rhodol chromophore with benzene or naphthalene rings (**61**, **118**) results in a bathochromic shift of both absorption and emission, however, a direct comparison with **44e** is not possible as spectra were measured in different solvents (Fig. 11). Compound **49** represents the generic structure of SNARF chromophores, which are vinyllogues of rhodol chromophores. Expanding the rhodol system by additional benzene ring leads to 60 nm bathochromic shift of the absorption maximum. In addition SNARF chromophores are characterized by higher Stokes shifts which can suggest bigger differences of the ground and excited state geometries. Therefore, SNARFs show emission maxima close to NIR spectral range (Fig. 11).^{77,81}

Compound **70** is a vinyllogue of rhodol with the conjugation chain lengthened by a phenyl ring. The comparison of the absorption properties of **70** with **44j** shows almost no difference in the maximum position. This can suggest that compound **70** mainly adopts a nonpolar structure with no charge separation. There is no fluorescence efficiency data for compound **70**, however, the Stokes shift is much larger than that for **44j** which often suggests low fluorescence quantum yield.

Within a series of bis-xanthene dyes, compounds **74–76** consist of the rhodol framework expanded with an additional π -system so that they represent a cross-conjugation between fluorescein–rhodol (**74**), two rhodols (**75**) and rhodamine–rhodol chromophores (**76**). Nevertheless, Fig. 11 shows that compounds **74–76** demonstrate almost identical spectroscopic properties comparable with annulated rhodol **118**.

Recently, the introduction of a second electron-donating amino group at the neighbouring position to the first has become a viable way to modulate the photophysical properties (**116–117**, Fig. 11).^{53,58} This modification leads to a strong increase in the Stokes shift (120–140 nm) resulting from red-shift of the emission maxima (to *ca.* 660 nm). The absorption maxima remain in the spectral range typical of substituted

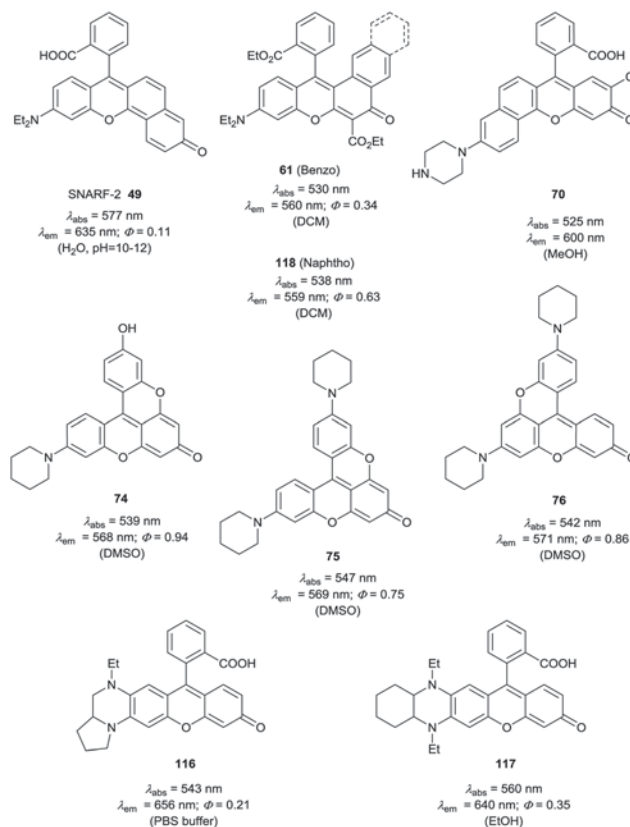


Fig. 11 The structure of π -expanded rhodol analogues.

rhodols. The most probable reason for this effect is that the dye molecule after excitation forms a charge transfer state.

A number of rhodol congeners with a bridging atom other than oxygen have been reported within the last decade. The study on the influence of polar substituents on the conjugation chain, and hence absorption spectra, of polymethine dyes including rhodamines is rationalized by the Dewar–Knott rule.^{101,102}

According to this rule, electron-donating groups at the *meso*- and bridge positions result in a hypsochromic shift of the absorption maxima, while electron-withdrawing groups show the reverse effect. On the basis of this rationale, rhodol analogues with a more electron withdrawing ‘bridge’ than oxygen atom should show a red-shift in both absorption and fluorescence maxima while electron donating moieties should show a hypsochromic shift (Fig. 12).

The position of both absorption and fluorescence maxima correlate with the average polar effect of the substituent. The electron-donor effect of oxygen bridge of O-rhodol **119** results in the somewhat blue-shift of the absorption maximum in comparison with unbridged chromophore **1** (Fig. 3).²² The increase of electron-withdrawing properties of the bridge atom leads to the bathochromic shift of the absorption and fluorescence maxima. According to Fig. 13 carborhodol **96**⁹³ demonstrates a significant red-shift which is the result of the absence of the resonance effect occurring for the O-bridge. At first glance Si-rhodol derivatives^{89,90,104,105} may be expected to have their absorption maxima slightly blue-shifted to that of carborhodol as silicon is less

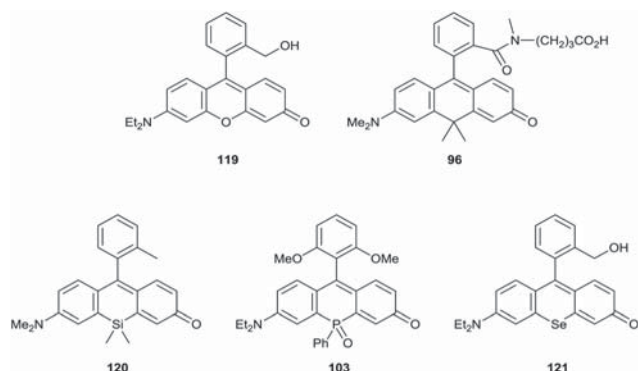


Fig. 12 Rhodol **119**,³⁷ carborhodol **96**,⁹³ Si-rhodol **120**,¹⁰³ P-rhodol **103**⁹⁴ and Se-rhodol **121**.⁹⁵

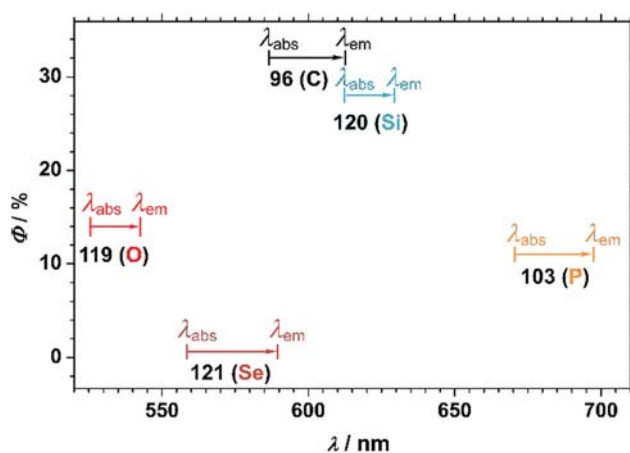


Fig. 13 Optical properties diagram for rhodol (**119**), carborhodol (**96**), P-rhodol (**103**), Si-rhodol (**120**) and Se-rhodol (**121**) in PBS buffer.

electronegative than a carbon atom. The truth is, however, that although the silicon atom is less electronegative compared to a carbon atom, an interaction of the chromophore LUMO with the pseudo- π^* of the silicon bridge^{106,107} ($\sigma^*-\pi^*$ hyperconjugation) decreases the LUMO energy thus resulting in the red-shift of both absorption and emission for derivative **121**¹⁰³ (Fig. 13).

P-rhodols tend to have the most bathochromically shifted absorption and fluorescence among other known rhodol-like molecules as the P-containing 'bridge' affects the π -system by means of electron withdrawing resonance interaction and $\sigma^*-\pi^*$ hyperconjugation similarly to Si-rhodols. Both effects result in a bathochromic shift of the absorption maximum, so that for compound **103** it almost reaches the NIR spectral region.^{94,108}

Oxygen and selenium, both belonging to group 16, affect the chromophore in the same manner. A bathochromic shift of the absorption band for Se-rhodol **121**⁹⁵ compared to rhodol **119** is the result of weakened $\sigma^*-\pi^*$ hyperconjugation with the larger Se atom. The presence of a heavy atom in the Se-rhodol structure also causes the quenching of fluorescence (Fig. 13). The small Stokes shifts for the rhodol-like structures **96**, **103**, **119**–**121** in such a polar medium as PBS buffer is due to the chromophores closely resembling the ideal polymethine state.⁹⁸

4.2. Non-linear optical properties

In contrast to both rhodamines and fluoresceins, the asymmetric, more polarized structure of rhodol displays more efficient two-photon (2P) absorption σ_2 due to increased intramolecular charge transfer (ICT). Only few reported rhodol chromophores have been examined with respect to 2P absorption and include **112**, **122** and **124** (Fig. 7, 14 and 16).^{69,73,100,109} Rhodols feature moderate 2P absorption cross-sections (up to 165 GM), although this is much higher than analogous rhodamines and fluoresceins. Additionally, rhodols show strong fluorescence efficiency which leads to the 2P brightness ($\sigma_2^{\text{max}} \cdot \Phi$) high enough for 2P excited fluorescence microscopy experiments (Fig. 14).

In summary, assuming the same pattern of substituents, the absorption and emission of rhodols is slightly hypsochromically shifted *versus* that of rhodamines and bathochromically *versus* fluoresceins. The position of both maxima are less pH-sensitive than for the two more popular chromophores. Except for SNARFs, the π -expansion of rhodol chromophore is not a viable pathway for realizing a notable bathochromic shift of absorption and fluorescence. The replacement of the oxygen atom in the bridging position with C, Si, Se and P turned out to be a much better strategy, with P-rhodols reaching record values ($\lambda_{\text{em}} = 695$ nm). Replacement of the oxygen atom bridge comes at a cost, however, and fluorescence quantum yields are lowered to 0.3 or below which leaves sizable room for further improvement.

5. Fluorescent imaging

5.1. Fluorescent reporters

Given the renewed interest in the use of small molecules as fluorescent probes,^{110–112} it is perhaps not surprising that the rhodol chromophore has become a popular scaffold for the design and implementation of fluorescence probes for a range of diverse biological studies. This is due to the many possible ways of functionalizing the rhodol moiety for different research purposes and to tune the photophysical properties of rhodol containing probes. Prior to the 21st century there were few

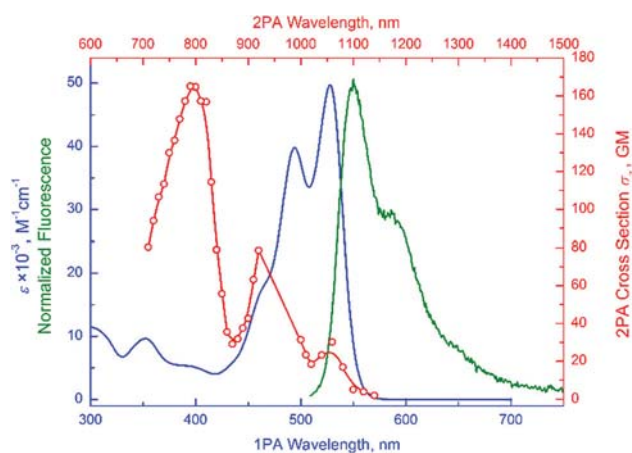


Fig. 14 1P and 2P absorption and fluorescence spectra for rhodol **112** in DCM. Reprinted with permission from *J. Org. Chem.*, 2013, **78**, 11721–11732. Copyright © 2013, American Chemical Society.

published reports of rhodols acting as fluorescent sensors⁵ possibly due to the plethora of classic and popular dyes such as cyanines, rhodamines and fluoresceins. Nevertheless, the use of rhodol chromophores has been progressively increasing in popularity over the last two decades, especially in more advanced biological studies.

The rhodol chromophore features certain structural elements commonly employed for modulation of the optical properties of the probe depending on its application (Fig. 15). The adjustment of the bridge atom and π -expansion allow the spectral range to be tuned. The dye/spiro form tautomerism governs fluorescence on/off signaling.^{40,48–50,60,113,114} O-Substitutions enforce the colorless spiroform, while the cleavage of the O-terminal group bond resumes the equilibrium and turns on rhodol fluorescence (Scheme 20).^{115–117} A combined approach using polar substituents at position 2, which allow excited state intramolecular proton transfer (ESIPT) between the hydroxy group of the spiroform and the polar substituent, enables another type of fluorescent signaling that allows switching between fluorescence regimes.^{118–120} Moreover, the terminal amino group is a linking position to introduce functional groups necessary for selective sensing or targeting.^{52,121,122} A range of rhodol probes employing a photo-induced electron transfer (PET) approach using either a one-photon (1P) or two-photon (2P) excitation regimes have been applied in fluorescence microscopy experiments and ratiometric fluorescence sensing.^{47,55}

As the polarization of the rhodol chromophore is a function of the external electric field stimulus, the study of neuron activity with a specifically designed rhodol probe has been achieved (Fig. 16).⁶⁹

Probe **122** features a rhodol chromophore modified with two chlorine atoms and a linear polyene substituent at the *meso*-position with a terminal electron-donor group. It exhibits absorption and emission in the range typical of rhodol dyes ($\lambda_{\text{abs}} = 520 \text{ nm}$, $\epsilon = 83\,000 \text{ cm}^{-1} \text{ M}^{-1}$, $\lambda_{\text{em}} = 535 \text{ nm}$, $\Phi = 0.27$; PBS, pH 7.4). The presence of the polyene chain makes this probe voltage sensitive as PET from the dimethylamino group to the rhodol chromophore causes fluorescence quenching. Indeed, probe **122** intercalated the plasma membrane where it is influenced by the membrane potential, which governs the strength of PET. The fluorescence efficiency decreases under hyperpolarized cellular conditions (typical resting neuronal membrane potential) as PET strengthens. In contrast, cellular depolarization weakens PET and leads to the increase of the

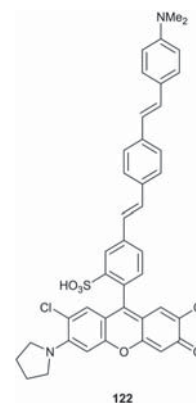


Fig. 16 Rhodol probe used to study neuron activity.

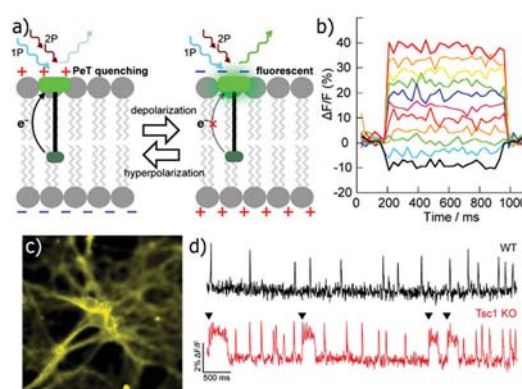


Fig. 17 Probe **122** voltage sensing via PET using 1P or 2P excitation. (a) At hyperpolarized or resting potentials fluorescence is quenched, whereas at depolarized potentials PET is inhibited by the electric field across the membrane, enhancing fluorescence. (b) Fractional change in fluorescence ($\Delta F/F$) vs. time in a patch-clamped HEK cells under 2P illumination (820 nm), held at -60 mV and then stepped to potentials ranging from -100 to $+100 \text{ mV}$ in 20 mV increments. (c) Assessing differences in spontaneous activity in WT and Tsc1 KO neurons with **122**. Wide-field fluorescence image of RVF5 staining in DIV 14 cultured Tsc1^{fl/fl} mouse hippocampal neurons infected with a virus encoding mCherry-Cre to knock out the Tsc1 gene (Tsc1 KO). (d) Representative optical recordings of spontaneous activity in pairs of wild-type (WT, upper, black trace) and Tsc1 KO cultures (Tsc1 KO, lower, red trace). Arrowheads (\blacktriangledown) indicate periods of 'burst' firing in the Tsc1 KO neuron. Reproduced from ref. 69 *Proc. Natl. Acad. Sci. U. S. A.*, 2017, **114**, 2813–2818.

fluorescence response thus enabling the detection of fast-spiking action potentials in neurons (Fig. 17).⁶⁹

The voltage sensitivity of **122** is comparable under both 1P and 2P conditions. Nevertheless, the improved 2P brightness compared with fluorescein-based voltage sensitive probes¹²³ allows the application of **122** in thick tissue or brain samples. In addition, the high photostability of **122** enables the probing of neuronal activity in a mouse model of the human genetic epilepsy disorder Tuberosus Sclerosis Complex (TSC), both in cultured neurons and in brain slices.

A number of reports demonstrate the design and application of metal ion probes employing both photoinduced electron transfer and the equilibrium between spiro and open forms of

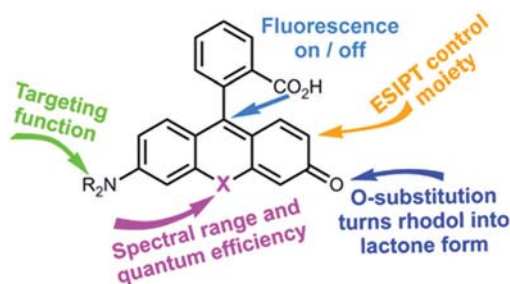


Fig. 15 Rhodol structural features used in probe design.

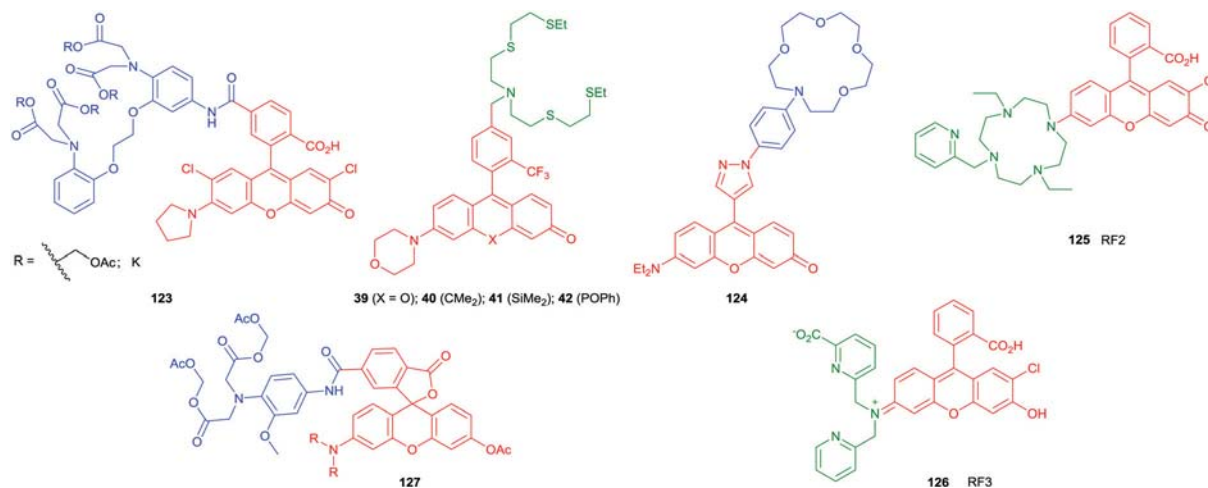


Fig. 18 Cation sensing rhodol based probes.

rhodol (Fig. 18). A rhodol chromophore functionalized with a BAPTA moiety (**123**) was developed to monitor spontaneous activity in cultured neurons and other intracellular processes connected with Ca^{2+} exchange. The formation of Ca^{2+} complexes leads to growth in the fluorescence response of sensor **123** due to a decrease in PET. In addition to conventional (1P) fluorescence microscopy techniques, microscopy experiments with 2P excitation were carried out and showed higher resolution fluorescence imaging (Fig. 19).⁷³

Copper is an endogenous regulator of lipolysis, the breakdown of fat, which is an essential process in maintaining body weight and energy stores.¹²⁴ A group of probes for Cu^+ built

upon O-, carbo-, Si- and P-rhodols **39–42** containing an identical sensing podand fragment were designed (Fig. 18). The podand moiety selectively binds with Cu^+ resulting in the growth of the fluorescence response. The probes showed absorption maxima in the range 510–570 nm depending on the bridging atom with weak fluorescence. By means of fluorescence microscopy these probes could detect changes in labile copper levels in living cells (Fig. 20).^{65,67}

Sensor molecule **124** uses an azacrown ether as the receptor to probe sodium cation concentration as the presence of Na^+ leads to a growth in the fluorescence response (Fig. 18). In addition, chelation of the sodium ion in the crown ether cavity leads to an increase in the two-photon absorption (2PA) cross-section. Experiments with the 2P excitation show a twelfold increase in the two-photon brightness of probe **124** in the presence of Na^+ .¹⁰⁹

For the construction of novel Zn^{2+} targeting ratiometric indicators the rhodol chromophore was modified with azacrown ether and dipicolylamine receptors. Both **125**⁵⁴ and **126**⁵⁷ exhibit visible absorption maxima at 514 nm and emission maxima around 540 nm, respectively (Fig. 18). Zinc coordination in **125**

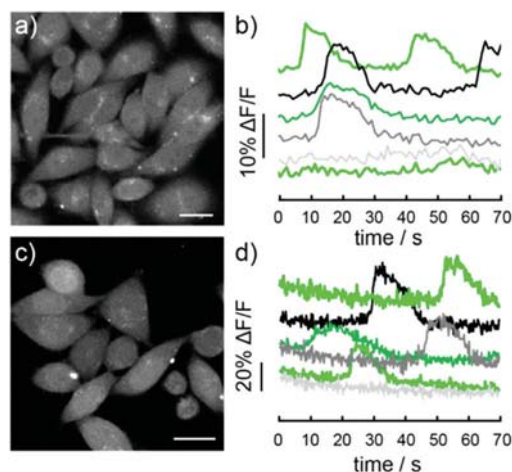


Fig. 19 Live-cell imaging of histamine-evoked Ca^{2+} fluctuations with rhodol Ca^{2+} sensor **123**. (a) Confocal fluorescence microscopy images (1P) of HeLa cells incubated with ester form of rhodol Ca^{2+} sensor (1.7 μM). Scale bar is 20 μm . (b) Quantification of intracellular Ca^{2+} concentration fluctuations measured in response to stimulation with histamine (5 μM). (c) 2P laser scanning fluorescence microscopy images of HeLa cells incubated with the ester form of rhodol Ca^{2+} sensor (1.7 μM). Scale bar is 20 μm . (d) Quantification of intracellular Ca^{2+} concentration fluctuations measured in response to stimulation with histamine (5 μM). Reprinted with permission from *Biochemistry*, 2018, **57**, 237–240. Copyright 2018 American Chemical Society.

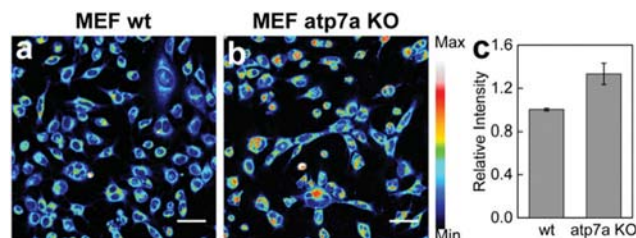


Fig. 20 Fluorescence imaging of labile copper pools in mouse embryonic fibroblast (MEF) wildtype (WT) and *Atp7a*^{-/-} knockout fibroblast cells with **40**. (a) MEF WT cells and (b) MEF *Atp7a*^{-/-} knockout cells were stained with 2 μM **40** for 10 min in DMEM, and their average fluorescence intensity was (c) quantified. Scale bars: 40 μm . Data were normalized to MEF *atp7a* wt cells and shown as average \pm s.d. (**40**, $n = 4$). Adapted with permission from *ACS Chem. Biol.*, 2018, **13**, 1844–1852. Copyright 2018 American Chemical Society.

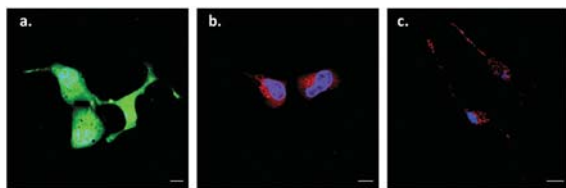


Fig. 21 Cellular localization of Thallos (a), **127** (R = Me) (b), and rhodamine 123 (c). Confocal microscopy images were obtained in HEK-293 cells co-expressing GIRK1 and GIRK2 following incubation with Thallos (1 μM), **127** (R = Me) (5 μM), or rhodamine-123 (1 μM) for 1 h and counterstained with Hoechst 33342 (1 $\mu\text{g mL}^{-1}$). Scale bar = 10 μm . Reproduced from ref. 75 with permission from The Royal Society of Chemistry.

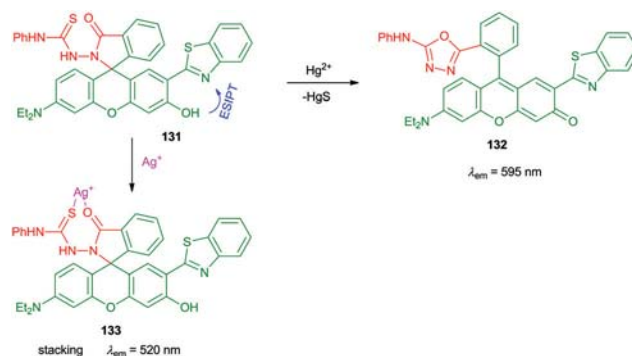
prompts a decrease in the absorption maximum and an increase of the fluorescence response from 0.36 to 0.56. Rhodol **126** responds to zinc coordination through a blue-shift in absorption to 495 nm and a blue-shift in emission to 523 nm combined with a subtle loss in fluorescence efficiency (from 0.62 to 0.52).

The Ti^+ flux assay coupled with a cell-permeable fluorescent indicator is used for imaging K^+ channel activity as it is compatible with kinetic imaging-based on high-throughput screening assays. A series of rhodol based Ti^+ sensitive probes with the general structure of **127** manifest themselves as versatile reagents for Ti^+ flux assays (Fig. 18).⁷⁵ Probe **127** (R = Me) localizes in the cytoplasm in an analogous manner to thallium targeting probe Thallos,¹²⁵ yet shows better pH tolerance and somewhat red-shifted absorption and emission spectra. The acetyloxy group is hydrolyzed in the intracellular volume thus opening the spiroform which activates the rhodol chromophore. Binding of the thallium ion gives rise to a more than fourfold increase in the fluorescence response (Fig. 21).

Using the ESIPT phenomenon simultaneously with spiro/dye tautomerism in rhodol-based probes offers a large advantage as it allows for the switching of fluorescence regimes. The ESIPT exclusively takes place in the closed form as only in that structure there is a phenolic OH group capable of acting as the hydrogen bond donor. The rhodol-based probe **128** in the absence of Hg^{2+} or ClO^- ions exists in a hydrogen bond stabilized spiroform (Scheme 21).¹²⁶ The mutual configuration of the benzothiazole moiety and the hydroxyl group leads to a blue emissive chromophore due to ESIPT. The presence of Hg^{2+} or ClO^- ions results in the activation of the rhodol chromophore and turns on fluorescence at 590 nm or 595 nm in **129** and **130**, respectively.¹²⁶



Scheme 21 Sensing mechanism of **128** for Hg^{2+} and ClO^- .

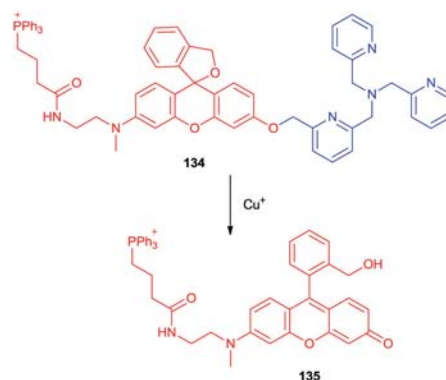


Scheme 22 Sensing mechanism of **131** for Hg^{2+} and Ag^+ .

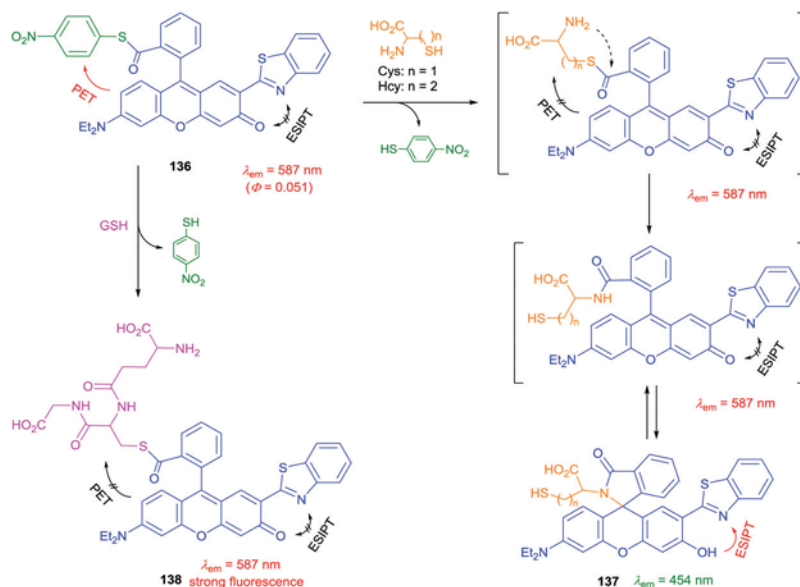
Besides several other reports on mercury ion sensing,^{127–131} Chen *et al.* demonstrated further development of sensor **128**. Compound **131** features the ability to selectively sense Hg^{2+} and Ag^+ ions through activation of the rhodol chromophore from its spiro form or through aggregation-induced emission (AIE), respectively (Scheme 22).¹³² Sensor molecule **131** reacts with a mercury cation which promotes the formation of an oxadiazole moiety and the rhodol chromophore **132** with a fluorescence maximum at 595 nm. In contrast, silver cations form a complex **133** with the sensor molecule in such a manner that significant stacking occurs and AIE with a fluorescence maximum at 520 nm is observed.

Molecule **134** is another rhodol probe for sensing metal ions based on the reaction of the spiroform functionality (Scheme 23). This sensor, for the intracellular fluorescence imaging of copper(i) ions features a phosphonium functional unit which facilitates mitochondria targeting. In turn, the formation of the triplicolylamine copper complex cleaves the terminal C–O bond thus recovering the emissive rhodol chromophore from its spiroform.³⁶

Employing various rhodol structural features in one sensor molecule makes it possible to construct polyfunctional fluorescent probes. A combination of the ESIPT and the labile *O*-substituted chelating group, which governs the spiro/open form equilibrium, allows for the design of dual function fluorescence probes for separate sensing of glutathione and cysteine/homocysteine,⁸³ the most abundant biological thiols. Rhodol probe **136** contains a benzothiazole moiety adjacent to the carbonyl group along



Scheme 23 Sensing mechanism of **134** for Cu^+ .

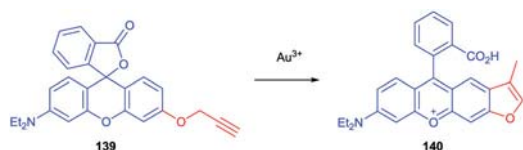
Scheme 24 Sensing mechanism of **136**.

with a nitrophenyl moiety (Scheme 24).¹³³ In the free form probe **136** shows dimmed fluorescence as the nitrophenyl moiety causes fluorescence quenching. The addition of a Cys moiety to probe **136** in DMF/buffer solution increases the emission at 587 nm as transesterification removes the nitroaryl moiety thus terminating PET-induced fluorescence quenching. Next, the intermediate product experiences intramolecular *S,N*-acyl shift followed by cyclization to the spiroform **137**. In the spiroform, the benzothiazole moiety in combination with the phenol group, enables the ESIPT with fluorescence at 454 nm. Since the cyclization is a reversible process, the fluorescence spectra after addition of Cys or Hcy, displays a strong band at 454 nm accompanied by weak emission at 587 nm. In the case of GSH the reaction stops at the transesterification step (**138**) as rearrangement is not possible, thus the addition of GSH leads to the growth of fluorescence at 587 nm.

In probe **139**, the spiroform of rhodol is secured by a propargyloxy group. In the presence of Au^{3+} ions intramolecular cyclization to **140** with a fused furanoxanthylum chromophore occurs showing strong absorption and fluorescence maxima at 493 and 526 nm, respectively (Scheme 25).¹³⁴ Due to the dramatic increase in emissive strength, a very high sensitivity for Au^{3+} is achieved (7 ppb).

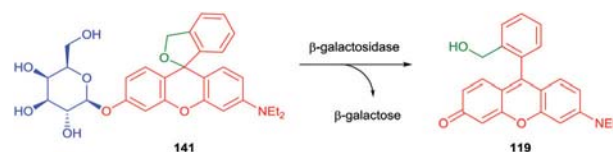
5.2. Biomolecule targeting

The design of probes where an enzymatic activity restores the rhodol chromophore from its spiroform has been found to be a

Scheme 25 The cyclization of **139** induced by Au^{3+} .

promising approach for targeted imaging.⁹ In the following series of studies, a rhodol chromophore was chosen for the visualization of metastases originating from ovarian cancers which show an enhanced enzymatic activity of β -galactosidase in comparison with normal ovaries. The terminal oxygen atom of the rhodol spiroform was modified with a β -galactopyranoside group to image cells with an increased activity of β -galactosidase as here the rhodol would be converted to the active (open) form in the cytoplasm of certain cells (Scheme 26).^{37,135} An analogue of β -galactosidase targeting probe **141**, Se-rhodol **142**, contains all the functionality of probe **141**, however, it exhibits a weak fluorescence response due to deactivation of the excited state *via* ISC to a greater extent.⁹⁵ The main application of dye **142** is rather in the phototherapy of cancer cells, where the formation of a triplet state is key to its functionality. The advantage of photosensitizer **142** is that the Se-rhodol is activated only in cells with the targeted enzyme, suppressing undesired phototoxicity (Fig. 22).

Probe **141** detects β -galactosidase activity in cultured cancer cells although it does not give adequate resolution due to high background fluorescence (Table 1).³⁷ On the basis of DFT calculations Urano and co-workers optimized the structure of probe **141** to shift the equilibrium towards the non-fluorescent spiroform. Within a series of rhodol-based derivatives probe **145** demonstrates superior fluorescence reporting properties as at pH 7.4, more than 99% of the probe exists in the spiroform thus weakening background fluorescence.¹³⁶ The detection

Scheme 26 Sensing mechanism of **141**.

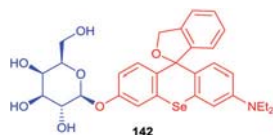


Fig. 22 Se-Rhodol photosensitizer.

Fig. 23 The structure of **152**.Table 1 Properties of β -galactosidase fluorescence probes¹³⁶

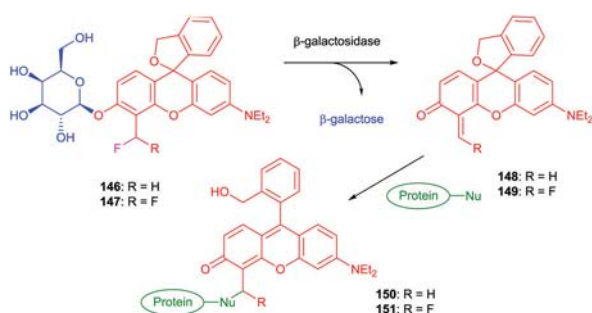
R ¹	R ²	pK _{cycl}	Fluorescence enhancement by β -galactosidase (fold)	
141	Et	Et	6.9	76.1 ³⁷
143	Et	H	6.3	313
144	(CH ₂) ₂ CF ₃	H	5.6	582
145	CH ₂ CF ₃	H	4.5	1420

limit of probe **145** to intracellular β -galactosidase activity in diverse ovarian cancer lines is very low and visualization of metastases as small as 1 mm *in vivo* can be achieved.

While enzyme targeting probe **141** shows high selectivity of staining, the main drawback is that the activated fluorescence chromophore tends to leak out of cells during prolonged incubation. The next generation of β -galactosidase targeting probes were designed in a manner so that after activation, the chromophore would be immobilized inside a cell. In addition, cellular studies on probes synthesized with anchoring moieties such as **146** revealed that they show enhanced fluorescence activation (Scheme 27).¹³⁷

To extend the utility of β -galactosidase probes with single-cell resolution in the red region, a Si-rhodol based β -galactosidase targeting probe was designed. Probe **152** emits at 638 nm in the open form and demonstrates all the sensing properties of **146** (Fig. 23). It can label cells of interest in combination with GFP markers and imagine multiple cell types at single-cell resolution in living samples.¹⁰³

Further development of specific cell targeting for analytical purposes requires the selective transport of therapeutic agents to a particular cell. The structure of the rhodol motif allows for

Scheme 27 Sensing mechanism of **146** and **147**.

the combination of cell targeting, drug release and activation of the chromophore to control the therapeutic effect. Rhodol based prodrug **153** consists of the biotin subunit as a moiety to provide tumor localization,¹³⁸ and the topoisomerase I inhibitor SN-38¹³⁹ connected *via* a linker with disulfide bonds. When prodrug **153** is localized in cancer cells it reacts with intracellular thiols to release SN-38 (**155**), one of the most efficient therapeutic agents used to treat various carcinomas, and activate the open form of rhodol probe **154** to monitor cytotoxicity (Scheme 28).^{140–142}

Probe **156** combines a rhodol chromophore in the spiroform modified with an arginine-glycine-aspartate motif (cRGD), which targets $\alpha_v\beta_3$ integrin overexpressed cancer cells. In addition, the probe **156** consists of a photosensitizer motif, which due to AIE¹⁴³ shows an emission maximum at 650 nm with a fluorescence quantum yield of 0.13 in a DMSO/water mixture and plays the role of an imaging agent to monitor endocytosis. When irradiated, probe **156** generates singlet oxygen and cleaves the aminoacrylate linker to release the green emissive rhodol **157** for *in situ* monitoring the singlet oxygen generation during PDT (Scheme 29).

Probe **159** demonstrates a rare instance where the rhodol chromophore is the targeting motif itself (Fig. 24). The fluorinated hydrophobic rhodol **159**, containing an electrophilic nitrofuranyl moiety, was revealed to accumulate in the endoplasmic reticulum (ER) due to the presence of the rhodol, and cause inhibition of the protein p97 of the ER.⁷⁶ Thus the fluorinated rhodol motif was found to be suitable for the transport of small molecules to the ER.

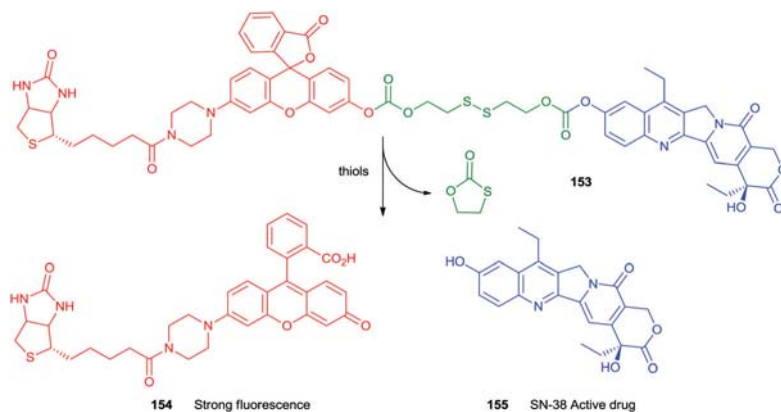
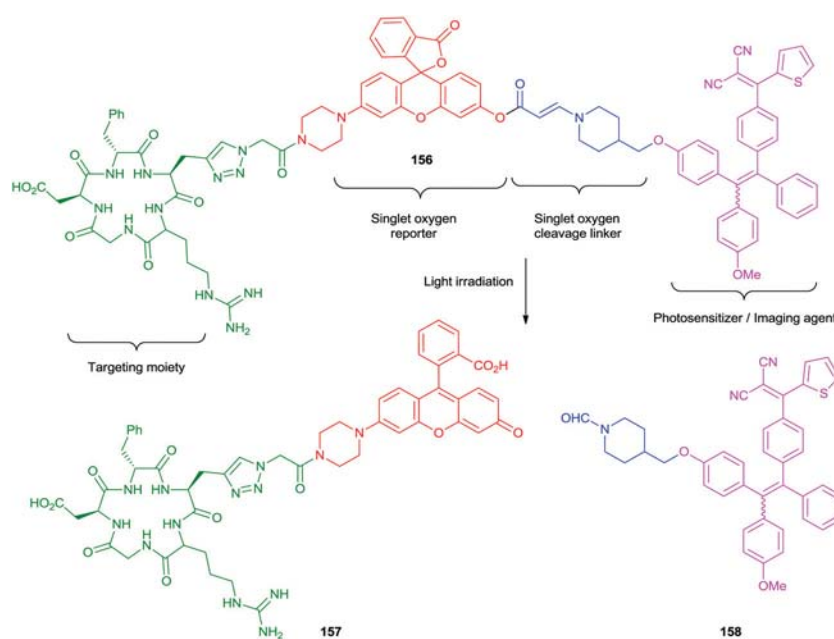
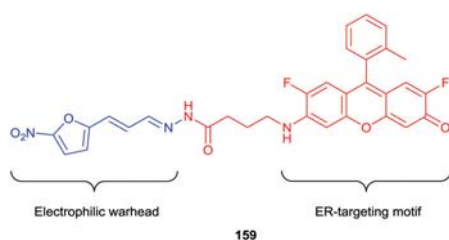
5.3. Rhodol based redox probes

The design of fluorescence probes for the study redox processes in biological systems can employ the rhodol motif as it allows versatile modification of the structure combined with excellent optical properties.

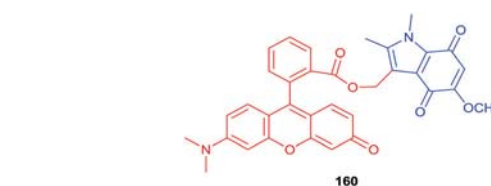
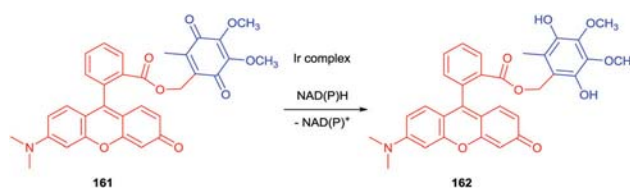
The sensing effect of the probe **160** relates to the position of the indoloquinone LUMO depending on the redox state. In the conjugate **160** the LUMO of the indoloquinone possesses a lower energy compared to the rhodol chromophore (Fig. 25).

As the result, probe **160** shows very weak fluorescence ($\lambda_{em} = 550$ nm, $\Phi = 0.0098$ in water) as the emission is quenched by the electron transfer from the rhodol LUMO to the indoloquinone LUMO. In the cellular imaging of a human lung adenocarcinoma cells, A549, the reaction of probe **160** with NADPH:cytochrome P450 reductase under hypoxic conditions (0.02% oxygen) releases free rhodol chromophore which shows strong fluorescence. Under aerobic conditions (20% oxygen) probe **160** shows no fluorescence growth.¹⁴⁴

Probe **161** features a ubiquinone moiety at the *meso*-position which makes this reporter sensitive to NAD(P)H (Scheme 30).

Scheme 28 Rhodol based prodrug **153**.Scheme 29 Rhodol based targeting agent **156**.Fig. 24 Rhodol based agent **159**.

It shows a strong fluorescence response for the quinone form ($\lambda_{em} = 518$ nm, $\Phi = 0.733$ in PBS buffer), while in the reduced form fluorescence of dye **162** is quenched. The fluorescence microscopy of HeLa cells visualizes the reaction of quinone probe **161** with NAD(P)H in the presence of artificial promoter $[(\eta^5\text{-C}_5\text{Me}_5)\text{Ir}(\text{phen})(\text{H}_2\text{O})]^{2+}$ which gives rise to an 8.6 fold decrease in the fluorescence efficiency over 10 min.¹²

Fig. 25 Redox probe **160**.Scheme 30 Rhodol based redox probe **161**.

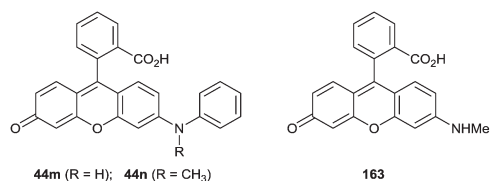


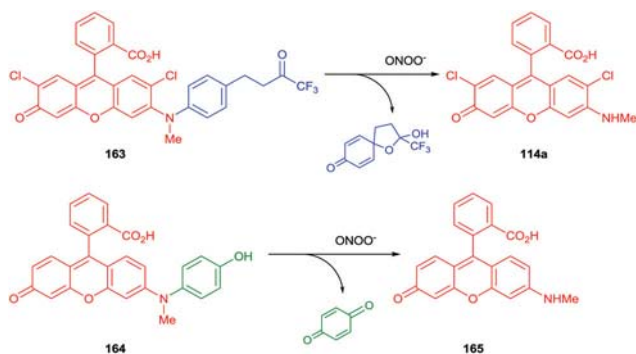
Fig. 26 Peroxynitrite sensitive rhodol probes **44n,m** and fluorophore **163** formed in the sensing process.

Despite the large structural similarity of rhodols **44m**, **44n**⁶⁸ and **163** these compounds show remarkably different fluorescence efficiency. Indeed, derivative **163** without *N*-aryl substituent is an efficient fluorophore, whereas both **44m** and **44n** show a fluorescence signal close to the background noise level (Fig. 26).

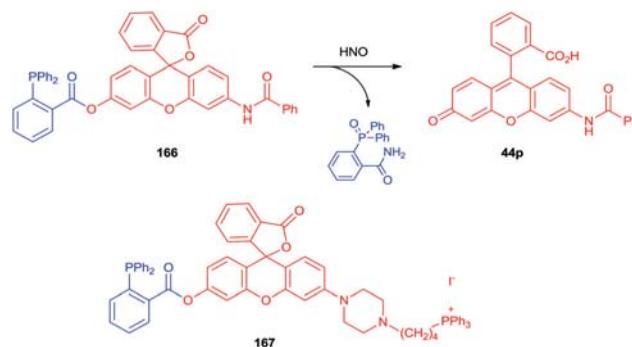
This difference in fluorescence response was used to design two families of rhodol-containing probes for the imaging of peroxynitrite (ONOO^-), a potent oxidant generated in cells from the reaction between nitric oxide (NO) and superoxide ($\text{O}_2^{\bullet-}$) (Scheme 31). This species contributes to tissue injury in a number of human diseases. Probes **163** and **164** are sensitive to the peroxynitrite species which cleave the *N*-aryl bond to form highly fluorescence rhodol derivatives **114a** and **165**. These probes demonstrate a great tolerance to reactive oxygen species and reactive nitrogen species (ROS and RNS) such as H_2O_2 , $^1\text{O}_2$, $\bullet\text{NO}$, $\text{O}_2^{\bullet-}$, ROO^\bullet and very weak sensitivity toward HOCl and $\bullet\text{OH}$. Still the fluorescence response over ONOO^- for probe **164** is more than 18 times higher than those for HOCl and $\bullet\text{OH}$.^{70,72,105,145}

As a probe for nitroxyl (HNO), which influences both the physiological and pathological processes in mammalian organisms and mediates their immune system response, a rhodol chromophore was modified with a triarylphosphine moiety. The reaction of rhodol probes **166**⁷¹ and **167**⁵⁹ with HNO selectively cleaves terminal ester bond converting them into fluorescent open forms (Scheme 32).

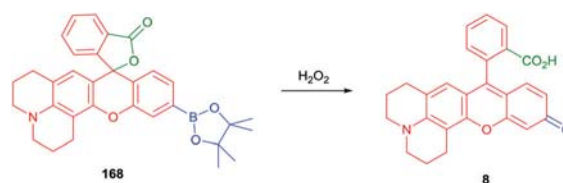
Fluorescence visualization of intracellular H_2O_2 employs the modified boronate-protected xanthene chromophore in the spiro-form **168**, which, in the presence of hydrogen peroxide cleaves the C–B bond to turn the chromophore into the fluorescent open form rhodol **8**. This probe, within a range of diverse xanthene-based multicolor probes,²⁸ shows a selective turn-on fluorescence response to H_2O_2 in live-cell imaging assays over a range of biologically relevant ROS (Scheme 33).⁴⁵



Scheme 31 The mechanism for peroxynitrite sensing of probes **163** and **164**.



Scheme 32 Nitroxyl sensing probes **166** and **167**.



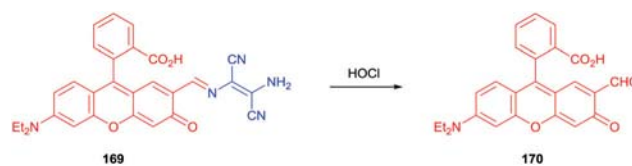
Scheme 33 H_2O_2 Sensing probe **168**.

Endogenous hypochlorous acid is a biologically important oxidative species. Sensors for the hypochlorite anion have been designed that contain the Schiff base fragment derived from formylrhodol. The barely fluorescent probe **169** ($\Phi = 0.04$) displays a high sensitivity and selectivity toward ClO^- to form formylrhodol **170** accompanied by an increase in fluorescence ($\Phi = 0.35$). Probe **169** shows a high efficiency of *in vivo* imaging ClO^- in living mice (Scheme 34).^{146,147}

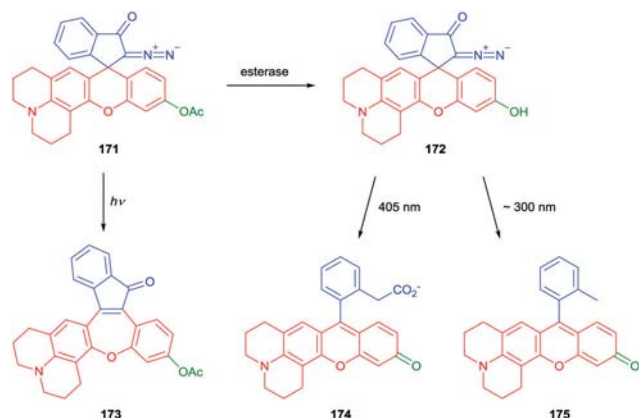
As rhodol dyes demonstrate high photostability⁶⁹ these molecules are suitable for super-resolution imaging techniques *i.e.* stimulated emission depletion (STED)⁹³ and photoactivated localization microscopy (PALM). Rhodol **171** is sensitive to light irradiation as it experiences light-induced Wolff rearrangement.

The photoproduct **173** consists of a seven-membered ring and demonstrates a very weak fluorescence response. Nevertheless, the removal of the acetyl group by carboxylesterases leads to hydroxyl derivative **172** which upon the light irradiation (depending on the wavelength) gives rise to either photoproduct **174** or **175**, both of which show bright emission (Scheme 35). Rhodol derivative **171** is an efficient reporter for probing esterase activity in live cells using PALM imaging technique as this molecule does not diffuse substantially from its activation site, allowing precise localization of the enzymatic event.¹⁴⁸

Scientists are chiefly attracted to rhodols over related xanthene dyes due to the combined beneficial aspects of better stability,



Scheme 34 Probe **169** for *in vivo* imaging of ClO^- .



Scheme 35 The efficient reporter for probing enzymatic activity in live cells using PALM imaging probe **171**.

strong fluorescence, their dipolar nature, better pH tolerance, higher sensitivity of fluorescence intensity to structural changes and the fact that they are comparatively under-explored. Importantly, they retain the advantage of lactone-forming switchability *i.e.* the transformation of the colorless spiro tautomer into the fluorescent dye (in analogy to fluoresceins and rhodamines). The nitrogen and oxygen atoms of rhodol are often used as linking positions to introduce active functional groups, which can govern fluorescence signaling in biological media and introduce extra functionality. Moreover, these features enable probes based on rhodol and its heteroanalogues to be used in super-resolution fluorescence microscopy. Paradoxically the very fact which is responsible for their relatively complex synthesis is also responsible for the ability to introduce various functionalities required for sensing. This in turn affords the construction of truly complex probes. In addition to the modular and adjustable design of the rhodol chromophore, enhanced two-photon absorption compared to other dyes commonly used in fluorescence imaging (*i.e.* rhodamines, fluoresceins, coumarins and BODIPY) enable the design of multifunctional fluorescence probes for sensing a range of ions, imaging thick tissue, biomolecules, intracellular redox processes, sensing enzymatic activity, intracellular targeting and intracellular drug delivery.

6. Summary and outlook

In 1990, it would have been impossible to imagine that within 30 years the chemistry of rhodols would expand to create an independent field of study. It can be hypothesized that such developments will continue with the recent emergence of various core-modified and π -expanded rhodols.

The synthesis of rhodols, unlike rhodamines and fluoresceins, still utilizes the most classical methodology *i.e.* the reaction of anhydrides with aminophenols followed by the reaction of a second nucleophile. Plausibly, this is related to the fact that many probes rely on the ring-opening/ring-closure transformation of the carboxyl group intrinsic to this synthesis. The accumulated knowledge of rhodol dyes over the last 130 years has allowed thorough analysis of their structures and properties. Bathochromic and hypsochromic shifts can be readily achieved through judicious

inclusion of functional groups or heteroatoms, and fluorescence efficiencies through amine substitution. As a result, a number of functional biological probes based upon the rhodol core have been prepared. Among rhodols and their analogues, a particularly promising and beneficial feature with respect to both rhodamines and fluoresceins is their dipolar nature, as this allows operating voltage sensitivity for in brain imaging without additional functional groups in the one- and two-photon excitation regimes. Interest in rhodols has shifted in the last few years from generic fluorescent dyes towards cutting-edge applications related to fluorescent imaging chiefly thanks to the work of Chang, Miller, Lavis, Rivera-Fuentes and Urano. Appreciation of rhodols' physicochemical properties have made them attractive scaffolds for fluorescence imaging. The possibility of flexible modification of the rhodol chromophore allows the design of multifunctional fluorescence probes for sensing intracellular redox processes, enzymatic activity, intracellular targeting, intracellular drug delivery, sensing of diverse biomolecules *etc.* Enhanced 2P absorption along with the high photostability of rhodol-like chromophores prompts applications related to fluorescence sensing of the membrane potential in cells. In addition, it enables the usage of probes based on rhodols and their heteroanalogues for state-of-the-art imaging techniques such as super-resolution fluorescence microscopy.

Needless to say a great deal of an additional effort is required to fully explore the possibilities of these molecules. We hope that this Review, in addition to organizing knowledge on this topic, will serve as a catalyst to spark further studies. Possible targets may be more densely substituted rhodol chromophores, modified in such a way to use the many benefits of this fluorescence platform in new fields of application. For practical applications, it is important to seek a balance between high fluorescence efficiency, large Stokes' shift and photostability. We believe that many scientific problems can be resolved and many yet unknown compounds can be discovered with the help of this Review and that some of them will find their way towards practical applications. The analysis of research performed within the last twenty years suggests that the variety of future compounds will be only limited by our imagination.

Conflicts of interest

There are no conflicts to declare.

Acknowledgements

We thank for financial support from the Foundation for Polish Science (grants FNP TEAM POIR.04.04.00-00-4232/17-00 and FNP TEAM POIR.04.04.00-00-3CF4/16-00) and from Global Research Laboratory Program (2014K1A1A2064569) through the National Research Foundation (NRF) funded by Ministry of Science, ICT & Future Planning, Korea.

Notes and references

- 1 Farbenfabriken vorm. Friedr. Bayer & Co. in Elberfeld, DE54085, 1889.
- 2 Badische Anilin- und Soda-Fabrik, DE54684, 1890.

- 3 J. T. Hewitt, *Dyestuffs Derived From Pyridine, Quinoline, Acridine And Xanthene*, Longmans, Green and Co, London, 1922.
- 4 N. Ghatak and S. Dutt, *J. Indian Chem. Soc.*, 1929, **6**, 465–471.
- 5 J. E. Whitaker, R. P. Haugland, D. Ryan, P. C. Hewitt, R. P. Haugland and F. G. Prendergast, *Anal. Biochem.*, 1992, **207**, 267–279.
- 6 G. A. Smith, J. C. Metcalfe and S. D. Clarke, *J. Chem. Soc., Perkin Trans. 2*, 1993, 1195.
- 7 K. R. Gee, M. Poot, D. H. Klaubert, W.-C. Sun, R. P. Haugland and F. Mao, US6162931(A), 1996.
- 8 F. Mao, W.-Y. Leung and R. P. Haugland, US6130101(A), 1997.
- 9 P. de Silva, J. Eilers and G. Zlokarnik, *Proc. Natl. Acad. Sci. U. S. A.*, 1999, **96**, 8336–8337.
- 10 K. Venkataraman, *The chemistry of synthetic dyes*, Academic Press, New York, 1952, vol. II.
- 11 I. S. Ioffe and V. F. Otten, *Zh. Org. Khim.*, 1965, **1**, 343–346.
- 12 H. Komatsu, Y. Shindo, K. Oka, J. P. Hill and K. Ariga, *Angew. Chem., Int. Ed.*, 2014, **53**, 3993–3995.
- 13 G. A. Reynolds, GB1410603, 1975.
- 14 P. R. Hammond, *J. Photochem.*, 1979, **10**, 467–471.
- 15 R. R. Sauers, S. N. Husain, A. P. Piechowski and G. R. Bird, *Dyes Pigm.*, 1987, **8**, 35–53.
- 16 L. G. Lee, G. M. Berry and C.-H. Chen, *Cytometry*, 1989, **10**, 151–164.
- 17 M. Kondo, M. Tanaka, N. Sakamoto and H. Ooyoshi, EP0511019(A2), 1992.
- 18 R. Alford, H. M. Simpson, J. Duberman, G. C. Hill, M. Ogawa, C. Regino, H. Kobayashi and P. L. Choyke, *Mol. Imaging*, 2009, **8**, 341–354.
- 19 H. Zheng, X. Q. Zhan, Q. N. Bian and X. J. Zhang, *Chem. Commun.*, 2013, **49**, 429–447.
- 20 J. Han and K. Burgess, *Chem. Rev.*, 2010, **110**, 2709–2728.
- 21 V. Z. Shirinian and A. A. Shimkin, *Heterocyclic Polymethine Dyes*, 2008, pp. 75–105.
- 22 S. Hünig, H. Schwegelberg and H. Schwarz, *Justus Liebigs Ann. Chem.*, 1954, **587**, 132–145.
- 23 K. Chulvi, A. M. Costero, L. E. Ochando, S. Gil, J. L. Vivanco and P. Gaviña, *Molecules*, 2015, **20**, 20688–20698.
- 24 E. A. Halabi, Z. Thiel, N. Trapp, D. Pinotsi and P. Rivera-Fuentes, *J. Am. Chem. Soc.*, 2017, **139**, 13200–13207.
- 25 S. S. Patil, K. G. Thorat, R. Mallah and N. Sekar, *J. Fluoresc.*, 2016, **26**, 2187–2197.
- 26 L. Geng, X. F. Yang, Y. Zhong, Z. Li and H. Li, *Dyes Pigm.*, 2015, **120**, 213–219.
- 27 H. J. Rivera-Jacquez and A. E. Masunov, *Spectrochim. Acta, Part A*, 2018, **198**, 123–135.
- 28 B. C. Dickinson, C. Huynh and C. J. Chang, *J. Am. Chem. Soc.*, 2010, **132**, 5906–5915.
- 29 S. V. Patel, M. P. Patel and R. G. Patel, *J. Serb. Chem. Soc.*, 2005, **70**, 931–936.
- 30 Z. Diwu, J. Liu and K. Gee, US2004147747(A1), 2004.
- 31 Z. Diwu, J. Liu, R. P. Haugland and K. Gee, WO0212195(A1), 2002.
- 32 Y. Zhao, Y. Ren, H. Li, T. Han, H. Chen and W. Guo, *Dyes Pigm.*, 2016, **132**, 255–261.
- 33 F. T. Chin, J. Klockow, K. Hettie and T. Glass, WO2016210054(A1), 2016.
- 34 G. S. Ghotekar, A. C. Shaikh and M. Muthukrishnan, *J. Org. Chem.*, 2019, **84**, 2269–2276.
- 35 K. Tiensomjit, R. Noorat, S. Chomngam, K. Wechakorn, S. Prappai, P. Kanjanasirirat, Y. Pewkliang, S. Borwornpinyo and P. Kongsaree, *Spectrochim. Acta, Part A*, 2018, **195**, 136–141.
- 36 M. Taki, K. Akaoka, K. Mitsui and Y. Yamamoto, *Org. Biomol. Chem.*, 2014, **12**, 4999–5005.
- 37 M. Kamiya, D. Asanuma, E. Kuranaga, A. Takeishi, M. Sakabe, M. Miura, T. Nagano and Y. Urano, *J. Am. Chem. Soc.*, 2011, **133**, 12960–12963.
- 38 S. Kamino, H. Ichikawa, S. I. Wada, Y. Horio, Y. Usami, T. Yamaguchi, T. Koda, A. Harada, K. Shimanuki, M. Arimoto, M. Doi and Y. Fujita, *Bioorg. Med. Chem. Lett.*, 2008, **18**, 4380–4384.
- 39 X. Jiao, C. Liu, K. Huang, S. Zhang, S. He, L. Zhao and X. Zeng, *Org. Biomol. Chem.*, 2015, **13**, 6647–6653.
- 40 W. Dong, H. Wen, X. F. Yang and H. Li, *Dyes Pigm.*, 2013, **96**, 653–658.
- 41 M. Niwa, T. Hirayama, K. Okuda and H. Nagasawa, *Org. Biomol. Chem.*, 2014, **12**, 6590–6597.
- 42 E. M. Poronik, M. P. Shandura and Y. P. Kovtun, *Chem. Heterocycl. Compd.*, 2005, **41**, 546–547.
- 43 Y. M. Poronik, M. P. Shandura and Y. P. Kovtun, *Dyes Pigm.*, 2007, **72**, 199–207.
- 44 W. Xuan, Y. Cao, J. Zhou and W. Wang, *Chem. Commun.*, 2013, **49**, 10474–10476.
- 45 B. C. Dickinson, Y. Tang, Z. Chang and C. J. Chang, *Chem. Biol.*, 2011, **18**, 943–948.
- 46 S. J. Lippard and S. Hilderbrand, US2003068275(A1), 2003.
- 47 S. J. Lippard and S. Burdette, US2003008405A1, 2003.
- 48 K. Huang, L. Yu, P. Xu, X. Zhang and W. Zeng, *RSC Adv.*, 2015, **5**, 17797–17801.
- 49 K. Huang, M. Liu, X. Wang, D. Cao, F. Gao, K. Zhou, W. Wang and W. Zeng, *Tetrahedron Lett.*, 2015, **56**, 3769–3773.
- 50 K. Huang, M. Liu, Z. Liu, D. Cao, J. Hou and W. Zeng, *Dyes Pigm.*, 2015, **118**, 88–94.
- 51 M. A. Clark, S. A. Hilderbrand and S. J. Lippard, *Tetrahedron Lett.*, 2004, **45**, 7129–7131.
- 52 M. A. Clark, K. Duffy, J. Tibrewala and S. J. Lippard, *Org. Lett.*, 2003, **5**, 2051–2054.
- 53 W. Chen, S. Xu, J. J. Day, D. Wang and M. Xian, *Angew. Chem., Int. Ed.*, 2017, **56**, 16611–16615.
- 54 S. C. Burdette and S. J. Lippard, *Inorg. Chem.*, 2002, **41**, 6816–6823.
- 55 S. J. Lippard and C. C. Woodrooffe, US2004224420A1, 2004.
- 56 X. Zhu, M. Xiong, H. Liu, G. Mao, L. Zhou, J. Zhang, X. Hu, X.-B. Zhang and W. Tan, *Chem. Commun.*, 2016, **52**, 733–736.
- 57 E. Tomat and S. J. Lippard, *Inorg. Chem.*, 2010, **49**, 9113–9115.
- 58 T.-B. Ren, W. Xu, W. Zhang, X.-X. Zhang, Z.-Y. Wang, Z. Xiang, L. Yuan and X.-B. Zhang, *J. Am. Chem. Soc.*, 2018, **140**, 7716–7722.
- 59 M. Ren, B. Deng, K. Zhou, J. Y. Wang, X. Kong and W. Lin, *J. Mater. Chem. B*, 2017, **5**, 1954–1961.

- 60 X. Lv, J. Liu, Y. Liu, Y. Zhao, M. Chen, P. Wang and W. Guo, *Sens. Actuators, B*, 2011, **158**, 405–410.
- 61 A. Chevalier, P. Y. Renard and A. Romieu, *Chem. – Eur. J.*, 2014, **20**, 8330–8337.
- 62 A. Chevalier, K. Renault, F. Boschetti, P. Y. Renard and A. Romieu, *Eur. J. Org. Chem.*, 2015, 152–165.
- 63 S. Orenga, V. Chalansonnet, A. Chevalier, P.-Y. Renard, A. Romieu and B. Roubinet, US2016146814A1, 2016.
- 64 J. Li and S. Q. Yao, *Org. Lett.*, 2009, **11**, 405–408.
- 65 S. C. Dodani, A. Firl, J. Chan, C. I. Nam, A. T. Aron, C. S. Onak, K. M. Ramos-Torres, J. Paek, C. M. Webster, M. B. Feller and C. J. Chang, *Proc. Natl. Acad. Sci. U. S. A.*, 2014, **111**, 16280–16285.
- 66 D. K. Sharma, S. T. Adams, K. L. Liebmann, A. Choi and S. C. Miller, *Org. Lett.*, 2019, **21**, 1641–1644.
- 67 S. Jia, K. M. Ramos-Torres, S. Kolemen, C. M. Ackerman and C. J. Chang, *ACS Chem. Biol.*, 2018, **13**, 1844–1852.
- 68 T. Peng and D. Yang, *Org. Lett.*, 2010, **12**, 496–499.
- 69 R. U. Kulkarni, D. J. Kramer, N. Pourmandi, K. Karbasi, H. S. Bateup and E. W. Miller, *Proc. Natl. Acad. Sci. U. S. A.*, 2017, **114**, 2813–2818.
- 70 T. Peng and D. Yang, *Org. Lett.*, 2010, **12**, 4932–4935.
- 71 K. Kawai, N. Ieda, K. Aizawa, T. Suzuki, N. Miyata and H. Nakagawa, *J. Am. Chem. Soc.*, 2013, **135**, 12690–12696.
- 72 T. Peng, N.-K. Wong, X. Chen, Y.-K. Chan, D. H.-H. Ho, Z. Sun, J. J. Hu, J. Shen, H. El-Nezami and D. Yang, *J. Am. Chem. Soc.*, 2014, **136**, 11728–11734.
- 73 A. A. Contractor and E. W. Miller, *Biochemistry*, 2018, **57**, 237–240.
- 74 D. Yang and T. Peng, US2009253143(A1), 2009.
- 75 B. F. Dutter, A. Ender, G. A. Sulikowski and C. D. Weaver, *Org. Biomol. Chem.*, 2018, **16**, 5575–5579.
- 76 J. M. Meinig, L. Fu and B. R. Peterson, *Angew. Chem., Int. Ed.*, 2015, **54**, 9696–9699.
- 77 J. E. Whitaker, R. P. Haugland and F. G. Prendergast, *Anal. Biochem.*, 1991, **194**, 330–344.
- 78 Y. Fu, M. M. Collinson and D. A. Higgins, *J. Am. Chem. Soc.*, 2004, **126**, 13838–13844.
- 79 E. Nakata, Y. Yukimachi, Y. Nazumi, Y. Uto, H. Maezawa, T. Hashimoto, Y. Okamoto and H. Hori, *Chem. Commun.*, 2010, **46**, 3526–3528.
- 80 J. Liu, Z. Diwu and W.-Y. Leung, *Bioorg. Med. Chem. Lett.*, 2001, **11**, 2903–2905.
- 81 S. A. Hilderbrand and R. Weissleder, *Tetrahedron Lett.*, 2007, **48**, 4383–4385.
- 82 C. Richter, N. P. Ernesting and R. Mahrwald, *Synthesis*, 2016, 1217–1225.
- 83 Y. Liu, K. Xiang, B. Tian and J. Zhang, *Luminescence*, 2017, **32**, 78–85.
- 84 L. Wang, C. W. Barth, M. Sibrian-Vazquez, J. O. Escobedo, M. Lowry, J. Muschler, H. Li, S. L. Gibbs and R. M. Strongin, *ACS Omega*, 2017, **2**, 154–163.
- 85 L. G. Wang, I. Munhenzva, M. Sibrian-Vazquez, J. O. Escobedo, C. H. Kitts, F. R. Fronczek and R. M. Strongin, *J. Org. Chem.*, 2019, **84**, 2585–2595.
- 86 K. Huang, X. Jiao, C. Liu, Q. Wang, X. Qiu, S. He, L. Zhao and X. Zeng, *Dyes Pigm.*, 2017, **145**, 561–569.
- 87 A. Yamagami, K. Kawano, S. Futaki, K. Kuramochi and K. Tsubaki, *Tetrahedron*, 2017, **73**, 7061–7066.
- 88 A. Yamagami, H. Ishimura, A. Katori, K. Kuramochi and K. Tsubaki, *Org. Biomol. Chem.*, 2016, **14**, 10963–10972.
- 89 T. Nagano, K. Hanaoka, T. Egawa, Y. Kushida, K. Numasawa, T. Myochin and W. Piao, EP2942352(A1), 2015.
- 90 A. Roth, H. Li, C. Anorma and J. Chan, *J. Am. Chem. Soc.*, 2015, **137**, 10890–10893.
- 91 J. B. Grimm, B. P. English, J. Chen, J. P. Slaughter, Z. Zhang, A. Revyakin, R. Patel, J. J. Macklin, D. Normanno, R. H. Singer, T. Lionnet and L. D. Lavis, *Nat. Methods*, 2015, **12**, 244–250.
- 92 J. B. Grimm, A. K. Muthusamy, Y. Liang, T. A. Brown, W. C. Lemon, R. Patel, R. Lu, J. J. Macklin, P. J. Keller, N. Ji and L. D. Lavis, *Nat. Methods*, 2017, **14**, 987–994.
- 93 M. V. Sednev, C. A. Wurm, V. N. Belov and S. W. Hell, *Bioconjugate Chem.*, 2013, **24**, 690–700.
- 94 M. Grzybowski, M. Taki and S. Yamaguchi, *Chem. – Eur. J.*, 2017, **23**, 13028–13032.
- 95 Y. Ichikawa, M. Kamiya, F. Obata, M. Miura, T. Terai, T. Komatsu, T. Ueno, K. Hanaoka, T. Nagano and Y. Urano, *Angew. Chem., Int. Ed.*, 2014, **53**, 6772–6775.
- 96 M. R. Detty, P. N. Prasad, D. J. Donnelly, T. Ohulchanskyy, S. L. Gibson and R. Hilf, *Bioorg. Med. Chem.*, 2004, **12**, 2537–2544.
- 97 D. J. Del Valle, D. J. Donnelly, J. J. Holt and M. R. Detty, *Organometallics*, 2005, **24**, 3807–3810.
- 98 S. Dähne, *Chimia*, 1991, **45**, 288–296.
- 99 H. Moustroph, J. Mistol, B. Senns, D. Keil, M. Findeisen and L. Hennig, *Angew. Chem., Int. Ed.*, 2009, **48**, 8773–8775.
- 100 Y. M. Poronik, G. Clermont, M. Blanchard-Desce and D. T. Gryko, *J. Org. Chem.*, 2013, **78**, 11721–11732.
- 101 M. J. S. Dewar, *J. Chem. Soc.*, 1950, 2329–2334.
- 102 J. Fabian and H. Hartmann, in *Reactivity and Structure Concepts in Organic Chemistry*, ed. K. Hafner, C. W. Rees, B. M. Trost, L.-M. Lehn, P. von Rague Schleyer and R. Zahnradnik, Springer-Verlag, Berlin Heidelberg New York, 1980, vol. 12, pp. 162–197.
- 103 H. Ito, Y. Kawamata, M. Kamiya, K. Tsuda-Sakurai, S. Tanaka, T. Ueno, T. Komatsu, K. Hanaoka, S. Okabe, M. Miura and Y. Urano, *Angew. Chem., Int. Ed.*, 2018, **57**, 15702–15706.
- 104 C. J. Chang, T. F. Brewer and J. Chan, WO2017034927A1, 2017.
- 105 D. Yang, P. Peng, J. Shen and X. Chen, WO2013113279(A1), 2013.
- 106 Y. Koide, Y. Urano, K. Hanaoka, T. Terai and T. Nagano, *ACS Chem. Biol.*, 2011, **6**, 600–608.
- 107 R. Emanuelsson, A. Wallner, E. A. M. Ng, J. R. Smith, D. Nauroozi, S. Ott and H. Ottosson, *Angew. Chem., Int. Ed.*, 2013, **52**, 983–987.
- 108 S. Yamaguchi, M. Taki and M. G. Grzybowski, WO2018181529A1, Nat. Univ. Corp. Nagoya Univ., 2018.
- 109 Y. M. Poronik, T. Bernaś, A. Wrzosek, M. Banasiewicz, A. Szweczyk and D. T. Gryko, *Asian J. Org. Chem.*, 2018, **7**, 411–415.
- 110 S. van de Linde, M. Heilemann and M. Sauer, *Annu. Rev. Phys. Chem.*, 2012, **63**, 519–540.

- 111 L. D. Lavis and R. T. Raines, *ACS Chem. Biol.*, 2014, **9**, 855–866.
- 112 L. D. Lavis, *Biochemistry*, 2017, **56**, 5165–5170.
- 113 K. Tiensomjit, R. Noorat, K. Wechakorn, S. Prabpai and K. Suksen, *Spectrochim. Acta, Part A*, 2017, **185**, 228–233.
- 114 W. Ming, J. Feng, S. Chang, K. Xiang, Z. Liu, B. Tian and J. Zhang, *Res. Chem. Intermed.*, 2017, **43**, 7387–7398.
- 115 J. Zhang, X. Y. Zhu, X. X. Hu, H. W. Liu, J. Li, L. L. Feng, X. Yin, X. B. Zhang and W. Tan, *Anal. Chem.*, 2016, **88**, 11892–11899.
- 116 X. Wang, S. Wang, K. Huang, Z. Liu, Y. Gao and W. Zeng, *Sens. Actuators, B*, 2017, **241**, 1188–1193.
- 117 Y. Ji, F. Dai and B. Zhou, *Talanta*, 2019, **197**, 631–637.
- 118 H. Wen, Q. Huang, X. F. Yang and H. Li, *Chem. Commun.*, 2013, **49**, 4956–4958.
- 119 Q. Wang, L. Zhou, L. Qiu, D. Lu, Y. Wu and X.-B. Zhang, *Analyst*, 2015, **140**, 5563–5569.
- 120 H. Wang, J. Guan, X. Han, S.-W. Chen, T. Li, Y. Zhang, M.-S. Yuan and J. Wang, *Talanta*, 2018, **189**, 39–44.
- 121 Y. Zhou, X. Zhang, S. Yang, Y. Li, Z. Qing, J. Zheng, J. Li and R. Yang, *Anal. Chem.*, 2017, **89**, 4587–4594.
- 122 Y. Zhou, K. N. Bobba, X. W. Lv, D. Yang, N. Velusamy, J. F. Zhang and S. Bhuniya, *Analyst*, 2017, **142**, 345–350.
- 123 C. R. Woodford, E. P. Frady, R. S. Smith, B. Morey, G. Canzi, S. F. Palida, R. C. Araneda, W. B. Kristan, C. P. Kubiak, E. W. Miller and R. Y. Tsien, *J. Am. Chem. Soc.*, 2015, **137**, 1817–1824.
- 124 L. Krishnamoorthy, J. A. Cotruvo, J. Chan, H. Kaluarachchi, A. Muchenditsi, V. S. Pendyala, S. Jia, A. T. Aron, C. M. Ackerman, M. N. V. Wal, T. Guan, L. P. Smaga, S. L. Farhi, E. J. New, S. Lutsenko and C. J. Chang, *Nat. Chem. Biol.*, 2016, **12**, 586–592.
- 125 D. C. Weaver, US9103791(B1), 2013.
- 126 A. Manna, D. Sarkar, S. Goswami, C. K. Quah and H. K. Fun, *RSC Adv.*, 2016, **6**, 57417–57423.
- 127 L. Li, S. Wang, H. Lan, G. Gong, Y. Zhu, Y. C. Tse and K. M. C. Wong, *ChemistryOpen*, 2018, **7**, 136–143.
- 128 K. Huang, X. Jiao, C. Liu, Q. Wang, X. Qiu, D. Zheng, S. He, L. Zhao and X. Zeng, *Dyes Pigm.*, 2017, **142**, 437–446.
- 129 Y. R. Zhang, Q. R. Wang, P. Su, F. Zhao, J. Huang and B. X. Zhao, *RSC Adv.*, 2015, **5**, 20634–20638.
- 130 H. G. Im, H. Y. Kim and S. K. Chang, *Sens. Actuators, B*, 2014, **191**, 854–859.
- 131 Q. Duan, M. Zhang, C. Sheng, C. Liu, L. Wu, Z. Ma, Q. Zhao, Z. Wang and B. Zhu, *Anal. Sci.*, 2017, **33**, 1169–1173.
- 132 S. Chen, W. Wang, M. Yan, Q. Tu, S. W. Chen, T. Li, M. Sen Yuan and J. Wang, *Sens. Actuators, B*, 2018, **255**, 2086–2094.
- 133 X. F. Yang, Q. Huang, Y. Zhong, Z. Li, H. Li, M. Lowry, J. O. Escobedo and R. M. Strongin, *Chem. Sci.*, 2014, **5**, 2177–2183.
- 134 K. Wechakorn, S. Prabpai, K. Suksen, P. Piyachaturawat and P. Kongsaree, *RSC Adv.*, 2016, **6**, 24752–24755.
- 135 E.-J. Kim, A. Podder, M. Maiti, J. M. Lee, B. G. Chung and S. Bhuniya, *Sens. Actuators, B*, 2018, **274**, 194–200.
- 136 D. Asanuma, M. Sakabe, M. Kamiya, K. Yamamoto, J. Hiratake, M. Ogawa, N. Kosaka, P. L. Choyke, T. Nagano, H. Kobayashi and Y. Urano, *Nat. Commun.*, 2015, **6**, 6463.
- 137 T. Doura, M. Kamiya, F. Obata, Y. Yamaguchi, T. Y. Hiyama, T. Matsuda, A. Fukamizu, M. Noda, M. Miura and Y. Urano, *Angew. Chem., Int. Ed.*, 2016, **55**, 9620–9624.
- 138 S. Chen, X. Zhao, J. Chen, J. Chen, L. Kuznetsova, S. S. Wong and I. Ojima, *Bioconjugate Chem.*, 2010, **21**, 979–987.
- 139 R. H. Mathijssen, R. J. van Alphen, J. Verweij, W. J. Loos, K. Nooter, G. Stoter and A. Sparreboom, *Clin. Cancer Res.*, 2001, **7**, 2182–2194.
- 140 S. Bhuniya, S. Maiti, E. J. Kim, H. Lee, J. L. Sessler, K. S. Hong and J. S. Kim, *Angew. Chem., Int. Ed.*, 2014, **53**, 4469–4474.
- 141 M. H. Lee, J. L. Sessler and J. S. Kim, *Acc. Chem. Res.*, 2015, **48**, 2935–2946.
- 142 D. Dutta, S. M. Alex, K. N. Bobba, K. K. Maiti and S. Bhuniya, *ACS Appl. Mater. Interfaces*, 2016, **8**, 33430–33438.
- 143 Y. Yuan, C.-J. Zhang, S. Xu and B. Liu, *Chem. Sci.*, 2016, **7**, 1862–1866.
- 144 H. Komatsu, H. Harada, K. Tanabe, M. Hiraoka and S. Nishimoto, *MedChemComm*, 2010, **1**, 50–53.
- 145 Q. Zhang, N. Zhang, Y.-T. Long, X. Qian and Y. Yang, *Bioconjugate Chem.*, 2016, **27**, 341–353.
- 146 Y. Zhang, L. Ma, C. Tang, S. Pan, D. Shi, S. Wang, M. Li, Y. Guo and J. Li, *J. Mater. Chem. B*, 2018, **6**, 725–731.
- 147 Y. Guo and S. Pan, CN107286173 A, Northwest Univ., 2017.
- 148 E. A. Halabi, Z. Thiel, N. Trapp, D. Pinotsi and P. Rivera-Fuentes, *J. Am. Chem. Soc.*, 2017, **139**, 13200–13207.


 Cite this: *Chem. Commun.*, 2021, 57, 7782

 Received 21st May 2021,
Accepted 6th July 2021

DOI: 10.1039/d1cc02687a

rsc.li/chemcomm

Red emissive sulfone-rhodols as mitochondrial imaging agents†

 Kateryna V. Vygranenko,^a Yevgen M. Poronik,^a Antoni Wrzosek,^b Adam Szewczyk*^b and Daniel T. Gryko *^a

The controlled hydrolysis of sulfone-rhodamines affords a series of core-modified red-emitting rhodols, the fluorescence of which is sensitive to solvent polarity with pronounced bathochromic shifts recorded in both DMSO and CH₃CN combined with an up to 8-fold increase in the fluorescence quantum yield.

The iconic fluorescent dyes fluorescein and rhodamine, were first reported by Baeyer and Ceresole in 1871 and 1888, respectively.^{1,2} These discoveries were the harbingers of modern fluorophore chemistry, which rapidly spread in the following years.^{3–10} One of the lesser known cousins of these two dyes is rhodol.¹¹ This dye, a structural hybrid of rhodamine and fluorescein, inherited their photophysical properties in terms of large extinction coefficient, high fluorescence quantum yield and solubility in a majority of solvents. Unlike rhodamines and fluoresceins, however, rhodols belong to merocyanines that contain a polymethine chain and two terminal heteroatoms in their chromophore. Numerous analogues of rhodol have been reported during last decade.^{12–17} More importantly they have been selected for several key applications such as fluorescent reporters in biological imaging, membrane potential sensors in cells and organelles, and photosensitizers in antitumor therapy.^{18–21} Over the years the motivation to shift both absorption and emission bathochromically to the red and NIR regions has increased in parallel with the importance of fluorescence imaging in cell biology.^{22–26} Along these lines, very recently the synthesis of a plethora of new fluorophores including sulfone-rhodamines, which exhibit both absorption and emission maxima in the near-infrared region, have been reported.²⁷ We reasoned that if the rhodamine scaffold is replaced by a rhodol, the resulting and

heretofore unknown sulfone-rhodols could possess attractive photophysical properties. Here we focus on realization of this vision.

The stepwise synthesis of sulfone-rhodols from benzene-based building blocks would be a long adventure. In an attempt to overcome this, we hypothesized that rhodamines possessing an endocyclic strong electron-withdrawing group may undergo basic hydrolysis to produce the corresponding sulfone-rhodols, in a similar manner to that observed for P-rhodamines.²⁸ Taking this into consideration, we have designed the following strategy: synthesis of 9-aryl substituted sulfone-rhodamines followed by conversion into the corresponding rhodols upon basic hydrolysis.

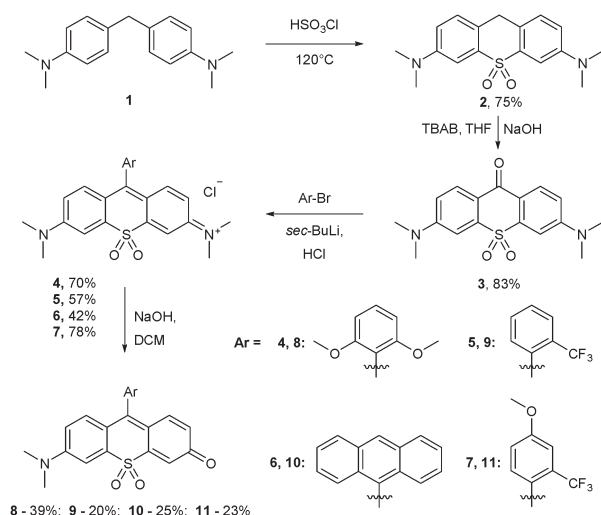
The design of a specific pattern of substituents on SO₂-rhodols is a very important issue, as relatively small structural changes can have a pivotal effect on photophysical properties. The aryl moiety plays a substantial role in rhodamines, fluoresceins and rhodols, governing some of their chemical and photophysical properties.^{29,30} Although, it is located orthogonally to the xanthenes scaffold and is not a part of the chromophore, it still decreases the sensitivity of the fluorophore's π-conjugation system to nucleophiles. Nucleophilic addition to the C9-position of unsubstituted rhodols results in discoloration of the dye due to interruption of the conjugation chain. Moreover, the size of the *ortho*-substituent also plays a crucial role in the stability of the chromophore towards nucleophilic attack. Consequently, P=O-rhodols possessing an *ortho*-tolyl group at the *meso*-position undergo slow discoloration under basic conditions because of the nucleophilic attack of the hydroxyl anion at the C9-position, while bulkier *ortho*-substituents, like CF₃ or OMe, prevent disruption of the chromophore's π-conjugation system.²⁶ For both rhodamines and fluoresceins, substituents at the *ortho*-position prevent the rotation of aryl groups, thus minimizing radiationless deactivation of the excited state and increasing the fluorescence efficiency. For the outlined reasons we decided to exclusively use sterically hindered substituents at the C9-position in this study.

^a Institute of Organic Chemistry, Polish Academy of Sciences, Kasprzaka 44/52, 01-224 Warsaw, Poland. E-mail: dtgryko@icho.edu.pl

^b Nencki Institute of Experimental Biology, Polish Academy of Sciences, Pasteura 3, 02-093 Warsaw, Poland. E-mail: a.szewczyk@nencki.edu.pl

† Electronic supplementary information (ESI) available: Experimental description, copies of ¹H and ¹³C NMR spectra as well as crystallographic details. CCDC 2084645. For ESI and crystallographic data in CIF or other electronic format see DOI: 10.1039/d1cc02687a

Communication

Scheme 1 The synthesis of sulfone-rhodols **8–11**.

We followed the method developed by Guo's group to obtain the necessary sulfone-rhodamines (Scheme 1). Adaptations such as employing the more available chlorosulfonic acid instead of oleum in the first step and using a NaOH–TBAB mixture in THF in the second, allowed us to increase the yields.

Sulfone-rhodols were synthesized in four steps from **4**, 4'-methylene-bis(*N,N*-dimethylaniline) (**1**) by: treatment of **1** with chlorosulfonic acid, followed by oxidation with NaOH in the presence of TBAB to produce sulfone-bridged bis(*N,N*-dimethylamino)-xanthone **3**.

Subsequently, ketone **3** was transformed into the corresponding rhodamines **4–7** utilizing a nucleophilic addition of lithiated aryl derivatives. The synthesis of rhodols **8–11** with an endocyclic sulfone group was performed *via* the hydrolytic deamination of the corresponding rhodamines **4–7** in an aqueous sodium hydroxide solution. Rhodol **11** was next subjected to demethylation conditions, followed by the alkylation of the

formed OH group with 1,6-dibromohexane to obtain fluorophore **13** (Scheme 2). Unexpectedly, the final step of the reaction was revealed to be very capricious towards the conditions. The condensation demands approximately 10 equivalents of triphenylphosphine, a high temperature, an inert atmosphere, a very short reaction time and a small amount of solvent. Prolonging the reaction time leads only to decomposition of both substrate and product.

As the sulfone-rhodol chromophore possesses the polarizable structure it gives rise to a strong solvatochromism. Indeed, in nonpolar toluene sulfone-rhodols exhibit broad absorption bands at around 540–550 nm (Fig. S2–S6, ESI[†]).

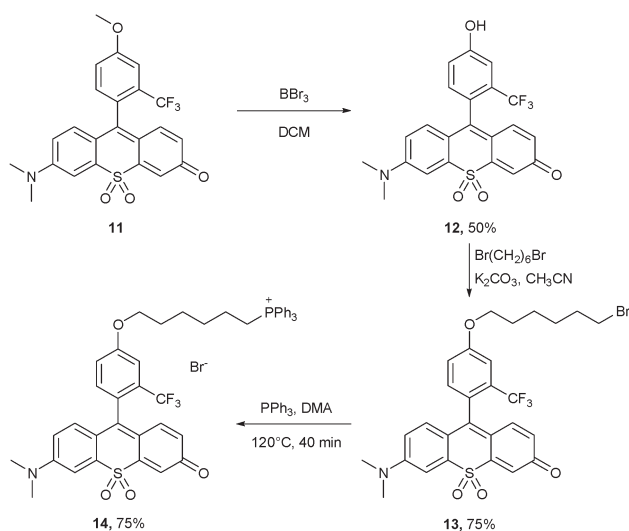
Compounds **8–11** exhibit a red-shift with the polarity increase and in the most polar DMSO–water mixtures exhibit the strongest red-shift with resolved cyanine-like absorption bands (Table 1 and Fig. 1). As the absorption bands narrow with the solvent polarity growth, SO₂-rhodols exhibit a decrease in the Stokes shifts on going from a toluene to a DMSO–water mixture. In non-polar toluene the fluorescence efficiency is weak as the rhodol chromophore possesses a mainly polyene character.³¹

The increase of media polarity makes the chromophore electronic structure closer to the cyanine limit³² that leads to

Table 1 Photophysical data of rhodols **8–12** and **14** measured in solution

Dye	Solvent	$\lambda_{\text{abs}}^{\text{max}}$ [nm] ($\epsilon \times 10^{-3}$) [M ⁻¹ cm ⁻¹]	$\lambda_{\text{em}}^{\text{max}}$ [nm]	Φ_{f}	$\Delta\bar{\nu}$ [cm ⁻¹]
8	Toluene	543 (35)	650	0.13 ^b	3000
	CH ₂ Cl ₂	571 (34)	674	0.43 ^c	2700
	CH ₃ CN	578 (33)	691	0.52 ^c	2800
	EtOH	595 (34)	699	0.33 ^c	2500
	DMSO	599 (32)	706	0.50 ^c	2500
	H ₂ O ^a	667	719	0.06 ^c	1100
9	Toluene	550 (27)	646	0.06 ^b	2700
	CH ₂ Cl ₂	574 (27)	672	0.46 ^c	2500
	CH ₃ CN	581 (24)	695	0.50 ^c	2800
	EtOH	595 (26)	702	0.29 ^c	2600
	DMSO	603 (27)	711	0.40 ^c	2500
	H ₂ O ^a	669	721	0.04 ^c	1100
10^d	Toluene	553 (27)	651	0.07 ^b	2700
	CH ₂ Cl ₂	579 (27)	678	0.13 ^c	2500
	CH ₃ CN	582 (27)	697	0.008 ^c	2800
	EtOH	599 (26)	703	0.003 ^c	2500
	DMSO	605 (28)	710	0.01 ^c	2400
	H ₂ O ^a	669	720	0.03 ^c	1100
11	Toluene	550 (26)	641	0.07 ^b	2600
	CH ₂ Cl ₂	575 (29)	676	0.50 ^c	2600
	CH ₃ CN	581 (27)	692	0.51 ^c	2800
	EtOH	595 (28)	703	0.26 ^c	2600
	DMSO	602 (29)	708	0.41 ^c	2500
	H ₂ O ^a	669	720	0.03 ^c	1100
12	Toluene	549 (27)	645	0.07 ^b	2700
	CH ₂ Cl ₂	575 (27)	675	0.50 ^c	2600
	CH ₃ CN	580 (26)	695	0.47 ^c	2800
	EtOH	595 (27)	702	0.26 ^c	2600
	DMSO	602 (31)	712	0.44 ^c	2600
	H ₂ O ^a	669	722	0.05 ^c	1100
14	DMSO	602	707	0.39 ^c	2500
	H ₂ O ^a	668	719	0.07 ^e	1100

^a Containing 2% DMSO. ^b Reference: sulforhodamine 101 in EtOH ($\Phi_{\text{f}} = 0.95$). ^c Reference: cresyl violet in EtOH ($\Phi_{\text{f}} = 0.54$). ^d Compound **10** was not measured in H₂O due to its poor solubility. ^e Reference: oxazine 1 in EtOH ($\Phi_{\text{f}} = 0.15$).

Scheme 2 The synthesis of sulfone-rhodol **14**.

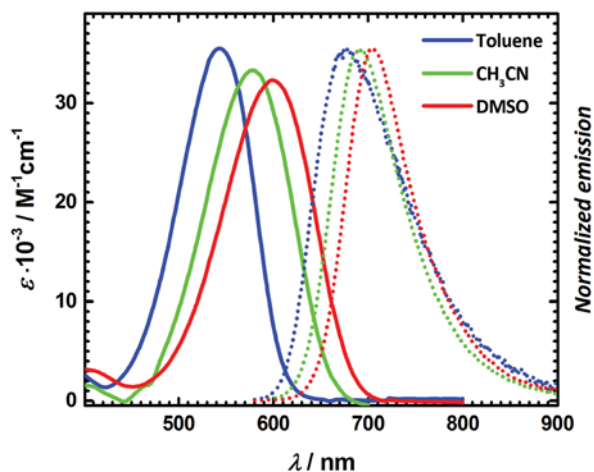


Fig. 1 Absorption (solid) and emission (dotted) spectra of compound **8** in toluene, CH₃CN and DMSO.

emission strengthening. The differences in λ_{abs} and λ_{em} within the series **8–12** is negligible confirming that aryl substituents at position 9 have no distinct influence on the photophysical properties of this type of dye. The only exception to this is a weak emission intensity in the case of **10**, which bears an anthracene-9-yl unit. In this case fluorescence is weak regardless of the solvent, which may be related to electron transfer as depicted in a ground-breaking paper by Urano and co-workers.³³ The lower Φ_f of anthracene-substituted fluoresceins and BODIPYs has been noticed by Nagano and co-workers and it was proven to be due to photoinduced electron transfer.^{34,35} Time-resolved fluorescence measurements partially prove this hypothesis as the fluorescence decay of **10** shows two-exponential profiles (Fig. S8, ESI[†]). The lifetimes were measured for two SO₂-rhodols **8** (4–5 ns) and **10** (0.3–0.4 ns) (Table S1, ESI[†]). These values correspond to $k_f \sim 1.0$ and 0.2, respectively.

Similar to other rhodols,¹¹ SO₂-rhodols are sensitive to a pH change and they turn into a protonated form in acidic media. In comparison to phospho-analogues, SO₂-rhodols are protonated at lower pH values.²⁸ The absorption spectra (Fig. S9–S12, Scheme S1, ESI[†]) clearly show a transition from a neutral SO₂-rhodol into a protonated form ($\lambda_{\text{abs}} \sim 550$ nm).

As heteroanalogues of rhodols, sulfone-rhodols show red-shifted absorption in comparison with rhodol derivatives due to the strong electron-withdrawing properties of the SO₂-bridge moiety, however, they possess lower molar extinction coefficients and show somewhat lower fluorescence responses yet larger Stokes shifts.¹¹

Similar to the previously reported phospho-analogues,²⁸ SO₂-rhodols also display positive solvatochromism, though they exhibit more red-shifted absorption and emission maxima (approx. 20 nm). Sulfone-rhodols tend to have comparable molar extinction coefficients to those of phosphorous analogues and somewhat lower fluorescence quantum yields. On the other hand, SO₂-rhodols demonstrate larger Stokes shifts compared with those of P-rhodols (Fig. 2).²⁸

The photostability of SO₂-rhodols was measured and compared with commercially available rhodamine 6G, cresyl violet

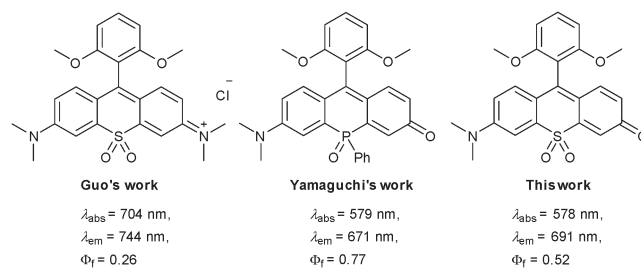


Fig. 2 Comparison of the photophysical properties of SO₂-rhodols with SO₂-rhodamines and P-rhodols measured in CH₃CN.

as well as with one of the diketopyrrolopyrroles (Fig. S14, ESI[†]). It turned out that sulfone-rhodols **8** and **10** have a comparable stability to rhodamine 6G whereas their analogs that possess less sterically hindered substituents display lower stability albeit still better than the DPPs. A comparative stability study performed in H₂O has revealed that the photostability of **8** and **12** is the same regardless of whether the pH is 1 or 7 whereas in the case of dyes **9** and **11** the stability at pH = 1 is very poor (Fig. S15, ESI[†]).

Both lipophilic triphenylphosphonium (TPP⁺) moieties^{36–39} and quaternary ammonium salts^{40–42} have been found to promote selective mitochondrial localization for fluorescent probes. With the goal of proving the usefulness of these new dyes, we performed studies on the localization of SO₂-rhodol **14** in cells. Fluorescence microscopy experiments showed the subcellular distribution of dye **14** in the cardiac H9C2 cell line.⁴³ Incubation with rhodol **14** produces a staining pattern corresponding to dye localization in the mitochondria, after only a short incubation loading time (15–30 min) (Fig. 3). The staining of mitochondria was confirmed by the co-localization with MitoTracker Green. As rhodol **14** is sensitive to the mitochondrial membrane potential, it accumulates in the mitochondrial matrix after incubation of the H9C2 cells at very

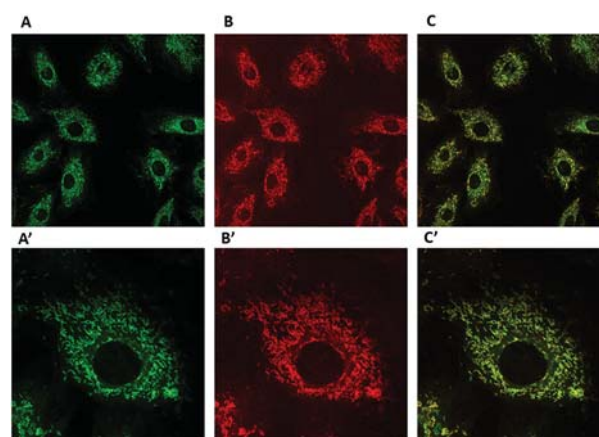


Fig. 3 Mitochondrial localization of dye **14** as detected using confocal fluorescence microscopy. (A and A') The fluorescence of MitoTracker[™] Green, (B and B') the fluorescence of **14** (red) ($\lambda_{\text{ex}} = 559$ nm) and emission range 610–750 nm, (C and C') overlay images recorded simultaneously for two fluorophores in a living H9C2 cell line. A', B' and C' are images of single cells chosen from the images above in a larger field of view.

low concentrations (150–500 nM). In the test experiment, staining of the cells was performed using dye **13** (Fig. S13, ESI†). Although dye **13** is cell-permeable it has an unlocalized distribution inside the H9C2 cells. In order to determine the cell viability under the influence of the sulfonrhodols **13** and **14**, an annexin V-based apoptosis and necrosis test was performed, revealing that these dyes are non-toxic within the concentrations applied during fluorescence imaging (Fig. S17, ESI†).

As a result of efforts to develop more stable merocyanine dyes, a synthesis for SO₂-rhodols was discovered. The presence of both the rhodol skeleton, electron-withdrawing SO₂ group and sterically hindered substituents at position 9 enhances their stability. The novel dyes bearing sterically hindered aryl substituents showed excellent photostability and after 1.5 hours exposure only 9% of the dye had degraded compared to 80% of *N,N*-dialkyldiketopyrrolopyrrole. Equipping SO₂-rhodols with a phosphonium moiety increases their sensitivity towards the mitochondrial membrane potential that allows selective penetration and accumulation in the mitochondrial matrix. This allows for well-resolved fluorescent imaging at nanomolar dye concentrations.

Conceptualization and investigation: K. V. V., Y. M. P., A. W.; supervision: D. T. G., A. S.; visualization: K. V. V., Y. M. P., A. W.; writing – original draft: K. V. V., Y. M. P., A. W., D. T. G.; writing – review and editing: D. T. G., A. S.

This work was financially supported by the Foundation for Polish Science (TEAM POIR.04.04.00-00-3CF4/16-00).

Conflicts of interest

There are no conflicts to declare.

Notes and references

- 1 A. Baeyer, *Berichte der Dtsch. Chem. Gesellschaft*, 1871, **4**, 555–558.
- 2 M. Ceresole, US377349A, 1888.
- 3 L. Cassar and A. Iqbal, EP0061426A1, 1982.
- 4 J. T. Hewitt, *Dyestuffs Derived From Pyridine, Quinoline, Acridine And Xanthene*, Longmans, Green and Co, London, 1922.
- 5 V. Prelog, L. Ruzicka and O. Metzler, *Helv. Chim. Acta*, 1947, **30**, 1883–1895.
- 6 S. Hünig, H. Schwegler and H. Schwarz, *Justus Liebigs Ann. Chem.*, 1954, **587**, 132–145.
- 7 R. Raue, H. Harnisch and K. H. Drexhage, *Dyestuff Lasers and Light Collectors—Two New Fields of Application for Fluorescent Heterocyclic Compounds*, 1984, vol. 21.
- 8 M. Q. Doja, *Chem. Rev.*, 1932, **11**, 273–321.
- 9 T. Koide, S. Iwamori, S. Koga, Y. Suzuki, J. Kawamata and Y. Hisaeda, *Dyes Pigm.*, 2020, **183**, 108667.
- 10 R. U. Kulkarni, M. Vandenberghe, M. Thunemann, F. James, O. A. Andreassen, S. Djurovic, A. Devor and E. W. Miller, *ACS Cent. Sci.*, 2018, **4**, 1371–1378.
- 11 Y. M. Poronik, K. V. Vygranenko, D. Gryko and D. T. Gryko, *Chem. Soc. Rev.*, 2019, **48**, 5242–5265.
- 12 R. R. Sauers, S. N. Husain, A. P. Piechowski and G. R. Bird, *Dyes Pigm.*, 1987, **8**, 35–53.
- 13 N. Ghatak and S. Dutt, *J. Indian Chem. Soc.*, 1929, **6**, 465–471.
- 14 J. E. Whitaker, R. P. Haugland, D. Ryan, P. C. Hewitt, R. P. Haugland and F. G. Prendergast, *Anal. Biochem.*, 1992, **207**, 267–279.
- 15 P. R. Hammond, *J. Photochem.*, 1979, **10**, 467–471.
- 16 L. G. Lee, G. M. Berry and C.-H. Chen, *Cytometry*, 1989, **10**, 151–164.
- 17 V. Z. Shirinian and A. A. Shimkin, *Heterocyclic Polymethine Dyes*, Springer Berlin Heidelberg, 2008, pp. 75–105.
- 18 R. U. Kulkarni, D. J. Kramer, N. Pourmandi, K. Karbasi, H. S. Bateup and E. W. Miller, *Proc. Natl. Acad. Sci. U. S. A.*, 2017, **114**, 2813–2818.
- 19 A. A. Contractor and E. W. Miller, *Biochemistry*, 2018, **57**, 237–240.
- 20 E.-J. Kim, A. Podder, M. Maiti, J. M. Lee, B. G. Chung and S. Bhuniya, *Sens. Actuators, B*, 2018, **274**, 194–200.
- 21 M. Kamiya, D. Asanuma, E. Kuranaga, A. Takeishi, M. Sakabe, M. Miura, T. Nagano and Y. Urano, *J. Am. Chem. Soc.*, 2011, **133**, 12960–12963.
- 22 L. Wang, W. Du, Z. Hu, K. Uvdal, L. Li and W. Huang, *Angew. Chem., Int. Ed.*, 2019, **58**, 14026–14043.
- 23 X. Lian, M. Y. Wei and Q. Ma, *Front. Bioeng. Biotechnol.*, 2019, **7**, 386.
- 24 C. Chen, R. Tian, Y. Zeng, C. Chu and G. Liu, *Bioconjugate Chem.*, 2020, **31**, 276–292.
- 25 Y. J. Gong, X. B. Zhang, G. J. Mao, L. Su, H. M. Meng, W. Tan, S. Feng and G. Zhang, *Chem. Sci.*, 2016, **7**, 2275–2285.
- 26 P. Xing, Y. Niu, R. Mu, Z. Wang, D. Xie, H. Li, L. Dong and C. Wang, *Nat. Commun.*, 2020, **11**, 1–9.
- 27 J. Liu, Y. Q. Sun, H. Zhang, H. Shi, Y. Shi and W. Guo, *ACS Appl. Mater. Interfaces*, 2016, **8**, 22953–22962.
- 28 M. Grzybowski, M. Taki and S. Yamaguchi, *Chem. – Eur. J.*, 2017, **23**, 13028–13032.
- 29 S. S. Patil, K. G. Thorat, R. Mallah and N. Sekar, *J. Fluoresc.*, 2016, **26**, 2187–2197.
- 30 L. Geng, X. F. Yang, Y. Zhong, Z. Li and H. Li, *Dyes Pigm.*, 2015, **120**, 213–219.
- 31 V. Z. Shirinian and A. A. Shimkin, *Heterocycl. Polymethine Dye*, 2008, pp. 75–105.
- 32 S. Dähne, *Chimia*, 1991, **45**, 288–296.
- 33 Y. Urano, M. Kamiya, K. Kanda, T. Ueno, K. Hirose and T. Nagano, *J. Am. Chem. Soc.*, 2005, **127**, 4888–4894.
- 34 H. Sunahara, Y. Urano, H. Kojima and T. Nagano, *J. Am. Chem. Soc.*, 2007, **129**, 5597–5604.
- 35 T. Miura, Y. Urano, K. Tanaka, T. Nagano, K. Ohkubo and S. Fukuzumi, *J. Am. Chem. Soc.*, 2003, **125**, 8666–8671.
- 36 Q. Hu, M. Gao, G. Feng and B. Liu, *Angew. Chem., Int. Ed.*, 2014, **53**, 14225–14229.
- 37 Roopa, N. Kumar, V. Bhalla and M. Kumar, *Chem. Commun.*, 2015, **51**, 15614–15628.
- 38 C. W. T. Leung, Y. Hong, S. Chen, E. Zhao, J. W. Y. Lam and B. Z. Tang, *J. Am. Chem. Soc.*, 2013, **135**, 62–65.
- 39 H. Ogasawara, Y. Tanaka, M. Taki and S. Yamaguchi, *Chem. Sci.*, 2021, **12**, 7902–7907.
- 40 W. Yang, P. Shan Chan, M. Shan Chan, K. Fai Li, P. Kwan Lo, N. Ki Mak, K. Wai Cheah and M. Shing Wong, *Chem. Commun.*, 2013, **49**, 3428–3430.
- 41 M. Grzybowski, E. Glodkowska-Mrowka, V. Hugues, W. Brutkowski, M. Blanchard-Desce and D. T. Gryko, *Chem. – Eur. J.*, 2015, **21**, 9101–9110.
- 42 S. Samanta, Y. He, A. Sharma, J. Kim, W. Pan, Z. Yang, J. Li, W. Yan, L. Liu, J. Qu and J. S. Kim, *Chem*, 2019, **5**, 1697–1726.
- 43 M. Laskowski, B. Augustynek, P. Bednarzyk, M. Żochowska, J. Kalisz, B. O'Rourke, A. Szewczyk and B. Kulawiak, *Int. J. Mol. Sci.*, 2019, **20**, 5323.

Supporting information

Red emissive sulfone-rhodols as mitochondrial imaging agents

Kateryna V. Vygranenko,^a Yevgen M. Poronik,^a Antoni Wrzosek,^b Adam Szewczyk,^{b*} and Daniel T. Gryko^{a*}

a. *Institute of Organic Chemistry, Polish Academy of Sciences, Kasprzaka 44/52, 01-224 Warsaw, Poland.
E-mail: dtgryko@icho.edu.pl.*

b. *Nencki Institute of Experimental Biology of Polish Academy of Sciences, Pasteura 3, 02-093 Warsaw, Poland. E-mail: a.szewczyk@nencki.gov.pl*

Table of Contents

Instrumentation and Materials	S1
Experimental Part.....	S2
¹ H, ¹⁹ F and ¹³ C NMR Spectra	S8
X-Ray structure of compound 11	S16
Absorption and emission spectra of compounds 8-12, 14	S17
Time-resolved fluorescence data.....	S20
Absorption dependence on pH.....	S21
Photostability measurements	S24
Cell culture conditions	S25
Fluorescence localization of 14 within the cells	S25

Instrumentation and Materials

All chemicals were used as received unless otherwise noted. All reported ¹H NMR spectra were collected using 500 MHz and 600 MHz spectrometers. Chemical shifts (δ ppm) were determined with TMS as the internal reference; *J* values are given in Hz. Chromatography was performed on silicagel (230-400 mesh). Preparative thin layer chromatography (TLC) was carried out using Merck PLC Silica gel 60 F₂₅₄ 1 mm plates. The mass spectra were obtained via electron ionization (EI-MS) or electrospray ionization (ESI-MS). All photophysical studies have been performed with freshly-prepared air-equilibrated solutions at room temperature (298 K).

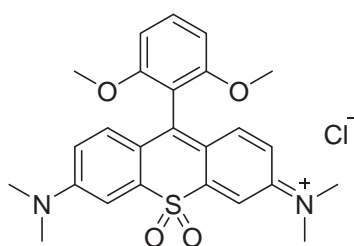
A Shimadzu UV-3600i Plus spectrophotometer and an Edinburgh Instruments Spectrofluorometer FS5 equipped with Hamamatsu R13456 PMT were used to acquire the absorption and emission spectra. Fluorescence lifetimes were measured on Fluorolog TCSPC Horiba. Spectrophotometric grade solvents were used without further purification. Fluorescence quantum yields were determined in toluene, CH₂Cl₂, CH₃CN, EtOH, DMSO and H₂O (with 2% DMSO) using cresyl violet in EtOH (for measurements in CH₂Cl₂, CH₃CN, EtOH, DMSO and H₂O) and sulforhodamine SR101 (for measurements in toluene) as standards. Photostability was determined using an Asahi Spectra Max-350 as a light source and Shimadzu UV-3600i Plus spectrophotometer. FluoroBrite™ DMEM, Foetal Bowine Serum (FBS), 0.25% Trypsin-EDTA, antibiotics (Penicillin/Streptomycin), L-Glutamine were purchased from Gibco, and DMEM High Glucose, Dulbecco's Phosphate Buffered Saline from Biowest. The MitoTracker™ Green FM was purchased from Molecular Probes.

Experimental part

General procedure for the preparation of compounds **4-7**.

To a solution of bromoarene (2.4 mmol) in 9 mL of anhydrous THF was slowly added sec-BuLi (1.4 M in cyclohexane, 1.7 mL, 2.4 mmol) at -78 °C and the resulting mixture was stirred for 2 h at the same temperature. A suspension of ketone **3** (200 mg, 0.6 mmol) in THF (25 mL) was added dropwise over 20 min. The reaction mixture was allowed to warm up to room temperature overnight. To the solution, 30 mL of 2 M HCl was added and the stirring was continued for 18 h. During this time, the color of the mixture changed from brown to deep green. The mixture was diluted with water and washed five times with Et₂O to remove unreacted xanthone and byproducts. The aqueous layer was then extracted three times with CH₂Cl₂. The combined CH₂Cl₂ layers were dried over Na₂SO₄. The drying agent was filtered off and the filtrate was evaporated. The product was recrystallized from the mixture of Et₂O/DCM/MeOH. However, the pure product was not obtained due to the fast cleavage of methyl group from diethylamino fragment.

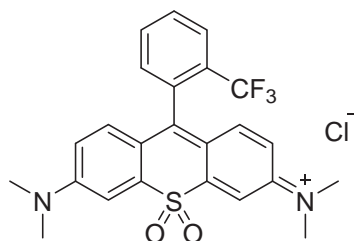
Compound **4**. Yield 70%.



4

It was not possible to get clean NMR spectra, though MS spectrum suggests product **4**. HRMS (ESI) calcd. for $C_{25}H_{27}N_2O_4S$ 451.1692 $[M]^{+}$, found 451.1696.

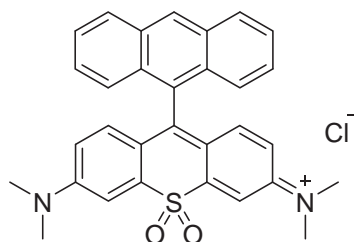
Compound **5**. Yield 57%.



5

It was not possible to get clean NMR spectra, though MS spectrum suggests product **5**. HRMS (ESI) calcd. for $C_{24}H_{22}N_2O_2F_3S$ 459.1354 $[M]^{+}$, found 459.1318.

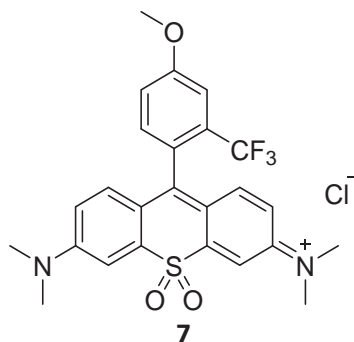
Compound **6**. Yield 42%.



6

It was not possible to get clean NMR spectra, though MS spectrum suggests product **6**. HRMS (ESI) calcd. for $C_{31}H_{27}N_2O_2S$ 491.1793 $[M]^{+}$, found 491.1793.

Compound **7**. Yield 78%.

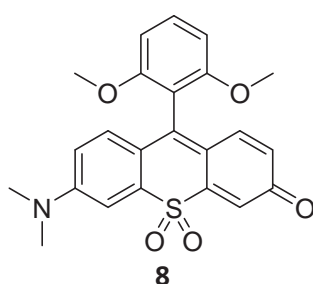


7

It was not possible to get clean NMR spectra, though MS spectrum suggests product 4d. HRMS (ESI) calcd. for $C_{25}H_{24}N_2O_3F_3S$ 489.1460 $[M]^{+}$, found 489.1460.

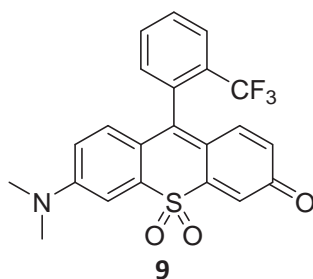
General procedure for the preparation of compounds **8-11**. To a solution of SO_2 -Rhodamine (0.040 mmol) in 50.0 mL of CH_2Cl_2 and 20.0 mL of 0.5 M NaOH aq. was added. The mixture was stirred for 1 h at room temperature, diluted with DCM, and washed four times with water. The organic layer was dried over Na_2SO_4 . The drying agent was filtered off and solvents were evaporated under reduced pressure. The product was purified using column chromatography (silica, CH_2Cl_2 : acetone 95:5). After evaporation of the solvent and drying under vacuum rhodols were obtained as violet-blue solids.

Compound **8**. Yield 25%. M.p. 224-225°C



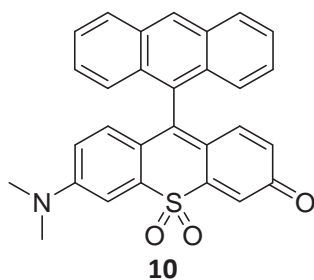
1H NMR (500 MHz, $CDCl_3$) δ : 7.45 (t, 1H, $J = 8.4$ Hz), 7.39 (d, 1H, $J = 2.7$ Hz), 7.28 (d, 1H, $J = 1.9$ Hz), 6.94 (d, 1H, $J = 9.9$ Hz), 6.92 (d, 1H, $J = 9.2$ Hz), 6.68 (d, 2H, $J = 8.4$ Hz), 6.60 (dd, 1H, $J_1 = 8.4$ Hz, $J_2 = 2.7$ Hz), 6.28 (dd, 1H, $J_1 = 9.9$ Hz, $J_2 = 1.9$ Hz), 3.69 (s, 6H), 3.14 (s, 6H); ^{13}C NMR (126 MHz, $CDCl_3$) δ : 186.9, 160.8, 154.7, 148.1 (2), 143.1, 141.3, 136.6, 134.1, 130.2, 128.5, 124.1, 122.0, 117.2, 115.0, 110.0, 106.7, 58.9, 43.1; HRMS (ESI) calc. for $C_{23}H_{21}NO_5SNa$ 446.1038 $[M + Na]^+$, found 446.1034.

Compound **9**. Yield 25%. M.p. 210-212°C



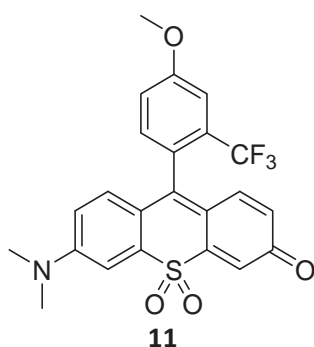
Yield 39%. 1H NMR (500 MHz, $CDCl_3$) δ : 7.89 (d, 1H, $J = 7.6$ Hz), 7.73 (t, 1H, $J = 7.3$ Hz), 7.69 (t, 1H, $J = 7.5$ Hz), 7.43 (d, 1H, $J = 2.4$ Hz), 7.33 (d, 2H, $J = 9.1$ Hz), 6.68 (t, 1H, $J = 10.1$ Hz), 6.65 (s, 1H), 6.58 (dd, 1H, $J_1 = 9.1$ Hz, $J_2 = 2.4$ Hz), 6.27 (dm, 1H), 3.17 (s, 6H); ^{13}C NMR (126 MHz, $CDCl_3$) δ : 183.6, 151.9, 145.6, 144.9, 140.0, 137.7, 134.6, 133.7, 132.1, 131.2, 129.6, 127.5, 126.9, 126.9, 126.5, 120.8, 118.9, 114.0, 107.5, 40.3; HRMS (ESI) calcd. for $C_{22}H_{17}NO_3SF_3$ 432.0881 $[M + H]^+$, found 432.0874.

Compound **10**. Yield 11%. M.p. 250°C(dec.)



^1H NMR (600 MHz, CDCl_3) δ : 8.65 (s, 1H), 8.11 (d, 2H, $J = 8.52$ Hz), 7.69 (d, 2H, $J = 8.7$ Hz), 7.51 (m, 3H), 7.44 (m, 3H), 6.50 (d, 1H, $J = 10$ Hz), 6.42 (d, 1H, $J = 9.3$ Hz), 6.36 (dd, 1H, $J_1 = 9.2$ Hz, $J_2 = 2.8$ Hz), 6.10 (dd, 1H, $J_1 = 9.9$ Hz, $J_2 = 1.7$ Hz), 3.13 (s, 6H); ^{13}C NMR (151 MHz, CDCl_3) δ : 183.4, 152.0, 148.1, 144.7, 140.2, 138.1, 135.1, 130.9, 130.2, 128.8, 128.7, 128.3, 127.8, 127.4, 126.0, 125.9, 125.5, 122.3, 119.5, 114.5, 107.5, 40.3; HRMS (ESI) calcd. for $\text{C}_{29}\text{H}_{22}\text{NO}_3\text{S}$ 464.1320 $[\text{M} + \text{H}]^+$, found 464.1337.

Compound **11**. Yield 25%. M.p. 238-240°C

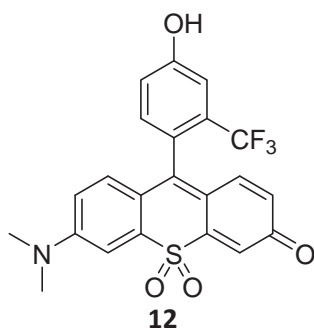


^1H NMR (500 MHz, CDCl_3) δ : 7.42 (d, 1H, $J = 2.8$ Hz), 7.36 (d, 1H, $J = 1.9$ Hz), 7.31 (d, 1H, $J = 2.0$ Hz), 7.21 (d, 2H, $J = 1.6$ Hz), 6.74 (dd, 2H, $J_1 = 19.4$ Hz, $J_2 = 9.6$ Hz), 6.59 (dd, 1H, $J_1 = 9.2$ Hz, $J_2 = 2.8$ Hz), 6.28 (dd, 1H, $J_1 = 10.0$ Hz, $J_2 = 2.0$ Hz), 3.95 (s, 3H), 3.17 (s, 6H); ^{13}C NMR (126 MHz, CDCl_3) δ : 182.6, 160.2, 151.9, 146.0, 145.0, 140.0, 137.9, 134.7, 132.5, 130.8, 127.5, 126.4, 125.2, 121.3, 119.3, 117.4, 114.0, 107.4, 55.8, 40.3; HRMS (ESI) calcd. for $\text{C}_{23}\text{H}_{19}\text{NO}_4\text{SF}_3$ 462.0987 $[\text{M} + \text{H}]^+$, found 462.0983.

Compound **12**.

A solution of **11** (400 mg, 0.87 mmol) in dry DCM (50 ml) under Ar was cooled to at 0°C and boron tribromide (225 mg, 0.9 mmol, 0.085 ml) was added dropwise upon stirring. The reaction was allowed to warm to rt and left stirring overnight. The mixture was diluted with 25 ml of saturated sodium bicarbonate and organic layer was separated, dried over sodium sulfate, filtrated and concentrated under the low pressure. The product was purified utilizing column chromatography (CH_2Cl_2 : acetone 95:5).

Yield 50%. M.p. 186-188°C

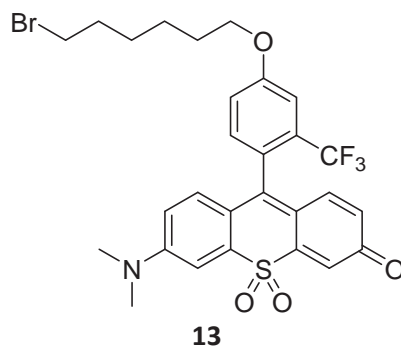


¹H NMR (500 MHz, DMSO-*d*₆) δ: 10.59 (s, 1H), 7.35 (1H, d, *J* = 3 Hz), 7.28 (2H, m), 7.20 (1H, dd, *J*₁ = 8.5 Hz, *J*₂ = 2.5 Hz), 7.01 (1H, d, *J* = 2 Hz), 6.86 (1H, dd, *J*₁ = 9 Hz, *J*₂ = 2.5 Hz), 6.79 (1H, d, *J* = 10 Hz), 6.72 (1H, d, *J* = 9.5 Hz), 6.27 (1H, dd, *J*₁ = 10 Hz, *J*₂ = 3 Hz), 3.15 (6H, s); ¹³C NMR (126 MHz, DMSO- *d*₆) δ: 182.26, 158.40, 151.95, 147.30, 144.88, 139.42, 138.05, 134.86, 133.02, 128.88, 128.64, 128.40, 126.72, 124.52, 124.24, 122.70, 122.34, 119.53, 119.41, 117.91, 114.82, 113.17, 113.13, 107.06; ¹⁹F NMR (500 MHz, CDCl₃) δ: -58.42; HRMS (ESI) calcd. for C₂₂H₁₇NO₄SF₃ 448.0830 [M + H]⁺, found 448.0820.

Compound **13**.

Compound **12** (194 mg, 0.43 mmol) was dissolved in dry CH₃CN (10 ml) followed by the addition of K₂CO₃ (240 mg, 1.74 mmol). 1,6-dibromohexane (159 mg, 0.65 mmol, 0.1 ml) was added under Ar and the reaction mixture was left refluxing for 18h. After the reaction complete, the solvent was evaporated under reduced pressure and the residue was dissolved in 50 ml of DCM. The organic layer was washed 3 times with water (50 ml), dried over Na₂SO₄ and concentrated in vacuo. The obtained solid was next boiled in 20 ml of hexane, filtered and washed again with hexane. The product was next purified via column chromatography (CH₂Cl₂ : acetone 95:5).

Yield 50%. M.p. 125-127°C(dec.)

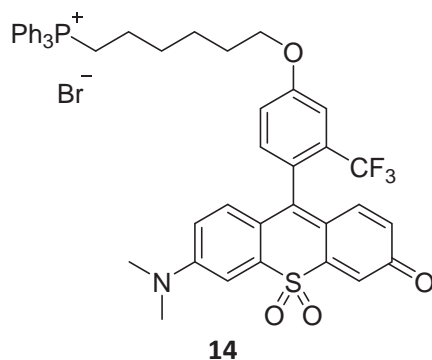


^1H NMR (500 MHz, CDCl_3) δ : 7.41 (d, 1H, $J = 2$ Hz), 7.35 (d, H, $J = 2$ Hz), 7.31 (d, 1H, $J = 2$ Hz), 7.19 (m, 2H), 6.77 (d, 1H, $J = 10$ Hz), 6.73 (d, 1H, $J = 9$ Hz), 6.58 (dd, 1H, $J_1 = 9.5$ Hz, $J_2 = 3$ Hz), 6.28 (dd, 1H, $J_1 = 10$ Hz, $J_2 = 3$ Hz), 4.09 (t, 2H, $J = 6$ Hz), 3.46 (t, 2H, $J = 6$ Hz), 3.17 (s, 6H), 1.92 (dq, 4H, $J_1 = 22$ Hz, $J_2 = 7$ Hz), 1.57 (m, 4H); ^{19}F NMR (500 MHz, CDCl_3) δ : -59.53; ^{13}C NMR (126 MHz, CDCl_3) δ : 183.63, 159.64, 151.80, 146.11, 144.92, 139.97, 137.94, 134.78, 132.46, 130.67, 127.41, 126.32, 124.94, 121.20, 119.29, 117.64, 113.97, 113.01, 107.38, 77.25, 77.00, 76.75, 68.42, 40.27, 33.70, 32.59, 28.90, 27.83, 25.25. HRMS (ESI) calcd. for $\text{C}_{28}\text{H}_{27}\text{NO}_4\text{SBrF}_3\text{Na}$ 632.0694 $[\text{M} + \text{Na}]^+$, found 632.0658.

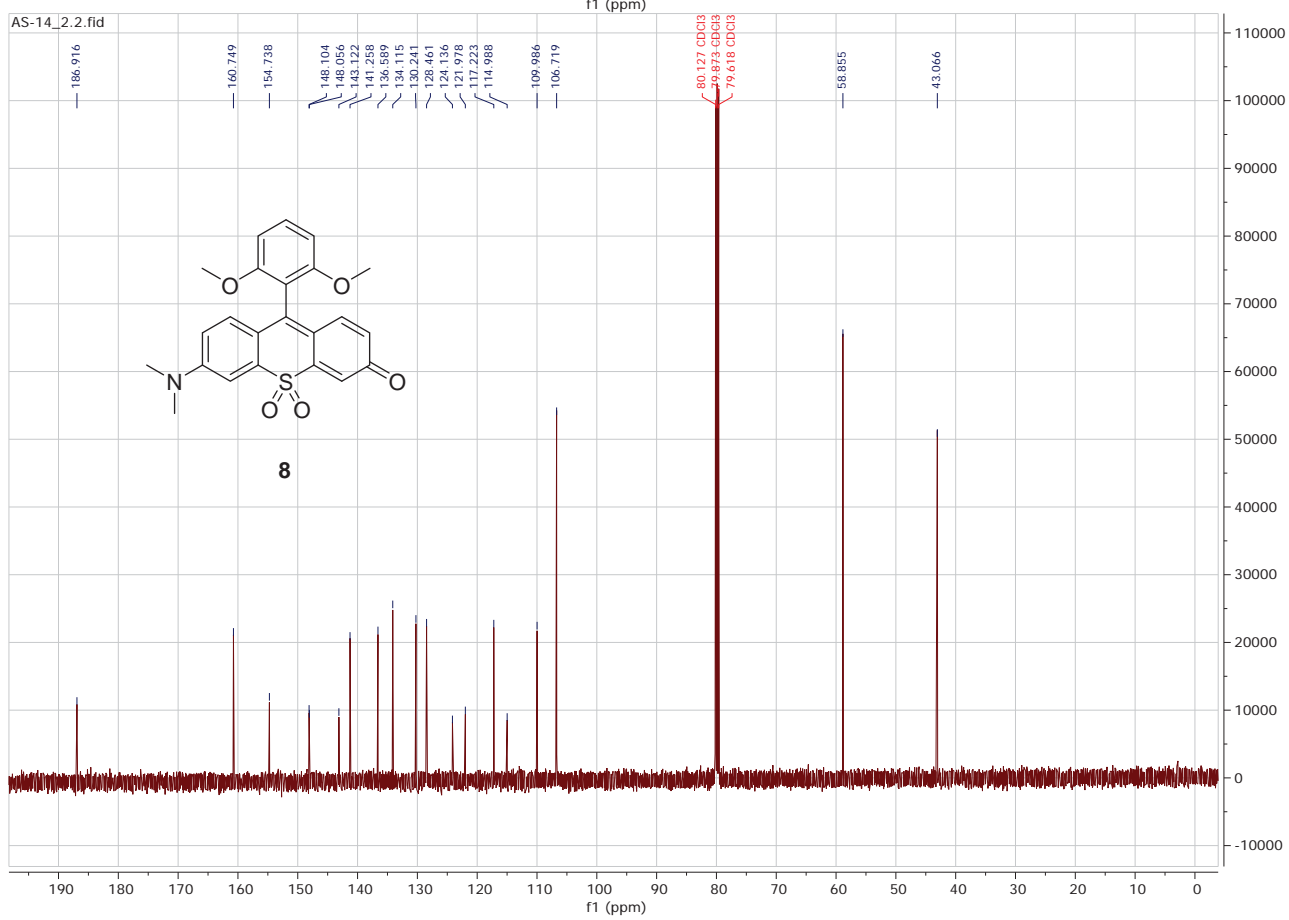
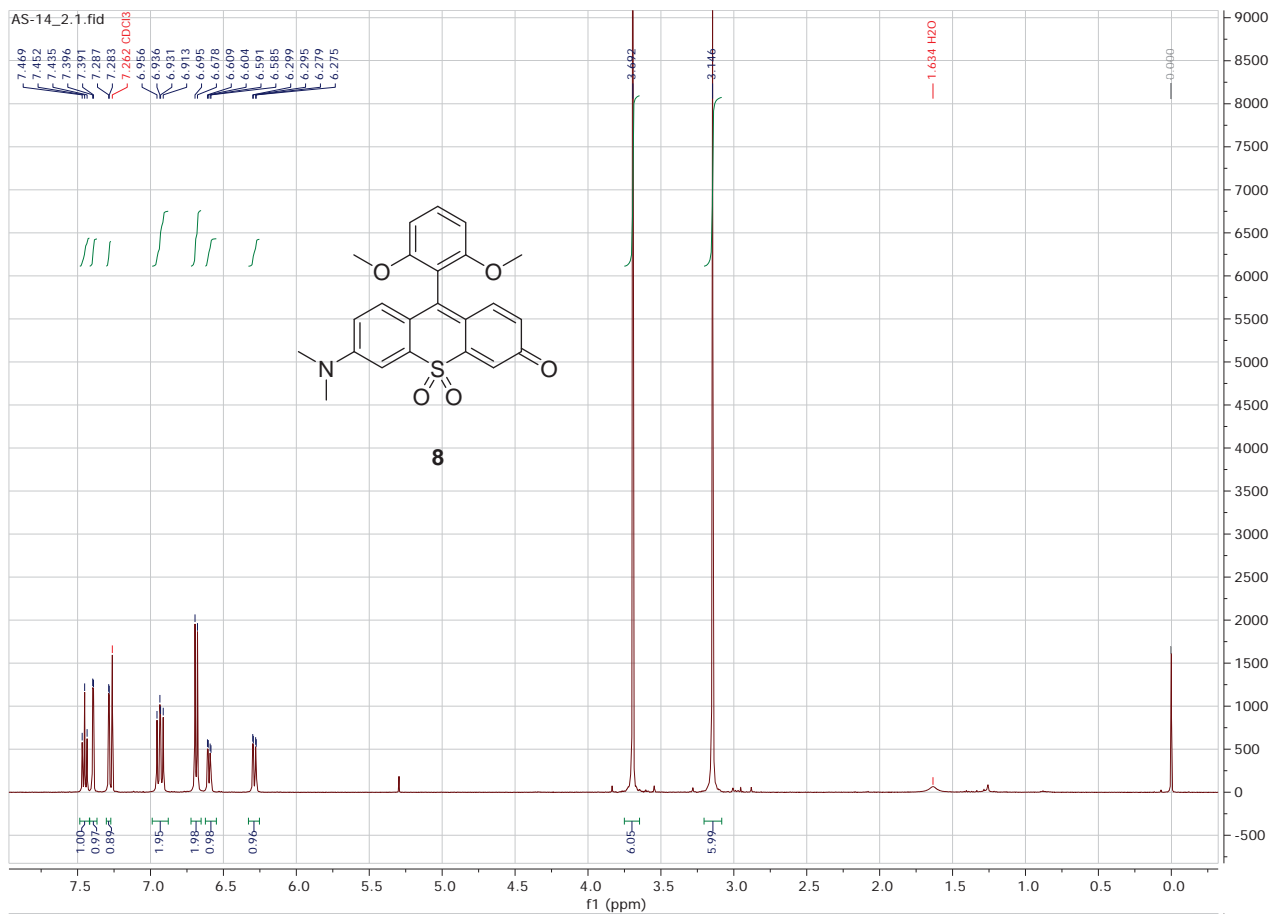
Compound **14**.

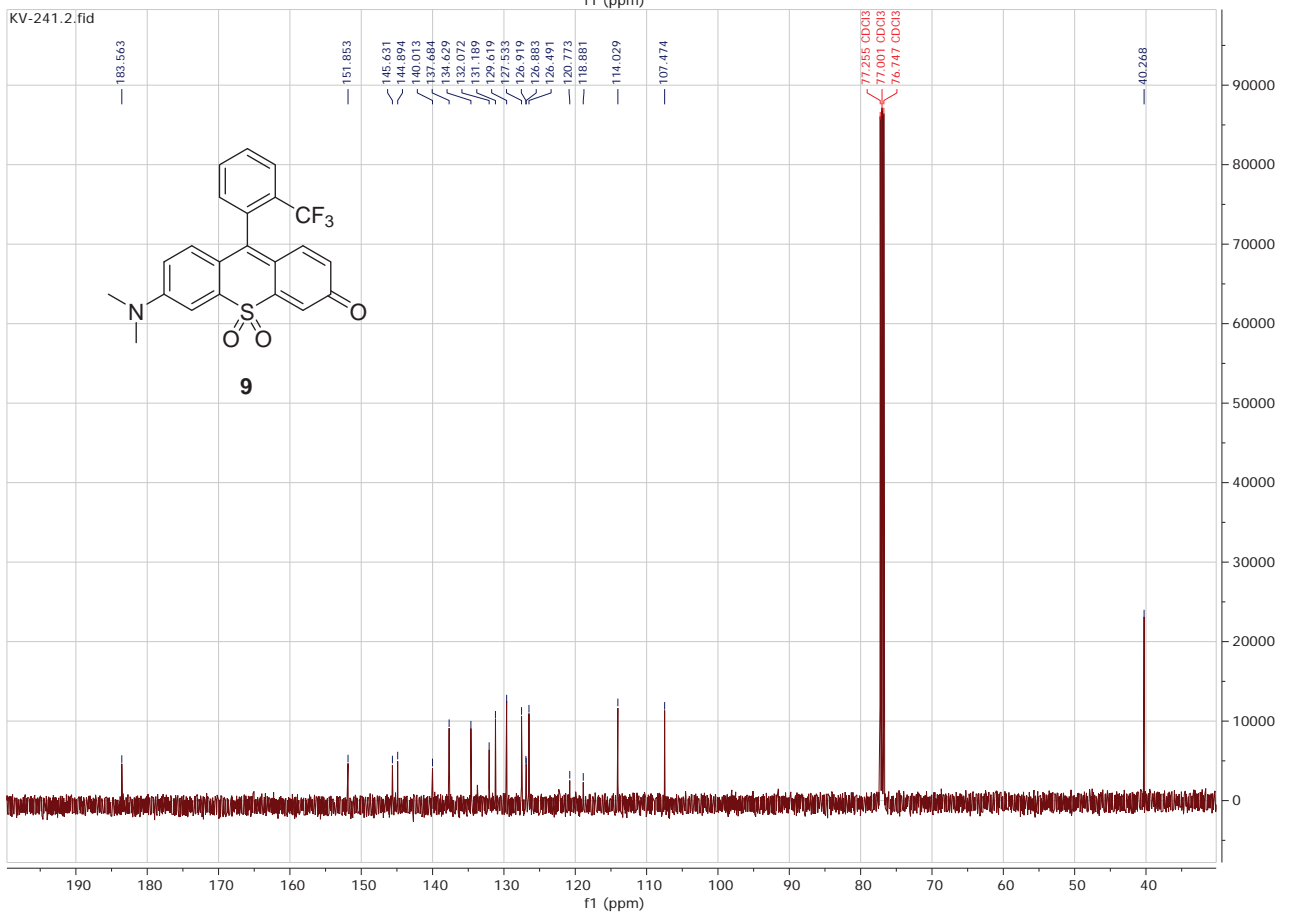
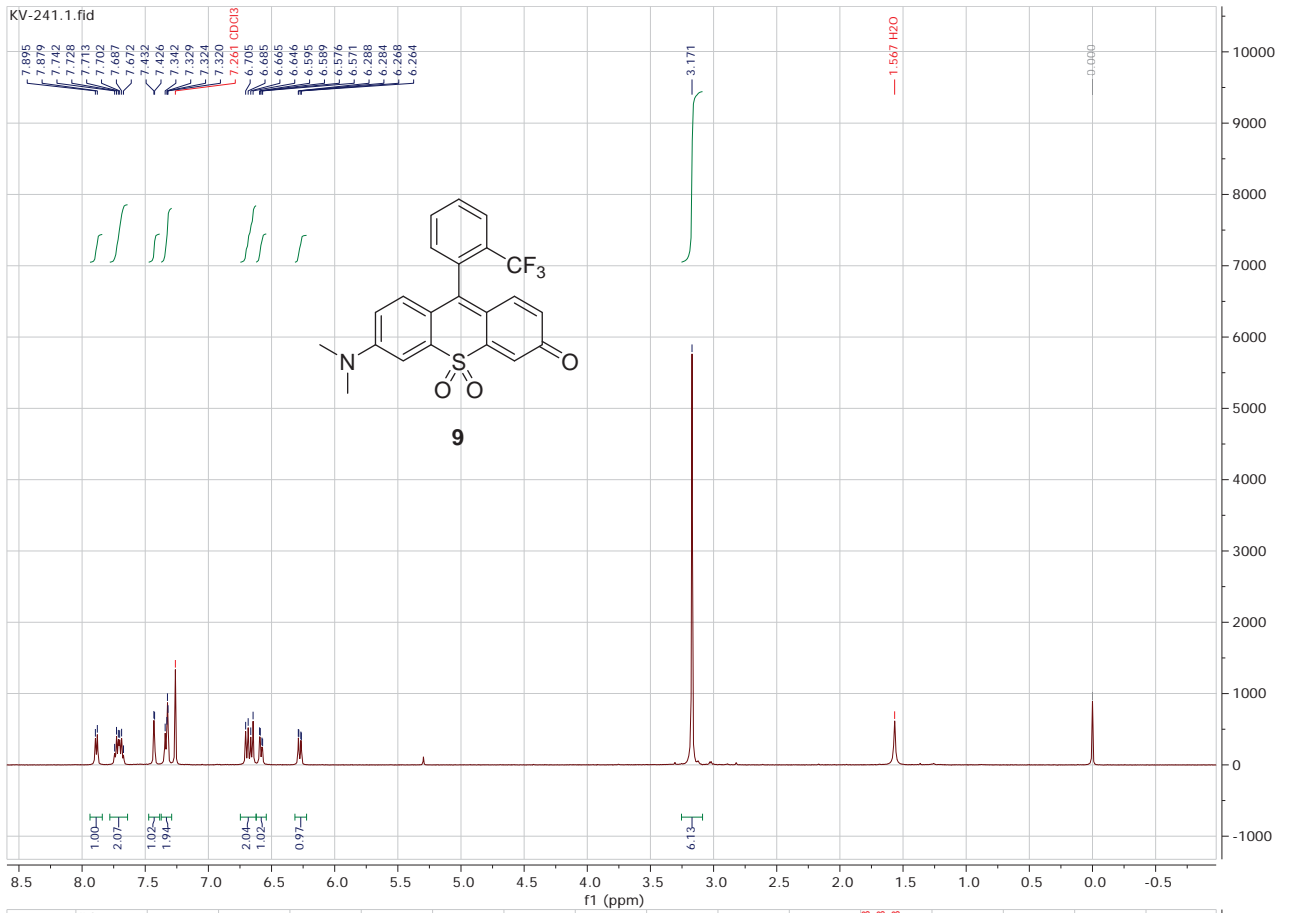
73 mg (0,12 mmol) of **13** with 0,31g (1,2 mmol) of triphenylphosphine in 0,3 ml of DMA was heated at 120° for 35 min under Argon. After cooling the reaction was diluted with a mixture hexane/ Et_2O , the crude product was filtered and washed again and next purified via column chromatography on a reversed phase (RP-18) in CH_3CN . After evaporation of the solvent the product was washed with EtOAc for 1h to give 12 mg of the product.

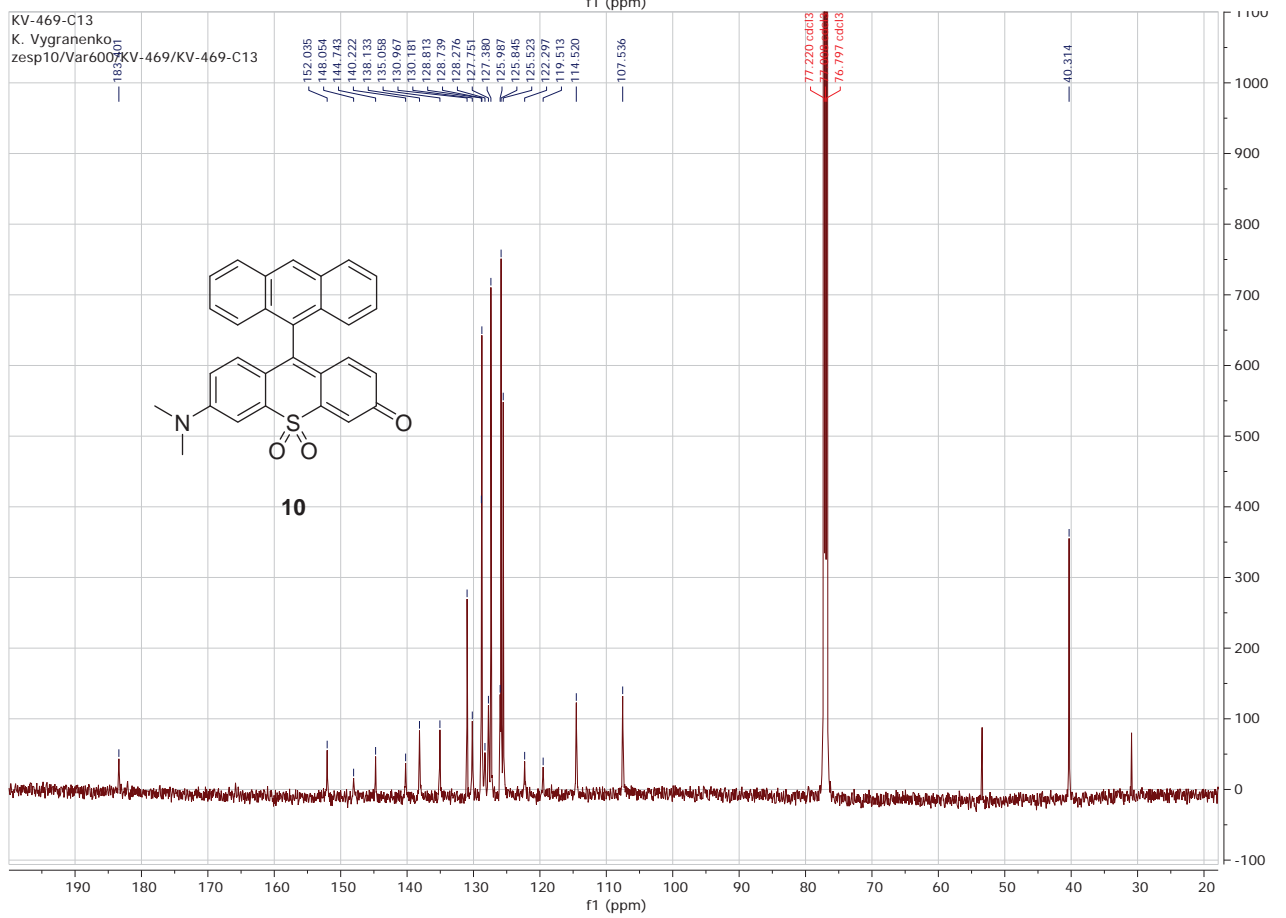
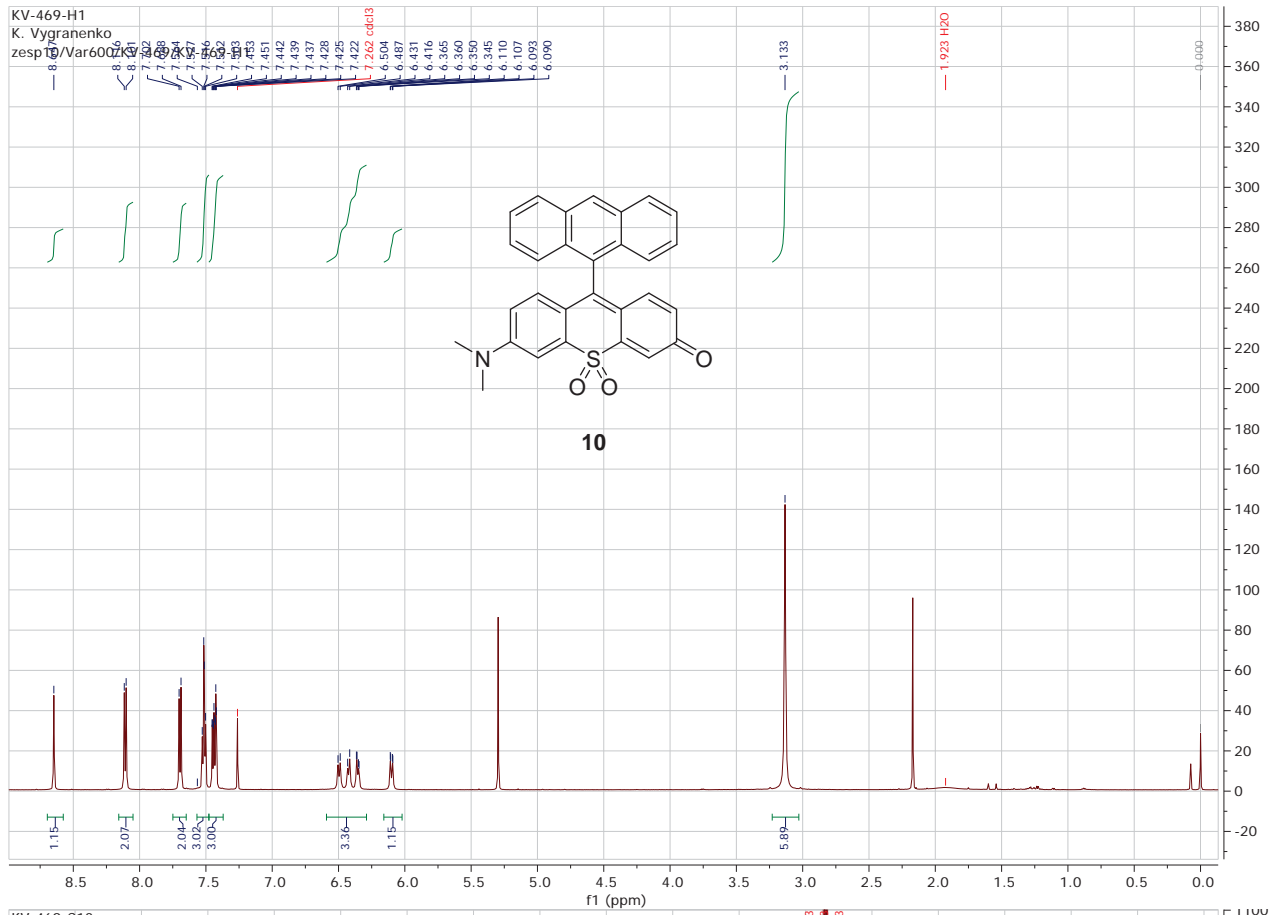
Yield 11%. M.p. $137\text{-}139^\circ\text{C}$ (dec.)

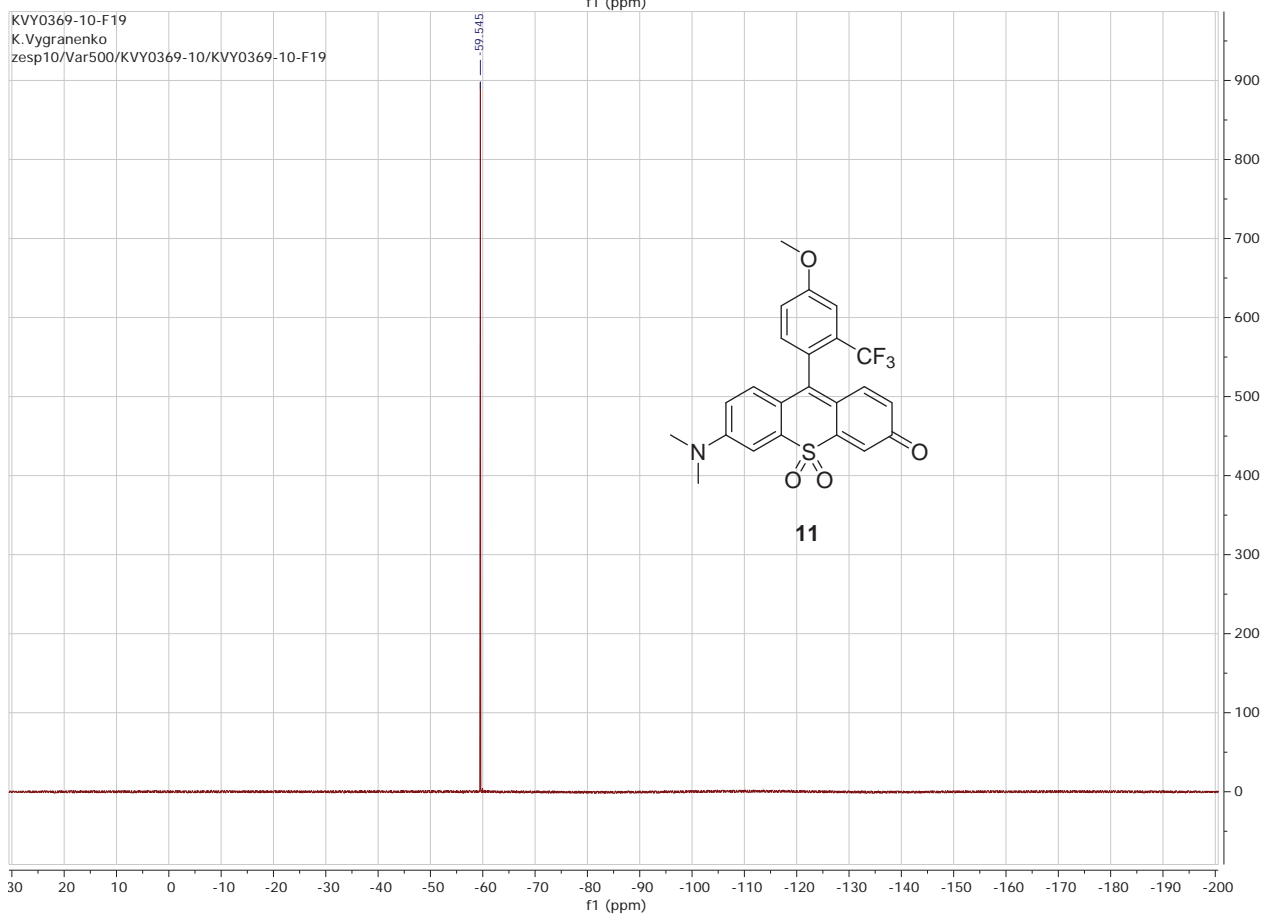
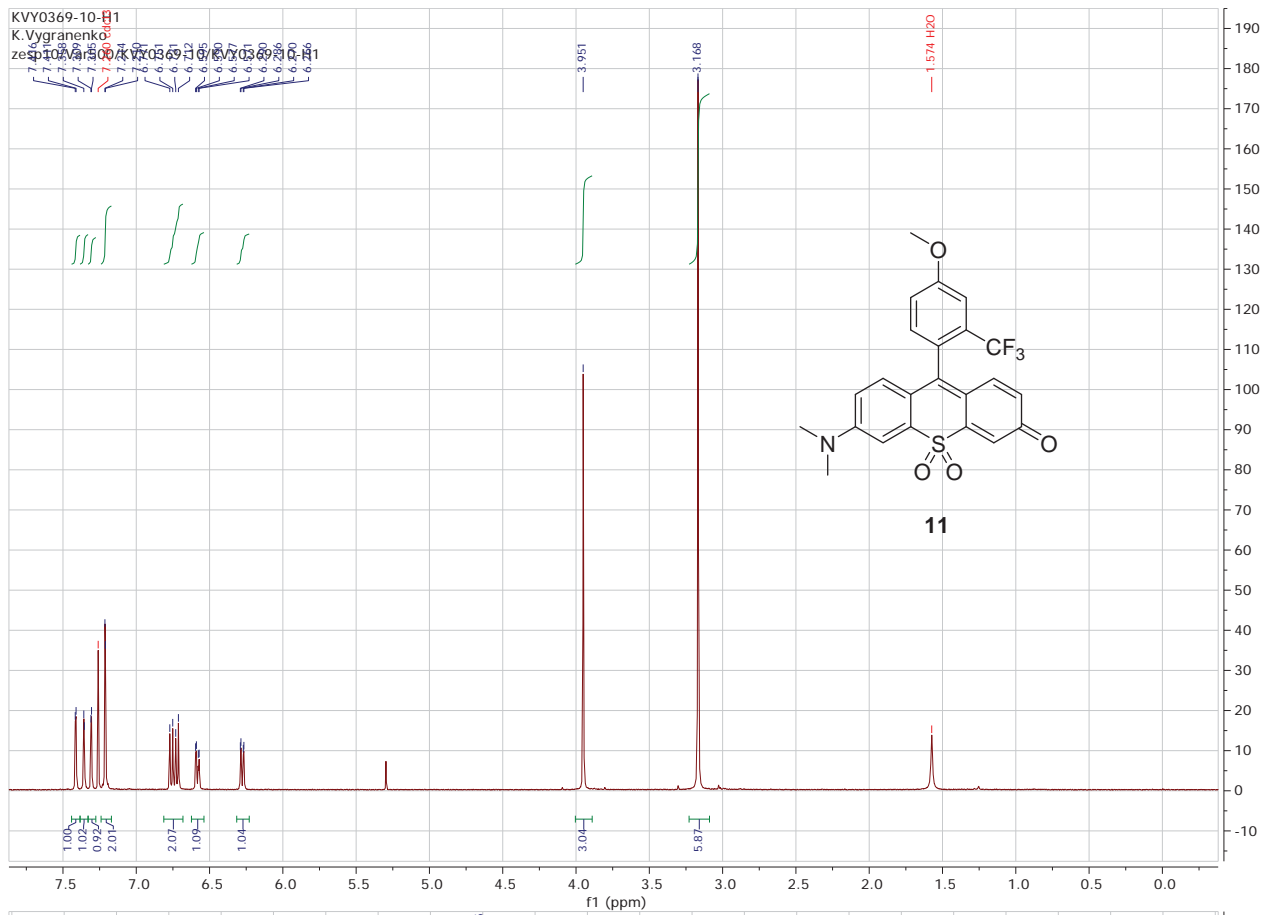


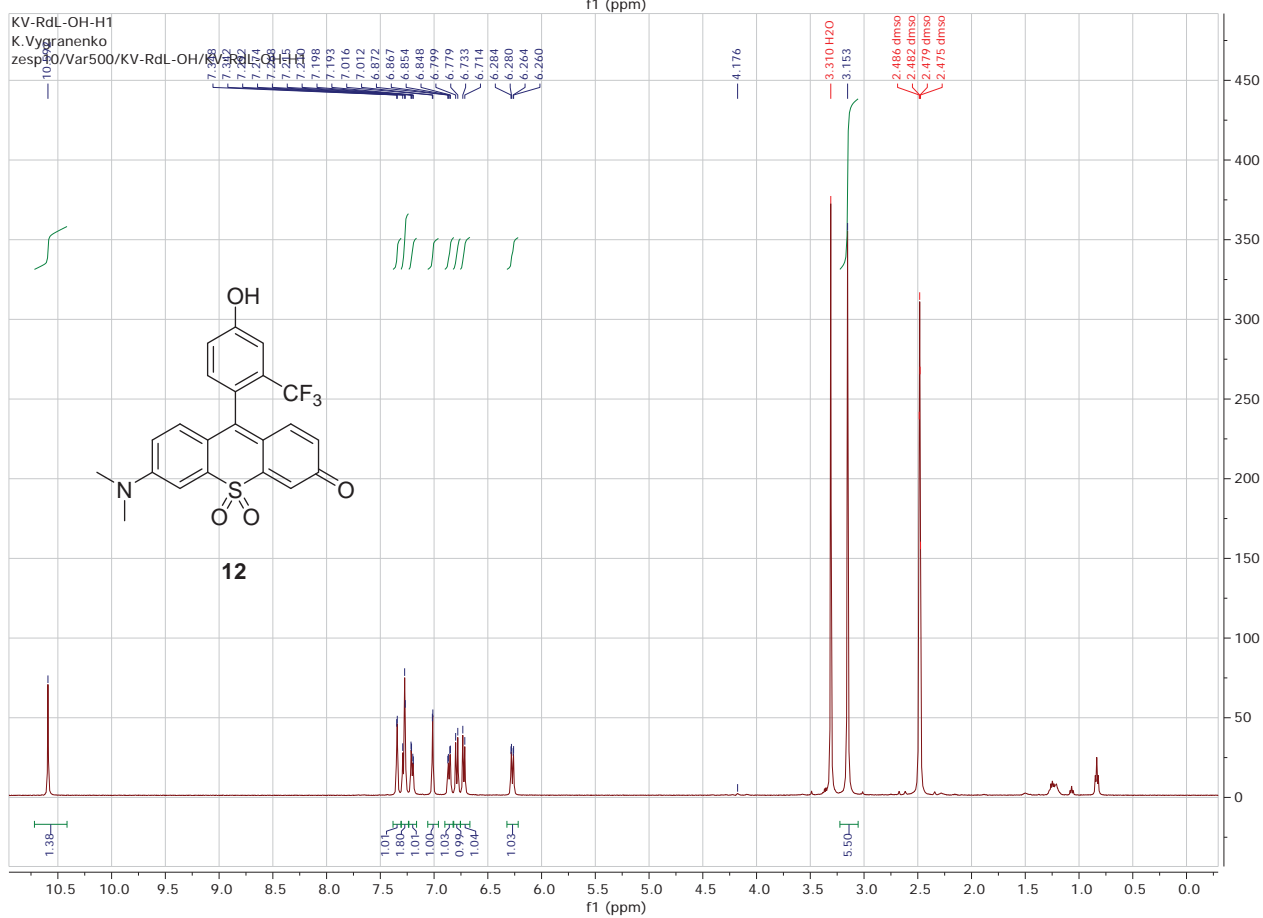
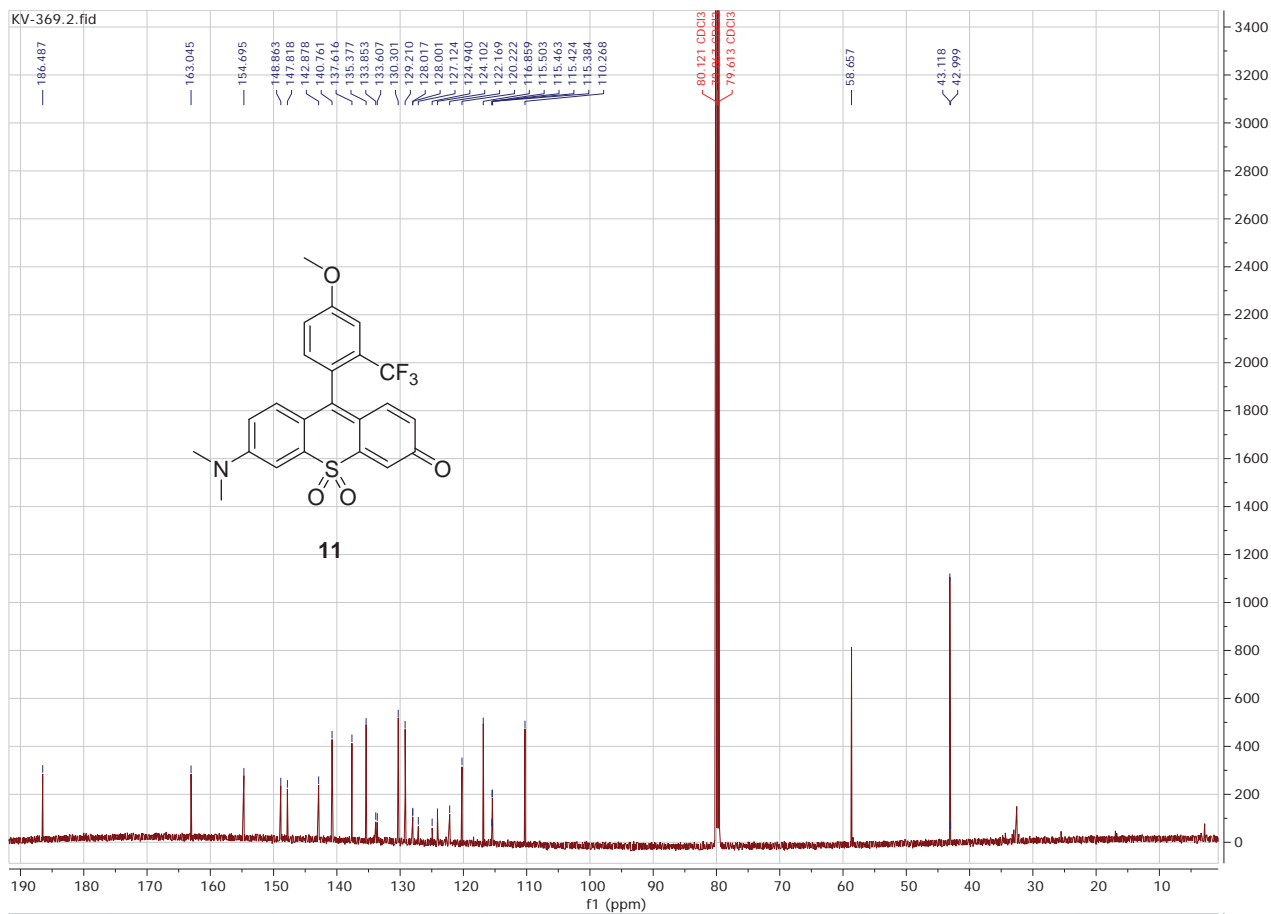
^1H NMR (500 MHz, CD_3CN) δ : 7.74 (bm, 15H), 7.42 (bd, 2H, $J_1 = 6.5$ Hz), 7.3 (bs, 2H), 7.13 (bs, 1H), 6.83 (d, 1H, $J = 10$ Hz), 6.79 (d, 1H, $J = 9.5$ Hz), 6.73 (dd, 1H, $J_1 = 9$ Hz, $J_2 = 3$ Hz), 6.22 (dd, 1H, $J_1 = 9$ Hz, $J_2 = 2$ Hz), 4.11 (t, 2H, $J = 6.5$ Hz), 3.27 (bm, 2H), 3.17 (s, 6H), 1.78 (q, 2H, $J = 7.5$ Hz), 1.7 (q, 2H, $J = 7.5$ Hz), 1.63 (q, 2H, $J = 7.5$ Hz), 1.54 (q, 2H, $J = 7.5$ Hz); ^{19}F NMR (500 MHz, CD_3CN) δ : -59.95; HRMS (ESI) calcd. for $\text{C}_{46}\text{H}_{42}\text{NO}_4\text{SF}_3\text{P}$ 792.2524 $[\text{M}]^+$, found 792.2505.

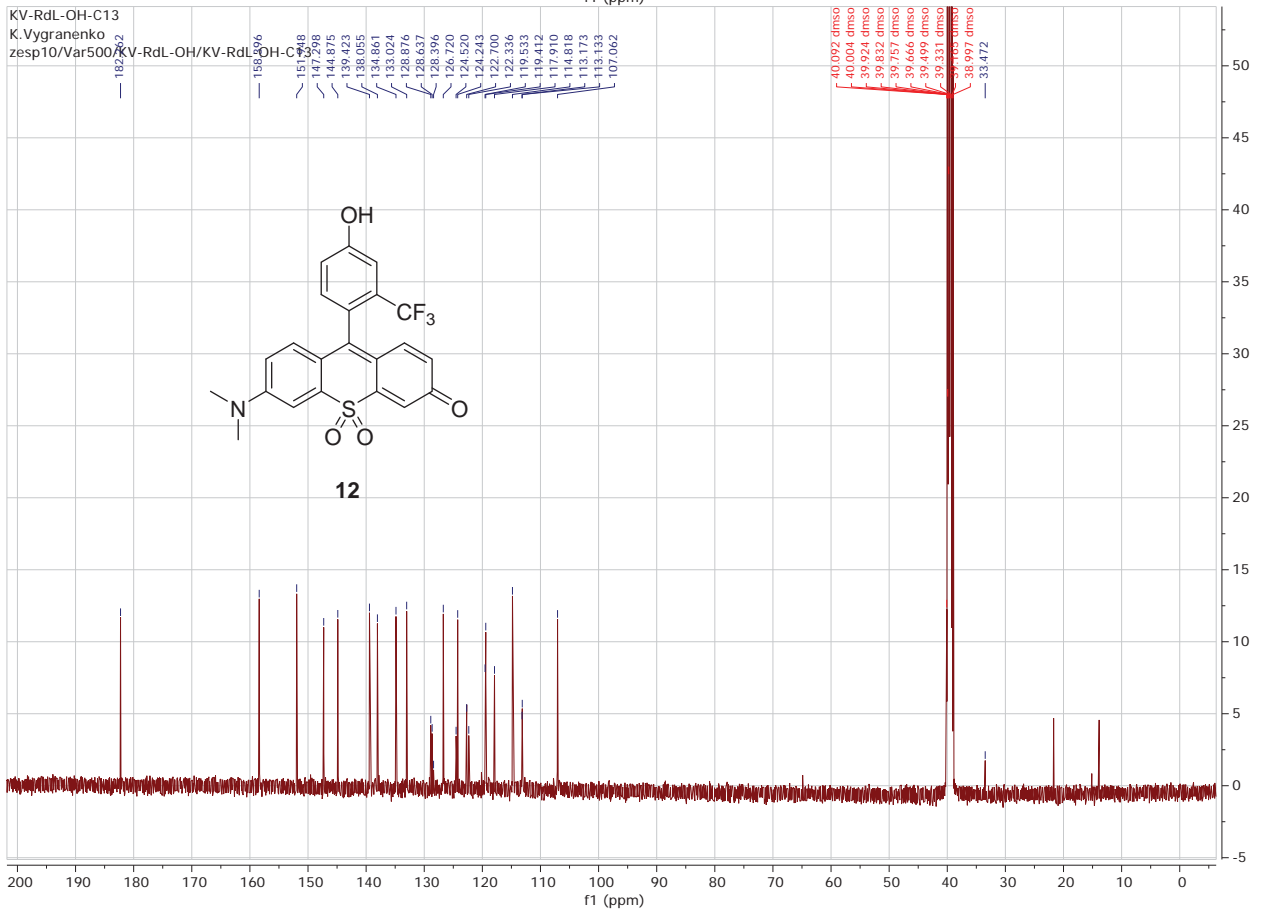
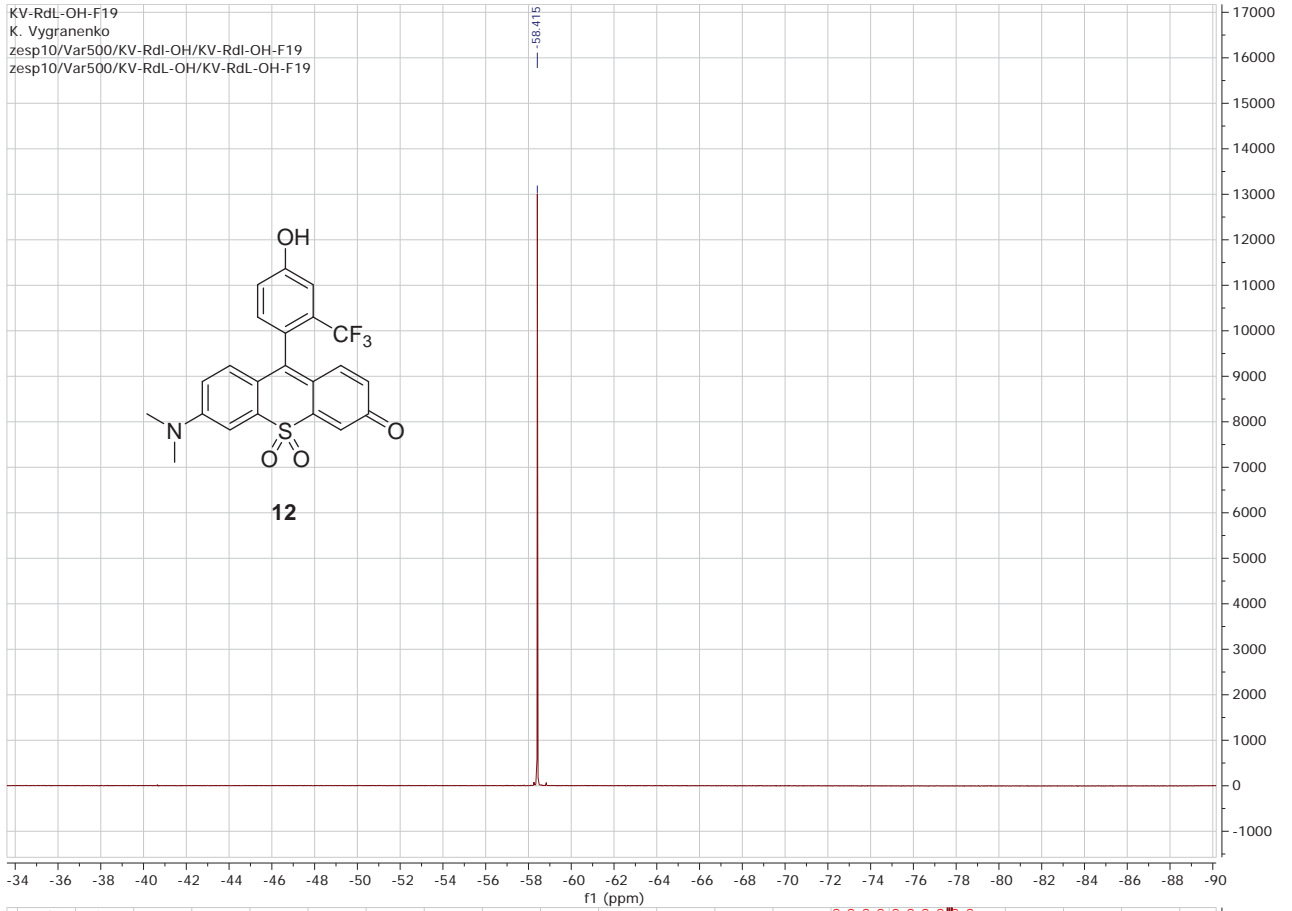


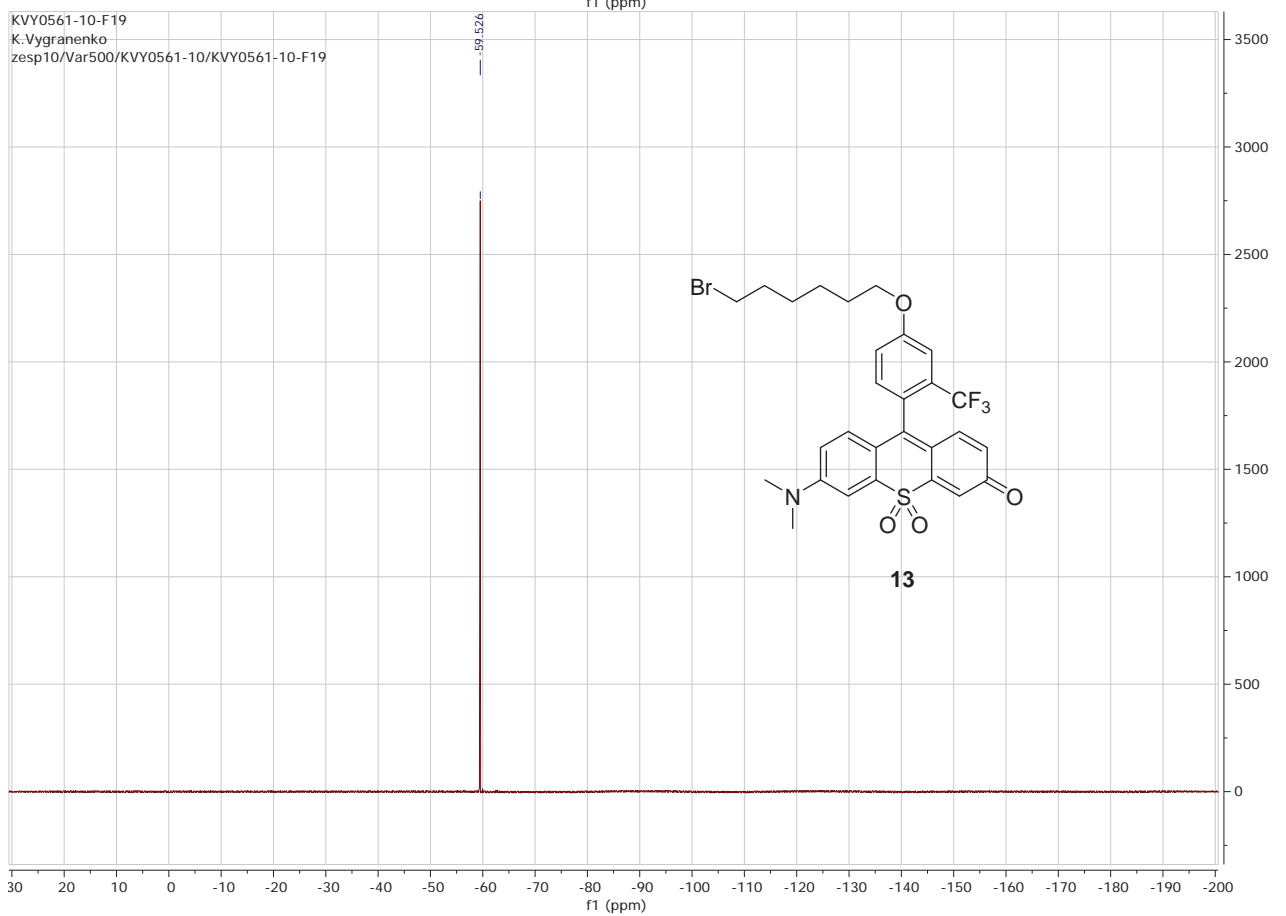
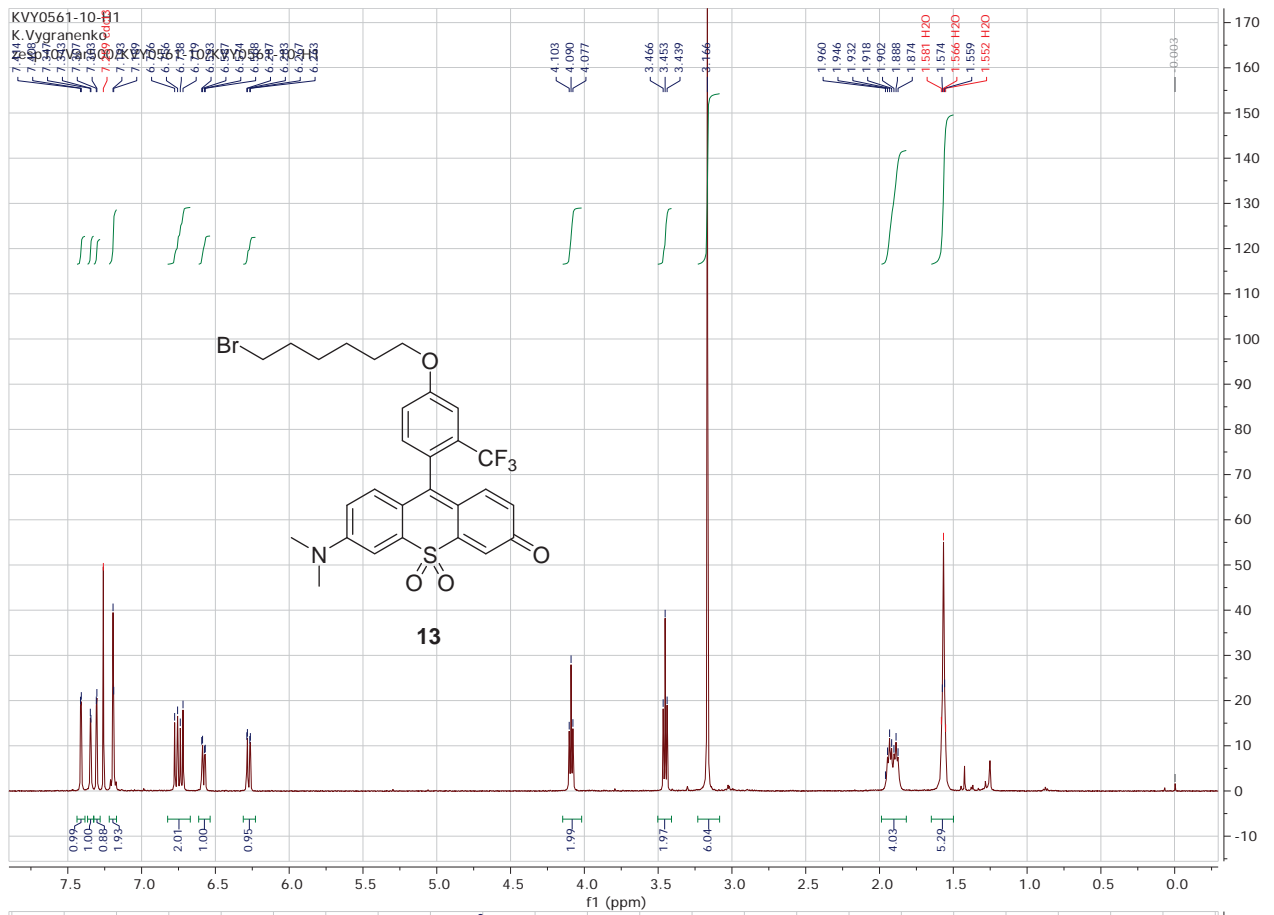


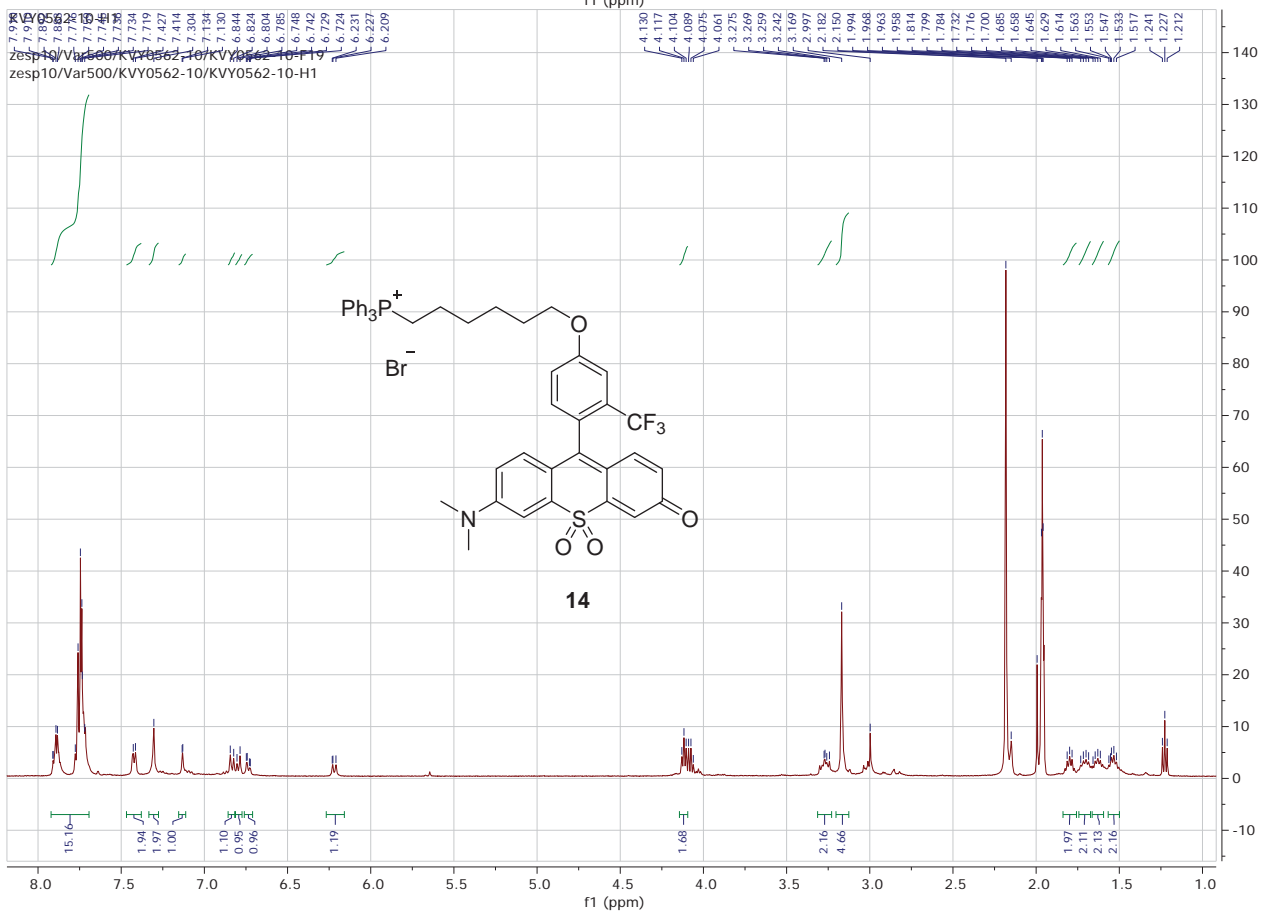
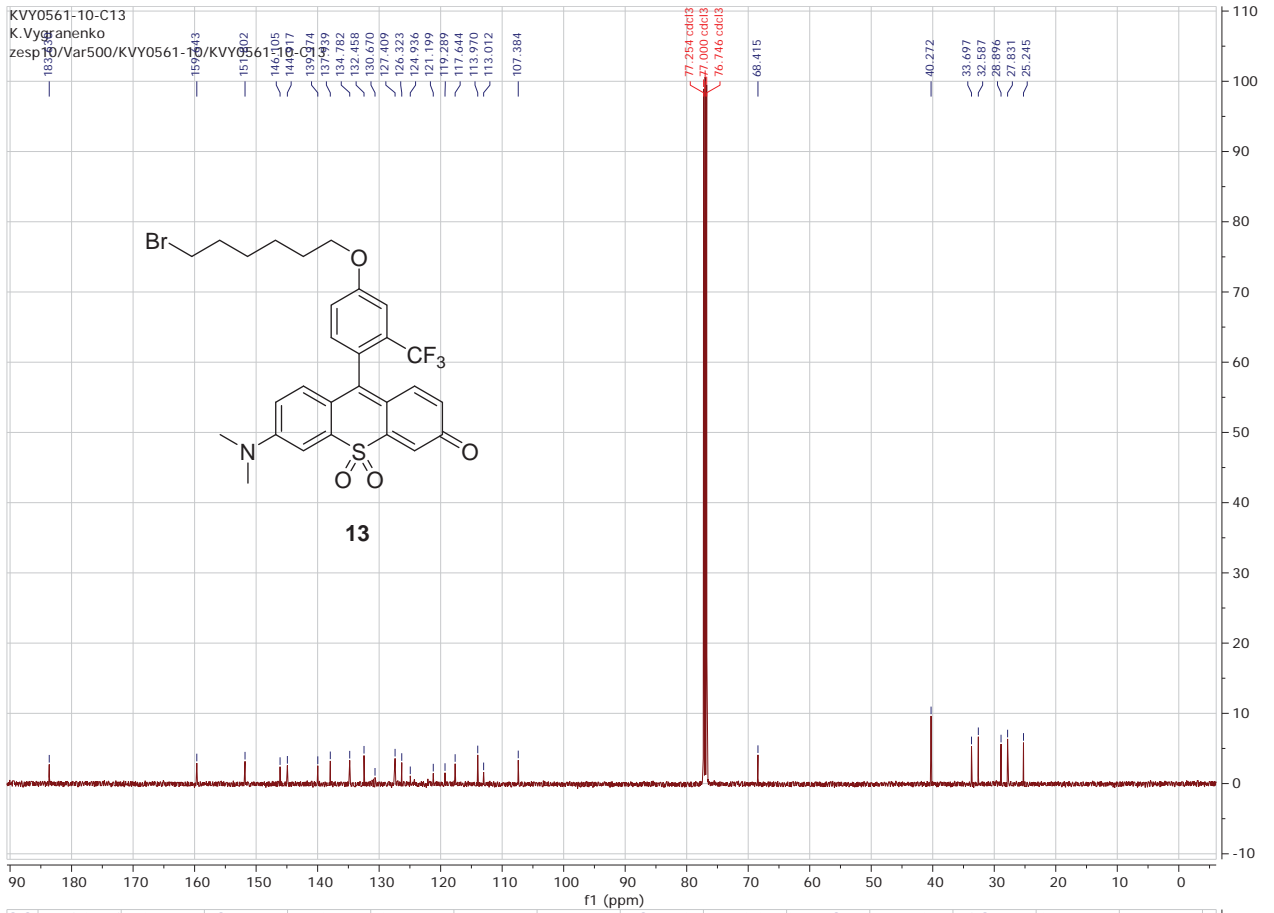












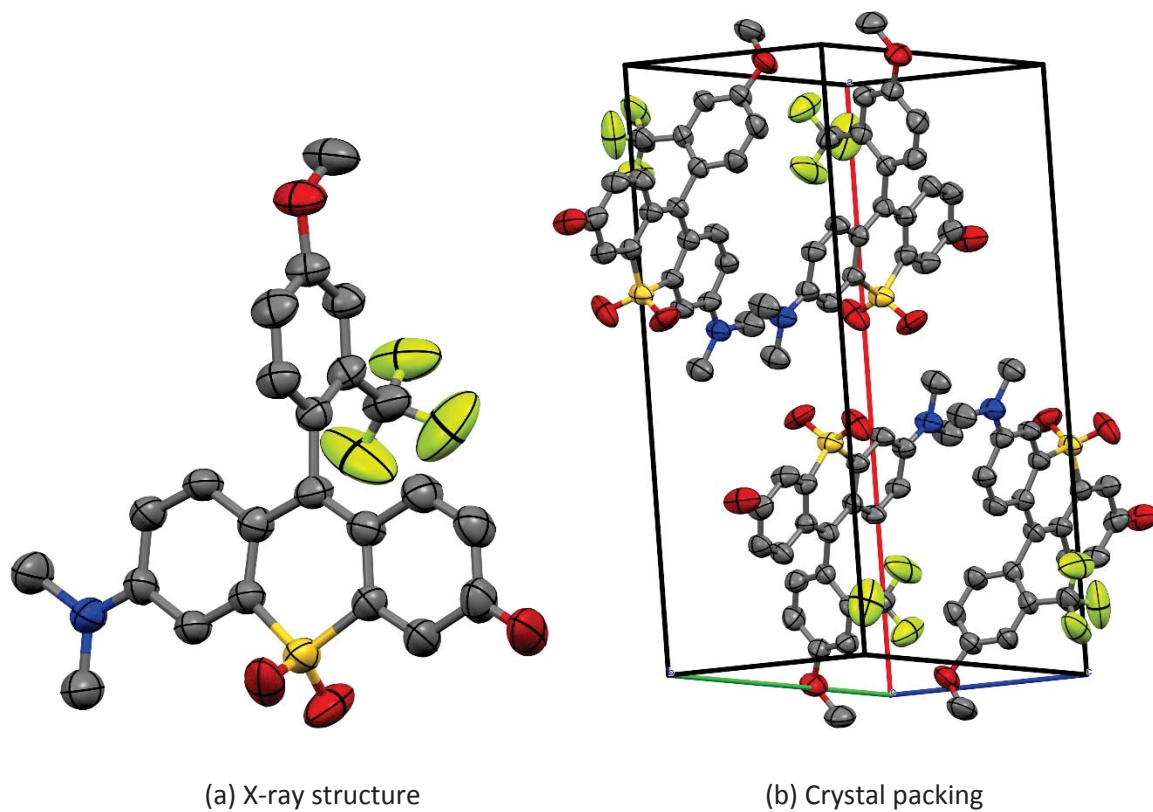
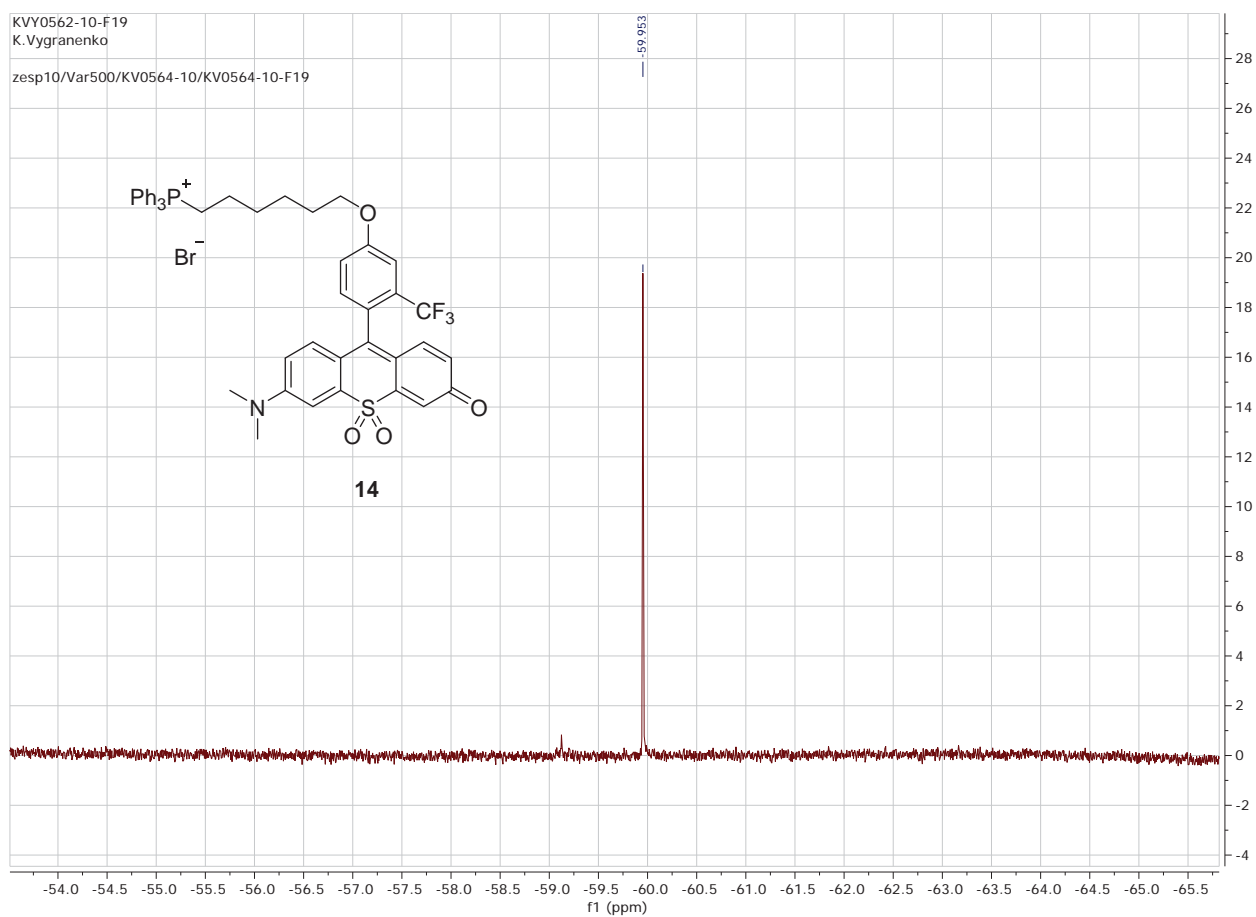


Figure S1. X-Ray structure of compound **11** (a) and crystal packing (b).

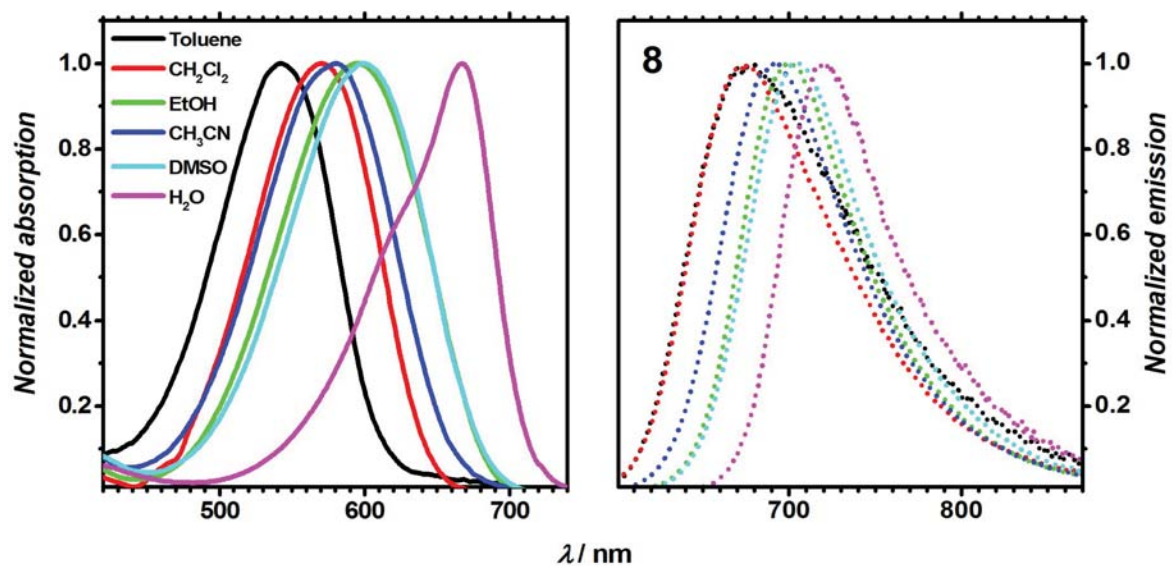


Figure S2. Absorption (solid) and emission (dotted) of compound **8** in toluene, CH₂Cl₂, EtOH, CH₃CN, DMSO, H₂O (containing 2% DMSO).

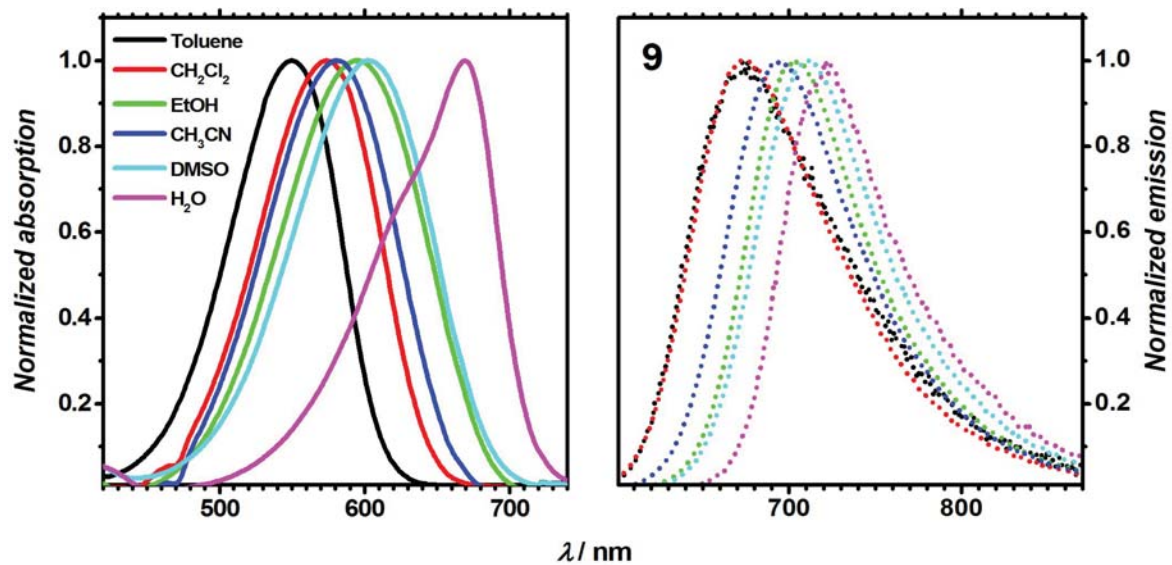


Figure S3. Absorption (solid) and emission (dotted) of compound **9** in toluene, CH₂Cl₂, EtOH, CH₃CN, DMSO, H₂O (containing 2% DMSO).

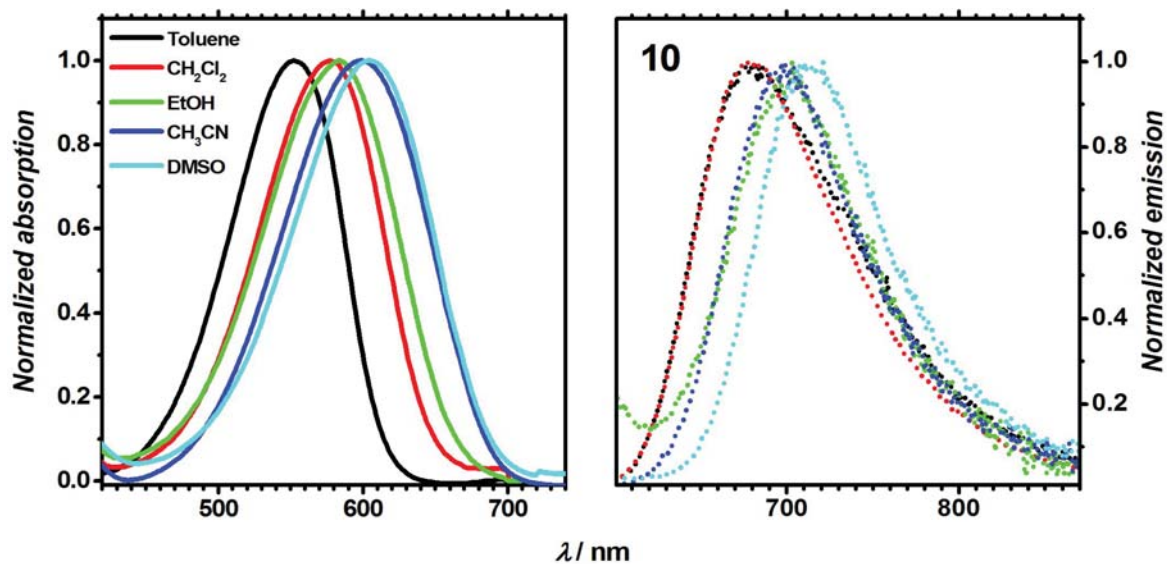


Figure S4. Absorption (solid) and emission (dotted) of compound **10** in toluene, CH₂Cl₂, EtOH, CH₃CN, DMSO, H₂O (containing 2% DMSO).

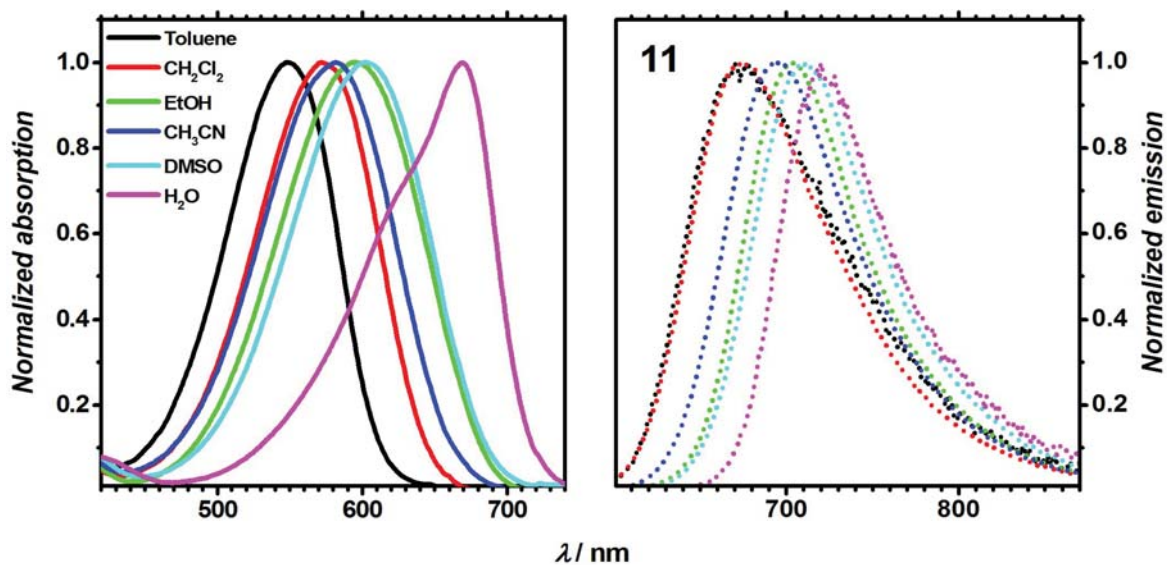


Figure S5. Absorption (solid) and emission (dotted) of compound **11** in toluene, CH₂Cl₂, EtOH, CH₃CN, DMSO, H₂O (containing 2% DMSO).

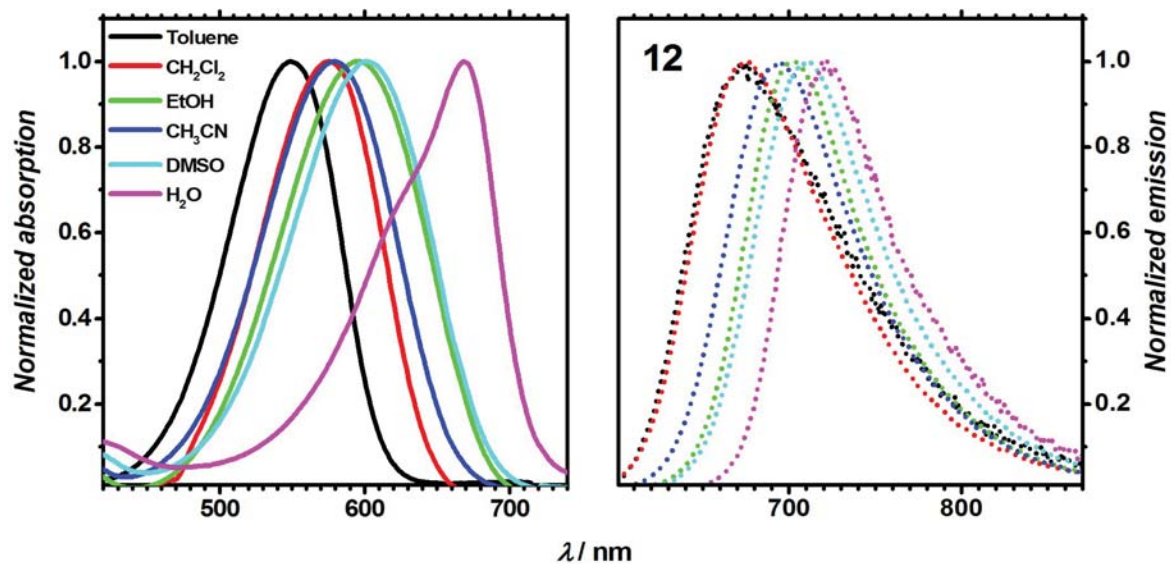


Figure S6. Absorption (solid) and emission (dotted) of compound **12** in toluene, CH_2Cl_2 , EtOH, CH_3CN , DMSO, H_2O (containing 2% DMSO).

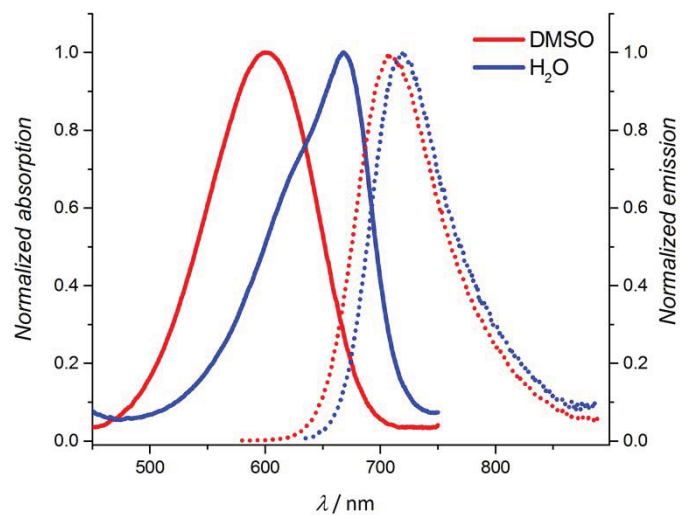


Figure S7. Absorption (solid) and emission (dotted) of compound **14** in DMSO and H_2O (2% of DMSO).

Time-resolved fluorescence data

Table S1. Fluorescence decay data for compounds **8** and **10**.^a

Comp.	Solvent	$\lambda_{\text{exc}} / \text{nm}$	$\lambda_{\text{obs}} / \text{nm}$	A_1	A_2	τ_1 / ns	$\tau_2 [\text{ns}]$	$k_r \cdot 10^{-8} / \text{s}^{-1}$	$k_{\text{nr}} \cdot 10^{-8} / \text{s}^{-1}$
8	CH ₂ Cl ₂	336	670			4.20		1.02	1.36
	CH ₃ CN	336	700			5.24		0.99	0.92
	DMSO	336	700			4.33		1.15	1.16
10	CH ₂ Cl ₂	336	670	38	62	0.46	2.06	2.83	18.9
	CH ₃ CN	336	700	100		0.32		0.25	31.0
	DMSO	336	700	94	6	0.32	6.13	0.31	31.1

^a: The values of the radiative k_r and non-radiative k_{nr} rates are approximated on the basis of equations:

$$k_r = \Phi_f / \tau_1 \text{ and } k_{\text{nr}} = 1 / \tau_1 - k_r$$

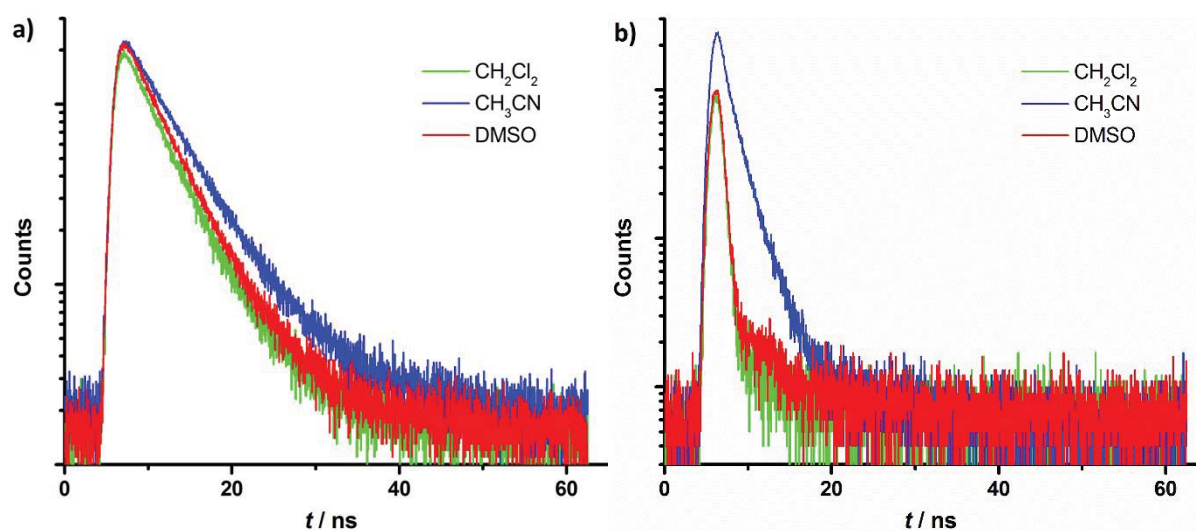
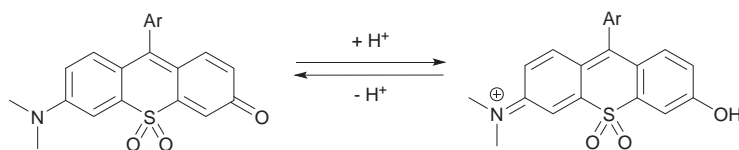


Figure S8. Fluorescence decay for **8** (a) and **10** (b) in CH₂Cl₂, CH₃CN and DMSO.

Absorption dependence on pH



Scheme S1. SO₂-rhodol protonation

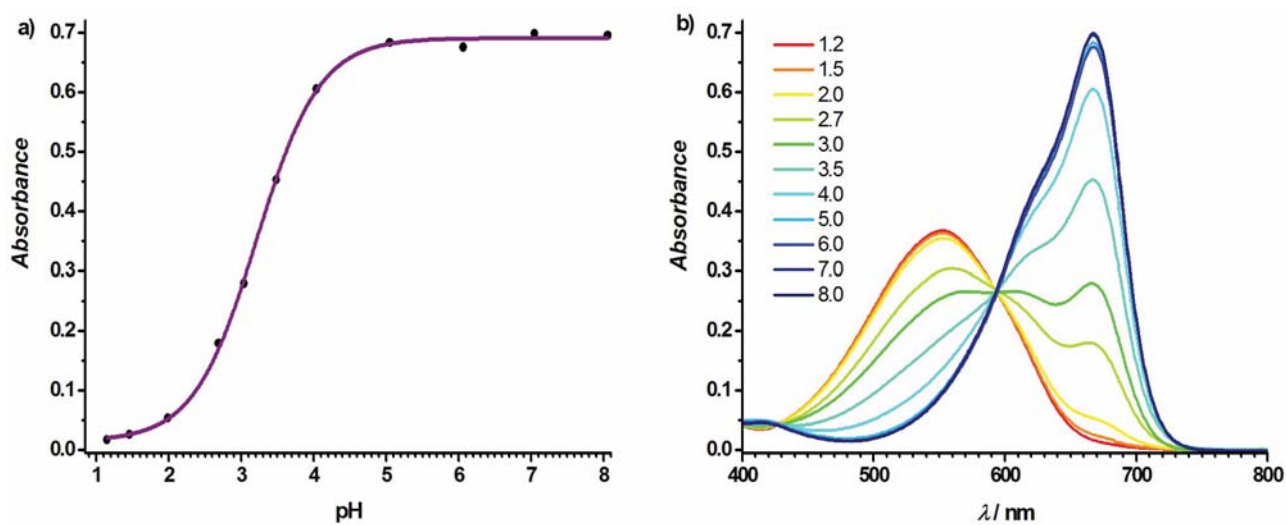


Figure S9. a) Absorption spectra of compound **8** at various pH values. b) The plots of absorbance of compound **8** at 667 nm as function of pH value and their fitting curve ($pK_a = 3.21$, $r = 0.9994$).

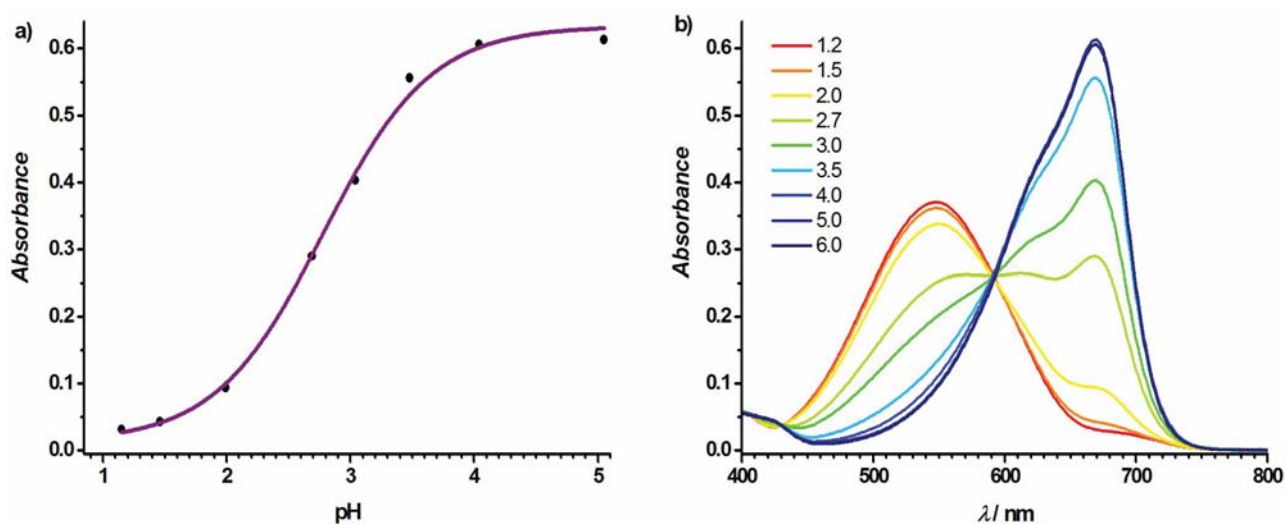


Figure S10. a) Absorption spectra of compound **9** at various pH values. b) The plots of absorbance of compound **9** at 669 nm as function of pH value and their fitting curve ($pK_a = 2.78$, $r = 0.9964$).

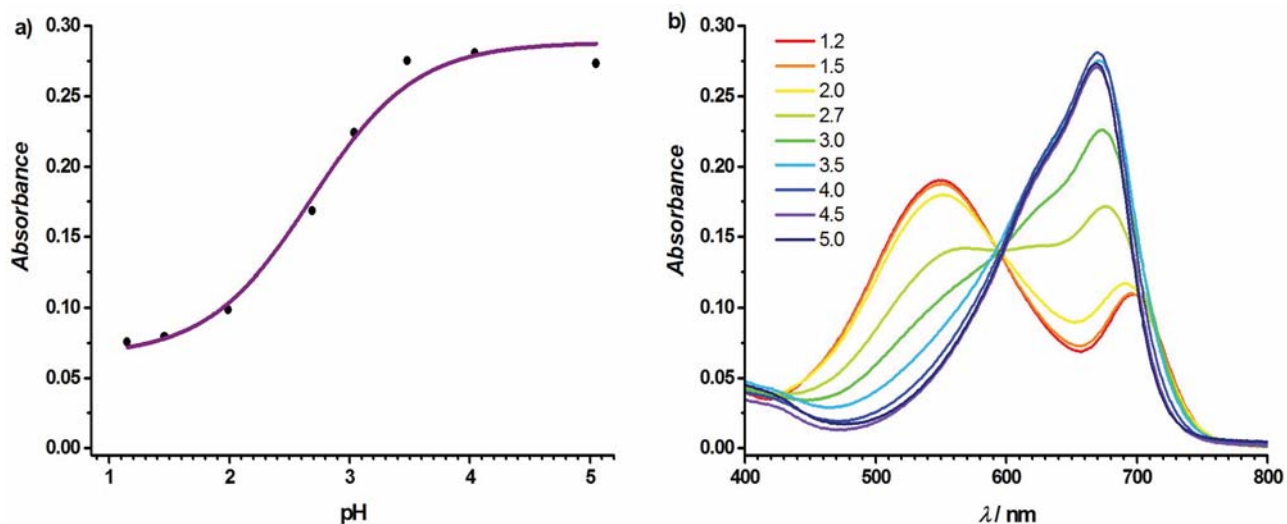


Figure S11. a) Absorption spectra of compound **11** at various pH values. b) The plots of absorbance of compound **11** at 669 nm as function of pH value and their fitting curve ($pK_a = 2.68$, $r = 0.9841$).

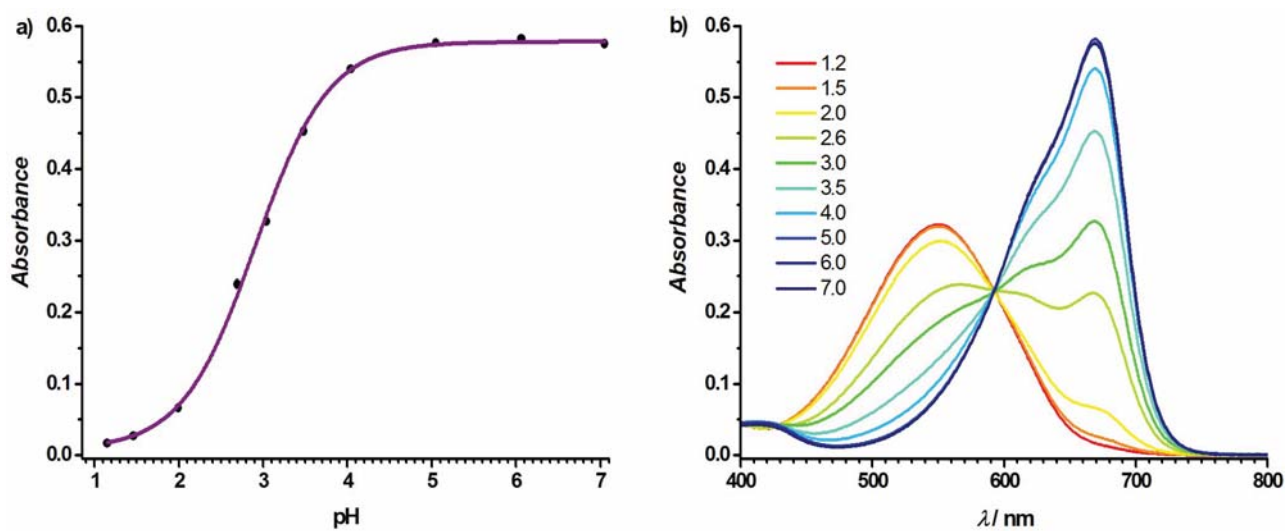


Figure S12. a) Absorption spectra of compound **12** at various pH values. b) The plots of absorbance of compound **12** at 669 nm as function of pH value and their fitting curve ($pK_a = 2.91$, $r = 0.99894$).

Compound **10** undergoes the formation of aggregates in DMSO-water media. The latter is not sensitive to a pH change.

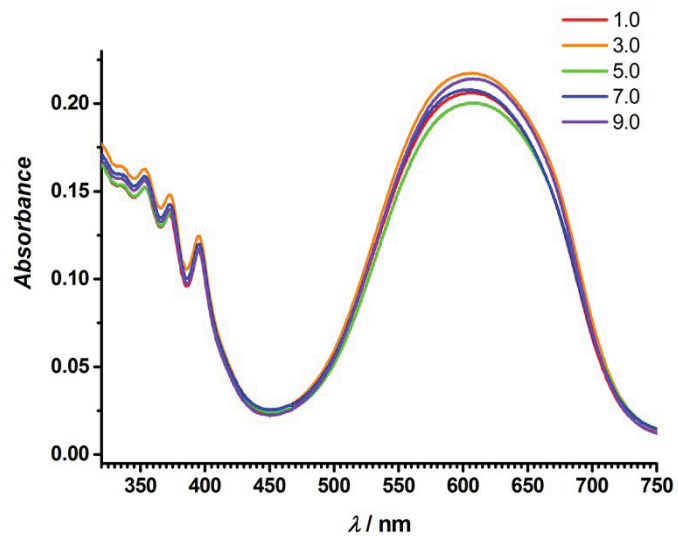


Figure S13. Absorption spectra of compound **10** at various pH values.

Photostability measurements

Photostability was determined through the variation in absorption of each sample at the appropriate absorption maximum wavelength (λ_{abs}) with respect to irradiation time. Ethanol was selected as the solvent. Concentrations giving similar optical densities ($A \approx 1$) were used. Quartz cells of samples were irradiated with a 300 W Xe lamp (Asahi spectra MAX-350, light power: 0.16 W/cm²) for 150 min at 25 °C equipped with a UV/vis mirror module through a glass fiber. The absorption spectra were measured at appropriate times during the irradiation. Cresyl violet, Rhodamine 6G and DPP (2,5-dimethyl-3,6-bis(3,4-dimethoxyphenyl)pyrrolo[3,4-c]pyrrole-1,4(2H,5H)-dione) were used as references.

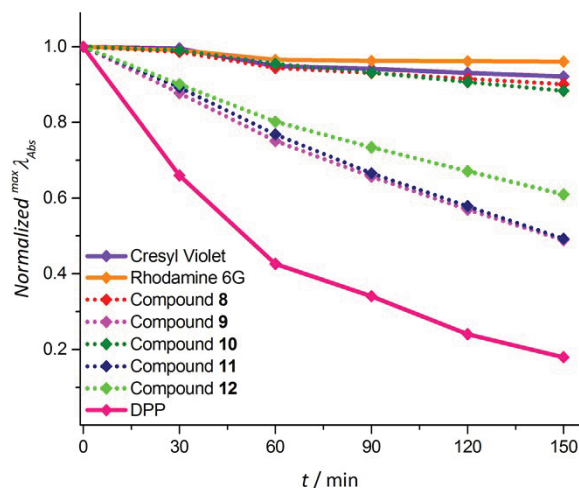


Figure S14. Photostability of sulfone-rhodols compared to the Rhodamine 6G, Cresyl Violet and DPP (2,5-dibutyl-3,6-bis(3,4-dimethoxyphenyl)pyrrolo[3,4-c]pyrrole-1,4(2H,5H)-dione) measured in EtOH using a collimated light source from a 300W Xe lamp.

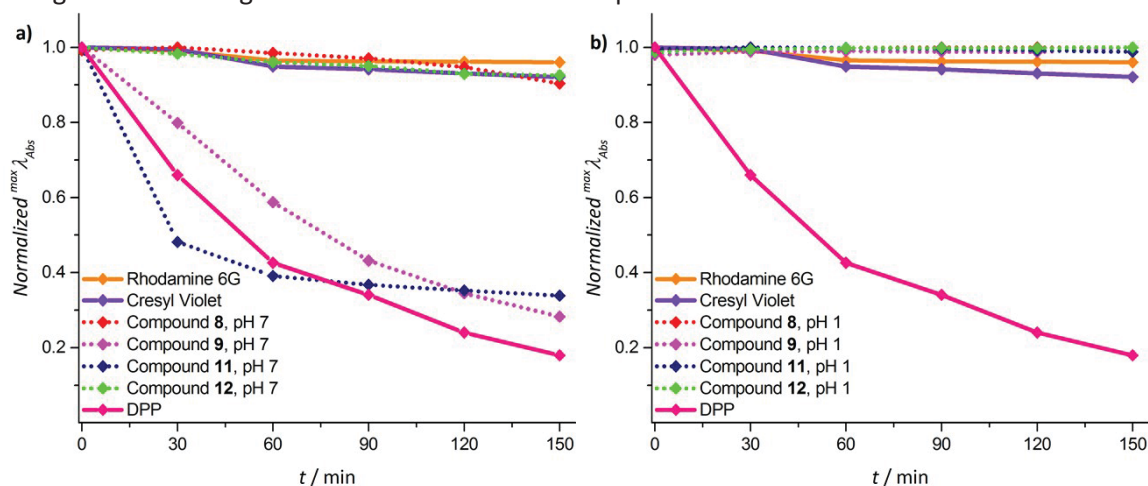


Figure S15. Photostability of sulfone-rhodols at pH 7 (a) and at pH 1 (b) (in H₂O containing 2% DMSO) compared to the Rhodamine 6G, Cresyl Violet and DPP (2,5-dibutyl-3,6-bis(3,4-dimethoxyphenyl)pyrrolo[3,4-c]pyrrole-1,4(2H,5H)-dione) in EtOH measured using a collimated light source from a 300W Xe lamp.

Stability experiments were not performed for compound **10** as it precipitated in course of the stability test.

Cell culture conditions

The rat embryonic cardiomyoblast-derived cell line H9C2 were cultured at 37°C in a humidified atmosphere containing 5% CO₂ in DMEM supplemented with 10% foetal bovine serum, 2 mM glutamine, 100 U/ml penicillin, and 100 g/ml streptomycin.

Fluorescence localization of **14** within the cells

The H9C2 cells were loaded with fluorophores in DMEM medium supplemented with 10% foetal bovine serum, 2 mM glutamine, 100 U/ml penicillin, and 100 g/ml streptomycin at 37°C in a humidified atmosphere containing 5% CO₂ for 15-30 minutes with the **14** compound at the final concentration ranging from 200 to 500 nM. The final concentration of the MitoTracker™ Green FM was 150 nM. Both fluorophores were dissolved in DMSO and for the loading were supplemented with 20% Pluronic-127. The final concentration of the Pluronic-127 was kept below 0.05% in the loading buffer. Before measurements, the incubation medium was replaced with FluoroBrite™ DMEM. The measurements were performed on Olympus IX83 confocal microscope with the water objective 60x UPLSAPO 60XW. The data were transferred to the ImageJ and prepared for presentation.

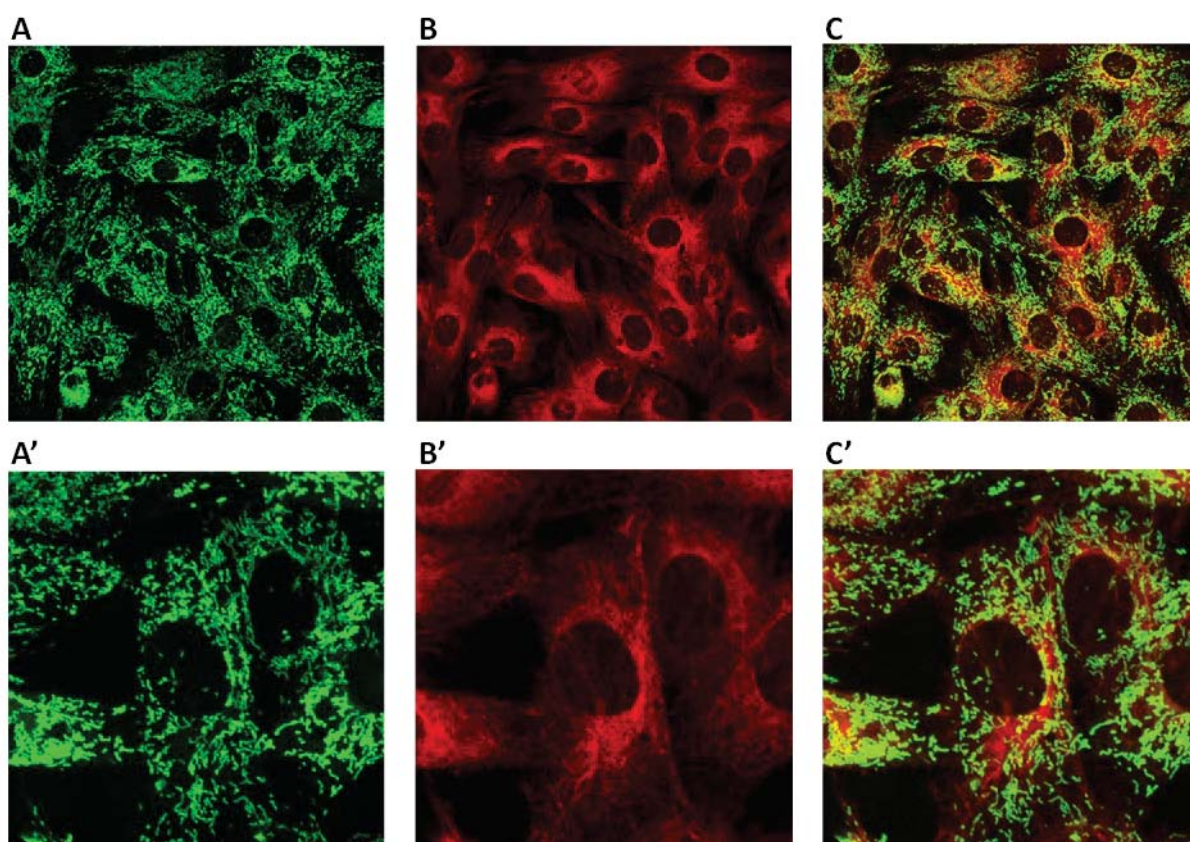


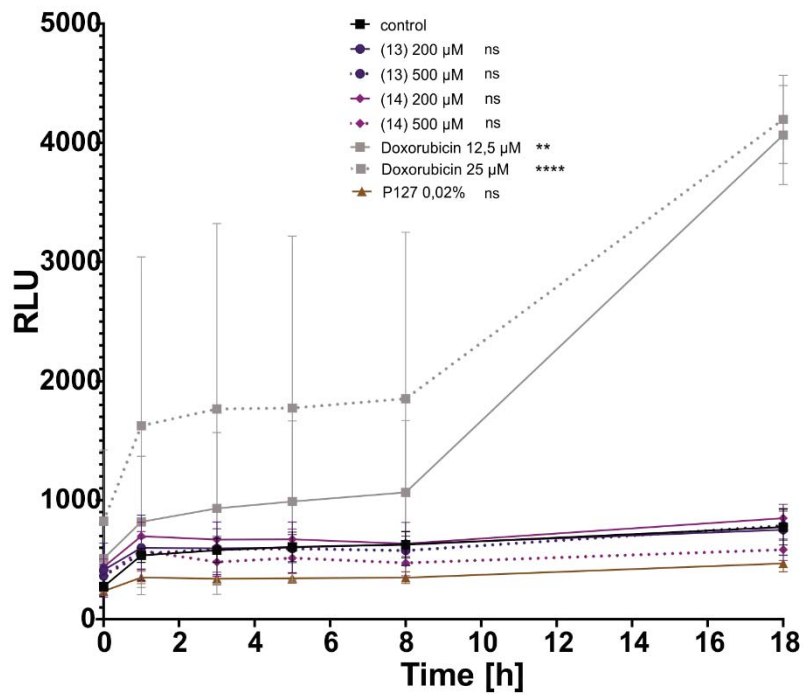
Figure S16. Intracellular localization of **13** compound as detected using confocal fluorescence microscopy. (A; A') The fluorescence of MitoTracker™ Green (green) as a well-established marker for

mitochondria, (B; B') the fluorescence of the **13** (red) recorded with 559 nm excitation wavelength and emission range 610–750 nm, (C; C') overlay picture recorded simultaneously for two fluorophore in living H9C2 cells line. A', B', C' pictures recorded for with higher magnification 3x.

Results

The dye **13** has a unlocalized distribution inside the H9C2 cells.

APOPTOSIS



NECROSIS

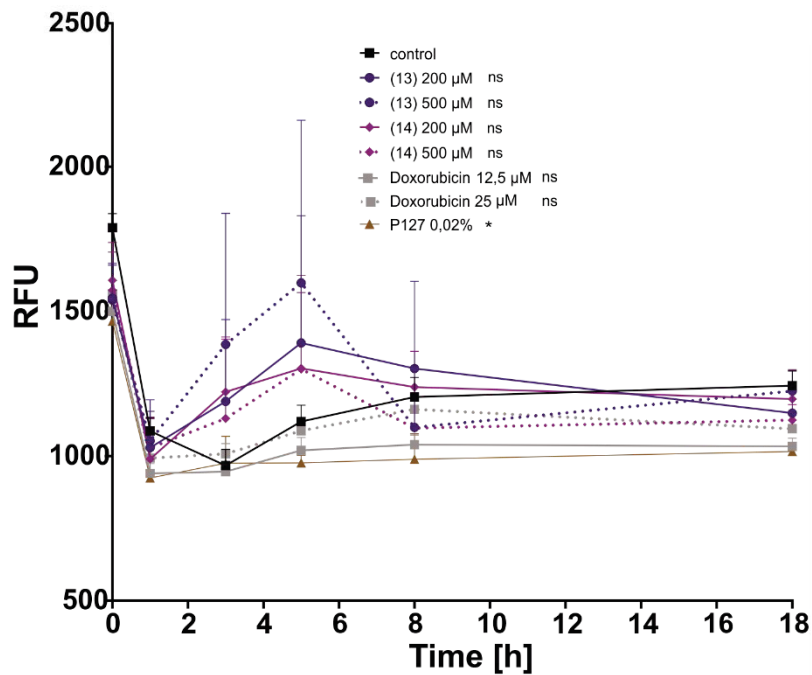


Figure S17. Effect of red emissive sulfonorhodols on apoptosis and necrosis of the H9C2 cells. Change in luminescence (RLU) as a measure of apoptosis and fluorescence (RFU) over the time. Statistical significance relative to the control was determined by two-way ANOVA with Tukey post-hoc test; $p > 0.05$ (ns), $p < 0.05$ (*), $p < 0.01$ (**), $p < 0.0001$ (****); $n = 9$

Methods

In order to determine the viability of cells under the influence of the tested red emissive sulfonorhodols **13** and **14**, an annexin V-based apoptosis and necrosis test (RealTime-Glo™ Annexin V Apoptosis and Necrosis Assay, Promega) was performed, allowing the simultaneous examination of the effect of the substances on the induction of apoptotic and necrotic cell death.

Materials

RealTime-Glo™ Annexin V Apoptosis and Necrosis Assay, Promega JA1011.


 Cite this: *Chem. Commun.*, 2022, **58**, 1542

 Received 8th December 2021,
 Accepted 31st December 2021

DOI: 10.1039/d1cc06924a

rsc.li/chemcomm

Direct transformation of coumarins into orange-red emitting rhodols†

 Kateryna V. Vygranenko,^a Yevgen M. Poronik,^a Manon H. E. Bousquet,^b Olena Vakuliuk,^a Denis Jacquemin^b *^b and Daniel T. Gryko^b *^a

The lactone carbonyl group of coumarin derivatives has been shown to participate in intramolecular Knoevenagel condensations, enabling the unprecedented direct transformation of coumarins into rhodols. The resulting rhodols, possessing two ester groups, have very intense orange-red fluorescence.

Rhodols are merocyanine dyes occupying an intermediate position between rhodamines and fluoresceins.¹ Recently they have been successfully utilized to build various sensors for intracellular fluorescence imaging, examination of neuronal excitability and visualization of metastases.^{2–6} Although various methods for the synthesis of rhodols and their analogues have been developed over the last decades they lack versatility and efficiency.^{7–12} In particular they are not compatible with certain functional groups being present on substrates.

To overcome these limits we envisioned an entirely new retrosynthetic disconnection relying on 3-formylcoumarins and dimethyl 1,3-acetonedicarboxylate, that may in principle lead to rhodols *via* double Knoevenagel condensation (Scheme 1). The direct inspiration for this endeavour was Prelog's work on the synthesis of benzene derivatives from aliphatic precursors.^{13,14} If successful this strategy would lead to heretofore unknown rhodols possessing two ester groups at positions 2 and 4.

Given the poor electrophilic properties of the carbon atom of the pyran-2-one heterocycle, Marchán and co-workers transformed coumarin into thionocoumarin in order to enable its further reaction with various nucleophiles.^{15,16} Our application of this approach for V-shaped bis-coumarin gave the corresponding rhodol in 30% yield (see the ESI,† Scheme S4).

This prompted us to attempt the direct one-pot transformation of 3-formylcoumarins into rhodols. Our initial experiments have proven that for the reaction of 7-diethylamino-3-formylcoumarin with dimethyl 1,3-acetonedicarboxylate, the double Knoevenagel condensation proceeds only in the presence of indium chloride¹⁷ and acetic anhydride. The yield of the expected product, however, was very low and its stability was poor due to the absence of any substituent at position 9 of the final rhodol. This position is subjected to nucleophilic attack by many nucleophiles, including water and methanol. Facing this obstacle we resolved to block the methine carbon atom with an *ortho*-substituted aryl group.¹² The additional advantage of this strategy is that the presence of a sterically hindered aryl group is known to be beneficial for increasing the fluorescence quantum yield of the resulting rhodol.^{12,18,19}

To implement this approach we developed a synthetic route towards 4-aryl-3-formylcoumarins. Triflated hydroxycoumarins **S1** and **S9** were subjected to Suzuki coupling to form coumarins **S2–S5** and **S10–S13** which were converted into two series of aldehydes **1**, **S6–S8** and **S14–S17** respectively (see the ESI,† Schemes S2 and S3).^{20,21}

The first attempts at performing the Knoevenagel condensation of formyl-coumarin **1** as a model substrate with dimethyl 1,3-acetonedicarboxylate (**2**) in the presence of InCl₃ and acetic acid anhydride resulted in the formation of the rhodol **4** in a very low yield accompanied by sizable quantity of intermediate **3** (Table 1 and Scheme 2). Various bases and Lewis acids in different solvents were trialled to improve this reaction (Table 1). Optimization resulted in finding that 2,6-lutidine is an optimal catalysts system

^a Institute of Organic Chemistry, Polish Academy of Sciences, Kasprzaka 44/52, 01-224 Warsaw, Poland. E-mail: dtgryko@icho.edu.pl

^b CEISAM Lab—UMR 6230, CNRS, University of Nantes, Nantes, France. E-mail: Denis.Jacquemin@univ-nantes.fr

 † Electronic supplementary information (ESI) available: Quantum chemical calculation and experimental data, synthetic procedures as well as, ¹H and ¹³C{¹H} NMR spectra. CCDC 2125095 and 2125096. For ESI and crystallographic data in CIF or other electronic format see DOI: 10.1039/d1cc06924a


Scheme 1 Retrosynthetic concept of the coumarin into rhodol transformation.

Communication

Table 1 Optimization of the synthesis of rhodol 4

Entry	Catalyst	Solvent	Temp. (°C)	Time (h)	Yield (%)
1	InCl ₃ , Ac ₂ O	<i>o</i> -DCB	140	18	1
2	EtONa	Neat	100	18	0
3	B(C ₆ F ₅) ₃	EtOH	rt	48	0
4	B(C ₆ F ₅) ₃	CH ₂ Cl ₂	rt	48	0
5	B(C ₆ F ₅) ₃	HFIP	rt	48	0
6	None	HFIP	rt	48	0
7	<i>t</i> -BuONa	Pyridine	60	18	18
8	2,6-Lutidine	Neat	100	18	26
9	2,6-Lutidine, mol. sieves	Neat	100	18	25

giving rise to the formation of rhodols 4 in 26% yield (Table 1, entry 8).

During the scope and limitations studies however, it turned out that for aldehyde **S6** possessing 2,6-dimethoxyphenyl substituent, these conditions fail resulting in the formation of only traces of rhodols 5. As the reaction workup is time consuming and the substrates are not easily accessible we performed a new set of optimization experiments estimating the formation of rhodols by the characteristic band ($\lambda_{\text{abs}} \approx 537$ nm) compared to $\lambda_{\text{abs}}(\mathbf{S6}) = 437$ nm and $\lambda_{\text{abs}}(\mathbf{S20}) = 448$ nm.²² The use of lutidine both as catalyst and solvent led to the formation of enormous amount of by-products making the purification challenging. Eventually we found that piperidine is an efficient catalyst for this double Knoevenagel condensation. Reaction of **S6** with ester **2** performed in methanol showed much cleaner formation of the desired product **5** under milder conditions compared to other experiments.

Changing the amount of diester **2** affects both kinetics and the conversion of substrates into rhodol **5**. Using a two-fold excess of **2** shows inefficient conversion, while 5-fold excess leads to much higher estimated yield of **5**. When 10 eq. of

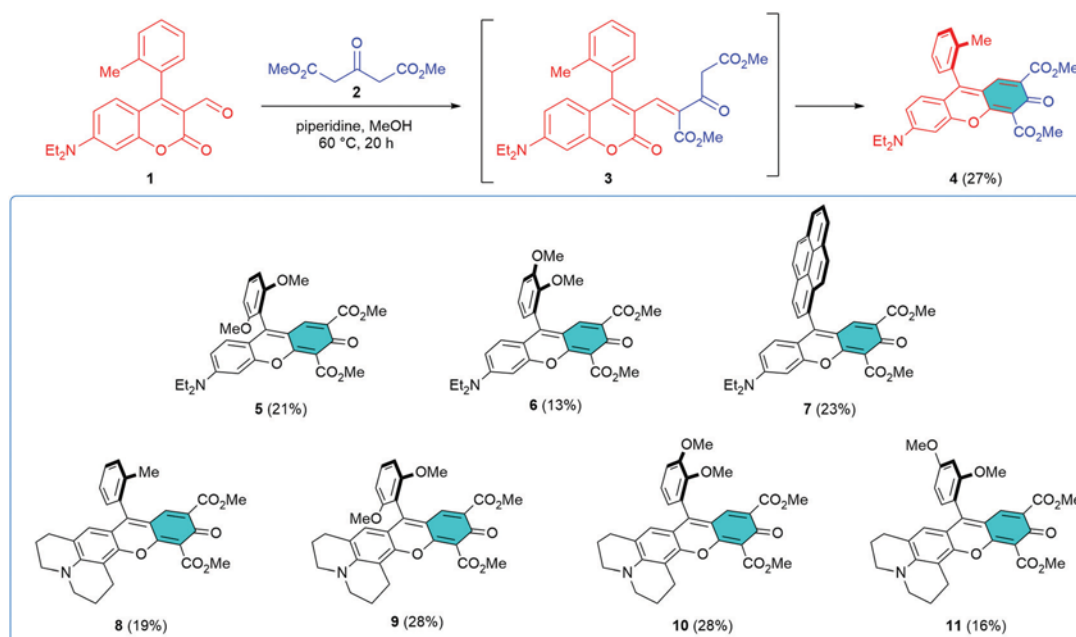
diester **2** were utilized, the formation of rhodol **5** was much faster and the most efficient, though longer reaction time caused a product decay. Consequently, we found that the conditions with 10-fold excess of **2** at 60 °C with the reaction time not exceeding 20 h were optimal.

Having optimized conditions in hand (10 eq. of ester **2**, 1 eq. of piperidine, MeOH, 60 °C, 20 h) we prepared the family of rhodols **4–11** from 2-aryl-3-formyl-coumarins and dimethyl 1,3-acetonedicarboxylate (Scheme 2). The yields of the desired products were in the range 13–39%.

We also resolved to study whether the condensation of 3-formyl coumarins **S18** and **S19** with diester **2** under the optimized conditions would also lead to the formation of corresponding rhodols with hydrogen and chlorine atoms at position 9, respectively. Surprisingly, two different products were formed possessing the same molecular mass. Notably X-ray diffraction analysis revealed that these two structurally related aldehydes lead to the formation of two unexpected products **12** and **13**, which originate from the reactivity of the position 4 of coumarin (Scheme 3).

Compound **12** shows absorption maxima at 418 nm and exhibits the strong emission response ($\lambda_{\text{em}} = 520$ nm, $\Phi_{\text{fl}} = 0.73$), while **13** has the absorption at 491 nm and shows the weak emission (Fig. S9 and Table S21 in the ESI†). The emission characteristics of dye **12** is comparable to other known benzo[*c*]coumarins.

The spectroscopic properties of the synthesized rhodols are typical of efficiently conjugated polymethine chromophores. Changing the solvent polarity hardly affects the position of the absorption maxima. Moreover, in the excited state rhodol molecules experience only small geometry changes evidenced by the negligible Stokes shifts, never exceeding 1000 cm⁻¹ (Table 2 and Fig. 1).



Scheme 2 Synthesis of rhodols **4–11** (10 eq. of ester **2**, 1 eq. of piperidine, MeOH, 60 °C, 20 h).



Scheme 3 The condensation of coumarins **S18** and **S19** with dimethyl-1,3-acetonedicarboxylate leading to dyes **12** and **13**.

Table 2 Photophysical data of rhodols **4–11** measured in solution

Dye	Solvent	$\epsilon \cdot 10^{-3}$ [$M^{-1} \text{cm}^{-1}$]	$\lambda_{\text{abs}}^{\text{max}}$ [nm]	$\lambda_{\text{em}}^{\text{max}}$ [nm]	Φ_{fl}	$\Delta\bar{\nu}$ [cm^{-1}]
4	CH ₂ Cl ₂	536 (70)	561	572	0.57 ^a	830
	DMSO	544 (73)	572	584	0.58 ^a	900
5	CH ₂ Cl ₂	537 (70)	566	576	0.65 ^a	950
	DMSO	547 (79)	576	588	0.68 ^a	920
6	CH ₂ Cl ₂	536 (81)	561	572	0.57 ^a	830
	DMSO	545 (86)	572	584	0.70 ^a	870
7	CH ₂ Cl ₂	540 (67)	567	578	0.47 ^a	880
	DMSO	548 (75)	578	589	0.63 ^a	950
8	CH ₂ Cl ₂	550 (83)	574	584	0.97 ^a	760
	DMSO	559 (85)	584	595	0.99 ^b	770
9	CH ₂ Cl ₂	552 (86)	579	589	1.00 ^a	840
	DMSO	562 (92)	589	600	0.98 ^b	820
10	CH ₂ Cl ₂	552 (71)	578	588	0.99 ^a	810
	DMSO	561 (74)	588	598	0.89 ^b	820
11	CH ₂ Cl ₂	551 (60)	575	585	0.86 ^a	760
	DMSO	559 (71)	585	595	0.91 ^b	800

^a Reference: Rhodamine 6G in EtOH ($\Phi_{\text{fl}} = 0.95$). ^b Reference: Sulforhodamine 101 in EtOH ($\Phi_{\text{fl}} = 0.95$).

Tethering the nitrogen atom (**8–11**) gives rise to a moderate red shift of the absorption maxima and to a significant growth of the fluorescence quantum yields (0.86–1.00) as this

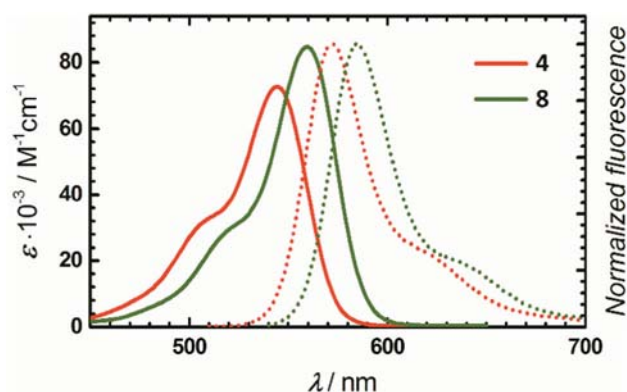


Fig. 1 Absorption (solid line) and normalized fluorescence (dotted line) spectra of rhodol **4** and **8** measured in DMSO. Legend specifies colours of lines.

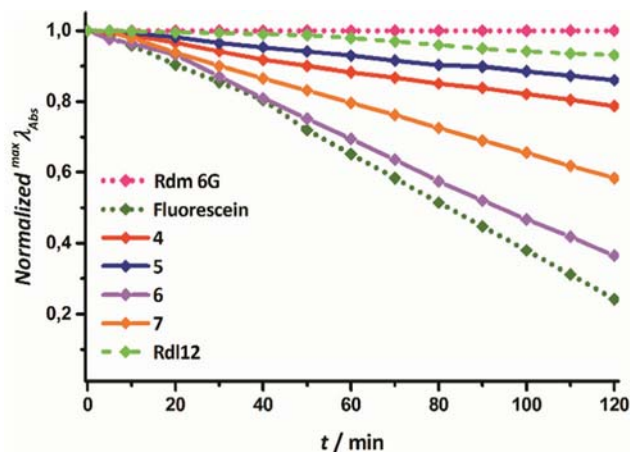


Fig. 2 Photostability of rhodols **4–7** compared to the **Rhodamine 6G** in EtOH, **Fluorescein** in 0.1 M NaOH aqueous solution and **Rh12** (for structure see ESI† Fig. S10) measured in DMSO using a collimated light source from a 300W Xe lamp. Legend specifies colours of lines.

diminishes the possibility of radiationless relaxation pathways compared to rhodols **4–7** bearing diethylamino fragments. In turn, the aryl moieties impact neither the absorption/emission maxima nor fluorescence quantum yield. Referencing known rhodol chromophores,^{1,23} introduction of the two ester groups only has a minor influence on the spectroscopic properties leading to 10–15 nm bathochromic shifts.

The photostability of **8–11** in DMSO is much lower than that of dyes **4–7**. Surprisingly all rhodols **4–11** are much less photostable in CH₂Cl₂ and after 15–30 min the absorption maxima are shifted in a blue region (Fig. 2, Fig. S11 and S12 in the ESI†).

We have performed theoretical calculations to explore the photophysical properties of dyes **4–11**. First, we found that TD-DFT overshoots the 0–0 energies as compared to experiment observations, a typical trend in cyanine derivatives, and that this trend can be corrected with ADC(2).²⁴

Both TD-DFT and ADC(2) nevertheless recover the slight redshift of the absorption and emission bands when going from series **4–7** to **8–11** (see the ESI†). The typical band shape of cyanine derivatives is also restored by the calculations, together with an ϵ in the correct experimental range (see the ESI†). The excited state topologies of **4** and **8** in the form of density difference plots shown on Fig. 3, demonstrate that the amino group acts as a donor, whereas the central moiety of the rhodols is an accepting unit. Consistent with the small impact of the substituent of the substitution of the benzene ring noticed experimentally (Table 2), this orthogonal ring does not play any role in the excited state. Interestingly, the rhodols were found to be strongly polarized, with *e.g.*, ground state dipole moments of 16.4 and 17.7 D for **4** and **8**, respectively, but this dipole only increases very slightly in the excited state (19.4 and 20.4 D, respectively), indicating a very small charge-transfer nature in these systems. Eventually, for the most rigid rhodols **8–11**, we have computed the radiative and internal conversion rate constants from first principles. For **8**, we obtain a k_{r} of $3.4 \cdot 10^8 \text{ s}^{-1}$, and a k_{ic} of $1.5 \cdot 10^8 \text{ s}^{-1}$, leading to an

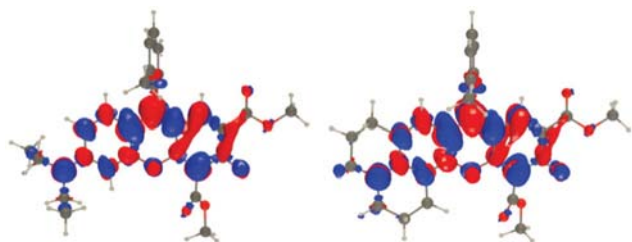


Fig. 3 Density difference plots for the three lowest transitions of **4** (left) and **8** (right). The crimson and blueberry lobes indicate an increase and decrease of density upon excitation, respectively. Contour threshold: 0.001 au.

estimated quantum yield of 70%, a very large value consistent with the experimental trends. The value of k_{ic} is small given the emission wavelength of the considered systems. As noticed in the measurements, these large values are maintained in the **8–11** series.

In summary a method offering a practical and atom-economic access to novel rhodols has been discovered. The key step in this synthesis involves the carbonyl group of a lactone, originating from a coumarin scaffold, participating in an intramolecular Knoevenagel condensation²⁵ allowing for the production of rhodols in a one-pot, two-step process. Novel rhodols are strongly emissive with a λ_{em} range of 560–590 nm. This programmed strategy is compatible with a broader range of substituents than traditional synthetic approaches based on Friedel–Crafts acylation.

Conceptualization: D. T. G. and K. V.; investigation: K. V. V., Y. M. P., M. H. E. B., O. V.; supervision: D. T. G.; visualization: K. V. V., Y. M. P.; calculation: D. J.; writing – original draft: K. V. V., Y. M. P., D. J.; D. T. G.; writing – review & editing: D. T. G.

The work was financially supported by the Polish National Science Centre, Poland (HARMONIA 2018/30/M/ST5/00460), the Foundation for Polish Science (TEAM POIR.04.04.00-00-3CF4/16-00). This project received funding from European Union's Horizon 2020 research and innovation programme under Grant Agreement No 860762. The authors also thank Dr David C. Young for proofreading the manuscript. M. H. E. and D. J. thank the CCIPL computational center installed in Nantes for generous allocation of computational time.

Conflicts of interest

There are no conflicts to declare.

Notes and references

- 1 Y. M. Poronik, K. V. Vygranenko, D. Gryko and D. T. Gryko, *Chem. Soc. Rev.*, 2019, **48**, 5242–5265.
- 2 D. Asanuma, M. Sakabe, M. Kamiya, K. Yamamoto, J. Hiratake, M. Ogawa, N. Kosaka, P. L. Choyke, T. Nagano, H. Kobayashi and Y. Urano, *Nat. Commun.*, 2015, **6**, 1–7.
- 3 R. U. Kulkarni, D. J. Kramer, N. Pourmandi, K. Karbasi, H. S. Bateup and E. W. Miller, *Proc. Natl. Acad. Sci. U. S. A.*, 2017, **114**, 2813–2818.
- 4 S. Chen, X. Zhao, J. Chen, J. Chen, L. Kuznetsova, S. S. Wong and I. Ojima, *Bioconjugate Chem.*, 2010, **21**, 979–987.
- 5 T. Doura, M. Kamiya, F. Obata, Y. Yamaguchi, T. Y. Hiyama, T. Matsuda, A. Fukamizu, M. Noda, M. Miura and Y. Urano, *Angew. Chem., Int. Ed.*, 2016, **55**, 9620–9624.
- 6 A. A. Contractor and E. W. Miller, *Biochemistry*, 2018, **57**, 237–240.
- 7 Y. M. Poronik, M. P. Shandura and Y. P. Kovtun, *Dyes Pigm.*, 2007, **72**, 199–207.
- 8 R. R. Sauers, S. N. Husain, A. P. Piechowski and G. R. Bird, *Dyes Pigm.*, 1987, **8**, 35–53.
- 9 T. Peng and D. Yang, *Org. Lett.*, 2010, **12**, 496–499.
- 10 M. Dai, Y. J. Reo, C. W. Song, Y. J. Yang and K. H. Ahn, *Chem. Sci.*, 2020, **11**, 8901–8911.
- 11 G. S. Ghotekar, A. C. Shaikh and M. Muthukrishnan, *J. Org. Chem.*, 2019, **84**, 2269–2276.
- 12 M. Grzybowski, M. Taki and S. Yamaguchi, *Chem. – Eur. J.*, 2017, **23**, 13028–13032.
- 13 V. Prelog, L. Ruzicka and O. Metzler, *Helv. Chim. Acta*, 1947, **30**, 1883–1895.
- 14 L. Ruzicka, V. Prelog and J. Battegay, *Helv. Chim. Acta*, 1948, **31**, 1296–1301.
- 15 A. Gandioso, M. Palau, R. Bresoli-Obach, A. Galindo, A. Rovira, M. Bosch, S. Nonell and V. Marchán, *J. Org. Chem.*, 2018, **83**, 11519–11531.
- 16 A. Gandioso, R. Bresoli-Obach, A. Nin-Hill, M. Bosch, M. Palau, A. Galindo, S. Contreras, A. Rovira, C. Rovira, S. Nonell and V. Marchán, *J. Org. Chem.*, 2018, **83**, 1185–1195.
- 17 Y. Ogiwara, K. Takahashi, T. Kitazawa and N. Sakai, *J. Org. Chem.*, 2015, **80**, 3101–3110.
- 18 S. S. Patil, K. G. Thorat, R. Mallah and N. Sekar, *J. Fluoresc.*, 2016, **26**, 2187–2197.
- 19 L. Geng, X. F. Yang, Y. Zhong, Z. Li and H. Li, *Dyes Pigm.*, 2015, **120**, 213–219.
- 20 L. Schmidt, T. Doroshenko, P. Barbie, A. Grüter, G. Jung and U. Kazmaier, *Synthesis*, 2016, 3077–3086.
- 21 R. S. Coleman and M. L. Madaras, *J. Org. Chem.*, 1998, **63**, 5700–5703.
- 22 G. R. Geier, J. A. Riggs and J. S. Lindsey, *J. Porphyrins Phthalocyanines*, 2001, **05**, 681–690.
- 23 Y. M. Poronik, G. Clermont, M. Blanchard-Desce and D. T. Gryko, *J. Org. Chem.*, 2013, **78**, 11721–11732.
- 24 B. Le Guennic and D. Jacquemin, *Acc. Chem. Res.*, 2015, **48**, 530–537.
- 25 D. R. Caldwell, S. M. Usama and M. J. Schnermann, *Org. Lett.*, 2021, **23**, 8857–8861.

Supporting information

Direct transformation of coumarins into orange-red emitting rhodols

Kateryna V. Vygranenko,^a Yevgen M. Poronik,^a Manon H. E. Bousquet,^b Olena Vakuliuk,^a Denis Jacquemin^{*b} and Daniel T. Gryko^{*a}

- a. *Institute of Organic Chemistry, Polish Academy of Sciences, Kasprzaka 44/52, 01-224 Warsaw, Poland. E-mail: dtgryko@icho.edu.pl.*
- b. *CEISAM Lab—UMR 6230, CNRS, University of Nantes, Nantes, France. E-mail : Denis.Jacquemin@univ-nantes.fr*

Table of Contents

Instrumentation and Materials	S1
Optimization of reaction conditions for the rhodol synthesis	S2
Experimental Part.....	S5
¹ H and ¹³ C NMR Spectra	S20
X-Ray data for compounds 12 and 13	S48
Absorption and emission spectra of compounds 4-13	S71
Photostability measurements	S74
Theoretical methods	S76
Notes and references	S79

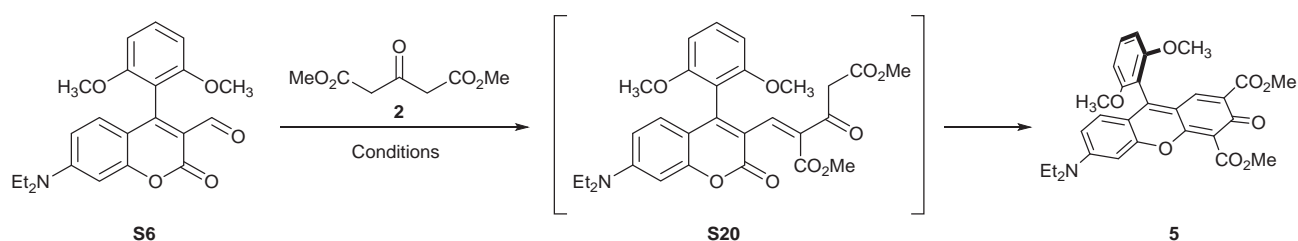
Instrumentation and Materials

All chemicals were used as received unless otherwise noted. All reported ¹H and ¹³C NMR spectra were collected using 500 MHz and 600 MHz spectrometers. Chemical shifts (δ ppm) were determined with TMS as the internal reference; *J* values are given in Hz. Chromatography was performed on silicagel (230-400 mesh). Preparative thin layer chromatography (TLC) was carried out using Merck PLC Silica gel 60 F₂₅₄ 1 mm plates. The mass spectra were obtained via electron ionization (EI-MS) or electrospray ionization (ESI-MS). All photophysical studies have been performed with freshly-prepared air-equilibrated solutions at room temperature (298 K).

A Shimadzu UV-3600i Plus spectrophotometer and an Edinburgh Instruments Spectrofluorometer FS5 equipped with Hamamatsu R13456 PMT were used to acquire the absorption and emission spectra. Spectrophotometric grade solvents were used without further purification. Fluorescence quantum yields were determined in CH₂Cl₂ and DMSO using Rhodamine 6G in EtOH and sulforhodamine SR101 (for measurements of compounds **8-11** in DMSO) as standards. Photostability was determined using an Asahi Spectra Max-350 as a light source and Shimadzu UV-3600i Plus spectrophotometer.

Optimization of reaction conditions for the rhodol synthesis

As a model reaction we chose the formation of rhodol **5** from coumarin aldehyde **S6** through intermediate **S20** (Scheme S2)



Scheme S1. The formation rhodol **5** from coumarin aldehyde **S6**.

Optical absorption measurement was chosen as a convenient instrumental method for the rhodol formation. The samples of coumarin aldehyde substrate were weighed with a 10⁻² mg precision, that allows keeping the concentration of the substrate within the same range for all optimization experiments. First we determined molar absorptivity (ϵ) of coumarin aldehyde substrate, the intermediate and the rhodol product (Fig. S1). The concentration (c) of the substrate and the reaction product was calculated based on the Beer–Lambert law (Eq. 1), where A is absorbance and l is optical path length in cm:

$$A = \epsilon lc \quad (1)$$

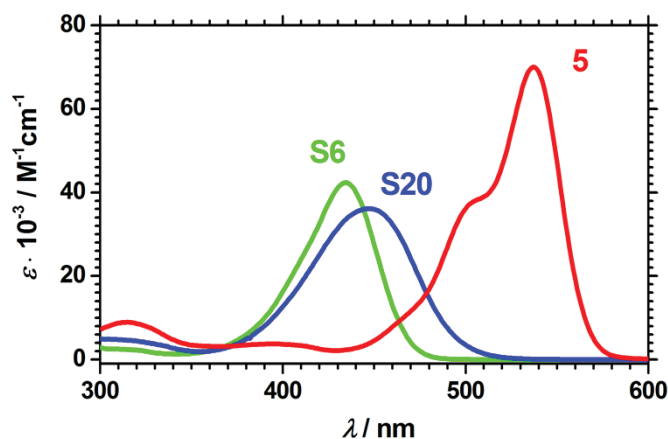


Figure S1. The absorption spectrum for **S6**, **S20** and **5** in CH_2Cl_2 .

The standard procedure for all optimization experiments was chosen as follows:

Coumarin aldehyde (1mg) was dissolved in 1 mL of an appropriate solvent with a certain excess of **2** in the presence of basic catalyst at certain conditions. To check the concentration an 20 μL aliquot was taken from the reaction mixture and diluted to 5 mL with CH_2Cl_2 . The absorption at the maxima was taken into account to calculate the concentration and the reaction yield of rhodol. Before the experiment started the exact amount of coumarin substrate was determined. In course of the reaction the concentrations of coumarin substrate and rhodol were monitored at equal time periods specified for each experiments. A dependence of the reaction yield on time allowed us finding optimal conditions for this type of transformation (Fig. S2).

To eliminate misinterpretations in the analysis of experiments we consider both spectroscopic data and TLC as in a number of experiments side reaction occurred that distorted the absorption data. For instance, all experiments in acetic anhydride as a solvent led to a formation of side products that has absorption in the same range as rhodol **5**, though rhodol formed very fast. We observed the similar situation for tests performed in pyridine or quinoline. The reactions were not efficient, besides that side products formed.

Studying model reaction in methanol in the presence of 1 eq. of piperidine we found that the use of 10eq. of dimethylacetondicarboxylate **2** leads to efficient conversion towards rhodol **5** with a minimum of side reactions, though due to the presence of little amount of side products having absorption at the spectral range of rhodol the reaction yield was overestimated (Fig. S2).

Using this method we have studied other rhodol formation to find the standard synthetic procedure. The chosen examples of the dependencies are shown in Fig. S2.

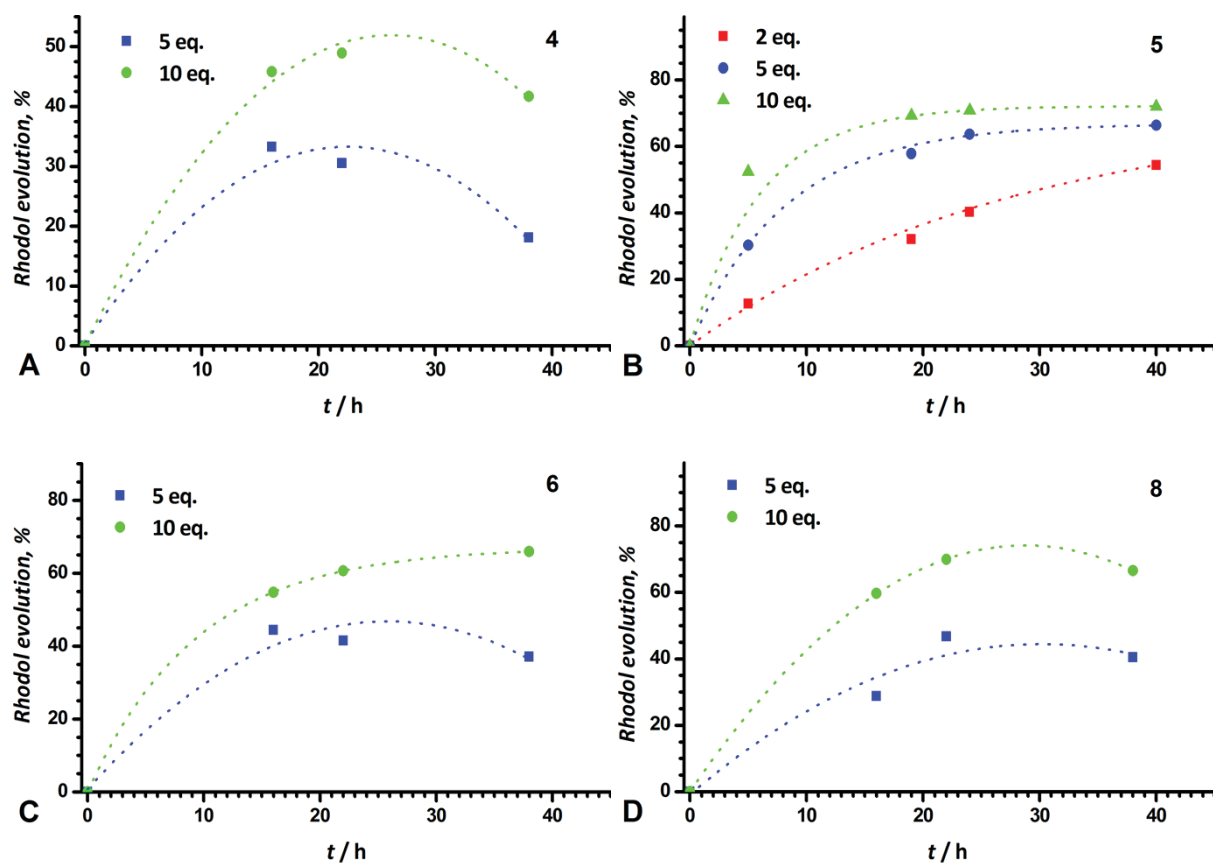
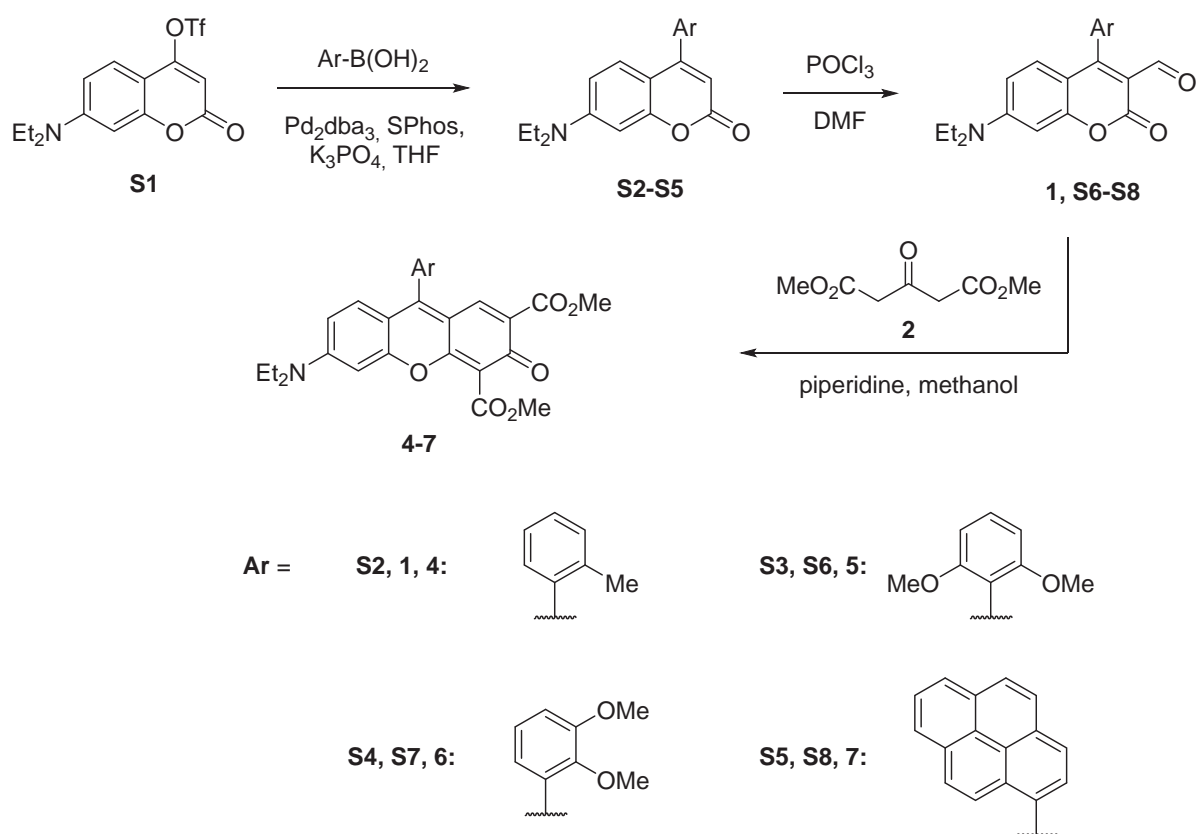


Figure S2. The optimization for the rhodols synthesis (A: Rhodol 4; B: Rhodol 5; C: Rhodol 6; B: Rhodol 8.). The rhodol evolution at using different excess of 2 based on the absorption at the correspondent absorption maxima. The intensity of rhodol signal is overestimated due to residual absorption of contaminants in this region.

Experimental part

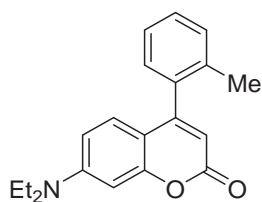


Scheme S2. Synthetic route from coumarin **S1** to rhodols **4-7**.

General procedure for the preparation of compounds **S2-S5**.

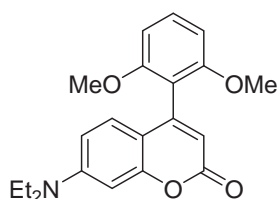
Compound **S1** (10 mmol), arylboronic acid (15 mmol), bis(dibenzylideneacetone)-palladium(0) (0,25 mmol), 2-dicyclohexylphosphino-2',6'-dimethoxybiphenyl (SPhos) (0,75 mmol) and tribasic potassium phosphate (40 mmol) were placed under Ar in a flame-dried Schlenk flask. Dry and degassed THF (50 ml) was added and the reaction mixture was stirred at 70°C for 4h under inert atmosphere. After the reaction was complete the mixture was diluted with DCM, filtered through celite and washed with NaHCO₃ solution (3 × 150 ml). The organic layer was dried over Na₂SO₄ and concentrated under vacuo. The residue was purified using column chromatography (hexane : EtOAc 1:1 + 1% AcOH).

Compound **S2**. Yield 97%. M.p. 95-96°C



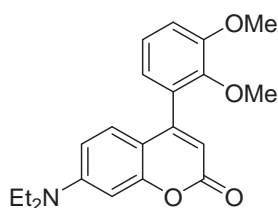
^1H NMR (500 MHz, CDCl_3) δ 7.35 (m, 1H, H-Ar), 7.32 – 7.27 (m, 2H, H-Ar), 7.16 (dd, $J = 7.5, 1.5$ Hz, 1H, H-Ar), 6.82 (d, $J = 9.0$ Hz, 1H, H-Ar), 6.56 (d, $J = 2.6$ Hz, 1H, H-Ar), 6.45 (dd, $J = 9.0, 2.6$ Hz, 1H, H-Ar), 5.94 (s, 1H, C-H), 3.40 (q, $J = 7.1$ Hz, 4H, CH_2), 2.18 (s, 3H, CH_3 -Ar), 1.20 (t, $J = 7.1$ Hz, 6H, CH_3); ^{13}C NMR (126 MHz, CDCl_3) δ 162.2, 156.4 (2), 150.7, 135.8, 135.3, 130.3, 128.7, 128.3, 127.8, 125.8, 108.8, 108.6, 108.5, 97.6, 44.7, 19.7, 12.4; HRMS (ESI) calc. for $\text{C}_{20}\text{H}_{21}\text{NO}_2\text{Na}$ 330.1470 $[\text{M} + \text{Na}]^+$, found 330.1465.

Compound **S3**. Yield 76%. M.p. 136-138°C



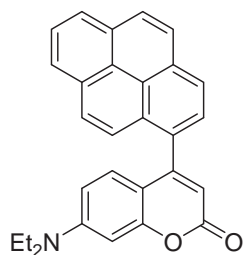
^1H NMR (500 MHz, CDCl_3) δ 7.36 (t, $J = 8.4$ Hz, 1H, H-Ar), 6.85 (d, $J = 8.9$ Hz, 1H, H-Ar), 6.66 (d, $J = 8.4$ Hz, 2H, H-Ar), 6.55 (d, $J = 2.5$ Hz, 1H, H-Ar), 6.45 (d, $J = 8.9$ Hz, 1H, H-Ar), 5.98 (s, 1H, C-H), 3.71 (s, 6H, OCH_3), 3.39 (q, $J = 7.1$ Hz, 4H, CH_2), 1.19 (t, $J = 7.1$ Hz, 6H, CH_3); ^{13}C NMR (126 MHz, CDCl_3) δ 162.6, 157.6, 156.3, 150.4, 130.3, 127.4, 113.5, 111.0, 109.2, 108.3, 104.0, 99.7, 55.9, 44.8, 12.5; HRMS (ESI) calc. for $\text{C}_{21}\text{H}_{23}\text{NO}_4\text{Na}$ 376.1525 $[\text{M} + \text{Na}]^+$, found 376.1535.

Compound **S4**. Yield 92%. M.p. 123-124°C



^1H NMR (500 MHz, CDCl_3) δ 7.14 (t, $J = 7.9$ Hz, 1H, Ar), 7.05 – 6.98 (m, 2H, Ar), 6.81 (dd, $J = 7.6, 1.6$ Hz, 1H, Ar), 6.58 (d, $J = 2.5$ Hz, 1H, Ar), 6.53 – 6.47 (m, 1H, Ar), 6.04 (s, 1H, C-H), 3.93 (s, 3H, OCH_3), 3.67 (s, 3H, OCH_3), 3.40 (q, $J = 7.1$ Hz, 4H, CH_2), 1.20 (t, $J = 7.1$ Hz, 6H, CH_3); ^{13}C NMR (126 MHz, CDCl_3) δ 162.2, 156.3, 153.7, 152.9, 150.6, 146.3, 130.6, 128.9, 124.2, 121.6, 113.1, 109.1, 108.5, 108.4, 97.4, 61.3, 55.9, 44.7, 12.4; HRMS (ESI) calc. for $\text{C}_{21}\text{H}_{23}\text{NO}_4\text{Na}$ 376.1525 $[\text{M} + \text{Na}]^+$, found 376.1532.

Compound **S5**. Yield 86%. M.p. 130-131°C

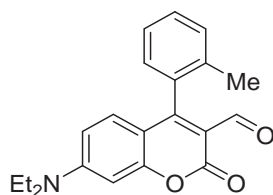


^1H NMR (500 MHz, CDCl_3) δ 8.28 – 8.22 (m, 2H, Ar), 8.19 (dd, $J = 7.6, 1.2$ Hz, 1H, Ar), 8.18 – 8.10 (m, 2H, Ar), 8.07 – 7.99 (m, 2H, Ar), 7.95 – 7.89 (m, 2H, Ar), 6.75 (d, $J = 9.1$ Hz, 1H, Ar), 6.64 (d, $J = 2.6$ Hz, 1H, Ar), 6.33 (dd, $J = 9.1, 2.6$ Hz, 1H, Ar), 6.24 (s, 1H, C-H), 3.39 (q, $J = 7.1$ Hz, 4H, CH_2), 1.19 (t, $J = 7.1$ Hz, 6H, CH_3); ^{13}C NMR (126 MHz, CDCl_3) δ 162.1, 156.5, 155.9, 150.8, 131.7, 131.3, 130.8, 128.6, 128.5, 128.2, 127.2, 126.3 (2), 125.7, 125.5, 124.7, 124.6 (2), 110.4, 109.5, 108.6, 97.6, 44.8, 12.4; HRMS (ESI) calc. for $\text{C}_{29}\text{H}_{23}\text{NO}_2\text{Na}$ 440.1626 $[\text{M} + \text{Na}]^+$, found 440.1613.

General procedure for the preparation of compounds **1**, **S6-S8**.

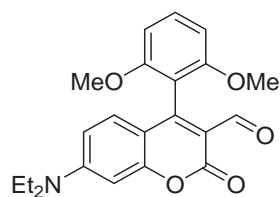
Phosphorus oxychloride (7,7 mmol) was added dropwise to a solution of 7-diethylamino-4-aryl-coumarin (**S2-S5**) (5 mmol) in DMF (15 ml) upon cooling on ice. The reaction mixture was allowed to stir at 50°C for 24h. The solution then was cooled to room temperature, poured into NaHCO_3 aqueous solution (20 g in 100 ml H_2O) with 300 ml of crashed ice. The precipitate which formed was filtered, washed with distilled water, dried under vacuum and purified via recrystallization from hexane + 2-propanol.

Compound **1**. Yield 60%. M.p. $160\text{-}161^\circ\text{C}$



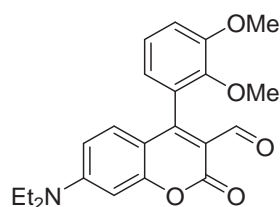
^1H NMR (500 MHz, CDCl_3) δ 9.83 (s, 1H, CHO), 7.39 (td, $J = 7.5, 1.4$ Hz, 1H, H-Ar), 7.35 – 7.26 (m, 2H, H-Ar), 7.06 (dd, $J = 7.5, 1.4$ Hz, 1H, H-Ar), 6.80 (d, $J = 9.2$ Hz, 1H, H-Ar), 6.52 (d, $J = 2.6$ Hz, 1H, H-Ar), 6.48 (dd, $J = 9.2, 2.6$ Hz, 1H, H-Ar), 3.45 (q, $J = 7.1$ Hz, 4H, CH_2), 2.10 (s, $J = 2.4$ Hz, 3H, $\text{CH}_3\text{-Ar}$), 1.23 (t, $J = 7.1$ Hz, 6H, CH_3); ^{13}C NMR (126 MHz, CDCl_3) δ 188.2, 162.0, 160.0, 157.8, 153.2, 135.1, 133.0, 130.5, 130.1, 128.9, 127.6, 125.8, 112.2, 109.8, 108.7, 97.0, 45.1, 19.4, 12.4; HRMS (ESI) calc. for $\text{C}_{21}\text{H}_{21}\text{NO}_3\text{Na}$ 358.1419 $[\text{M} + \text{Na}]^+$, found 358.1415.

Compound **S6**. Yield 50%. M.p. $213\text{-}215^\circ\text{C}$



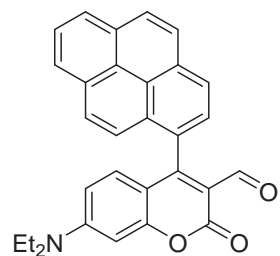
^1H NMR (500 MHz, CDCl_3) δ 9.81 (s, 1H, CHO), 7.41 (t, $J = 8.4$ Hz, 1H, H-Ar), 6.92 (d, $J = 9.1$ Hz, 1H, H-Ar), 6.67 (d, $J = 8.4$ Hz, 2H, H-Ar), 6.52 – 6.44 (m, 2H, H-Ar), 3.69 (s, 6H, OCH_3), 3.43 (q, $J = 7.1$ Hz, 4H, CH_2), 1.22 (t, $J = 7.1$ Hz, 6H, CH_3); ^{13}C NMR (126 MHz, CDCl_3) δ 188.7, 160.2, 157.7, 157.4, 157.1, 152.9, 130.9, 129.9, 113.4, 110.3, 109.4, 109.0, 103.9, 96.9, 55.9, 45.0, 12.5; HRMS (ESI) calc. for $\text{C}_{22}\text{H}_{23}\text{NO}_5\text{Na}$ 404.1474 $[\text{M} + \text{Na}]^+$, found 404.1486.

Compound **S7**. Yield 28%. M.p. 163-164°C



^1H NMR (500 MHz, CDCl_3) δ 9.98 (s, 1H, CHO), 7.16 (t, $J = 7.9$ Hz, 1H, H-Ar), 7.05 (d, $J = 8.2$ Hz, 1H, H-Ar), 6.93 (d, $J = 9.1$ Hz, 1H, H-Ar), 6.66 (d, $J = 7.6$ Hz, 1H, H-Ar), 6.53 – 6.45 (m, 2H, H-Ar), 3.94 (s, 3H, OCH_3), 3.67 (s, 3H, OCH_3), 3.43 (q, $J = 7.1$ Hz, 4H, CH_2), 1.22 (t, $J = 7.1$ Hz, 6H, CH_3); ^{13}C NMR (126 MHz, CDCl_3) δ 188.4, 160.5, 158.8, 157.6, 153.0, 152.7, 145.7, 130.9, 128.0, 124.2, 120.7, 113.1, 112.5, 109.7, 109.2, 97.0, 60.9, 55.8, 45.1, 12.4; HRMS (ESI) calc. for $\text{C}_{22}\text{H}_{23}\text{NO}_5\text{Na}$ 404.1474 $[\text{M} + \text{Na}]^+$, found 404.1479.

Compound **S8**. Yield 80%. M.p. 169-171°C

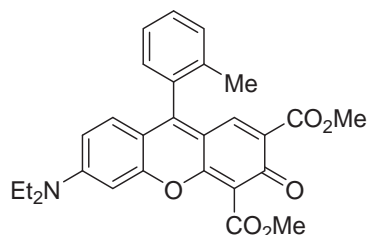


^1H NMR (500 MHz, CDCl_3) δ 9.79 (s, 1H, CHO), 8.30 - 8.22 (m, 2H, H-Ar), 8.21 – 8.12 (m, 3H, H-Ar), 8.04 (t, $J = 7.6$ Hz, 1H, H-Ar), 8.01 (d, $J = 9.1$ Hz, 1H, H-Ar), 7.83 (d, $J = 7.8$ Hz, 1H, H-Ar), 7.72 (d, $J = 9.1$ Hz, 1H, H-Ar), 6.63 – 6.55 (m, 2H, H-Ar), 6.30 (dd, $J = 9.3, 2.6$ Hz, 1H, H-Ar), 3.41 (q, $J = 7.1$ Hz, 4H, CH_2), 1.19 (t, $J = 7.1$ Hz, 6H, CH_3); ^{13}C NMR (126 MHz, CDCl_3) δ 188.0, 161.4, 160.0, 157.8, 153.2, 131.8, 131.3, 131.2, 130.8, 128.8, 128.7, 128.3, 128.0, 127.3, 126.4, 125.9 (2), 125.7, 124.5 (3), 124.1, 113.6, 109.9, 109.8, 97.0, 45.2, 12.4; HRMS (ESI) calc. for $\text{C}_{30}\text{H}_{24}\text{NO}_3$ 446.1756 $[\text{M} + \text{H}]^+$, found 446.1761.

General procedure for the preparation of compounds **4-7**.

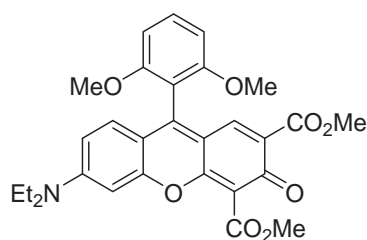
Aldehyde (**1**, **S6-S8**) (1 mmol), dimethyl-1,3-acetonedicarboxylate (**2**) (10 mmol) and piperidine (1 mmol) were dissolved in methanol (3 ml) and allowed to stir at 60°C for 20h. The solvent was evaporated and the residue was washed with diethyl ether. The crude product was purified via column chromatography (CH₂Cl₂ : MeOH 93:7).

Compound **4**. Yield 28%. M.p. 258-260°C



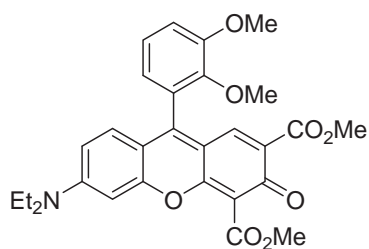
¹H NMR (500 MHz, CDCl₃) δ 7.52 (s, 1H, H-Ar), 7.45 (td, *J* = 7.6, 1.4 Hz, 1H, H-Ar), 7.4 – 7.33 (m, 2H, H-Ar), 7.12 (d, *J* = 7.5 Hz, 1H, H-Ar), 6.90 (d, *J* = 9.1 Hz, 1H, H-Ar), 6.62 – 6.55 (m, 2H, H-Ar), 4.01 (s, 3H, OCH₃), 3.81 (s, 3H, OCH₃), 3.50 (q, *J* = 7.3 Hz, 4H, CH₂), 2.06 (s, 3H, CH₃ - Ar), 1.26 (t, *J* = 7.1 Hz, 6H, CH₃); ¹³C NMR (126 MHz, CDCl₃) δ 176.7, 167.1, 166.4, 156.2, 155.6, 155.3, 153.6, 136.0, 135.1, 132.1, 130.7 (2), 129.7, 129.0, 128.2, 126.1, 113.0, 112.1, 111.1, 110.9, 96.9, 52.3, 52.2, 45.3, 19.6, 12.6; HRMS (ESI) calc. for C₂₈H₂₈NO₆ 474.1917 [M + H]⁺, found 474.1903.

Compound **5**. Yield 21%. M.p. 217-218°C



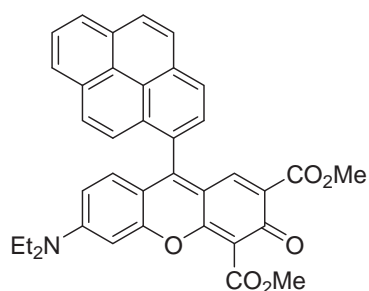
¹H NMR (500 MHz, CDCl₃) δ 7.61 (s, 1H, H-Ar), 7.51 – 7.41 (t, *J* = 8.4 Hz, 1H, H-Ar), 7.02 – 6.96 (m, 1H, H-Ar), 6.73 – 6.67 (m, 2H, H-Ar), 6.59 – 6.53 (m, 2H, H-Ar), 4.00 (s, 3H, OCH₃), 3.82 (s, 3H, OCH₃), 3.66 (s, 6H, OCH₃), 3.48 (q, *J* = 7.1 Hz, 4H, CH₂), 1.25 (t, *J* = 7.1 Hz, 6H, CH₃); ¹³C NMR (126 MHz, CDCl₃) δ 176.8, 167.5, 166.7, 157.7, 156.3, 156.0, 153.4, 151.3, 135.8, 131.6, 130.4, 127.5, 113.3, 112.5, 111.5, 110.8, 109.5, 104.1, 96.7, 55.9, 52.2, 52.0, 45.1, 12.6; HRMS (ESI) calc. for C₂₉H₃₀NO₈ 520.1971 [M + H]⁺, found 520.1978.

Compound **6**. Yield 13%. M.p. 210-211°C

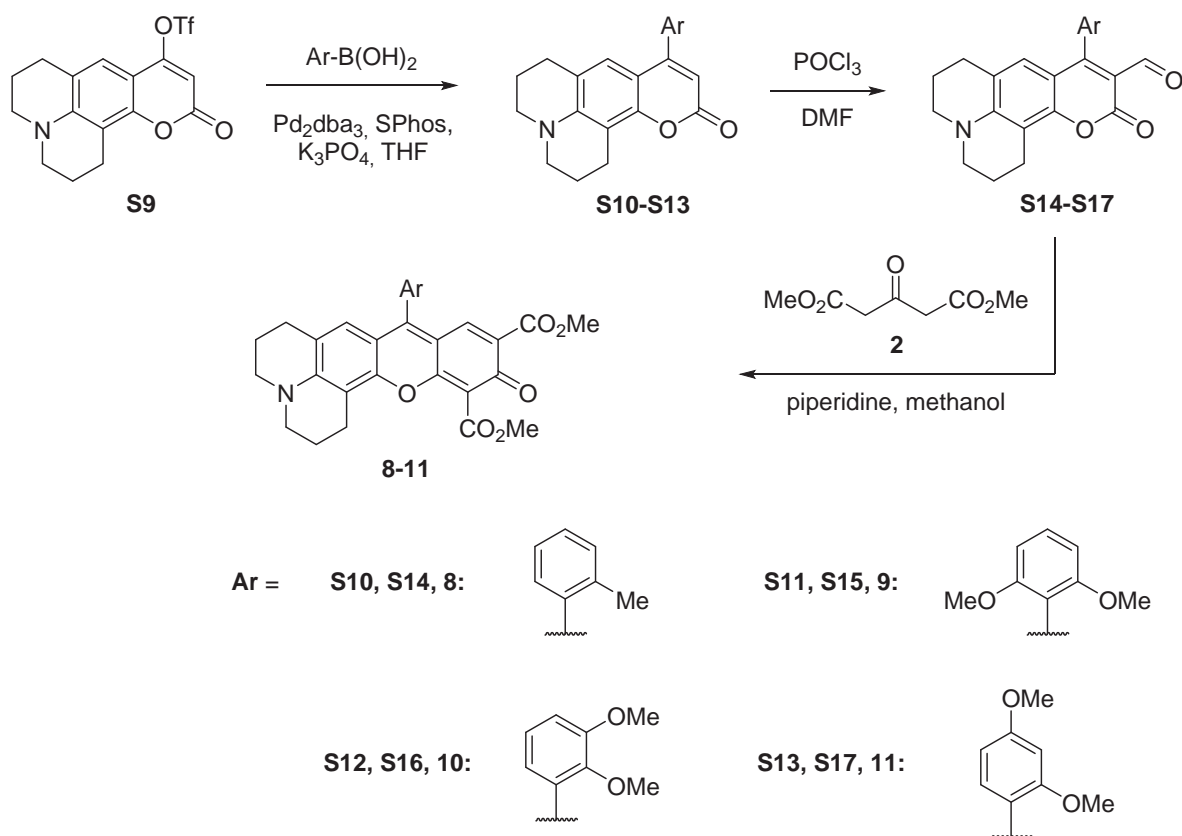


^1H NMR (500 MHz, CDCl_3) δ 7.70 (s, 1H, H-Ar), 7.21 (t, $J = 7.9$ Hz, 1H, H-Ar), 7.11 (dd, $J = 8.3, 1.5$ Hz, 1H, H-Ar), 7.06 – 7.01 (m, 1H, H-Ar), 6.73 (dd, $J = 7.7, 1.5$ Hz, 1H, H-Ar), 6.61 – 6.55 (m, 2H, H-Ar), 4.01 (s, 3H, OCH_3), 3.96 (s, 3H, OCH_3), 3.82 (s, 3H, OCH_3), 3.61 (s, 3H, OCH_3), 3.49 (q, $J = 7.2$ Hz, 4H, CH_2), 1.25 (t, $J = 7.1$ Hz, 6H, CH_3); ^{13}C NMR (126 MHz, CDCl_3) δ 176.6, 167.1, 166.4, 156.1, 155.6, 153.6, 152.9, 152.8, 146.5, 135.4, 131.0, 127.7, 126.7, 124.4, 121.8, 113.8, 112.8, 112.4, 111.2, 110.9, 96.7, 61.2, 55.8, 52.2, 52.0, 45.2, 12.5; HRMS (ESI) calc. for $\text{C}_{29}\text{H}_{30}\text{NO}_8$ 520.1977 $[\text{M} + \text{H}]^+$, found 520.1978.

Compound **7**. Yield 23%. M.p. 211-213°C



^1H NMR (500 MHz, CDCl_3) δ 8.33 (d, $J = 7.8$ Hz, 1H, H-Ar), 8.29 (d, $J = 7.7$ Hz, 1H, H-Ar), 8.25 – 8.15 (m, 3H, H-Ar), 8.07 (t, $J = 7.6$ Hz, 1H, H-Ar), 8.01 (d, $J = 9.1$ Hz, 1H, H-Ar), 7.86 (d, $J = 7.8$ Hz, 1H, H-Ar), 7.61 (d, $J = 9.1$ Hz, 1H, H-Ar), 7.43 (s, 1H, H-Ar), 6.73 (d, $J = 9.4$ Hz, 1H, H-Ar), 6.67 (d, $J = 2.5$ Hz, 1H, H-Ar), 6.41 (dd, $J = 9.4, 2.5$ Hz, 1H, H-Ar), 4.05 (s, 3H, OCH_3), 3.64 (s, 3H, OCH_3), 3.47 (q, $J = 7.2$ Hz, 4H, CH_2), 1.24 (t, $J = 7.1$ Hz, 6H, CH_3); ^{13}C NMR (126 MHz, CDCl_3) δ 176.7, 166.8, 166.4, 156.1, 155.6, 154.7, 153.6, 135.3, 132.3, 131.3, 130.8, 129.5, 129.1, 128.8, 128.3, 127.2, 126.9, 126.8, 126.6, 126.2, 126.0, 124.6 (2), 124.4, 124.1, 113.6, 113.0, 112.1, 111.1, 96.9, 52.4, 52.0, 45.3, 12.6; HRMS (ESI) calc. for $\text{C}_{37}\text{H}_{30}\text{NO}_6$ 584.2073 $[\text{M} + \text{H}]^+$, found 584.2075.

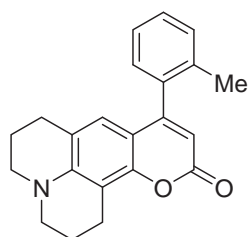


Scheme S3. Synthetic route from coumarin **S9** to rhodols **8-11**.

General procedure for the preparation of compounds **S10-S13**.

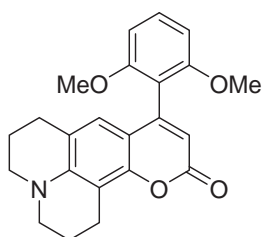
Compound **S9** (10 mmol), arylboronic acid (15 mmol), bis(dibenzylideneacetone)-palladium(0) (0.25 mmol), 2-dicyclohexylphosphino-2',6'-dimethoxybiphenyl (SPhos) (0.75 mmol) and tribasic potassium phosphate (40 mmol) were placed under Ar in a flame-dried Schlenk flask. Dry and degassed THF (75 ml) was added and the reaction mixture was stirred at 70°C for 7h under inert atmosphere. After the reaction was complete the mixture was diluted with DCM, filtered through celite and washed with NaHCO₃ solution (3 × 150 ml). The organic layer was dried over Na₂SO₄ and concentrated under vacuo. The residue was recrystallized from methanol.

Compound **S10**. Yield 90%. M.p. 166-167°C



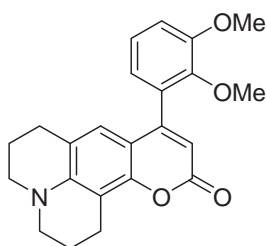
^1H NMR (600 MHz, CDCl_3) δ 7.37 – 7.34 (m, 1H, H-Ar), 7.32 – 7.26 (m, 2H, H-Ar), 7.14 (dd, J = 7.6, 1.4 Hz, 1H, H-Ar), 6.39 (s, 1H, H-Ar), 5.89 (s, 1H, C-H), 3.29 – 3.21 (m, 4H, CH_2), 2.95 (t, J = 6.5 Hz, 2H, CH_2), 2.60 (t, J = 6.5 Hz, 2H, CH_2), 2.17 (s, 3H, CH_3 -Ar), 2.02 – 1.97 (m, 2H, CH_2), 1.93 – 1.88 (m, J = 7.9, 5.5 Hz, 2H, CH_2); ^{13}C NMR (151 MHz, CDCl_3) δ 162.5, 156.6, 151.4, 145.9, 136.2, 135.3, 130.2, 128.5, 128.4, 125.7, 123.8, 118.2, 108.3, 108.2, 106.8, 49.9, 49.5, 27.5, 21.5, 20.6, 20.5, 19.7; HRMS (ESI) calc. for $\text{C}_{22}\text{H}_{21}\text{NO}_2\text{Na}$ 354.1470 $[\text{M} + \text{Na}]^+$, found 354.1469.

Compound **S11**. Yield 94%.



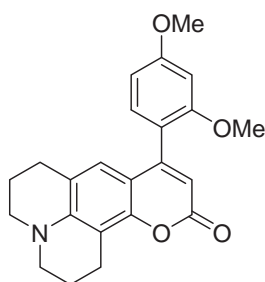
^1H NMR (500 MHz, CDCl_3) δ 7.36 (t, J = 8.4 Hz, 1H, H-Ar), 6.66 (d, J = 8.4 Hz, 2H, H-Ar), 6.43 (s, 1H, H-Ar), 5.92 (s, 1H, C-H), 3.70 (s, 6H, OCH_3), 3.23 – 3.19 (m, 4H, CH_2), 2.94 (t, J = 6.6 Hz, 2H, CH_2), 2.62 (t, J = 6.4 Hz, 2H, CH_2), 2.02 – 1.99 (m, 2H, CH_2), 1.97 – 1.93 (m, 2H, CH_2); ^{13}C NMR (126 MHz, CDCl_3) δ 162.9, 157.6, 151.4, 150.7, 145.6, 130.1, 123.4, 117.9, 114.0, 110.3, 109.0, 106.7, 104.1, 56.0, 50.0, 49.6, 27.5, 21.6, 20.8, 20.6; HRMS (ESI) calc. for $\text{C}_{23}\text{H}_{23}\text{NO}_4\text{Na}$ 400.1525 $[\text{M} + \text{Na}]^+$, found 400.1529.

Compound **S12**. Yield 89%. M.p. 208-210°C



^1H NMR (500 MHz, CDCl_3) δ 7.13 (t, J = 7.9 Hz, 1H, H-Ar), 7.02 (dd, J = 8.3, 1.5 Hz, 1H, H-Ar), 6.78 (dd, J = 7.7, 1.5 Hz, 1H, H-Ar), 6.56 (s, 1H, H-Ar), 5.97 (s, 1H, C-H), 3.93 (s, 3H, OCH_3), 3.67 (s, 3H, OCH_3), 3.27 – 3.20 (m, 4H, CH_2), 2.94 (t, J = 6.5 Hz, 2H, CH_2), 2.69 – 2.55 (m, 2H, CH_2), 2.02 – 1.96 (m, 2H, CH_2), 1.92 – 1.87 (m, 2H, CH_2); ^{13}C NMR (126 MHz, CDCl_3) δ 162.5, 153.9, 152.8, 151.3, 146.2, 145.9, 131.0, 124.2, 124.1, 121.6, 118.1, 112.8, 108.4, 108.4, 106.6, 61.3, 55.8, 50.0, 49.5, 27.5, 21.5, 20.7, 20.5; HRMS (ESI) calc. for $\text{C}_{23}\text{H}_{23}\text{NO}_4\text{Na}$ 400.1525 $[\text{M} + \text{Na}]^+$, found 400.1522.

Compound **S13**. Yield 84%. M.p. 201-203°C

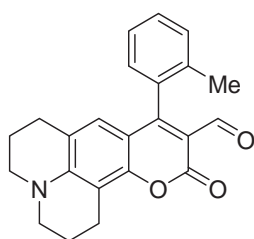


^1H NMR (500 MHz, CDCl_3) δ 7.13 – 7.08 (m, 1H, H-Ar), 6.59 – 6.57 (m, 3H, H-Ar), 5.95 (s, 1H, C-H), 3.87 (s, 3H, OCH_3), 3.73 (s, 3H, OCH_3), 3.23 (t, $J = 5.8$ Hz, 4H, CH_2), 2.93 (t, $J = 6.5$ Hz, 2H, CH_2), 2.64 (t, $J = 6.4$ Hz, 2H, CH_2), 2.01 - 1.96 (m, $J = 6.2$ Hz, 2H, CH_2), 1.94 – 1.89 (d, $J = 6.0$ Hz, 2H, CH_2); ^{13}C NMR (126 MHz, CDCl_3) δ 162.8, 161.5, 157.6, 153.9, 151.3, 145.6, 130.8, 124.2, 118.3, 117.8, 109.2, 108.8, 106.7, 104.5, 99.0, 55.6, 55.5, 49.9, 49.6, 27.6, 21.6, 20.8, 20.5; HRMS (ESI) calc. for $\text{C}_{23}\text{H}_{23}\text{NO}_4\text{Na}$ 400.1525 $[\text{M} + \text{Na}]^+$, found 400.1530.

General procedure for the preparation of compounds **S14-S17**.

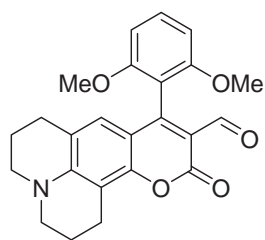
Phosphorus oxychloride (7.7 mmol) was added dropwise to a solution of 7-diethylamino-4-aryl coumarin (**S10-S13**) (5 mmol) in DMF (15 ml) upon cooling on ice. The reaction mixture was allowed to stir at 50°C for 24h. The solution then was cooled to room temperature, poured into NaHCO_3 aqueous solution (20 g in 100 ml H_2O) with 300 ml of crashed ice. The precipitate which formed was filtered, washed with distilled water and methanol, dried under vacuo and purified via recrystallization from $\text{MeOH}/\text{CH}_2\text{Cl}_2$.

Compound **S14**. Yield 84%. M.p. $201\text{-}203^\circ\text{C}$



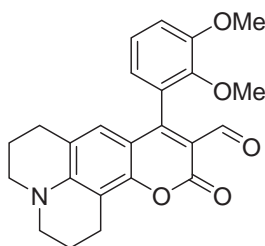
^1H NMR (500 MHz, CDCl_3) δ 9.80 (s, 1H, CHO), 7.38 (t, $J = 7.5$ Hz, 1H, H-Ar), 7.33 – 7.24 (m, 2H, H-Ar), 7.03 (d, $J = 7.5$ Hz, 1H, H-Ar), 6.35 (s, 1H, H-Ar), 3.36 – 3.32 (m, 4H, CH_2), 2.94 (t, $J = 6.4$ Hz, 2H, CH_2), 2.57 (t, $J = 6.2$ Hz, 2H, CH_2), 2.08 (s, 3H, $\text{CH}_3\text{-Ar}$), 2.00 (quint, $J = 6.2$ Hz, 2H, CH_2), 1.90 (quint, $J = 6.3$ Hz, 2H, CH_2); ^{13}C NMR (126 MHz, CDCl_3) δ 188.4, 161.6, 160.3, 152.9, 149.0, 135.2, 133.5, 130.0, 128.7, 127.8, 126.1, 125.7, 119.5, 111.3, 108.4, 106.0, 50.3, 49.9, 27.5, 21.1, 20.2, 20.2, 19.5; HRMS (ESI) calc. for $\text{C}_{23}\text{H}_{22}\text{NO}_3$ 360.1600 $[\text{M} + \text{H}]^+$, found 360.1588.

Compound **S15**. Yield 87%. M.p. $263\text{-}265^\circ\text{C}$



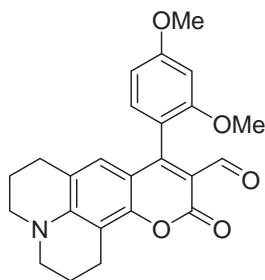
^1H NMR (500 MHz, CDCl_3) δ 9.77 (s, 1H, CHO), 7.41 (t, $J = 8.4$ Hz, 1H, H-Ar), 6.66 (d, $J = 8.4$ Hz, 2H, H-Ar), 6.49 (s, 1H, H-Ar), 3.68 (s, 6H, OCH_3), 3.34 – 3.28 (m, 4H, CH_2), 2.92 (t, $J = 6.4$ Hz, 2H, CH_2), 2.60 (t, $J = 6.3$ Hz, 2H, CH_2), 1.97 (quint, $J = 6.1$ Hz, 2H, CH_2), 1.91 (quint, $J = 6.1$ Hz, 2H, CH_2); ^{13}C NMR (126 MHz, CDCl_3) δ 188.8, 160.4, 157.3, 157.1, 152.8, 148.7, 130.7, 125.5, 119.1, 112.3, 110.8, 108.7, 105.8, 103.9, 56.0, 50.2, 49.9, 49.6, 27.5, 21.1, 20.3 (2); HRMS (ESI) calc. for $\text{C}_{24}\text{H}_{23}\text{NO}_5\text{Na}$ 428.1474 $[\text{M} + \text{Na}]^+$, found 428.1472.

Compound **S16**. Yield 86%. M.p. 242-244°C



^1H NMR (500 MHz, CDCl_3) δ 9.89 (s, 1H, CHO), 7.15 (t, $J = 7.9$ Hz, 1H, H-Ar), 7.06 (d, $J = 8.2$ Hz, 1H, H-Ar), 6.64 (d, $J = 7.6$ Hz, 1H, H-Ar), 6.50 (s, 1H, H-Ar), 3.94 (s, 3H, OCH_3), 3.66 (s, 3H, OCH_3), 3.36 – 3.32 (m, 4H, CH_2), 2.91 (t, $J = 6.4$ Hz, 2H, CH_2), 2.59 (t, $J = 6.4$ Hz, 2H, CH_2), 1.97 (quint, $J = 6.2$ Hz, 2H, CH_2), 1.89 (quint, $J = 6.0$ Hz, 2H, CH_2); ^{13}C NMR (126 MHz, CDCl_3) δ 188.0, 160.1, 158.4, 152.3, 152.2, 148.7, 145.2, 127.8, 126.0, 123.7, 120.3, 119.2, 112.6, 110.6, 108.3, 105.3, 60.4, 55.4, 49.9, 49.4, 27.0, 20.5, 19.7 (2); HRMS (ESI) calc. for $\text{C}_{24}\text{H}_{23}\text{NO}_5\text{Na}$ 428.1474 $[\text{M} + \text{Na}]^+$, found 428.1481.

Compound **S17**. Yield 32%. M.p. 210-211°C



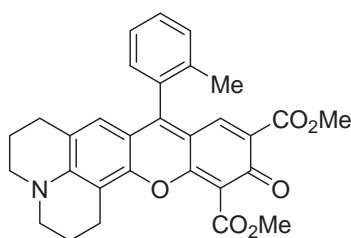
^1H NMR (500 MHz, CDCl_3) δ 9.80 (s, 1H, CHO), 6.97 (d, $J = 8.3$ Hz, 1H, H-Ar), 6.60 (dd, $J = 8.3, 2.3$ Hz, 1H, H-Ar), 6.57-6.56 (m, 2H, H-Ar), 3.88 (s, 3H, OCH_3), 3.70 (s, 3H, OCH_3), 3.35 – 3.29 (m, 4H, CH_2), 2.92 (t,

$J = 6.4$ Hz, 2H, CH₂), 2.64 – 2.58 (m, 2H, CH₂), 2.02 – 1.95 (m, 2H, CH₂), 1.93 – 1.88 (m, 2H, CH₂); ¹³C NMR (126 MHz, CDCl₃) δ 188.9, 161.7, 160.3, 159.1, 157.7, 152.9, 148.6, 130.3, 126.3, 119.1, 114.8, 112.1, 109.1, 106.0, 104.5, 98.7, 55.7, 55.5, 50.2, 49.9, 27.5, 21.1, 20.3 (2); HRMS (ESI) calc. for C₂₄H₂₃NO₅Na 428.1474 [M + Na]⁺, found 428.1472.

General procedure for the preparation of compounds **8-11**.

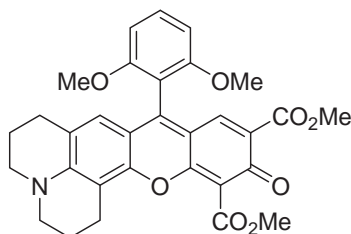
3-formyl coumarin (**S14-S17**) (1 mmol), dimethyl-1,3-acetonedicarboxylate (**2**) (10 mmol) and piperidine (1 mmol) were dissolved in methanol (5 ml) and allowed to stir at 60°C for 20h. The solvent was evaporated and the residue was washed with diethyl ether. The crude product was purified via column chromatography (CH₂Cl₂ : MeOH 9:1).

Compound **8**. Yield 19%. M.p. 265-266°C



¹H NMR (500 MHz, CDCl₃) δ 7.49 – 7.41 (m, 2H, H-Ar), 7.38 – 7.33 (m, 2H, H-Ar), 7.10 – 7.08 (m, 1H, H-Ar), 6.47 (s, 1H, H-Ar), 3.98 (s, 3H, OCH₃), 3.80 (s, 3H, OCH₃), 3.41 -3.37 (m, 4H, CH₂), 2.95 – 2.91 (m, 2H, CH₂), 2.63 (t, $J = 6.2$ Hz, 2H, CH₂), 2.08 – 1.99 (m, 5H, CH₃-Ar, CH₂), 1.98 – 1.89 (m, 2H, CH₂); ¹³C NMR (126 MHz, CDCl₃) δ 176.2, 167.4, 166.6, 155.8, 155.0, 151.1, 149.7, 136.0, 134.8, 132.5, 130.6, 129.5, 129.0, 127.8, 126.1, 126.0, 121.2, 112.2, 111.1, 110.8, 105.8, 52.2, 52.1, 50.5, 50.2, 27.5, 20.9, 20.0, 19.8, 19.6; HRMS (ESI) calc. for C₃₀H₂₈NO₆ 498.1917 [M + H]⁺, found 498.1921.

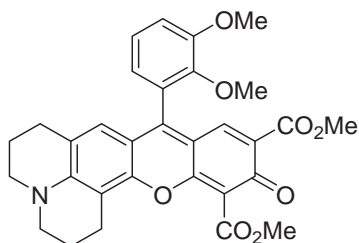
Compound **9**. Yield 28%. M.p. 260-262°C



¹H NMR (500 MHz, CDCl₃) δ 7.57 (s, 1H, H-Ar), 7.46 (t, $J = 8.4$ Hz, 1H, H-Ar), 6.70 (d, $J = 8.4$ Hz, 2H, H-Ar), 6.57 (s, 1H, H-Ar), 3.98 (s, 3H, OCH₃), 3.82 (s, 3H, OCH₃), 3.65 (s, 6H, OCH₃), 3.41 – 3.34 (m, 4H, CH₂), 2.93 (t, $J = 6.4$ Hz, 2H, CH₂), 2.65 (t, $J = 6.2$ Hz, 2H, CH₂), 2.03 - 1.98 (m, 2H, CH₂), 1.97 – 1.92 (m, 2H, CH₂); ¹³C NMR (126 MHz, CDCl₃) δ 176.4, 167.9, 166.9, 157.7, 156.3, 151.3, 151.0, 149.6, 135.5,

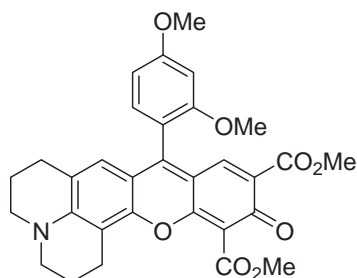
131.5, 127.0, 126.1, 120.9, 112.1, 111.8, 111.5, 109.9, 105.5, 104.1, 56.0, 52.1, 52.0, 50.5, 50.2, 27.6, 21.1, 20.2, 19.8; HRMS (ESI) calc. for $C_{31}H_{30}NO_8$ 544.1971 $[M + H]^+$, found 544.1970.

Compound **10**. Yield 28%. M.p. 200°C (dec.)



1H NMR (500 MHz, $CDCl_3$) δ 7.66 (s, 1H, H-Ar), 7.21 (t, $J = 7.9$ Hz, 1H, H-Ar), 7.10 (d, $J = 8.2$ Hz, 1H, H-Ar), 6.74 – 6.68 (m, 1H, H-Ar), 6.60 (s, 1H, H-Ar), 3.98 (s, 3H, OCH_3), 3.97 (s, 3H, OCH_3), 3.81 (s, 3H, OCH_3), 3.59 (s, 3H, OCH_3), 3.41 – 3.37 (m, 4H, CH_2), 2.92 (t, $J = 6.4$ Hz, 2H, CH_2), 2.65 – 2.62 (m, 2H, CH_2), 2.03 – 2.00 (m, 2H, CH_2), 1.95 – 1.90 (m, 2H, CH_2); ^{13}C NMR (126 MHz, $CDCl_3$) δ 176.2, 167.6, 166.6, 152.9, 146.5, 135.3, 127.1 (2), 126.6, 124.3, 121.9, 113.6, 111.4, 105.6, 61.2, 55.8, 52.1, 52.0, 50.5, 50.2, 27.5, 20.9, 20.1, 19.8; HRMS (ESI) calc. for $C_{31}H_{30}NO_8$ 544.1971 $[M + H]^+$, found 544.1974.

Compound **11**. Yield 16%. M.p. 181°C(dec.)

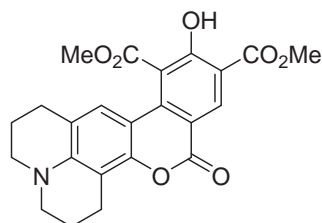


1H NMR (500 MHz, $CDCl_3$) δ 7.64 (s, 1H, H-Ar), 7.02 (d, $J = 8.3$ Hz, 1H, H-Ar), 6.68 – 6.60 (m, 3H, H-Ar), 3.97 (s, 3H, OCH_3), 3.91 (s, 3H, OCH_3), 3.82 (s, 3H, OCH_3), 3.68 (s, 3H, OCH_3), 3.40 – 3.36 (m, 4H, CH_2), 2.92 (t, $J = 6.3$ Hz, 2H, CH_2), 2.66 (t, $J = 6.3$ Hz, 2H, CH_2), 2.01 (quint, $J = 6.2$ Hz, 2H, CH_2), 1.99 – 1.90 (m, 2H, CH_2); ^{13}C NMR (126 MHz, $CDCl_3$) δ 176.2, 167.7, 166.7, 162.2, 158.0, 156.1, 153.1, 151.3, 149.5, 135.8, 131.4, 127.1, 126.6, 120.8, 114.0, 112.0, 111.9, 111.5, 105.6, 104.9, 99.1, 55.7, 55.5, 52.1, 52.0, 50.5, 50.2, 27.6, 21.0, 20.1, 19.8; HRMS (ESI) calc. for $C_{31}H_{30}NO_8$ 544.1971 $[M + H]^+$, found 544.1975.

General procedure for the preparation of compounds **12**, **13**.

3-formyl coumarin (**S18**, **S19**) (1 mmol), dimethyl-1,3-acetonedicarboxylate (**2**) (10 mmol) and piperidine (1 mmol) were dissolved in methanol (5 ml) and allowed to stir at 60°C for 20h. The precipitate which formed was filtered and recrystallized from MeOH/CH₂Cl₂.

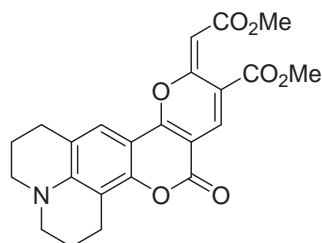
Compound **12**. Yield 21%. M.p. 250°C(dec.)



Starting compound **S18** was synthesized following a procedure described in the literature.¹

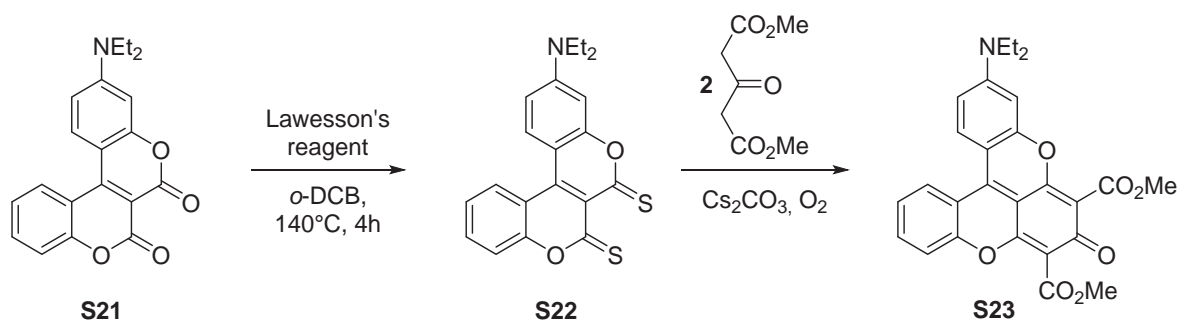
¹H NMR (500 MHz, CDCl₃) δ 11.66 (s, 1H, OH), 8.92 (s, 1H, H-Ar), 7.09 (s, 1H, H-Ar), 4.01 (s, 3H, OCH₃), 3.99 (s, 3H, OCH₃), 3.28 – 3.24 (m, 4H, CH₂), 2.89 (t, *J* = 6.5 Hz, 2H, CH₂), 2.74 (t, *J* = 6.3 Hz, 2H, CH₂), 1.98 (quint, *J* = 6.1 Hz, 4H, CH₂); ¹³C NMR (126 MHz, CDCl₃) δ 169.5, 168.4, 162.6, 160.8, 149.4, 146.1, 139.0, 135.6, 122.9, 117.9, 115.6, 111.7, 110.5, 107.4, 103.4, 52.9, 52.7, 49.9, 49.3, 27.9, 21.5, 20.7, 20.6; HRMS (EI) calc. for C₂₃H₂₁NO₇ 423.1318 M⁺, found 423.1302.

Compound **30**. Yield 60%. M.p. 288-289°C



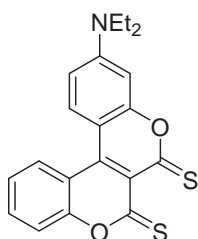
Starting compound **S19** was synthesized following a procedure described in the literature.²

¹H NMR (500 MHz, 1,1,2,2-CD₂Cl₄) δ 8.04 (s, 1H), 7.58 (s, 1H), 6.38 (s, 1H), 3.82 (s, 3H, OCH₃), 3.76 (s, 3H, OCH₃), 3.37 – 3.32 (m, 4H, CH₂), 2.85 – 2.82 (m, 4H, CH₂), 1.99 – 1.94 (m, 4H, CH₂); ¹³C NMR (500 MHz, 1,1,2,2- CD₂Cl₄) δ 165.6, 163.4, 161.6, 159.6, 154.6, 151.9, 149.0, 136.9, 121.6, 119.9, 113.3, 106.0, 99.8, 95.8, 94.6, 52.2, 51.0, 50.2, 49.7, 27.7, 20.9, 20.1, 19.9; HRMS (ESI) calc. for C₂₃H₂₁NO₇Na 446.1216 [M + Na]⁺, found 446.1218.



Scheme S4. Transformation of bis-coumarins into V-shaped rhodols.

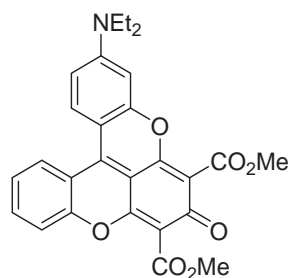
Compound **S22**. Yield 18%. M.p. 170-171°C



The starting compound **S21** was synthesized according to the literature procedure.³ The bis-coumarin **S21** (1 mmol) together with Lawesson's reagent (1,25 mmol) were dissolved in 25 ml of dry *o*-DCB and the reaction was heated at 140°C for 4 hours. After the solvent was evaporated under the vacuo, the residue was filtered through a silica pad, washed with mixture of hexane and CH₂Cl₂ (1:1) and concentrated under vacuo. The product was next purified via DCVC (CH₂Cl₂ : hexane 1:2) followed by the recrystallization from the mixture of hexane and CH₂Cl₂.

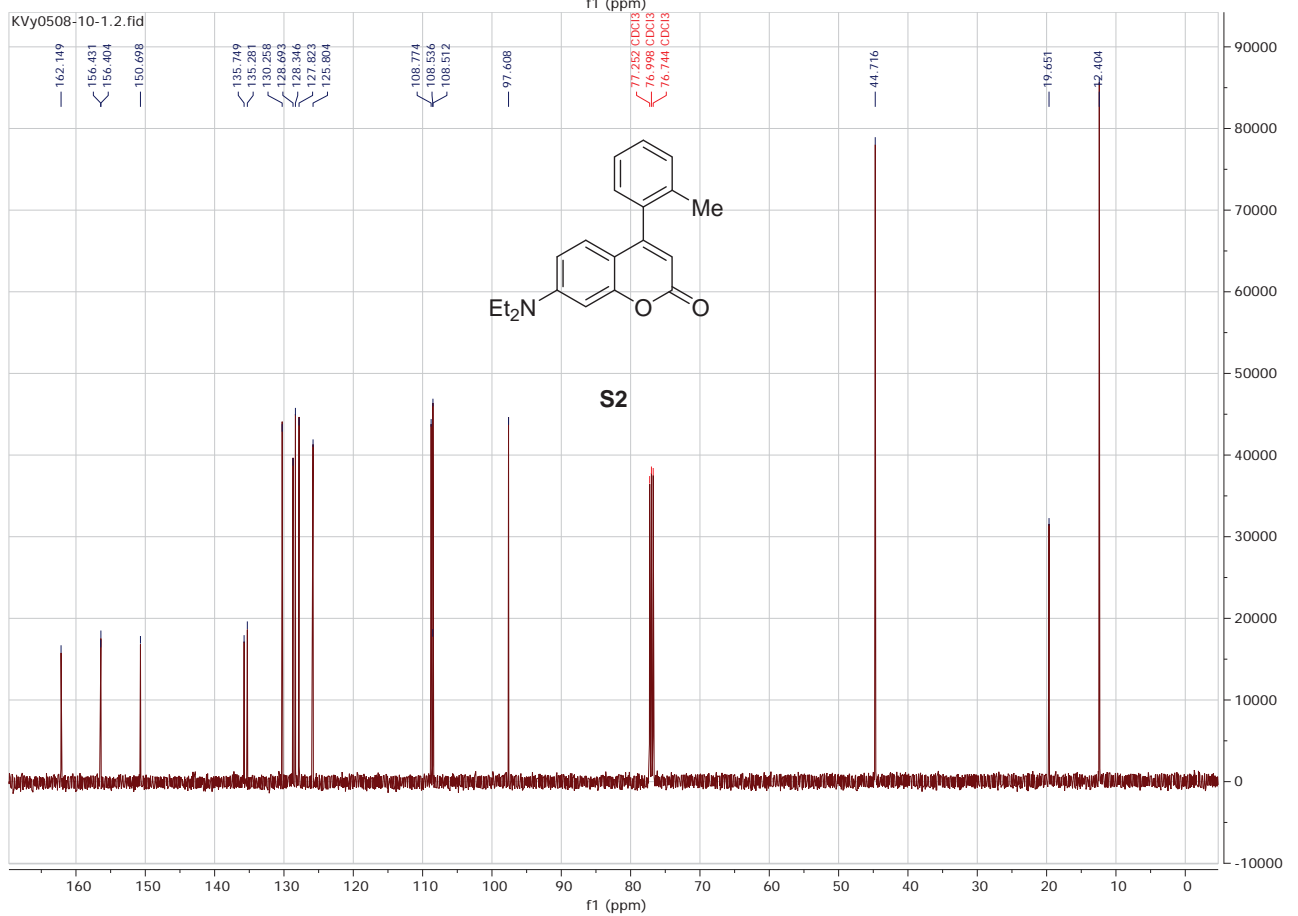
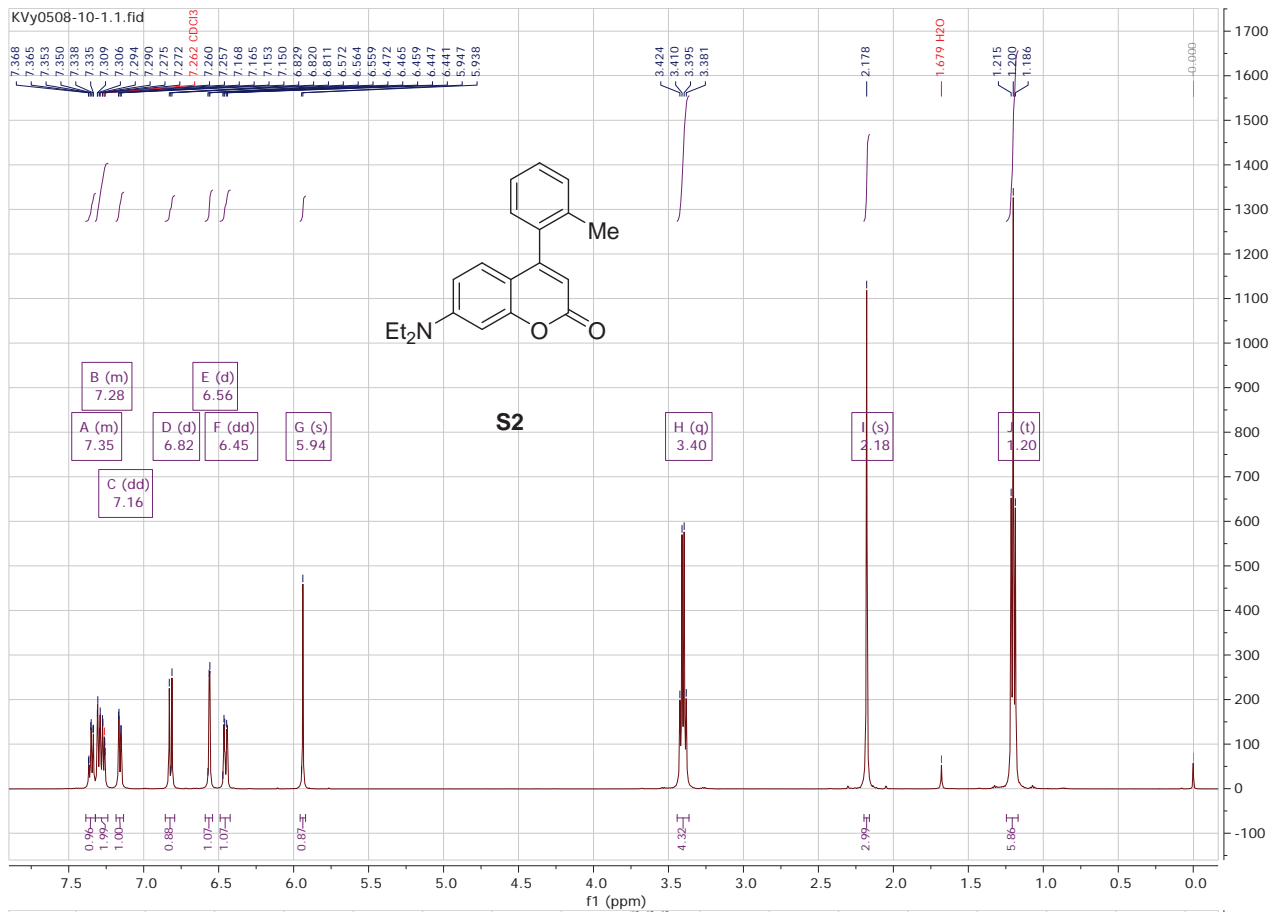
¹H NMR (500 MHz, CDCl₃) δ 8.07 (dd, *J* = 8.1, 1.5 Hz, 1H, H-Ar), 7.96 (d, *J* = 9.3 Hz, 1H, H-Ar), 7.66 (ddd, *J* = 8.5, 7.2, 1.5 Hz, 1H, H-Ar), 7.42 (dd, *J* = 8.4, 1.2 Hz, 1H, H-Ar), 7.35 (ddd, *J* = 8.3, 7.3, 1.3 Hz, 1H, H-Ar), 6.75 (dd, *J* = 9.4, 2.7 Hz, 1H, H-Ar), 6.60 (d, *J* = 2.6 Hz, 1H, H-Ar), 3.50 (q, *J* = 7.2 Hz, 4H, CH₂), 1.28 (t, *J* = 7.2 Hz, 6H, CH₃); ¹³C NMR (126 MHz, CDCl₃) δ 190.6, 190.5, 158.6, 155.2, 153.3, 139.8, 134.1, 131.0, 129.2, 124.8, 121.1, 117.3, 117.0, 111.3, 105.6, 97.0, 45.4, 12.5; HRMS (EI) calc. for C₂₀H₁₇NO₂S₂ 367.0701 M⁺, found 367.0706.

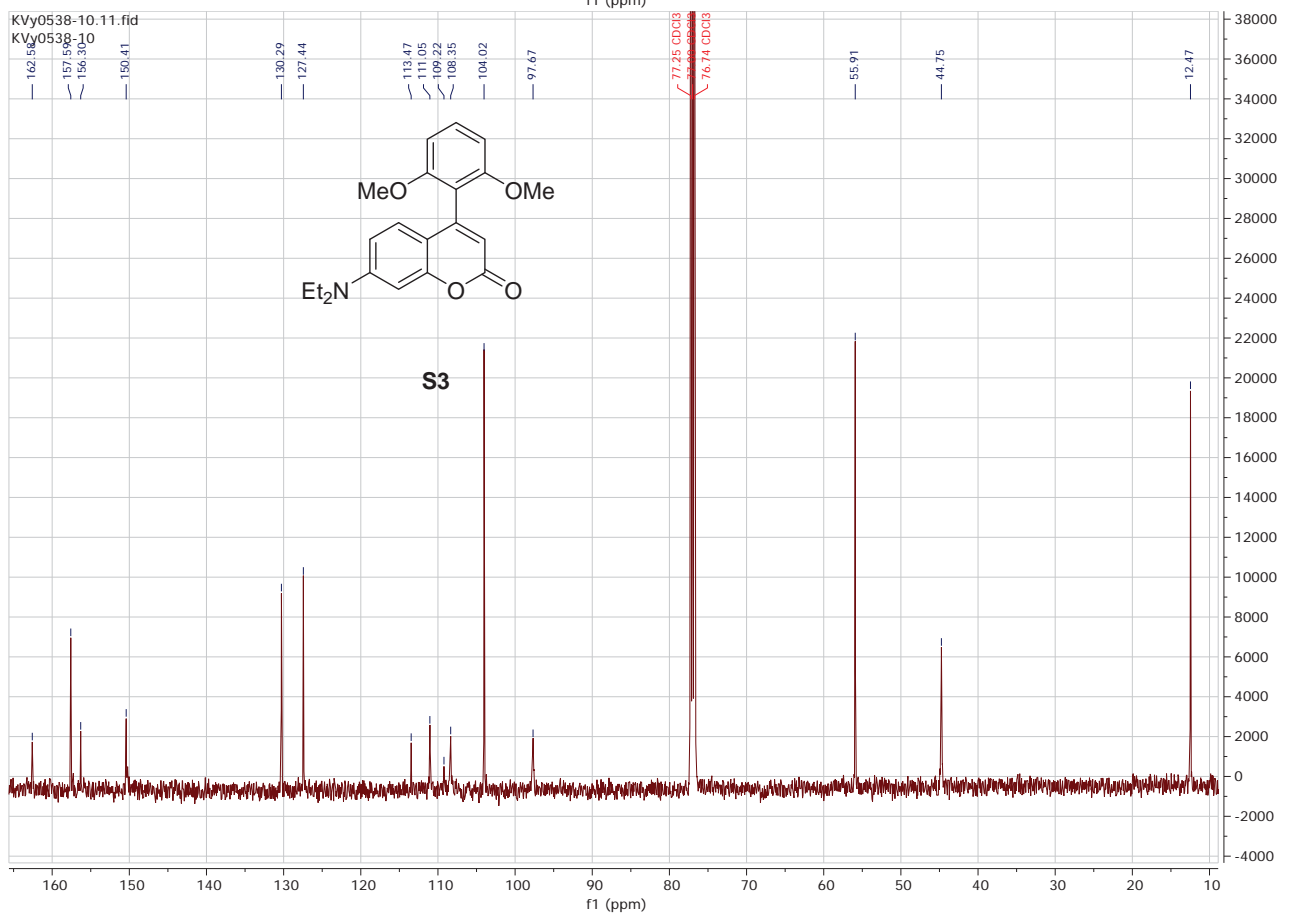
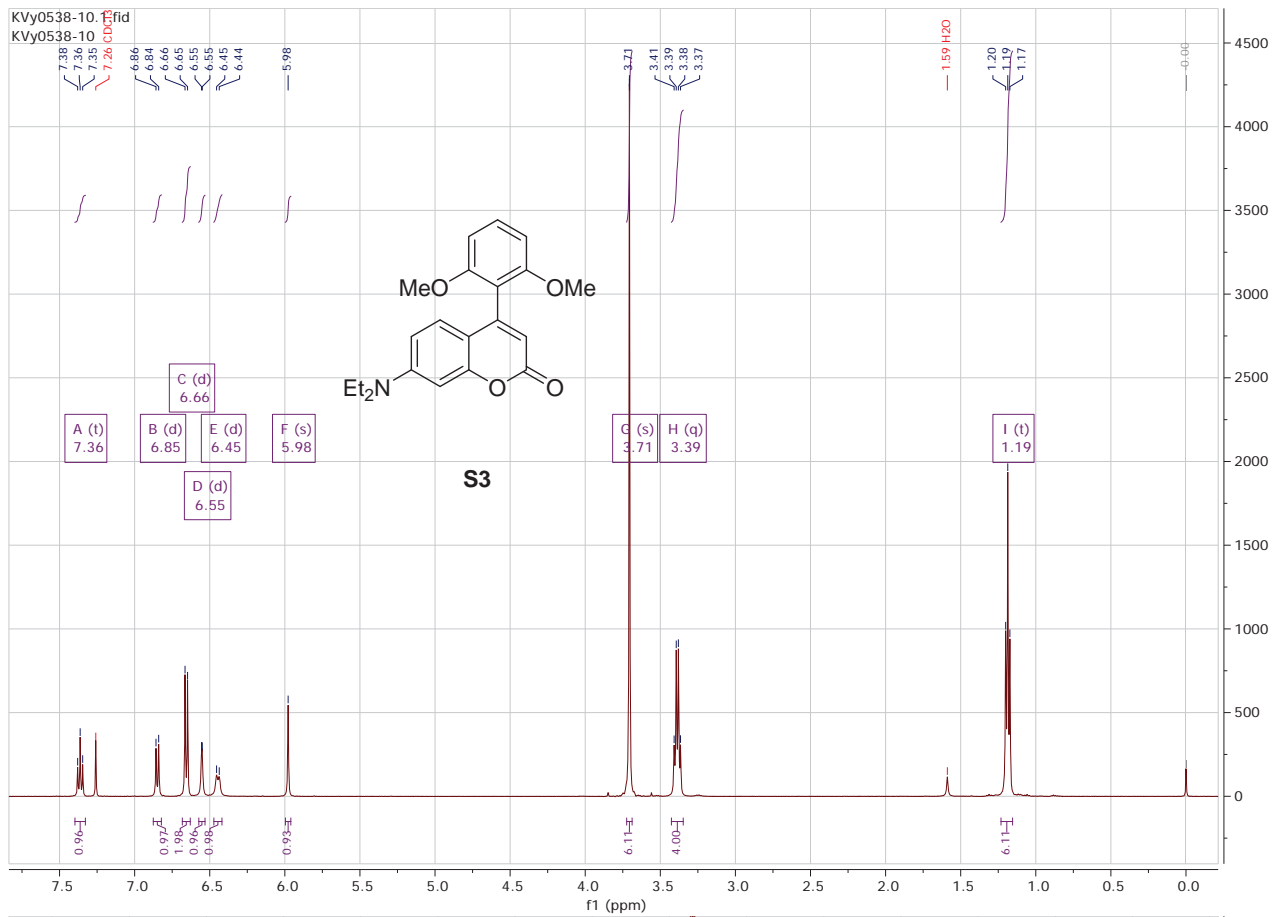
Compound **S23**. Yield 30%. M.p. 294-295°C

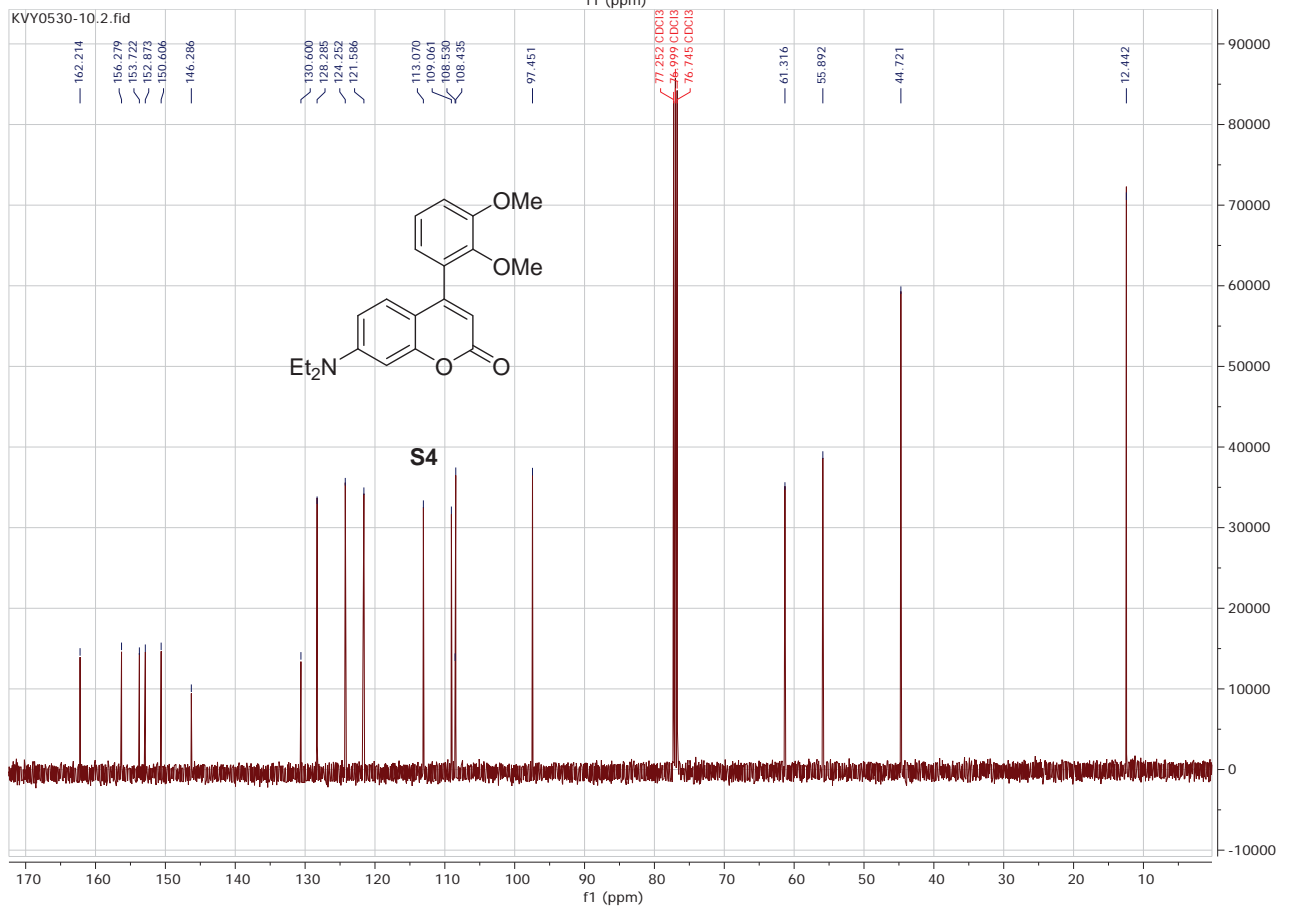
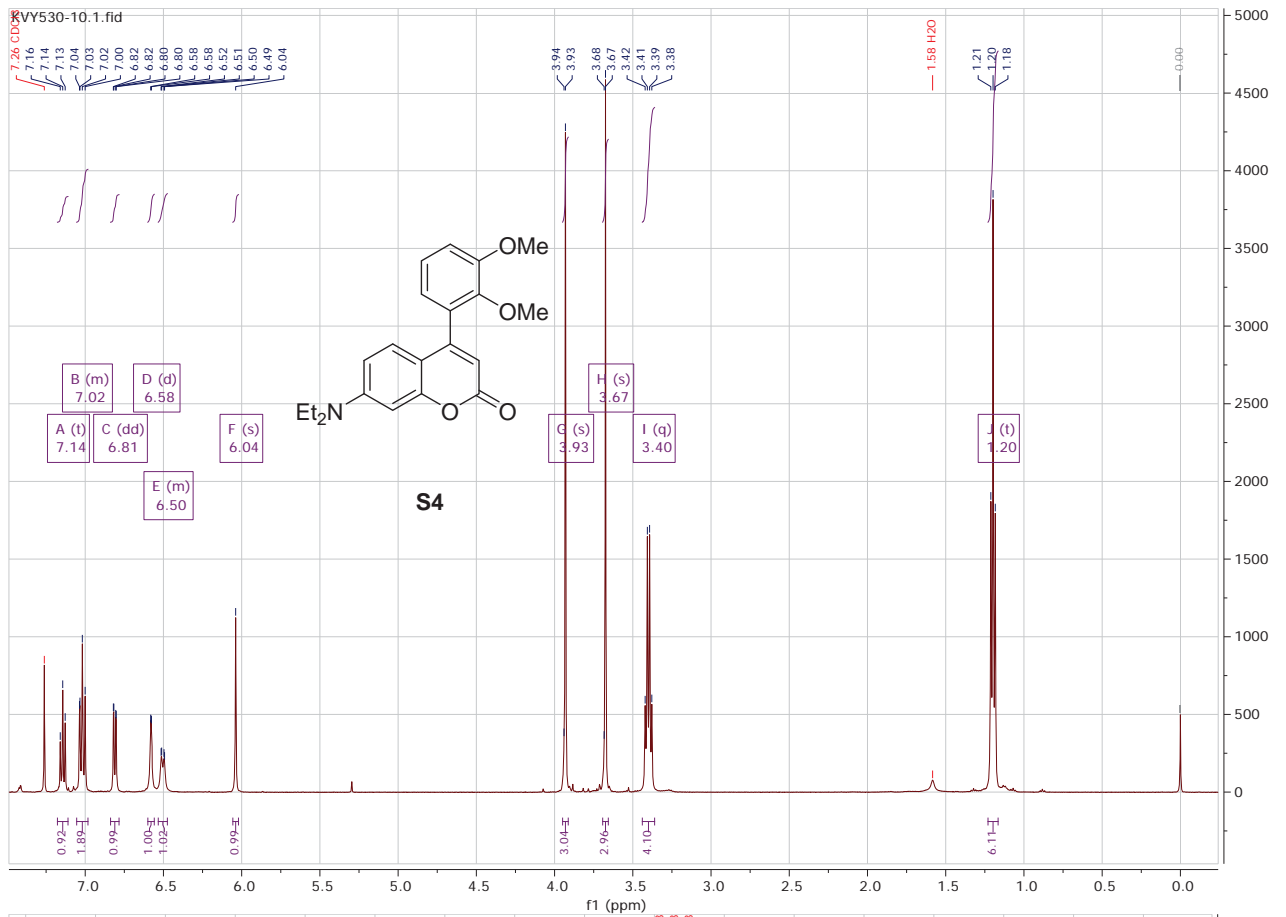


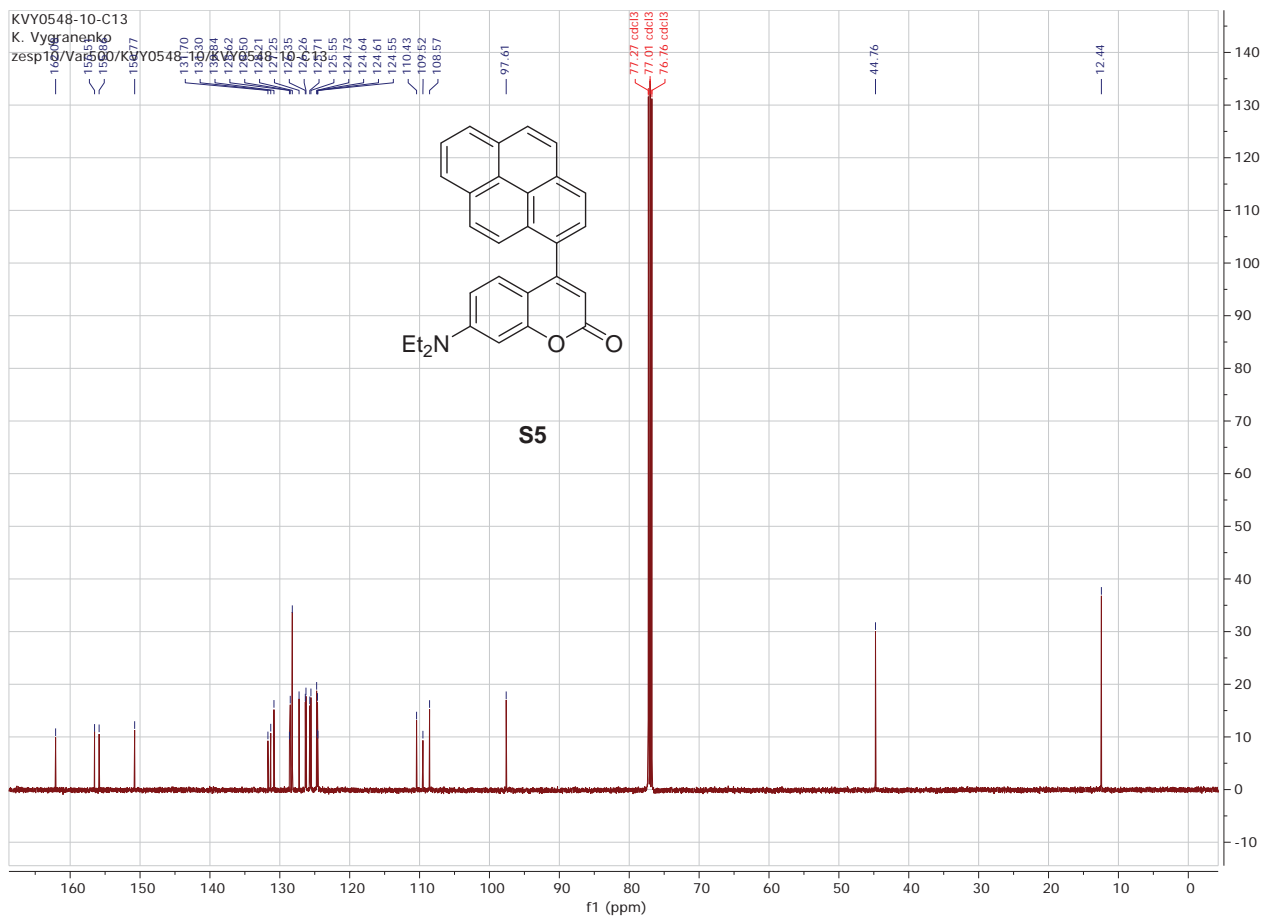
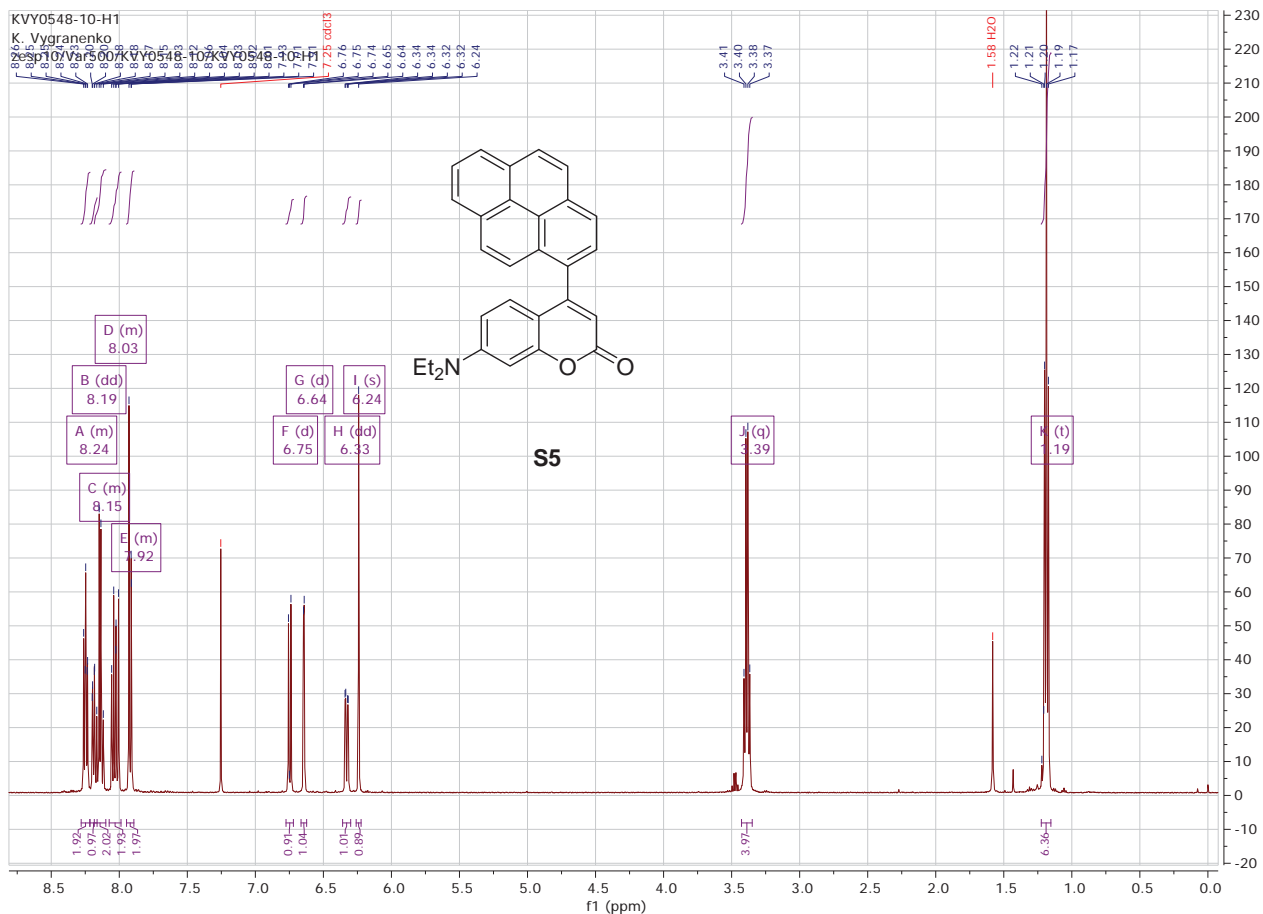
0,03 mmol of compound **S22**, 0,072 mmol of Cs_2CO_3 and 0,3 mmol of dimethyl 1,3-acetonedicarboxylate were mixed together in 2 ml of CH_3CN and were allowed to stir at r.t. overnight. The solvent was evaporated and the residue was purified using DCVC (0,1-2% MeOH in CH_2Cl_2).

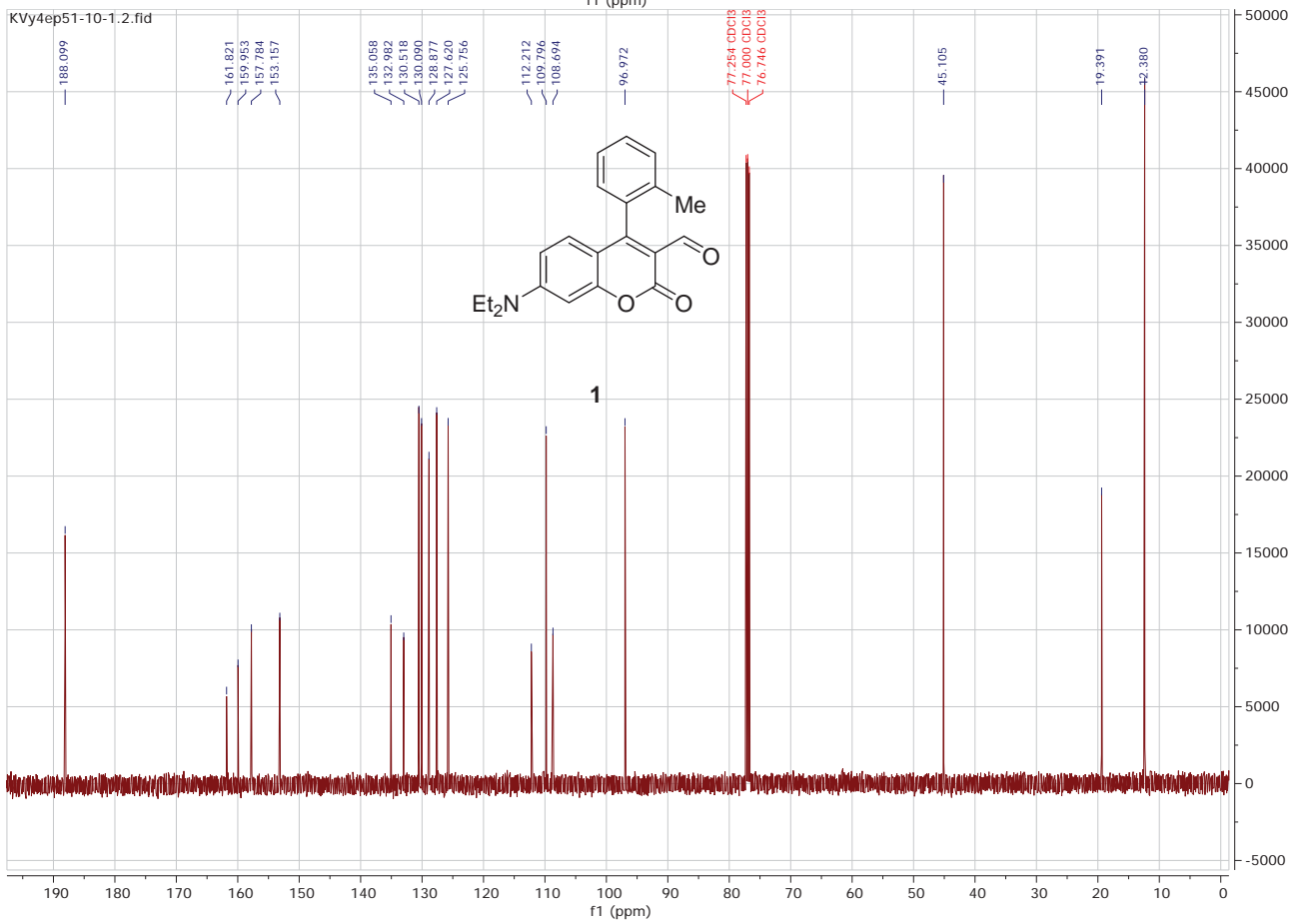
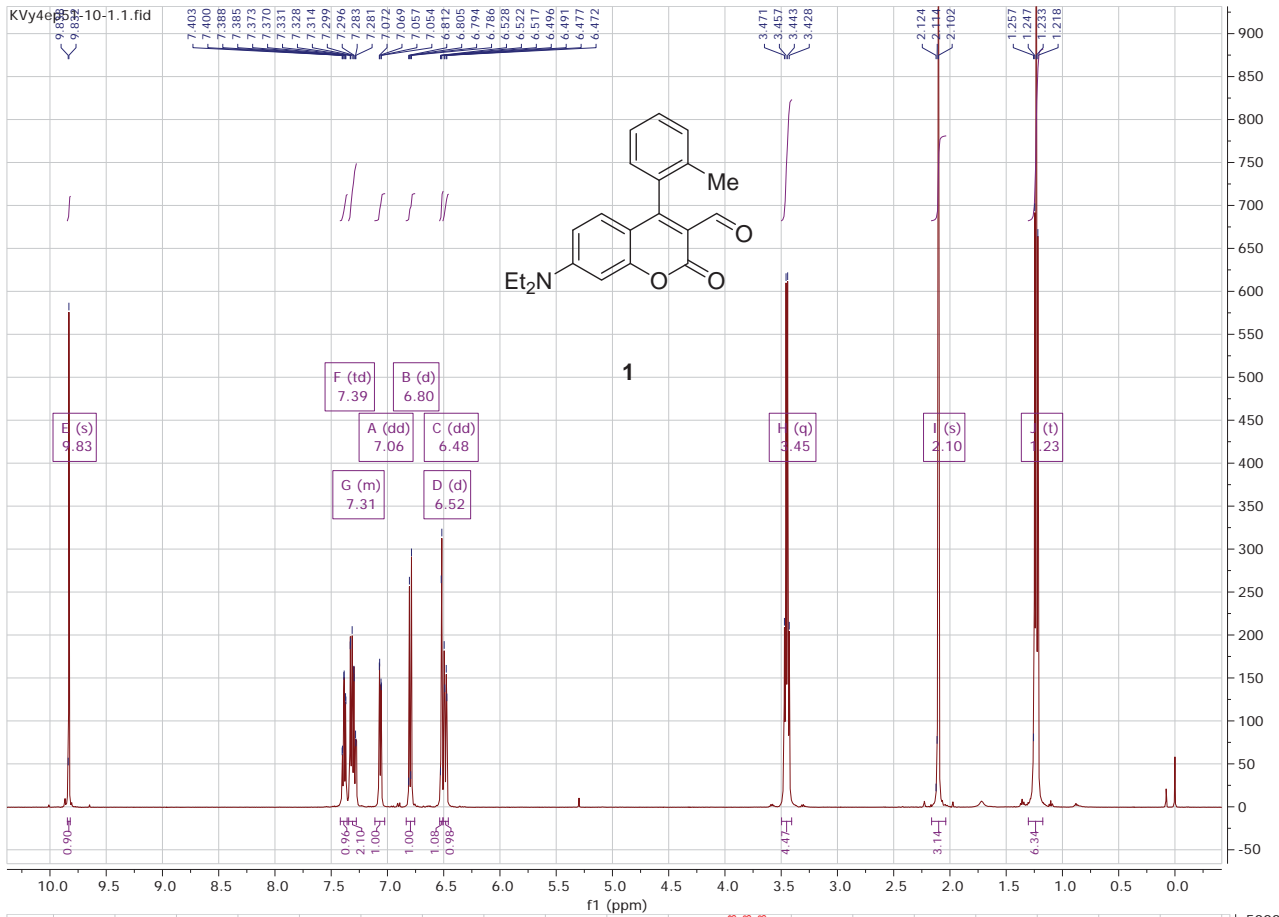
^1H NMR (500 MHz, CDCl_3) δ 8.27 (d, $J = 8.1$ Hz, 1H, H-Ar), 8.14 (d, $J = 9.4$ Hz, 1H, H-Ar), 7.65 (t, $J = 7.8$ Hz, 1H, H-Ar), 7.46 (d, $J = 8.3$ Hz, 1H, H-Ar), 7.37 (t, $J = 7.7$ Hz, 1H, H-Ar), 6.74 (dd, $J = 9.4, 2.7$ Hz, 1H, H-Ar), 6.55 (d, $J = 2.6$ Hz, 1H, H-Ar), 3.98 (d, $J = 7.1$ Hz, 6H, OCH_3), 3.51 (q, $J = 7.1$ Hz, 4H, CH_2), 1.29 (t, $J = 7.1$ Hz, 6H, CH_3); ^{13}C NMR (126 MHz, CDCl_3) δ 175.4, 165.6, 165.4, 157.3, 154.2, 152.8, 151.3, 150.7, 140.1, 134.0, 129.7, 128.2, 124.5, 118.8, 116.3, 110.5, 105.4, 105.1, 98.1, 52.3, 52.3, 45.1, 12.6; HRMS (EI) calc. for $\text{C}_{27}\text{H}_{23}\text{NO}_7$ 473.1457 M^+ , found 473.1470.

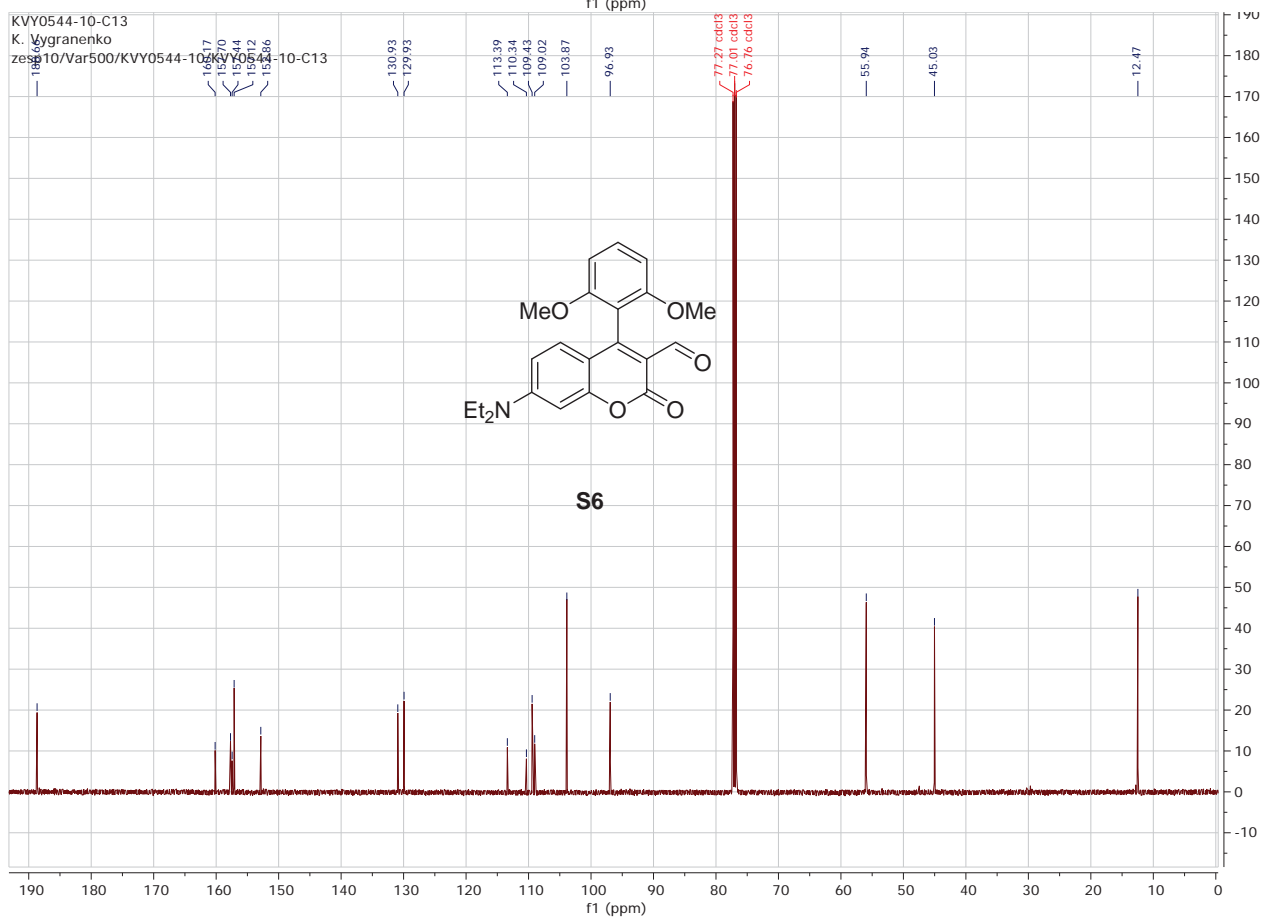
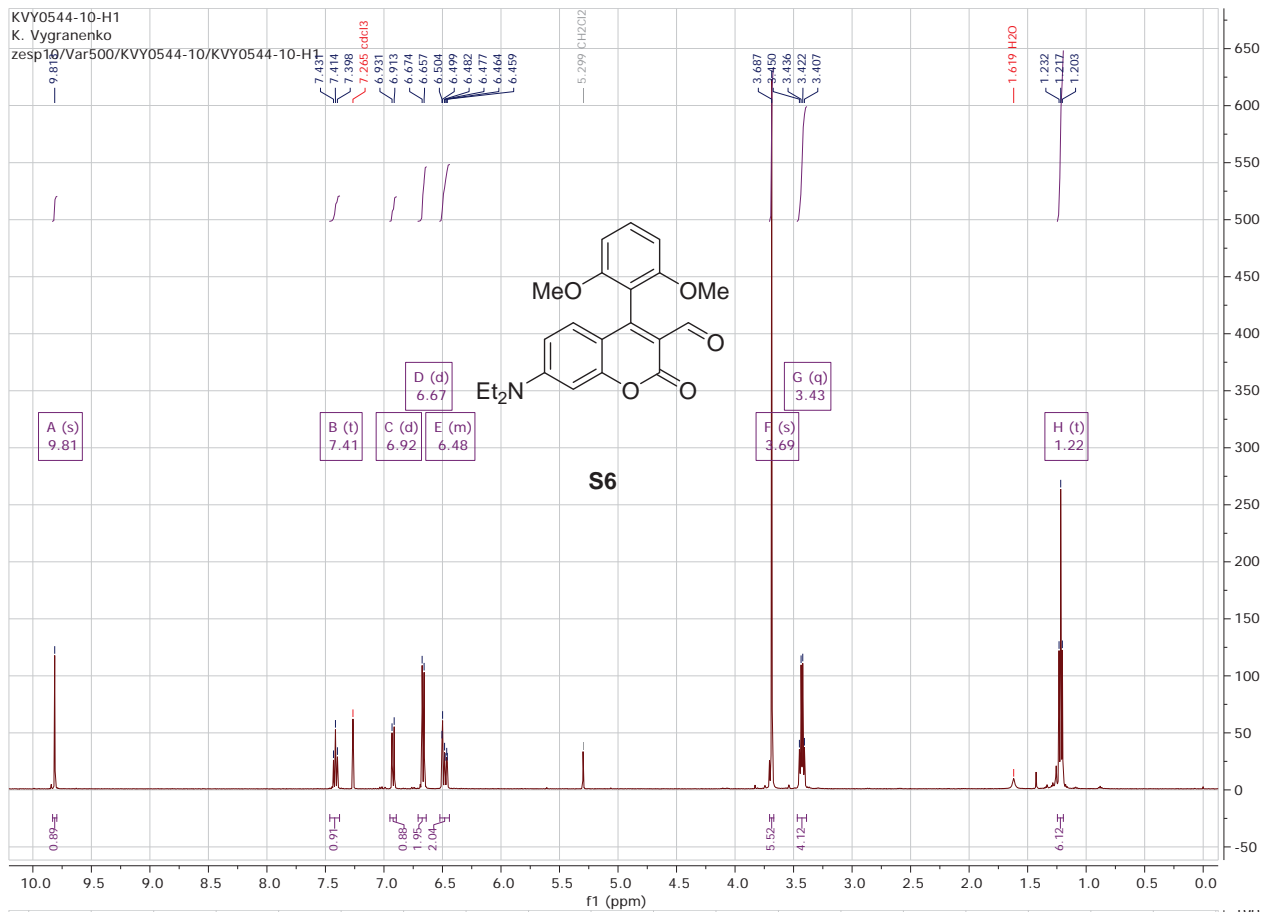


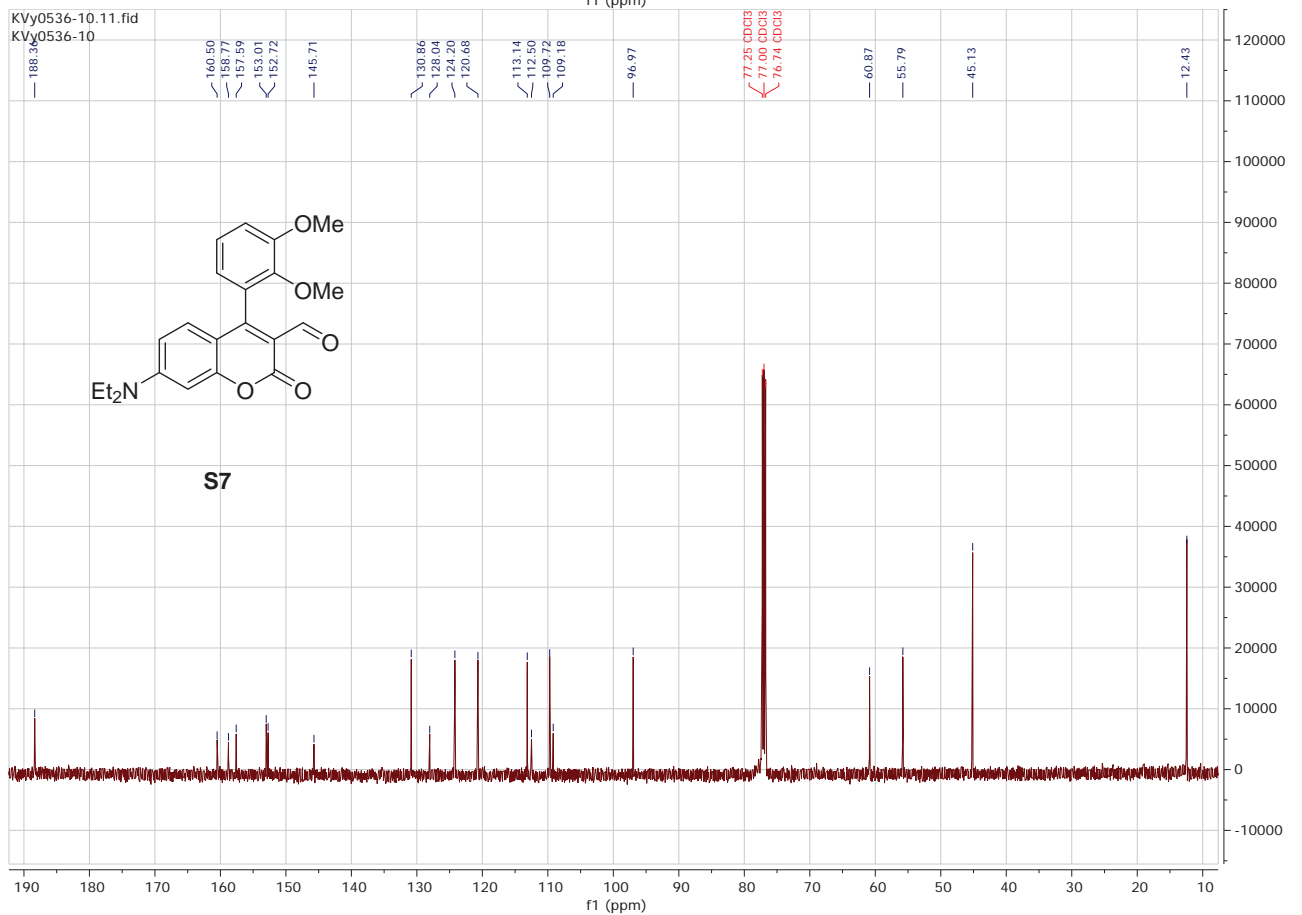
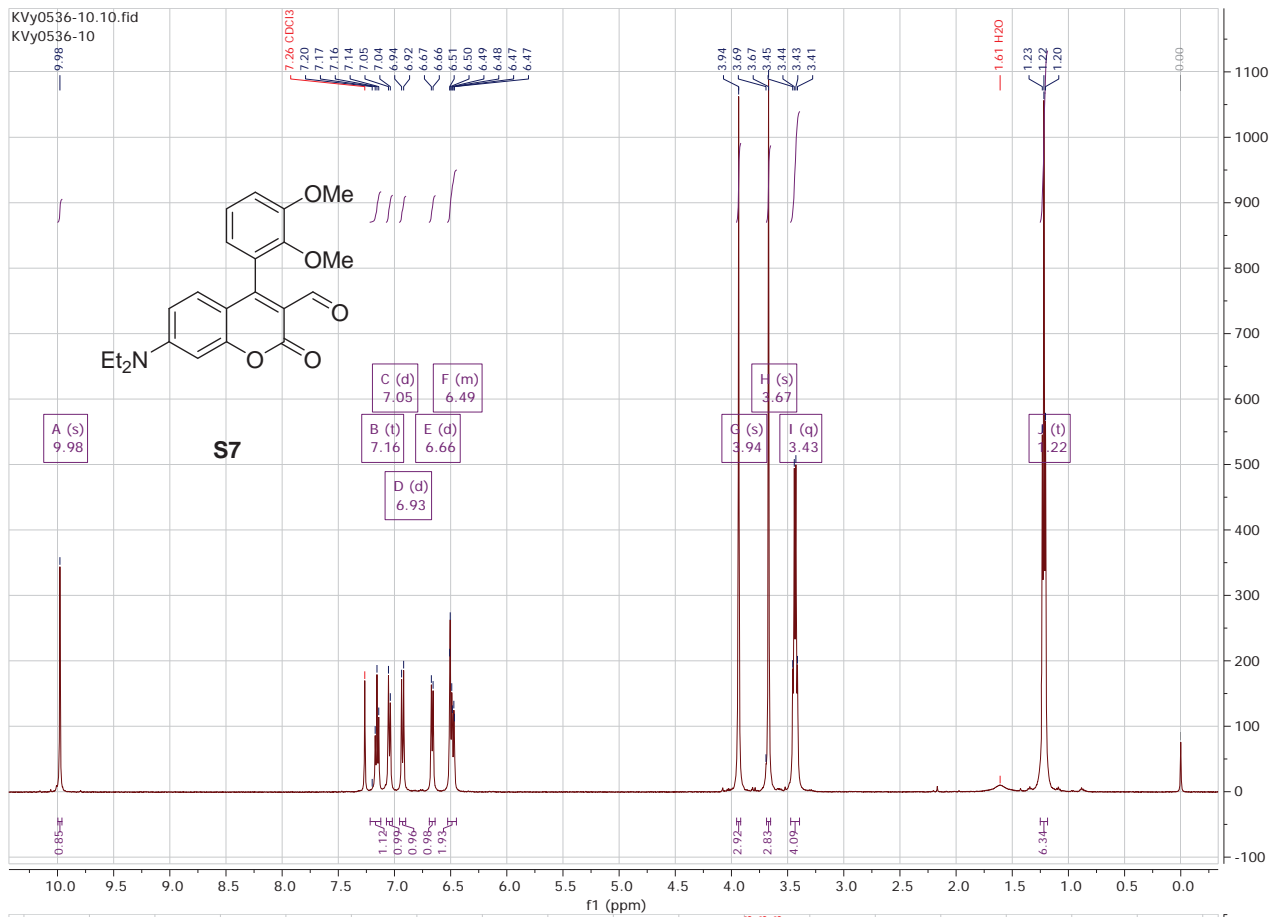


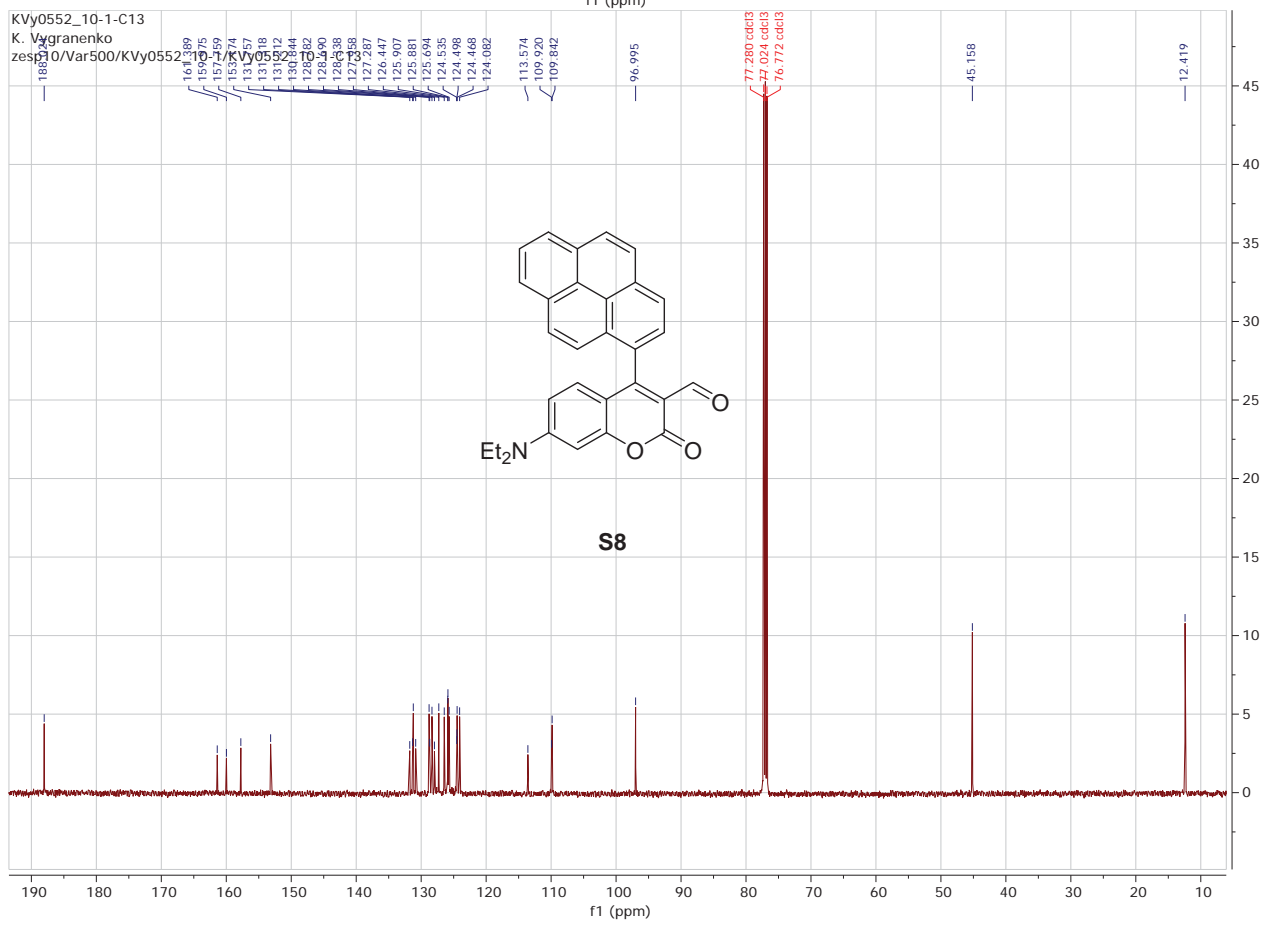
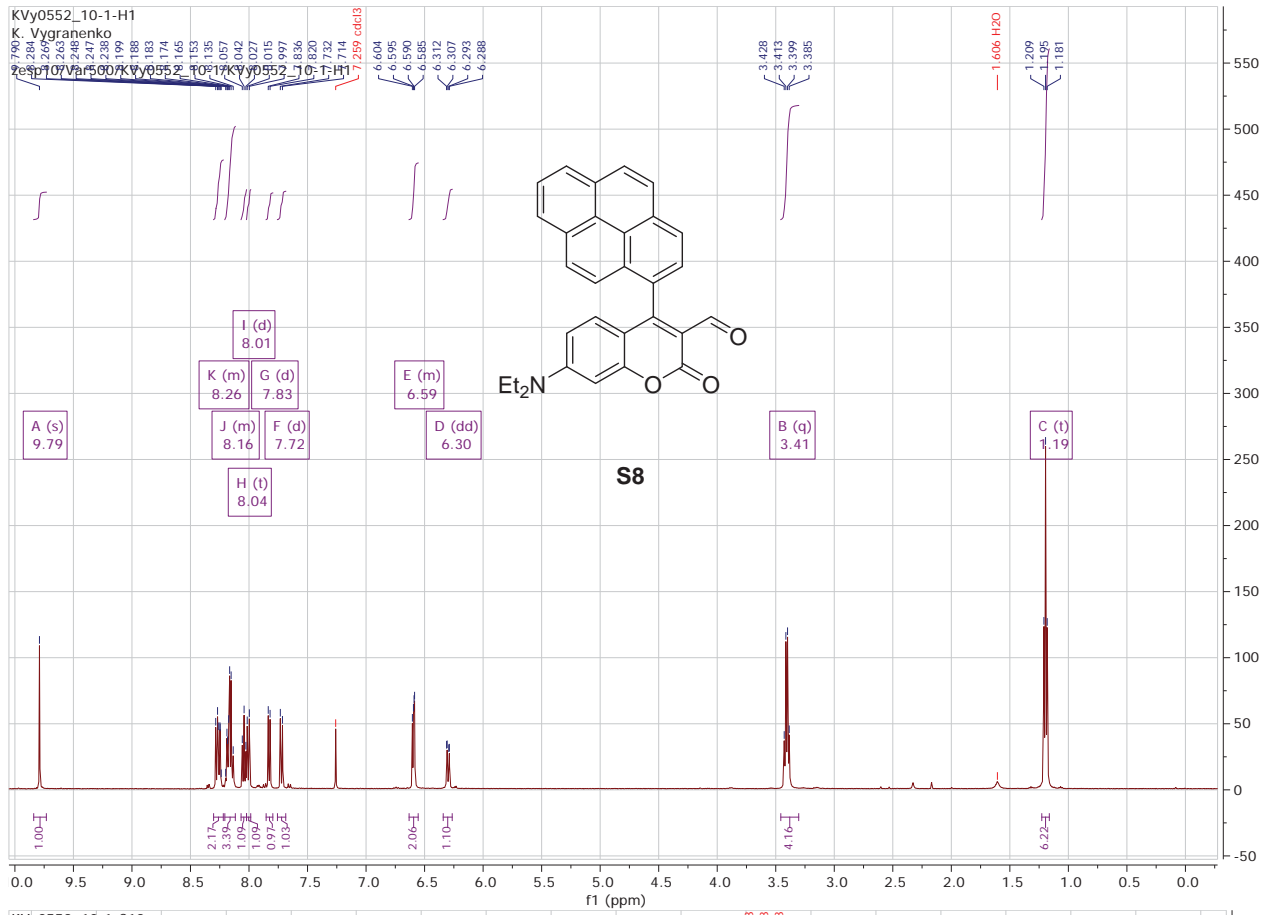


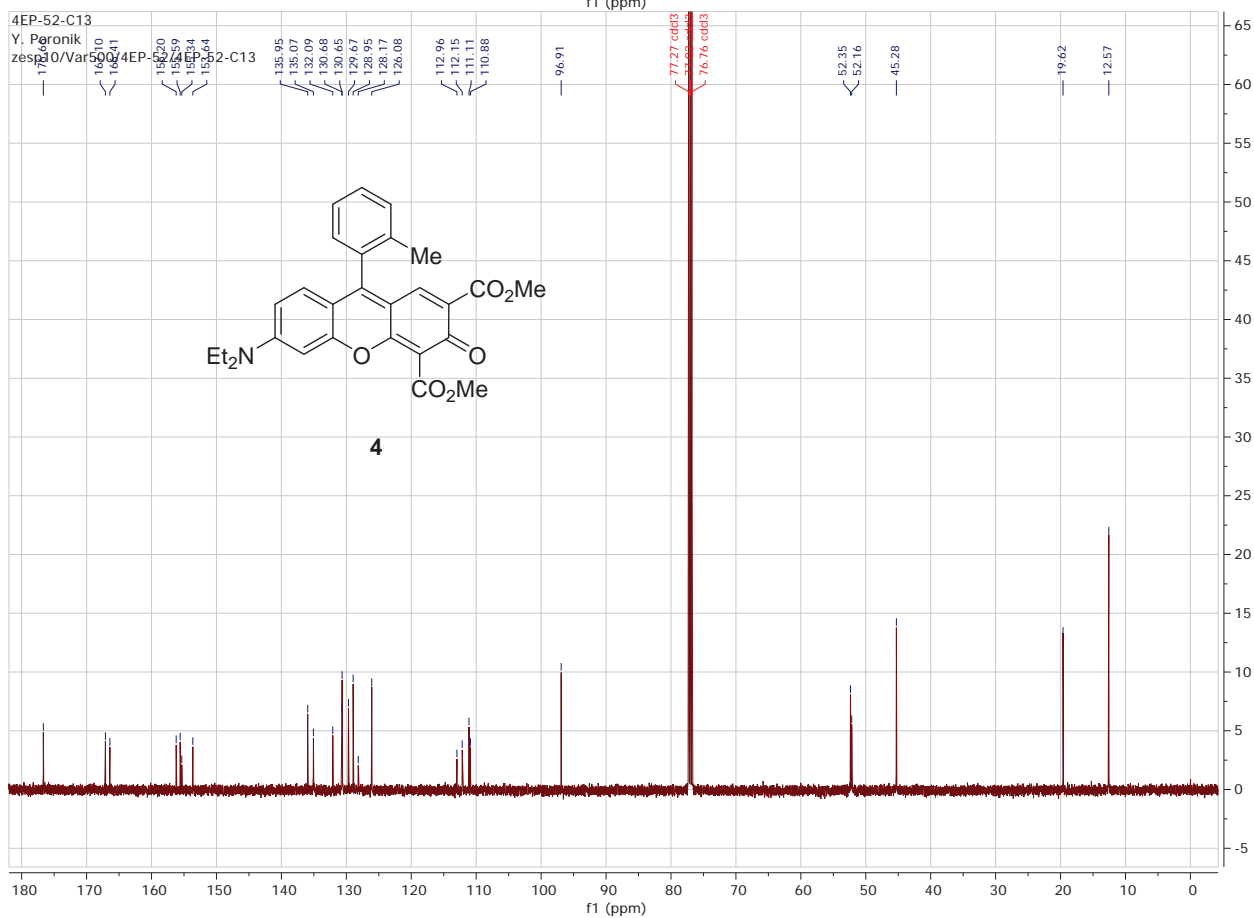
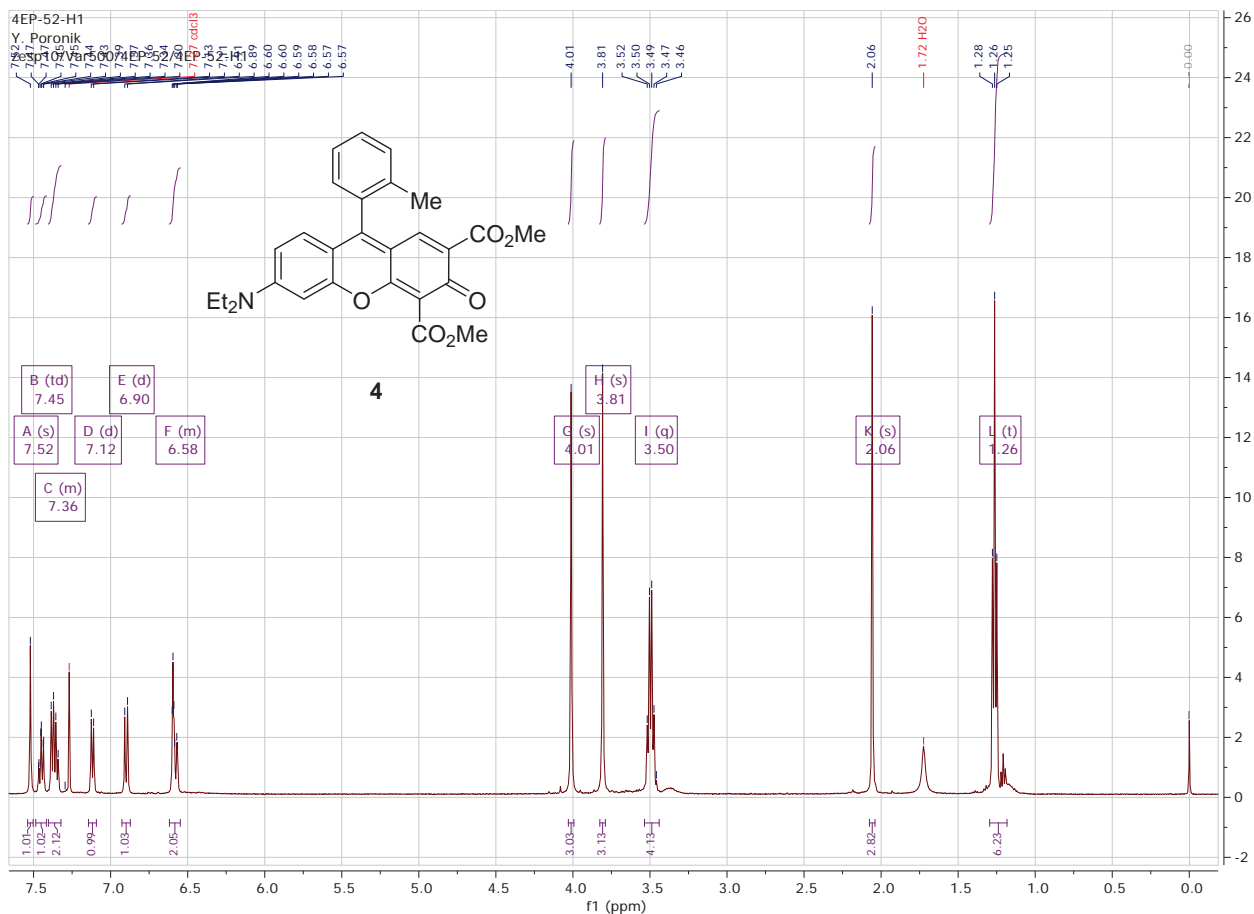


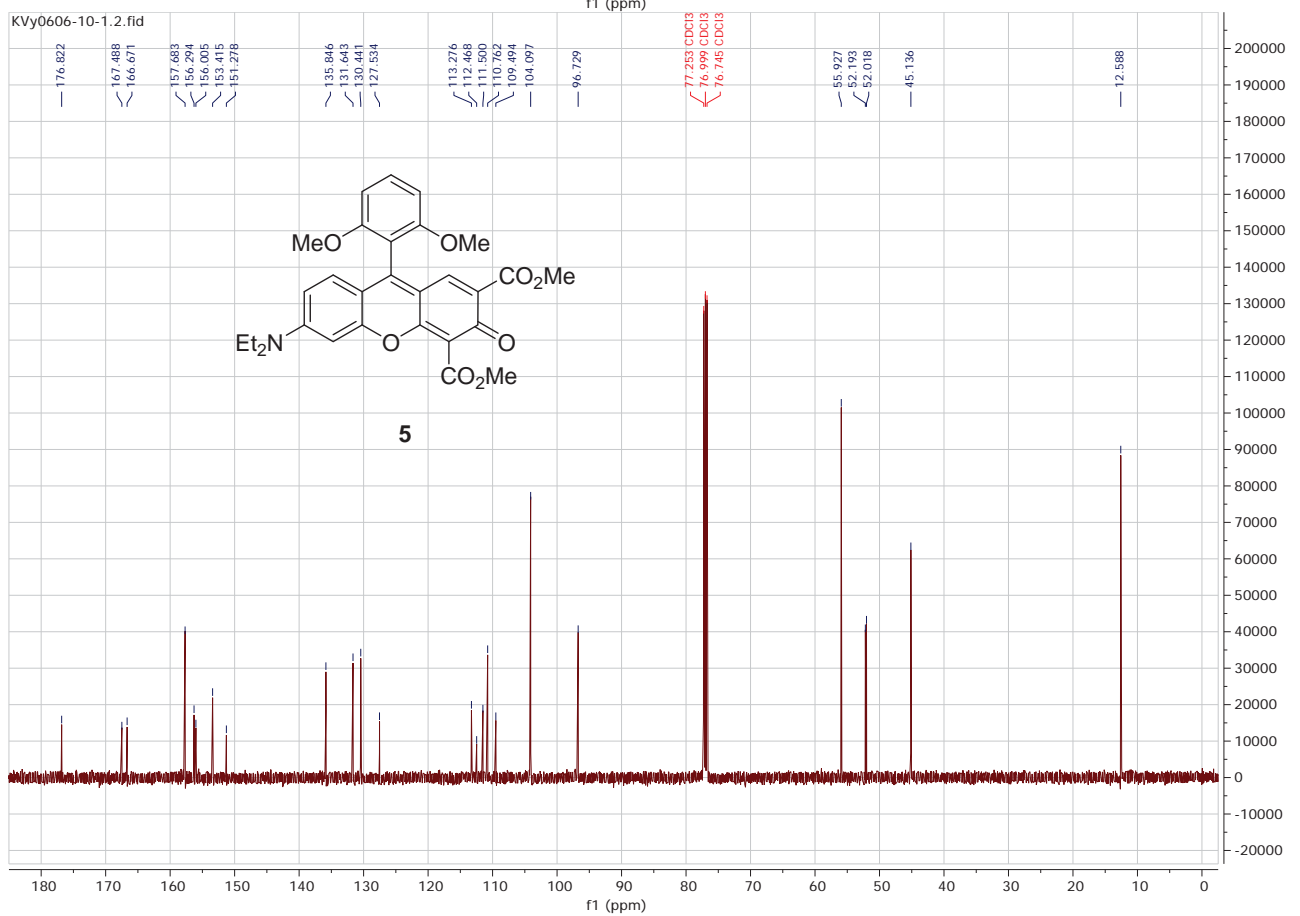
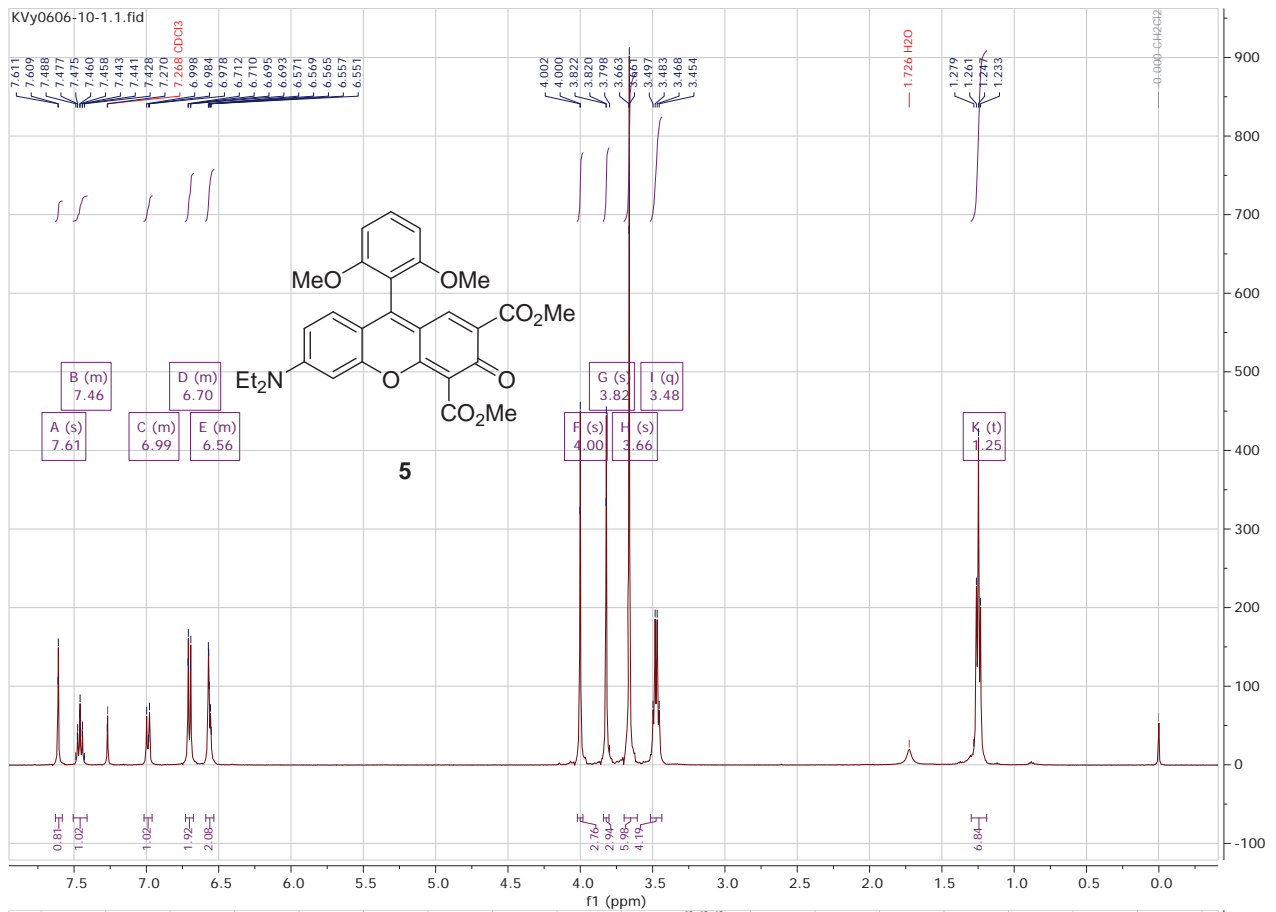


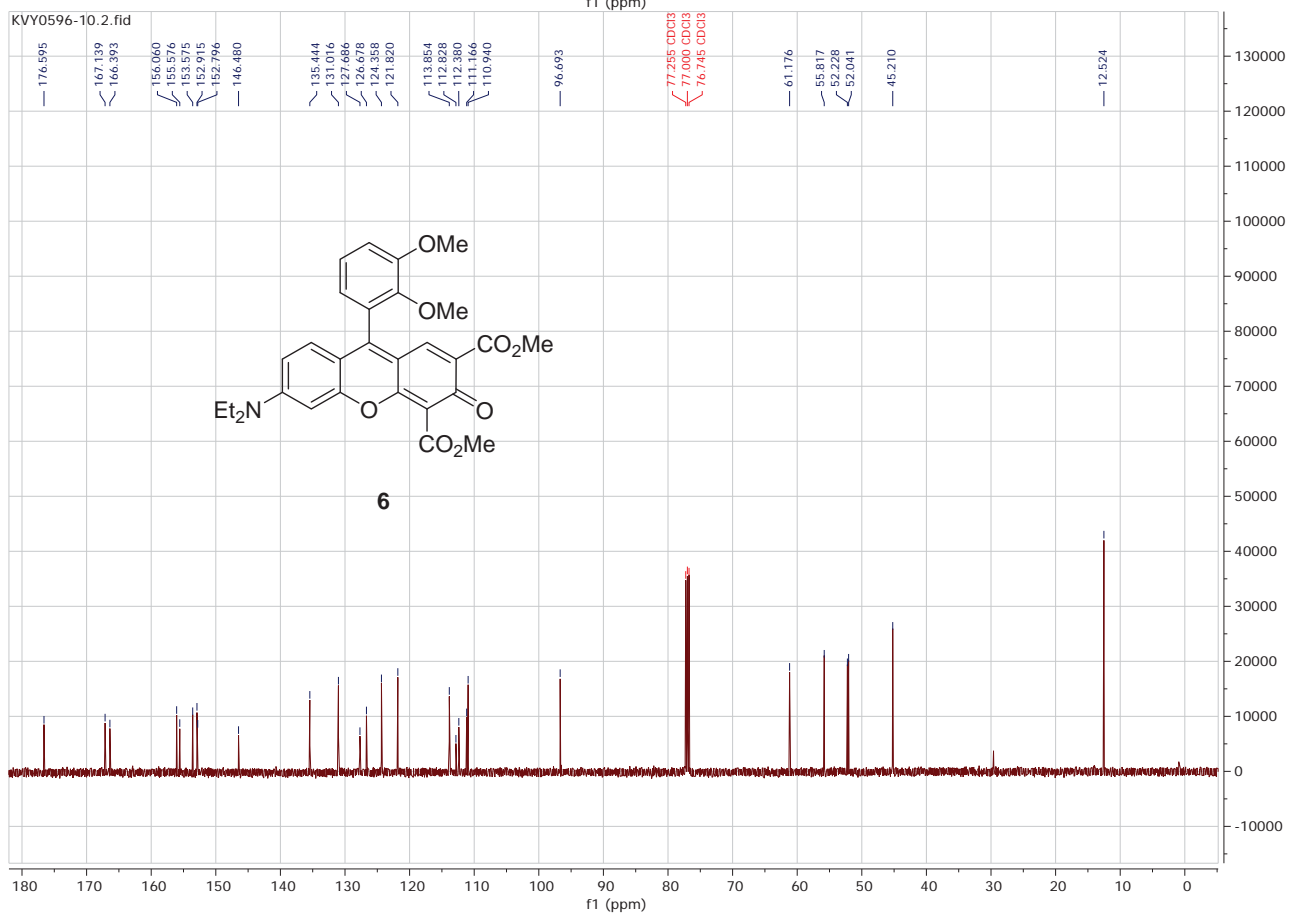
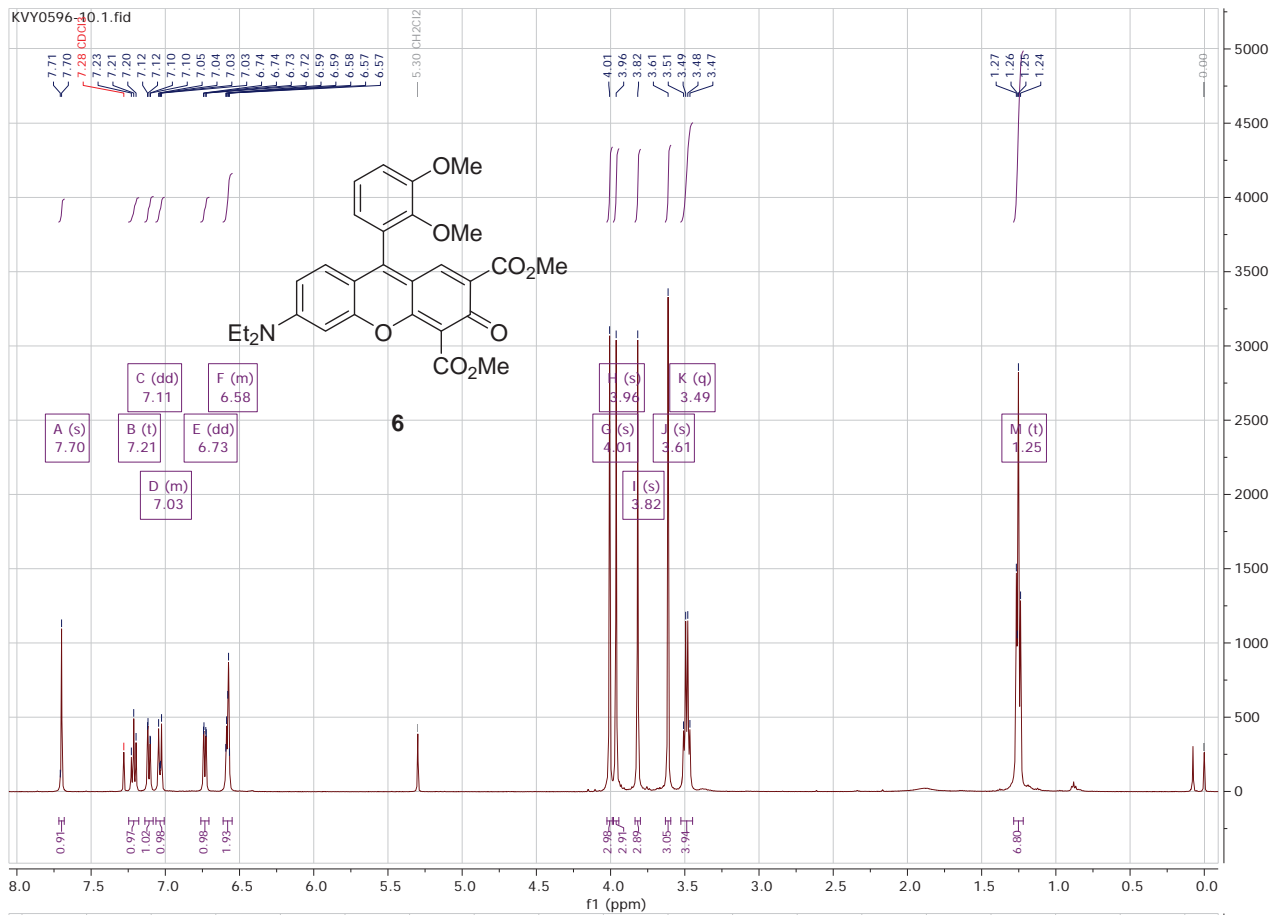


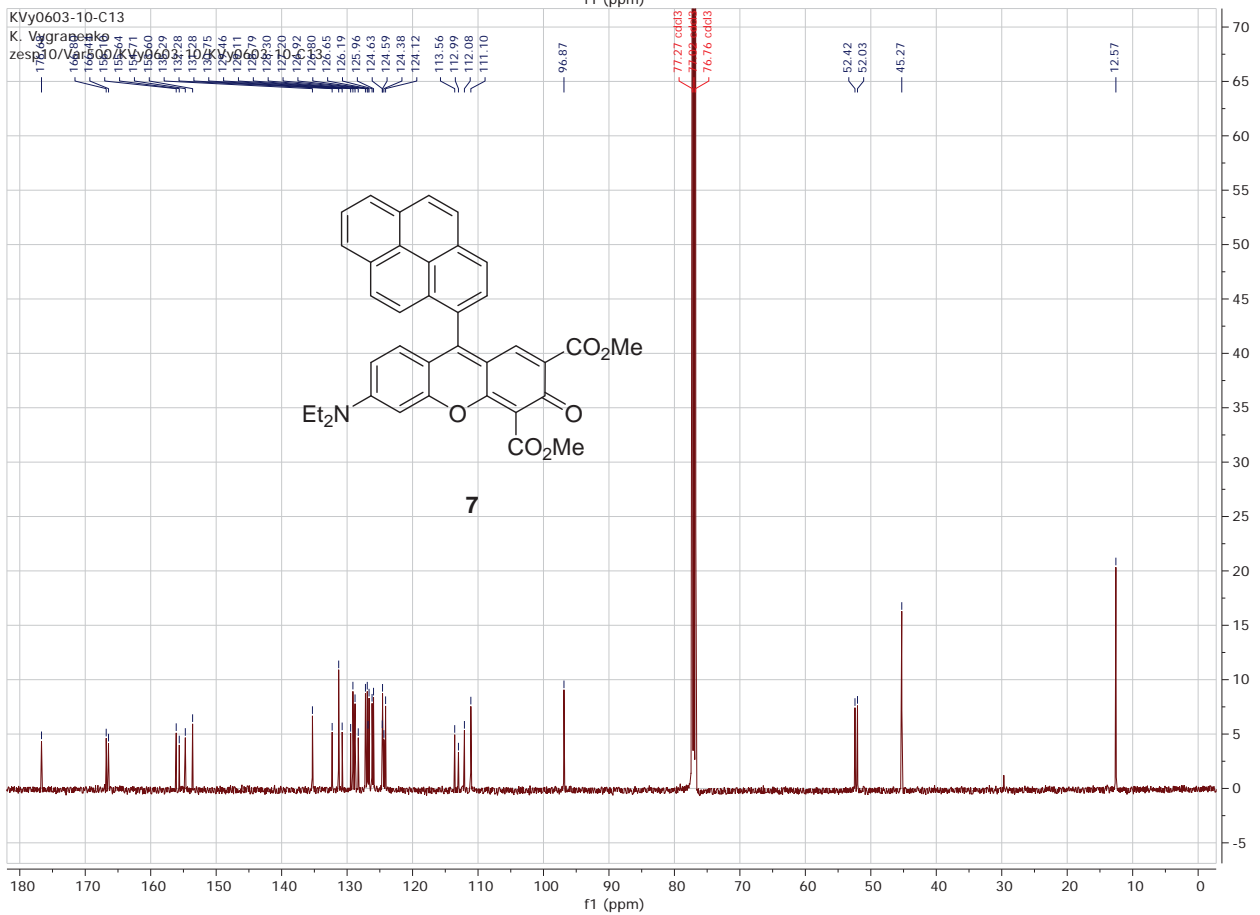
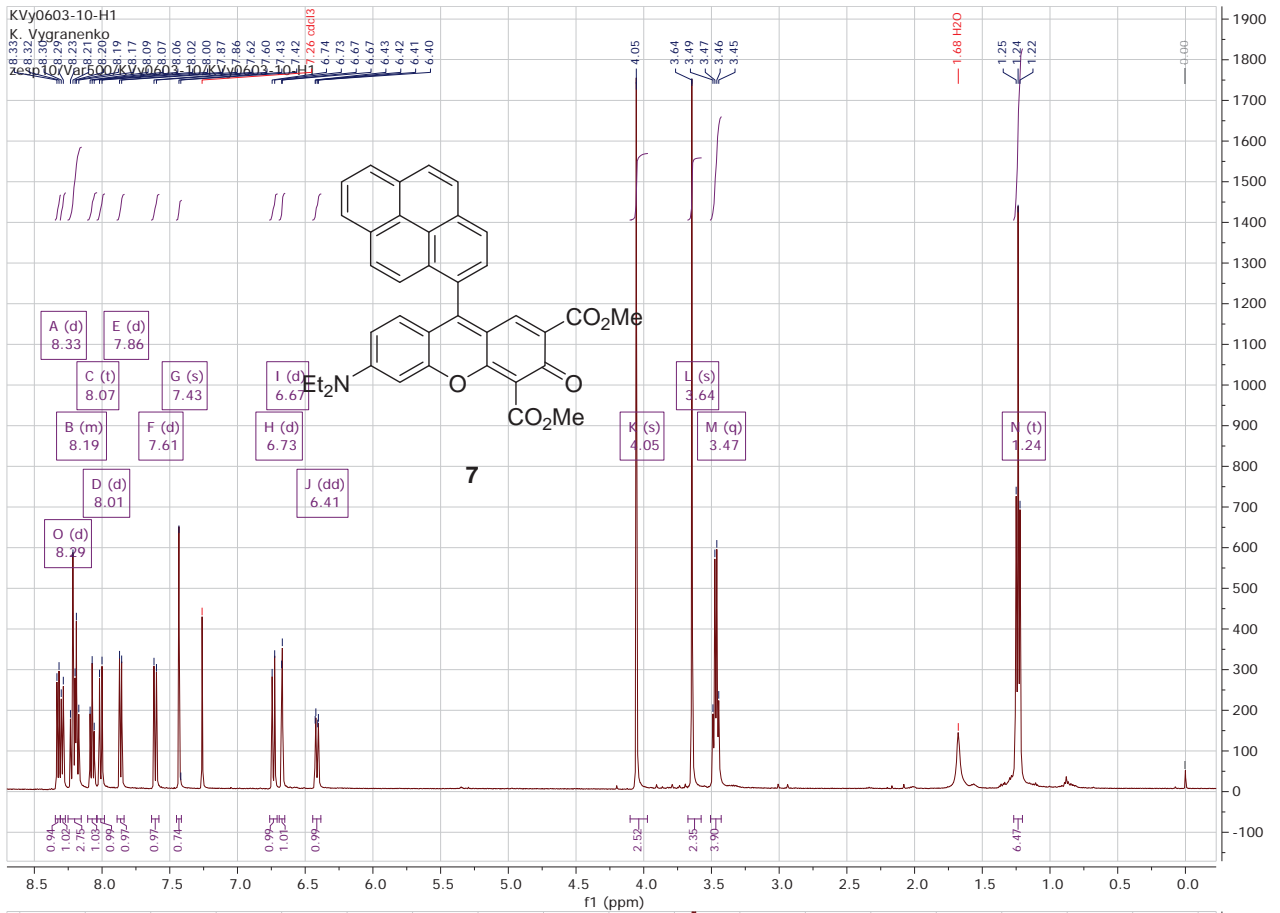


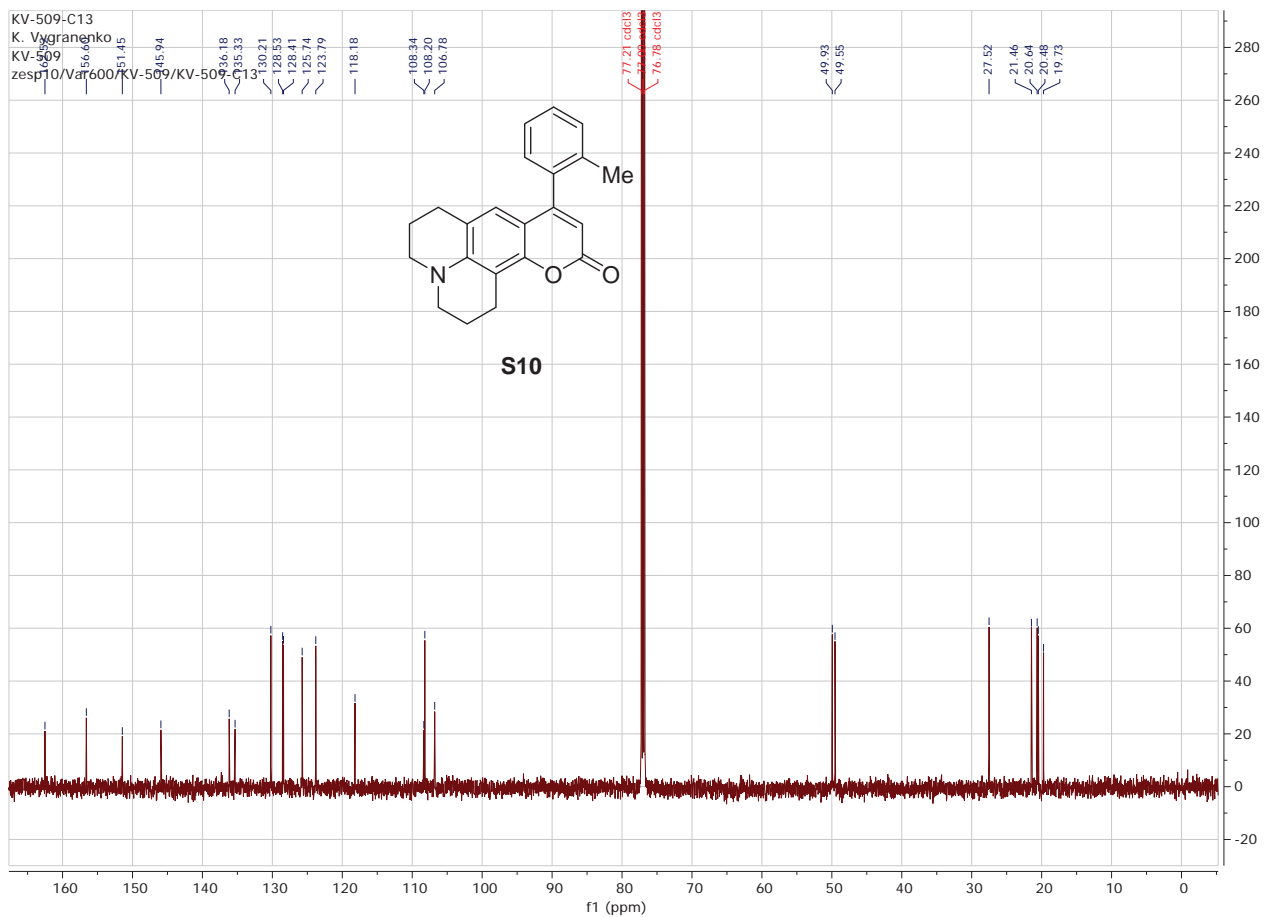
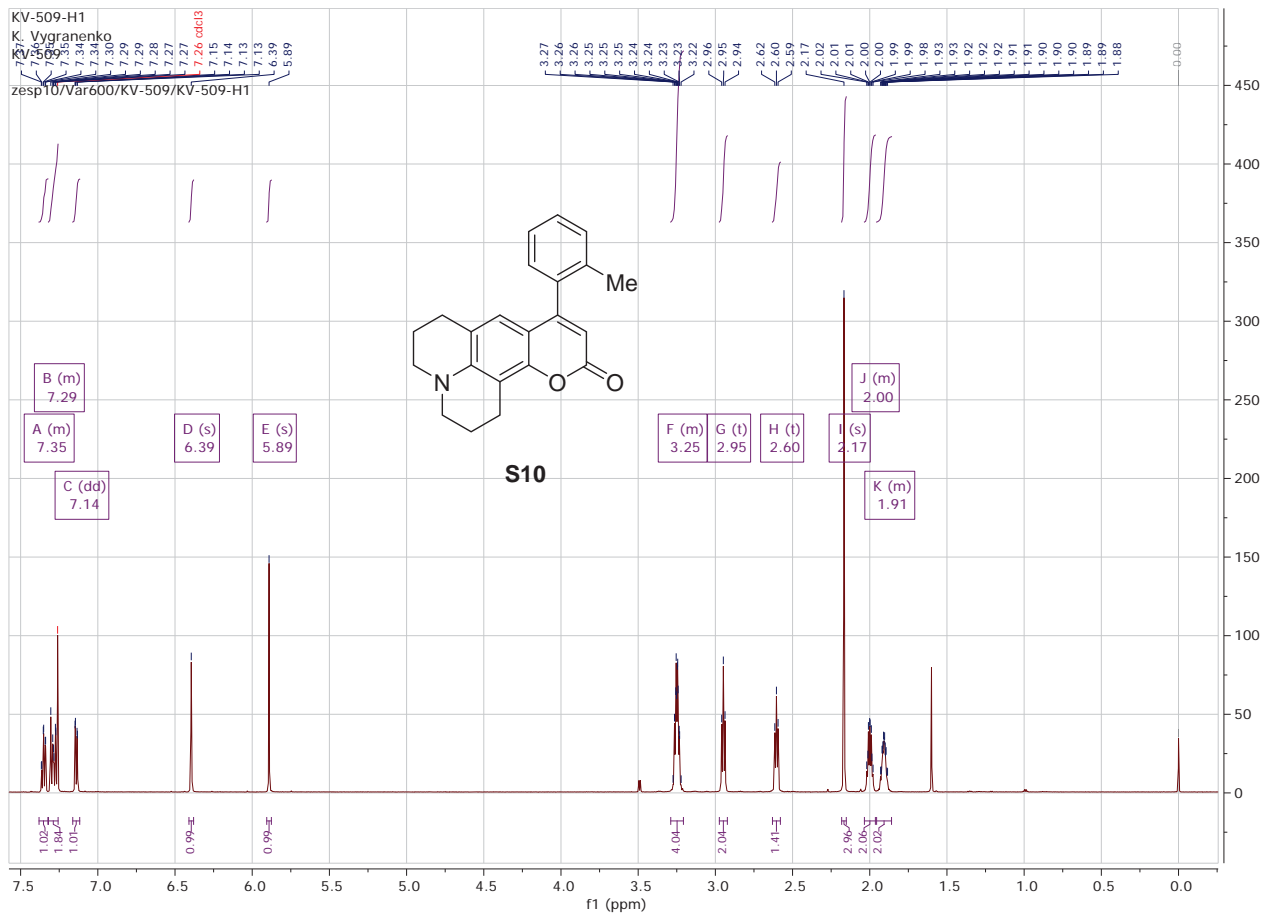


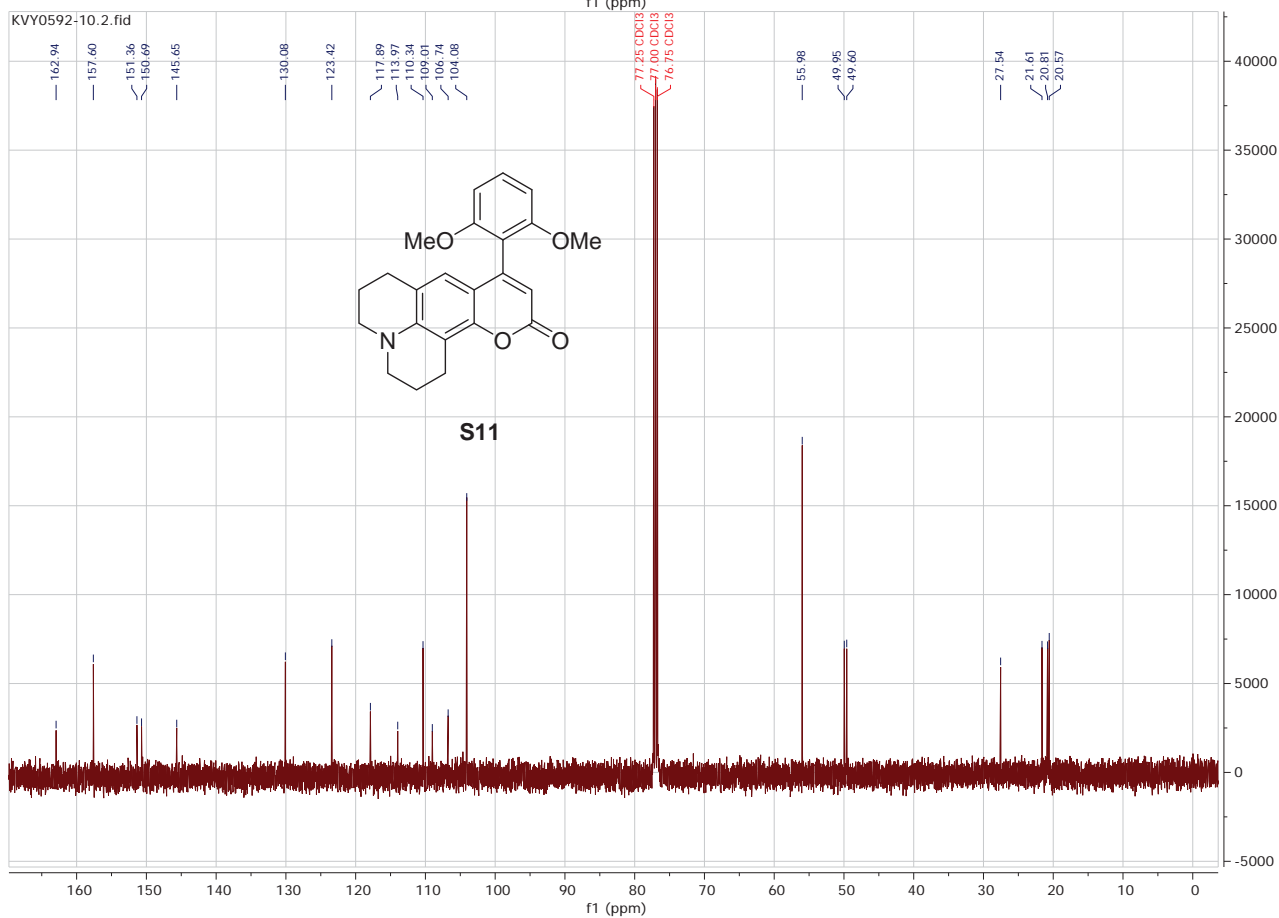
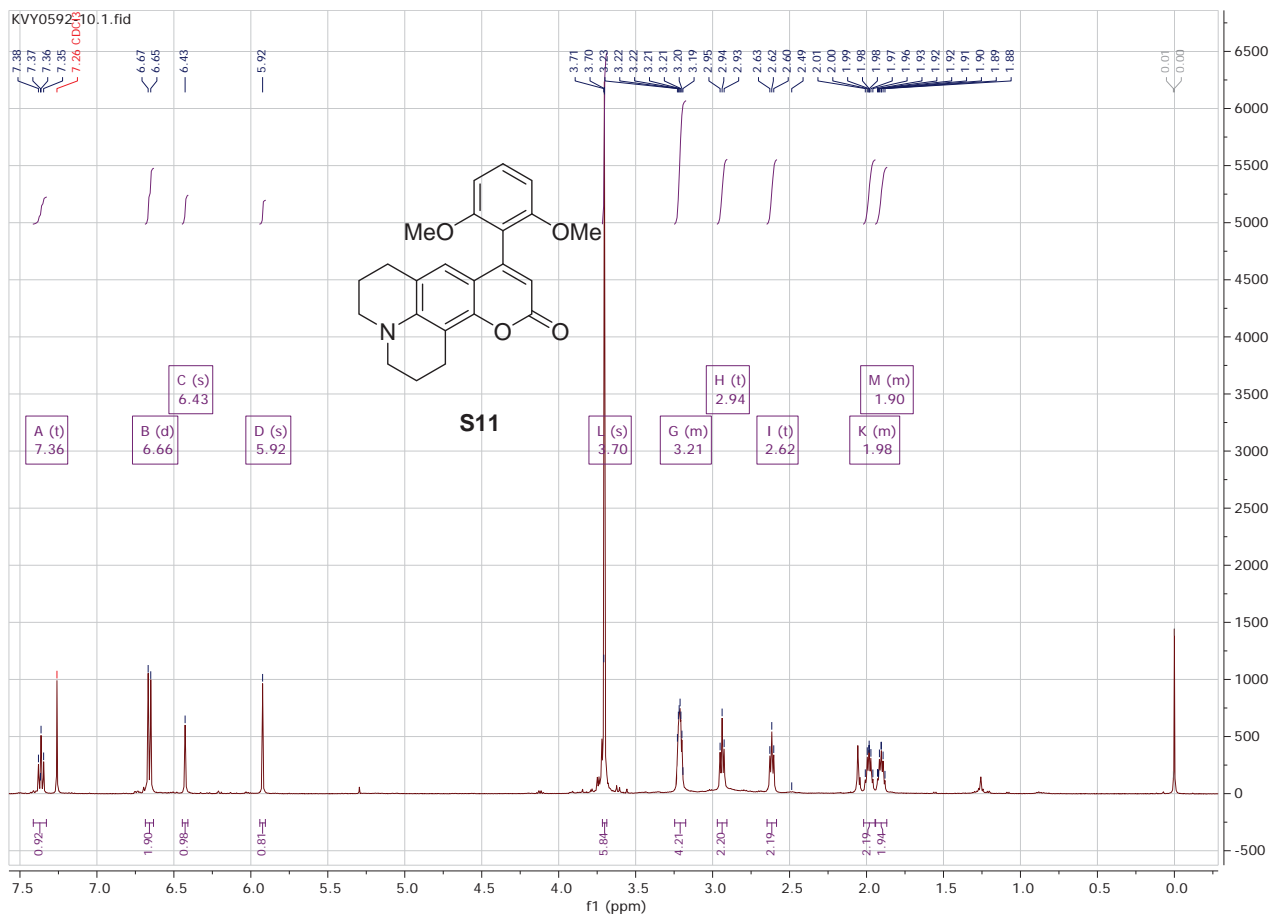


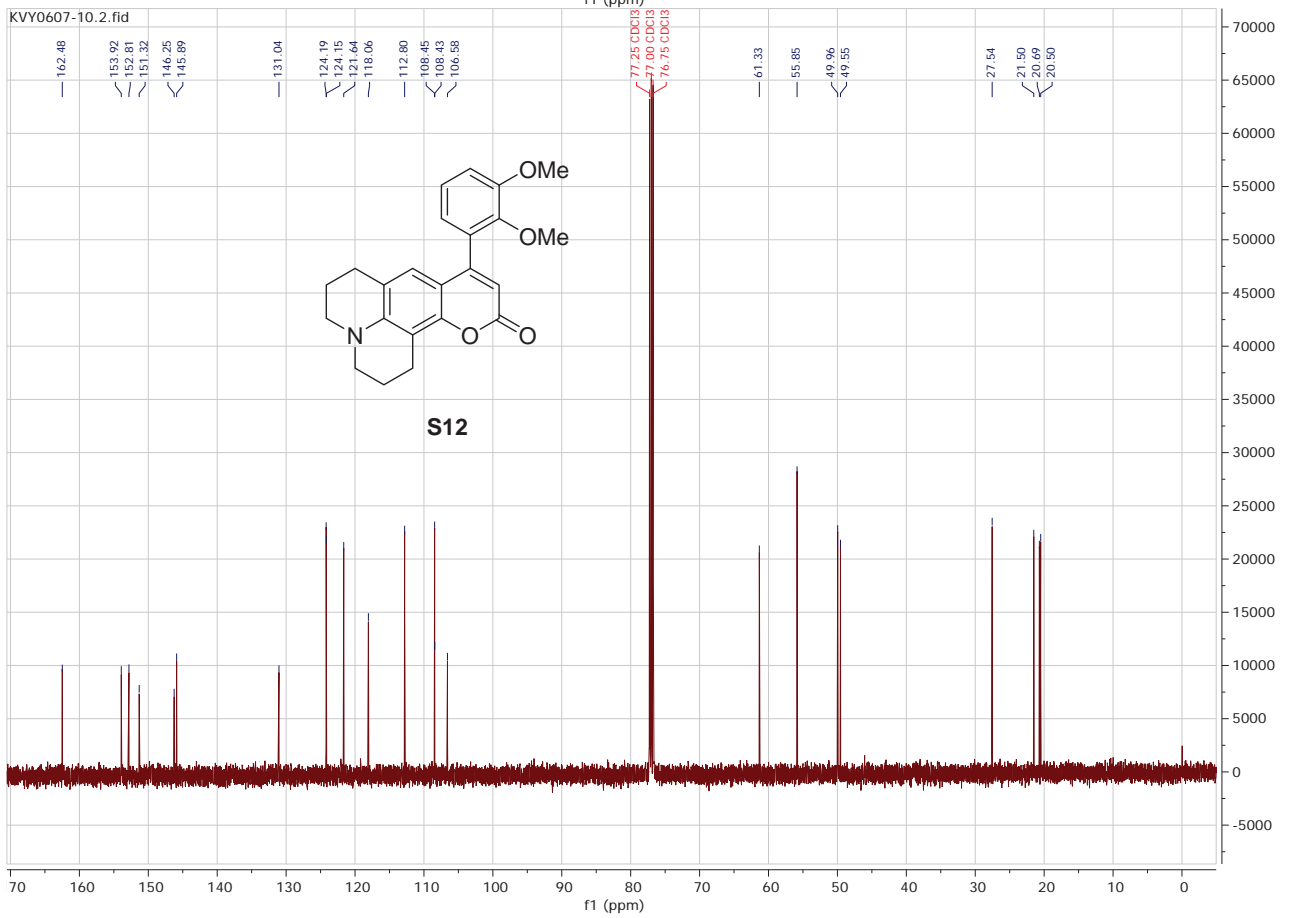
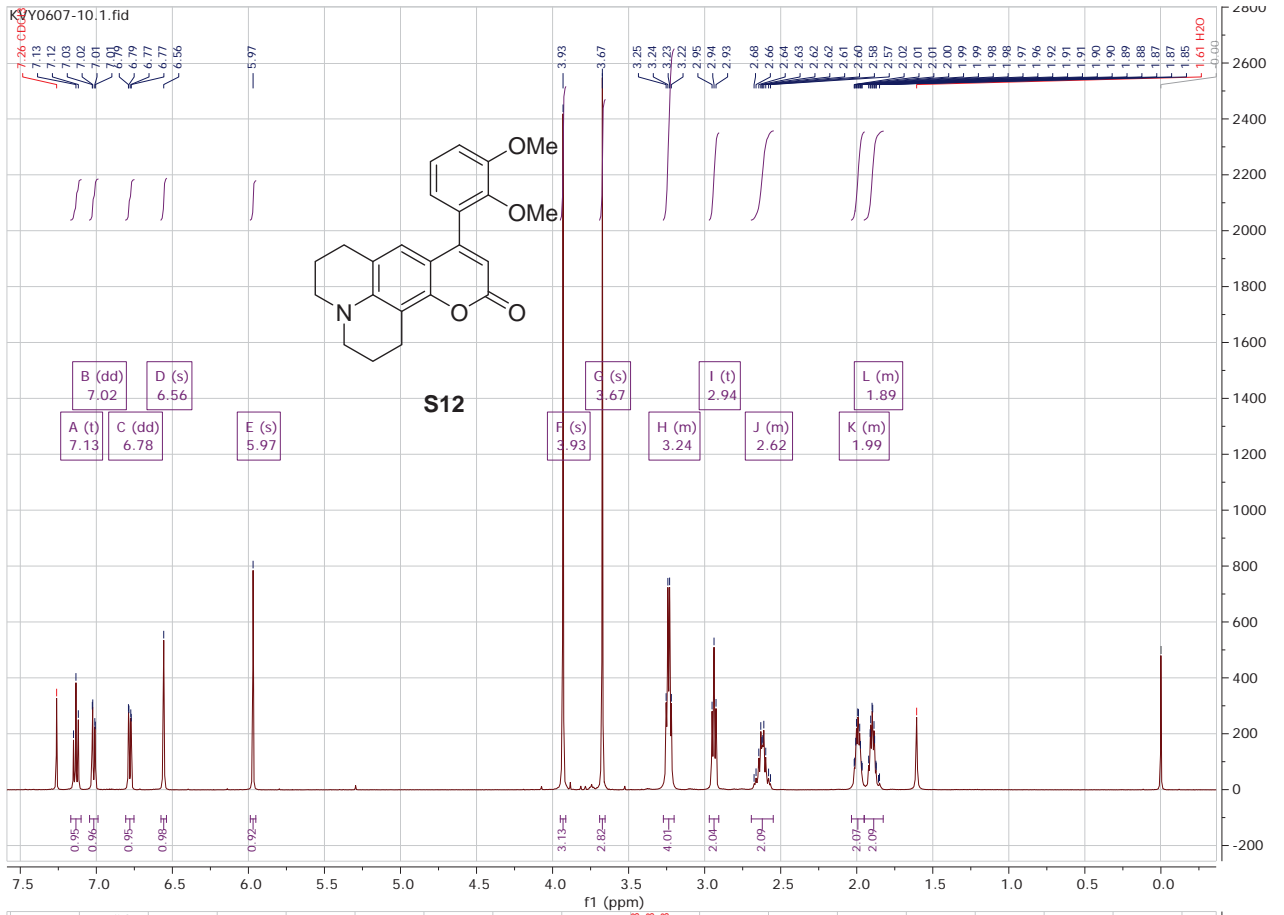


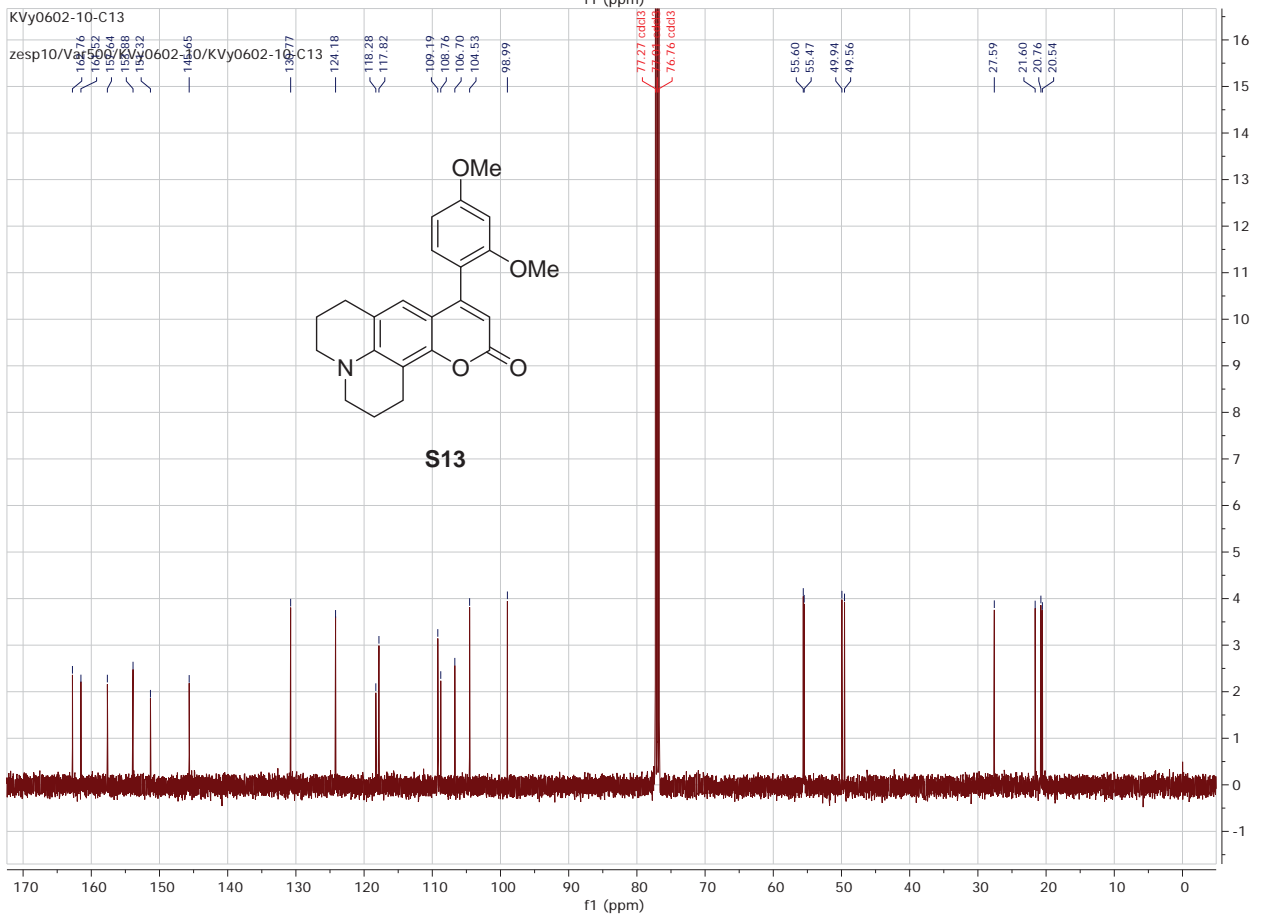
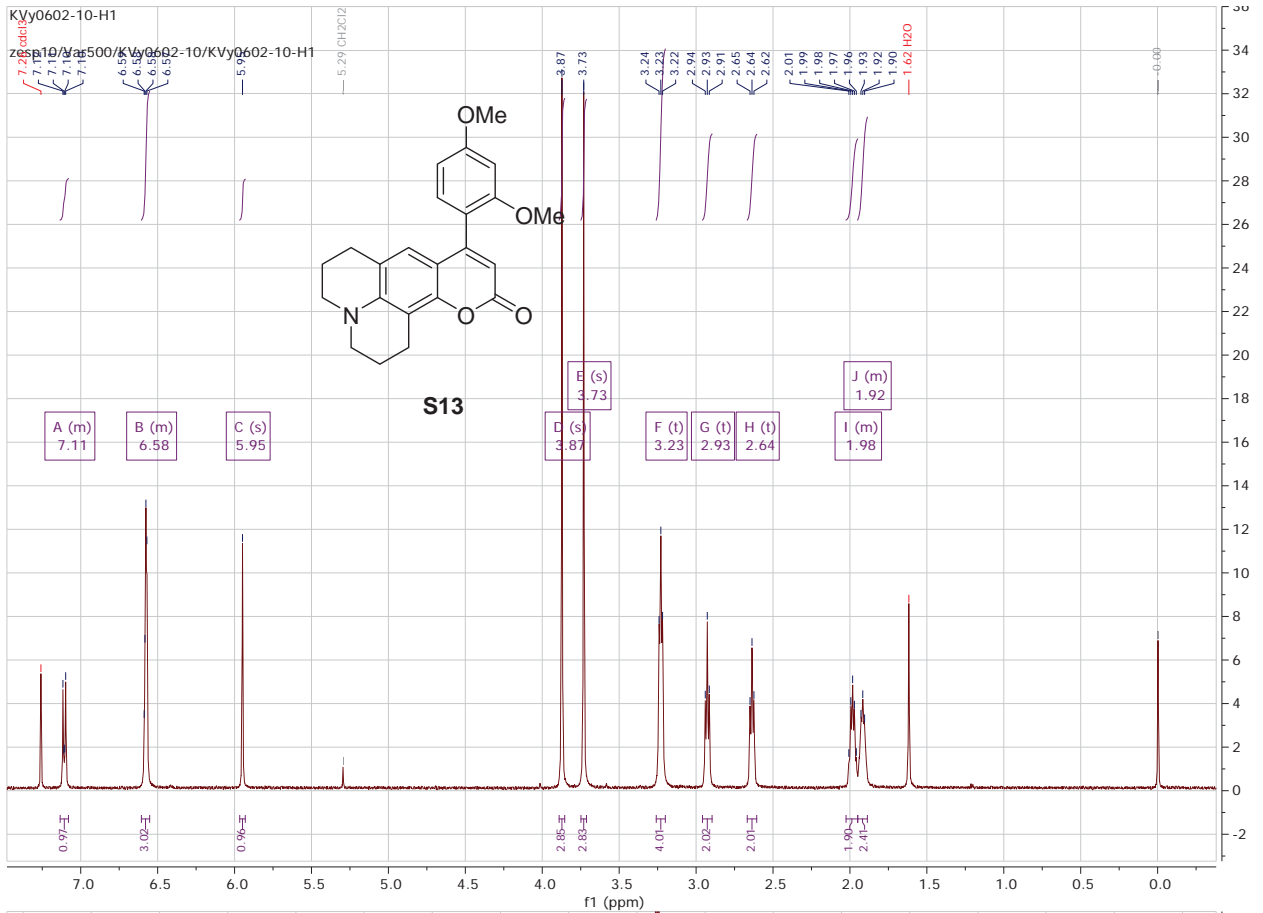


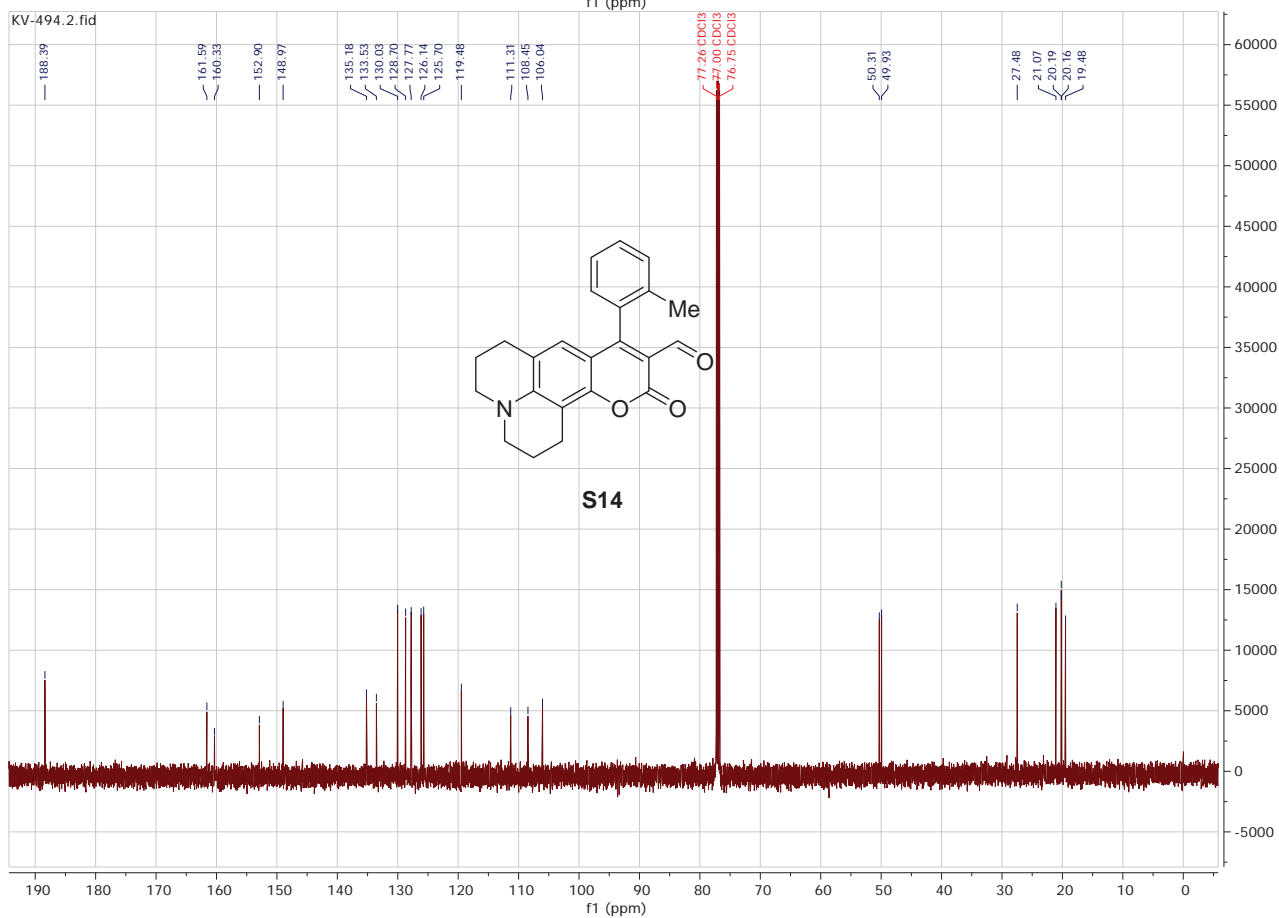
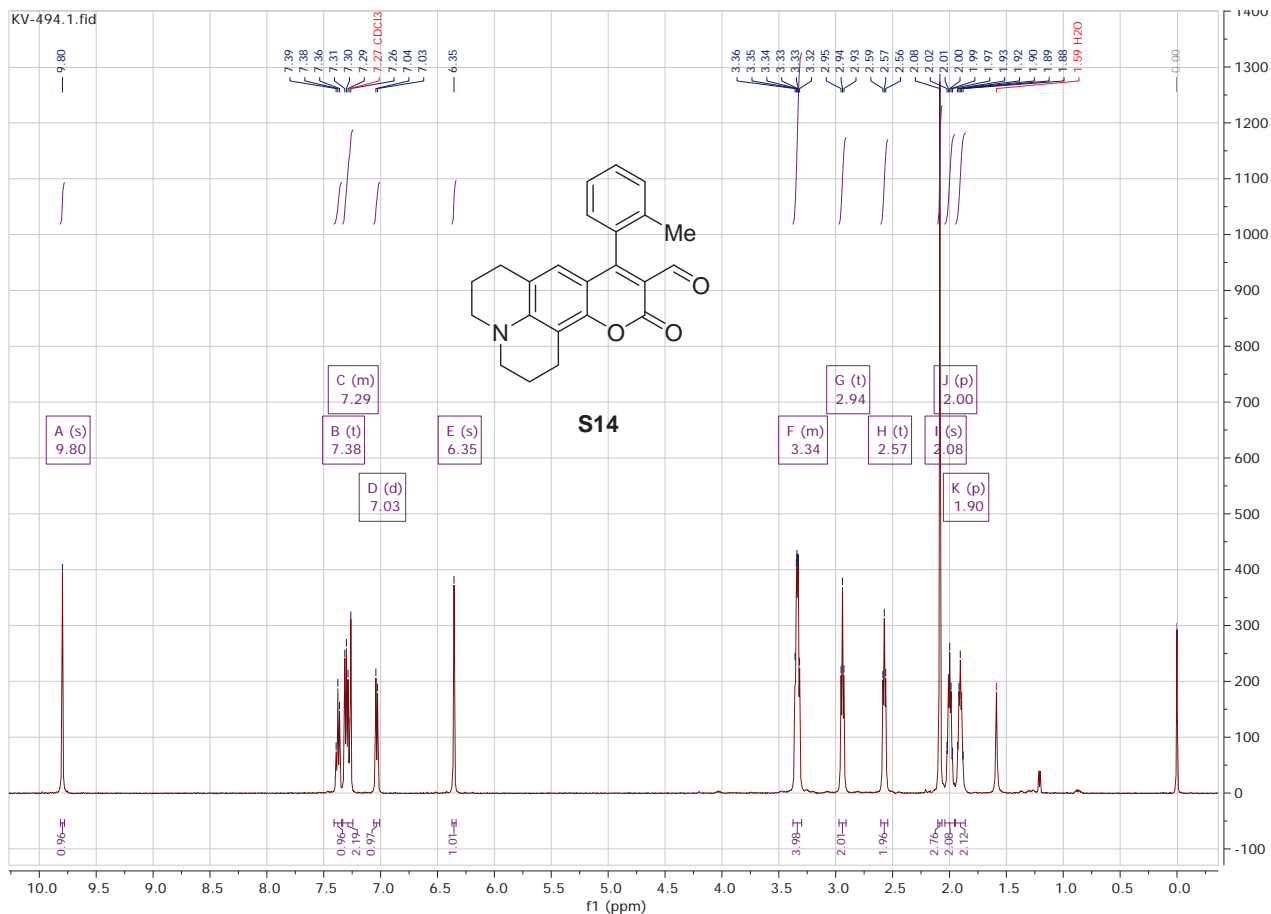


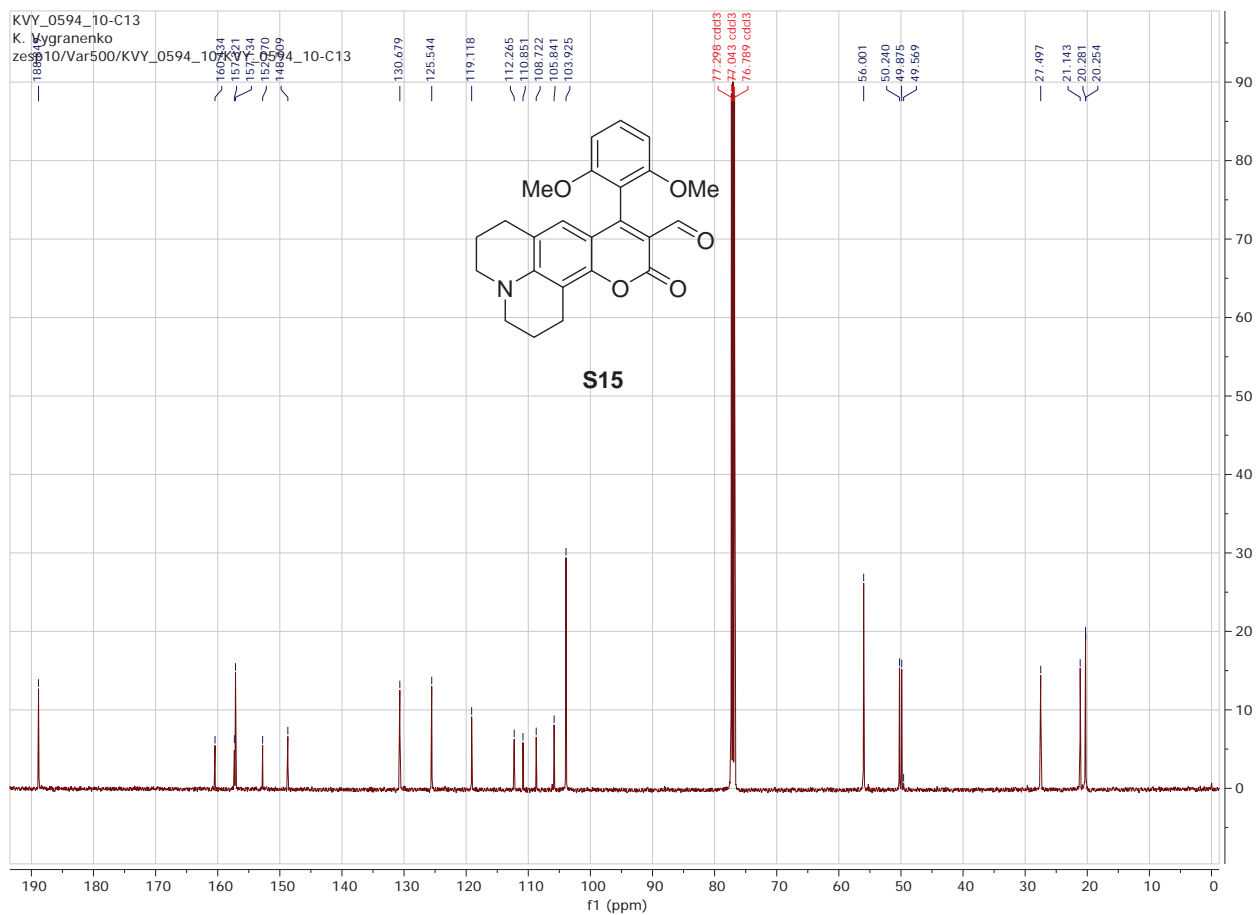
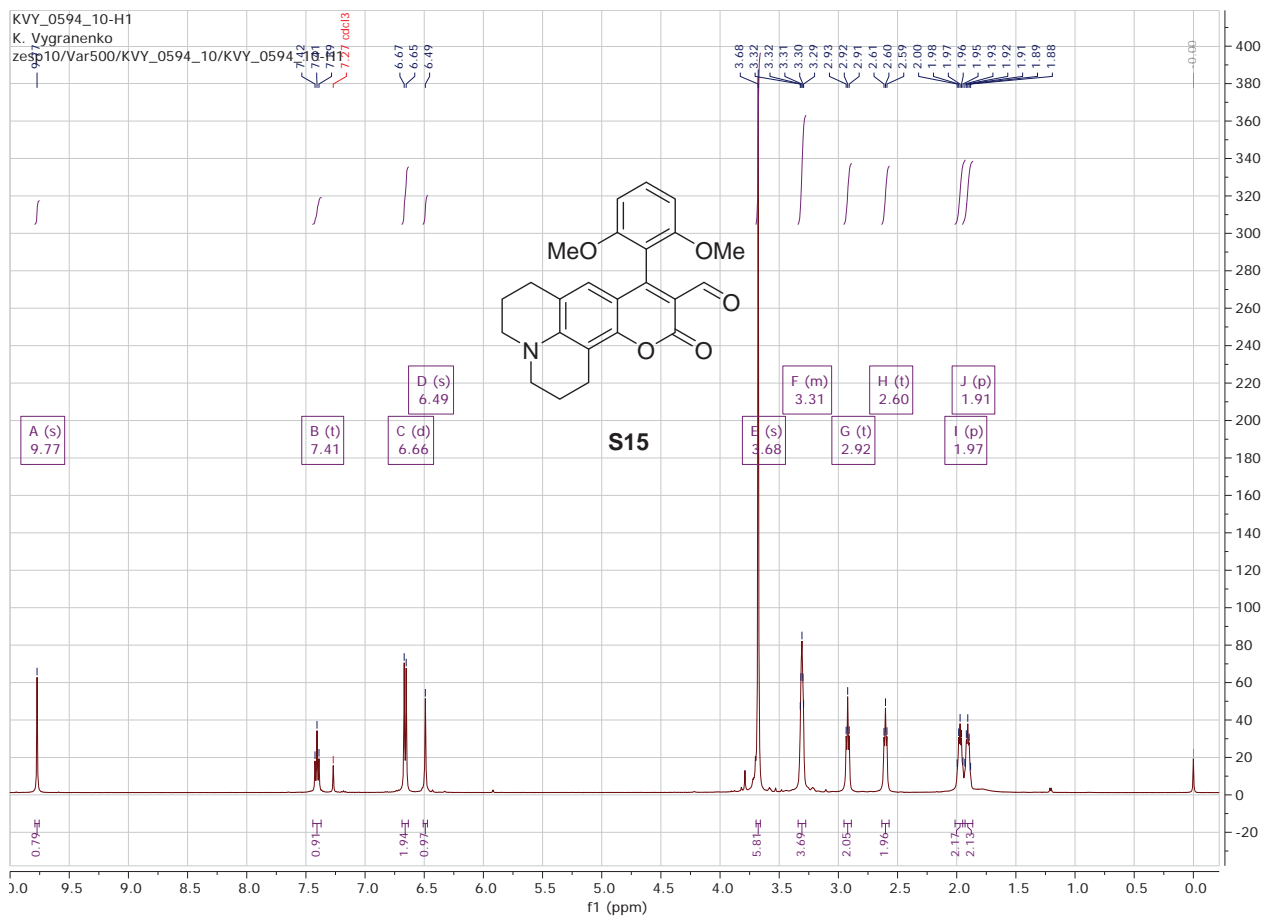


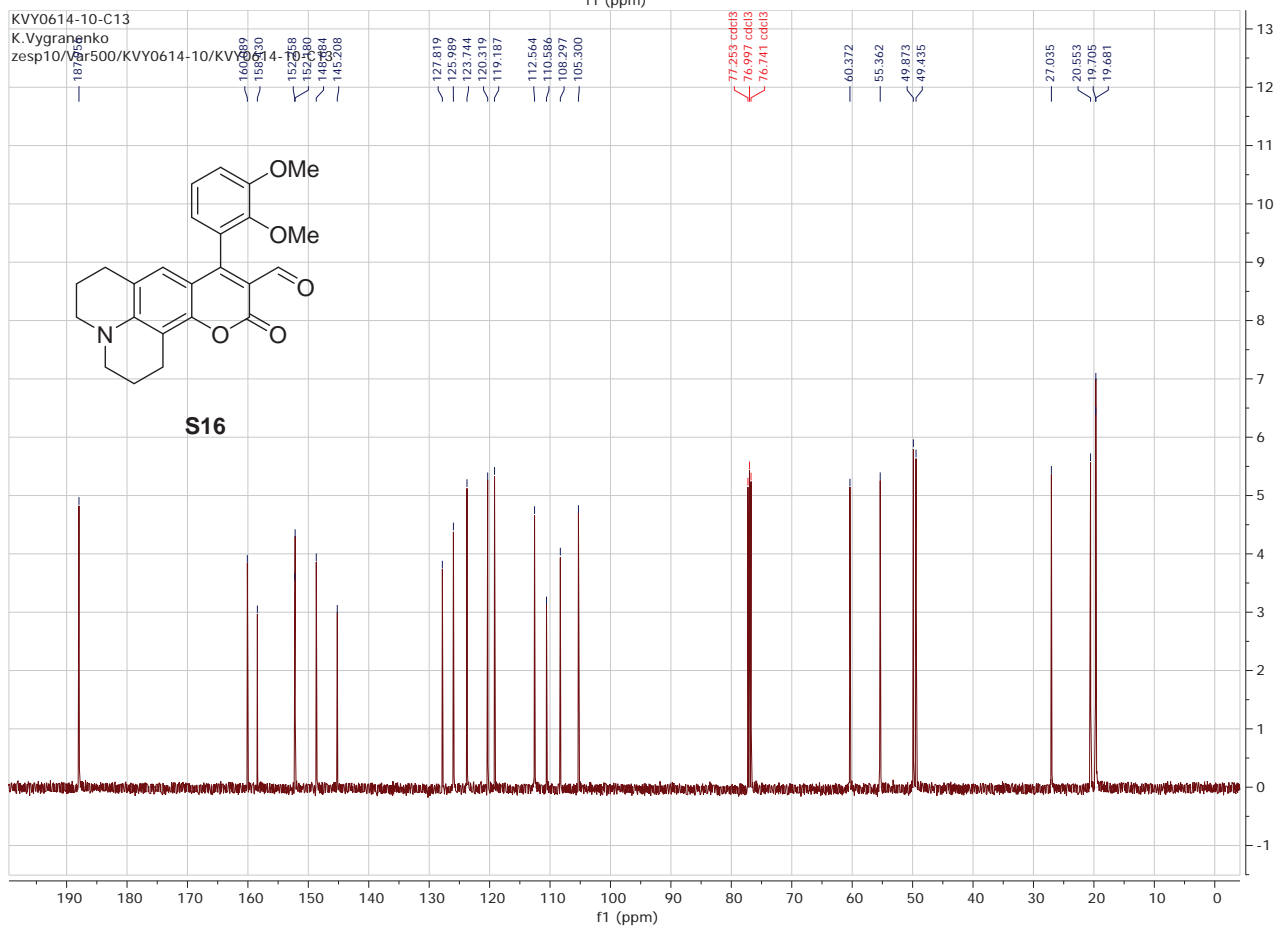
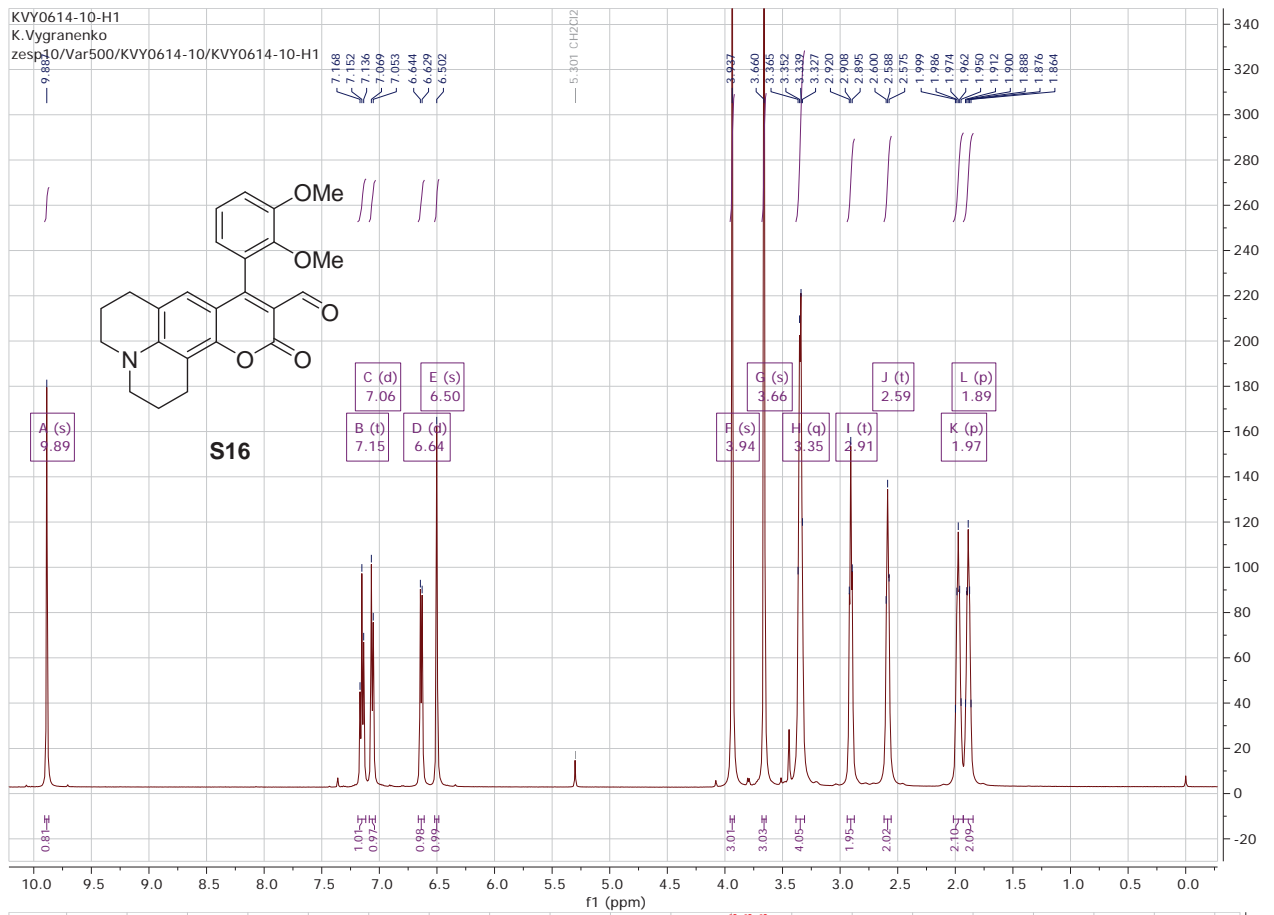


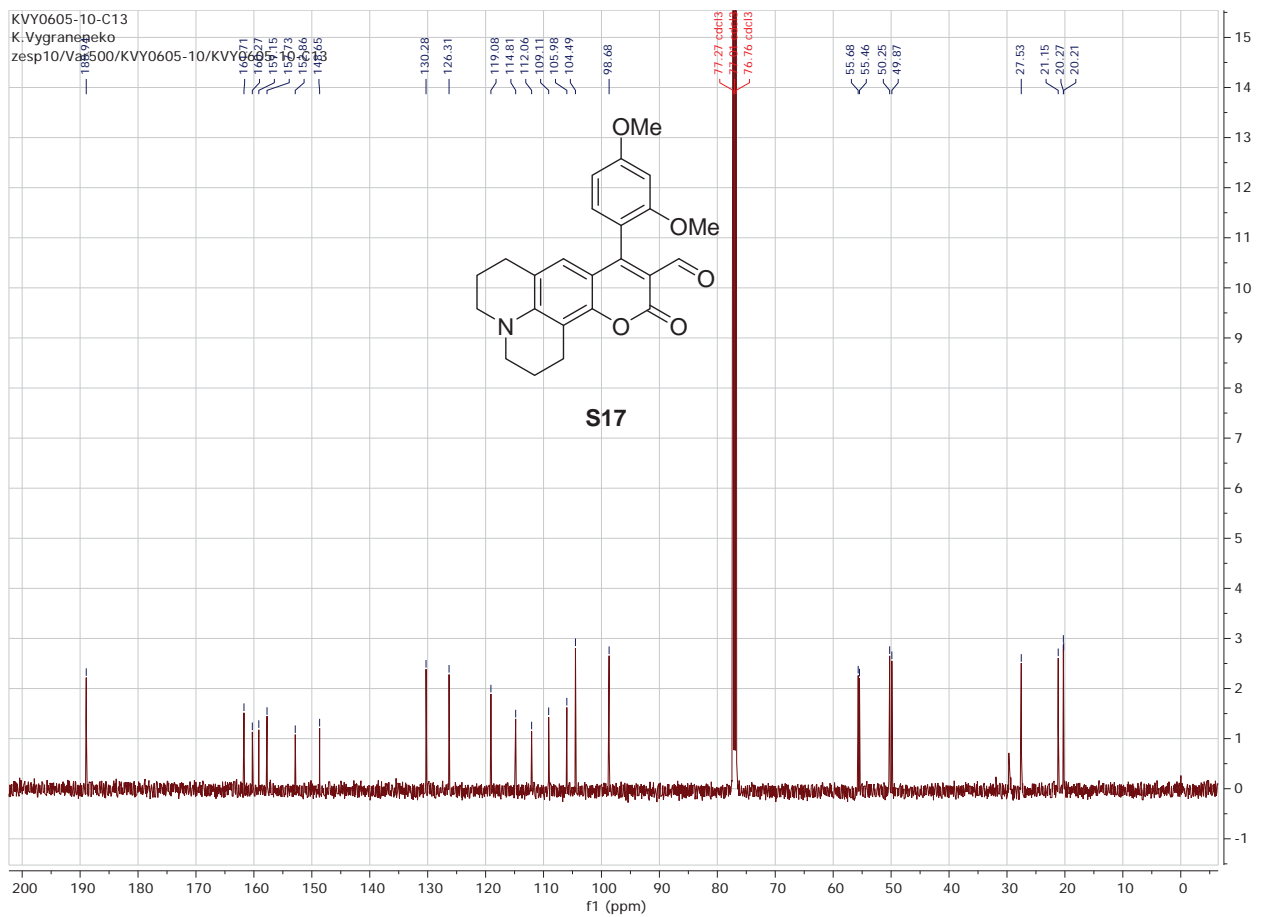
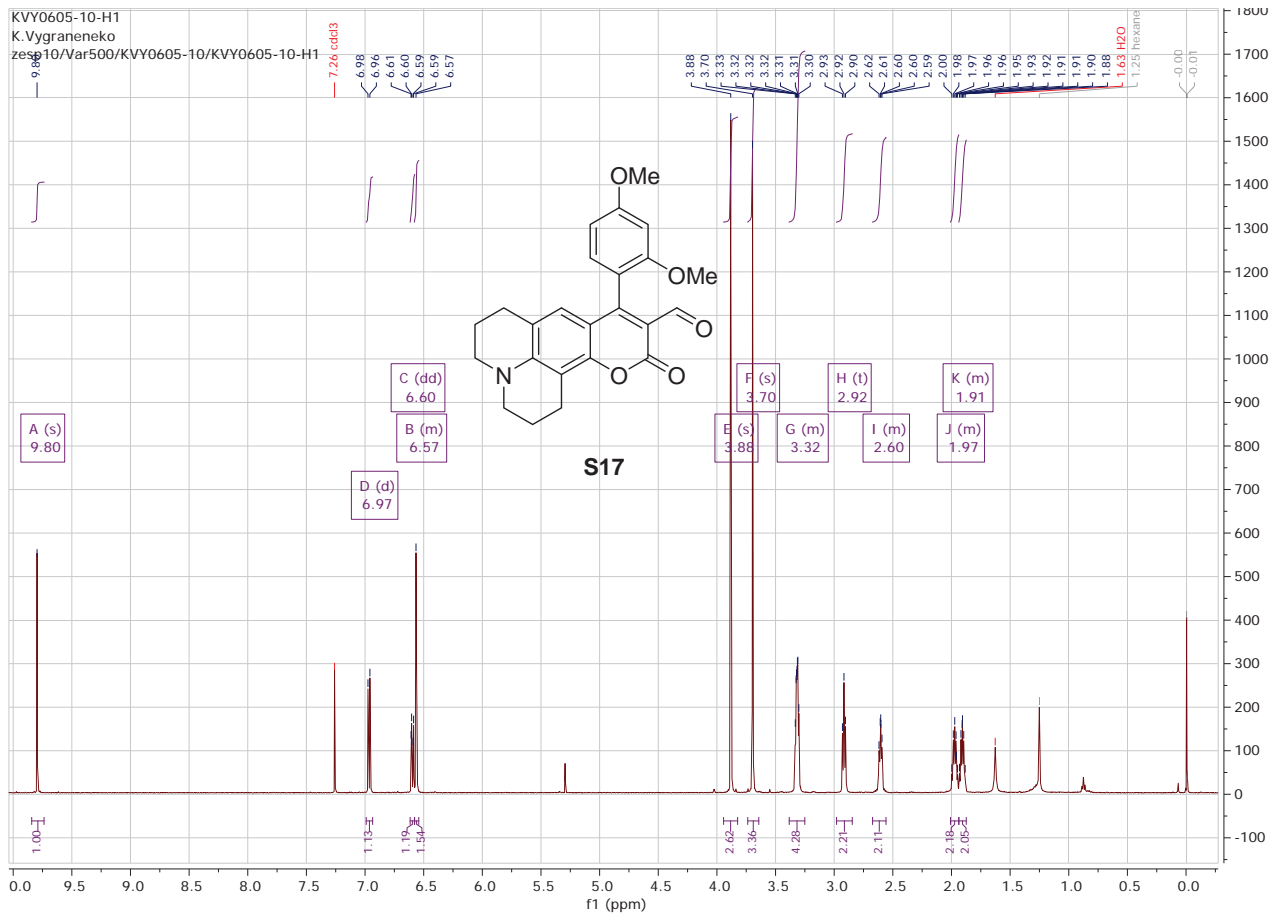


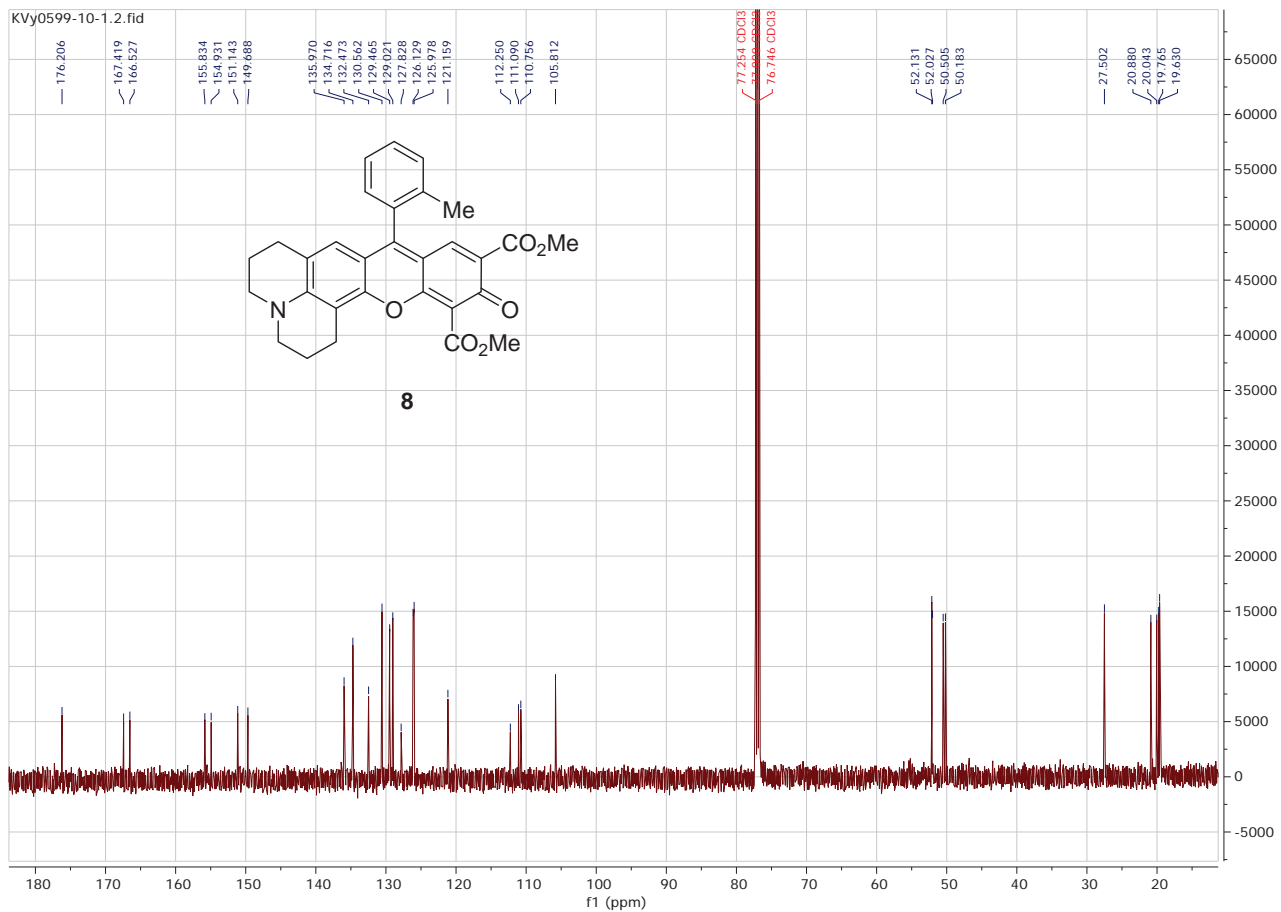
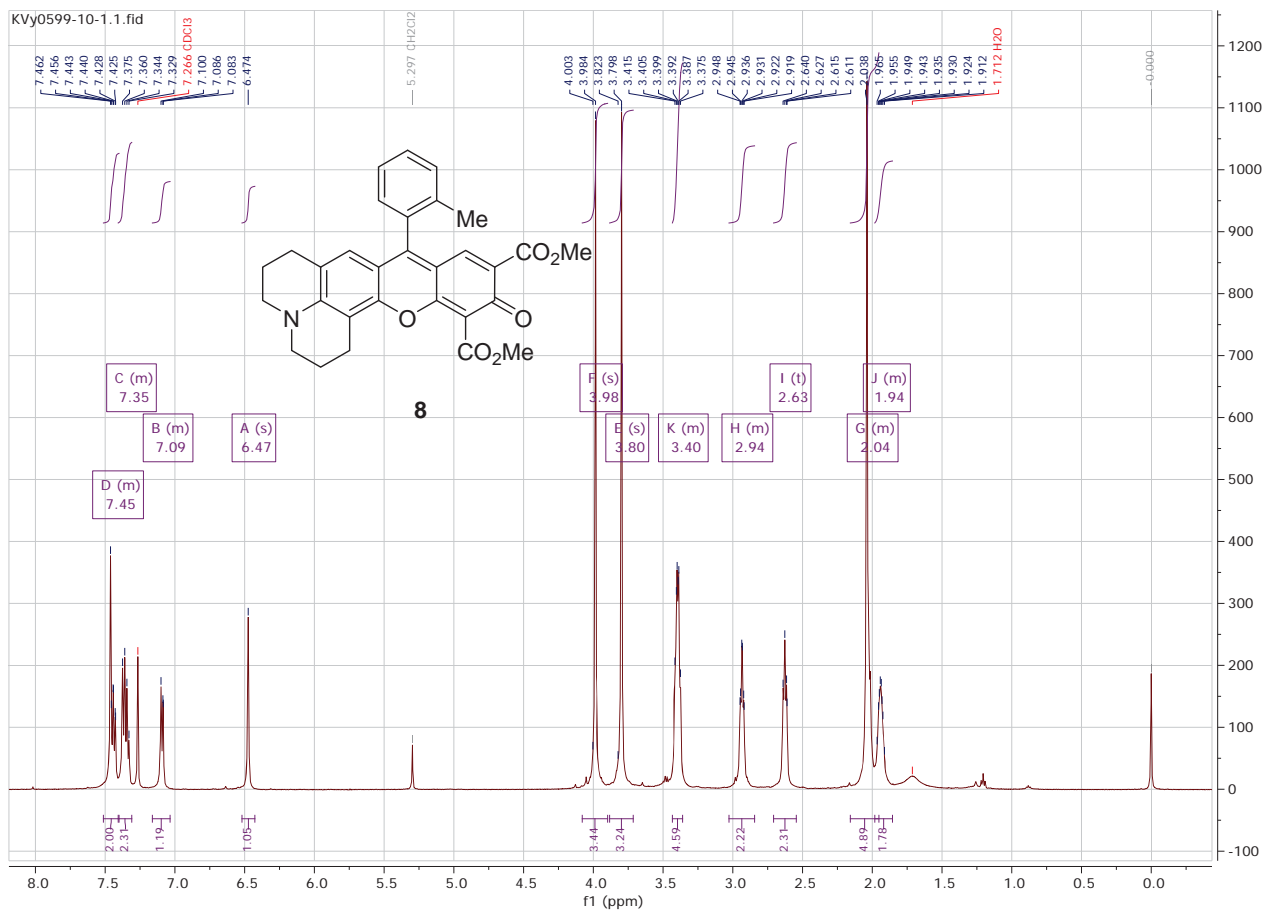


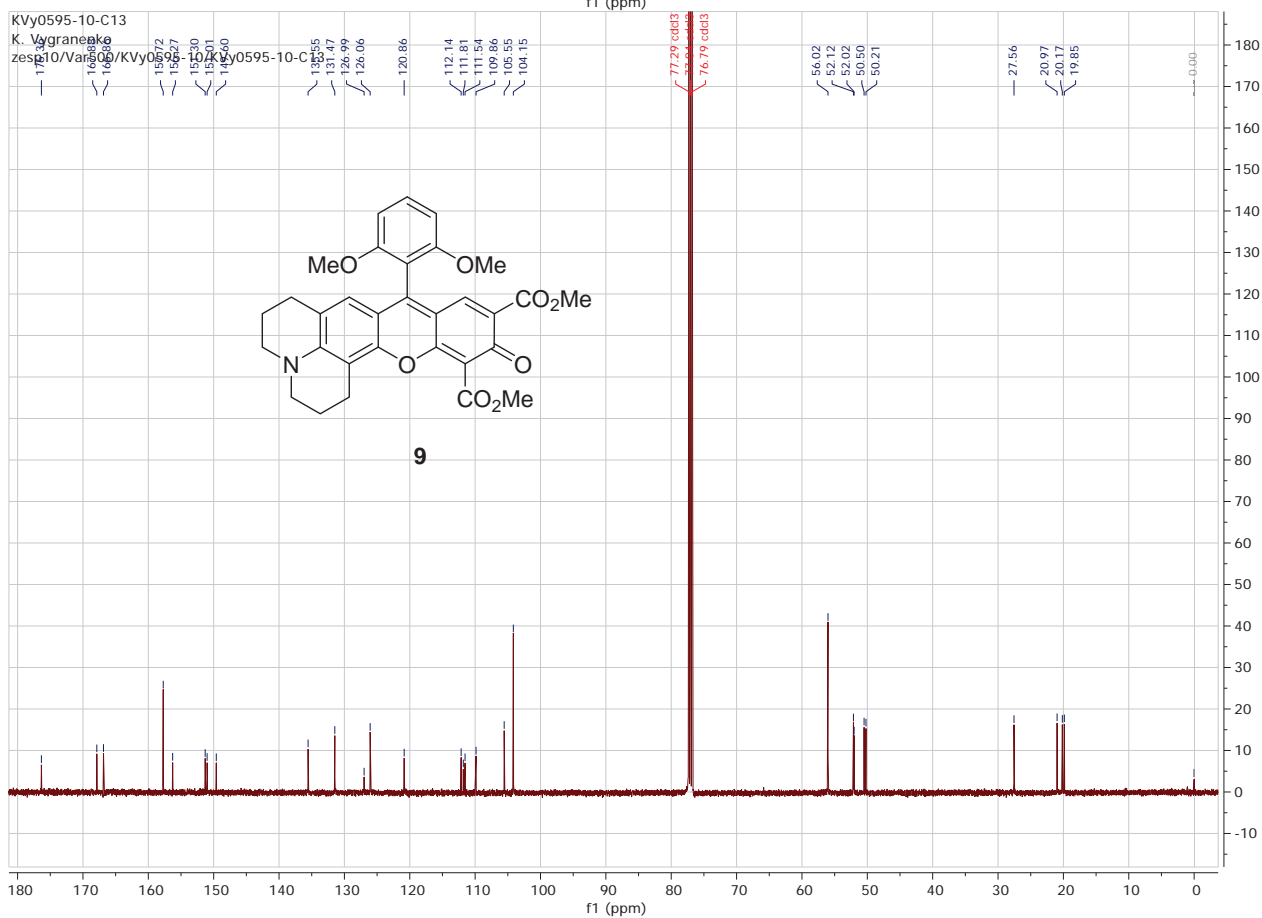
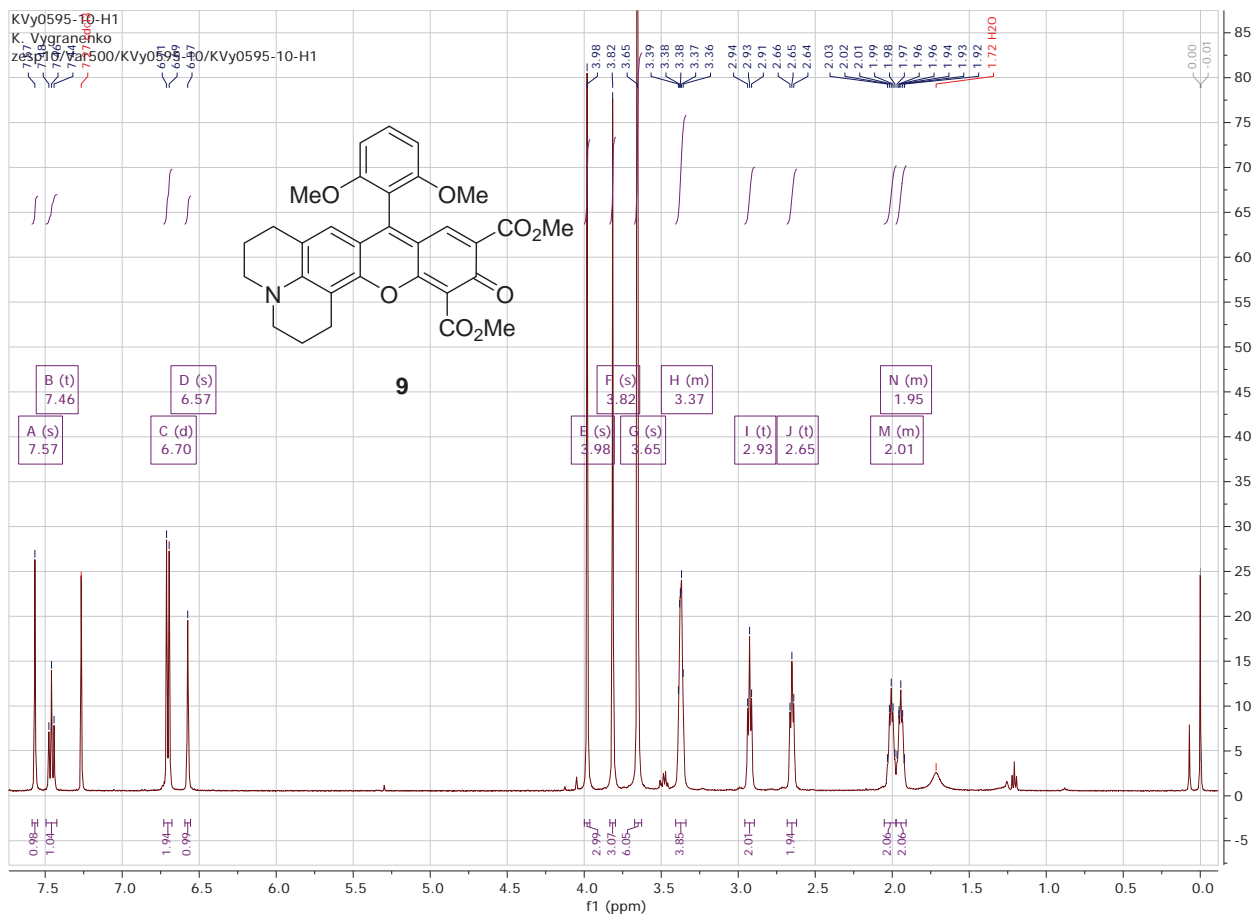


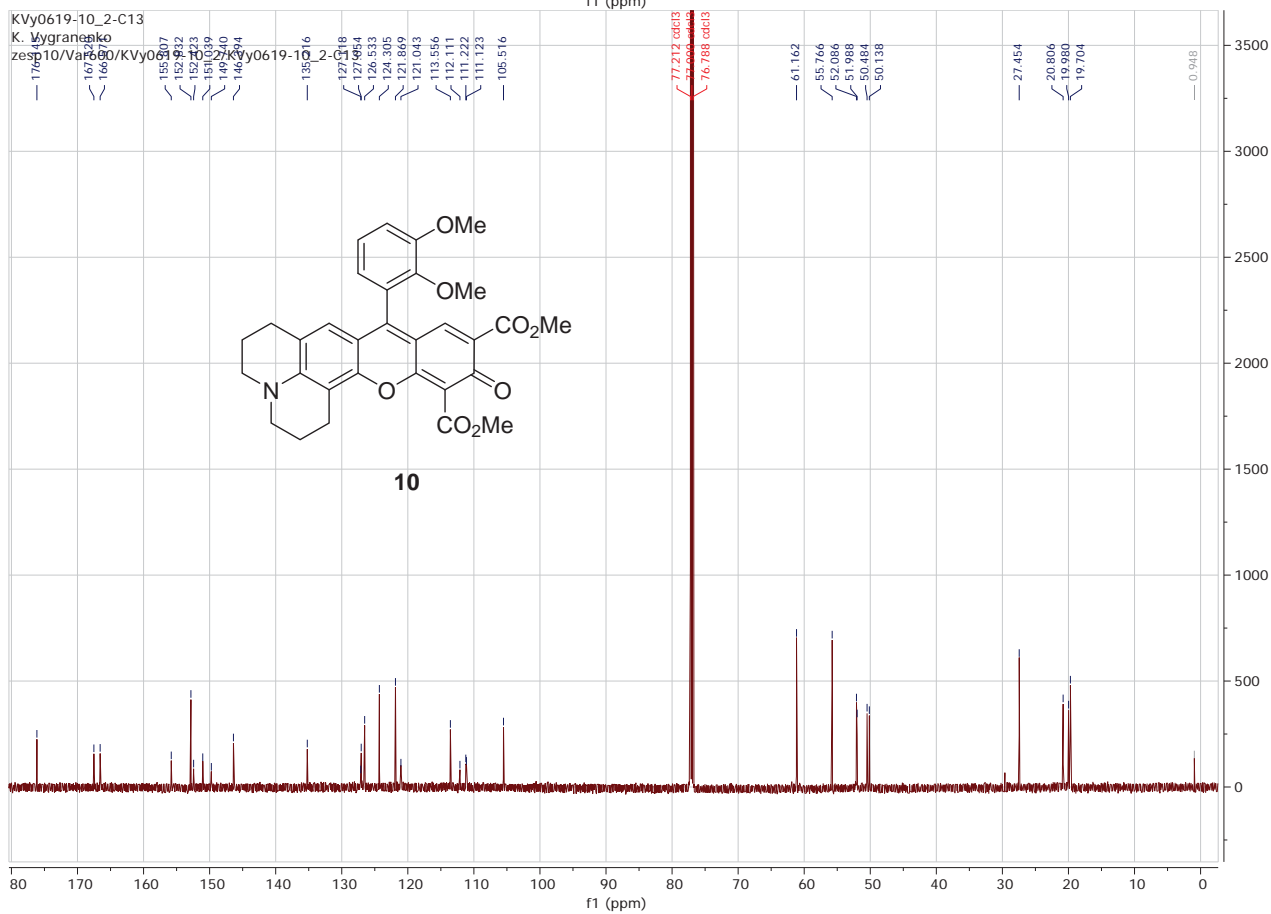
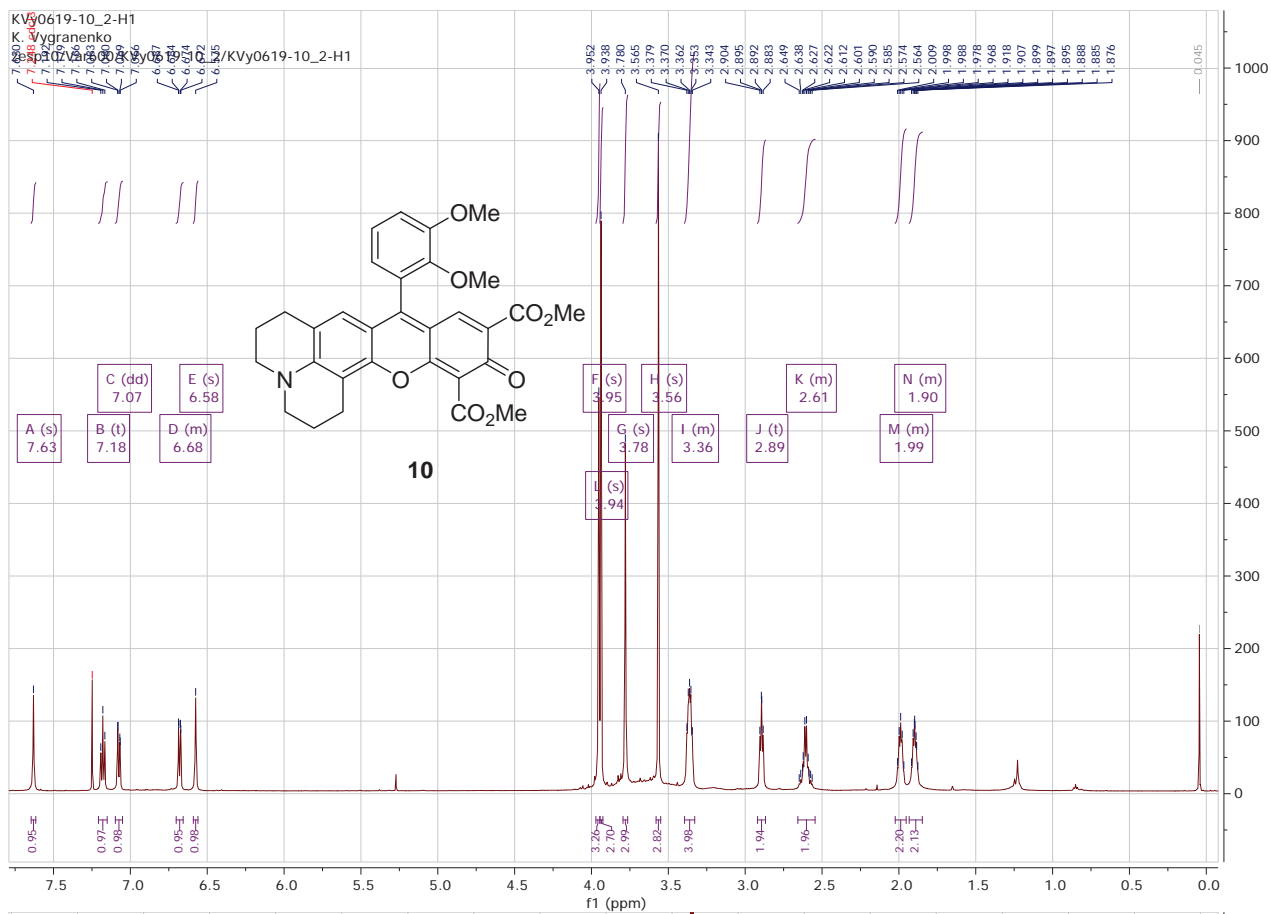


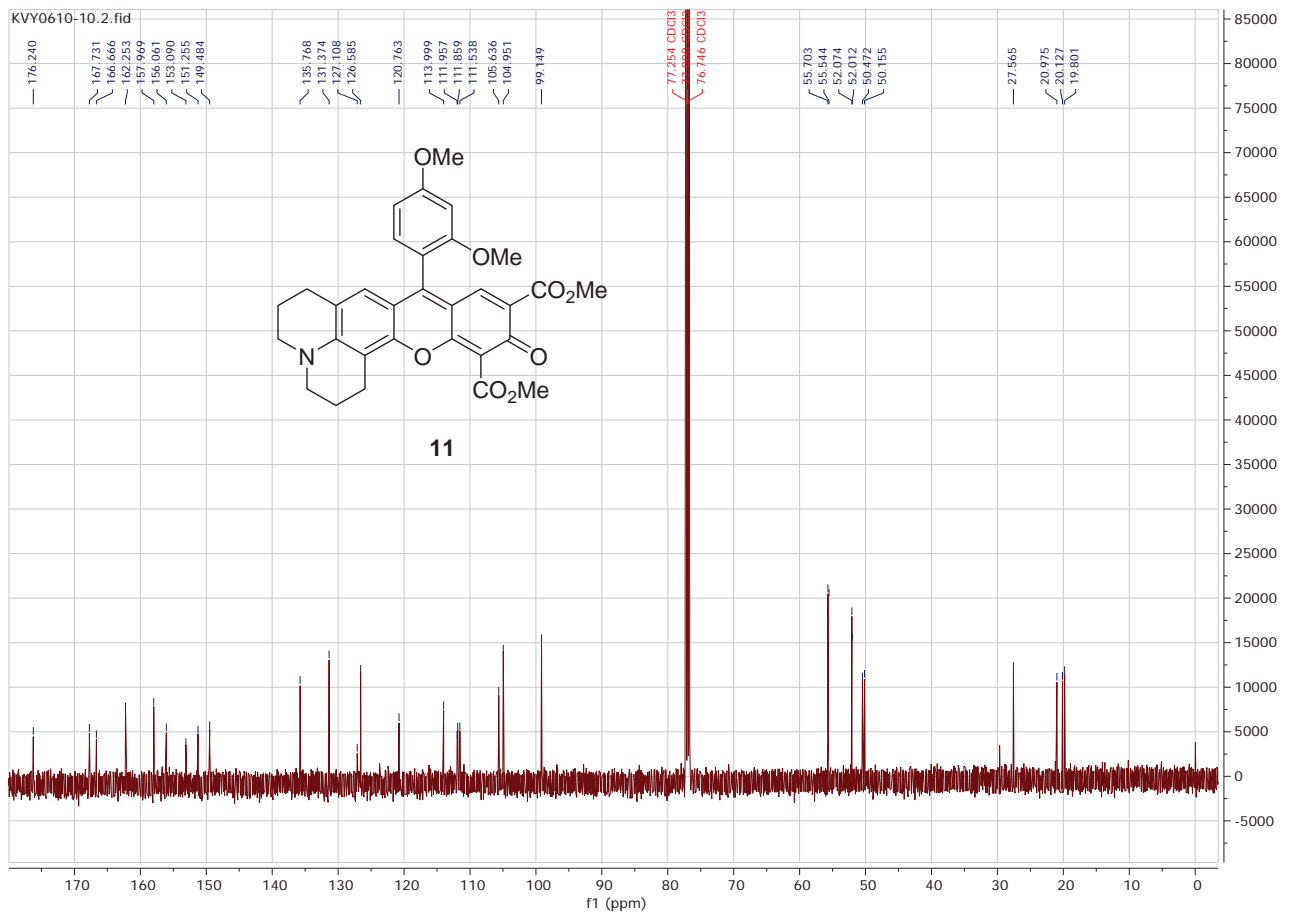
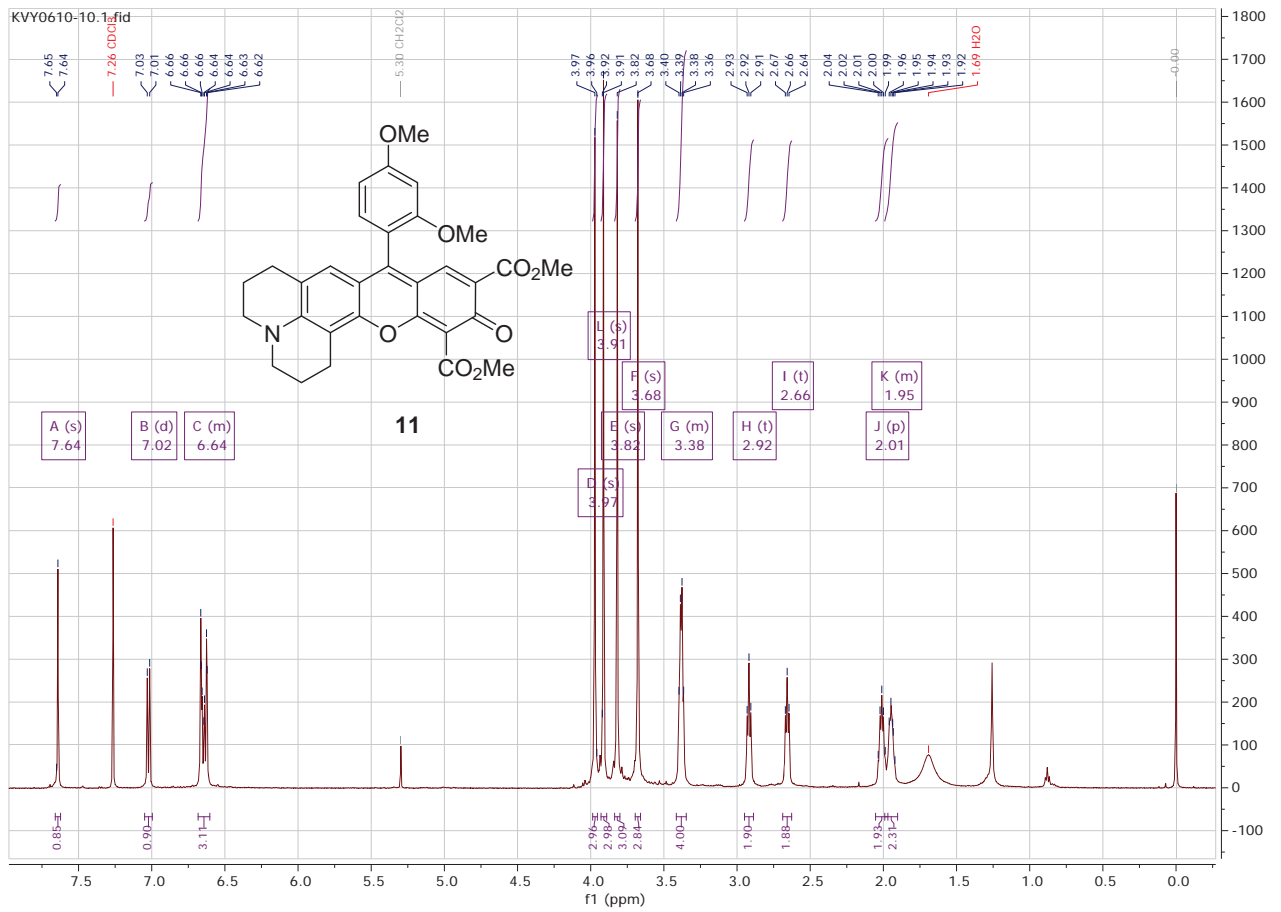


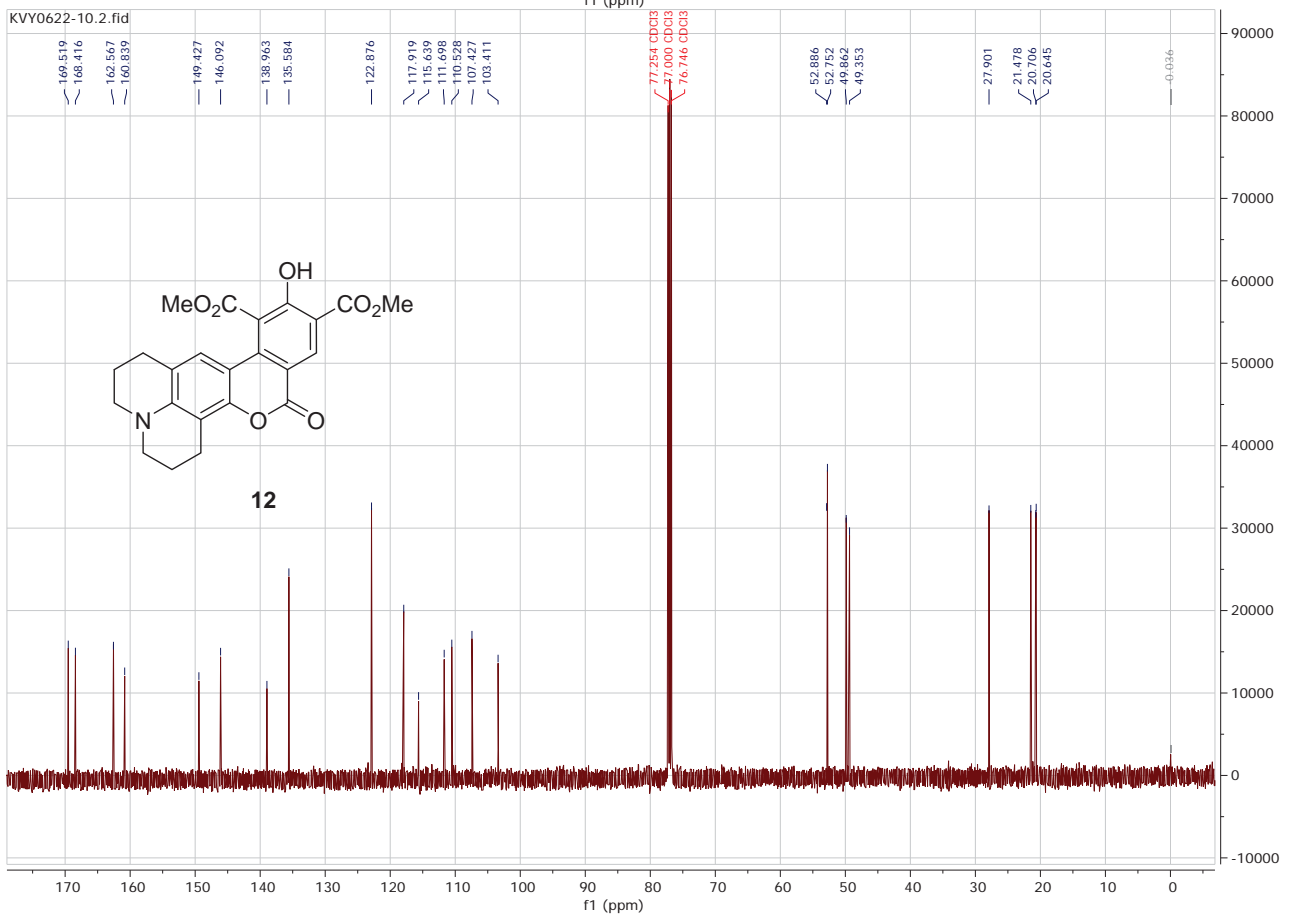
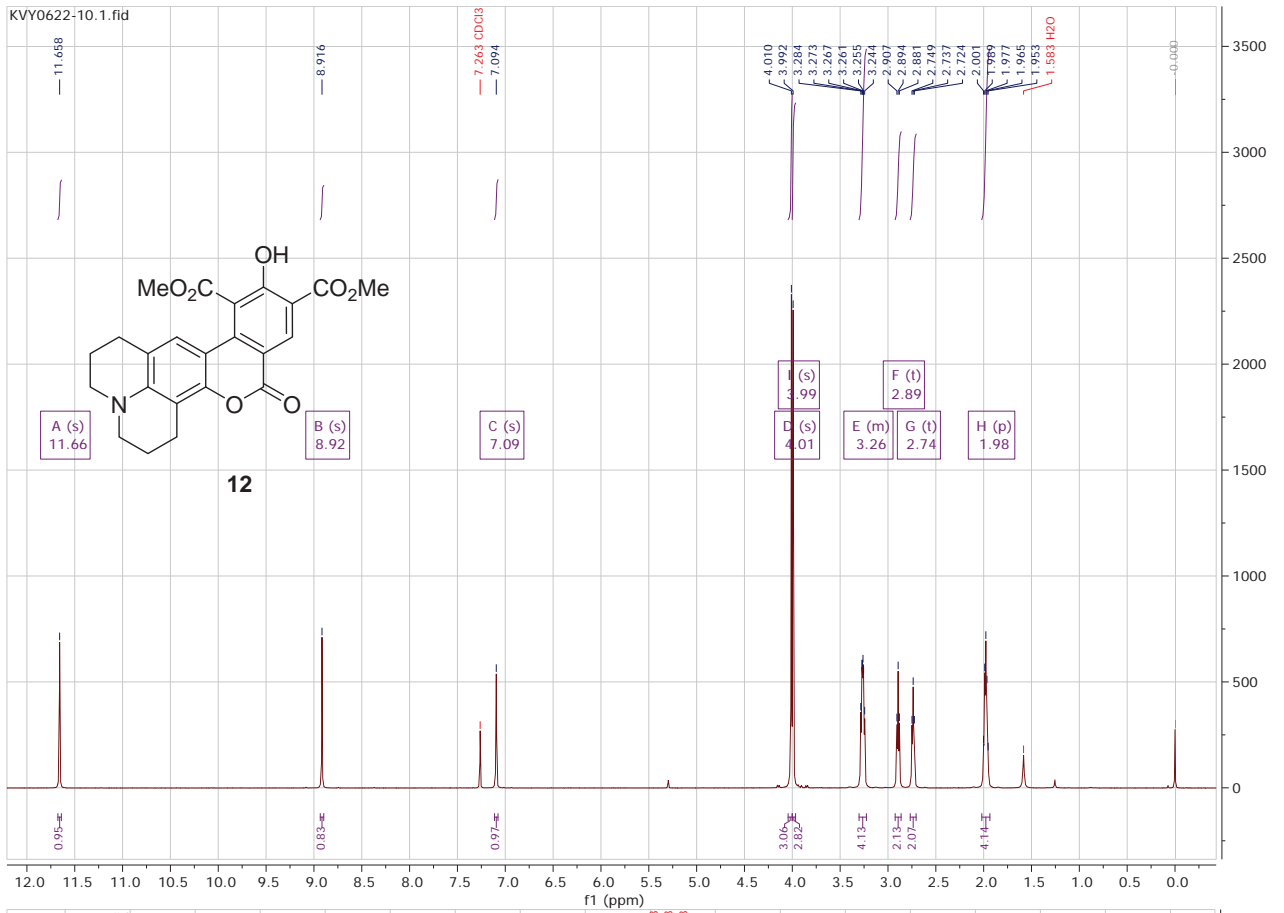


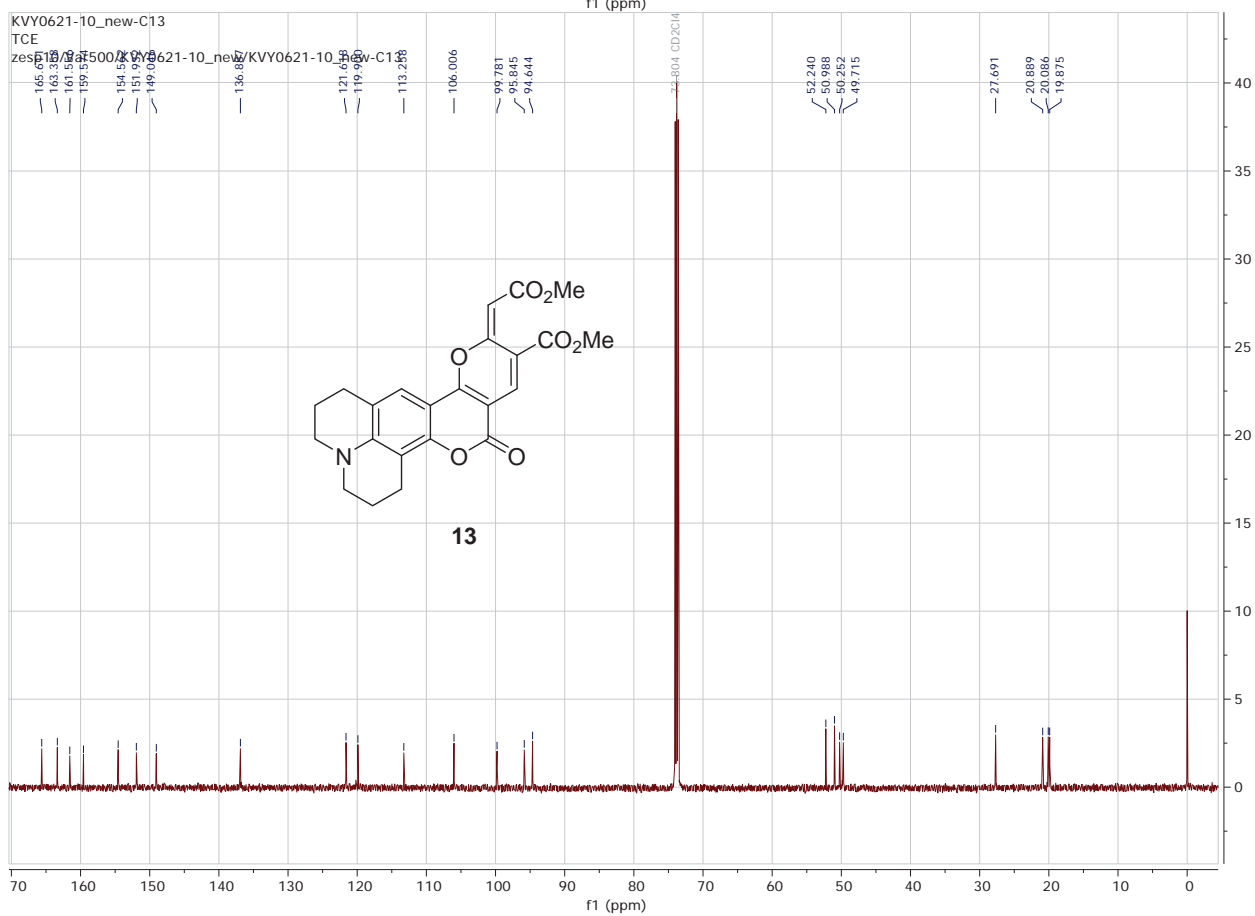
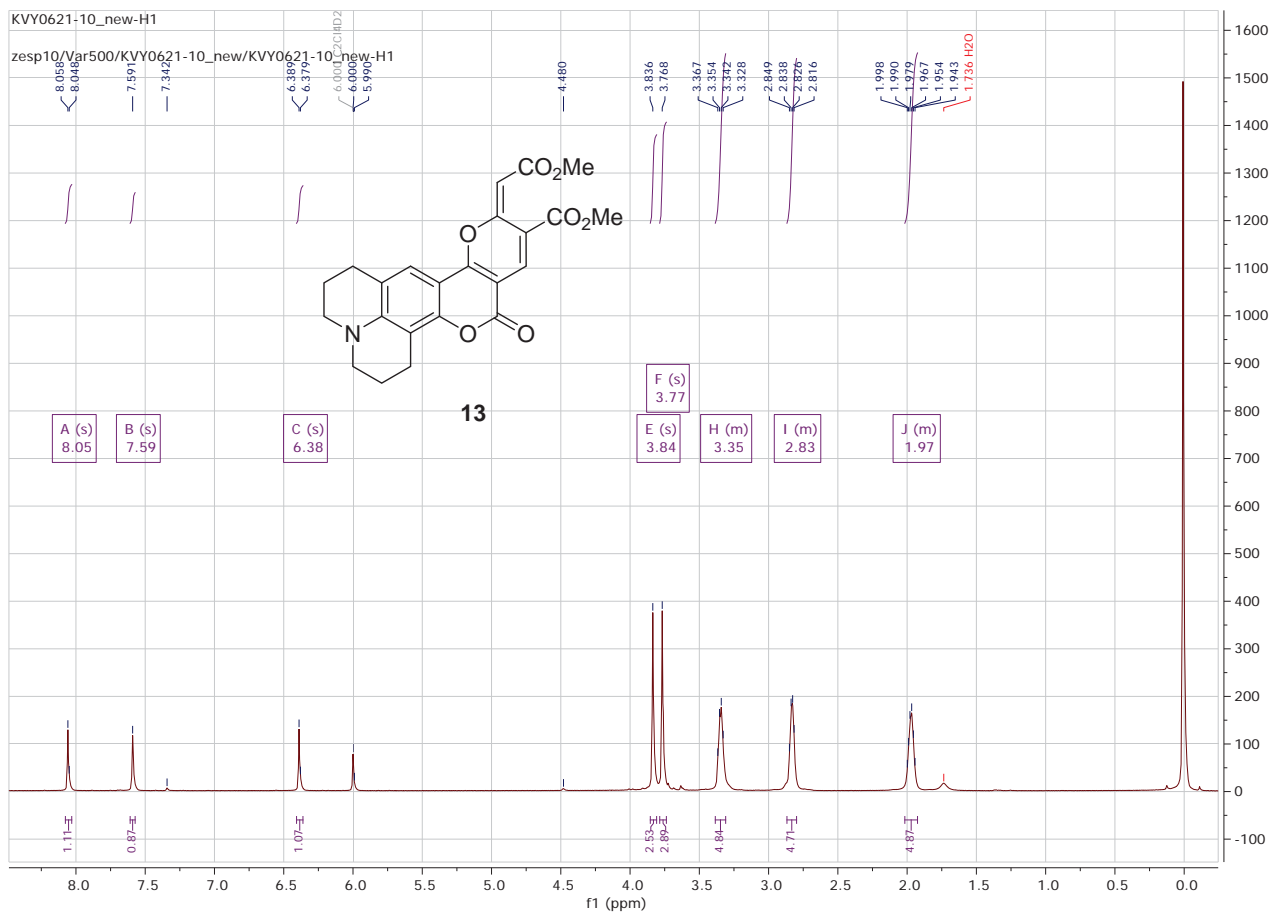


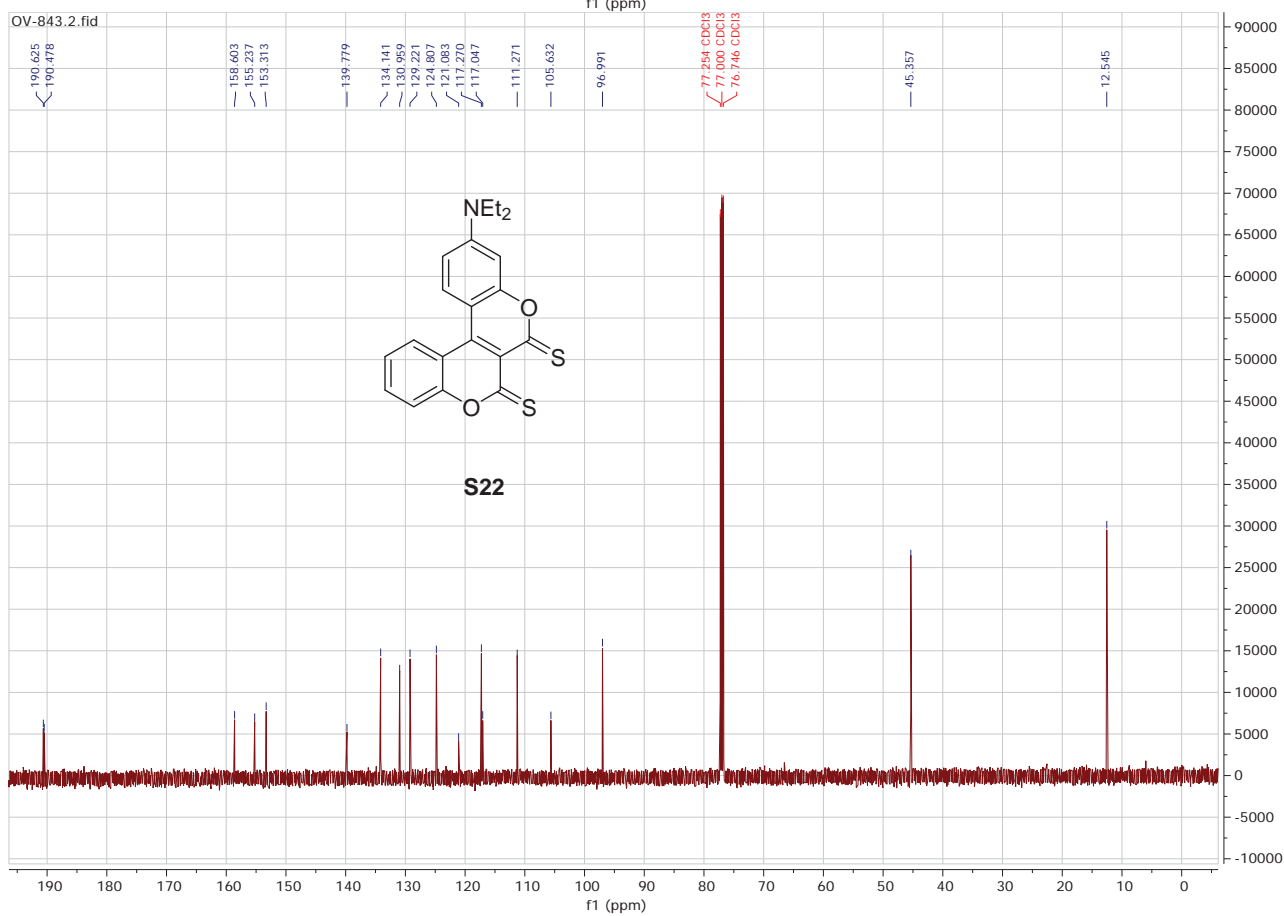
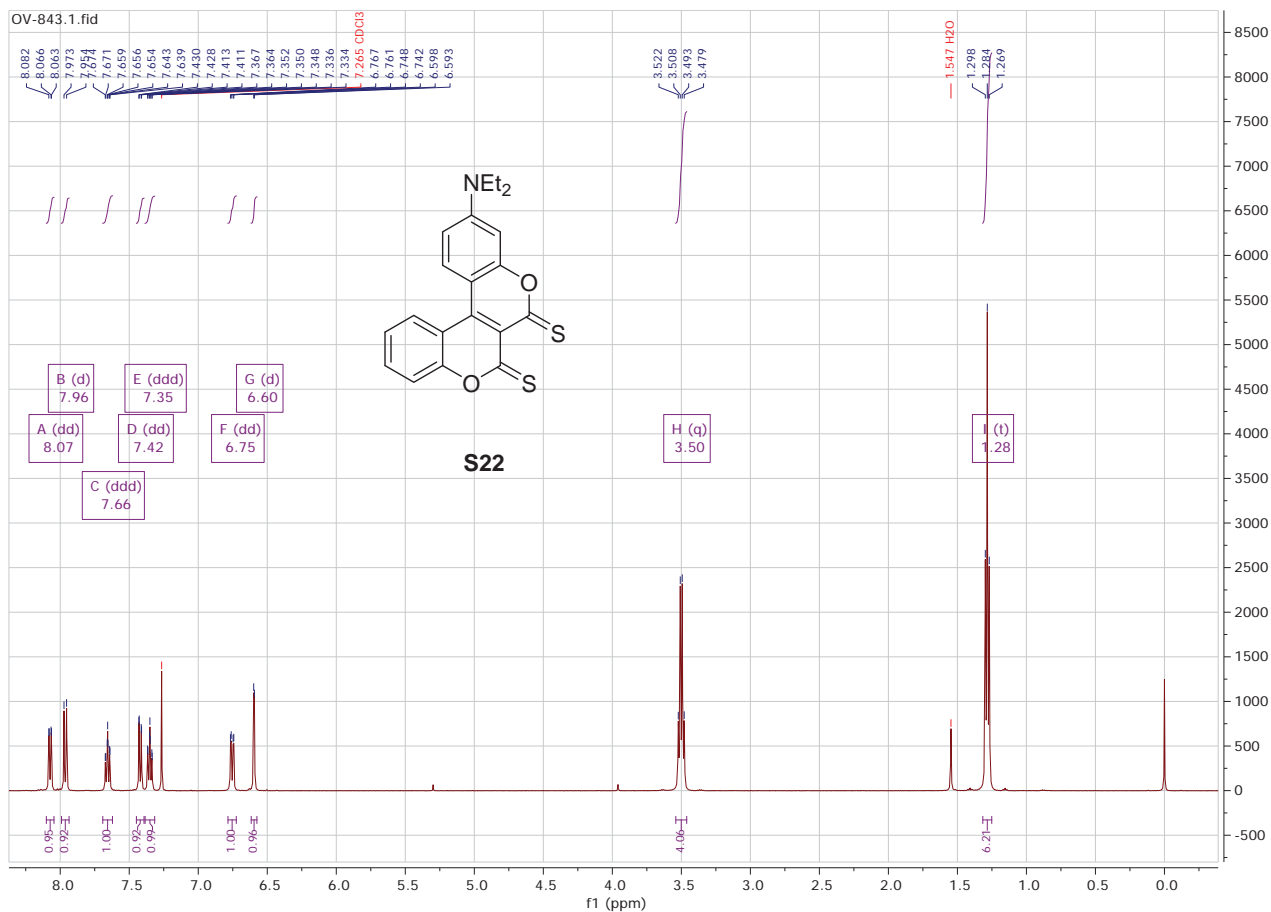


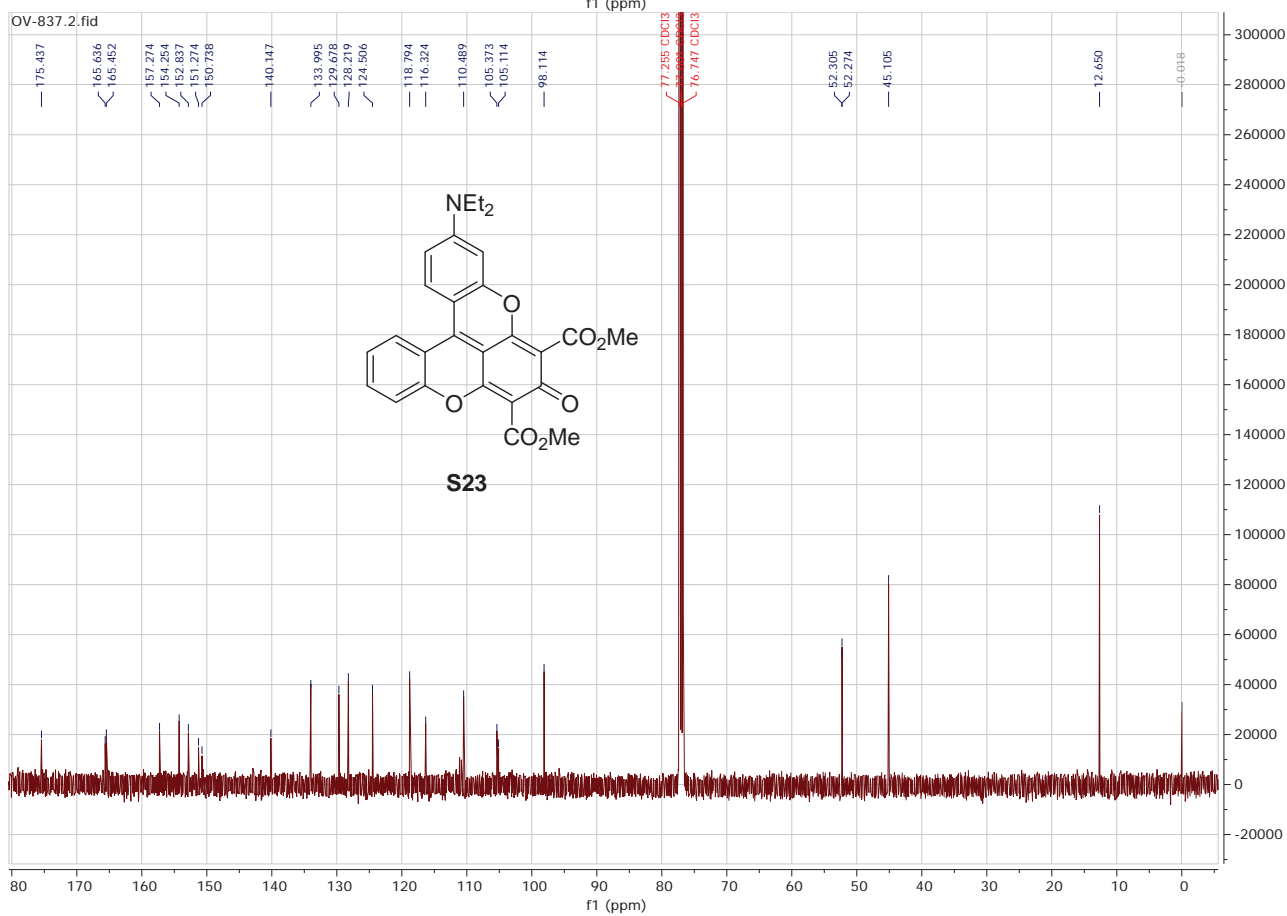
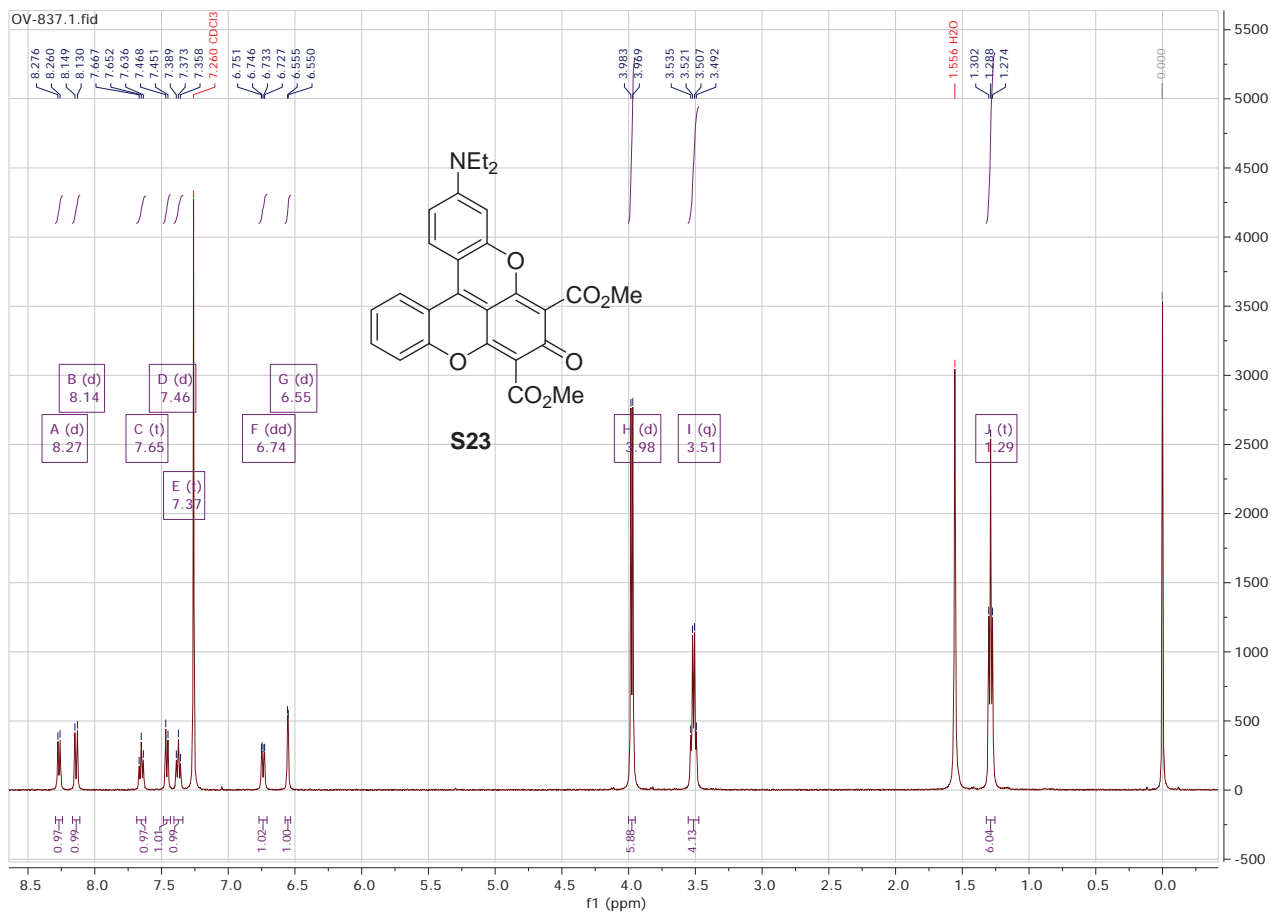












Crystal Structure Report for 12

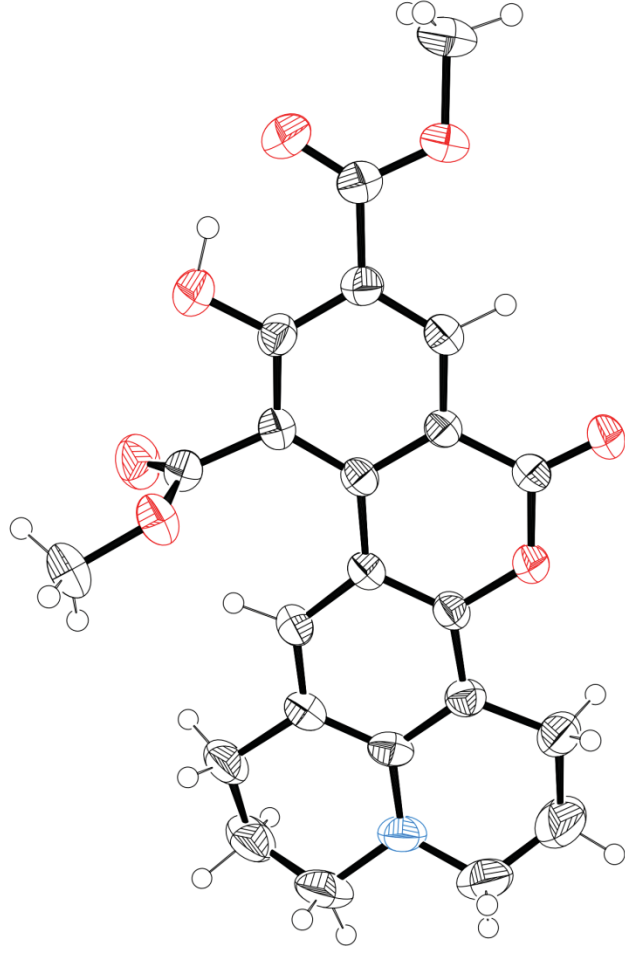


Figure S3. The ORTEP drawing⁴ of X-ray diffraction analysis for compound **12**. CCDC 2125095.

A yellow prisms-like specimen of $C_{23}H_{21}NO_7$, approximate dimensions 0.194 mm x 0.244 mm x 0.368 mm, was used for the X-ray crystallographic analysis. The X-ray intensity data were measured.

Table S1. Data collection details for **12**.

Axis	dx/mm	2 θ /°	ω /°	ϕ /°	χ /°	Width/°	Frames	Time/s	Wavelength/Å	Voltage/kV	Current/mA	Temperature/K
Omega	39.835	-97.72	-192.85	-178.62	24.03	2.00	54	88.00	1.54184	45	30.0	n/a
Omega	39.835	-101.63	-206.31	-24.27	43.23	2.00	56	88.00	1.54184	45	30.0	n/a
Omega	39.835	-101.30	-209.35	-83.58	50.32	2.00	57	88.00	1.54184	45	30.0	n/a
Phi	39.835	-18.13	-3.92	-116.00	23.00	2.00	92	88.00	1.54184	45	30.0	n/a
Omega	39.835	-100.90	-111.03	-90.42	-30.05	2.00	54	88.00	1.54184	45	30.0	n/a
Omega	39.835	-100.79	-203.51	-119.88	40.40	2.00	55	88.00	1.54184	45	30.0	n/a
Omega	39.835	36.11	-52.45	-114.35	52.48	2.00	47	88.00	1.54184	45	30.0	n/a
Phi	39.835	85.61	-280.32	0.00	-58.06	2.00	180	88.00	1.54184	45	30.0	n/a
Omega	39.835	27.38	-337.08	0.00	-54.74	2.00	57	88.00	1.54184	45	30.0	n/a
Omega	39.835	-101.22	-108.86	19.45	-42.31	2.00	56	88.00	1.54184	45	30.0	n/a
Omega	39.835	-100.90	-205.62	22.16	43.34	2.00	56	88.00	1.54184	45	30.0	n/a
Omega	39.835	-100.87	-206.52	-166.47	46.12	2.00	56	88.00	1.54184	45	30.0	n/a
Omega	39.835	-101.30	-204.15	-50.83	40.80	2.00	55	88.00	1.54184	45	30.0	n/a
Omega	39.835	-99.71	-200.88	-223.75	36.03	2.00	55	88.00	1.54184	45	30.0	n/a
Omega	39.835	84.67	-280.79	90.00	-54.74	2.00	58	88.00	1.54184	45	30.0	n/a
Omega	39.835	-101.22	-209.09	-148.00	49.76	2.00	57	88.00	1.54184	45	30.0	n/a
Omega	39.835	84.67	-280.79	180.00	-54.74	2.00	58	88.00	1.54184	45	30.0	n/a
Omega	39.835	84.67	-280.79	0.00	-54.74	2.00	58	88.00	1.54184	45	30.0	n/a
Omega	39.835	-100.35	-109.65	72.81	-32.08	2.00	54	88.00	1.54184	45	30.0	n/a
Omega	39.835	27.38	-337.08	153.00	-54.74	2.00	57	88.00	1.54184	45	30.0	n/a
Phi	39.835	-100.61	-174.76	-44.00	23.00	2.00	28	88.00	1.54184	45	30.0	n/a
Omega	39.835	84.67	-280.79	270.00	-54.74	2.00	58	88.00	1.54184	45	30.0	n/a
Omega	39.835	-101.52	-206.51	57.38	44.15	2.00	56	88.00	1.54184	45	30.0	n/a
Omega	39.835	-100.23	-106.60	-144.54	-49.09	2.00	57	88.00	1.54184	45	30.0	n/a
Omega	39.835	-100.91	-106.03	-34.93	-55.74	2.00	58	88.00	1.54184	45	30.0	n/a
Omega	39.835	-101.15	-205.37	80.53	41.85	2.00	56	88.00	1.54184	45	30.0	n/a
Omega	39.835	12.38	-353.08	270.00	-54.74	2.00	58	88.00	1.54184	45	30.0	n/a

Axis	dx/mm	$2\theta/^\circ$	$\omega/^\circ$	$\phi/^\circ$	$\chi/^\circ$	Width/ $^\circ$	Frames	Time/s	Wavelength/ \AA	Voltage/kV	Current/mA	Temperature/K
Omega	39.835	-97.67	-64.94	-136.03	-74.84	2.00	46	88.00	1.54184	45	30.0	n/a
Phi	39.835	70.61	-295.32	0.00	-58.06	2.00	180	88.00	1.54184	45	30.0	n/a

A total of 1869 frames were collected. The total exposure time was 45.69 hours. The frames were integrated with the Bruker SAINT software package using a narrow-frame algorithm. The integration of the data using a monoclinic unit cell yielded a total of 20848 reflections to a maximum θ angle of 68.75° (0.83 \AA resolution), of which 3496 were independent (average redundancy 5.963, completeness = 97.3%, $R_{\text{int}} = 6.44\%$, $R_{\text{sig}} = 4.22\%$) and 2521 (72.11%) were greater than $2\sigma(F^2)$. The final cell constants of $a = 11.7140(13) \text{ \AA}$, $b = 9.9926(12) \text{ \AA}$, $c = 16.775(2) \text{ \AA}$, $\beta = 98.713(7)^\circ$, volume = $1940.9(4) \text{ \AA}^3$, are based upon the refinement of the XYZ-centroids of 7169 reflections above $20 \sigma(I)$ with $5.329^\circ < 2\theta < 136.6^\circ$. Data were corrected for absorption effects using the numerical method (SADABS). The ratio of minimum to maximum apparent transmission was 0.825. The calculated minimum and maximum transmission coefficients (based on crystal size) are 0.7320 and 0.8440.

The structure was solved and refined using the Bruker SHELXTL Software Package, using the space group $P 1 21/n 1$, with $Z = 4$ for the formula unit, $C_{23}H_{21}NO_7$. The final anisotropic full-matrix least-squares refinement on F^2 with 326 variables converged at $R1 = 4.93\%$, for the observed data and $wR2 = 13.29\%$ for all data. The goodness-of-fit was 1.015. The largest peak in the final difference electron density synthesis was $0.650 \text{ e}/\text{\AA}^3$ and the largest hole was $-0.324 \text{ e}/\text{\AA}^3$ with an RMS deviation of $0.044 \text{ e}/\text{\AA}^3$. On the basis of the final model, the calculated density was $1.449 \text{ g}/\text{cm}^3$ and $F(000)$, 888 e^- .

Table S2. Sample and crystal data for **12**.

Identification code	KVY0620A	
Chemical formula	$C_{23}H_{21}NO_7$	
Formula weight	423.41 g/mol	
Temperature	296(2) K	
Wavelength	1.54178 \AA	
Crystal size	0.194 x 0.244 x 0.368 mm	
Crystal habit	yellow prisms	
Crystal system	monoclinic	
Space group	$P 1 21/n 1$	
Unit cell dimensions	$a = 11.7140(13) \text{ \AA}$	$\alpha = 90^\circ$
	$b = 9.9926(12) \text{ \AA}$	$\beta = 98.713(7)^\circ$
	$c = 16.775(2) \text{ \AA}$	$\gamma = 90^\circ$
Volume	$1940.9(4) \text{ \AA}^3$	
Z	4	
Density (calculated)	$1.449 \text{ g}/\text{cm}^3$	
Absorption coefficient	0.903 mm^{-1}	
$F(000)$	888	

Table S3. Data collection and structure refinement for **12**.

Theta range for data collection	4.31 to 68.75°
Index ranges	$-14 \leq h \leq 14$, $-11 \leq k \leq 10$, $-20 \leq l \leq 20$
Reflections collected	20848
Independent reflections	3496 [$R(\text{int}) = 0.0644$]
Coverage of independent reflections	97.3%
Absorption correction	numerical
Max. and min. transmission	0.8440 and 0.7320
Structure solution technique	direct methods

Structure solution program	SHELXL-2014 (Sheldrick, 2014)	
Refinement method	Full-matrix least-squares on F ²	
Refinement program	SHELXL-2014 (Sheldrick, 2014)	
Function minimized	$\Sigma w(F_o^2 - F_c^2)^2$	
Data / restraints / parameters	3496 / 0 / 326	
Goodness-of-fit on F ²	1.015	
Final R indices	2521 data; $l > 2\sigma(l)$	R1 = 0.0493, wR2 = 0.1180
	all data	R1 = 0.0726, wR2 = 0.1329
Weighting scheme	$w=1/[\sigma^2(F_o^2)+(0.0563P)^2+0.9257P]$ where $P=(F_o^2+2F_c^2)/3$	
Largest diff. peak and hole	0.650 and -0.324 eÅ ⁻³	
R.M.S. deviation from mean	0.044 eÅ ⁻³	

Table S4. Atomic coordinates and equivalent isotropic atomic displacement parameters (Å²) for **12**. U(eq) is defined as one third of the trace of the orthogonalized U_{ij} tensor.

	x/a	y/b	z/c	U(eq)
N1	0.79545(16)	0.8429(2)	0.96972(13)	0.0496(5)
O1	0.40679(11)	0.73599(15)	0.98848(9)	0.0430(4)
O2	0.22301(12)	0.69230(18)	0.98329(10)	0.0534(5)
O3	0.42098(15)	0.32825(19)	0.27994(10)	0.0564(5)
O4	0.65852(14)	0.33896(17)	0.22349(11)	0.0592(5)
O5	0.63780(12)	0.53689(17)	0.28201(9)	0.0484(4)
O6	0.20390(14)	0.27387(19)	0.26422(11)	0.0596(5)
O7	0.08283(13)	0.38296(18)	0.17120(11)	0.0560(5)
C1	0.9165(2)	0.8403(3)	0.0081(2)	0.0665(8)
C2	0.9551(2)	0.7029(3)	0.0347(2)	0.0626(8)
C3	0.88157(19)	0.6484(3)	0.09211(18)	0.0543(7)
C4	0.75485(17)	0.6737(2)	0.06535(13)	0.0387(5)
C5	0.71712(17)	0.7696(2)	0.00534(14)	0.0383(5)
C6	0.59773(17)	0.7873(2)	0.98031(13)	0.0369(5)
C7	0.5524(2)	0.8849(3)	0.91468(18)	0.0501(6)
C8	0.6456(3)	0.9451(4)	0.8743(2)	0.0893(11)

	x/a	y/b	z/c	U(eq)
)
C9	0.7564(2)	0.9621(3)	0.9255(2)	0.0719(9)
C10	0.67491(17)	0.6033(2)	0.10043(14)	0.0377(5)
C11	0.55527(16)	0.6212(2)	0.08003(13)	0.0335(5)
C12	0.52187(16)	0.7126(2)	0.01808(13)	0.0343(5)
C13	0.31944(16)	0.6681(2)	0.01591(13)	0.0365(5)
C14	0.35030(16)	0.5755(2)	0.08252(12)	0.0316(5)
C15	0.46661(16)	0.5535(2)	0.11724(12)	0.0314(5)
C16	0.48664(17)	0.4678(2)	0.18456(13)	0.0351(5)
C17	0.39510(18)	0.4064(2)	0.21439(13)	0.0381(5)
C18	0.28036(17)	0.4263(2)	0.17743(13)	0.0370(5)
C19	0.26035(17)	0.5115(2)	0.11245(13)	0.0356(5)
C20	0.60377(18)	0.4383(2)	0.23082(14)	0.0394(5)
C21	0.7529(2)	0.5265(3)	0.32706(17)	0.0644(8)
C22	0.18693(19)	0.3537(2)	0.20899(14)	0.0430(6)
C23	0.9883(2)	0.3055(4)	0.1955(2)	0.0831(10)

Table S5. Bond lengths (Å) for **12**.

N1-C5	1.379(3)	N1-C9	1.441(3)
N1-C1	1.466(3)	O1-C13	1.364(2)
O1-C12	1.384(2)	O2-C13	1.203(2)
O3-C17	1.345(3)	O3-H3	0.95(3)
O4-C20	1.198(3)	O5-C20	1.328(3)
O5-C21	1.446(3)	O6-C22	1.216(3)
O7-C22	1.319(3)	O7-C23	1.458(3)
C1-C2	1.492(4)	C1-H1A	0.99(3)
C1-H1B	1.08(4)	C2-C3	1.489(4)
C2-H2A	0.98(3)	C2-H2B	1.06(3)
C3-C4	1.506(3)	C3-H3A	0.99(3)
C3-H3B	1.00(3)	C4-C10	1.373(3)
C4-C5	1.411(3)	C5-C6	1.409(3)
C6-C12	1.385(3)	C6-C7	1.506(3)

C7-C8	1.496(4)	C7-H7A	0.95(3)
C7-H7B	0.95(3)	C8-C9	1.454(4)
C8-H8A	0.97	C8-H8B	0.97
C9-H9A	0.97	C9-H9B	0.97
C10-C11	1.403(3)	C10-H10	0.97(3)
C11-C12	1.395(3)	C11-C15	1.457(3)
C13-C14	1.454(3)	C14-C19	1.390(3)
C14-C15	1.415(3)	C15-C16	1.408(3)
C16-C17	1.393(3)	C16-C20	1.500(3)
C17-C18	1.406(3)	C18-C19	1.375(3)
C18-C22	1.476(3)	C19-H19	0.98(2)
C21-H21A	0.96	C21-H21B	0.96
C21-H21C	0.96	C23-H23A	0.96
C23-H23B	0.96	C23-H23C	0.96

Table S6. Bond angles (°) for **12**.

C5-N1-C9	118.8(2)	C5-N1-C1	117.6(2)
C9-N1-C1	116.8(2)	C13-O1-C12	122.32(17)
C17-O3-H3	104.4(17)	C20-O5-C21	116.72(19)
C22-O7-C23	115.7(2)	N1-C1-C2	112.1(2)
N1-C1-H1A	102.2(18)	C2-C1-H1A	113.6(18)
N1-C1-H1B	110.9(19)	C2-C1-H1B	108.8(19)
H1A-C1-H1B	109.(3)	C1-C2-C3	110.6(3)
C1-C2-H2A	107.3(16)	C3-C2-H2A	111.0(16)
C1-C2-H2B	108.8(15)	C3-C2-H2B	110.8(15)
H2A-C2-H2B	108.(2)	C2-C3-C4	112.7(2)
C2-C3-H3A	113.8(18)	C4-C3-H3A	107.4(18)
C2-C3-H3B	113.8(19)	C4-C3-H3B	107.4(18)
H3A-C3-H3B	101.(3)	C10-C4-C5	119.56(19)
C10-C4-C3	119.5(2)	C5-C4-C3	121.0(2)
N1-C5-C4	120.84(19)	N1-C5-C6	120.0(2)
C4-C5-C6	119.16(19)	C12-C6-C5	118.2(2)
C12-C6-C7	120.25(19)	C5-C6-C7	121.5(2)
C8-C7-C6	113.0(2)	C8-C7-H7A	108.1(19)
C6-C7-H7A	111.(2)	C8-C7-H7B	109.0(19)
C6-C7-H7B	112.0(19)	H7A-C7-H7B	103.(3)
C9-C8-C7	115.2(3)	C9-C8-H8A	108.5
C7-C8-H8A	108.5	C9-C8-H8B	108.5
C7-C8-H8B	108.5	H8A-C8-H8B	107.5
N1-C9-C8	113.1(2)	N1-C9-H9A	109.0
C8-C9-H9A	109.0	N1-C9-H9B	109.0
C8-C9-H9B	109.0	H9A-C9-H9B	107.8
C4-C10-C11	123.4(2)	C4-C10-H10	115.0(14)
C11-C10-H10	121.5(14)	C12-C11-C10	114.99(19)
C12-C11-C15	119.07(17)	C10-C11-C15	125.9(2)

C6-C12-O1	113.74(18)	C6-C12-C11	124.53(18)
O1-C12-C11	121.73(18)	O2-C13-O1	116.56(19)
O2-C13-C14	125.79(19)	O1-C13-C14	117.63(17)
C19-C14-C15	121.01(19)	C19-C14-C13	117.17(18)
C15-C14-C13	121.80(17)	C16-C15-C14	117.22(18)
C16-C15-C11	125.66(18)	C14-C15-C11	117.12(18)
C17-C16-C15	120.82(18)	C17-C16-C20	114.90(19)
C15-C16-C20	124.26(18)	O3-C17-C16	117.33(19)
O3-C17-C18	121.62(19)	C16-C17-C18	121.0(2)
C19-C18-C17	118.28(19)	C19-C18-C22	122.8(2)
C17-C18-C22	118.9(2)	C18-C19-C14	121.59(19)
C18-C19-H19	122.0(12)	C14-C19-H19	116.4(12)
O4-C20-O5	124.6(2)	O4-C20-C16	124.9(2)
O5-C20-C16	110.47(18)	O5-C21-H21A	109.5
O5-C21-H21B	109.5	H21A-C21-H21B	109.5
O5-C21-H21C	109.5	H21A-C21-H21C	109.5
H21B-C21-H21C	109.5	O6-C22-O7	123.0(2)
O6-C22-C18	123.4(2)	O7-C22-C18	113.6(2)
O7-C23-H23A	109.5	O7-C23-H23B	109.5
H23A-C23-H23B	109.5	O7-C23-H23C	109.5
H23A-C23-H23C	109.5	H23B-C23-H23C	109.5

Table S7. Torsion angles (°) for **12**.

C5-N1-C1-C2	42.9(4)	C9-N1-C1-C2	-166.2(3)
N1-C1-C2-C3	-58.2(4)	C1-C2-C3-C4	44.2(4)
C2-C3-C4-C10	164.4(3)	C2-C3-C4-C5	-16.2(4)
C9-N1-C5-C4	-163.7(2)	C1-N1-C5-C4	-13.4(3)
C9-N1-C5-C6	18.1(3)	C1-N1-C5-C6	168.3(2)
C10-C4-C5-N1	179.2(2)	C3-C4-C5-N1	-0.1(3)
C10-C4-C5-C6	-2.5(3)	C3-C4-C5-C6	178.1(2)
N1-C5-C6-C12	-179.4(2)	C4-C5-C6-C12	2.3(3)
N1-C5-C6-C7	0.2(3)	C4-C5-C6-C7	-178.0(2)
C12-C6-C7-C8	-173.4(3)	C5-C6-C7-C8	6.9(4)
C6-C7-C8-C9	-31.8(4)	C5-N1-C9-C8	-43.1(4)
C1-N1-C9-C8	166.4(3)	C7-C8-C9-N1	49.8(4)
C5-C4-C10-C11	-0.1(3)	C3-C4-C10-C11	179.3(2)
C4-C10-C11-C12	2.8(3)	C4-C10-C11-C15	-177.4(2)
C5-C6-C12-O1	-179.19(18)	C7-C6-C12-O1	1.1(3)
C5-C6-C12-C11	0.5(3)	C7-C6-C12-C11	-179.1(2)
C13-O1-C12-C6	177.40(19)	C13-O1-C12-C11	-2.3(3)
C10-C11-C12-C6	-3.0(3)	C15-C11-C12-C6	177.2(2)
C10-C11-C12-O1	176.71(19)	C15-C11-C12-O1	-3.1(3)
C12-O1-C13-O2	-176.7(2)	C12-O1-C13-C14	4.5(3)
O2-C13-C14-C19	-1.6(3)	O1-C13-C14-C19	177.10(19)

O2-C13-C14-C15	-179.9(2)	O1-C13-C14-C15	-1.2(3)
C19-C14-C15-C16	-2.0(3)	C13-C14-C15-C16	176.32(19)
C19-C14-C15-C11	177.85(19)	C13-C14-C15-C11	-3.9(3)
C12-C11-C15-C16	-174.23(19)	C10-C11-C15-C16	6.0(3)
C12-C11-C15-C14	6.0(3)	C10-C11-C15-C14	-173.8(2)
C14-C15-C16-C17	0.9(3)	C11-C15-C16-C17	-178.9(2)
C14-C15-C16-C20	-177.24(19)	C11-C15-C16-C20	3.0(3)
C15-C16-C17-O3	-178.59(19)	C20-C16-C17-O3	-0.3(3)
C15-C16-C17-C18	1.1(3)	C20-C16-C17-C18	179.4(2)
O3-C17-C18-C19	177.6(2)	C16-C17-C18-C19	-2.0(3)
O3-C17-C18-C22	-3.3(3)	C16-C17-C18-C22	177.1(2)
C17-C18-C19-C14	1.0(3)	C22-C18-C19-C14	-178.1(2)
C15-C14-C19-C18	1.0(3)	C13-C14-C19-C18	-177.3(2)
C21-O5-C20-O4	4.9(3)	C21-O5-C20-C16	-175.93(19)
C17-C16-C20-O4	81.0(3)	C15-C16-C20-O4	-100.7(3)
C17-C16-C20-O5	-98.1(2)	C15-C16-C20-O5	80.2(3)
C23-O7-C22-O6	-4.6(4)	C23-O7-C22-C18	174.9(2)
C19-C18-C22-O6	176.8(2)	C17-C18-C22-O6	-2.3(4)
C19-C18-C22-O7	-2.7(3)	C17-C18-C22-O7	178.2(2)

Table S8. Anisotropic atomic displacement parameters (\AA^2) for **12**. The anisotropic atomic displacement factor exponent takes the form: $-2\pi^2 [h^2 a^{*2} U_{11} + \dots + 2 h k a^* b^* U_{12}]$

	U_{11}	U_{22}	U_{33}	U_{23}	U_{13}	U_{12}
N1	0.0406(10)	0.0441(12)	0.0659(14)	0.0033(11)	0.0139(9)	-0.0097(8)
O1	0.0297(7)	0.0482(9)	0.0505(10)	0.0159(8)	0.0039(7)	0.0018(6)
O2	0.0299(8)	0.0651(11)	0.0631(11)	0.0227(9)	0.0001(7)	0.0034(7)
O3	0.0484(10)	0.0705(12)	0.0493(10)	0.0254(10)	0.0039(8)	-0.0008(9)
O4	0.0514(10)	0.0502(11)	0.0725(13)	0.0008(10)	-0.0022(9)	0.0149(8)
O5	0.0397(8)	0.0566(10)	0.0448(9)	-0.0050(9)	-0.0068(7)	0.0010(7)
O6	0.0534(10)	0.0658(12)	0.0614(11)	0.0255(10)	0.0142(8)	-0.0031(8)
O7	0.0361(8)	0.0679(12)	0.0637(11)	0.0178(10)	0.0065(8)	-0.0126(8)
C1	0.0414(14)	0.068(2)	0.091(2)	-0.0046(19)	0.0163(14)	-0.0207(13)
C2	0.0343(13)	0.084(2)	0.0692(19)	-0.0005(18)	0.0073(12)	-0.0056(13)
C3	0.0299(11)	0.072(2)	0.0597(18)	0.0020(16)	0.0019(11)	-0.0039(11)
C4	0.0312(10)	0.0423(13)	0.0420(13)	-0.0067(11)	0.0038(9)	-0.0038(9)
C5	0.0355(11)	0.0342(12)	0.0464(13)	-0.0087(11)	0.0102(10)	-0.0077(9)
C6	0.0360(11)	0.0335(12)	0.0420(13)	-0.0006(10)	0.0084(9)	-0.0007(9)
C7	0.0500(14)	0.0473(15)	0.0545(16)	0.0124(14)	0.0124(13)	0.0041(12)
C8	0.0664(19)	0.093(2)	0.111(3)	0.055(2)	0.0226(18)	0.0008(17)
C9	0.0626(17)	0.0553(17)	0.100(2)	0.0191(18)	0.0196(16)	-0.0132(14)
C10	0.0313(10)	0.0439(13)	0.0364(12)	-0.0001(11)	0.0008(9)	0.0016(9)
C11	0.0285(10)	0.0358(12)	0.0357(12)	-0.0021(10)	0.0034(8)	-0.0001(8)
C12	0.0286(10)	0.0350(12)	0.0386(12)	-0.0013(10)	0.0026(9)	0.0014(8)
C13	0.0296(10)	0.0380(12)	0.0417(12)	0.0037(11)	0.0052(9)	0.0003(9)
C14	0.0303(10)	0.0324(11)	0.0318(11)	-0.0016(10)	0.0036(8)	-0.0007(8)

	U ₁₁	U ₂₂	U ₃₃	U ₂₃	U ₁₃	U ₁₂
C15	0.0295(10)	0.0328(11)	0.0315(11)	-0.0048(10)	0.0029(8)	0.0001(8)
C16	0.0336(10)	0.0372(12)	0.0334(11)	-0.0011(10)	0.0012(9)	0.0020(9)
C17	0.0418(11)	0.0400(12)	0.0322(12)	0.0047(11)	0.0049(9)	0.0009(9)
C18	0.0363(11)	0.0379(12)	0.0373(12)	0.0004(11)	0.0076(9)	-0.0026(9)
C19	0.0304(10)	0.0375(12)	0.0379(12)	-0.0028(10)	0.0022(9)	-0.0001(9)
C20	0.0379(11)	0.0413(13)	0.0385(12)	0.0068(11)	0.0038(9)	0.0008(10)
C21	0.0457(14)	0.080(2)	0.0594(17)	0.0042(16)	-0.0169(12)	-0.0061(13)
C22	0.0425(12)	0.0440(13)	0.0432(14)	0.0039(12)	0.0086(10)	-0.0035(10)
C23	0.0462(15)	0.108(3)	0.094(2)	0.034(2)	0.0067(15)	-0.0303(16)

Table S9. Hydrogen atomic coordinates and isotropic atomic displacement parameters (Å²) for **12**.

	x/a	y/b	z/c	U(eq)
H8A	0.6568	0.8888	-0.1710	0.107
H8B	0.6195	1.0319	-0.1471	0.107
H9A	0.8136	0.9883	-0.1077	0.086
H9B	0.7501	1.0341	-0.0366	0.086
H21A	0.7632	0.4395	0.3513	0.097
H21B	0.7633	0.5937	0.3685	0.097
H21C	0.8087	0.5396	0.2913	0.097
H23A	0.0067	0.2119	0.1949	0.125
H23B	-0.0812	0.3223	0.1586	0.125
H23C	-0.0227	0.3313	0.2489	0.125
H10	0.707(2)	0.539(3)	0.1413(15)	0.054(7)
H19	0.1821(18)	0.532(2)	0.0856(12)	0.036(6)
H1A	0.957(3)	0.877(3)	-0.0349(18)	0.083(10)
H2A	1.036(2)	0.709(3)	0.0601(16)	0.064(8)
H3A	0.901(3)	0.684(3)	0.148(2)	0.087(10)
H3B	0.891(3)	0.550(4)	0.102(2)	0.091(11)
H7A	0.511(3)	0.956(3)	-0.0652(19)	0.086(10)
H2B	0.951(2)	0.641(3)	-0.0168(18)	0.070(9)
H7B	0.496(3)	0.846(3)	-0.1249(19)	0.080(10)
H1B	0.930(3)	0.906(4)	0.060(2)	0.110(12)
H3	0.349(3)	0.292(3)	0.2888(17)	0.074(9)

Table S10. Hydrogen bond distances (Å) and angles (°) for **12**.

	Donor-H	Acceptor-H	Donor-Acceptor	Angle
O3-H3...O6	0.95(3)	1.69(3)	2.574(2)	152.(3)
C2-H2B...O7	1.06(3)	2.57(3)	3.521(4)	149.(2)
C23-H23A...O5	0.96	2.5	3.115(3)	121.4

Crystal Structure Report for 13

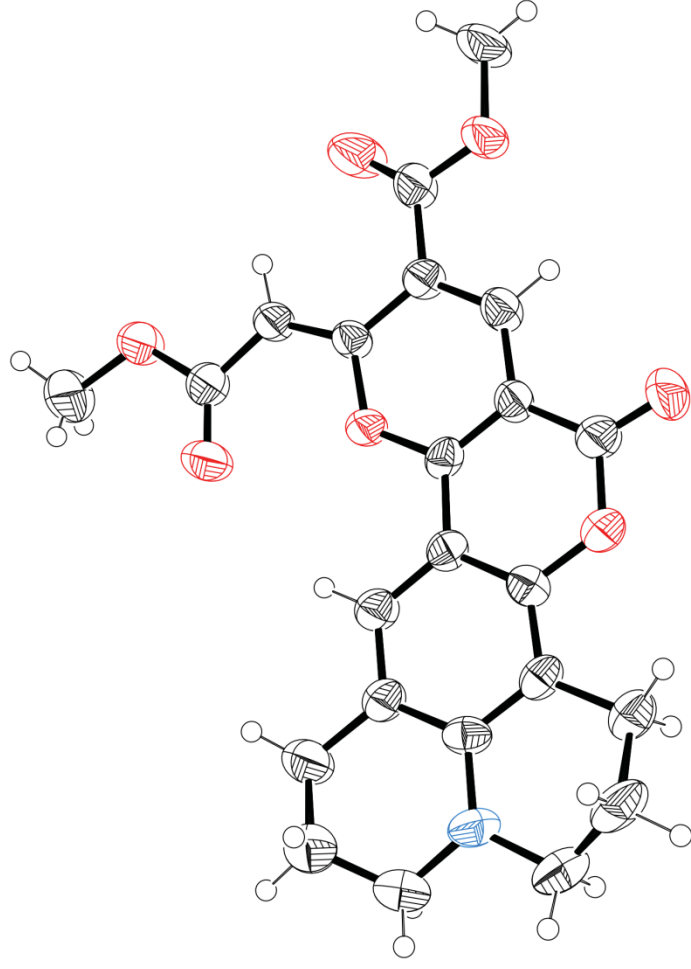


Figure S4. The ORTEP drawing⁴ of X-ray diffraction analysis for compound **13**. CCDC 2125096.

A red needle-like specimen of $C_{23}H_{21}NO_7$, approximate dimensions 0.093 mm x 0.118 mm x 0.654 mm, was used for the X-ray crystallographic analysis. The X-ray intensity data were measured.

Table S11. Data collection details for **13**.

Axis	dx/mm	2 θ /°	ω /°	ϕ /°	χ /°	Width/°	Fra-mes	Time/s	Wave-length/Å	Volta-ge/kV	Current/mA	Tempe-rature/K
Omega	39.875	-99.52	-196.16	0.05	26.30	1.60	68	24.00	1.54184	45	30.0	n/a
Omega	39.875	-100.83	-210.20	-187.67	52.45	1.60	72	24.00	1.54184	45	30.0	n/a
Omega	39.875	-100.46	-106.07	105.38	-57.83	1.60	74	24.00	1.54184	45	30.0	n/a

Axis	dx/mm	2 θ /°	ω /°	ϕ /°	χ /°	Width/°	Fra-mes	Time/s	Wave-length/Å	Volta-ge/kV	Current/mA	Tempe- rature/K
Omega	39.875	-100.80	-200.04	-257.00	32.48	1.60	68	24.00	1.54184	45	30.0	n/a
Omega	39.875	-101.00	-203.00	-126.64	37.78	1.60	69	24.00	1.54184	45	30.0	n/a
Omega	39.875	39.67	-326.19	270.00	-54.74	1.60	73	24.00	1.54184	45	30.0	n/a
Omega	39.875	-99.90	-197.24	-57.68	27.86	1.60	68	24.00	1.54184	45	30.0	n/a
Omega	39.875	44.78	-38.43	75.16	69.29	1.60	55	24.00	1.54184	45	30.0	n/a
Phi	39.875	85.61	-280.32	0.00	-58.06	1.60	225	24.00	1.54184	45	30.0	n/a
Omega	39.875	-97.67	-103.69	-113.67	-56.62	1.60	74	24.00	1.54184	45	30.0	n/a
Omega	39.875	39.67	-326.19	90.00	-54.74	1.60	73	24.00	1.54184	45	30.0	n/a
Omega	39.875	-94.23	-62.72	37.64	-80.63	1.60	62	24.00	1.54184	45	30.0	n/a
Omega	39.875	39.67	-326.19	0.00	-54.74	1.60	73	24.00	1.54184	45	30.0	n/a
Omega	39.875	-100.72	-200.75	42.15	34.55	1.60	68	24.00	1.54184	45	30.0	n/a
Omega	39.875	39.67	-326.19	180.00	-54.74	1.60	73	24.00	1.54184	45	30.0	n/a
Omega	39.875	-96.19	-196.73	-227.77	35.95	1.60	68	24.00	1.54184	45	30.0	n/a
Omega	39.875	-100.83	-106.04	47.01	-58.93	1.60	74	24.00	1.54184	45	30.0	n/a
Omega	39.875	82.64	-36.62	-58.22	77.11	1.60	63	24.00	1.54184	45	30.0	n/a
Omega	39.875	-100.85	-110.62	134.78	-31.95	1.60	68	24.00	1.54184	45	30.0	n/a
Omega	39.875	-99.90	-202.81	-86.05	40.42	1.60	69	24.00	1.54184	45	30.0	n/a
Omega	39.875	-101.52	-208.03	75.65	46.31	1.60	71	24.00	1.54184	45	30.0	n/a
Omega	39.875	-100.86	-210.38	-164.63	52.92	1.60	72	24.00	1.54184	45	30.0	n/a
Omega	39.875	69.67	-296.19	0.00	-54.74	1.60	73	24.00	1.54184	45	30.0	n/a
Omega	39.875	-100.21	-75.75	-33.75	-65.22	1.60	58	24.00	1.54184	45	30.0	n/a
Omega	39.875	69.67	-296.19	90.00	-54.74	1.60	73	24.00	1.54184	45	30.0	n/a
Phi	39.875	70.61	-295.32	0.00	-58.06	1.60	225	24.00	1.54184	45	30.0	n/a
Omega	39.875	-91.39	-190.44	-37.93	31.98	1.60	68	24.00	1.54184	45	30.0	n/a
Omega	39.875	93.00	-382.07	7.02	62.00	1.60	75	24.00	1.54184	45	30.0	n/a
Omega	39.875	-98.85	-106.83	44.61	-38.97	1.60	69	24.00	1.54184	45	30.0	n/a
Omega	39.875	-2.62	-113.72	270.00	54.74	1.60	73	24.00	1.54184	45	30.0	n/a

Axis	dx/mm	2 θ /°	ω /°	ϕ /°	χ /°	Width/°	Fra-mes	Time/s	Wave-length/Å	Volta-ge/kV	Current/mA	Tempe- rature/K
Omega	39.875	84.67	-281.19	180.00	-54.74	1.60	73	24.00	1.54184	45	30.0	n/a
Omega	39.875	84.67	-281.19	0.00	-54.74	1.60	73	24.00	1.54184	45	30.0	n/a
Omega	39.875	54.67	-311.19	270.00	-54.74	1.60	73	24.00	1.54184	45	30.0	n/a
Omega	39.875	-99.76	-110.47	-109.53	-29.62	1.60	68	24.00	1.54184	45	30.0	n/a
Omega	39.875	54.67	-311.19	90.00	-54.74	1.60	73	24.00	1.54184	45	30.0	n/a
Omega	39.875	54.67	-311.19	180.00	-54.74	1.60	73	24.00	1.54184	45	30.0	n/a
Omega	39.875	54.67	-311.19	0.00	-54.74	1.60	73	24.00	1.54184	45	30.0	n/a
Omega	39.875	84.67	-281.19	90.00	-54.74	1.60	73	24.00	1.54184	45	30.0	n/a
Omega	39.875	87.22	-37.01	-42.42	81.01	1.60	62	24.00	1.54184	45	30.0	n/a
Omega	39.875	84.67	-281.19	270.00	-54.74	1.60	73	24.00	1.54184	45	30.0	n/a
Phi	39.875	55.61	49.69	0.00	-58.06	1.60	225	24.00	1.54184	45	30.0	n/a
Omega	39.875	27.38	-337.68	-105.00	-54.74	1.60	72	24.00	1.54184	45	30.0	n/a
Phi	39.875	-18.13	-3.92	0.00	23.00	1.60	225	24.00	1.54184	45	30.0	n/a
Omega	39.875	69.67	-296.19	270.00	-54.74	1.60	73	24.00	1.54184	45	30.0	n/a
Omega	39.875	91.50	-381.45	-46.60	58.28	1.60	74	24.00	1.54184	45	30.0	n/a
Phi	39.875	43.16	28.95	0.00	-23.00	1.60	225	24.00	1.54184	45	30.0	n/a
Phi	39.875	-18.13	-12.20	0.00	58.06	1.60	225	24.00	1.54184	45	30.0	n/a
Omega	39.875	27.38	-337.68	-156.00	-54.74	1.60	72	24.00	1.54184	45	30.0	n/a
Omega	39.875	27.38	-337.68	-54.00	-54.74	1.60	72	24.00	1.54184	45	30.0	n/a
Omega	39.875	91.71	-373.51	-178.35	44.85	1.60	70	24.00	1.54184	45	30.0	n/a
Omega	39.875	69.67	-296.19	180.00	-54.74	1.60	73	24.00	1.54184	45	30.0	n/a
Omega	39.875	93.00	-366.21	62.22	32.38	1.60	68	24.00	1.54184	45	30.0	n/a
Phi	39.875	40.61	34.69	0.00	-58.06	1.60	225	24.00	1.54184	45	30.0	n/a
Omega	39.875	27.38	-337.68	0.00	-54.74	1.60	72	24.00	1.54184	45	30.0	n/a
Omega	39.875	27.38	-337.68	153.00	-54.74	1.60	72	24.00	1.54184	45	30.0	n/a
Phi	39.875	43.16	37.23	0.00	-58.06	1.60	225	24.00	1.54184	45	30.0	n/a
Omega	39.875	-81.15	-181.41	-167.12	35.16	1.60	68	24.00	1.54184	45	30.0	n/a

Axis	dx/mm	$2\theta/^\circ$	$\omega/^\circ$	$\phi/^\circ$	$\chi/^\circ$	Width/ $^\circ$	Fra-mes	Time/s	Wave-length/ Å	Volta-ge/kV	Current/mA	Tempe-rature/K
Omega	39.875	27.38	-337.68	51.00	-54.74	1.60	72	24.00	1.54184	45	30.0	n/a
Omega	39.875	-2.62	-113.72	0.00	54.74	1.60	73	24.00	1.54184	45	30.0	n/a
Omega	39.875	27.38	-337.68	102.00	-54.74	1.60	72	24.00	1.54184	45	30.0	n/a
Omega	39.875	-2.62	-113.72	90.00	54.74	1.60	73	24.00	1.54184	45	30.0	n/a
Omega	39.875	-2.62	-113.72	180.00	54.74	1.60	73	24.00	1.54184	45	30.0	n/a
Omega	39.875	12.38	-353.48	0.00	-54.74	1.60	73	24.00	1.54184	45	30.0	n/a

A total of 5680 frames were collected. The total exposure time was 37.87 hours. The frames were integrated with the Bruker SAINT software package using a narrow-frame algorithm. The integration of the data using a monoclinic unit cell yielded a total of 45603 reflections to a maximum θ angle of 66.19° (0.84 Å resolution), of which 3201 were independent (average redundancy 14.246, completeness = 91.9%, R_{int} = 14.21%, R_{sig} = 12.25%) and 1257 (39.27%) were greater than $2\sigma(F_2)$. The final cell constants of $a = 11.3428(5)$ Å, $b = 20.3876(9)$ Å, $c = 8.5895(4)$ Å, $\beta = 93.145(3)^\circ$, volume = 1983.35(15) Å³, are based upon the refinement of the XYZ-centroids of 7323 reflections above $20\sigma(I)$ with $7.806^\circ < 2\theta < 111.6^\circ$. Data were corrected for absorption effects using the multi-scan method (SADABS). The ratio of minimum to maximum apparent transmission was 0.772. The calculated minimum and maximum transmission coefficients (based on crystal size) are 0.5960 and 0.9220.

The structure was solved and refined using the Bruker SHELXTL Software Package, using the space group P 1 21/c 1, with $Z = 4$ for the formula unit, C₂₃H₂₁NO₇. The final anisotropic full-matrix least-squares refinement on F₂ with 283 variables converged at $R_1 = 7.38\%$, for the observed data and $wR_2 = 23.70\%$ for all data. The goodness-of-fit was 0.989. The largest peak in the final difference electron density synthesis was 0.273 e-/Å³ and the largest hole was -0.257 e-/Å³ with an RMS deviation of 0.060 e-/Å³. On the basis of the final model, the calculated density was 1.418 g/cm³ and $F(000)$, 888 e-.

Table S12. Sample and crystal data for **13**.

Identification code	KVy0615_10	
Chemical formula	C ₂₃ H ₂₁ NO ₇	
Formula weight	423.41 g/mol	
Temperature	296(2) K	
Wavelength	1.54178 Å	
Crystal size	0.093 x 0.118 x 0.654 mm	
Crystal habit	red needle	
Crystal system	monoclinic	
Space group	P 1 21/c 1	
Unit cell dimensions	$a = 11.3428(5)$ Å	$\alpha = 90^\circ$
	$b = 20.3876(9)$ Å	$\beta = 93.145(3)^\circ$
	$c = 8.5895(4)$ Å	$\gamma = 90^\circ$
Volume	1983.35(15) Å ³	
Z	4	
Density (calculated)	1.418 g/cm ³	
Absorption coefficient	0.884 mm ⁻¹	
$F(000)$	888	

Table S13. Data collection and structure refinement for **13**.

Theta range for data collection	3.90 to 66.19°
Index ranges	$-12 \leq h \leq 12$, $-22 \leq k \leq 23$, $-9 \leq l \leq 9$
Reflections collected	45603
Independent reflections	3201 [R_{int} = 0.1421]
Coverage of independent reflections	91.9%

Absorption correction	multi-scan	
Max. and min. transmission	0.9220 and 0.5960	
Structure solution technique	direct methods	
Structure solution program	SHELXL-2014 (Sheldrick, 2014)	
Refinement method	Full-matrix least-squares on F ²	
Refinement program	SHELXL-2014 (Sheldrick, 2014)	
Function minimized	$\sum w(\text{Fo}^2 - \text{Fc}^2)^2$	
Data / restraints / parameters	3201 / 0 / 283	
Goodness-of-fit on F ²	0.989	
$\Delta/\sigma_{\text{max}}$	0.006	
Final R indices	1257 data; $I > 2\sigma(I)$	R1 = 0.0738, wR2 = 0.1727
	all data	R1 = 0.2244, wR2 = 0.2370
Weighting scheme	$w = 1/[\sigma^2(\text{Fo}^2) + (0.0977P)^2 + 1.3622P]$ where $P = (\text{Fo}^2 + 2\text{Fc}^2)/3$	
Extinction coefficient	0.0002(1)	
Largest diff. peak and hole	0.273 and -0.257 e ^Å -3	
R.M.S. deviation from mean	0.060 e ^Å -3	

Table S14. Atomic coordinates and equivalent isotropic atomic displacement parameters (Å^2) for **13**. $U(\text{eq})$ is defined as one third of the trace of the orthogonalized U_{ij} tensor.

	x/a	y/b	z/c	U(eq)
N1	0.0470(4)	0.3526(2)	0.3296(5)	0.0535(13)
O1	0.8548(3)	0.15605(17)	0.1646(4)	0.0513(10)
O2	0.7813(3)	0.06119(18)	0.0827(4)	0.0723(13)
O3	0.6111(3)	0.25900(14)	0.8953(4)	0.0442(9)
O4	0.5256(3)	0.37712(17)	0.8099(5)	0.0805(14)
O5	0.3723(3)	0.37069(16)	0.6370(4)	0.0668(12)
O6	0.3440(4)	0.15007(18)	0.6299(5)	0.0871(15)
O7	0.4453(3)	0.06125(17)	0.6947(4)	0.0679(12)
C1	0.0523(5)	0.4238(3)	0.3430(7)	0.0765(19)
C2	0.9991(6)	0.4567(3)	0.2021(8)	0.097(2)
C3	0.8758(5)	0.4335(3)	0.1653(7)	0.0699(18)
C4	0.8695(4)	0.3599(2)	0.1623(6)	0.0457(14)
C5	0.9545(4)	0.3217(3)	0.2509(6)	0.0421(13)
C6	0.9487(4)	0.2528(3)	0.2506(6)	0.0413(13)
C7	0.0401(4)	0.2123(2)	0.3416(6)	0.0513(15)
C8	0.1558(4)	0.2492(3)	0.3616(7)	0.0655(17)
C9	0.1351(5)	0.3165(3)	0.4257(7)	0.0669(18)
C10	0.7817(4)	0.3281(2)	0.0759(6)	0.0458(14)
C11	0.7731(4)	0.2596(2)	0.0732(6)	0.0390(13)
C12	0.8576(4)	0.2240(2)	0.1620(6)	0.0423(14)
C13	0.6902(4)	0.2230(3)	0.9827(5)	0.0373(13)
C14	0.6871(4)	0.1562(2)	0.9792(6)	0.0420(14)

	x/a	y/b	z/c	U(eq)
C15	0.7727(4)	0.1203(3)	0.0748(6)	0.0493(15)
C16	0.5999(4)	0.1252(2)	0.8818(6)	0.0462(14)
C17	0.5200(4)	0.1599(2)	0.7928(6)	0.0410(13)
C18	0.5235(4)	0.2310(2)	0.7979(6)	0.0386(14)
C19	0.4527(4)	0.2732(2)	0.7190(6)	0.0436(14)
C20	0.4593(5)	0.3437(3)	0.7318(6)	0.0500(15)
C21	0.3689(5)	0.4415(3)	0.6327(7)	0.089(2)
C22	0.4273(5)	0.1257(3)	0.6972(7)	0.0514(15)
C23	0.3583(5)	0.0224(2)	0.6063(7)	0.0743(19)

Table S15. Bond lengths (Å) for **13**.

N1-C5	1.369(6)	N1-C1	1.457(6)
N1-C9	1.460(6)	O1-C15	1.384(5)
O1-C12	1.385(5)	O2-C15	1.210(5)
O3-C13	1.354(5)	O3-C18	1.387(5)
O4-C20	1.194(5)	O5-C20	1.360(5)
O5-C21	1.444(6)	O6-C22	1.190(5)
O7-C22	1.330(5)	O7-C23	1.447(5)
C1-C2	1.483(7)	C1-H1A	0.97
C1-H1B	0.97	C2-C3	1.494(7)
C2-H2A	0.97	C2-H2B	0.97
C3-C4	1.504(6)	C3-H3A	0.97
C3-H3B	0.97	C4-C10	1.372(6)
C4-C5	1.426(6)	C5-C6	1.406(6)
C6-C12	1.381(6)	C6-C7	1.509(6)
C7-C8	1.514(6)	C7-H7A	0.97
C7-H7B	0.97	C8-C9	1.502(7)
C8-H8A	0.97	C8-H8B	0.97
C9-H9A	0.97	C9-H9B	0.97
C10-C11	1.400(6)	C10-H10	0.93
C11-C12	1.396(6)	C11-C13	1.402(6)
C13-C14	1.363(6)	C14-C16	1.409(6)
C14-C15	1.437(6)	C16-C17	1.353(6)
C16-H16	0.93	C17-C18	1.450(6)
C17-C22	1.474(7)	C18-C19	1.336(6)
C19-C20	1.443(6)	C19-H19	0.93
C21-H21A	0.96	C21-H21B	0.96
C21-H21C	0.96	C23-H23A	0.96
C23-H23B	0.96	C23-H23C	0.96

Table S16. Bond angles (°) for **13**.

C5-N1-C1	121.6(5)	C5-N1-C9	122.0(5)
C1-N1-C9	115.7(5)	C15-O1-C12	122.2(4)

C13-O3-C18	122.8(4)	C20-O5-C21	115.9(4)
C22-O7-C23	116.7(4)	N1-C1-C2	111.9(5)
N1-C1-H1A	109.2	C2-C1-H1A	109.2
N1-C1-H1B	109.2	C2-C1-H1B	109.2
H1A-C1-H1B	107.9	C1-C2-C3	111.3(5)
C1-C2-H2A	109.4	C3-C2-H2A	109.4
C1-C2-H2B	109.4	C3-C2-H2B	109.4
H2A-C2-H2B	108.0	C2-C3-C4	111.2(5)
C2-C3-H3A	109.4	C4-C3-H3A	109.4
C2-C3-H3B	109.4	C4-C3-H3B	109.4
H3A-C3-H3B	108.0	C10-C4-C5	118.8(5)
C10-C4-C3	120.8(5)	C5-C4-C3	120.4(5)
N1-C5-C6	119.6(5)	N1-C5-C4	119.3(5)
C6-C5-C4	120.9(5)	C12-C6-C5	117.4(5)
C12-C6-C7	121.6(5)	C5-C6-C7	121.0(5)
C6-C7-C8	110.7(4)	C6-C7-H7A	109.5
C8-C7-H7A	109.5	C6-C7-H7B	109.5
C8-C7-H7B	109.5	H7A-C7-H7B	108.1
C9-C8-C7	110.0(5)	C9-C8-H8A	109.7
C7-C8-H8A	109.7	C9-C8-H8B	109.7
C7-C8-H8B	109.7	H8A-C8-H8B	108.2
N1-C9-C8	111.7(4)	N1-C9-H9A	109.3
C8-C9-H9A	109.3	N1-C9-H9B	109.3
C8-C9-H9B	109.3	H9A-C9-H9B	107.9
C4-C10-C11	121.8(5)	C4-C10-H10	119.1
C11-C10-H10	119.1	C12-C11-C10	117.7(5)
C12-C11-C13	116.4(5)	C10-C11-C13	125.8(5)
C6-C12-O1	115.7(5)	C6-C12-C11	123.3(5)
O1-C12-C11	120.9(5)	O3-C13-C14	121.0(4)
O3-C13-C11	114.9(5)	C14-C13-C11	124.1(5)
C13-C14-C16	118.5(4)	C13-C14-C15	118.7(5)
C16-C14-C15	122.8(5)	O2-C15-O1	116.3(5)
O2-C15-C14	126.1(5)	O1-C15-C14	117.6(5)
C17-C16-C14	121.8(4)	C17-C16-H16	119.1
C14-C16-H16	119.1	C16-C17-C18	119.3(5)
C16-C17-C22	120.1(5)	C18-C17-C22	120.5(5)
C19-C18-O3	115.6(4)	C19-C18-C17	127.8(5)
O3-C18-C17	116.6(4)	C18-C19-C20	125.2(5)
C18-C19-H19	117.4	C20-C19-H19	117.4
O4-C20-O5	121.3(5)	O4-C20-C19	129.8(5)
O5-C20-C19	109.0(5)	O5-C21-H21A	109.5
O5-C21-H21B	109.5	H21A-C21-H21B	109.5
O5-C21-H21C	109.5	H21A-C21-H21C	109.5
H21B-C21-H21C	109.5	O6-C22-O7	121.5(5)
O6-C22-C17	126.7(5)	O7-C22-C17	111.8(5)

O7-C23-H23A	109.5	O7-C23-H23B	109.5
H23A-C23-H23B	109.5	O7-C23-H23C	109.5
H23A-C23-H23C	109.5	H23B-C23-H23C	109.5

Table S17. Torsion angles (°) for **13**.

C5-N1-C1-C2	-33.8(7)	C9-N1-C1-C2	155.8(5)
N1-C1-C2-C3	54.5(7)	C1-C2-C3-C4	-50.5(7)
C2-C3-C4-C10	-154.4(5)	C2-C3-C4-C5	26.2(7)
C1-N1-C5-C6	-175.3(5)	C9-N1-C5-C6	-5.6(7)
C1-N1-C5-C4	8.6(7)	C9-N1-C5-C4	178.3(5)
C10-C4-C5-N1	175.8(4)	C3-C4-C5-N1	-4.8(7)
C10-C4-C5-C6	-0.2(7)	C3-C4-C5-C6	179.1(5)
N1-C5-C6-C12	-176.2(4)	C4-C5-C6-C12	-0.2(7)
N1-C5-C6-C7	2.6(7)	C4-C5-C6-C7	178.7(4)
C12-C6-C7-C8	152.5(5)	C5-C6-C7-C8	-26.3(6)
C6-C7-C8-C9	51.4(6)	C5-N1-C9-C8	32.4(7)
C1-N1-C9-C8	-157.3(5)	C7-C8-C9-N1	-54.8(6)
C5-C4-C10-C11	0.4(7)	C3-C4-C10-C11	-179.0(5)
C4-C10-C11-C12	-0.1(7)	C4-C10-C11-C13	-176.7(5)
C5-C6-C12-O1	179.9(4)	C7-C6-C12-O1	1.1(7)
C5-C6-C12-C11	0.5(7)	C7-C6-C12-C11	-178.3(4)
C15-O1-C12-C6	-176.4(4)	C15-O1-C12-C11	3.1(7)
C10-C11-C12-C6	-0.4(7)	C13-C11-C12-C6	176.5(4)
C10-C11-C12-O1	-179.8(4)	C13-C11-C12-O1	-2.9(7)
C18-O3-C13-C14	-0.2(7)	C18-O3-C13-C11	179.4(4)
C12-C11-C13-O3	-178.6(4)	C10-C11-C13-O3	-1.9(7)
C12-C11-C13-C14	1.0(7)	C10-C11-C13-C14	177.7(5)
O3-C13-C14-C16	0.3(7)	C11-C13-C14-C16	-179.3(4)
O3-C13-C14-C15	-179.7(4)	C11-C13-C14-C15	0.7(8)
C12-O1-C15-O2	177.6(4)	C12-O1-C15-C14	-1.2(7)
C13-C14-C15-O2	-179.3(5)	C16-C14-C15-O2	0.7(8)
C13-C14-C15-O1	-0.6(7)	C16-C14-C15-O1	179.4(4)
C13-C14-C16-C17	0.0(7)	C15-C14-C16-C17	180.0(5)
C14-C16-C17-C18	-0.3(7)	C14-C16-C17-C22	-177.6(5)
C13-O3-C18-C19	-179.8(4)	C13-O3-C18-C17	-0.1(6)
C16-C17-C18-C19	180.0(5)	C22-C17-C18-C19	-2.7(8)
C16-C17-C18-O3	0.4(7)	C22-C17-C18-O3	177.7(4)
O3-C18-C19-C20	-1.8(7)	C17-C18-C19-C20	178.6(5)
C21-O5-C20-O4	2.4(8)	C21-O5-C20-C19	-178.2(4)
C18-C19-C20-O4	0.5(9)	C18-C19-C20-O5	-178.9(5)
C23-O7-C22-O6	-0.1(8)	C23-O7-C22-C17	178.9(4)
C16-C17-C22-O6	169.9(6)	C18-C17-C22-O6	-7.4(9)
C16-C17-C22-O7	-9.1(7)	C18-C17-C22-O7	173.6(4)

Table S18. Anisotropic atomic displacement parameters (Å²) for **13**. The anisotropic atomic displacement factor exponent takes the form: $-2\pi^2[h^2 a^*^2 U_{11} + \dots + 2 h k a^* b^* U_{12}]$

	U11	U22	U33	U23	U13	U12
N1	0.042(3)	0.062(3)	0.055(3)	-0.005(3)	-0.012(2)	-0.009(3)
O1	0.044(2)	0.051(2)	0.057(2)	0.002(2)	-0.0133(19)	0.0024(19)
O2	0.071(3)	0.039(2)	0.104(3)	0.006(2)	-0.028(2)	0.007(2)
O3	0.036(2)	0.039(2)	0.055(2)	-0.0009(18)	-0.0126(18)	-0.0015(18)
O4	0.082(3)	0.044(3)	0.110(4)	-0.004(2)	-0.047(3)	-0.005(2)
O5	0.061(3)	0.041(2)	0.093(3)	-0.001(2)	-0.035(2)	0.009(2)
O6	0.063(3)	0.053(3)	0.140(4)	-0.019(2)	-0.052(3)	0.008(2)
O7	0.061(3)	0.040(2)	0.098(3)	-0.001(2)	-0.038(2)	-0.007(2)
C1	0.077(5)	0.063(5)	0.086(5)	-0.003(4)	-0.022(4)	-0.024(4)
C2	0.093(5)	0.072(5)	0.119(6)	0.023(4)	-0.048(5)	-0.026(4)
C3	0.061(4)	0.048(4)	0.098(5)	-0.001(3)	-0.020(4)	-0.007(3)
C4	0.038(3)	0.048(3)	0.051(4)	0.001(3)	-0.006(3)	0.004(3)
C5	0.033(3)	0.051(4)	0.043(3)	-0.006(3)	0.005(3)	-0.010(3)
C6	0.031(3)	0.055(4)	0.038(3)	0.003(3)	0.001(3)	0.005(3)
C7	0.040(3)	0.066(4)	0.048(4)	0.007(3)	-0.001(3)	0.004(3)
C8	0.031(3)	0.099(5)	0.065(4)	0.011(4)	-0.014(3)	0.000(3)
C9	0.051(4)	0.086(5)	0.060(4)	-0.003(4)	-0.020(3)	0.001(3)
C10	0.037(3)	0.046(4)	0.053(4)	-0.002(3)	-0.004(3)	0.003(3)
C11	0.028(3)	0.044(3)	0.045(3)	0.001(3)	-0.001(3)	0.003(3)
C12	0.041(4)	0.039(3)	0.047(4)	-0.002(3)	0.004(3)	-0.003(3)
C13	0.025(3)	0.044(3)	0.042(4)	0.005(3)	-0.002(3)	0.004(3)
C14	0.034(3)	0.037(3)	0.054(4)	0.005(3)	-0.004(3)	0.000(3)
C15	0.039(4)	0.048(4)	0.059(4)	-0.002(3)	-0.007(3)	0.001(3)
C16	0.037(3)	0.037(3)	0.064(4)	0.002(3)	-0.001(3)	0.000(3)
C17	0.029(3)	0.042(3)	0.052(4)	-0.002(3)	-0.003(3)	0.002(3)
C18	0.030(3)	0.035(3)	0.050(4)	0.000(3)	-0.001(3)	-0.003(3)
C19	0.035(3)	0.038(3)	0.057(4)	0.000(3)	-0.009(3)	0.000(3)
C20	0.042(4)	0.046(4)	0.061(4)	0.002(3)	-0.007(3)	0.004(3)
C21	0.112(6)	0.039(4)	0.112(6)	-0.003(4)	-0.034(4)	0.022(4)
C22	0.039(4)	0.042(4)	0.072(4)	0.001(3)	-0.008(3)	0.005(3)
C23	0.063(4)	0.044(3)	0.112(5)	-0.010(3)	-0.030(4)	-0.016(3)

Table S19. Hydrogen atomic coordinates and isotropic atomic displacement parameters (Å²) for **13**.

	x/a	y/b	z/c	U(eq)
H1A	1.1340	0.4373	0.3590	0.092
H1B	1.0107	0.4374	0.4333	0.092
H2A	1.0468	0.4478	0.1141	0.116
H2B	0.9987	0.5038	0.2188	0.116
H3A	0.8477	0.4507	0.0647	0.084

	x/a	y/b	z/c	U(eq)
H3B	0.8247	0.4501	0.2432	0.084
H7A	1.0524	0.1715	0.2870	0.062
H7B	1.0118	0.2019	0.4432	0.062
H8A	1.2099	0.2253	0.4322	0.079
H8B	1.1913	0.2528	0.2618	0.079
H9A	1.1087	0.3126	0.5308	0.08
H9B	1.2088	0.3407	0.4308	0.08
H10	0.7263	0.3528	0.0174	0.055
H16	0.5971	0.0796	-0.1213	0.055
H19	0.3946	0.2558	-0.3496	0.052
H21A	0.4479	0.4583	-0.3695	0.134
H21B	0.3329	0.4576	-0.2762	0.134
H21C	0.3237	0.4556	-0.4589	0.134
H23A	0.2900	0.0166	-0.3339	0.112
H23B	0.3913	-0.0197	-0.4163	0.112
H23C	0.3359	0.0445	-0.4895	0.112

Table S20. Hydrogen bond distances (Å) and angles (°) for **13**.

	Donor-H	Acceptor-H	Donor-Acceptor	Angle
C23-H23B...O4	0.96	2.46	3.305(6)	146.6
C19-H19...O6	0.93	2.24	2.882(6)	126.1
C9-H9B...O5	0.97	2.57	3.350(6)	137.8

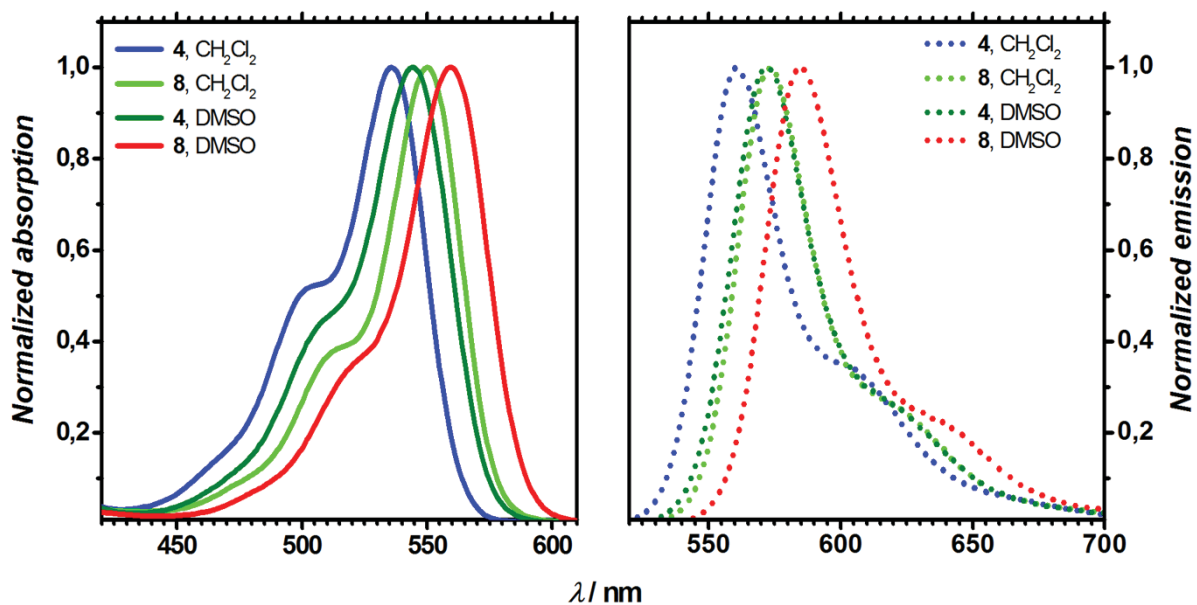


Figure S5. Absorption (solid) and emission (dotted) of compounds 4 and 23 in CH_2Cl_2 and DMSO.

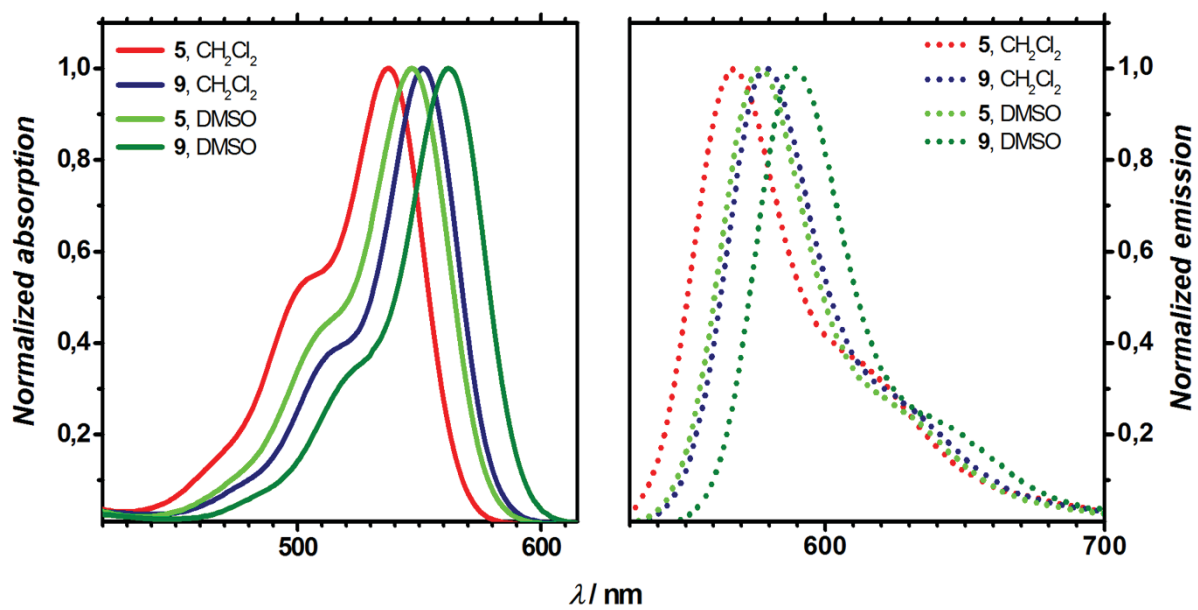


Figure S6. Absorption (solid) and emission (dotted) of compounds 5 and 9 in CH_2Cl_2 and DMSO.

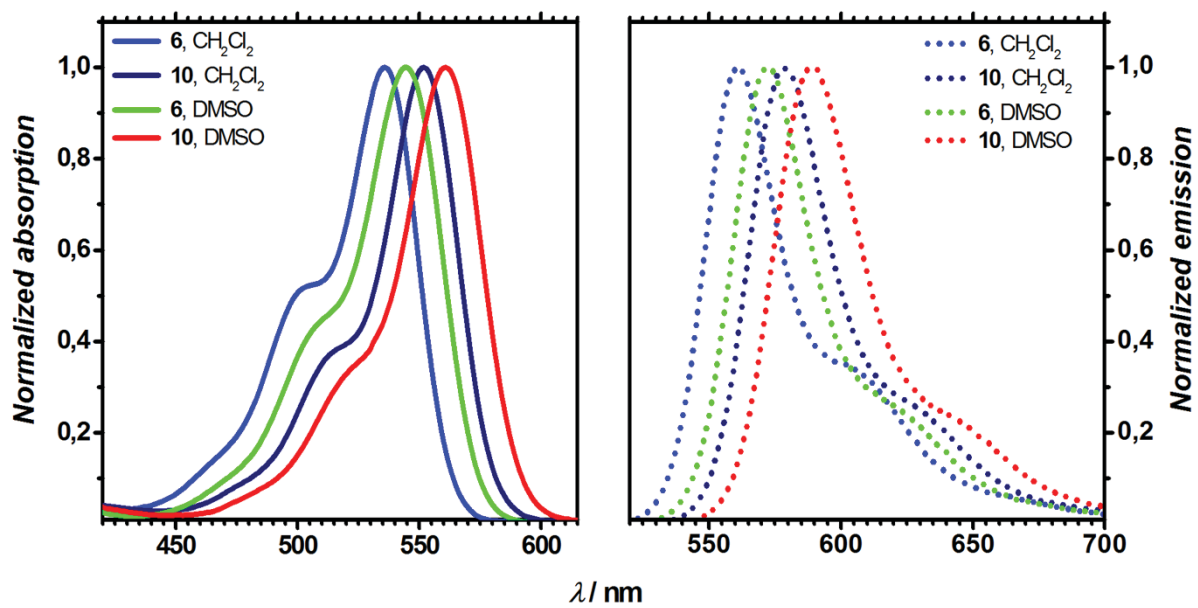


Figure S7. Absorption (solid) and emission (dotted) of compounds **6** and **10** in CH_2Cl_2 and DMSO.

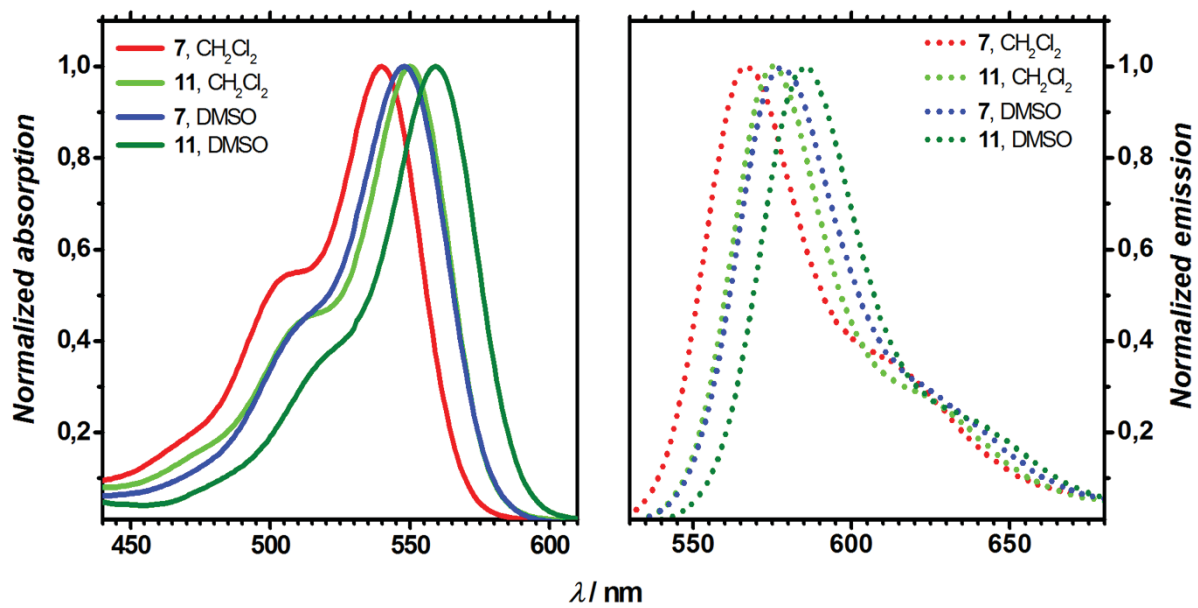


Figure S8. Absorption (solid) and emission (dotted) of compounds **7** and **11** in CH_2Cl_2 and DMSO.

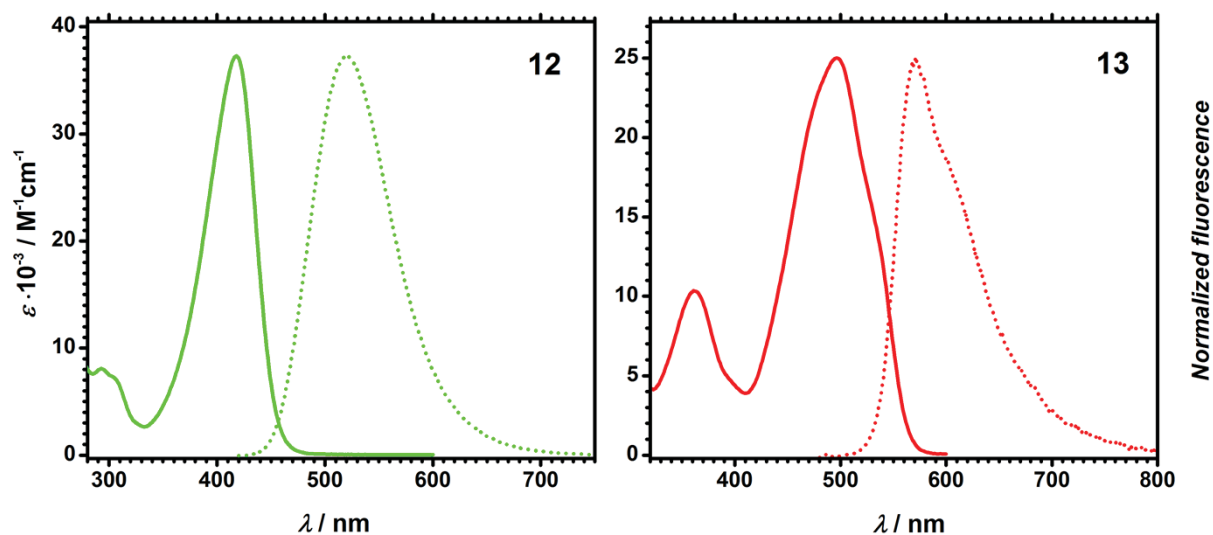


Figure S9. Absorption (solid) and emission (dotted) spectra for compounds **12** (in CH₂Cl₂) and **13** (in DMSO).

Table S21. The spectroscopic properties for compounds **12** and **13**.

Dye	Solvent	$\lambda_{\text{abs}}^{\text{max}}$ [nm]	$\epsilon \cdot 10^{-3}$ [M ⁻¹ cm ⁻¹]	$\lambda_{\text{em}}^{\text{max}}$ [nm]	$\Delta\bar{\nu}$ [cm ⁻¹]	Φ_{fl}
12 ^a	CH ₂ Cl ₂	418	37	520	4700	0.73
13	CH ₂ Cl ₂	491	32	– ^b		
	DMSO	497	25	571	2600	0.037

^a – Compound **12** in DMSO does not show linear dependence of the absorption vs. concentration.

^b – In the fluorescence spectrum compound **13** in CH₂Cl₂ shows emission from two forms.

Photostability measurements

Photostability was determined through the variation in absorption of each sample at the appropriate absorption maximum wavelength (λ_{abs}) with respect to irradiation time. Ethanol was selected as the solvent. Concentrations giving similar optical densities ($A \approx 1$) were used. Quartz cells of samples were irradiated with a 300 W Xe lamp (Asahi spectra MAX-350) for 120 min (for compounds **4-7** in DMSO), 50 min (for compounds **8-11** in DMSO) and 30 min for all dyes in DCM at 25 °C equipped with a UV/vis mirror module through a glass fiber. The absorption spectra were measured at appropriate times during the irradiation. **Rhodamine 6G**, **Fluorescein** and **Rdl12**⁵ in appropriate solvents were used as references.

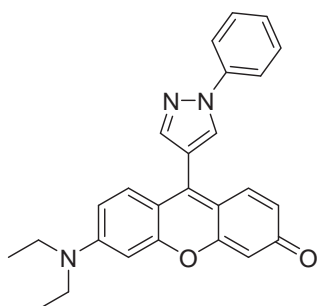


Figure S10. The structure of **Rdl12**.

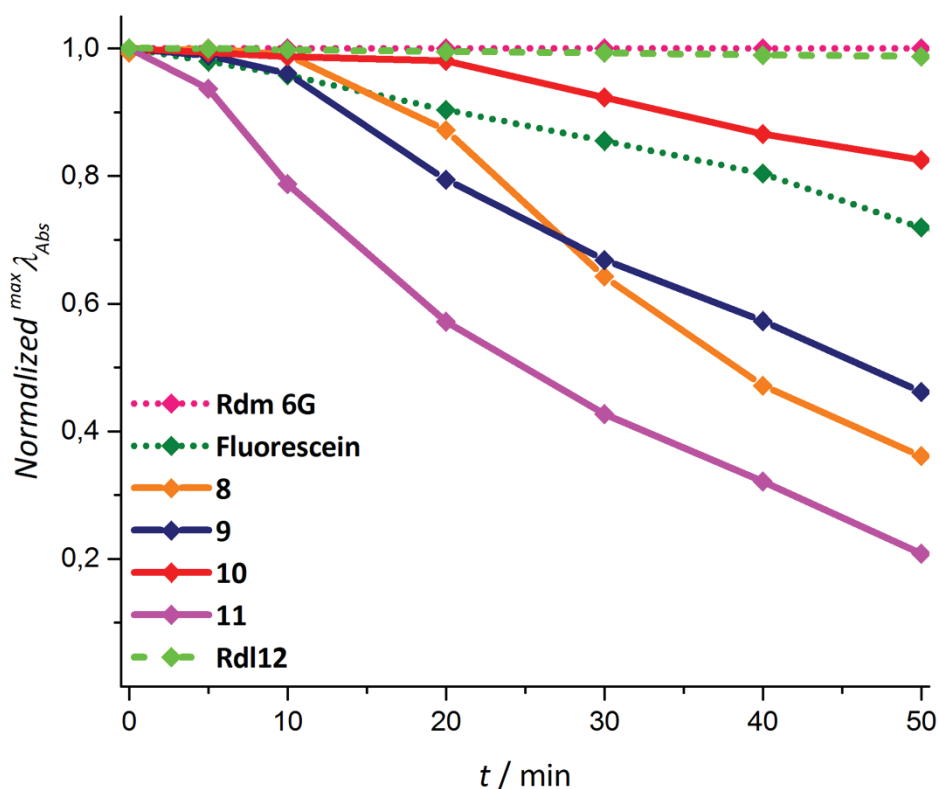


Figure S11. Photostability of rhodols **8-11** compared to the Rhodamine 6G in EtOH, fluorescein in 0,1M NaOH aqueous solution and **Rdl12** measured in DMSO using a collimated light source from a 300W Xe lamp.

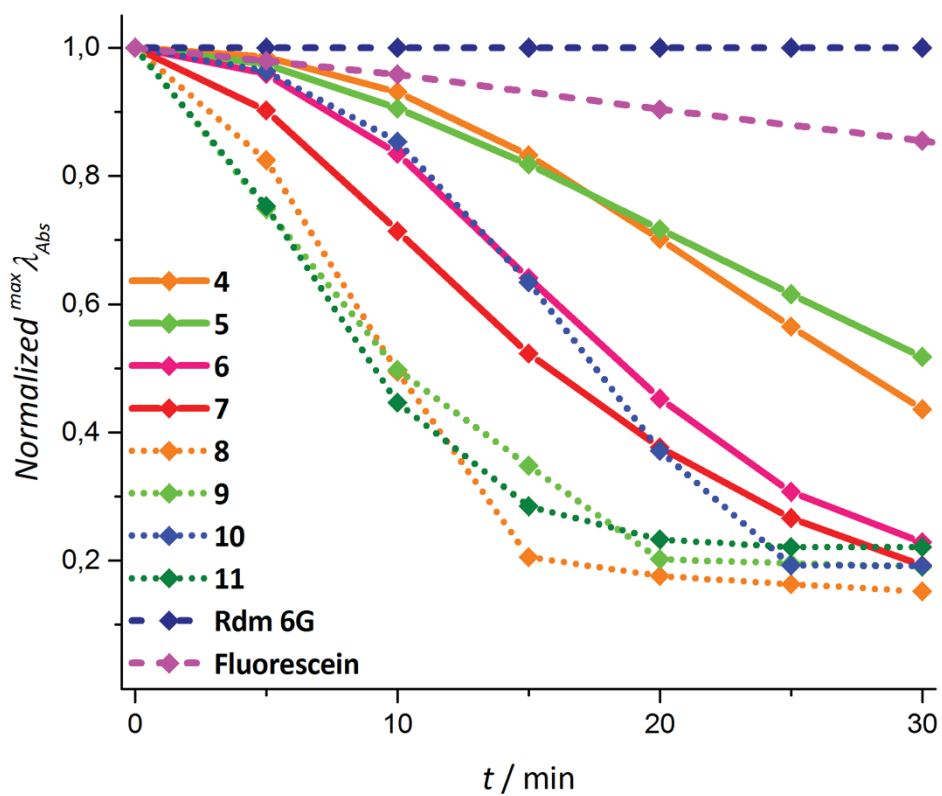


Figure S12. Photostability of rhodols 4-11 compared to the **Rhodamine 6G** in EtOH and **Fluorescein** in 0,1M NaOH aqueous solution measured in CH_2Cl_2 using a collimated light source from a 300W Xe lamp.

Theoretical methods

We have performed the DFT and TD-DFT calculations with the Gaussian 16 code⁶ on all dyes. For **4**, we performed a conformational search on the side esters groups and only the most stable ones were used. Default Gaussian16 thresholds and algorithms were used but for an improved optimization threshold (10^{-5} au on average residual forces), a stricter self-consistent field convergence criterion (10^{-10} a.u.) and the use of the *ultrafine* DFT integration grid.

Firstly, the S_0 geometries have been optimized with DFT and the vibrational frequencies have been analytically determined, using the M06-2X *meta*-GGA hybrid exchange-correlation functional.⁷ These calculations were performed with the 6-311G(d,p) atomic basis set and account for solvent effects through the linear-response PCM approach considering DCM as solvent.⁸ Secondly, starting from the optimal ground-state geometries, we have used TD-DFT with the same functional and basis set to optimize the S_1 geometry and compute the vibrational frequencies. All optimized structures correspond to true minima of the potential energy surface. Thirdly, the vertical transition energies were determined with TD-DFT and the same functional, but a larger basis set, namely 6-311+G(2d,p), in gas-phase as well as in solution using the cLR² variant of the PCM,⁹ in its *non-equilibrium* limit.

As the shortcomings of TD-DFT for cyanine derivatives¹⁰ are known, the obtained transition energies were also computed using COSMO-ADC(2)¹¹ with the Turbomole 7.3 code.¹² These ADC(2) energies were calculated in gas phase applying the resolution of identity scheme, and using the *aug-cc-pVDZ* atomic basis set.

The vibrationally resolved spectrum were determined with the FCClasses 3 program.^{13,14} We used a time-dependent formulation, applied the FC approximation (HT effects were neglected), and selected the so-called *Vertical Gradient*¹⁵ vibronic model for the band topologies on the basis of the TD-DFT data only. We used a simulation temperature of 298K. The obtained stick spectrum were convoluted with Gaussian having HWHM of 300 cm^{-1} . The radiative and internal conversion rates have been obtained using the TVCF formalism.¹⁶ These calculations were made within the time-dependent formulation, the same FC approach and the *Vertical Gradient* model.¹⁵ For the radiative part, we used the same broadening as for the band shapes, i.e., a 300 cm^{-1} Gaussian, but this is known to be not important for the radiative rate.¹⁷ For the IC part, we used a 10 cm^{-1} broadening Lorentzian, which is a typical value in the literature.^{17,18}

Additional theoretical data

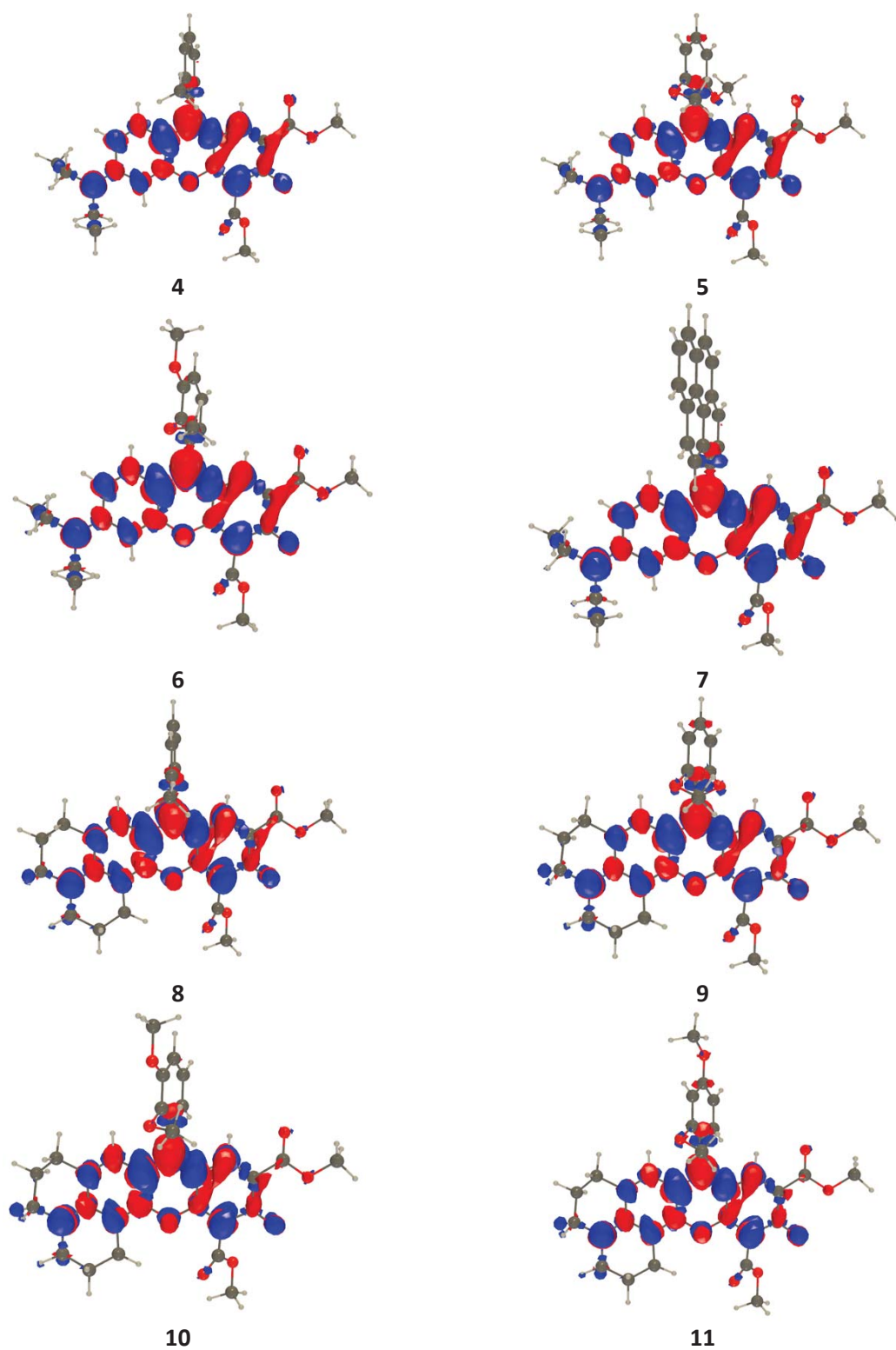


Figure S13. Electron density difference (EDD) plots for the lowest excited states of compounds **4-11**, as obtained with TD-DFT. The blue and red lobes correspond to regions of decrease and increase of electron density respectively. Contour threshold: 0.001 au.

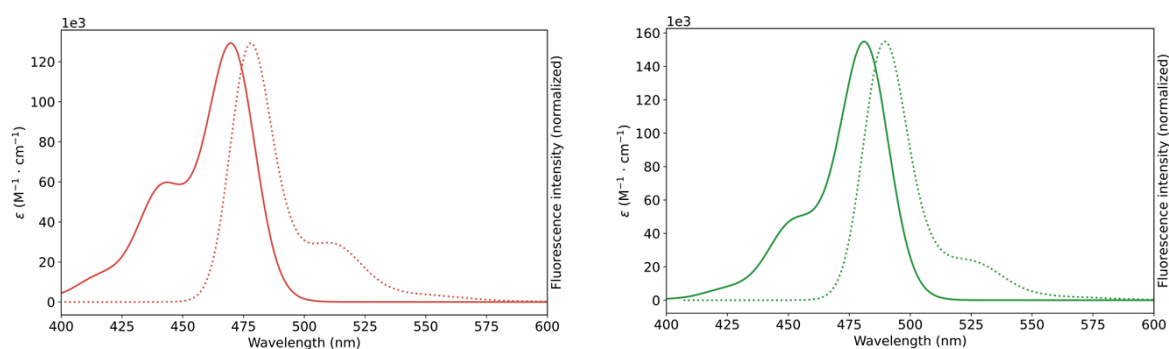


Figure S14. Computed vibrationaly-resolved absorption and emission spectra for **4** (left) and **8** (right). The presence of the typical “cyanine shoulder” is clear in all cases.

Table S22. Computed vertical absorption, vertical emission, and 0-0 wavelengths with TD-DFT and ADC(2) for rhodols **4-11**. All values are given in nm. We recall here that vertical transition energies cannot be directly compared to experimental λ_{max} , and that, in contrast, 0-0 values can be rigorously to the experimental crossing point between the absorption and fluorescence curves. It can be noted that the experimental values are bracketed by the TD-DFT and ADC(2) estimates, but closer from the latter.

	cLR ² -PCM-TD-DFT			COSMO-ADC(2)		
	$\lambda_{\text{vert-abso}}$	$\lambda_{\text{vert-fluo}}$	λ_{0-0}	$\lambda_{\text{vert-abso}}$	$\lambda_{\text{vert-fluo}}$	λ_{0-0}
4	440	471	466	562	625	603
5	452	491	479	585	665	640
6	445	480	472	573	643	620
7	443	478	472	570	640	617
8	452	478	477	592	641	622
9	467	496	492	621	681	663
10	456	487	482	601	660	642
11	460	486	485	607	659	640

Table S23. Computed radiative and international conversion rates (10^8 s^{-1}) and deduced quantum yield of emission.

	k_r	k_{ic}	ϕ_f
8	3.44	1.48	0.70
9	2.97	1.65	0.64
10	3.23	1.56	0.67
11	3.22	1.54	0.68

Notes and references

- 1 L. Yuan, W. Lin, J. Song and Y. Yang, *Chem. Commun.*, 2011, **47**, 12691–12693.
- 2 G. Yin, T. Niu, T. Yu, Y. Gan, X. Sun, P. Yin, H. Chen, Y. Zhang, H. Li and S. Yao, *Angew. Chem. Int. Ed.*, 2019, **58**, 4557–4561.
- 3 M. Tasior, Y. M. Poronik, O. Vakuliuk, B. Sadowski, M. Karczewski and D. T. Gryko, *J. Org. Chem.*, 2014, **79**, 8723–8732.
- 4 L. J. Farrugia, *J. Appl. Crystallogr.*, 2012, **45**, 849–854.
- 5 Y. M. Poronik, G. Clermont, M. Blanchard-Desce and D. T. Gryko, *J. Org. Chem.*, 2013, **78**, 11721–11732.
- 6 M. J. Frisch, G. W. Trucks, H. B. Schlegel, G. E. Scuseria, M. A. Robb, J. R. Cheeseman, G. Scalmani, V. Barone, G. A. Petersson, H. Nakatsuji, X. Li, M. Caricato, A. V. Marenich, J. Bloino, B. G. Janesko, R. Gomperts, B. Mennucci, H. P. Hratchian, J. V. Ortiz, A. F. Izmaylov, J. L. Sonnenberg, D. Williams-Young, F. Ding, F. Lipparini, F. Egidi, J. Goings, B. Peng, A. Petrone, T. Henderson, D. Ranasinghe, V. G. Zakrzewski, J. Gao, N. Rega, G. Zheng, W. Liang, M. Hada, M. Ehara, K. Toyota, R. Fukuda, J. Hasegawa, M. Ishida, T. Nakajima, Y. Honda, O. Kitao, H. Nakai, T. Vreven, K. Throssell, J. A. Montgomery Jr., J. E. Peralta, F. Ogliaro, M. J. Bearpark, J. J. Heyd, E. N. Brothers, K. N. Kudin, V. N. Staroverov, T. A. Keith, R. Kobayashi, J. Normand, K. Raghavachari, A. P. Rendell, J. C. Burant, S. S. Iyengar, J. Tomasi, M. Cossi, J. M. Millam, M. Klene, C. Adamo, R. Cammi, J. W. Ochterski, R. L. Martin, K. Morokuma, O. Farkas, J. B. Foresman and D. J. Fox, *Gaussian 16 Revision A.03*, Gaussian, Inc., Wallingford CT, 2016.
- 7 Y. Zhao and D. G. Truhlar, *Theor. Chem. Acc.*, 2008, **120**, 215–241.
- 8 J. Tomasi, B. Mennucci and R. Cammi, *Chem. Rev.*, 2005, **105**, 2999–3093.
- 9 C. A. Guido, A. Chrayteh, G. Scalmani, B. Mennucci and D. Jacquemin, *J. Chem. Theory Comput.*, 2021, **17**, 5155–5164.
- 10 B. Le Guennic and D. Jacquemin, *Acc. Chem. Res.*, 2015, **48**, 530–537.
- 11 A. Dreuw and M. Wormit, *Wiley Interdiscip. Rev. Comput. Mol. Sci.*, 2015, **5**, 82–95.
- 12 *TURBOMOLE V7.3*, A development of University of Karlsruhe and Forschungszentrum Karlsruhe GmbH, 1989–2007, TURBOMOLE GmbH. <http://www.turbomole.com>, 2007.
- 13 J. Cerezo and F. Santoro, *FCClasses 3.0*, <http://www.pi.iccom.cnr.it/fcclasses>.
- 14 F. Santoro, R. Improta, A. Lami, J. Bloino and V. Barone, *J. Chem. Phys.*, 2007, **126**, 084509.
- 15 F. Santoro and D. Jacquemin, *Wiley Interdiscip. Rev. Comput. Mol. Sci.*, 2016, **6**, 460–486.
- 16 Q. Peng, Y. Yi, Z. Shuai and J. Shao, *J. Chem. Phys.*, 2007, **126**, 114302.
- 17 A. Humeniuk, M. Bužančić, J. Hoche, J. Cerezo, R. Mitrić, F. Santoro and V. Bonačić-Koutecký, *J. Chem. Phys.*, 2020, **152**, 054107.
- 18 Q. Ou, Q. Peng and Z. Shuai, *J. Phys. Chem. Lett.*, 2020, **11**, 7790–7797.

Excellence in Chemistry Research



Announcing our new flagship journal

- Gold Open Access
- Publishing charges waived
- Preprints welcome
- Edited by active scientists

Meet the Editors of *ChemistryEurope*



Luisa De Cola
Università degli Studi
di Milano Statale, Italy



Ive Hermans
University of
Wisconsin-Madison, USA



Ken Tanaka
Tokyo Institute of
Technology, Japan

Chemistry A European Journal

 **Chemistry
Europe**
European Chemical
Societies Publishing

Accepted Article

Title: A Novel Method for the Synthesis of Merocyanines: New Photophysical Possibilities for a Well-Known Class of Fluorophores

Authors: Brunella Bardi, Katerina V. Vygranenko, Beata Koszarna, Olena Vakuliuk, Łukasz Dobrzycki, Daniel T. Gryko, Francesca Terenziani, and Anna Painelli

This manuscript has been accepted after peer review and appears as an Accepted Article online prior to editing, proofing, and formal publication of the final Version of Record (VoR). The VoR will be published online in Early View as soon as possible and may be different to this Accepted Article as a result of editing. Readers should obtain the VoR from the journal website shown below when it is published to ensure accuracy of information. The authors are responsible for the content of this Accepted Article.

To be cited as: *Chem. Eur. J.* **2023**, e202300979

Link to VoR: <https://doi.org/10.1002/chem.202300979>

RESEARCH ARTICLE

A Novel Method for the Synthesis of Merocyanines: New Photophysical Possibilities for a Well-Known Class of Fluorophores

Brunella Bardi,^{[a]†} Katerina V. Vygranenko,^{[b]†} Beata Koszarna,^[b] Olena Vakuliuk,^[b] Łukasz Dobrzycki,^[c] Daniel T. Gryko,^{*[b]} Francesca Terenziani,^{*[a]} and Anna Painelli^[a]

- [a] Dr. B. Bardi, Prof. F. Terenziani, Prof. A. Painelli
Department of Chemistry, Life Sciences and Environmental Sustainability
University of Parma, Parco Area delle Scienze 17/a 43124 Parma, Italy
E-mail: francesca.terenziani@unipr.it
- [b] K. V. Vygranenko, Dr. B. Koszarna, Dr. O. Vakuliuk, Prof. D. T. Gryko
Institute of Organic Chemistry Polish Academy of Sciences, Warsaw, Poland
E-mail: dtgryko@icho.edu.pl
- [c] Prof. L. Dobrzycki
Faculty of Chemistry, University of Warsaw, Żwirki i Wigury 101, 02-089 Warsaw, Poland
E-mail: mkc@chem.uw.edu.pl
- † These authors contributed equally

Supporting information for this article is given via a link at the end of the document

Abstract: A new, transformative methodology for the preparation of rhodols and other merocyanines from readily available tetrafluorohydroxybenzaldehyde and aminophenols has been developed. It is now possible to prepare merocyanines bearing three fluorine atoms and additional conjugated rings and the whole one-pot process occurs under neutral, mild conditions. Three heretofore unknown merocyanine-based architectures were prepared using this strategy from aminonaphthols and 4-hydroxycoumarins. The ability to change the structure of original rhodol chromophore into π -expanded merocyanines translates to a comprehensive method for the modulation of photophysical properties such as shifting the absorption and emission bands across almost the entire visible spectrum, reaching a huge Stokes shift i.e. 4800 cm^{-1} , brightness ca. 80,000 $\text{M}^{-1} \text{cm}^{-1}$, two-photon absorption cross-section above 150 GM and switching-on/off solvatofluorochromism. A detailed investigation allowed to rationalize the different spectroscopic behavior of rhodols and novel merocyanines, addressing solvatochromism and two-photon absorption.

Introduction

Rhodamines, fluoresceins and rhodols are iconic fluorophores which, although developed in the 19th century, are still popular objects of research,^[1] because of their large brightness combined with their straightforward preparation. The synthesis from phenols/aminophenols and phthalic anhydride, however, limited the studies on the relationship between the structure of these dyes and their photophysical properties to substituents at position 9 (see numbering in Scheme 1). During the last two decades, the second bridging atom, i.e. oxygen, was replaced with silicon,^[2–4] phosphorus,^[5,6] sulfur,^[7] or carbon^[8–10] in rhodamine,^[11–14] fluorescein,^[15,16] and rhodol^[17] scaffolds or it was removed entirely,^[18] with spectacular success in terms of bathochromic shift of fluorescence and increased stability. The remaining positions 1, 2, 4, 5, 7 and 8 were dormant, although in Alexa-type

fluoresceins two fluorine atoms are inserted at the left ring, featuring increased stability.^[19] Vygranenko et al. have recently proposed a novel strategy showing that the reaction of 3-formyl-7-dialkylaminocoumarins with dimethyl ketoglutarate leads to the formation of rhodols in one step, which possess CO_2Me substituents at positions 2 and 4.^[20]

Here we report an even simpler methodology leading to rhodols with three fluorine atoms at positions 1, 2 and 4. It is well-known that activated fluoroarenes undergo nucleophilic aromatic substitution with phenols,^[21] as well as aromatic aldehydes react with 3-dialkylaminophenols or other electron-rich aromatics.^[22–24] Performing these two-steps simultaneously can in principle lead to the formation of a six-membered ring bridging two benzene rings in a linear fashion, opening the possibility to devise an entirely new retrosynthetic pathway towards xanthene dyes. We show this new concept with the synthesis of a library of trifluororhodols and related π -expanded merocyanines, and compare their photophysics with rhodols possessing two ester groups, characterized by different electron-withdrawing substituents, specifically two ester groups.^[20] Extensive spectroscopic characterization revealed interesting differences between rhodols and merocyanines, which were fully rationalized through in-depth computational investigation and theoretical modeling.

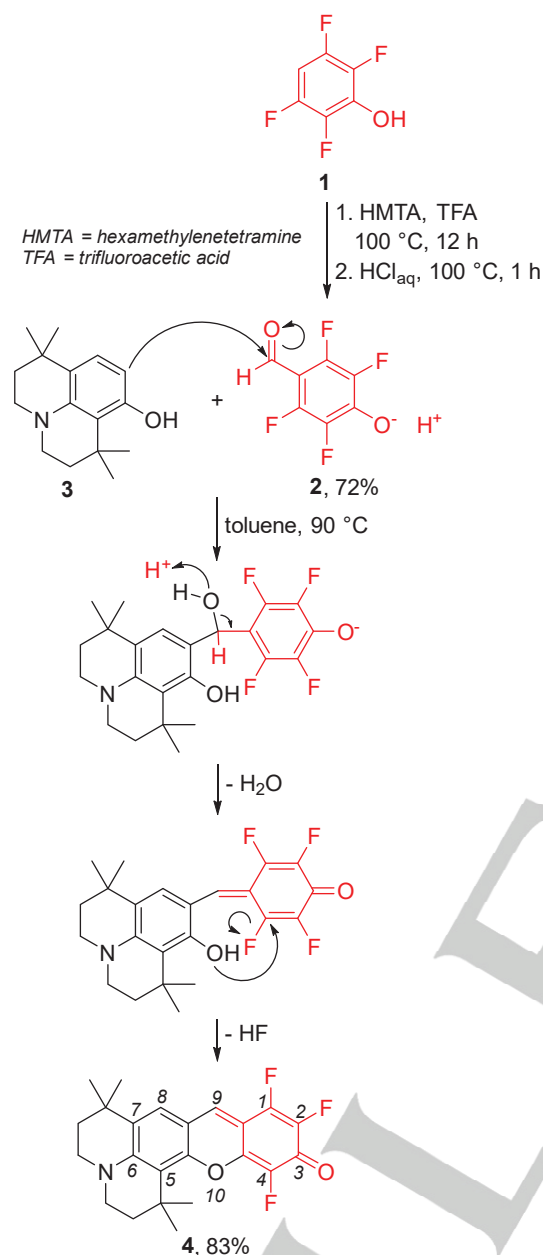
Results and Discussion

Design and synthesis

In the envisioned synthetic strategy, we have chosen 3-dialkylaminophenol as the model substrate. On the other hand, the second molecule, besides being 2-fluorobenzaldehyde, must consider three strict requirements: (1) The reactivity of the formyl group will be enhanced by the presence of four moderately electron-withdrawing fluorine atoms; (2) The reactivity of the C-F bonds towards nucleophilic aromatic substitution will be

RESEARCH ARTICLE

enhanced by the electron-withdrawing CHO group; (3) The strategically placed OH group will become rhodol's C=O functionality. Their combination points towards 4-hydroxybenzaldehyde possessing four fluorine atoms.



Scheme 1. Synthesis of rhodol 4.

Consequently the project started with the synthesis of 4-hydroxy-2,3,5,6-tetrafluorobenzaldehyde (**2**) from tetrafluorophenol (**1**) via a Duff reaction,^[25–27] (Scheme 1). As outlined earlier, we designed the new approach towards rhodols based on a combination of the Friedel-Crafts reaction and an aromatic nucleophilic substitution of a fluorine atom. Our initial experiments revealed that simply heating of 2,3,5,6-tetrafluoro-4-hydroxybenzaldehyde (**2**) with 8-hydroxy-1,1,7,7-tetramethyljulolidine (**3**) in toluene leads to the formation of the targeted rhodol **4**.

The novel rhodol **4** was used as a model for further investigation and optimization of the reaction conditions. When the reaction was carried out in toluene at 60 °C, product **4** was obtained in low

yield and with a sizable amount of unidentified side-products (Table 1, entry 1).

The first factor we decided to investigate was temperature. Increasing the reaction temperature significantly improved the yield of dye **4** and shortened the reaction time (Table 1, entry 2). Further increase of the reaction temperature to reflux (i.e. 110 °C) led to the formation of a higher number of side-products which hampered the purification (Table 1, entry 3). Since the first step of the studied transformation is an electrophilic aromatic substitution, we have selected two Lewis acids known for their efficiency as catalysts in Friedel-Crafts acylation and alkylation, namely aluminum(III) chloride and scandium(III) triflate.^[28–30] The reaction performed in the presence of AlCl₃ and Sc(OTf)₃ led however to slightly lower yield of rhodol **4** (Table 1, entries 4–5). Our next move resulted from the combination of the following arguments: (a) the second step, i.e. nucleophilic aromatic substitution would benefit from the presence of a base; (b) reactions of reactive aldehydes with strongly electrophilic partners are known to occur in the presence of bases.^[31] We found that the addition of sterically hindered 2,4,6-tri(*tert*-butyl)pyridine^[32] did not affect the reaction yield (Table 1, entry 6), whereas strong non-nucleophilic phosphazene-type base stopped the reaction (Table 1, entry 7). Replacement of toluene with other solvents, such as DMSO (polar, aprotic), THF (moderately polar, aprotic) and hexafluoroisopropanol (HFIP) (polar, protic, slightly acidic) led to detrimental results (Table 1, entries 8–10). Finally, the higher-boiling analogs of toluene turned out not to be better solvents than toluene for the formation of rhodol **4** (Table 1, entries 11–12). The optimization process brought us to the conclusion that the conversion of the aminophenols into the corresponding rhodols shows the best outcome in nonpolar solvents at high temperature without any catalyst. In all probability the process starts from the Friedel-Crafts alkylation of electron-rich phenol **3** by the formyl group, with H⁺ originating from highly acidic phenol **2** as possible catalyst. Once the carbon-carbon bond is formed, an intramolecular S_NAr reaction occurs with elimination of weakly acidic HF.

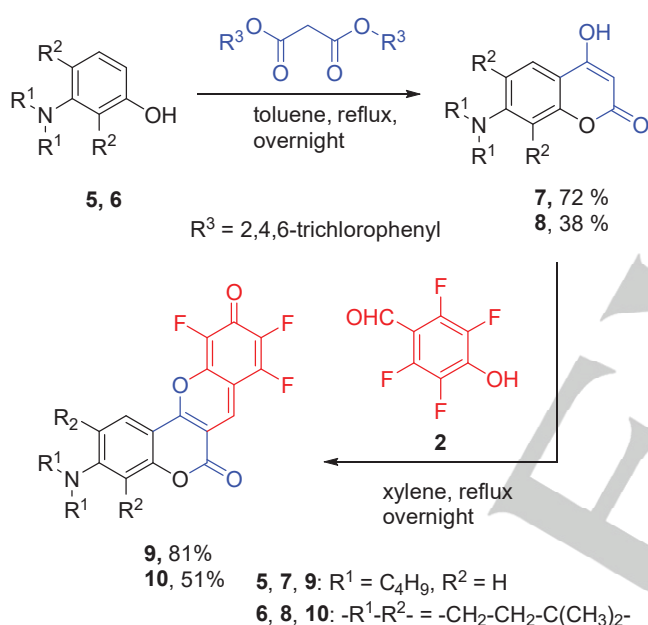
Table 1. Conditions for the optimization of the condensation of aldehyde **2** with phenol **3**.

Entry	solvent	T / °C	catalyst	time / h	yield
1	toluene	60	none	12	37%
2	toluene	90	none	1	83%
3	toluene	reflux	none	1	80%
4	toluene	90	AlCl ₃	1	68%
5	toluene	90	Sc(OTf) ₃	1	70%
6	toluene	90	2,4,6-tri- <i>tert</i> -butylpyridine	1	78%
7	toluene	90	phosphazene base P ₁ -t-Bu	1	trace
8	DMSO	80	none	1	0%
9	THF	60	none	12	23%
10	HFIP	80	none	1	0%
11	mesitylene	reflux	none	1	75%
12	xylenes	135	none	1	75%

RESEARCH ARTICLE

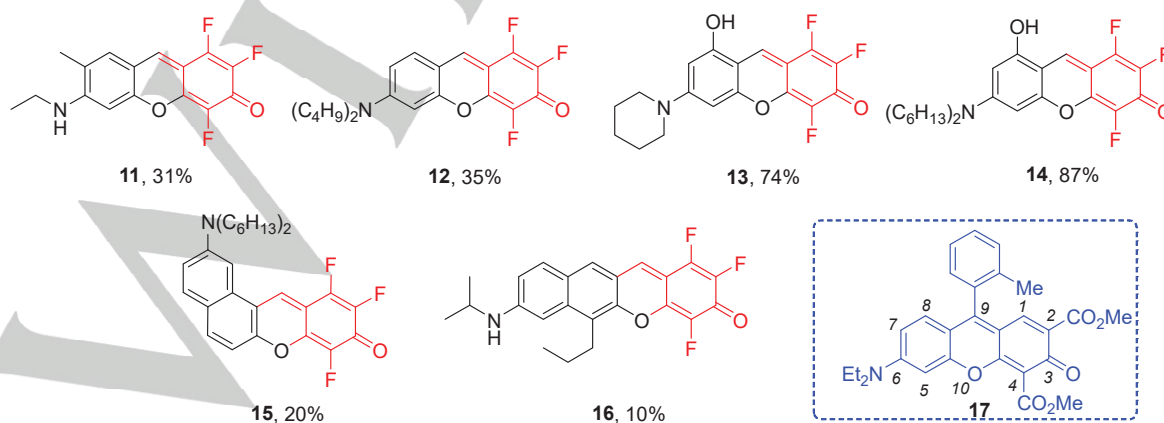
To test the synthetic utility of the optimized reaction conditions, we employed various aminophenols. Rhodols **11-14** were prepared in 31-87% yield (Scheme 3).

Recognizing that the biggest advantage of the new methodology can lie in forging an access to heretofore non-existing rhodols-type fluorophores, we subsequently employed 4-hydroxy-7-dialkylaminocoumarins (Scheme 2 and 3). During the scope and limitations studies, it turned out that condensation of 4-hydroxycoumarins **7** and **8** with aldehyde **2** produces hybrid coumarino-merocyanines **9** and **10** with very poor yield due to the slow conversion of the intermediate products into the desired rhodols. For this reason, we replaced toluene with xylenes (hence we increased reaction temperature) in order to achieve higher conversion and reasonable yields of dyes **9** and **10**. This result was attributed to the fact that 4-hydroxycoumarins **7** and **8** do not belong to phenols, and consequently their reactivity towards both electrophilic aromatic substitution and nucleophilic substitution is different.



Scheme 2. Synthesis of coumarins **7, 8** and their transformation into the corresponding merocyanines **9** and **10**.

The new methodology enabled, for the first time, the synthesis of an unprecedented linear rhodols-type merocyanines, whose



Scheme 3. Synthesized rhodols and merocyanines, as well as the molecular structure of the "reference" rhodol **17**, together with position numbering.

photophysical properties could be compared with those of the twisted one. First, we have synthesized 7-(dihexylamino)naphthalen-2-ol (**S1**) and subjected it to condensation with aldehyde **2** in xylenes for 7 hours (see ESI, Scheme S1). We have obtained only the angular merocyanine **15**, because position 1 of derivative **S1** is much more reactive than position 3. The use of naphthalene precursor **S5** with blocked position 1 enabled a selective reaction leading to a linear product (see ESI, Scheme S2). The substrate was prepared by condensation of diisopropylamine with 2,7-dihydroxynaphthalene under Bucherer conditions, followed by alkylation of the hydroxy group with allyl bromide and Claisen rearrangement. Reduction of the double bond with the Pd catalyst in the hydrogen atmosphere led to the formation of the precursor of merocyanine **16**.

Due to the poor reactivity of the 3-position of naphthalene, we were forced to increase condensation time (72 hours) and temperature (160 °C). The desired dye **16** was obtained with 10% yield as dark blue crystals. Its structure has been confirmed by X-ray crystallography (ESI, CCDC 2250222).

Spectroscopic characterization

The linear absorption and emission spectra of rhodols **4, 11-14** and **17** and merocyanines **9, 10, 15** and **16** were collected in different solvents, spanning a wide range of polarities. The main spectroscopic data are summarized in Table 2 and S12, while spectra of selected dyes are presented in Figure 1 (spectra of the other compounds can be found in Figure S2).

Absorption spectra of the dyes with a rhodol core (**4, 11-14** and **17**) feature an intense band located in the 490-540 nm region (in toluene), and weak features below 400 nm. Corresponding emission spectra cover a narrow spectral region with maxima at ~ 550 nm (in toluene). The absorption solvatochromism of these new rhodols is moderate. Conversely, the vibronic bandshape is largely affected by the solvent polarity, with the contribution from the 0-0 line increasing in polar solvents at the expense of higher replicas. This effect is responsible for a red-shift of the $\lambda_{\text{abs}}^{\text{max}}$ up to 17200 cm^{-1} for compound **11**, when replacing toluene with DMSO. Emission is also weakly solvatochromic, suggesting that these dyes have similar polarity in the ground and the first excited state. The fluorescence quantum yield (ϕ_f), already large in non-polar solvents, further increases up to more than 0.8 in strongly polar DMSO and acetonitrile solvents. Emission lifetimes, in the 3.5-4 ns range, are marginally affected by the solvent.

RESEARCH ARTICLE

The replacement of dialkylamino substituent at position 6 (dye **12**) with secondary amine (dye **11**) is accompanied by a 1430 cm^{-1} hypsochromic shift of the absorption maximum in toluene, related to the different vibronic band structure. The blue-shift reduces to only $\sim 380 \text{ cm}^{-1}$ in chloroform, where the two dyes have a similar bandshape (Figure S3). On the other hand, the rigidification of amine substituent (**12**→**4**) induces instead a bathochromic shift. All these changes have minor impact on ϕ_{fl} . The insertion of OH group at position 8 (dyes **13** and **14**) marginally affects the photophysics of rhodols.

The main photophysical properties of the trifluororhodols (intense absorption in the visible, narrow orange emission, marginal effect of solvent polarity) are qualitatively and quantitatively similar to those of rhodol **17**, substituted with ester groups instead of fluorine atoms.¹⁶ However, trifluororhodols **4** and **11-14** have a larger fluorescence quantum yield with respect to **17**.

The π -expansion of rhodol **12** towards angular merocyanine **15** leads to a red-shift and to a sizeable broadening of the absorption band, that covers most of the visible window (400-700 nm in polar solvents). The emission of **15** is bathochromically shifted compared to **12**, and is highly sensitive to solvent polarity: its vibronic structure, well resolved in low-polarity environments (hexane), blurs as the solvent polarity increases. Concomitantly, the emission shifts to the red, with $\lambda_{\text{em}}^{\text{max}} = 578 \text{ nm}$ in hexane and $\approx 800 \text{ nm}$ in acetone. Its fluorescence intensity decreases fast in polar solvents, and vanishes in acetonitrile. The different behavior of merocyanine **15** is related to its specific structure that puts it apart from the rhodol family.

Further modification towards fully linear architecture (**15**→**16**) results in a hypsochromic shift of absorption and emission (e.g. 665 nm vs. 739 nm in CHCl_3). As for **15**, the absorption spectrum of the linear dye **16** features a broad, almost featureless and marginally solvatochromic band in the visible. Similarly, its fluorescence spectrum is remarkably red-shifted as the solvent polarity is increased ($\lambda_{\text{em}}^{\text{max}}$ moves from $\sim 600 \text{ nm}$ in toluene to $> 700 \text{ nm}$ in acetonitrile).

Merocyanines **9** and **10** are very interesting. Their absorption resembles that of rhodols **4** and **12**, with analogous influence of rigidification of amine substituent (i.e. a bathochromic shift of both absorption and emission bands, see Figure S3). These dyes show a stronger solvatofluorochromism compared to their rhodol analogues, and their emission red-shifts by approx. 50-70 nm ($1200\text{-}1700 \text{ cm}^{-1}$) from toluene to CH_3CN . Their fluorescence quantum yields are low in non-polar solvents, reach maximum values (up to 0.7) in solvents of moderate polarity, and drop again to 0.2-0.5 in CH_3CN .

The dependences of the emission wavenumbers of all the dyes upon two commonly used solvent polarity parameters are shown in Figure S4. In particular, we selected the $f(\epsilon_{\text{st}}) - f(\epsilon_{\text{opt}})$ parameter, to have Lippert-Mataga plots^[33,34] (see Eq. S4 and successive discussion for the definition of f) and Reichardt's $E_T(30)$.^[35] Only dyes **10**, **15** and **16** are significantly solvatofluorochromic, with a monotonic and almost linear dependence. The greater slope is shown by dye **15**, followed by **16** and then **10**.

Rhodol-type merocyanines **9** and **10** represent the architectures which were heretofore unknown, whereas a merocyanine possessing essentially the same chromophore as **16** was recently published by Ahn and co-workers.^[36] Benzo[*b*]xantene-3-one derivative reported by these authors (**ABXO 1**, Figure S5), in analogy to merocyanine **16**, features a strong absorption band at

540-550 nm, and similar fluorescence quantum yield (10% for **ABXO 1** vs 8% for **16**). Importantly, the lack of fluorine atoms shifts hypsochromically the emission of **ABXO 1** (36 nm in polar media), positioning this dye among deep-red fluorophores, while compound **16** emits in the near infra-red region.

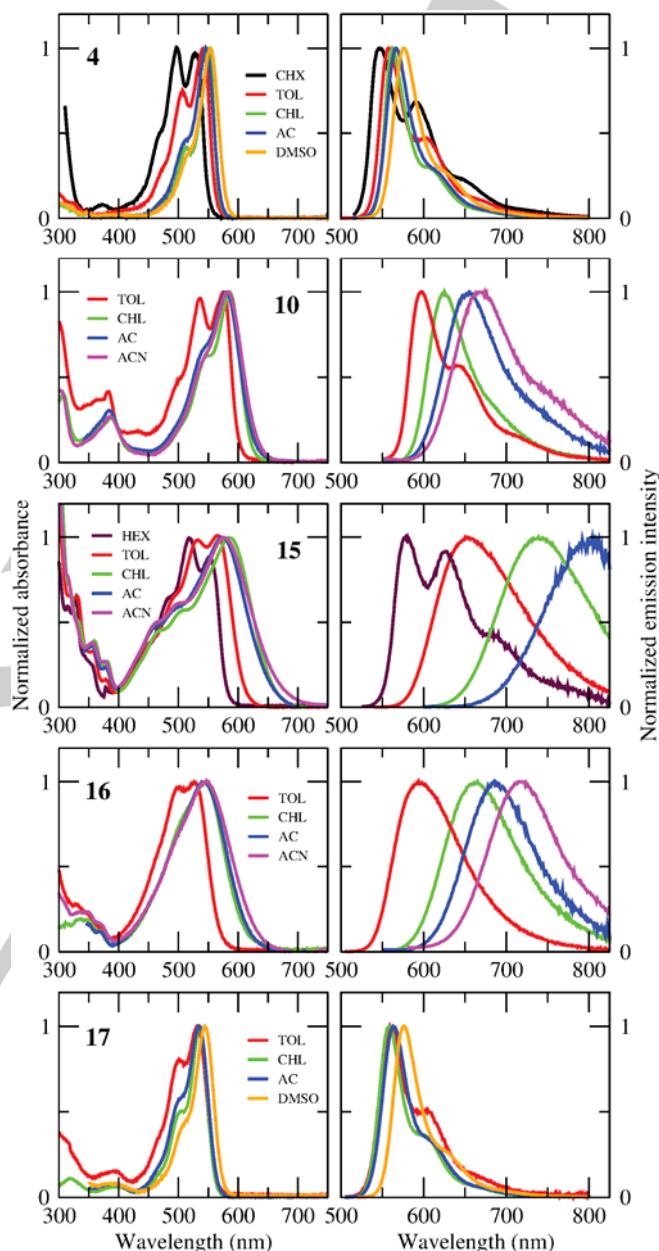


Figure 1. Normalized absorption (left) and emission (right) spectra of compounds **4**, **10**, **15**, **16** and **17** in solvents of different polarity (CHX: cyclohexane, HEX: hexane, TOL: toluene, CHL: chloroform, AC: acetone, ACN: acetonitrile, DMSO: dimethyl sulfoxide).

Among other rhodol-type merocyanines or π -expanded rhodols known in the literature, particularly interesting is **BRosol** (Figure S5),^[37] vinylogous to rhodol **4** with the conjugation chain extended by a benzene ring. It shows moderate solvatofluorochromism in contrast to dye **4**, however, the direct comparison is not possible as spectra were measured in different solvents. Nonetheless, a pronounced difference can be clearly observed in the emission intensity, with fluorescence quantum yield reaching 27% in DCM for **BRosol** vs ca. 85% in chloroform,

RESEARCH ARTICLE

acetone and DMSO for **4**, favoring the latter dye in bioimaging applications.

Table 2. Spectroscopic properties of target rhodols and merocyanines in different solvents: absorption and emission maxima ($\lambda_{\text{abs}}^{\text{max}}$ and $\lambda_{\text{em}}^{\text{max}}$), Stokes shifts, fluorescence quantum yield (ϕ_{fl}) and emission lifetime.

Solvent	$\lambda_{\text{abs}}^{\text{max}}$ /nm	$\lambda_{\text{em}}^{\text{max}}$ /nm	Stokes shift /cm ⁻¹	ϕ_{fl} [a]	Lifetime /ns	
4	Cyclohexane	498	546	1800	0.67	3.93
	Toluene	542	558	500	0.68	3.76
	Chloroform	551	562	350	0.84	3.81
	Acetone	546	567	700	0.85	4.04
	DMSO	554	576	700	0.85	3.70
9	Toluene	528	586	1900	0.21	1.31
	Chloroform	572	596	700	0.72	3.33
	Acetone	566	619	1500	0.71	3.56
	Acetonitrile	566	629	1800	0.52	2.74
10	Toluene	575	598	700	0.51	2.80
	Chloroform	586	625	1100	0.73	3.86
	Acetone	581	655	2000	0.38	2.33
	Acetonitrile	583	667	2200	0.13	..[b]
11	Toluene	491	550	2200	0.43	3.03
	Chloroform	530	546	550	0.75	3.95
	Acetone	527	547	700	0.77	4.08
	DMSO	536	555	600	0.91	3.51
12	Hexane	485	539	2100	0.72	3.46
	Toluene	528	550	750	0.68	3.57
	Chloroform	541	554	400	0.91	3.69
	Acetone	533	557	800	0.89	3.58
	DMSO	542	567	800	0.66	2.58
13	Chloroform	536	550	500	0.91	3.57
	Acetone	533	555	750	0.91	3.73
	Acetonitrile	533	555	750	0.73	3.24
	Toluene	527	550	800	0.68	3.56
14	Chloroform	537	548	400	0.96	3.56
	Acetone	534	552	600	0.90	3.80
	Acetonitrile	534	554	700	0.53	3.62
	Hexane	519	578	2000	0.10	0.81 (62%); 1.18 (38%) ^[c]
15	Toluene	566	650	2300	0.50	4.69
	Chloroform	584	739	3600	0.10	1.40
	Acetone	575	798	4900	0.01	..[d]
	Acetonitrile	578	..[d]	..[d]	..[d]	..[d]
	Toluene	527	594	2200	0.52	1.31 (21%); 2.45 (79%) ^[c]
16	Chloroform	545	665	3300	0.44	2.63
	Acetone	545	685	3750	0.34	2.16
	Acetonitrile	547	721	4400	0.08	0.59 (93%); 1.73 (7%) ^[c]
	Toluene	531	559	950	0.08	0.47 (73%); 2.83 (27%) ^[c]
17	Chloroform	536	558	700	0.62	2.82
	Acetone	534	563	1000	0.40	1.98
	DMSO	544	571	900	0.62	2.55

[a] Standard: fluorescein in NaOH(aq) 0.1 M. [b] Too short to be estimated (\ll 1 ns). [c] Amplitude in brackets. [d] Weak emission.

Benzo[c]xanthene-based seminaphthorhodafluor (**SNARF 1**, Figure S5) reported by the the Strongin's group,^[38] possesses an angular structure similar to the one in dye **15**. Even though there

is no sufficient fluorescence data for these emitters, comparison of the fluorescence spectra reveals significant influence of the substitution pattern and nature of substituents on the emission maxima. Whilst a tiny Stokes shift is observed for **SNARF 1** in polar media, merocyanine **15** is characterized by significant red-shift of the fluorescence band (located at ca. 800 nm in acetone), with a Stokes shift up to 4800 cm⁻¹.

On the other hand, reported by the same group, regioisomeric benzo[c]xanthene-based **SNARFs 2** (Figure S5)^[39] possesses π -expanded core from the electron-acceptor side of the dye. Even though such modification did not result in a striking bathochromic shift of the absorption maxima (up to 556 nm in MeOH), the emission of **SNARFs 2** appeared in the red part of the spectrum (up to 630 nm) with maximum efficiency on \sim 20% (in MeOH), which is however less favorable compared to the optical properties of **15** in terms of future applications.

The photochemical stability of some representative compounds (trifluororhodol **4**, non-fluorinated rhodol **17**, merocyanines **10**, **15** and **16**) was investigated in chloroform solution. Photodecomposition quantum yields^[40] were estimated adopting the method proposed by Belfield et al.^[41], based on the time-dependent variation of the optical density of a solution irradiated with a continuous light source (details in the Supporting Information and Figure S5). The photodecomposition quantum yield, ϕ_D , estimated for the trifluororhodol **4** (5×10^{-6}) is one order of magnitude lower than for the non-fluorinated analogue **17** (3×10^{-5}), indicating a positive effect of the new substitution pattern on photochemical stability. Compared to **4**, the two π -expanded rhodols **15** and **16** are more susceptible to photodecomposition, with the linear dye (**16**) being considerably less stable ($\phi_D = 7 \times 10^{-5}$) than the angular one (**15**, $\phi_D = 9 \times 10^{-6}$). Hybrid coumarino-rhodol **10**, instead, shows an excellent photochemical stability, with the smallest ϕ_D among all compounds ($\phi_D = 8 \times 10^{-7}$). Overall, the new dyes have ϕ_D comparable to literature values for fluorescein (2×10^{-5} - 1×10^{-4}) and rhodamine 6G (1×10^{-6} - 2×10^{-5}).^[40]

The two-photon absorption (2PA) spectra of selected dyes (Figure 2 and S7) were collected in chloroform, exploiting the 2PEF technique.^[42-44] The low symmetry of the dyes makes all electronic transitions allowed both in one-photon absorption (1PA) and 2PA processes.

In the experimentally accessible window (700-1300 nm), two bands dominate the 2PA spectrum of rhodols **4** and **17**. The lowest-energy band peaks around 1000 nm (photon energy) and matches the main 1PA band. However, the vibronic bandshape of the 1PA and 2PA bands are remarkably different: for both dyes, the most intense feature in the 1PA spectrum is due to the 0-0 transition, while in 2PA the most intense peak is related to the 0-1 transition, with a consequent apparent blue shift of the 2PA vs the 1PA band. The origin of this interesting feature will be discussed later on. A second featureless 2PA band occurs around 800 nm, in correspondence with a very weak 1PA feature. The 2PA cross-section amounts to $\sigma_2 \approx 40$ GM for the low-energy band of both dyes and reaches 40 GM and 120 GM for the higher energy 2PA band of **4** and **17**, respectively. These values are in line with available data for rhodols.^[45]

The 2PA spectrum of dye **10** has some qualitative analogies with that of rhodols: the lowest-energy 2PA band, corresponding to the main 1PA peak, has a resolved vibronic structure with an apparent blue shift vs 1PA due the different vibronic structure. However, the cross-section of **10** at the band maximum ($\sigma_2 \approx 150$

RESEARCH ARTICLE

GM) is more than three times larger than for rhodols **4** and **17**. An additional 2PA band at higher energy, with slightly higher similar cross-section, presents two maxima at 800 and 870 nm corresponding to two weak 1PA features. Merocyanines **15** and

16, instead, show a qualitatively different behavior (Figure 2). Their 2PA spectra show a broad band mimicking the shape of the corresponding 1PA spectra, with cross-sections up to 150-200 GM.

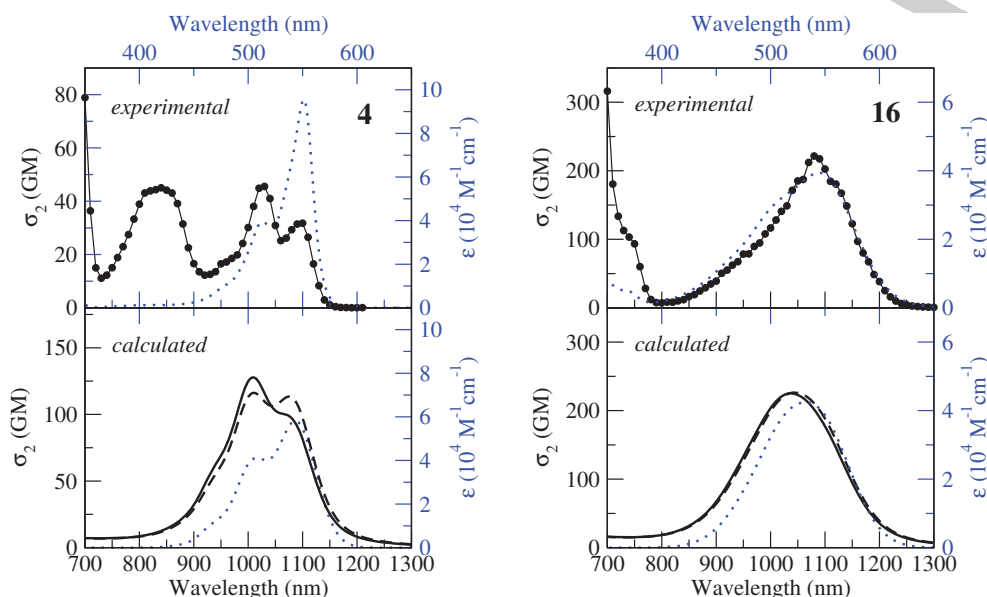


Figure 2. Top panels: experimental two-photon absorption cross-section σ_2 (black circles) and molar extinction coefficient ϵ (blue dotted line) of **4** and **16** collected in chloroform solution. Experimental uncertainties on σ_2 are $\sim 10\%$ for **4** and 20-25% for **16**. Bottom panels: 2PA (black) and 1PA (blue) spectra calculated in the essential-state model ($\epsilon_{\text{opt}} = 0.25$ eV for **4** and 0.38 eV for **16**). Calculated 2PA spectra shown as continuous lines refer to the full calculation, while 2PA spectra shown as dashed lines refer to spectra calculated without accounting for the vibrational channel. $1 \text{ GM} = 10^{-50} \text{ cm}^4 \text{ s photons}^{-1}$.

Excitation anisotropy of **4**, **10**, **15**, **16** and **17** (Figure S8) was collected in 2-methyltetrahydrofuran solution undercooled at 77 K to yield a transparent glass. At this temperature, the rotational motion of the dyes is frozen, so that the measured anisotropy value corresponds to the fundamental anisotropy r_0 . This quantity is related to the angle α between excitation and emission dipole moments:^[46,47]

$$r_0 = \frac{2}{5} \left(\frac{3\cos^2\alpha - 1}{2} \right) \quad (1)$$

Since, according to Kasha's rule, emission occurs from the (relaxed) lowest-energy excited state (S_1), r_0 gives information about the angle formed by transition dipole moments of the Kasha state and of the state reached upon absorption at each excitation wavelength, facilitating the individuation of the different electronic states contributing to the absorption spectrum.

For rhodols **4** and **17**, the flat anisotropy over the whole region of the main 1PA band confirms that only one state (S_1) is responsible for the absorption in that spectral region. The dip around 400 nm, in the same region of a weak 1PA signal and of the second 2PA band, suggests the presence of an excited state with different polarization ($\alpha \approx 50^\circ$ or an angle with the same squared cosine), responsible for both linear and nonlinear absorption. At shorter wavelengths ($\lambda < 400$ nm), instead, the behavior of the two dyes is different: the anisotropy of **4** amounts to 0.2 while that of **17** is lower (0.05-0.1), suggesting a different excited-state scenario for the two compounds. The analogy between the low-energy spectral features of **4** and **17** suggests a similar nature of the $S_0 \rightarrow S_1$ transition, irrespective of the different substituents. Therefore, this transition can be associated to the rhodol's merocyanine chromophore, while substitution mainly affects higher-energy states.

The anisotropy of dye **10** is high (~ 0.3) and constant over the 450-600 nm range, supporting the attribution of its intense

absorption band to the $S_0 \rightarrow S_1$ excitation. Moreover, r_0 shows two negative minima (≈ -0.1) at 430 nm and below 390 nm, separated by a local maximum at 415 nm (≈ 0.1), suggesting the presence of several excited states in this spectral region.

Excitation anisotropies of **15** and **16** offer information on the origin of the broad absorption features, and reveals a major difference between the two. For **16**, the anisotropy suggests that the band in the 400-600 nm window is due to a single excited state, S_1 ($r_0 \approx 0.3$ over all this wavelength range), while the second bright excited state is much higher in energy, and is spotted by a dip at $\lambda < 400$ nm ($r_0 \approx 0-0.05$). Conversely, the main absorption band of **15** originates from the contribution of at least two excited states, peaking around 600 and 500 nm respectively, which are revealed by a different anisotropy value (0.3 and 0.05).

Computational results

TDDFT results in gas phase

Additional insight into the electronic structure of the dyes was gathered from a computational investigation utilizing density functional theory (DFT) and its time-dependent extension (TDDFT).^[48-51] The ground-state geometry of the two rhodols **4** and **17**, and compounds **10**, **15** and **16** was optimized in the gas phase at the M06-2X/6-31G(d) level of theory,^[52] as implemented in the Gaussian16 package.^[53] In the computations, the long alkyl chains of **15** have been replaced by ethyl groups, with negligible effect on the electronic properties.

In all dyes, the π -conjugated backbone is almost planar. In dye **17**, the aryl substituent in position 9 is nearly orthogonal to the molecular plane (dihedral angle $\approx 77^\circ$), suggesting a poor conjugation with the rhodol skeleton.^[54]

Rhodols, as well as the other expanded dyes presented in this

RESEARCH ARTICLE

work, belong to the large family of merocyanine dyes. Merocyanines are characterized by a donor and an acceptor group connected by a π -conjugated bridge. Their low-energy photophysics is dominated by two limiting resonance structures: a neutral form and a zwitterionic form, in which one electron is transferred from the amino to the carbonyl group (Figure S9).^[17] The length of the two bonds of the conjugated bridge, b_1 and b_2 (Figure S9) can be viewed as an indicator of the weight of the two forms in the ground state. Bond lengths calculated for the target dyes (Table S13) indicate an intermediate character between a single and a double bond, as expected for a conjugated system. In more detail, the small difference between the two bonds points to a slight dominance of the neutral form over the zwitterionic form. Interestingly, the bond-length difference calculated for merocyanine **10** is similar to that of rhodols **4** and **17**, while the difference estimated for **15** and **16** is larger, indicating a smaller mixing between the two limiting structures.

To address excitations, we performed gas phase TDDFT calculations at the M06-2X/6-31G(d) level, on the ground-state optimized geometry. Table 3 summarizes the main results for the three lowest-energy transitions of the dyes. Frontier molecular orbitals (FMOs) involved in the optically-allowed transitions are shown in Figure 3.

Table 3. TDDFT data on selected dyes in the gas phase calculated at M06-2X/6-31G(d) level of theory: transition energy and wavelength λ , oscillator strength f , FMO contribution (>25%).

	Transition	Energy/eV	λ /nm	f	Type (%)
4	$S_0 \rightarrow S_1$	3.09	401	0.750	H \rightarrow L (94%)
	$S_0 \rightarrow S_2$	3.67	338	0.000	H-3 \rightarrow L (71%)
	$S_0 \rightarrow S_3$	3.73	332	0.077	H-1 \rightarrow L (86%)
10	$S_0 \rightarrow S_1$	2.94	421	0.771	H \rightarrow L (92%)
	$S_0 \rightarrow S_2$	3.67	338	0.000	H-4 \rightarrow L (64%)
	$S_0 \rightarrow S_3$	3.74	331	0.145	H-1 \rightarrow L (69%)
15	$S_0 \rightarrow S_1$	3.03	409	0.486	H \rightarrow L (90%)
	$S_0 \rightarrow S_2$	3.44	360	0.109	H-1 \rightarrow L (82%)
	$S_0 \rightarrow S_3$	3.60	344	0.000	H-4 \rightarrow L (72%)
16	$S_0 \rightarrow S_1$	3.12	397	1.022	H \rightarrow L (93%)
	$S_0 \rightarrow S_2$	3.22	385	0.006	H-1 \rightarrow L (89%)
	$S_0 \rightarrow S_3$	3.56	348	0.000	H-4 \rightarrow L (75%)
17	$S_0 \rightarrow S_1$	3.08	402	0.751	H \rightarrow L (96%)
	$S_0 \rightarrow S_2$	3.36	369	0.000	H-2 \rightarrow L (73%)
	$S_0 \rightarrow S_3$	3.92	316	0.147	H-1 \rightarrow L (85%)

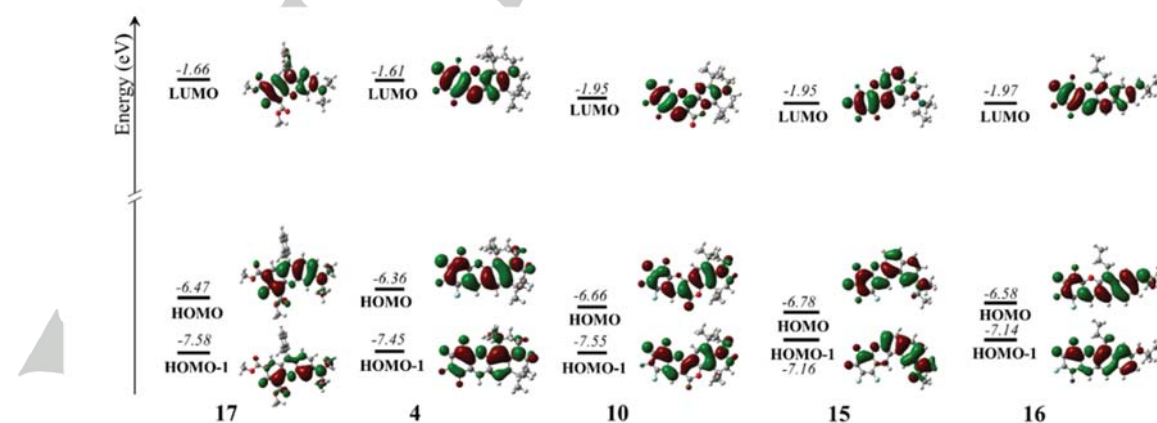


Figure 3. Frontier molecular orbitals (FMOs) of **4**, **10** and **15-17** (DFT M06-2X/6-31G(d) in gas phase; isovalue: 0.02).

For all the dyes, the $S_0 \rightarrow S_1$ is the most intense transition, and corresponds to an almost pure HOMO \rightarrow LUMO excitation. For rhodols **4** and **17**, as well as for the π -expanded dye **16**, this transition is predicted at similar energy (≈ 3.1 eV), while it is slightly red-shifted (up to 0.15 eV) for **15** and **10**, in agreement with the experimental trend. The main component of the associated transition dipole moment is aligned along the axis connecting the amino and the carbonyl groups.

To better understand the variation of the charge distribution upon photoexcitation, we arbitrarily partitioned the target molecules into two moieties (see Figure S10) and compared the cumulative Hirshfeld charges^[55] calculated in the two moieties in the ground state and in the S_1 (vertical) state (data in Table S14).

In the ground state, a small negative charge resides on the region containing the electron-withdrawing carbonyl group, while charge depletion is observed on the amino group, behaving as an electron donor. Upon photoexcitation to S_1 , the charge separation increases in the same direction, confirming the charge-transfer character of the transition.

Moving to higher energies, for dyes **4**, **10** and **17**, the $S_0 \rightarrow S_2$ transition has a $n \rightarrow \pi^*$ character and is dark, while the $S_0 \rightarrow S_3$, mainly a HOMO-1 \rightarrow LUMO excitation, is optically-allowed but its oscillator strength is almost one order of magnitude smaller compared to that of the $S_0 \rightarrow S_1$. The energy difference between $S_0 \rightarrow S_1$ and $S_0 \rightarrow S_3$ amounts to ≈ 0.8 eV for **10** and **17** and ≈ 0.6 eV for **4**, in good agreement with the experimental energy gap between the main absorption transition and the lowest-energy weak absorption feature corresponding to an anisotropy dip and to the secondary 2PA band.

The $S_0 \rightarrow S_1$ and $S_0 \rightarrow S_2$ transitions of the expanded merocyanine **15** are closer in energy (0.4 eV) with a comparable oscillator strength, in agreement with the peculiar broad absorption band made up by the contribution of two states, as revealed by anisotropy analysis. Unlike parent rhodols, whose FMOs extend over both amino and carbonyl groups suggesting strong conjugation, the HOMO-1 and LUMO of dye **15** are localized on the moieties containing the amino group (donor) and the carbonyl group (acceptor), respectively, indicating a stronger charge-transfer character of the $S_0 \rightarrow S_2$ transition, as confirmed by the large increase of charge separation (Table S14).

For the linear merocyanine **16**, instead, absorption is dominated by the $S_0 \rightarrow S_1$ transition, with charge-transfer nature.

RESEARCH ARTICLE

Computational results in solution

Solvation effects usually play an important role in the spectroscopy of polar and polarizable solutes like merocyanines. Thus, the proper description of the interaction with the solvent is crucial to understand solvatochromism and rationalize the different behavior of the dyes.

To address solvation, we adopt a method recently proposed^[56,57] to properly account for the different timescales of the two main solvation components. On one side, electronic solvation, related to the electronic degrees of freedom of the solvent, is very fast and will be dealt with in the antiadiabatic approximation. On the other side, polar solvation, related to the orientational motion of polar solvent molecules, is very slow and will be dealt with in the adiabatic approximation. The approach proposed in Ref.^[57], is shortly summarized in ESI.

Main results obtained for rhodol **4** and merocyanine **16** are presented in Figure 4, and describe the evolution with the solvent polarity of the transition energies and dipole moments for the three lowest-energy transitions (top and bottom panels, respectively) as well as the permanent dipole moments in the ground state and in the three lowest-energy electronic excited states (middle panels). Analogous figures for **10**, **15** and **17** are provided in ESI (Figures S11-S13).

The permanent dipole moment of **4** in the ground state is large (13-15 Debye) and is marginally affected by the solvent polarity. Upon vertical excitation to S_1 , the dipole moment shows a moderate increase to 20-23 Debye, explaining the observation of a small absorption solvatochromism. Conversely, in the relaxed S_1 geometry, S_0 and S_1 have similar polarity (15-20 Debye) in all the investigated solvents, pointing to a negligible solvatochromic effect. Indeed, calculated emission energies (2.5-2.6 eV) are

barely affected by the solvent polarity, in very good agreement with experimental data. Quantitatively similar results were obtained for rhodol **17** (Figure S13), in line with the similar photophysics of the two dyes.

Dye **16** also has a large permanent dipole moment in the ground state (15-20 Debye) but, at variance with **4** and **17**, the permanent dipole moment of its S_1 state is even larger, amounting to ≈ 35 Debye. This large variation of the dipole moment upon excitation justifies the pronounced positive emission solvatochromism of merocyanine **16**. The calculated shift from toluene to acetonitrile of ≈ 0.5 eV compares well with the experimental one (≈ 0.4 eV). Concerning absorption, S_1 and S_2 states, closely spaced in the gas phase, are separated by a wide energy gap in solution (> 0.9 eV), improving the agreement with experimental data.

The hybrid coumarino-merocyanine **10** (Figure S11) has an intermediate behavior between **4** and **16**: its permanent dipole moment shows a moderate increase upon excitation, from 13-15 Debye in the ground state to 25-30 Debye in S_1 , pointing to a more pronounced solvatochromism compared to rhodols.

Fairly accurate results are also obtained for dye **15**, notwithstanding its complex electronic structure with two nearby electronic states (Figure S12). In solution, even in nonpolar solvents, the state with the largest charge-transfer character is stabilized: the S_1 state is characterized by a sizable dipole moment (25-35 Debye), while S_2 has a similar polarity as the ground state. Accordingly, in absorption the $S_0 \rightarrow S_1$ transition moves slightly to the red with increasing solvent polarity, while $S_0 \rightarrow S_2$ remains unshifted, mimicking the experimental red-shift and widening of the band. As for **16**, the large increase of permanent dipole moment upon excitation also in the relaxed geometry leads to a sizeable emission solvatochromism.

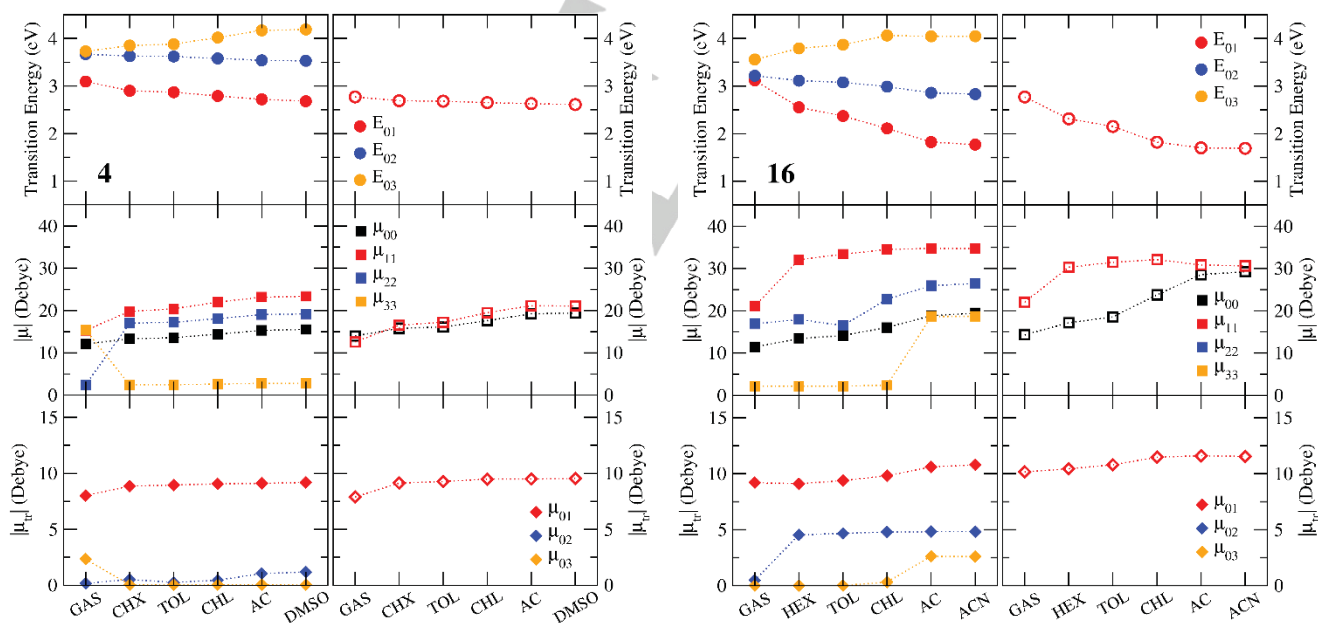


Figure 4. Properties of dyes **4** and **16** calculated in gas phase and in different solvents adopting the antiadiabatic approximation for electronic solvation and the adiabatic approximation for orientational solvation: transition energies E_{ij} (top panels), permanent dipole moments μ_{ii} (middle panels) and transition dipole moments μ_{ij} (bottom panels). HEX: hexane, CHX: cyclohexane, TOL: toluene, CHL: chloroform, AC: acetone, ACN: acetonitrile, DMSO: dimethyl sulfoxide, GAS: gas phase. Solid symbols are relevant to the absorption process, empty symbols to the emission process. Properties were calculated at the equilibrium value of the orientational component of the reaction field (F_{or} , see ESI) for the state of interest (S_0 for absorption and S_1 for emission).

Essential-state model

TDDFT analysis points to a fairly complex electronic structure of the target dyes. Nevertheless, their photophysics is dominated by

the lowest-energy transition, with a clear charge-transfer character. This invites to adopt a simple two-state model, extensively applied to describe the spectral properties of push-

RESEARCH ARTICLE

pull chromophores.^[58–60] Specifically, we focused on dyes **4** and **16**, that show distinctively different behavior.

We describe the two compounds as conjugated donor-acceptor $D-\pi-A$ dyes, resonating between two limiting structures, a neutral form ($D-\pi-A$) and a zwitterionic form ($D^+-\pi-A^-$), and we chose these two structures as the electronic basis states for the molecular Hamiltonian. The two states are mixed in a ground state with permanent dipole $\mu_0\rho$, where μ_0 is the dipole moment of the zwitterionic state, and ρ , also called ionicity, is its weight in the ground state. This minimal model for the electronic structure is extended to account for vibrational coupling and polar solvation (see ESI for further details) and allows for a detailed description of spectral band-shapes and their dependence on the solvent polarity.^[61,62]

Calculated absorption and emission spectra (Figure 5) provide a good description of the lowest-lying transition and reproduce the solvatochromic shifts as well as the evolution of the spectral bandshape with solvent polarity.

The estimated ground-state ionicity ρ of **4** at equilibrium goes from 0.21 in cyclohexane to 0.24 in dimethyl sulfoxide, while the ionicity of **16** stays almost constant at 0.15–0.16 in all solvents. This finding indicates that the charge separation in the ground state is lower for the π -expanded dye, in agreement with TDDFT results, and implies a larger polarity increase in the excited state, in line with a stronger solvatofluorochromism.

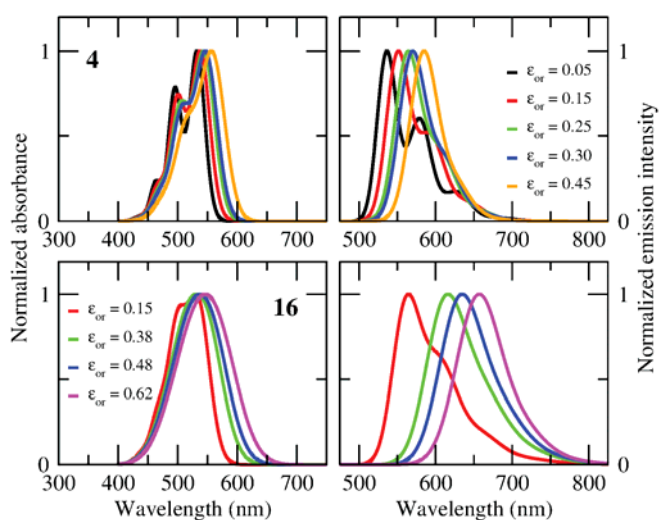


Figure 5. Normalized absorption (left) and emission (right) spectra of dyes **4** and **16** simulated with the two-state model in different solvents (different ϵ_{or} values, see legend). Model parameters for **4**: $z_0 = 0.80$ eV, $\sqrt{2}t = -1.00$ eV, $\mu_0 = 20.5$ D, $\omega_v = 0.20$ eV, $\omega_t = 0.10$ eV, $\epsilon_v = 0.625$ eV. Model parameters for **16**: $z_0 = 0.94$ eV, $\sqrt{2}t = -0.86$ eV, $\mu_0 = 23.5$ D, $\omega_v = 0.18$ eV, $\omega_t = 0.14$ eV, $\epsilon_v = 0.286$ eV. The spectral bandwidth γ (half-width at half-maximum) assigned to each vibronic transition was set to 0.06 eV. ϵ_{or} values mimicking different solvents are reported in eV.

Within this model, only the lowest-energy electronic transition can be addressed, but the relevant 2PA spectrum can be calculated fully accounting for the vibronic bandshape. In all investigated molecules, the lack of symmetry makes the lowest excited state allowed both in 1PA and 2PA. In spite of that, for rhodol **4** the linear and the nonlinear absorption spectra show a distinctively different shape, with the 0-0 vibronic line dominating the 1PA spectrum and the 0-1 vibronic line dominating 2PA. This result is well reproduced in the calculated spectra (Figure 2, bottom panels), fully in line with the behavior predicted more than 20 years back for dyes with sizable ρ .^[63] It is interesting to notice in

this context the sizable contributions of the “vibrational channels” to 2PA spectra, i.e. for the terms in the sum-over-state expression (Equation S9) involving the vibrational states in the electronic ground state manifold. Conversely, the 2PA spectrum of **16** lacks a vibronic structure and the shape of the 2PA band is more similar to the 1PA bandshape, as expected for a dye with a comparatively small ρ ,^[63] in good agreement with experiment.

Conclusions

A novel synthetic approach towards rhodols and rhodols-type merocyanines was developed. The reactivity of the formyl group in tetrafluorohydroxybenzaldehyde proved to be strong enough to induce the Friedel-Crafts reaction with 3-dialkylaminophenol without an external acidic catalyst. The subsequent nucleophilic aromatic substitution leads to the formation of a merocyanine chromophore in an overall one-pot process. This new synthetic strategy leads to heretofore inaccessible rhodols lacking a substituent at position 9 and having three fluorine atoms on the electron-accepting ring. We have proven that also hydroxy-amino-coumarins as well as aminonaphthalenols undergo this tandem reaction with 4-hydroxy-2,3,5,6-tetrafluorobenzaldehyde, giving rise to heretofore unknown classes of fluorophores.

A comprehensive photophysical characterization has shown that, in rhodols, the presence of three fluorine atoms marginally affects the degree of charge transfer and the sensitivity to the environment compared to other electron-withdrawing substituents like ester groups. However, the new substitution pattern allows to increase the brightness (up to 80,000 $M^{-1} cm^{-1}$) and achieve an excellent photochemical stability even though position 9 is free. The π -expansion of the rhodols-type core in a linear or angular fashion has a significant impact on the photophysical properties: not only it allows to shift absorption and emission across the visible window, but it also introduces a large emission solvatochromism, that is not seen in rhodols. A remarkable exception are hybrid coumarino-merocyanine that, in spite of a more complex π -conjugated architecture, basically retain a rhodol-like behavior.

Our computational investigation supported the description of the new fluorophores as merocyanine dyes. Indeed, the lowest absorption band has a charge-transfer character, suggesting that the ground and the first excited state can be described as resonating between a neutral and a charge-separated (zwitterionic) structure.

In rhodols, the contribution of the charge-separated state in the ground state is large, leading to sizeable permanent dipole moments. Upon excitation, the permanent dipole moment only slightly increases, explaining their weak solvatochromism and locating rhodols rather close to the cyanine limit. The progressive substantial loss of intensity of vibronic replicas (both in absorption and emission spectra) for increasing solvent polarity is similarly in line with a cyanine-like electronic structure. Conversely, π -expanded systems are characterized by a more neutral ground state, and a sizeable increase of permanent dipole moment upon charge-transfer occurs. Their highly polar S_1 state is stabilized in polar solvents, yielding large emission solvatochromic shifts.

Another interesting difference between the investigated dyes concerns 2PA. All dyes are noncentrosymmetric, so that the $S_0 \rightarrow S_1$ transition is symmetry-allowed both 1PA and 2PA. However, while for π -expanded dyes 1PA and 2PA bands are featureless and almost superimposable, for rhodol and rhodol-like systems

RESEARCH ARTICLE

the 2PA band, characterized by a prominent vibronic structure, is distorted with respect to the 1PA band, and the rescaled 2PA maximum is blue-shifted compared to the 1PA maximum.

The charge-transfer nature of the first electronic transition supported the description of the two representative rhodols through a minimal model only accounting for two basis states, corresponding to the limiting resonance forms. In this model electron-phonon coupling and inhomogeneous broadening effects from polar solvation can be investigated, addressing quantitatively the bandshape of linear and nonlinear spectra.

Along these lines, we were able to rationalize the observed blue-shift and different band-shape of 2PA vs 1PA of rhodols as due to a significant contribution of the “vibrational channel”.^[63] This finding further confirms that rhodols are not too far from the cyanine limit.

The moderate 2PA response of trifluororhodols and rhodol-like systems in the near-IR region, combined with orange-red emission, high fluorescence quantum yields (also in high polarity environments) and good photostability, make them suitable for application as fluorescent imaging probes in two-photon microscopy.

The reported new synthetic procedures offer new possibilities for fine-tuning the properties of an interesting and widespread class of fluorophores, a result of paramount importance particularly in view of their multifarious applications.

Acknowledgements

The authors thank the Foundation for Polish Science (TEAM POIR.04.04.00-00-3CF4/16-00) and the European Union Horizon 2020 research and innovation programme (GA 101007804, Micro4Nano). Work at UNIPR also received financial support from PNRR-MUR project ECS_00000033_ECOSISTER and benefited from the HPC (High Performance Computing) facility of the University of Parma and from the equipment and framework of the COMP-HUB and COMP-R Initiatives, funded by the ‘Departments of Excellence’ program of the Italian Ministry for University and Research (MIUR, 2018-2022 and MUR, 2023-2027). We thank Mr. Joseph Milton for amending the manuscript.

Keywords: dyes/pigments • fluorescent probes • intramolecular charge transfer • linear and nonlinear optical spectroscopy • theoretical modelling

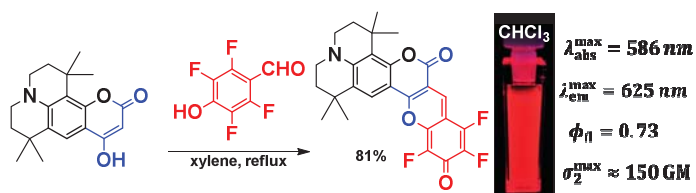
- [1] I. Johnson, M. T. Z. Spence, Eds., *Molecular Probes Handbook, A Guide to Fluorescent Probes and Labeling Technologies*, Life Technologies Corporation, 2010.
- [2] P. Shieh, V. T. Dien, B. J. Beahm, J. M. Castellano, T. Wyss-Coray, C. R. Bertozzi, *J. Am. Chem. Soc.* **2015**, *137*, 7145–7151.
- [3] G. Lukinavičius, L. Reymond, K. Umezawa, O. Sallin, E. D’Este, F. Göttfert, H. Ta, S. W. Hell, Y. Urano, K. Johnsson, *J. Am. Chem. Soc.* **2016**, *138*, 9365–9368.
- [4] T. Ikeno, T. Nagano, K. Hanaoka, *Chem. - An Asian J.* **2017**, *12*, 1435–1446.
- [5] M. Grzybowski, M. Taki, S. Yamaguchi, *Chem. - A Eur. J.* **2017**, *23*, 13028–13032.
- [6] M. Grzybowski, M. Taki, K. Kajiwara, S. Yamaguchi, *Chem. - A Eur. J.* **2020**, *26*, 7912–7917.
- [7] J. Liu, Y. Q. Sun, H. Zhang, H. Shi, Y. Shi, W. Guo, *ACS Appl. Mater. Interfaces* **2016**, *8*, 22953–22962.
- [8] A. N. Butkevich, G. Y. Mitronova, S. C. Sidenstein, J. L. Klocke, D. Kamin, D. N. H. Meineke, E. D’Este, P. T. Kraemer, J. G. Danzl, V. N. Belov, et al., *Angew. Chemie - Int. Ed.* **2016**, *55*, 3290–3294.
- [9] J. B. Grimm, A. J. Sung, W. R. Legant, P. Hulamm, S. M. Matlosz, E. Betzig, L. D. Lavis, *ACS Chem. Biol.* **2013**, *8*, 1303–1310.
- [10] M. V. Sednev, C. A. Wurm, V. N. Belov, S. W. Hell, *Bioconjug. Chem.* **2013**, *24*, 690–700.
- [11] S. Takahashi, Y. Kagami, K. Hanaoka, T. Terai, T. Komatsu, T. Ueno, M. Uchiyama, I. Koyama-Honda, N. Mizushima, T. Taguchi, et al., *J. Am. Chem. Soc.* **2018**, *140*, 5925–5933.
- [12] L. D. Lavis, *Biochemistry* **2017**, *56*, 5165–5170.
- [13] Y. J. Gong, X. B. Zhang, G. J. Mao, L. Su, H. M. Meng, W. Tan, S. Feng, G. Zhang, *Chem. Sci.* **2016**, *7*, 2275–2285.
- [14] J. Chan, S. C. Dodani, C. J. Chang, *Nat. Chem.* **2012**, *4*, 973–984.
- [15] C. Deo, S. H. Sheu, J. Seo, D. E. Clapham, L. D. Lavis, *J. Am. Chem. Soc.* **2019**, *141*, 13734–13738.
- [16] P. Shieh, M. J. Hangauer, C. R. Bertozzi, *J. Am. Chem. Soc.* **2012**, *134*, 17428–17431.
- [17] Y. M. Poronik, K. V. Vygranenko, D. Gryko, D. T. Gryko, *Chem. Soc. Rev.* **2019**, *48*, 5242–5265.
- [18] M. Grzybowski, O. Morawski, K. Nowak, P. Garbacz, *Chem. Commun.* **2022**, *58*, 5455–5458.
- [19] W. C. Sun, K. R. Gee, D. H. Klaubert, R. P. Haugland, *J. Org. Chem.* **1997**, *62*, 6469–6475.
- [20] K. V. Vygranenko, Y. M. Poronik, M. H. E. Bousquet, O. Vakuliuk, D. Jacquemin, D. T. Gryko, *Chem. Commun.* **2022**, *58*, 1542–1545.
- [21] D. T. Gryko, D. Wyrostek, A. Nowak-Król, K. Abramczyk, M. K. Rogacki, *Synthesis* **2008**, 4028–4032.
- [22] Q. He, E. W. Miller, A. P. Wong, C. J. Chang, *J. Am. Chem. Soc.* **2006**, *128*, 9316–9317.
- [23] A. C. Benniston, D. B. Rewinska, *Org. Biomol. Chem.* **2006**, *4*, 3886–3888.
- [24] R. Bandichhor, A. D. Petrescu, A. Vespa, A. B. Kier, F. Schroeder, K. Burgess, *Bioconjug. Chem.* **2006**, *17*, 1219–1225.
- [25] J. C. Duff, E. J. Bills, *J. Chem. Soc.* **1932**, 1987.
- [26] W. E. Smith, *J. Org. Chem.* **1972**, *37*, 3972.
- [27] K. Skonieczny, G. Charalambidis, M. Tasiar, M. Krzeszewski, A. Kalkan-Burat, A. G. Coutsolelos, D. T. Gryko, *Synthesis* **2012**, *44*, 3683–3687.
- [28] G. R. Geier, Y. Ciringh, F. Li, D. M. Haynes, J. S. Lindsey, *Org. Lett.* **2000**, *2*, 1745–1748.
- [29] S. Kobayashi, *Eur. J. Org. Chem.* **1999**, 15–27.
- [30] X. Wang, Y. Wang, D.-M. Du, J. Xu, *J. Mol. Catal. A Chem.* **2006**, *255*, 31–35.
- [31] Y. Terazono, E. J. North, A. L. Moore, T. A. Moore, D. Gust, *Org. Lett.* **2012**, *14*, 1776–1779.
- [32] J.-J. Zhang, M.-C. Tang, Y. Fu, K.-H. Low, J. Ma, L. Yang, J. J. Weigand, J. Liu, V. W.-W. Yam, X. Feng, *Angew. Chemie - Int. Ed.* **2020**, *60*, 2833–2838.
- [33] E. Lippert, *Z. Für Nat. A.* **1955**, *10*, 541–545.
- [34] N. Mataga, Y. Kaifu, M. Koizumi, *Bull. Chem. Soc. Jpn.* **1955**, *28*, 690–691.
- [35] C. Reichardt, *Chem. Rev.* **1994**, *94*, 2319–2358.
- [36] U. Tamima, C. W. Song, M. Santra, Y. J. Reo, H. Banna, M. R. Islam, K. H. Ahn, *Sensors Actuators, B Chem.* **2020**, *322*, 128588.
- [37] M. Dai, Y. J. Reo, C. W. Song, Y. J. Yang, K. H. Ahn, *Chem. Sci.* **2020**, *11*, 8901–8911.
- [38] L. Wang, C. W. Barth, M. Sibrian-Vazquez, J. O. Escobedo, M. Lowry, J. Muschler, H. Li, S. L. Gibbs, R. M. Strongin, *ACS Omega* **2017**, *2*, 154–163.
- [39] L. G. Wang, I. Munhenzva, M. Sibrian-Vazquez, J. O. Escobedo, C. H. Kitts, F. R. Fronczek, R. M. Strongin, *J. Org. Chem.* **2019**, *84*, 2585–2595.
- [40] C. Eggeling, J. Widengren, R. Rigler, C. A. M. Seidel, in *Appl. Fluoresc. Chem. Biol. Med.* (Eds.: W. Rettig, B. Strehmel, M. Schrader, H. Seifert), Springer-Verlag, Berlin Heidelberg, **1999**, pp. 193–240.
- [41] K. D. Belfield, M. V. Bondar, Y. Liu, O. V. Przhonska, *J. Phys. Org. Chem.* **2003**, *16*, 69–78.

RESEARCH ARTICLE

- [42] C. Xu, W. W. Webb, *J. Opt. Soc. Am. B* **1996**, *13*, 481.
- [43] F. Terenziani, C. Katan, E. Badaeva, S. Tretiak, M. Blanchard-Desce, *Adv. Mater.* **2008**, *20*, 4641–4678.
- [44] M. A. Albota, C. Xu, W. W. Webb, *Appl. Opt.* **1998**, *37*, 7352.
- [45] Y. M. Poronik, G. Clermont, M. Blanchard-Desce, D. T. Gryko, *J. Org. Chem.* **2013**, *78*, 11721–11732.
- [46] J. R. Lakowicz, *Principles of Fluorescence Spectroscopy*, Springer, New York, USA, **2006**.
- [47] B. Valeur, *Molecular Fluorescence. Principles and Applications*, Wiley-VCH Verlag GmbH, **2001**.
- [48] E. Runge, E. K. U. Gross, *Phys. Rev. Lett.* **1984**, *52*, 997–1000.
- [49] R. Bauernschmitt, R. Ahlrichs, *Chem. Phys. Lett.* **1996**, *256*, 454–464.
- [50] M. E. Casida, C. Jamorski, K. C. Casida, D. R. Salahub, *J. Chem. Phys.* **1998**, *108*, 4439–4449.
- [51] C. Adamo, D. Jacquemin, *Chem. Soc. Rev.* **2013**, *42*, 845–856.
- [52] Y. Zhao, D. G. Truhlar, *Theor. Chem. Acc.* **2008**, *120*, 215–241.
- [53] M. J. Frisch, G. W. Trucks, H. B. Schlegel, G. E. Scuseria, M. A. Robb, J. R. Cheeseman, G. Scalmani, V. Barone, G. A. Petersson, H. Nakatsuji, X. Li, M. Caricato, A. V. Marenich, J. Bloino, B. G. Janesko, R. Gomperts, B. Mennucci, H. P. Hratchian, J. V. Ortiz, A. F. Izmaylov, J. L. Sonnenberg, D. Williams-Young, F. Ding, F. Lipparini, F. Egidi, J. Goings, B. Peng, A. Petrone, T. Henderson, D. Ranasinghe, V. G. Zakrzewski, J. Gao, N. Rega, G. Zheng, W. Liang, M. Hada, M. Ehara, K. Toyota, R. Fukuda, J. Hasegawa, M. Ishida, T. Nakajima, Y. Honda, O. Kitao, H. Nakai, T. Vreven, K. Throssell, J. E. Montgomery, J. A., Jr. Peralta, F. Ogliaro, M. J. Bearpark, J. J. Heyd, E. N. Brothers, K. N. Kudin, V. N. Staroverov, T. A. Keith, R. Kobayashi, K. Normand, J. Raghavachari, A. P. Rendell, J. C. Burant, S. S. Iyengar, J. Tomasi, M. Cossi, J. M. Millam, M. Klene, C. Adamo, R. Cammi, J. W. Ochterski, R. L. Martin, K. Morokuma, O. Farkas, J. B. Foresman and D. J. Fox, Gaussian16, revision B.01, Gaussian, Inc., Wallingford CT, **2016**.
- [54] S. S. Patil, K. G. Thorat, R. Mallah, N. Sekar, *J. Fluoresc.* **2016**, *26*, 2187–2197.
- [55] F. L. Hirshfeld, *Theor. Chem. Acc.* **1977**, *44*, 129–138.
- [56] D. K. A. Phan Huu, R. Dhali, C. Pieroni, F. Di Maiolo, C. Sissa, F. Terenziani, A. Painelli, *Phys. Rev. Lett.* **2020**, *124*, 107401.
- [57] R. Dhali, D. K. A. Phan Huu, F. Terenziani, C. Sissa, A. Painelli, *J. Chem. Phys.* **2021**, *154*, 134112.
- [58] A. Painelli, F. Terenziani, *J. Phys. Chem. A* **2000**, *104*, 11041–11048.
- [59] B. Boldrini, E. Cavalli, A. Painelli, F. Terenziani, *J. Phys. Chem. A* **2002**, *106*, 6286–6294.
- [60] S. Sanyal, C. Sissa, F. Terenziani, S. K. Pati, A. Painelli, *Phys. Chem. Chem. Phys.* **2017**, *19*, 24979–24984.
- [61] A. Painelli, *Chem. Phys. Lett.* **1998**, *285*, 352–358.
- [62] A. Painelli, F. Terenziani, *Chem. Phys. Lett.* **1999**, *312*, 211–220.
- [63] A. Painelli, L. Del Freo, F. Terenziani, *Chem. Phys. Lett.* **2001**, *346*, 470–478.

RESEARCH ARTICLE

Entry for the Table of Contents



Friedel-Crafts reaction followed by nucleophilic aromatic substitution enables the assembly of rhodols and novel strongly emitting merocyanines from simple substrates.

A novel method for the programmed synthesis of merocyanines: unprecedented photophysical possibilities for a well-known class of fluorophores

Brunella Bardi,^{a†} Kateryna V. Vygranenko,^{b†} Beata Koszarna,^b Olena Vakuliuk,^b Łukasz Dobrzycki,^c Daniel T. Gryko,^{b*} Francesca Terenziani ^{a*} and Anna Painelli ^a

^a*Department of Chemistry, Life Sciences and Environmental Sustainability, University of Parma, Parco Area delle Scienze 17/a, 43124 Parma, Italy*

^b*Institute of Organic Chemistry Polish Academy of Sciences, Warsaw, Poland*

^c*Faculty of Chemistry, University of Warsaw, Żwirki i Wigury 101, 02-089 Warsaw, Poland*

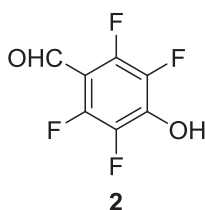
SUPPORTING INFORMATION

1. Experimental details

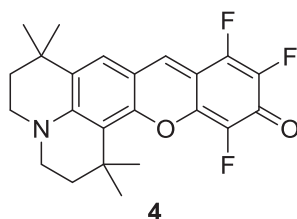
1.1. Synthesis

All chemicals were used as received unless otherwise noted. All reported ^1H and ^{13}C NMR spectra were collected using 500 MHz and 600 MHz spectrometers. Chemical shifts (δ ppm) were determined with TMS as the internal reference; J values are given in Hz. Chromatography was performed on silica gel (230-400 mesh). Thin layer chromatography (TLC) was carried out using Merck PLC Silica gel 60 F₂₅₄ 1 mm plates. The mass spectra were obtained via electron ionization (EI-MS) or electrospray ionization (ESI-MS).

1.1.1 Experimental part



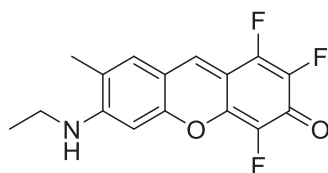
2,3,5,6-Tetrafluoro-4-hydroxybenzaldehyde (**2**): HMTA (1.1 eq, 0.165 mol, 23.1 g) was slowly added to the solution of 2,3,5,6-tetrafluorophenol (0.15 mol, 24.9 g) in TFA (120 mL) (exothermic reaction). The mixture was stirred under argon at 100 °C overnight. Subsequently 10% HCl_{aq} (150 mL) was added and the reaction mixture was stirred at 100 °C for another 1 h. The solution was cooled to room temperature, diluted with H₂O, and extracted with EtOAc (150 mL x 2) and CHCl₃ (150 mL x 1). The organic fractions were collected, dried over Na₂SO₄, and solvents were removed under reduced pressure. The product was purified using column chromatography (silica, hexane/EtOAc, 2:1 and then 1:1) and recrystallized from cold hexane to obtain the pure product (21 g, 72 %) as off-white crystals. ^1H NMR (500 MHz, DMSO) δ 10.1 (s, 1H). Spectroscopic properties are in agreement with the literature data.¹



Rhodol **4**: A solution of 2,3,5,6-tetrafluoro-4-hydroxybenzaldehyde (**2**, 1 mmol, 194 mg) and 8-hydroxy-1,1,7,7-tetramethyljulolidine (1 mmol, 245 mg) in toluene (30 ml) was stirred under argon at 90 °C overnight. The solution was cooled to room temperature and the precipitate was filtered and washed with toluene. The crude product was crystallized from Et₂O to give the pure product (333 mg, 83 %) as violet crystals. M.p. 235 – 236 °C (from Et₂O).

^1H NMR (500 MHz, CDCl₃) δ 8.02 (d, J = 1.5 Hz, 1H), 7.28 (s, 1H), 3.59 - 3.48 (m, 2H), 3.45 - 3.39 (m, 2H), 1.93 - 1.84 (m, 2H), 1.83 - 1.75 (m, 2H), 1.58 (s, 6H), 1.34 (s, 6H). ^{13}C NMR (126 MHz, CDCl₃) δ 165.5 (dd, J = 11.9; 6.0 Hz), 152.0, 149.3, 144.3 (dd, J = 259.4; 12.3 Hz), 141.7 (dt, J = 253.2; 7.3 Hz), 139.0 (dd, J = 241.9; 6.7 Hz), 139.0 (t, J = 9.3 Hz), 135.9 (m), 130.8, 125.5, 114.8, 110.5, 103.5 (d, J = 20.0 Hz), 47.9, 47.5, 38.5, 34.7,

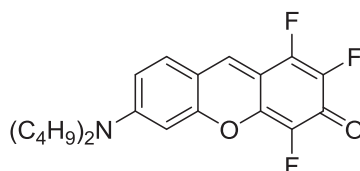
32.3, 32.2, 29.7, 28.2. ^{19}F NMR (470 MHz, CDCl_3) δ -153.4 (dd, $J = 17.6, 5.4$ Hz), -160.0 (dd, $J = 17.7, 14.5$ Hz), -168.3 (dd, $J = 14.0, 5.4$ Hz). HRMS (ESI) calc. for $\text{C}_{23}\text{H}_{23}\text{NO}_3\text{F}_3$ 402.1681 $[\text{M} + \text{H}]^+$, found 402.1679.



11

Rhodol **11**: 3-Ethylamino-*p*-cresol (2 mmol, 302 mg), 2,3,5,6-tetrafluoro-4-hydroxybenzaldehyde (2 mmol, 388 mg) and xylene (35 mL) were placed in a sealed tube. The resulting mixture was stirred under Ar at 135 °C for 1 h. After cooling to RT, the precipitate was filtered and washed with Et_2O . Recrystallization of crude product with $\text{MeOH}/\text{Et}_2\text{O}$ gave dark purple solid (188 mg, 31 %). M.p. 283 – 285 °C.

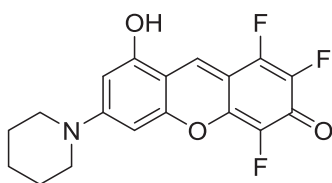
^1H NMR (500 MHz, pyridine- d_5) δ 8.17 (s, 1H), 7.39 – 7.35 (m, 1H), 7.32 (s, 1H), 6.79 (s, 1H), 3.39 (p, $J = 7.0$ Hz, 2H), 2.22 (s, 3H), 1.23 (t, $J = 7.2$ Hz, 3H). ^{13}C NMR (126 MHz, pyridine- d_5) δ 165.5 (dd, $J = 17.6; 6.3$ Hz), 155.6, 155.0, 145.1 (dd, $J = 258.9; 12.0$ Hz), 142.1 (dd, $J = 253.0; 7.4$ Hz), 139.9 (t, $J = 9.1$ Hz), 139.5 (dd, $J = 239.7; 7.1$ Hz), 136.3 (m), 131.0, 122.8, 110.2, 104.4 (d, $J = 20.2$ Hz), 95.0, 38.5, 17.5, 14.1. ^{19}F NMR (470 MHz, Pyridine- d_5) δ -152.2 (dd, $J = 18.1, 5.2$ Hz), -157.8 (dd, $J = 18.0, 13.5$ Hz), -166.7 (dd, $J = 14.2, 5.0$ Hz). HRMS (ESI) calc. for $\text{C}_{16}\text{H}_{13}\text{NO}_2\text{F}_3$ 308.0898 $[\text{M} + \text{H}]^+$, found 308.0901.



12

Rhodol **12**: A solution of 2,3,5,6-tetrafluoro-4-hydroxybenzaldehyde (**2**, 1 mmol, 194 mg) and *N,N*-di-*n*-butyl-3-aminophenol (1 mmol, 221 mg, 225 μL) in toluene (30 ml) was stirred under argon at 90 °C overnight. The reaction mixture was cooled to room temperature and concentrated under vacuum. The crude product was purified using column chromatography (silica, $\text{CH}_2\text{Cl}_2/\text{MeOH}$, 98:2) to give the pure product (130 mg, 35 %) as red crystals. M.p. 219 - 220 °C.

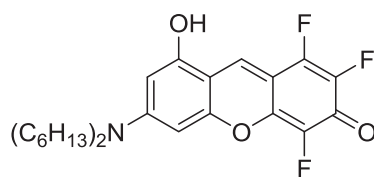
^1H NMR (500 MHz, CDCl_3) δ 8.01 (s, 1H), 7.43 (d, $J = 9.0$ Hz, 1H), 6.72 (dd, $J = 9.1, 2.4$ Hz, 1H), 6.60 (d, $J = 2.4$ Hz, 1H), 3.43 (t, $J = 7.9$ Hz, 4H), 1.70 - 1.63 (m, 4H), 1.47 – 1.38 (m, 4H), 1.01 (t, $J = 7.3$ Hz, 6H). ^{13}C NMR (126 MHz, CDCl_3) δ 166.2 (td, $J = 16.9, 5.5$ Hz), 155.7, 154.2, 144.5 (dd, $J = 260.7, 12.1$ Hz), 141.4 (dt, $J = 254.8, 7.4$ Hz), 139.3 (t, $J = 8.9$ Hz), 138.8 (dd, $J = 242.4, 6.6$ Hz), 135.5 (m), 131.5, 111.5, 109.7, 105.2, 96.8, 51.5, 29.3, 20.2, 13.9. ^{19}F NMR (470 MHz, CDCl_3) δ -149.9 (dd, $J = 17.4, 5.1$ Hz), -154.8 (dd, $J = 17.5, 13.0$ Hz), -164.4 (dd, $J = 12.9, 4.8$ Hz). HRMS (ESI) calc. for $\text{C}_{21}\text{H}_{23}\text{NO}_2\text{F}_3$ 378.1681 $[\text{M} + \text{H}]^+$, found 378.1687.



13

Rhodol **13**: A mixture of 2,3,5,6-tetrafluoro-4-hydroxybenzaldehyde (**2**, 1 mmol, 194 mg) and 5-(piperidin-1-yl)benzene-1,3-diol² (1 mmol, 193 mg) in xylene (30 ml) was stirred under argon at 160 °C overnight. The resulting precipitate was filtered and washed with boiling MeOH to give the pure product (259 mg, 74 %) as dark red crystals. M.p. > 350 °C.

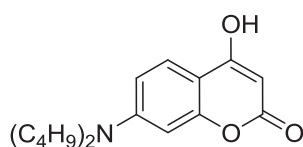
¹H NMR (500 MHz, CF₃COOD) δ 8.84 (s, 1H), 6.77 (s, 1H), 6.70 (s, 1H), 3.84 (br s, 4H), 1.87 (br s, 6H). ¹³C NMR (126 MHz, CF₃COOD) δ 160.0 (t, *J* = 5.2 Hz), 158.0 (dd, *J* = 186.4, 6.7 Hz), 144.9, 142.9 – 142.5 (m), 139.01 (dd, *J* = 9.6, 8.7 Hz), 138.12 (d, *J* = 8.2 Hz), 137.2, 135.3, 133.1, 104.2, 104.1, 97.0, 92.8, 50.5, 25.9, 23.1. Due to the poor solubility of compound **13** and the complexity of ¹³C NMR spectrum, it is not possible to assign all signals. ¹⁹F NMR (470 MHz, CF₃COOD) δ -146.6 (dd, *J* = 18.5, 11.3 Hz), -161.0 (d, *J* = 18.3 Hz), -162.5 (br d, *J* = 8.2 Hz). HRMS (ESI) calc. for C₁₈H₁₃NO₃F₃ 348.0848 [M-H]⁻, found 348.0843.



14

Rhodol **14**: A mixture of 2,3,5,6-tetrafluoro-4-hydroxybenzaldehyde (**2**, 1 mmol, 194 mg) and 5-*N,N*-dihexylamino-benzene-1,3-diol³ (1 mmol, 293 mg) in xylene (30 ml) was stirred under argon at 160 °C overnight. The resulting precipitate was filtered and recrystallized from CH₂Cl₂/MeOH to give the pure product (392 mg, 87 %) as dark red crystals. M.p. 301 - 303 °C.

¹H NMR (500 MHz, DMSO-*d*₆) δ 11.32 (s, 1H), 8.32 (s, 1H), 6.46 – 6.43 (m, 1H), 6.21 (d, *J* = 1.9 Hz, 1H), 3.43 (t, *J* = 7.8 Hz, 4H), 1.63 – 1.51 (m, 4H), 1.31 (br s, 12H), 0.88 (t, *J* = 6.9 Hz, 6H). ¹³C NMR (126 MHz, DMSO-*d*₆) δ 163.3 (td, *J* = 17.2, 4.9 Hz), 157.8, 155.2, 155.1, 145.5, 142.6 (dd, *J* = 230.3; 11.0 Hz), 139.6, 139.2, 139.0 (t, *J* = 8.8 Hz), 137.4, 131.6 (t, *J* = 14.4 Hz), 103.2, 100.1 (d, *J* = 20.1 Hz), 94.2, 90.2, 50.7, 30.9, 26.9, 25.8, 22.0, 13.8. Due to the poor solubility of compound **13** and the complexity of ¹³C NMR spectrum, it is not possible to assign all signals. ¹⁹F NMR (470 MHz, DMSO-*d*₆) δ -145.9 (dd, *J* = 19.8, 4.8 Hz), -154.3 (dd, *J* = 19.4, 14.6 Hz), -161.0 (dd, *J* = 13.9, 3.2 Hz). HRMS (ESI) calc. for C₂₅H₃₁NO₃F₃ 450.2256 [M + H]⁺, found 450.2257.

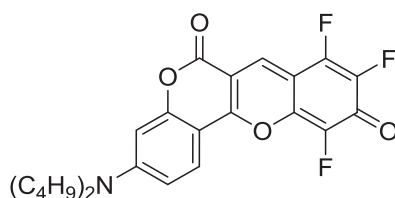


7

7-(Dibutylamino)-4-hydroxy-2H-chromen-2-one **7**: A mixture of *N,N*-di-*n*-butyl-3-aminophenol (**5**, 4.5 mmol, 1 g, 1.02 ml) and bis-(2,4,6-trichlorophenyl)-malonate (5.4 mmol, 2.5 g) in toluene (50 ml) was refluxed under

argon overnight. The reaction mixture was cooled to room temperature and the resulting precipitate was filtered, washed with toluene and pentane to give pure product (0.93 g, 72%) as pale yellow crystals. M.p. 206 – 208 °C.

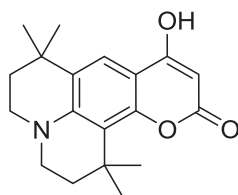
^1H NMR (500 MHz, DMSO- d_6) δ 11.89 (br s, 1H), 7.54 (d, J = 9.0 Hz, 1H), 6.64 (dd, J = 9.0, 2.4 Hz, 1H), 6.41 (d, J = 2.4 Hz, 1H), 5.26 (s, 1H), 3.33 (t, J = 7.7 Hz, 4H), 1.56 – 1.47 (m, 4H), 1.33 (h, J = 7.4 Hz, 4H), 0.92 (t, J = 7.3 Hz, 6H). ^{13}C NMR (126 MHz, DMSO- d_6) δ 166.9, 163.2, 156.5, 151.7, 124.5, 108.7, 103.9, 96.9, 86.5, 50.4, 29.3, 20.0, 14.3. HRMS (ESI) calc. for $\text{C}_{17}\text{H}_{24}\text{NO}_3$ 290.1756 $[\text{M} + \text{H}]^+$, found 290.1757.



9

Rhodol **9**: A mixture of 2,3,5,6-tetrafluoro-4-hydroxybenzaldehyde (**2**, 1 mmol, 194 mg) and coumarin **7** (1 mmol, 289 mg) in xylene (30 ml) was stirred under argon at 160 °C overnight. The reaction mixture was cooled to room temperature and the resulting precipitate was filtered to give the pure product (361 mg, 81 %) as dark green crystals. M.p. 279 – 280 °C.

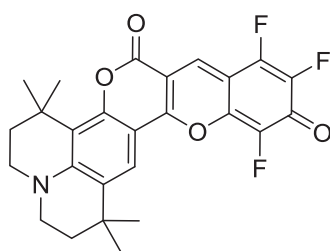
^1H NMR (600 MHz, CDCl_3) δ 8.38 (d, J = 1.5 Hz, 1H), 7.92 (d, J = 9.2 Hz, 1H), 6.73 (dd, J = 9.3, 2.4 Hz, 1H), 6.49 (d, J = 2.4 Hz, 1H), 3.45 – 3.40 (m, 4H), 1.69 – 1.61 (m, 4H), 1.42 (h, J = 7.4 Hz, 4H), 1.00 (t, J = 7.4 Hz, 6H). ^{13}C NMR (151 MHz, CDCl_3) δ 160.3, 158.9, 157.1, 154.7, 142.4 (dd, J = 260.7, 8.2 Hz), 139.2 (dd, J = 250.8, 6.4 Hz), 137.9, 133.4 – 133.3 (m), 125.7, 111.0, 108.4, 108.2, 100.1, 100.0, 97.7, 51.5, 29.3, 20.2, 13.9. Due to the poor solubility of compound **13** and the complexity of ^{13}C NMR spectrum, it is not possible to assign all signals. ^{19}F NMR (470 MHz, CDCl_3) -146.96 (dd, J = 16.0, 4.2 Hz), -150.29 (dd, J = 15.9, 12.9 Hz), -159.60 – -160.22 (m). HRMS (ESI) calc. for $\text{C}_{24}\text{H}_{23}\text{NO}_4\text{F}_3$ 446.1579 $[\text{M} + \text{H}]^+$, found 446.1582.



8

9-Hydroxy-1,1,7,7-tetramethyl-2,3,6,7-tetrahydro-1H,5H,11H-pyrano[2,3-*f*]pyrido[3,2-*1-ij*]quinolin-11-one (**8**): A mixture of 1,1,7,7-tetramethyl-8-hydroxyjulolidine (**6**, 4 mmol, 0.98 g) and bis-(2,4,6-trichlorophenyl)-malonate (4.8 mmol, 2.22 g) in toluene (50 ml) was refluxed under argon overnight. The reaction mixture was cooled to room temperature and the resulting precipitate was filtered, washed with hexane to give pure product (0.48 g, 38 %) as pale yellow crystals. M.p. 178 – 180 °C.

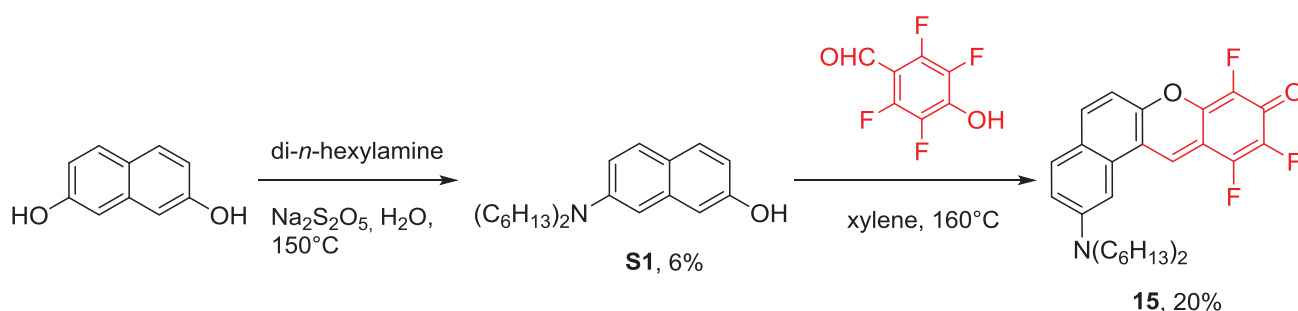
^1H NMR (500 MHz, DMSO- d_6) δ 11.76 (bs, 1H), 7.41 (s, 1H), 5.25 (s, 1H), 3.25 (t, J = 6.0 Hz, 2H), 3.21 – 3.15 (m, 2H), 1.76 – 1.71 (m, 2H), 1.68 (t, J = 6.0 Hz, 2H), 1.43 (s, 6H), 1.23 (s, 6H). ^{13}C NMR (126 MHz, DMSO- d_6) δ 167.1, 162.9, 152.7, 146.0, 127.4, 118.4, 114.4, 104.2, 86.1, 46.9, 46.4, 35.8, 32.3 (2), 31.2, 29.3. HRMS (ESI) calc. for $\text{C}_{19}\text{H}_{24}\text{NO}_3$ 314.1756 $[\text{M} + \text{H}]^+$, found 314.1762.



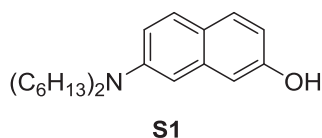
10

Rhodol (**10**): A mixture of 2,3,5,6-tetrafluoro-4-hydroxybenzaldehyde (**2**, 1 mmol, 194 mg) and coumarin **8** (1 mmol, 313 mg) in xylene (30 ml) was stirred under argon at 160 °C overnight. The reaction mixture was cooled to room temperature, concentrated under vacuum and purified using column chromatography (silica, CH₂Cl₂/Et₂O, 9:1) to give the pure product (240 mg, 51 %) as dark purple crystals. M.p. 304 – 306 °C.

¹H NMR (500 MHz, CDCl₃) δ 8.37 (d, *J* = 1.1 Hz, 1H), 7.69 (s, 1H), 3.49 (t, *J* = 6.2 Hz, 2H), 3.39 (t, *J* = 5.8 Hz, 2H), 1.87 – 1.83 (m, 2H), 1.79 (t, *J* = 6.2 Hz, 2H), 1.55 (s, 6H), 1.36 (s, 6H). ¹³C NMR (126 MHz, CDCl₃) δ 167.0 (td, *J* = 17.6; 5.8 Hz), 160.2, 158.5, 153.3, 149.9, 144.8 (dd, *J* = 264.4; 12.5 Hz), 142.2 (dt, *J* = 260.0; 7.1 Hz), 139.2 (dd, *J* = 249.2, 6.5 Hz), 138.1 – 137.9 (m), 134.2 – 133.1 (m), 130.4, 118.9, 115.4, 107.3, 107.1, 100.1, 99.5, 48.0, 47.3, 38.5, 34.7, 32.3, 29.6, 28.5. ¹⁹F NMR (470 MHz, CDCl₃) δ -147.2 (dd, *J* = 16.5, 4.4 Hz), -151.5 (dd, *J* = 16.4, 13.2 Hz), -160.5 (dd, *J* = 13.3, 2.9 Hz). HRMS (ESI) calc. for C₂₆H₂₃NO₄F₃ 470.1579 [M + H]⁺, found 470.1585.



Scheme S1. Synthesis of π -expanded rhodol **15**.

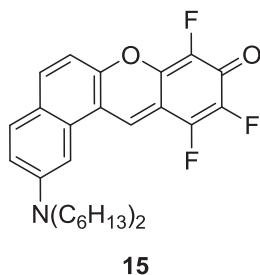


S1

7-(dihexylamino)naphthalen-2-ol (**S1**): The mixture of 2,7-dihydroxynaphthalene (3.2 g, 20 mmol), *N,N*-di-*n*-hexylamine (40 mmol, 7.4 g, 9.3 ml) and sodium metabisulfite (42 mmol, 8 g) in 120 ml of water was placed in pressure tube and stirred upon heating at 150 °C for 2 hours. The reaction mixture was cooled to room temperature, diluted with 300 ml of water and extracted with DCM (3 x 150 ml). The organic layer was dried over Na₂SO₄ and concentrated under vacuum. The residue was purified using column chromatography (silica, hexane /EtOAc, 4:1) to give pure product (380 mg, 6 %) as colourless oil.

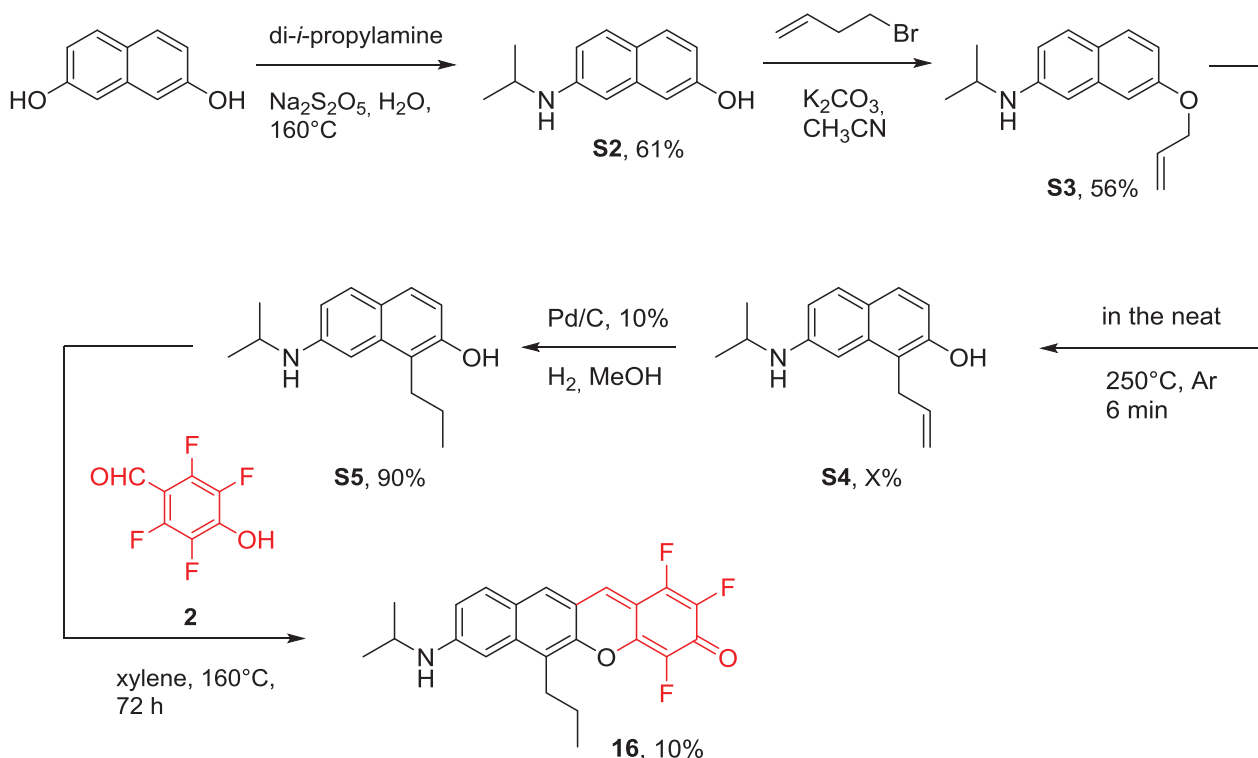
¹H NMR (500 MHz, CDCl₃) δ 7.58 (d, *J* = 9.0 Hz, 1H), 7.54 (d, *J* = 8.6 Hz, 1H), 6.95 – 6.87 (m, 2H), 6.76 (dd, *J* = 8.7, 2.5 Hz, 1H), 6.66 (d, *J* = 2.6 Hz, 1H), 3.34 (t, *J* = 7.7 Hz, 4H), 1.66 – 1.58 (m, 6H), 1.40 – 1.31 (m, 12H), 0.91

(t, $J = 7.1$ Hz, 6H). ^{13}C NMR (126 MHz, CDCl_3) δ 153.9, 146.7, 136.6, 129.3, 128.7, 121.6, 113.6, 113.0, 107.6, 103.8, 51.2, 31.8, 27.3, 26.9, 22.7, 14.1. HRMS (ESI) calc. for $\text{C}_{22}\text{H}_{34}\text{NO}$ 328.2640 $[\text{M} + \text{H}]^+$, found 328.2642

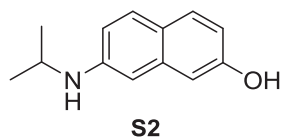


Rhodol (15): A mixture of 2,3,5,6-tetrafluoro-4-hydroxybenzaldehyde (**2**, 1 mmol, 194 mg) and naphthalene **S1** (1 mmol, 327 mg) in xylene (30 ml) was stirred under argon at 160 °C for 7 h. The reaction mixture was cooled to room temperature, concentrated under vacuum and purified via column chromatography (silica, $\text{CH}_2\text{Cl}_2/\text{Et}_2\text{O}$, 9:1) to give pure product (97 mg, 20 %) as dark blue crystals. M.p. 152 – 153 °C.

^1H NMR (500 MHz, CD_2Cl_2) δ 8.63 (s, 1H), 7.91 (d, $J = 8.8$ Hz, 1H), 7.69 (d, $J = 9.1$ Hz, 1H), 7.18 (d, $J = 8.8$ Hz, 1H), 7.15 (br s, 1H), 7.08 (dd, $J = 9.1, 1.9$ Hz, 1H), 3.47 (t, $J = 7.9$ Hz, 4H), 1.75 – 1.68 (m, 4H), 1.47 – 1.35 (m, 12H), 0.94 (t, $J = 7.1$ Hz, 6H). ^{13}C NMR (126 MHz, CD_2Cl_2) δ 166.6 (m), 154.1, 149.1, 143.9 (dd, $J = 262.4, 12.7$ Hz), 140.9 – 140.7 (m), 138.1 (dd, $J = 207.7, 7.3$ Hz), 137.1, 131.7, 130.7, 122.1, 115.1, 112.0, 110.2, 109.8, 109.6, 98.5, 96.6, 51.1, 31.6, 27.1, 26.7, 22.7, 13.7. ^{19}F NMR (470 MHz, CD_2Cl_2) δ -148.65 (dd, $J = 15.9, 5.1$ Hz), -149.94 (dd, $J = 15.8, 11.9$ Hz), -163.26 (dd, $J = 12.2, 4.9$ Hz). HRMS (ESI) calc. for $\text{C}_{29}\text{H}_{33}\text{NO}_2\text{F}_3$ 484.2463 $[\text{M} + \text{H}]^+$, found 484.2462.

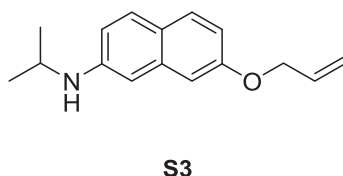


Scheme S2. Synthesis of linear π -expanded rhodol (**16**).



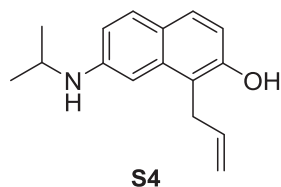
7-(Isopropylamino)naphthalen-2-ol (**S2**): The mixture of 2,7-dihydroxynaphthalene (10 g, 62.5 mmol), *N,N*-diisopropylamine (125 mmol, 12.63 g, 17.65 ml) and sodium metabisulfite (131.25 mmol, 24.94 g) in H₂O (100 ml) was stirred in the pressure tube at 120 °C for 24 hours. The reaction mixture was cooled to room temperature and extracted with EtOAc (3 x 300 ml). The organic phases were collected, dried over Na₂SO₄ and concentrated under vacuum. The residue was purified using column chromatography (silica, hexane/EtOAc, 3:1) to give pure product (7.61 mg, 61 %) as off-white crystals. M.p. 139 – 140 °C.

¹H NMR (500 MHz, CDCl₃) δ 7.54 (t, *J* = 8.2 Hz, 2H), 6.89 (d, *J* = 2.6 Hz, 1H), 6.78 (dd, *J* = 8.7, 2.5 Hz, 1H), 6.69 (dd, *J* = 8.8, 2.3 Hz, 1H), 6.63 (d, *J* = 2.3 Hz, 1H), 3.74 (hept, *J* = 6.3 Hz, 1H), 1.27 (d, *J* = 6.3 Hz, 6H). ¹³C NMR (126 MHz, CDCl₃) δ 153.9, 145.7, 136.6, 129.5, 128.9, 122.8, 116.0, 113.3, 107.8, 103.8, 44.3, 22.9. HRMS (ESI) calc. for C₁₃H₁₆NO 202.1232 [M + H]⁺, found 202.1234.



7-(Allyloxy)-*N*-isopropyl-naphthalen-2-amine (**S3**): To the mixture of 7-(*N*-isopropylamino)naftalen-2-ol (7.5 g, 0.037 mol) and K₂CO₃ (12.7 g, 0.092 mol) in acetone (350 ml) allyl bromide (4 ml, 0.046 mol) was added. The reaction mixture was stirred at room temperature overnight. The solid was filtered off, the solvent was evaporated and the residue was purified via column chromatography (silica, heksan/EtOAc, 100:1). The product was obtained in 56 % yield as yellow oil. M.p. 46 – 47 °C.

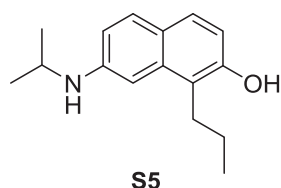
¹H NMR (500 MHz, CDCl₃) δ 7.56 – 7.49 (m, 2H), 6.93 (d, *J* = 2.5 Hz, 1H), 6.87 (dd, *J* = 8.8, 2.5 Hz, 1H), 6.70 – 6.66 (m, 2H), 6.17 - 6.06 (m, 1H), 5.45 (dq, *J* = 17.2; 1.6, 1H), 5.30 (dq, *J* = 10.4; 1.4, 1H), 4.62 (dt, *J* = 5.3, 1.6 Hz, 2H), 3.74 (hept, *J* = 6.3 Hz, 1H), 3.60 (s, 1H), 1.26 (d, *J* = 6.2 Hz, 6H). ¹³C NMR (126 MHz, CDCl₃) δ 157.2, 145.7, 136.5, 133.5, 129.1, 128.7, 122.7, 117.5, 115.8, 114.4, 105.7, 104.3, 68.7, 44.2, 22.9. HRMS (EI) calc. for C₁₆H₁₉NO 241.1467 [M⁺], found 241.1464.



1-Allyl-7-(isopropylamino)naphthalen-2-ol (**S4**): 7-allyloxy-2-(*N*-isopropylamino)naftalen (5 g, 0.02 mol) was placed in a round-bottom flask under argon atmosphere and heated with heatgun (approx. 250 °C) till the moment when the color of the oil changes to light brown (≈ 4 - 6 min). The reaction mixture was purified via column chromatography (silica, hexane/EtOAc, 1:1). The product was obtained in 50 % yield as beige solid. M.p. 105 - 107 °C.

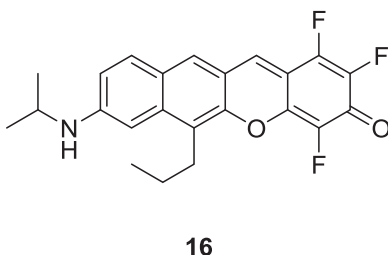
¹H NMR (500 MHz, CDCl₃) δ 7.56 (d, *J* = 8.7 Hz, 1H), 7.48 (d, *J* = 8.6 Hz, 1H), 6.84 (d, *J* = 2.3 Hz, 1H), 6.78 (d, *J* = 8.7 Hz, 1H), 6.72 (dd, *J* = 8.7, 2.3 Hz, 1H), 6.13 – 6.01 (m, 1H), 5.15 – 5.09 (m, 2H), 4.38 (br s, 1H), 3.82 –

3.72 (m, 3H), 1.31 -1.26 (m, 7H). ^{13}C NMR (126 MHz, CDCl_3) δ 151.6, 145.7, 136.1, 135.1, 129.7, 127.9, 123.1, 115.5, 115.2, 114.7, 113.5, 101.2, 44.3, 29.5, 22.8. HRMS (EI) calc. for $\text{C}_{16}\text{H}_{19}\text{NO}$ 241.1467 [M^+], found 241.1460.



7-(Isopropylamino)-1-propylnaphthalen-2-ol (**S5**): To the solution of 1-allyl-7-*N*-isopropylaminonaphthalene-2-ol (2.4 g, 0.01 mol) in methanol (100 ml) was added 10 % Pd/C (85 mg). The flask was filled with hydrogen and the reaction mixture was stirred at rt for 3h. The resulting solid was filtered off and washed with 30 ml of methanol. The filtrate was concentrated under vacuum to give the product in 90 % yield as yellow solid. M.p. 112 - 113 °C.

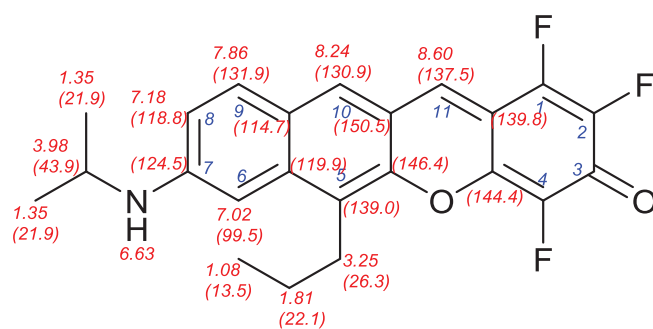
^1H NMR (500 MHz, CDCl_3) δ 7.53 (d, J = 8.7 Hz, 1H), 7.42 (d, J = 8.6 Hz, 1H), 6.83 (d, J = 2.3 Hz, 1H), 6.75 (d, J = 8.6 Hz, 1H), 6.70 (dd, J = 8.7, 2.3 Hz, 1H), 4.73 (br s, 1H), 3.77 (hept, J = 6.3 Hz, 1H), 3.65 (br s, 1H), 2.95 - 2.88 (m, 2H), 1.70 (h, J = 7.4 Hz, 2H), 1.28 (d, J = 6.3 Hz, 6H), 1.05 (t, J = 7.4 Hz, 3H). ^{13}C NMR (126 MHz, CDCl_3) δ 150.9, 145.6, 135.0, 129.7, 127.3, 123.2, 117.8, 115.0, 113.3, 101.3, 44.3, 27.1, 22.9, 22.5, 14.4. HRMS (ESI) calc. for $\text{C}_{16}\text{H}_{22}\text{NO}$ 244.1701 [$\text{M} + \text{H}$] $^+$, found 244.1702.



1,2,4-Trifluoro-8-(isopropylamino)-6-propyl-3H-benzo[*b*]xanthen-3-one (**16**): A mixture of 2,3,5,6-tetrafluoro-4-hydroxybenzaldehyde (**2**, 1 mmol, 194 mg) and naphthalene **S5** (1 mmol, 243 mg) in xylene (30 ml) was stirred under argon at 160 °C for 72 h. The reaction mixture was cooled to room temperature, concentrated under vacuum and purified via column chromatography (silica, $\text{CH}_2\text{Cl}_2/\text{MeOH}$, 95:5). Resulting solid was washed with boiling MeOH to give pure product (40 mg, 10 %) as dark purple crystals. M.p. 325 - 326 °C.

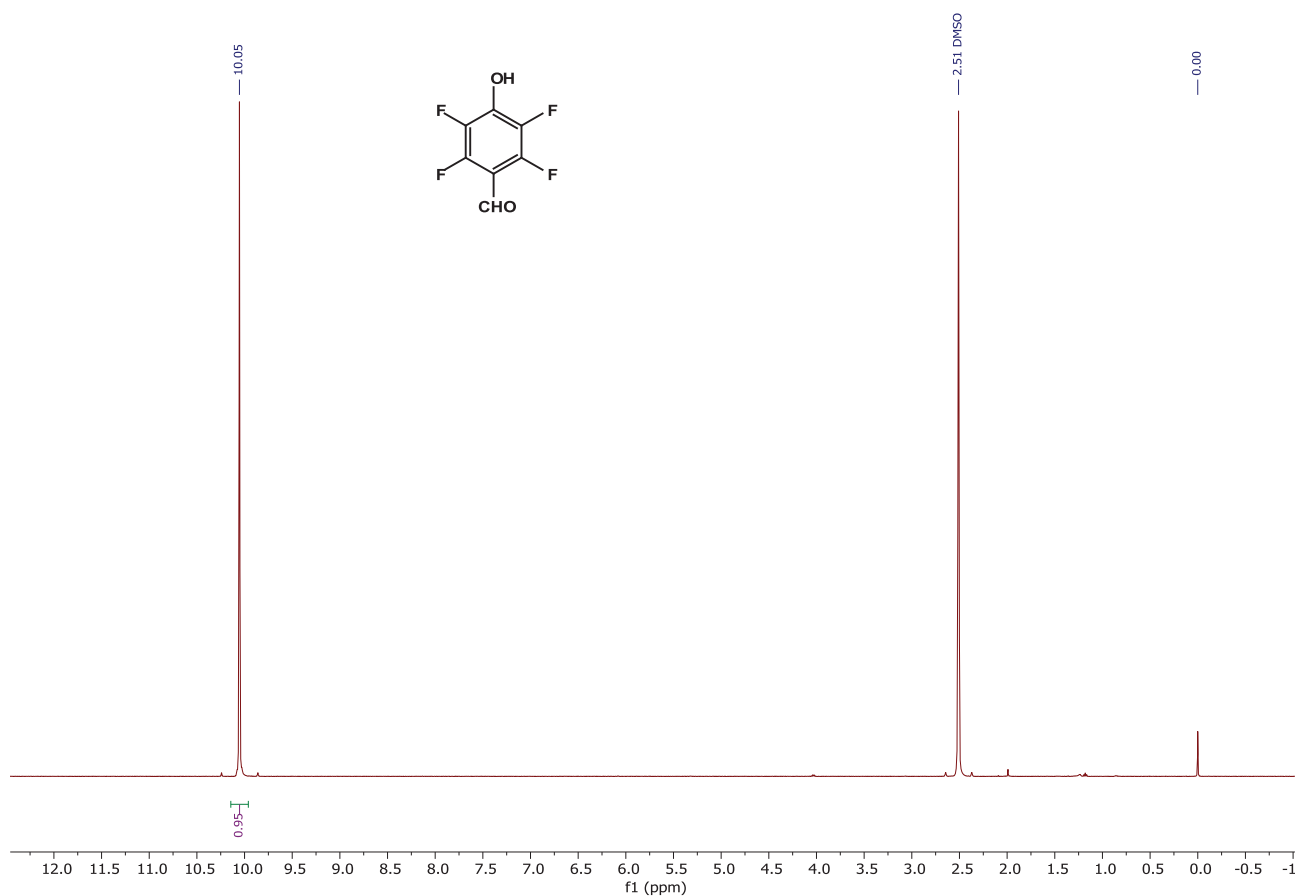
In spite of all our attempts to dry compound **16**, we did not manage to get rid of some solvents and their peaks are present on ^1H NMR spectrum.

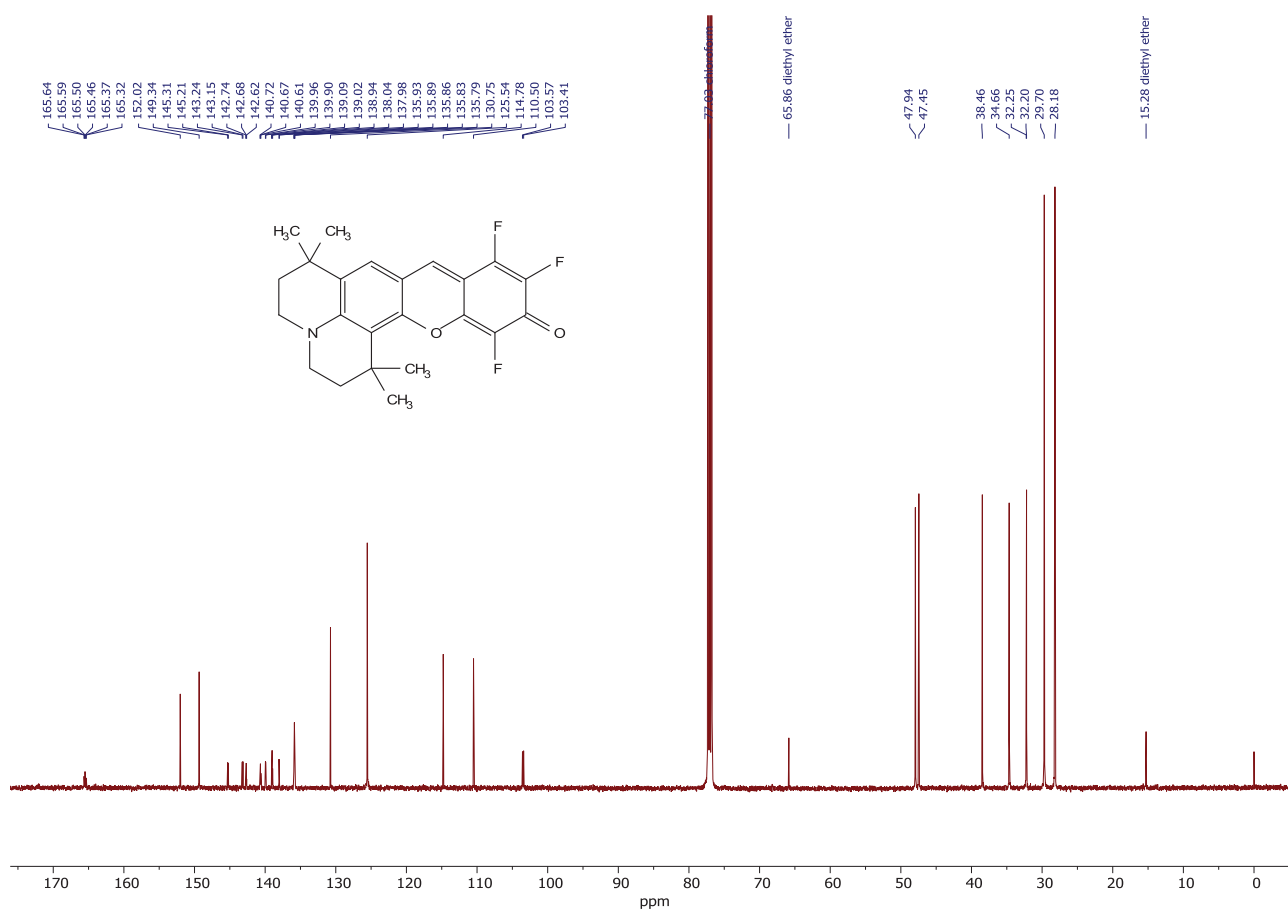
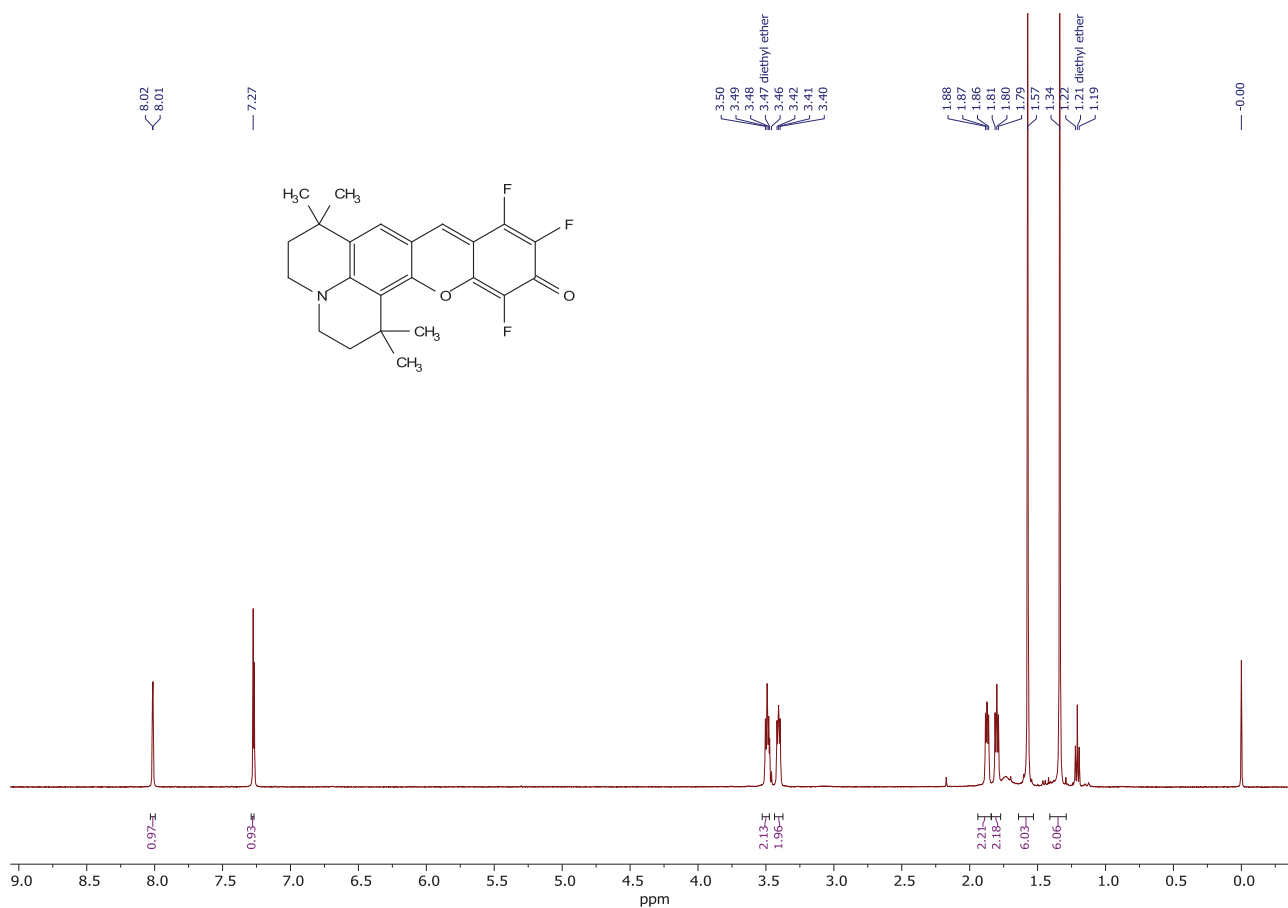
^1H NMR (500 MHz, DMF-d_7) δ 8.60 (s, 1H), 8.24 (s, 1H), 7.87 (d, J = 9.1 Hz, 1H), 7.19 (dd, J = 9.0, 2.1 Hz, 1H), 7.02 (d, J = 2.2 Hz, 1H), 6.63 (d, J = 7.4 Hz, 1H), 3.98 (h, J = 6.5 Hz, 1H), 3.25 (t, J = 7.5 Hz, 2H), 1.83 (h, J = 7.4 Hz, 2H), 1.35 (d, J = 6.3 Hz, 6H), 1.09 (t, J = 7.4 Hz, 3H). Due to the poor solubility of compound **13** and the complexity of ^{13}C NMR spectrum, it is not possible to assign all signals. ^{13}C NMR (126 MHz, DMF-d_7) δ 150.5, 146.4, 139.0, 137.5, 131.9, 130.9, 124.5, 119.9, 118.8, 114.7, 108.8, 99.4, 43.7, 34.2, 34.0, 29.1, 26.3, 22.1, 21.9, 13.5. ^{19}F NMR (470 MHz, DMF-d_7) δ -150.2 (dd, J = 15.3, 4.5 Hz), -157.3 (dd, J = 15.4, 10.6 Hz), -165.8 (ddd, J = 10.5, 4.5, 1.8 Hz). HRMS (ESI) calc. for $\text{C}_{23}\text{H}_{21}\text{NO}_2\text{F}_3$ 400.1524 [$\text{M} + \text{H}$] $^+$, found 400.1523.

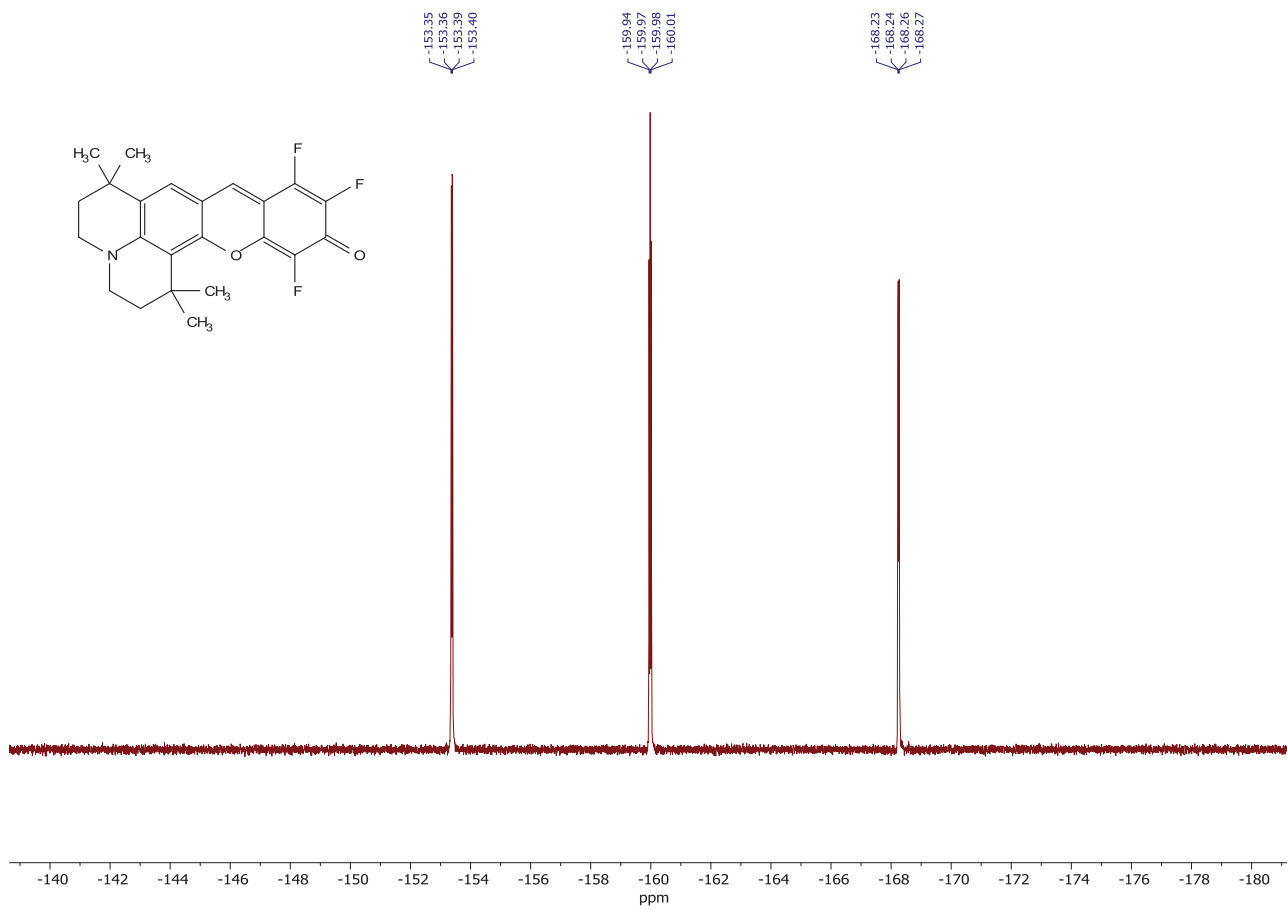


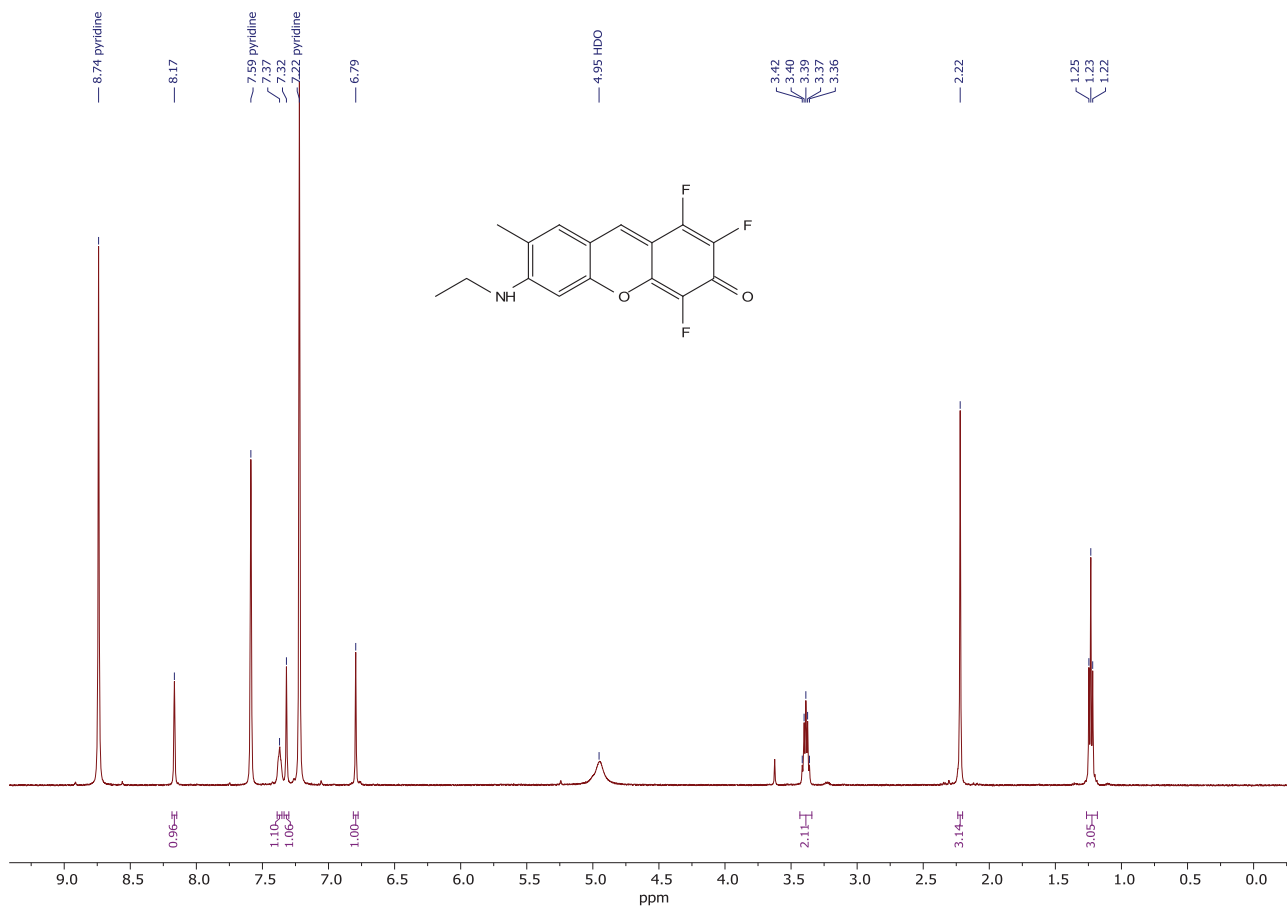
A thorough analysis of one-dimensional (1D) NMR and two-dimensional (2D) NMR spectra provides sufficient structural information about compound **16**. ^1H NMR spectrum shows NH-*i*Pr group as doublet with chemical shift 6.63 ppm (NH) together with doublet (1.35 ppm) and septet (3.98 ppm) of isopropyl group. Propyl group appears as two triplets (1.09 ppm and 3.25 ppm) and sextet (1.82 ppm). Moreover, 5 peaks were detected in aromatic area in ^1H NMR spectra. The correlations in $^1\text{H}^{13}\text{C}$ HSQC, and $^{13}\text{C}^{13}\text{C}$ HMBC spectra allow to assign most of the signals belonging to the molecule with the exception of quaternary carbons 1, 2, 3 and 4. Correlations in $^{13}\text{C}^{13}\text{C}$ HMBC fully support the linear structure of rhodol **16**, that was further confirmed by single crystal X-ray analysis.

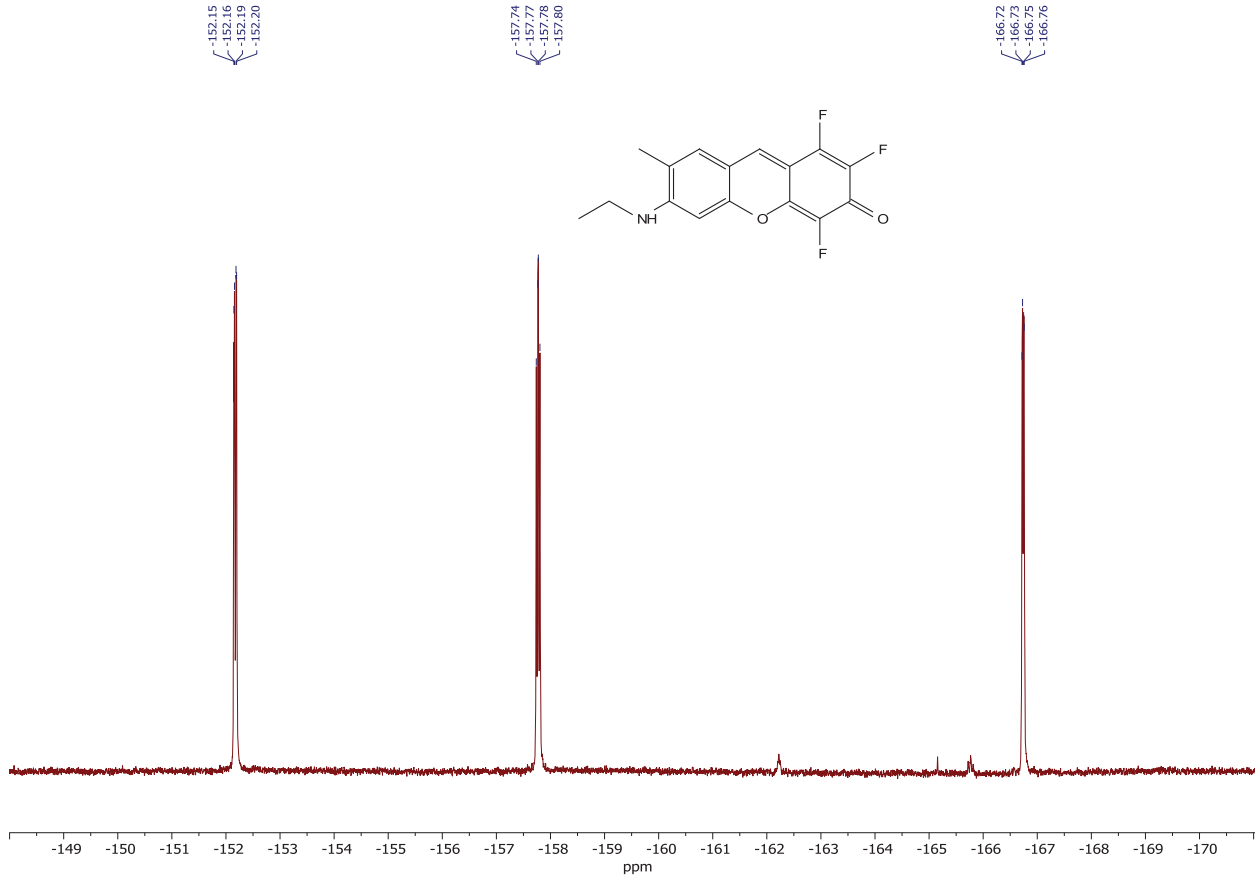
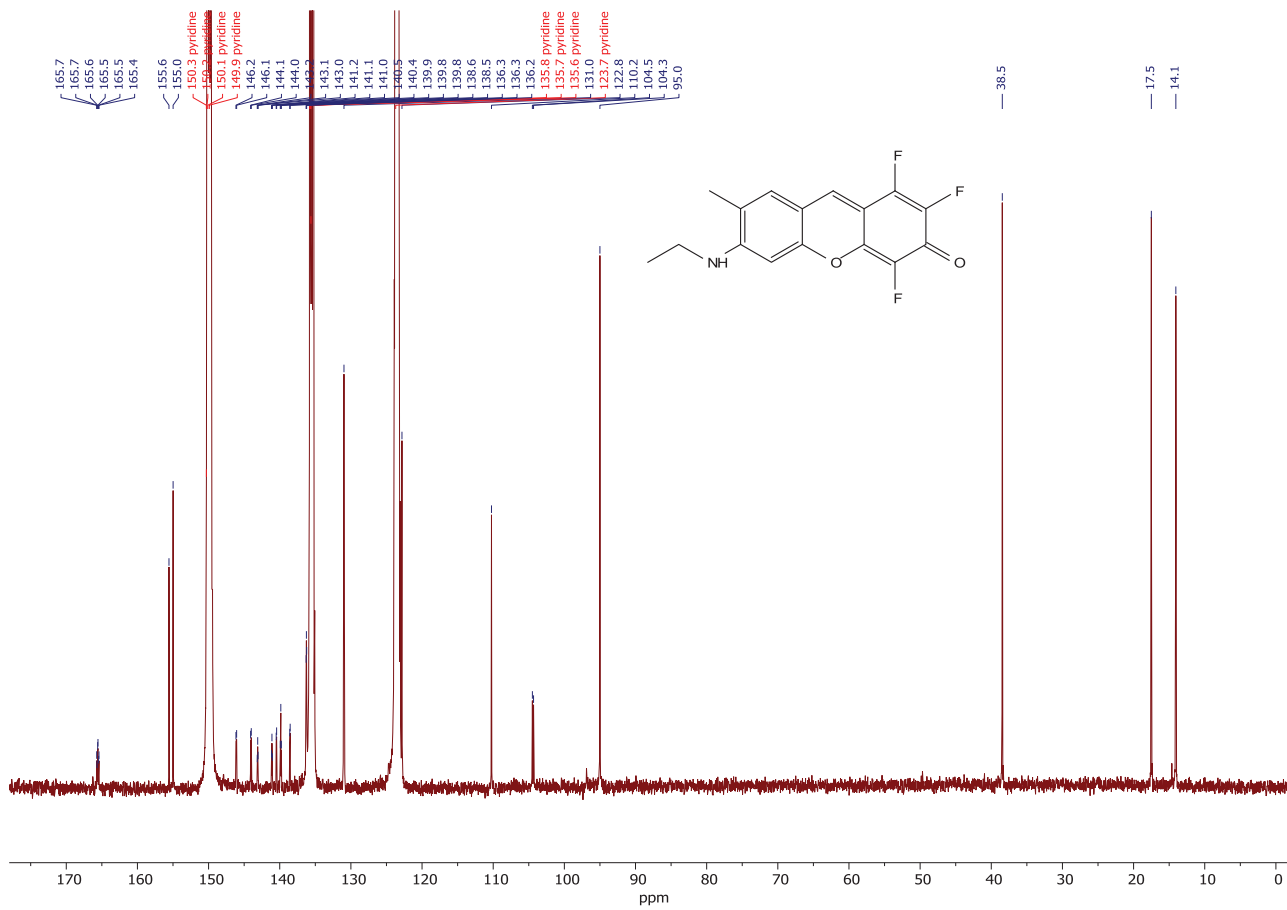
1.1.2 ^1H and ^{13}C NMR spectra for synthesized compounds

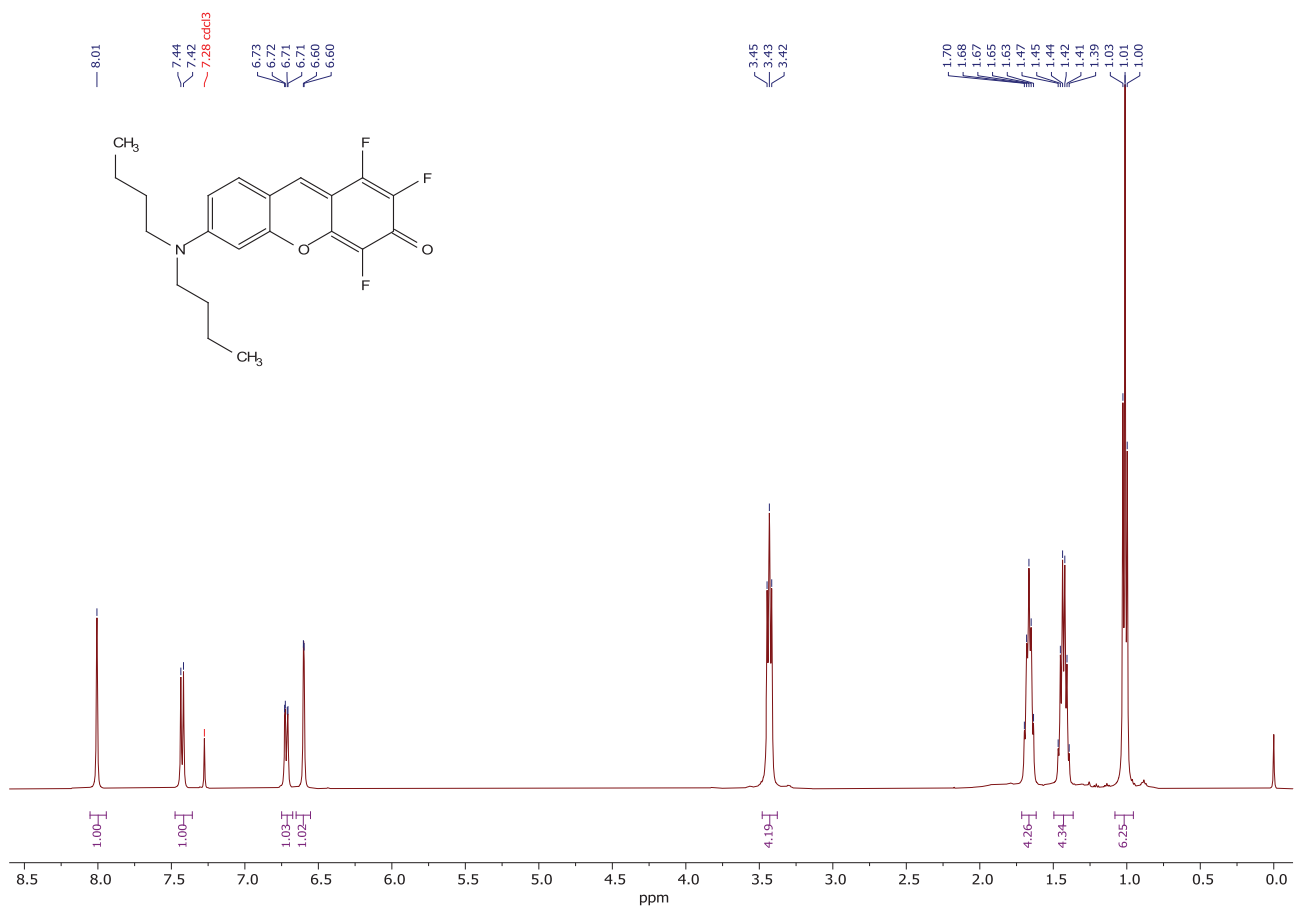


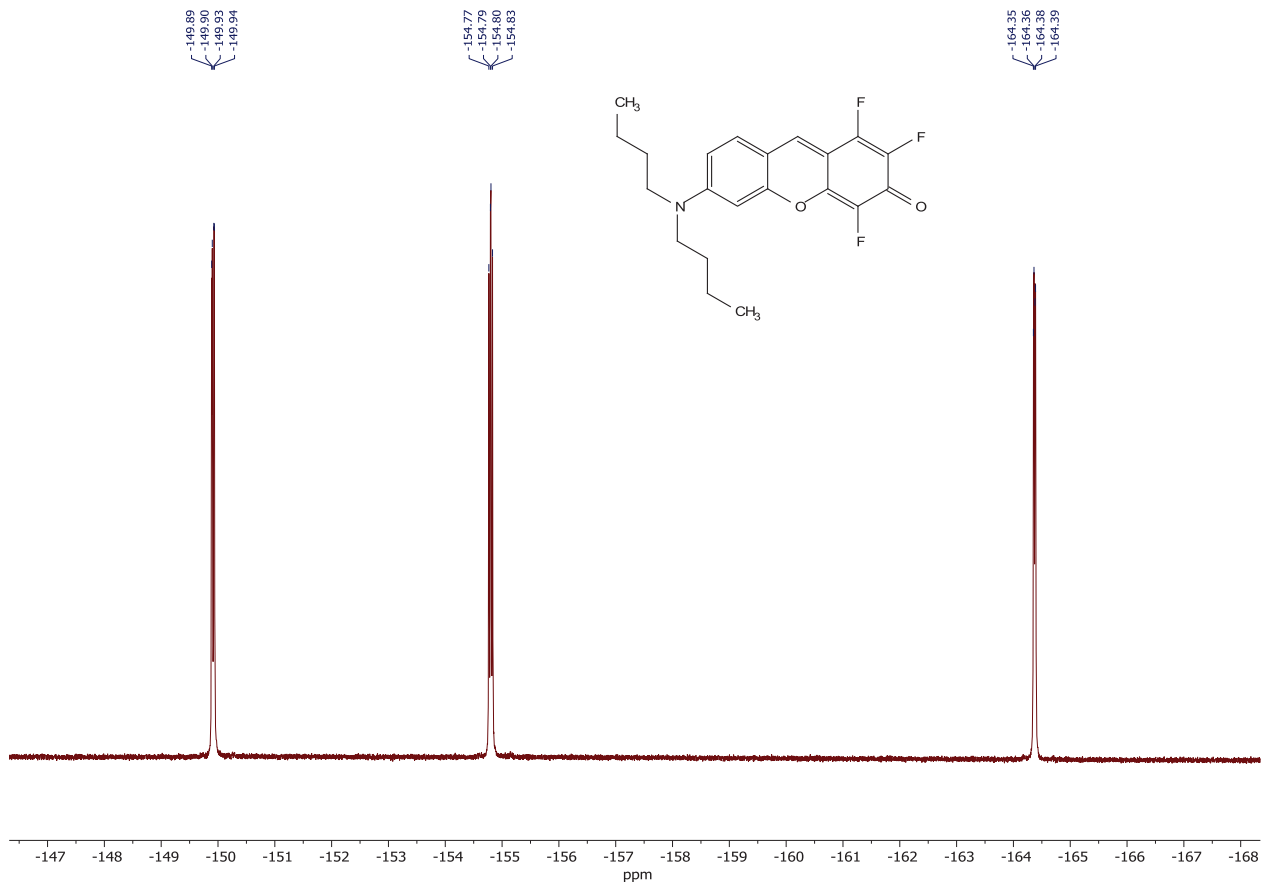
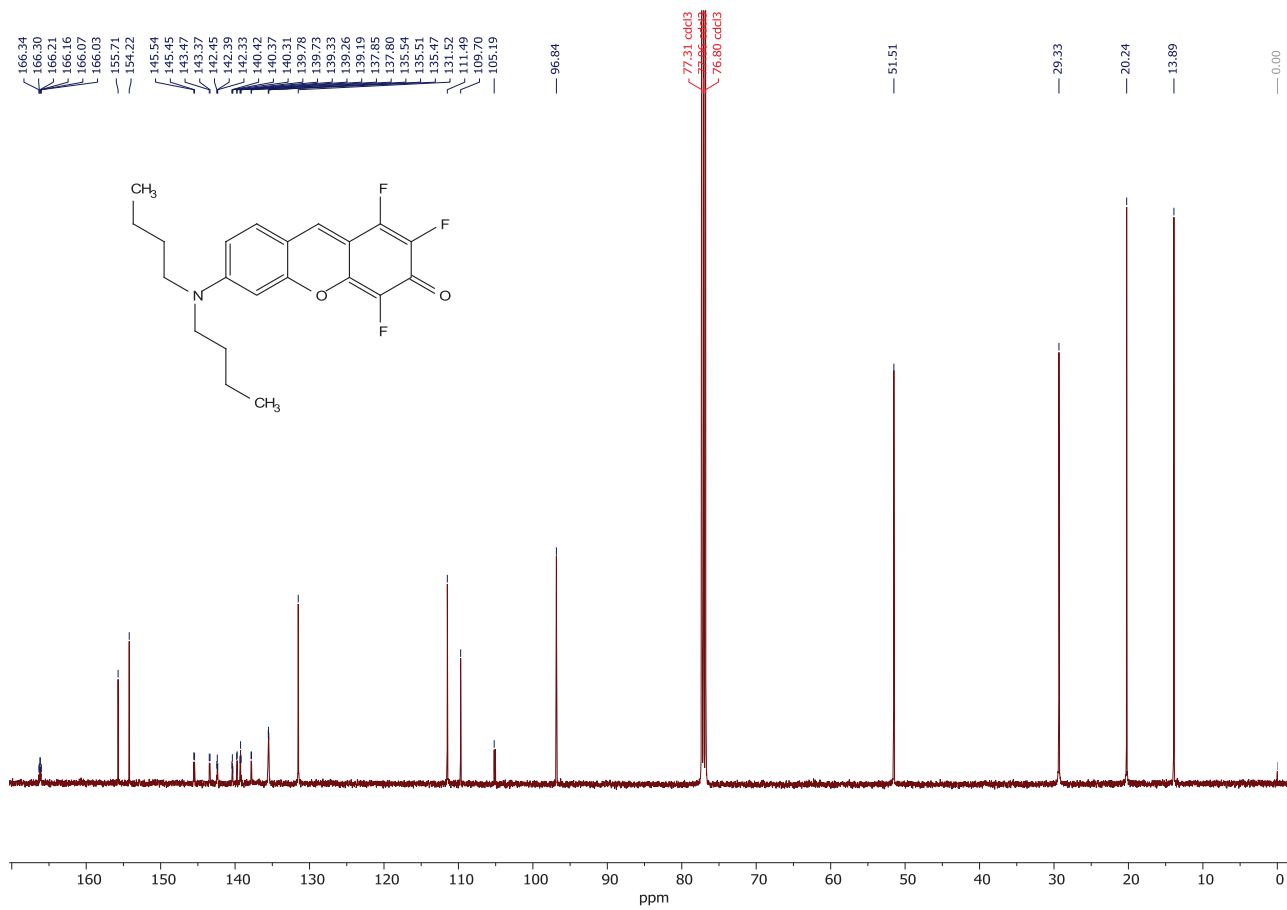


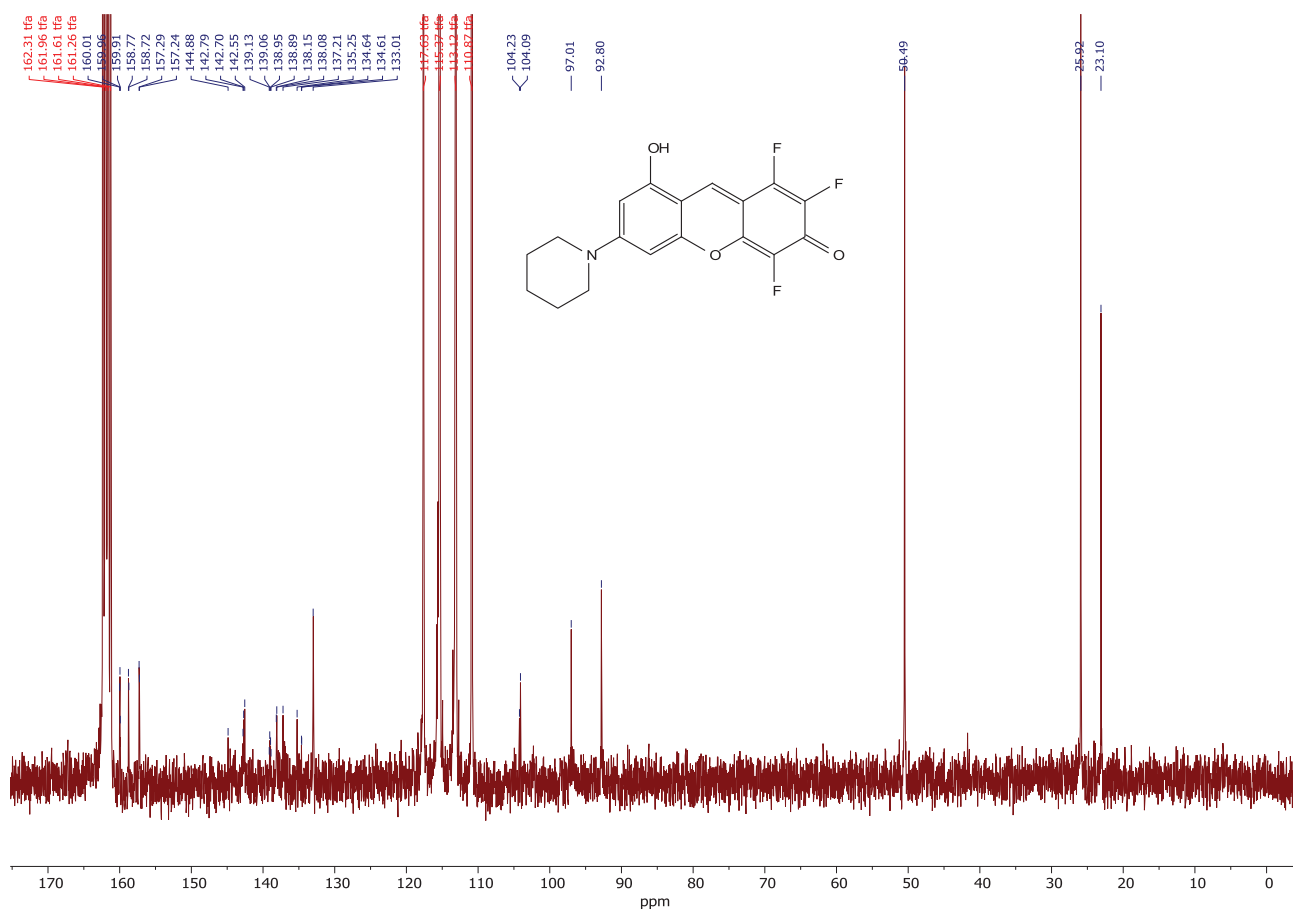
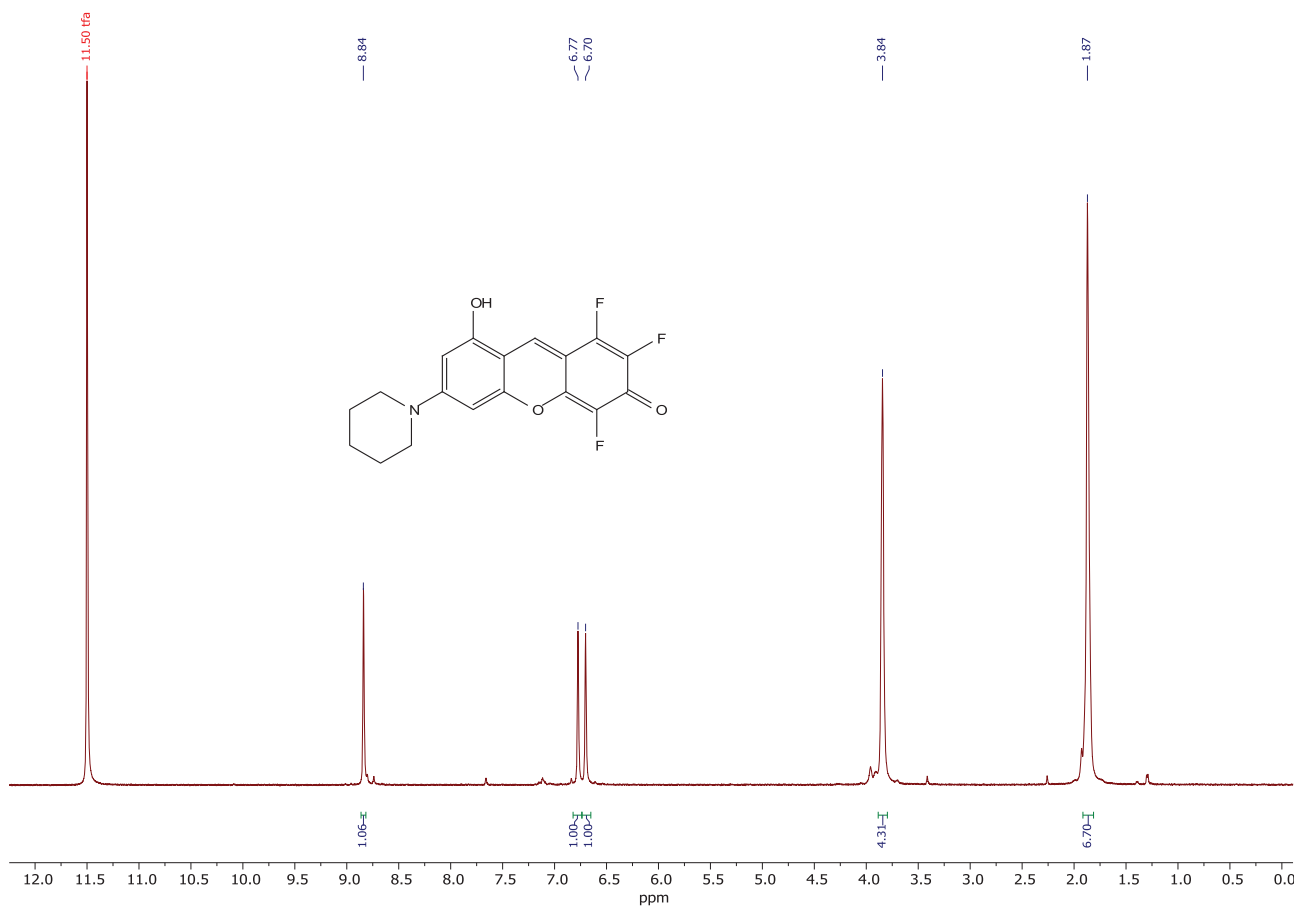


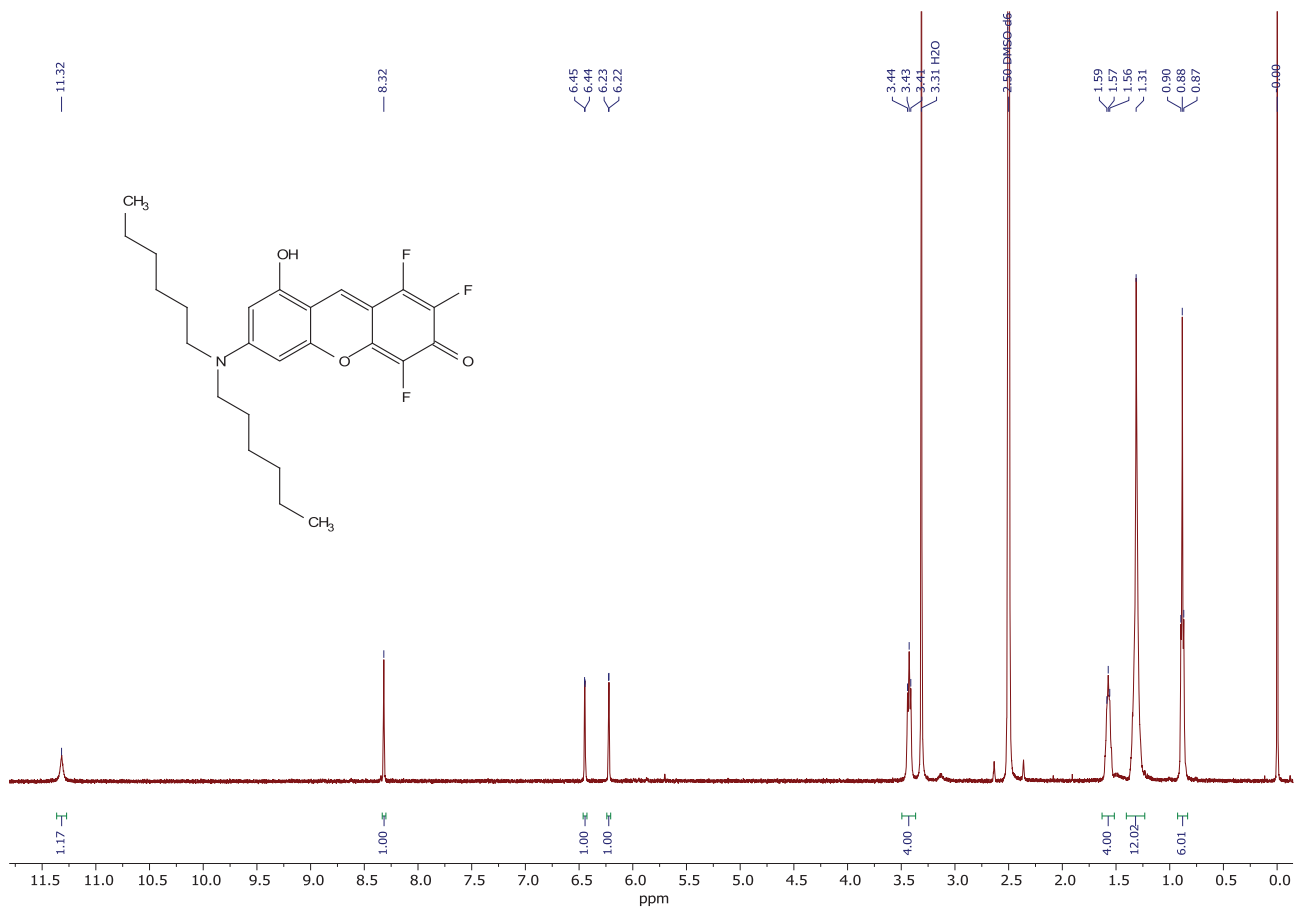
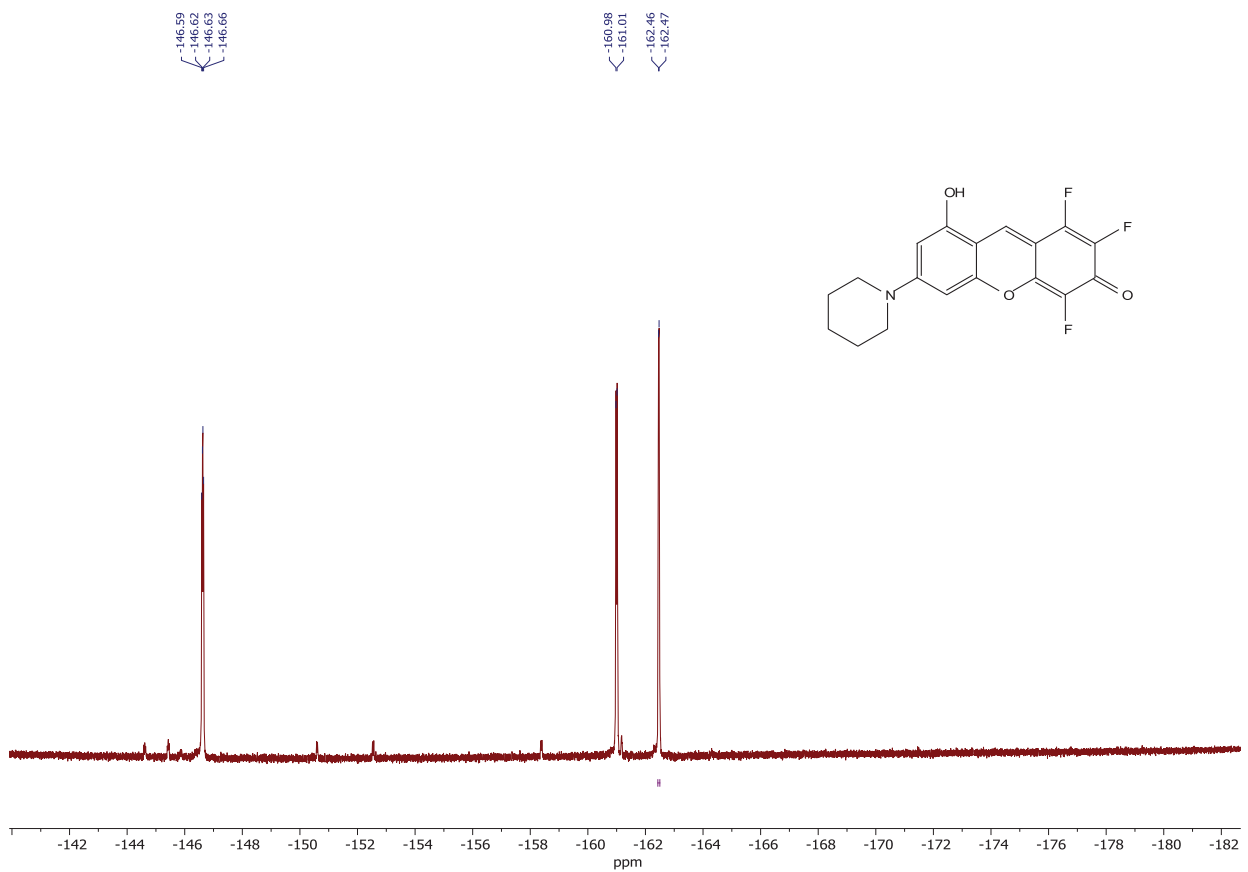


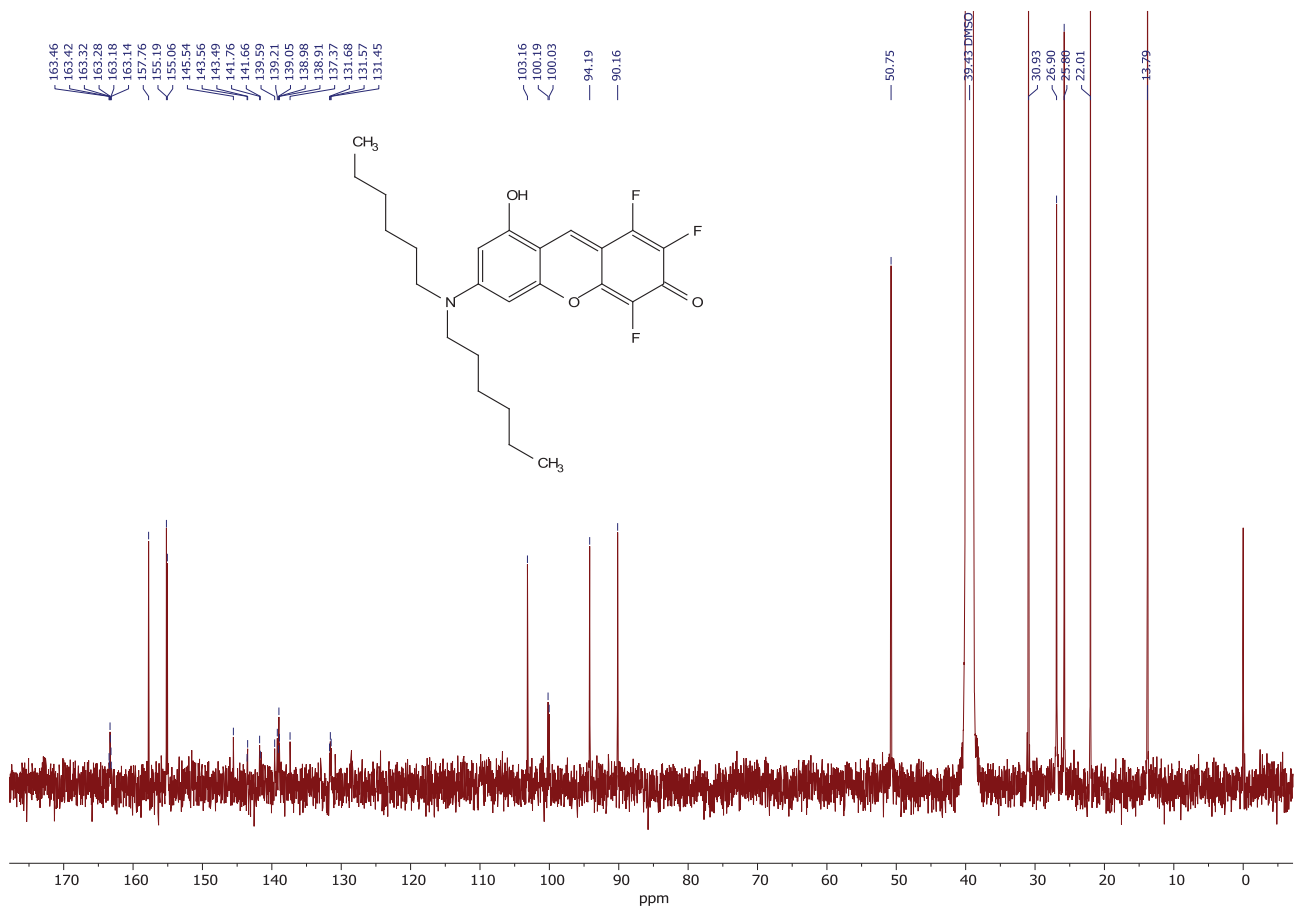


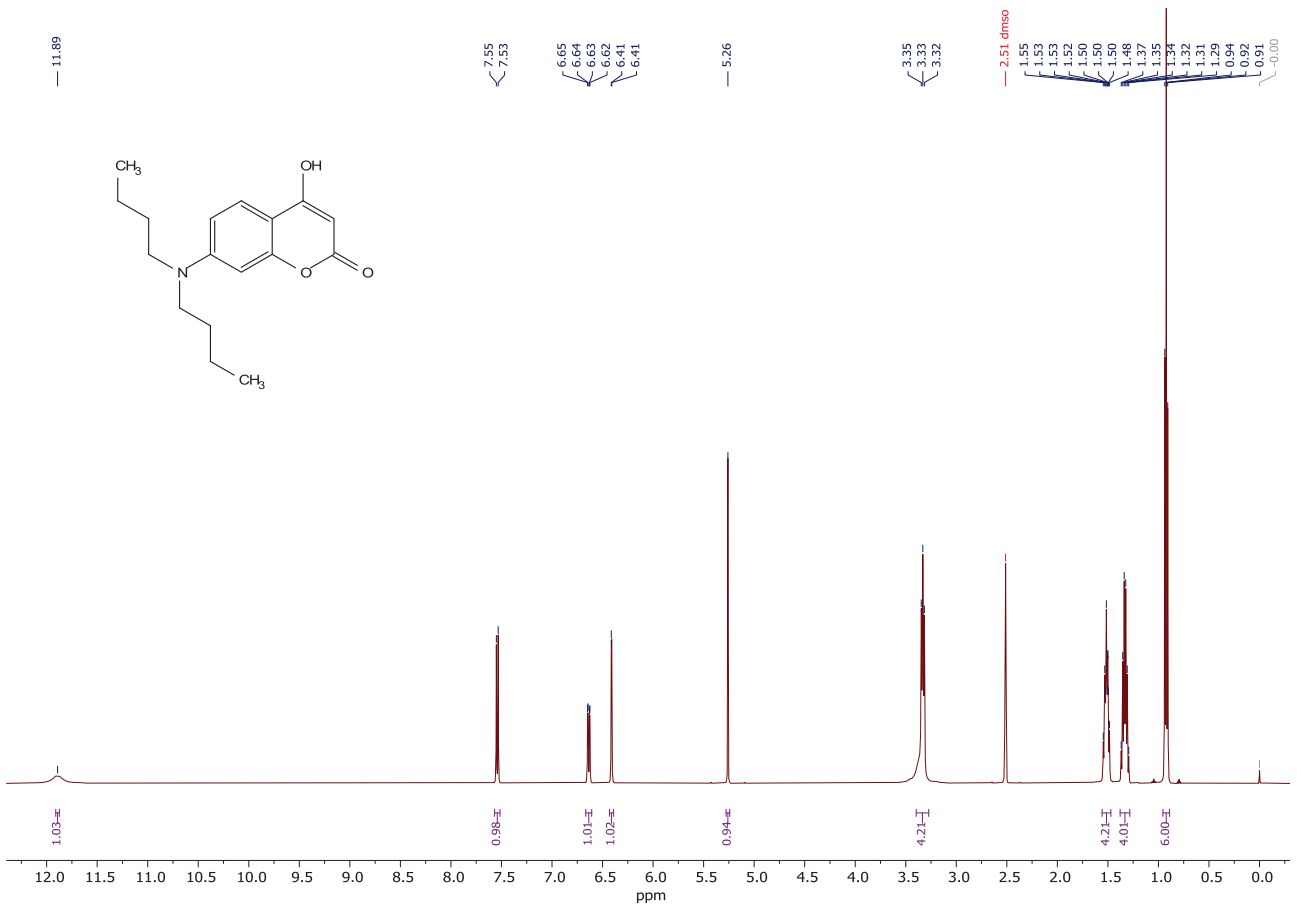
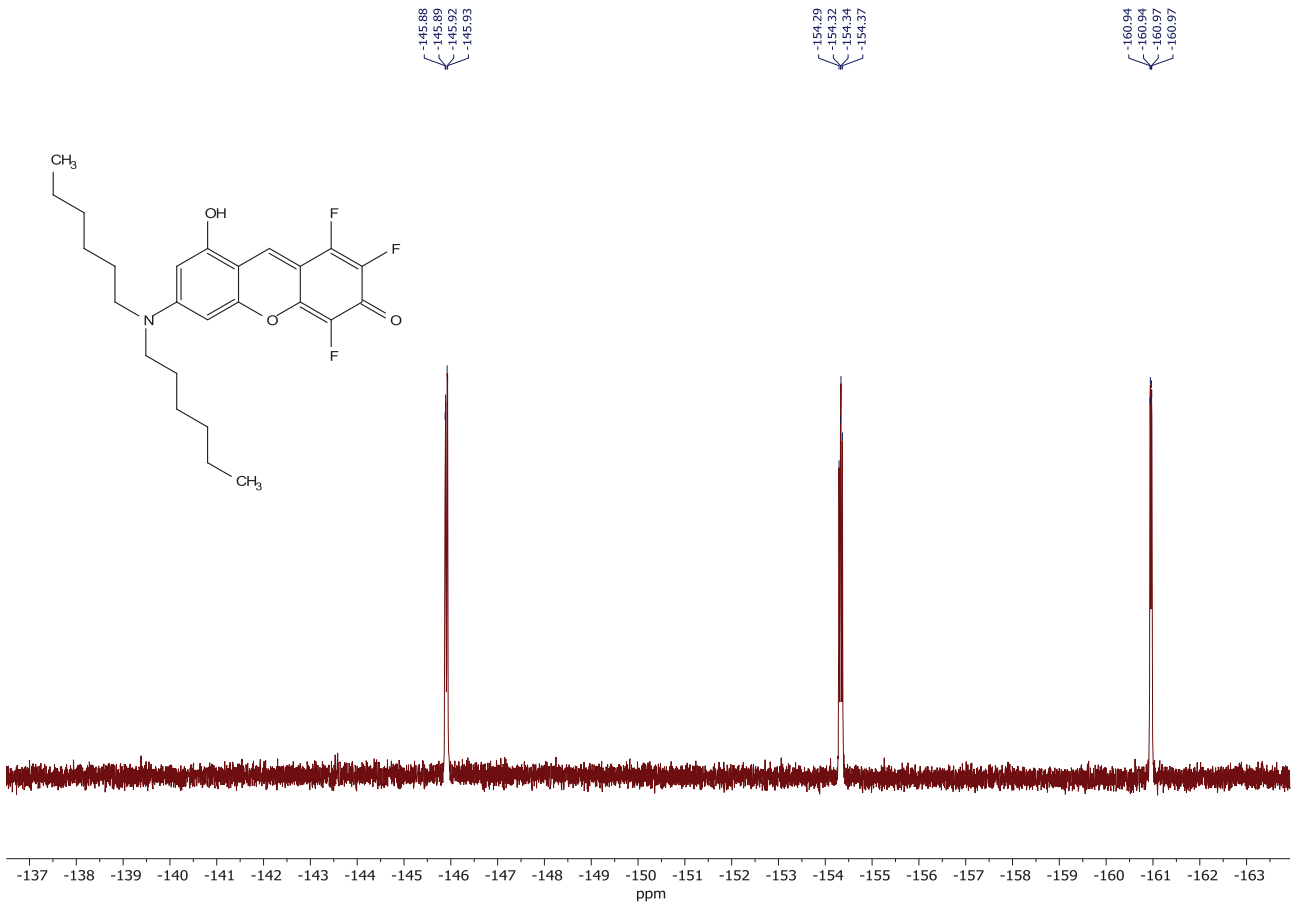


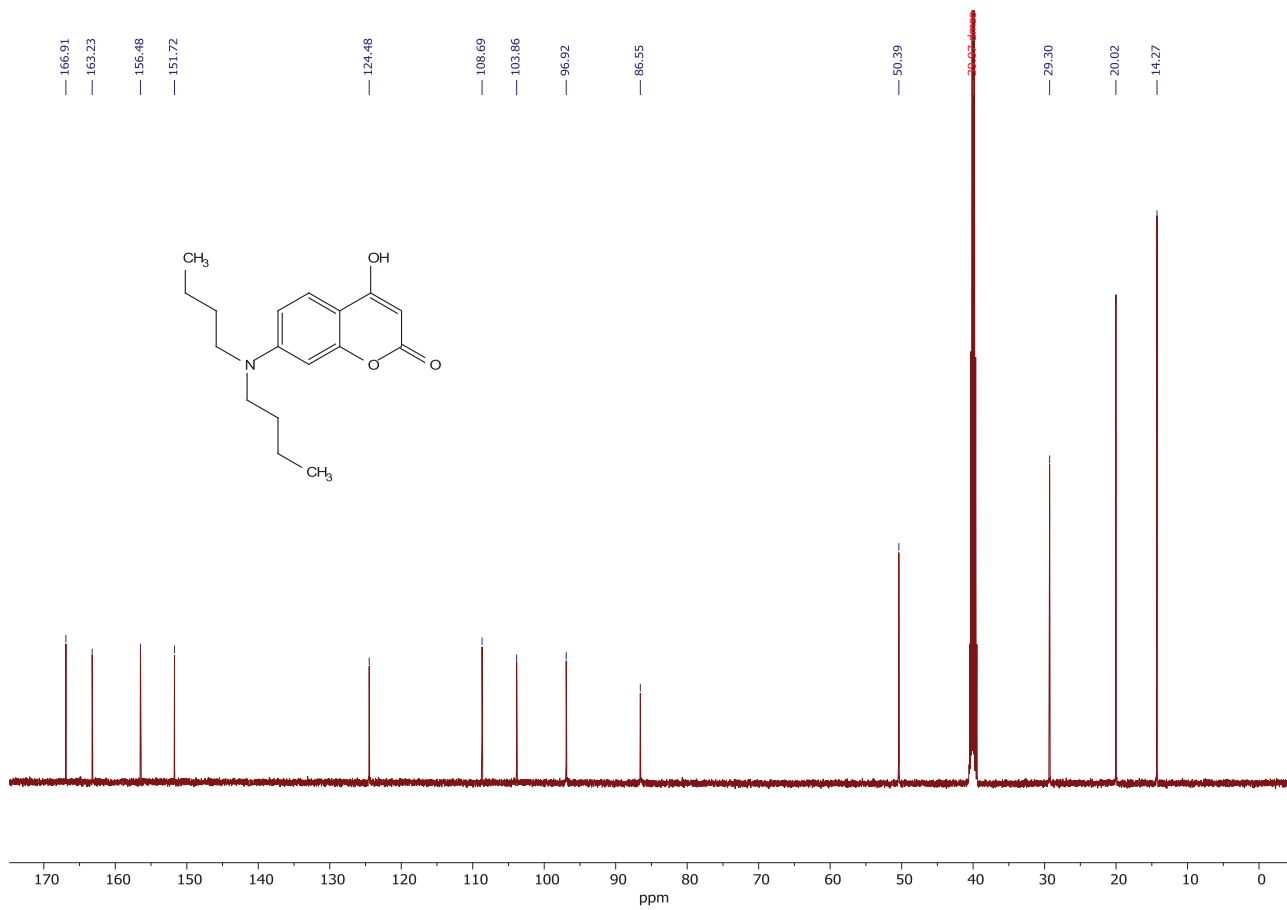


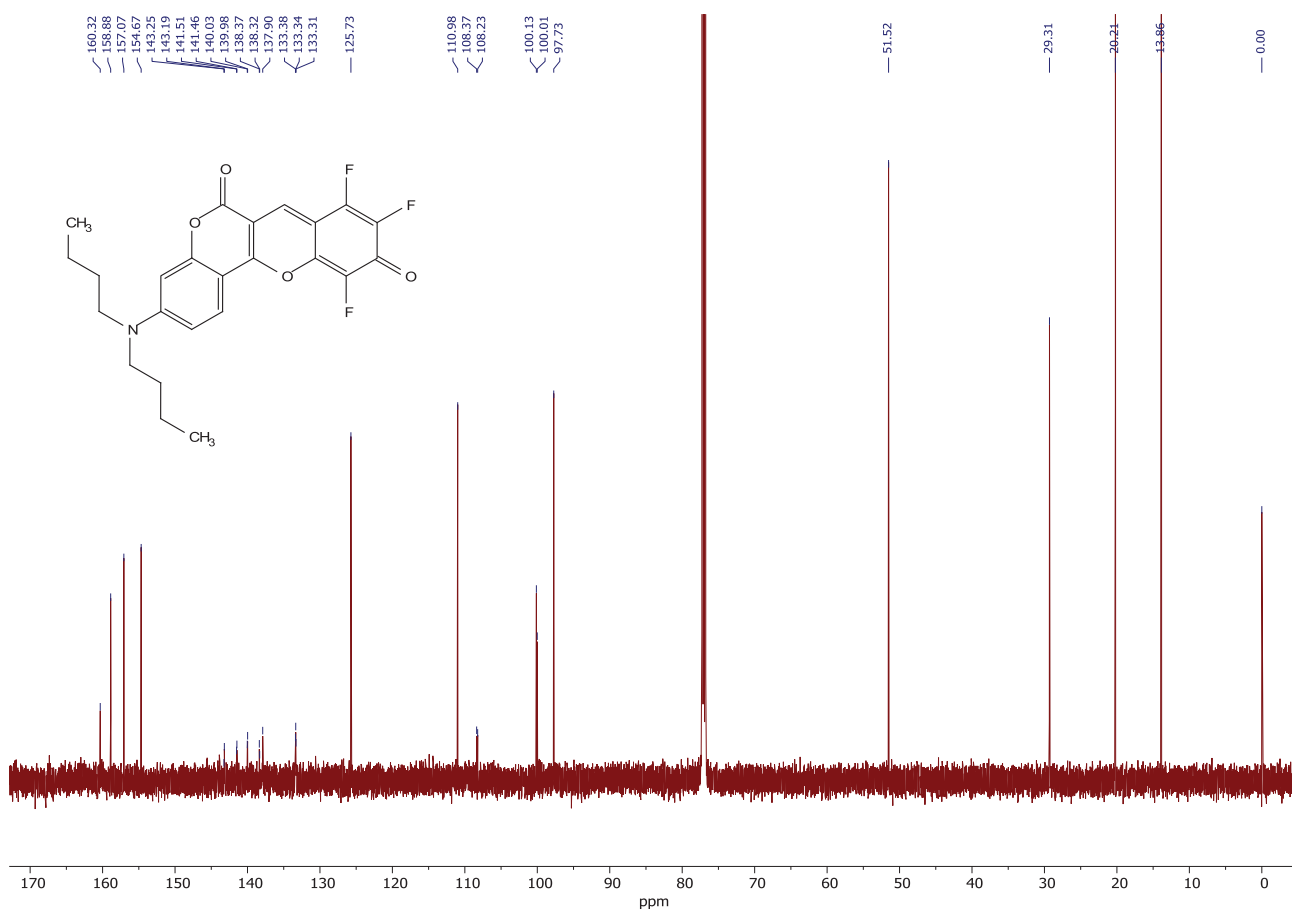
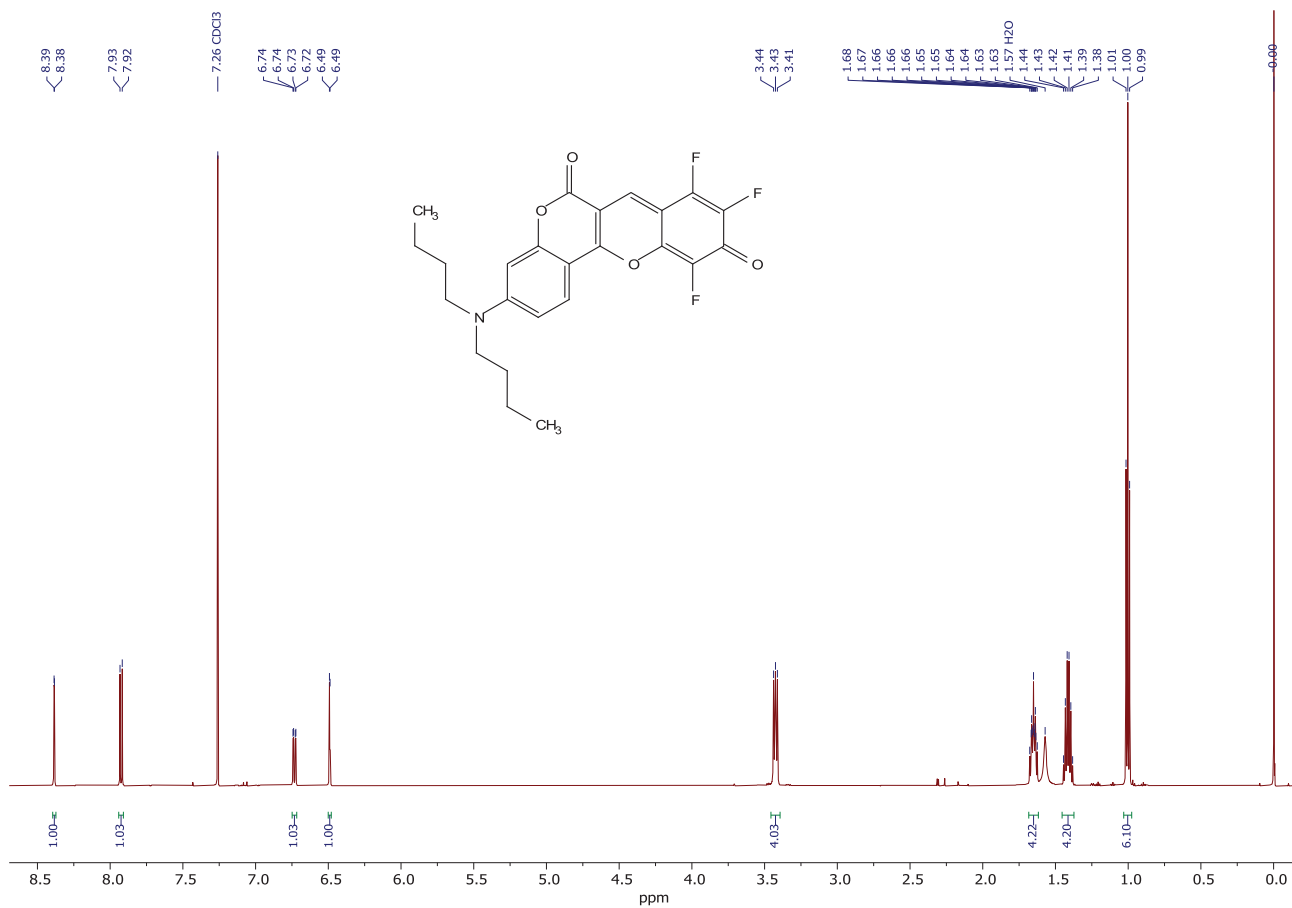


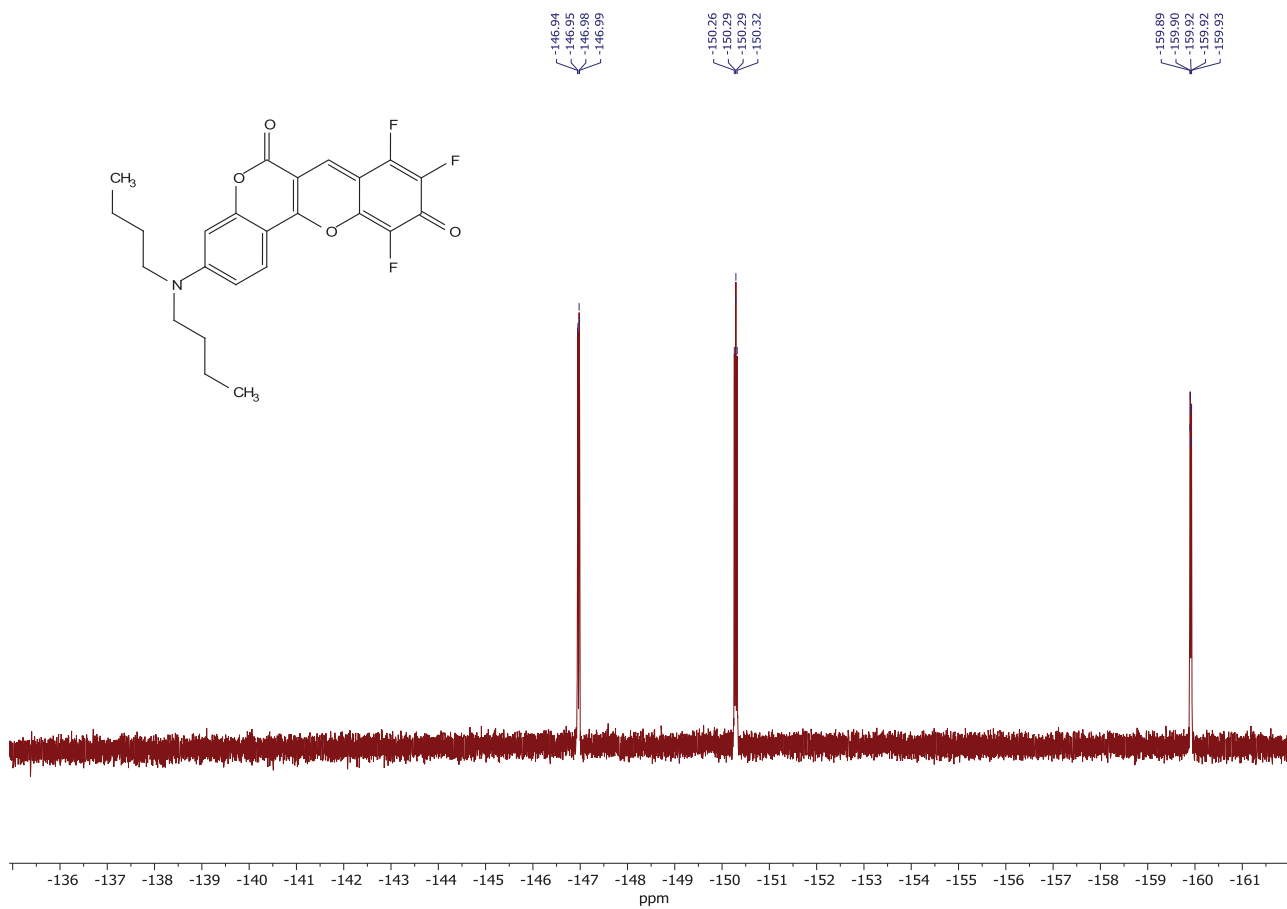


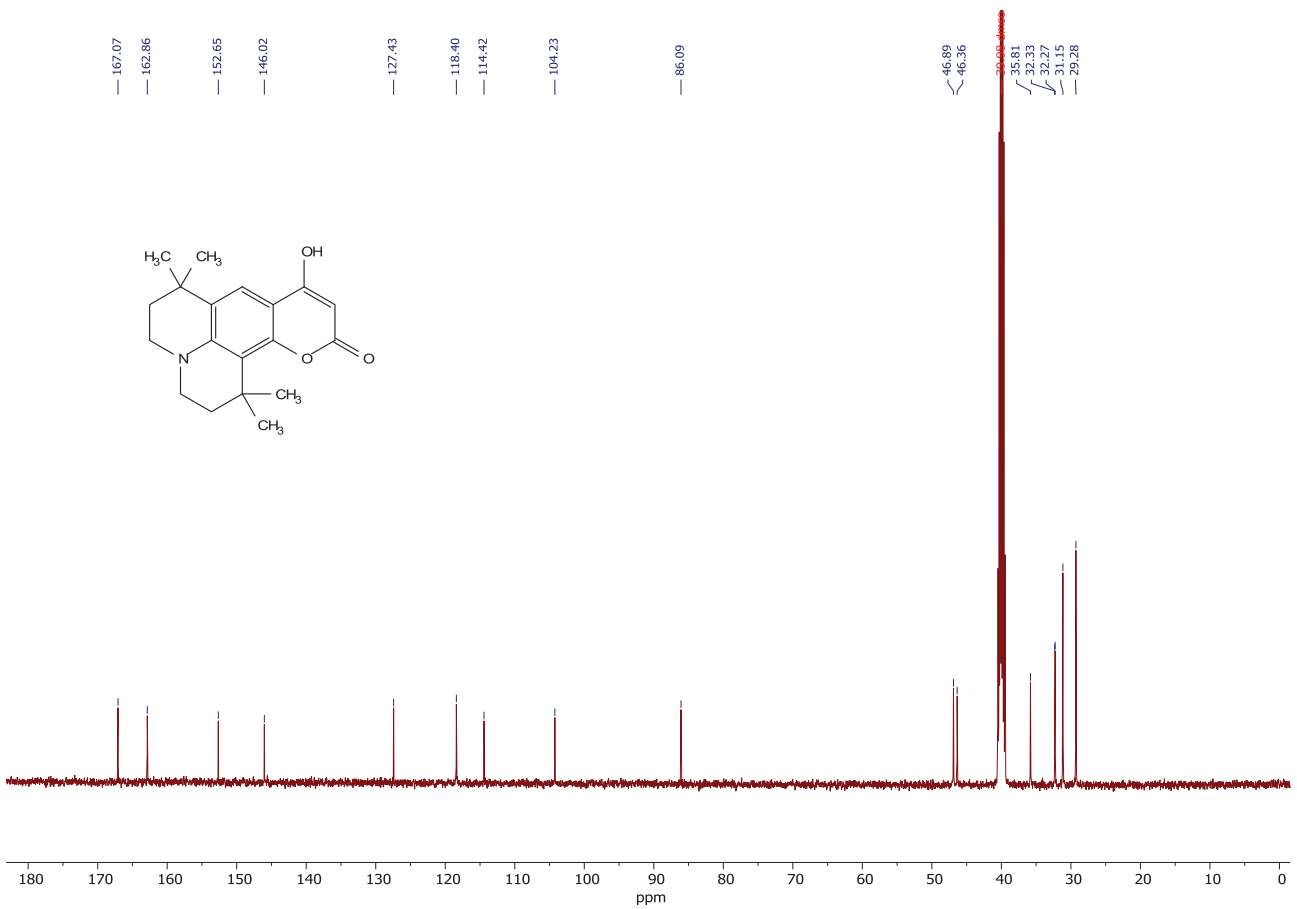
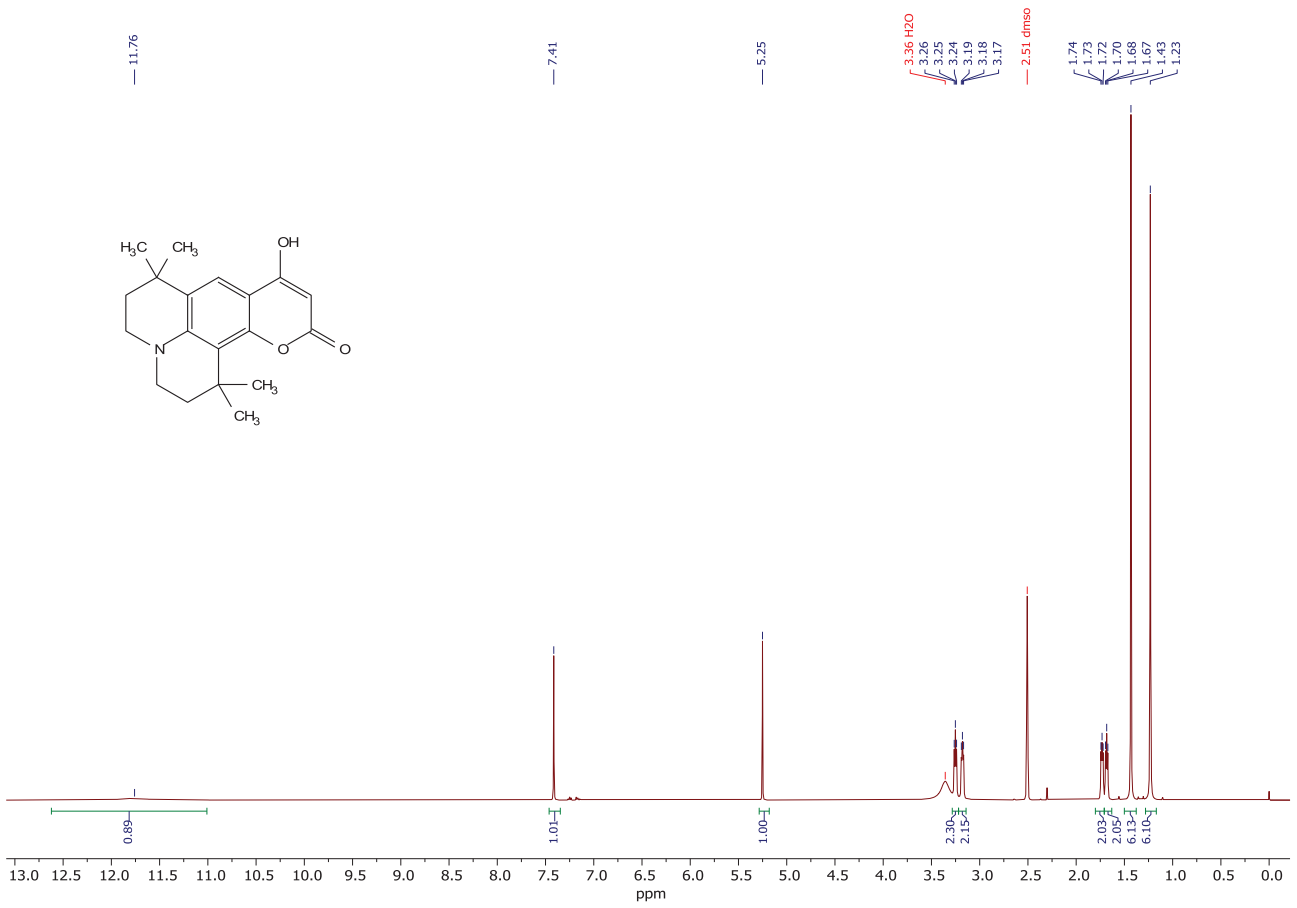


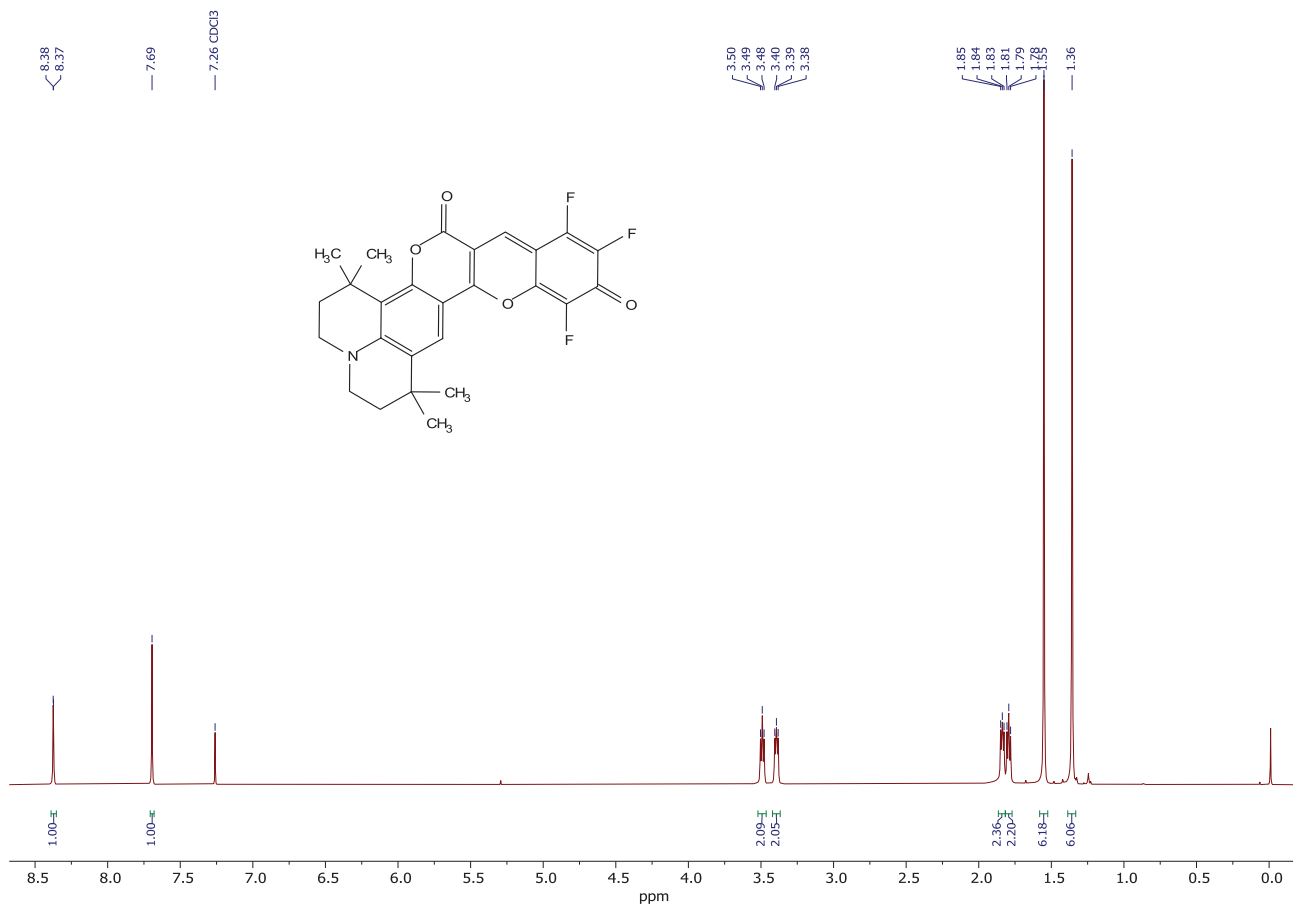


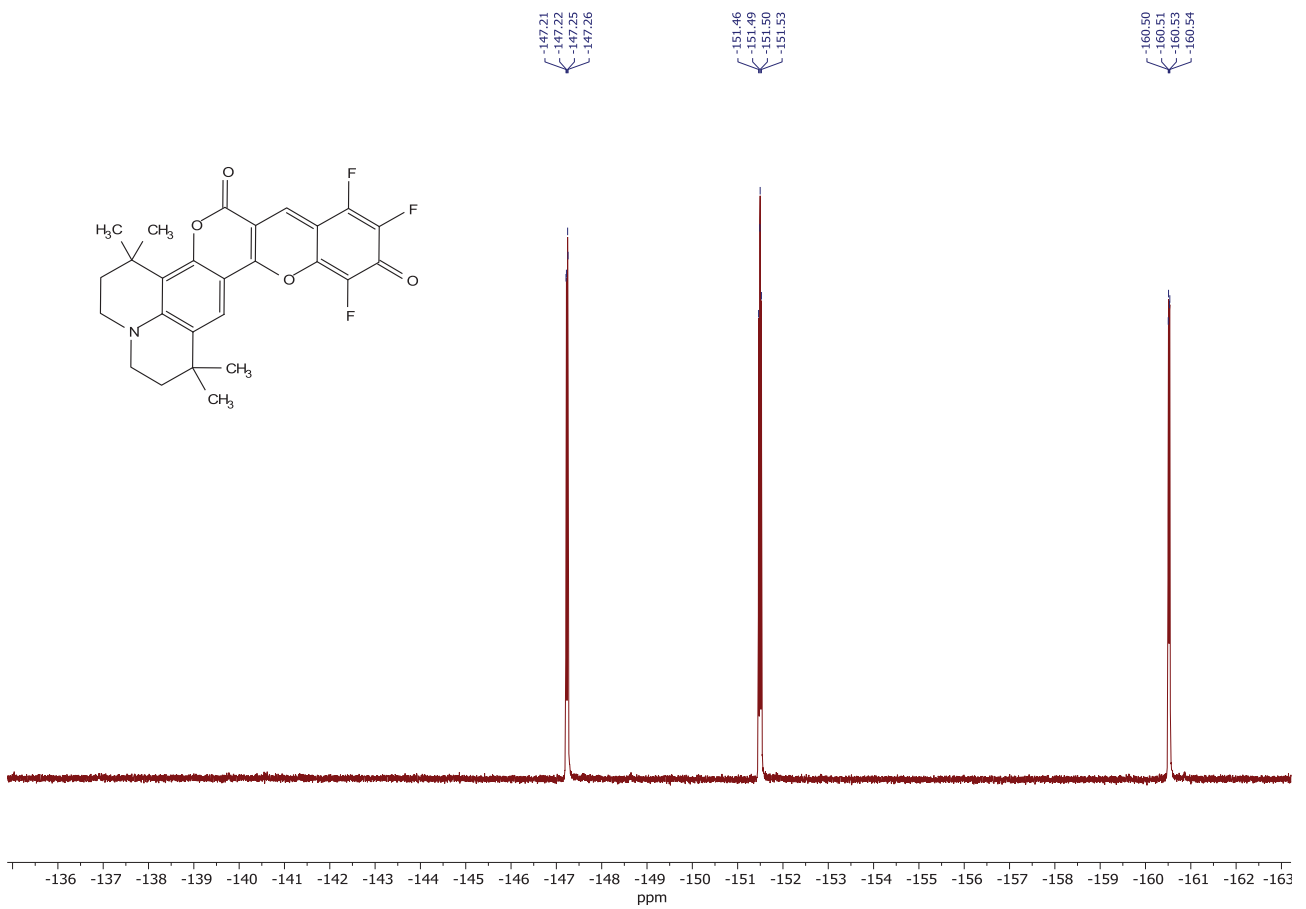
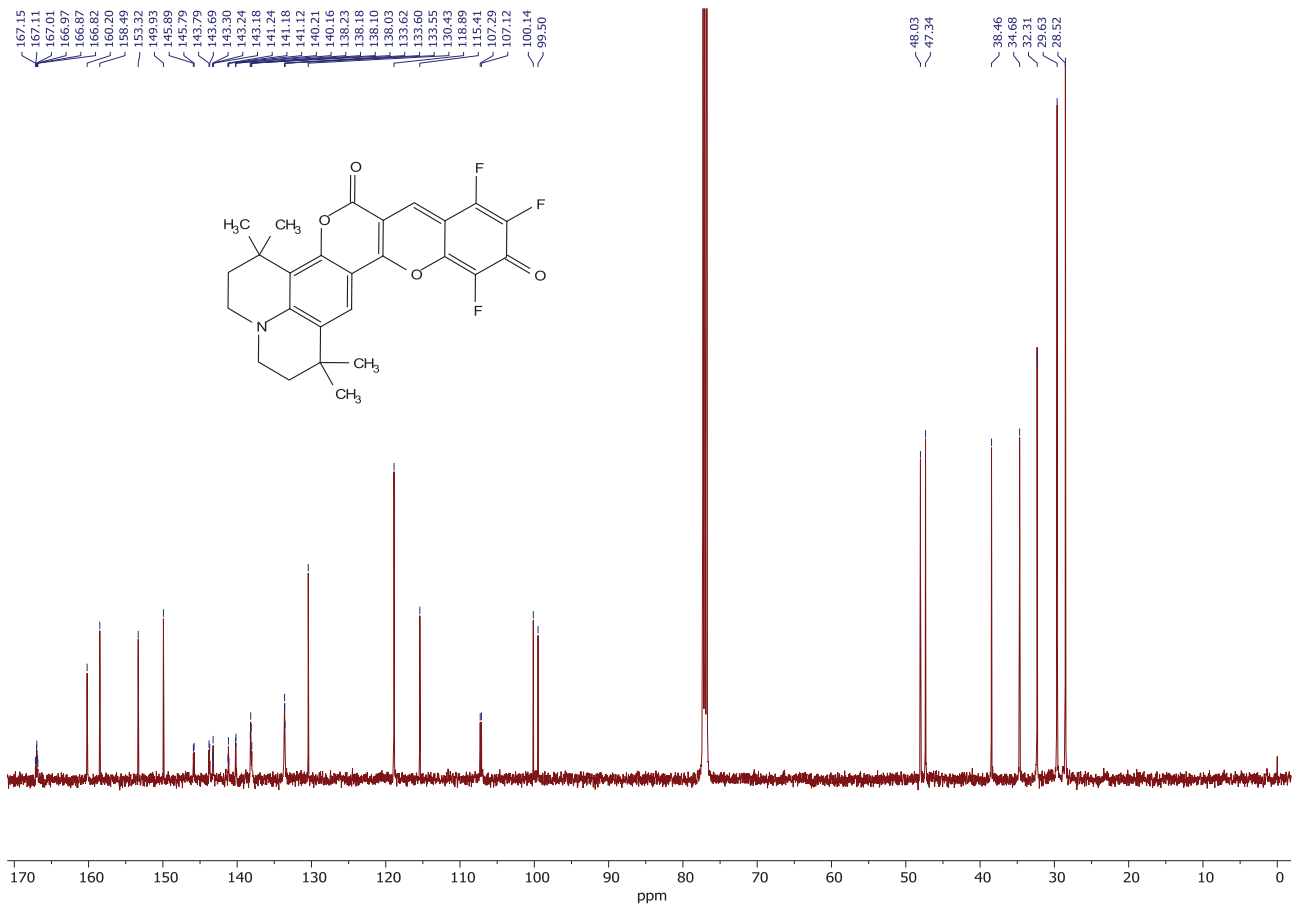


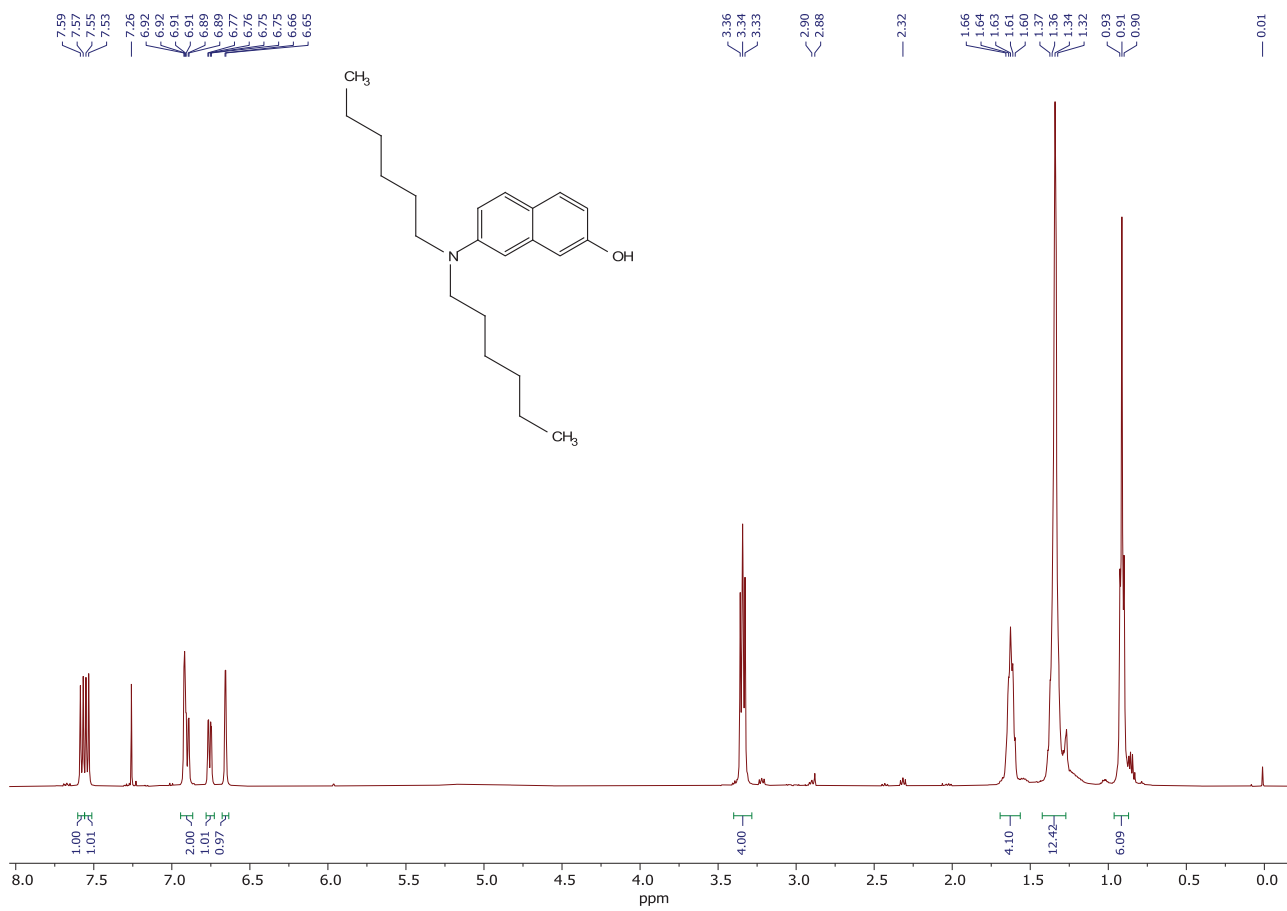


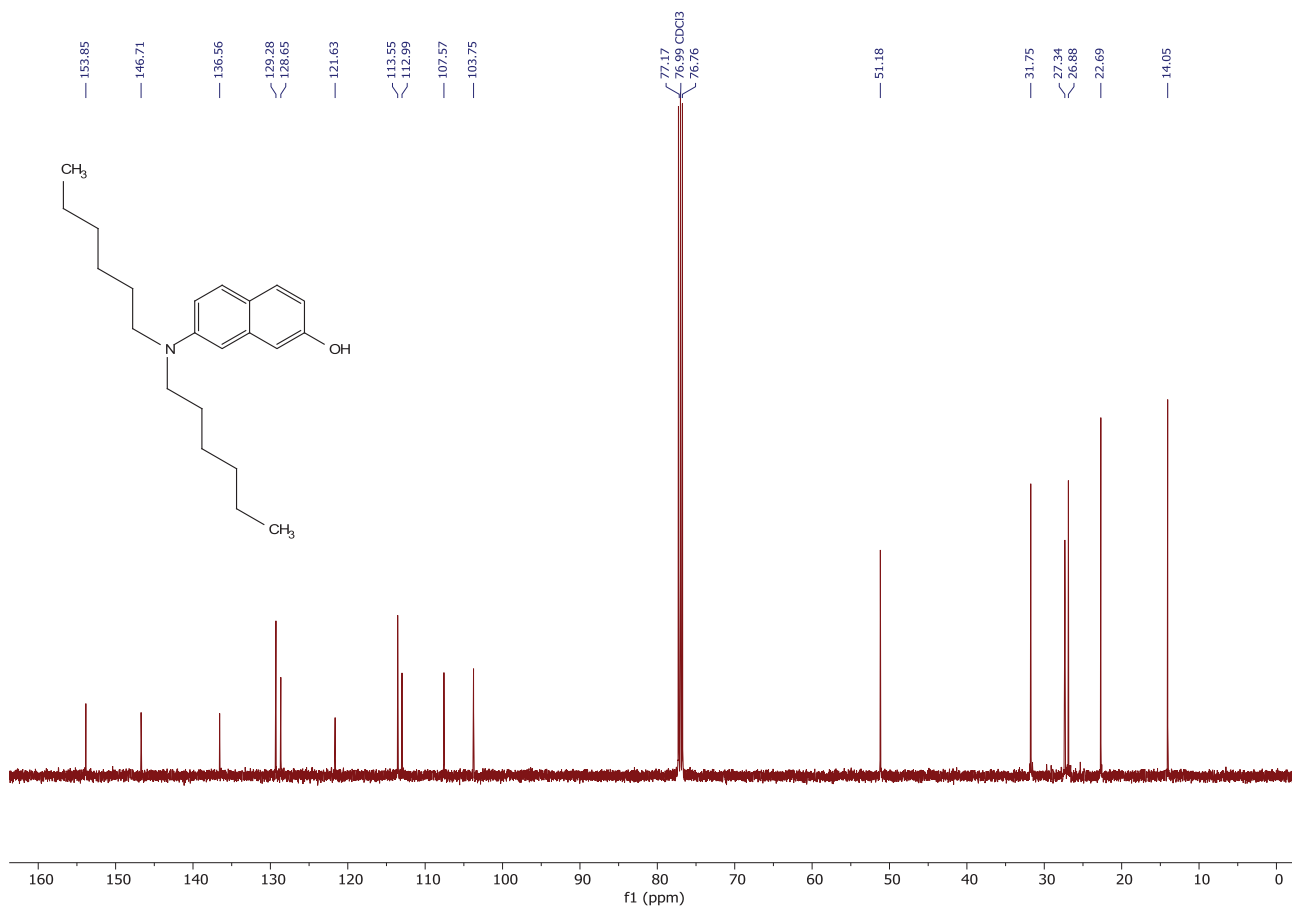


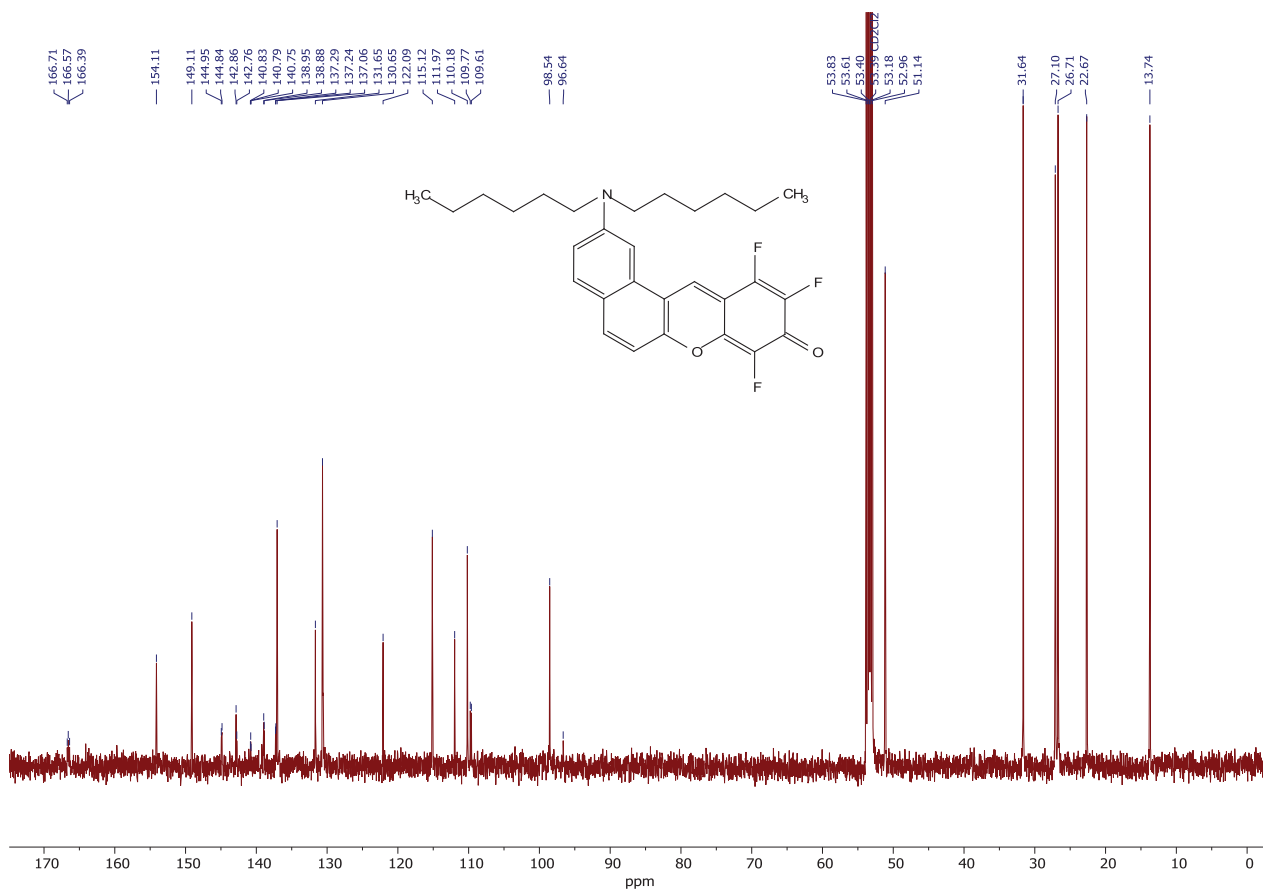
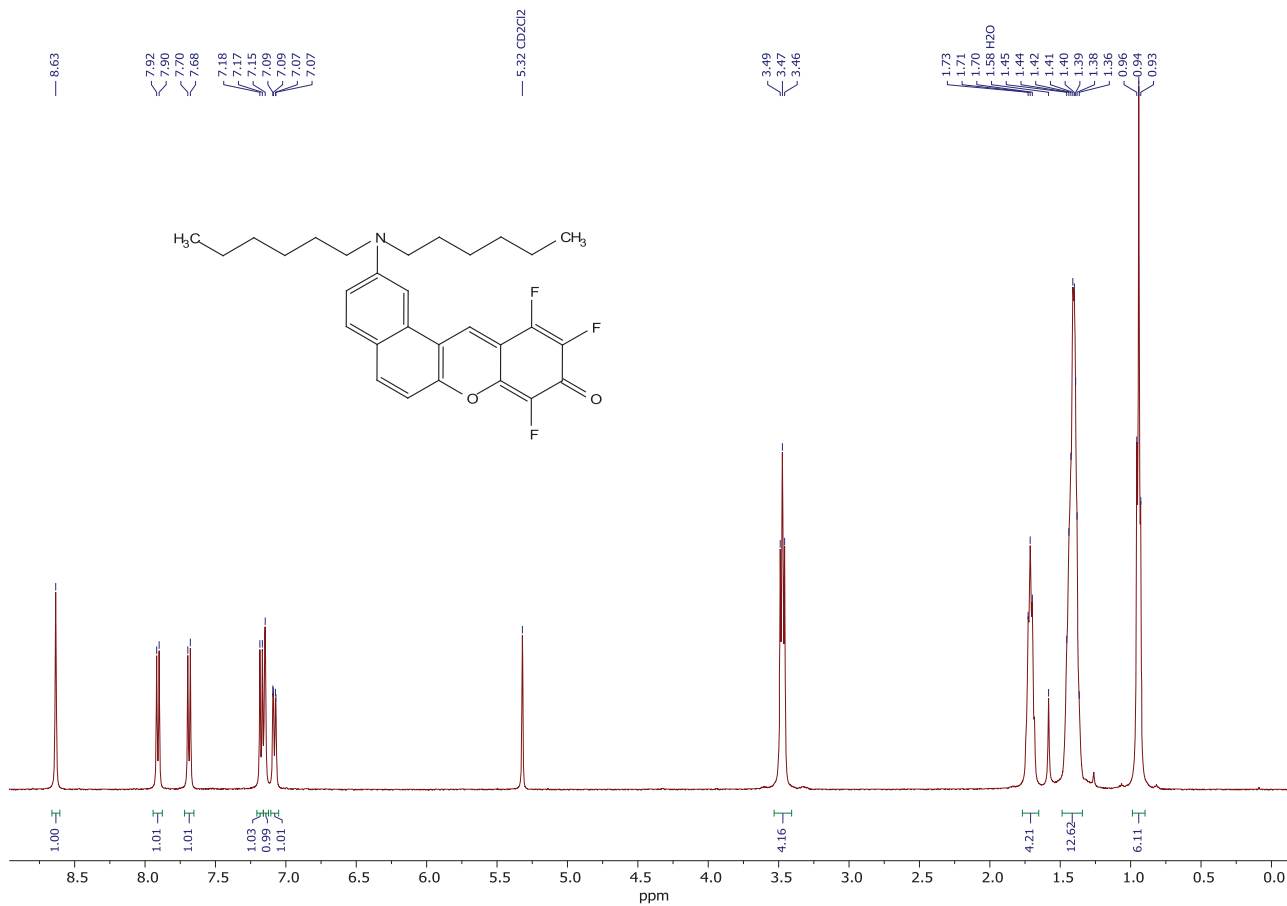


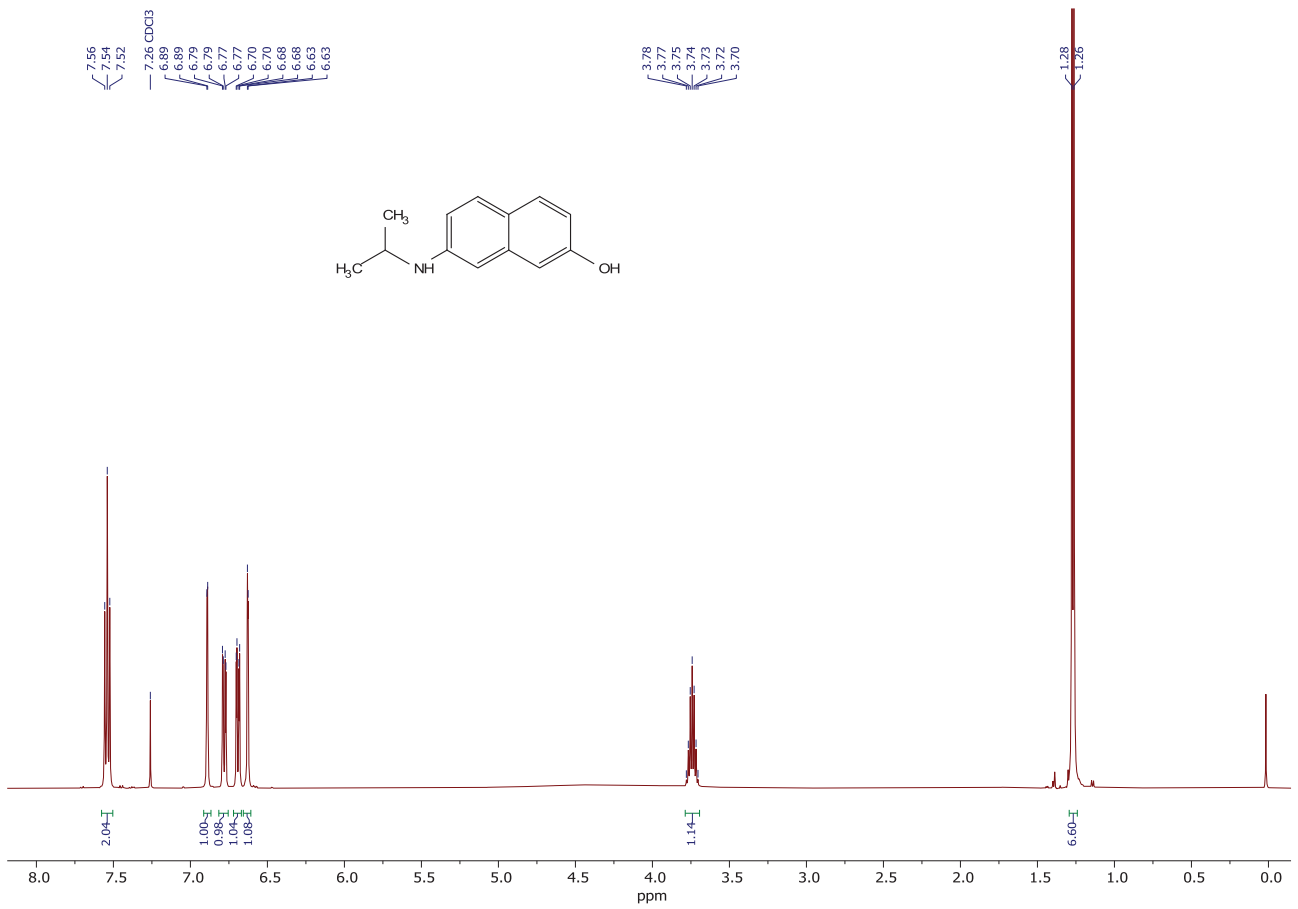
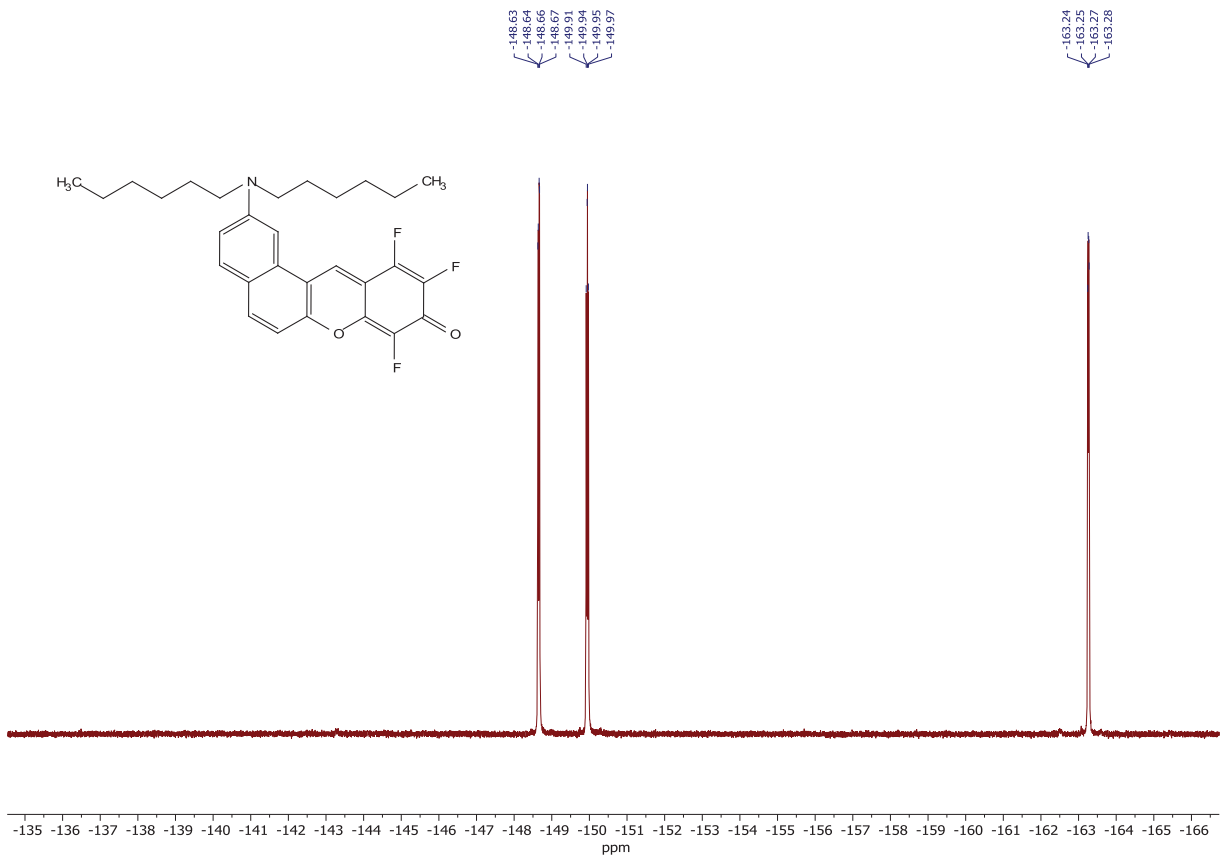


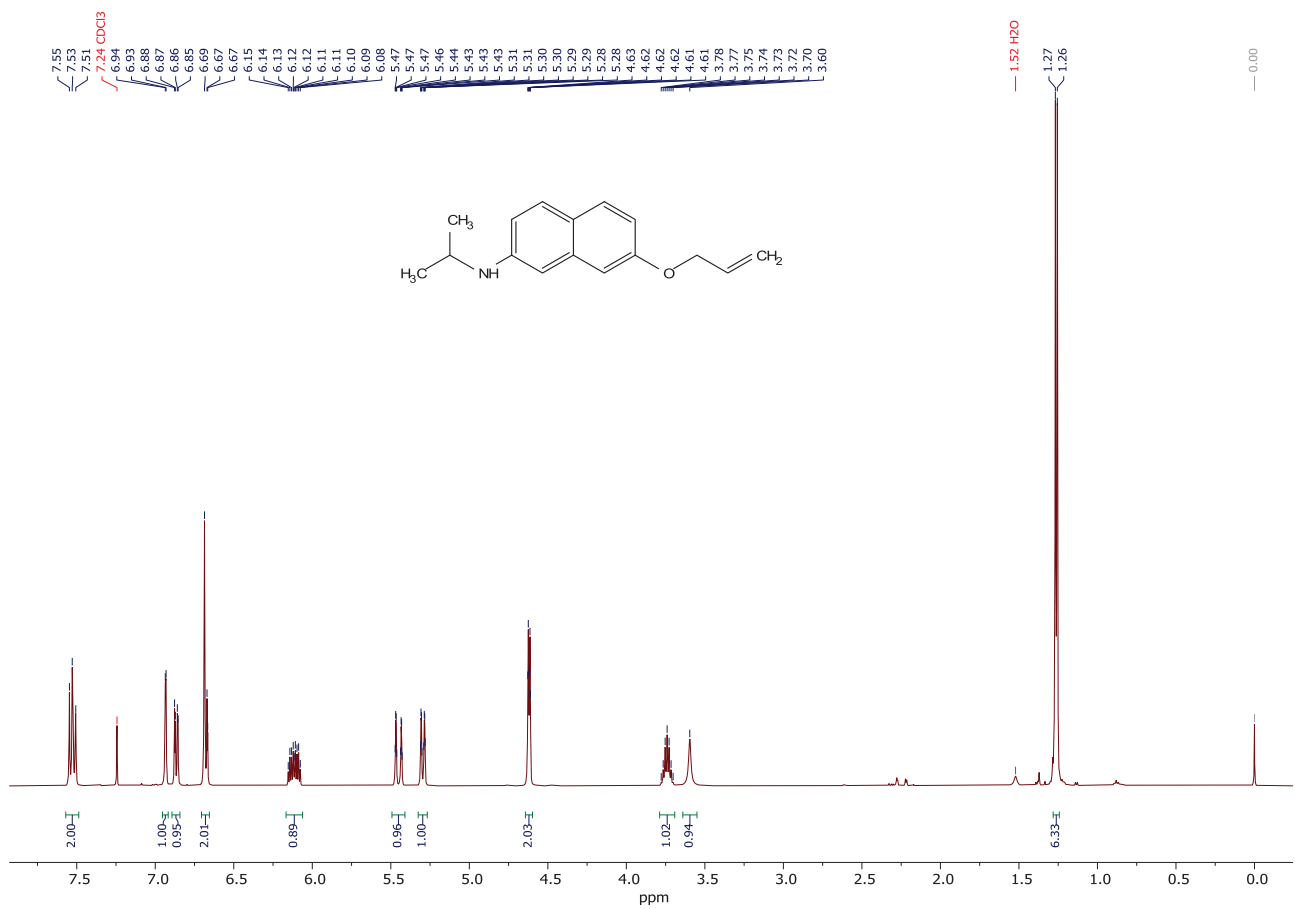
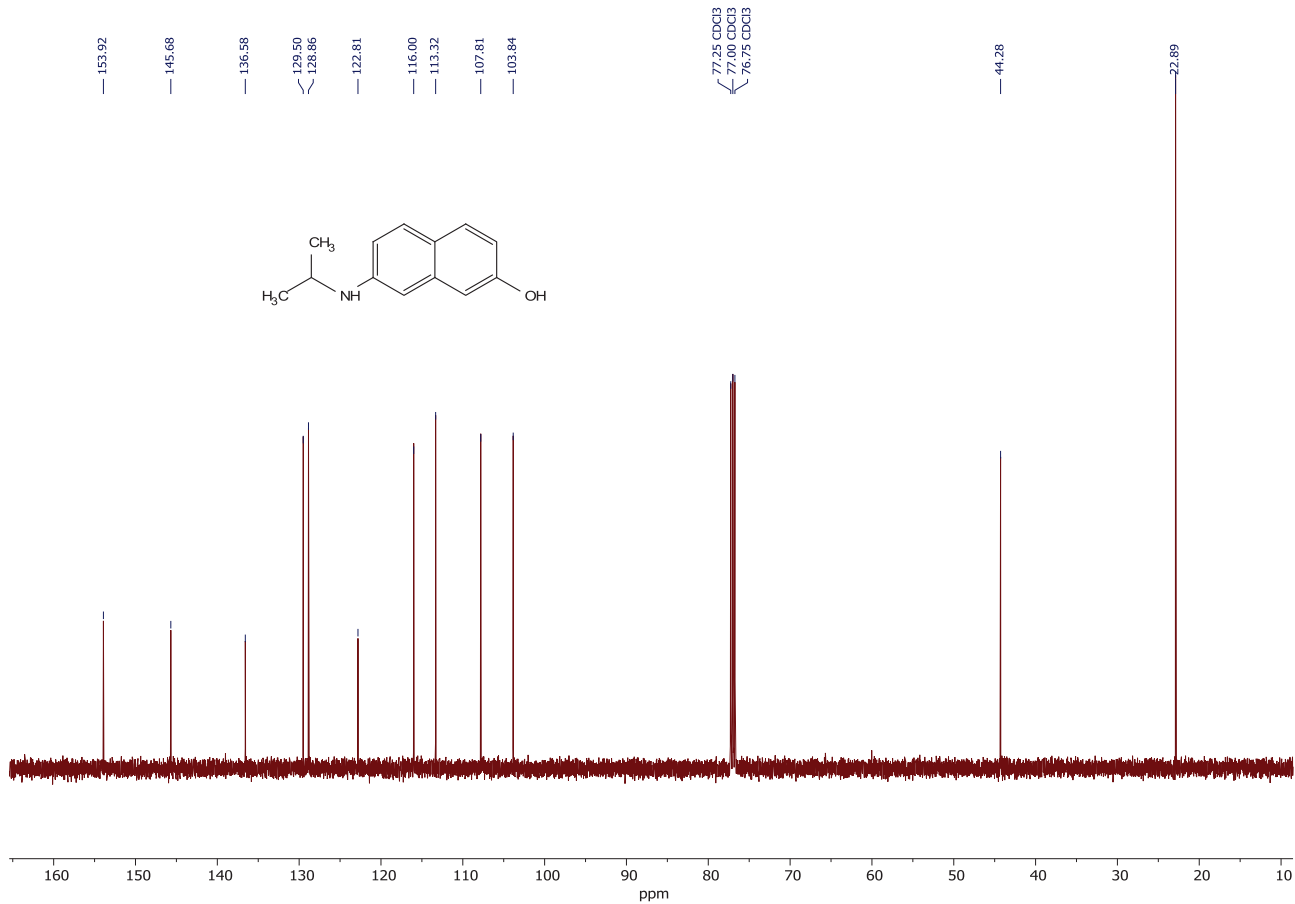


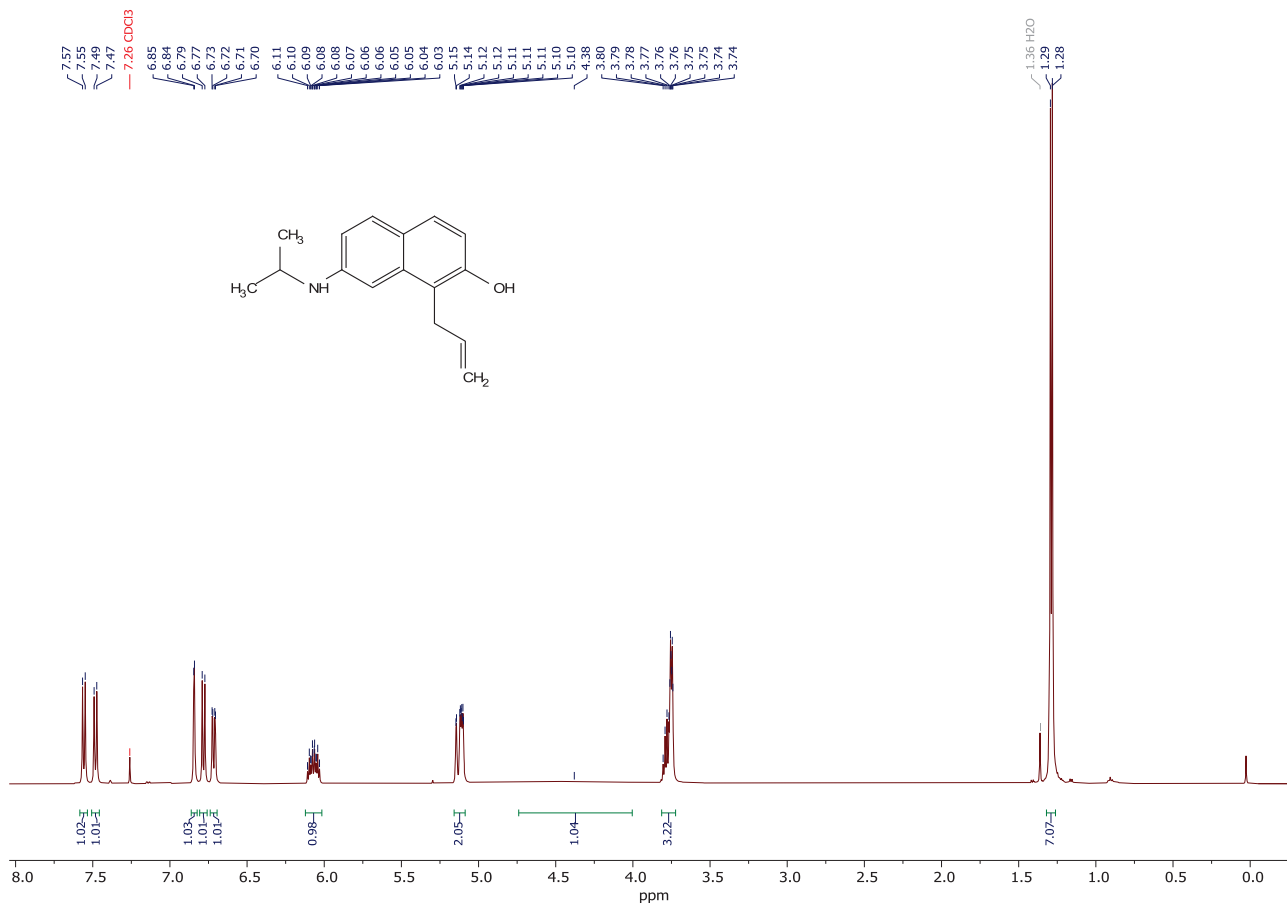
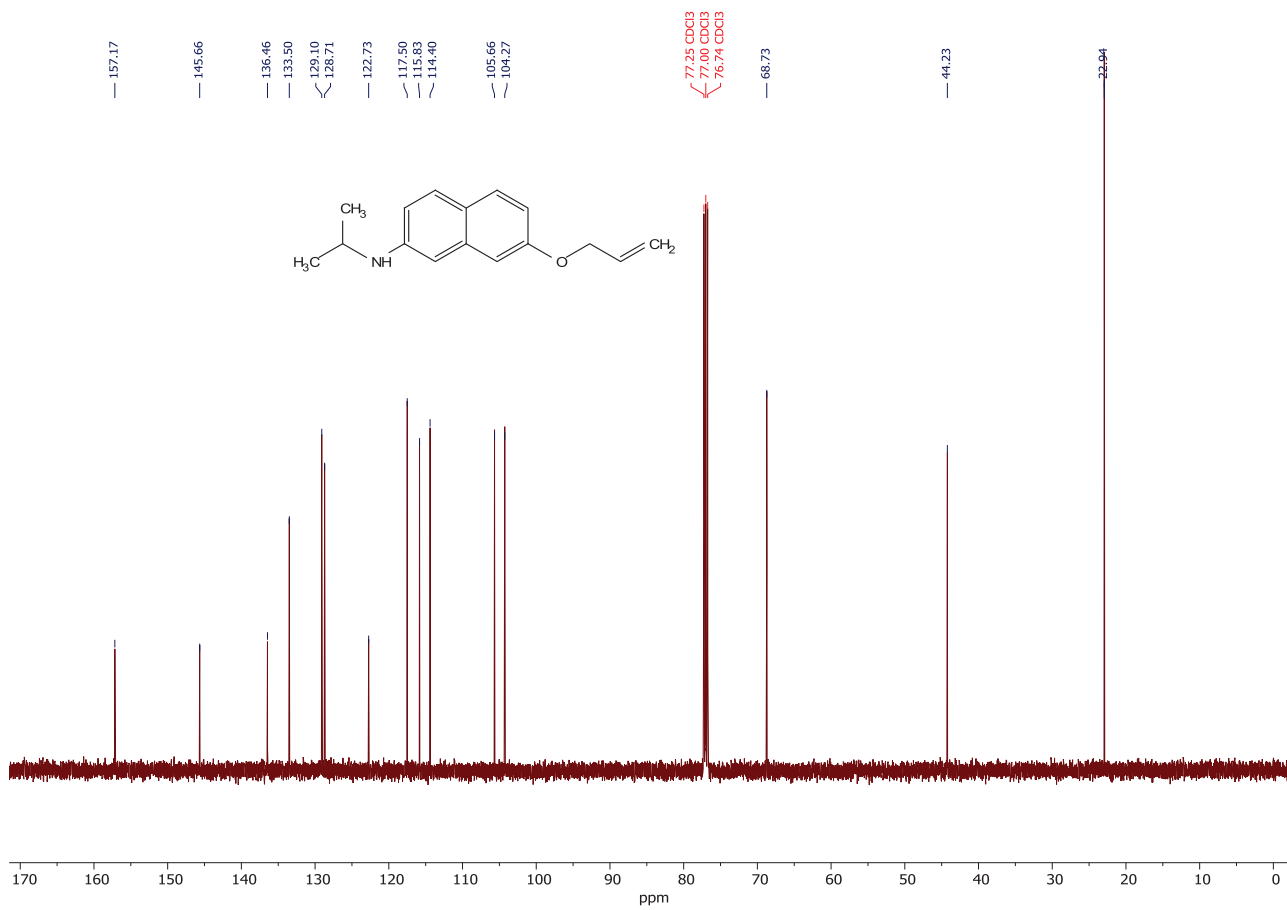


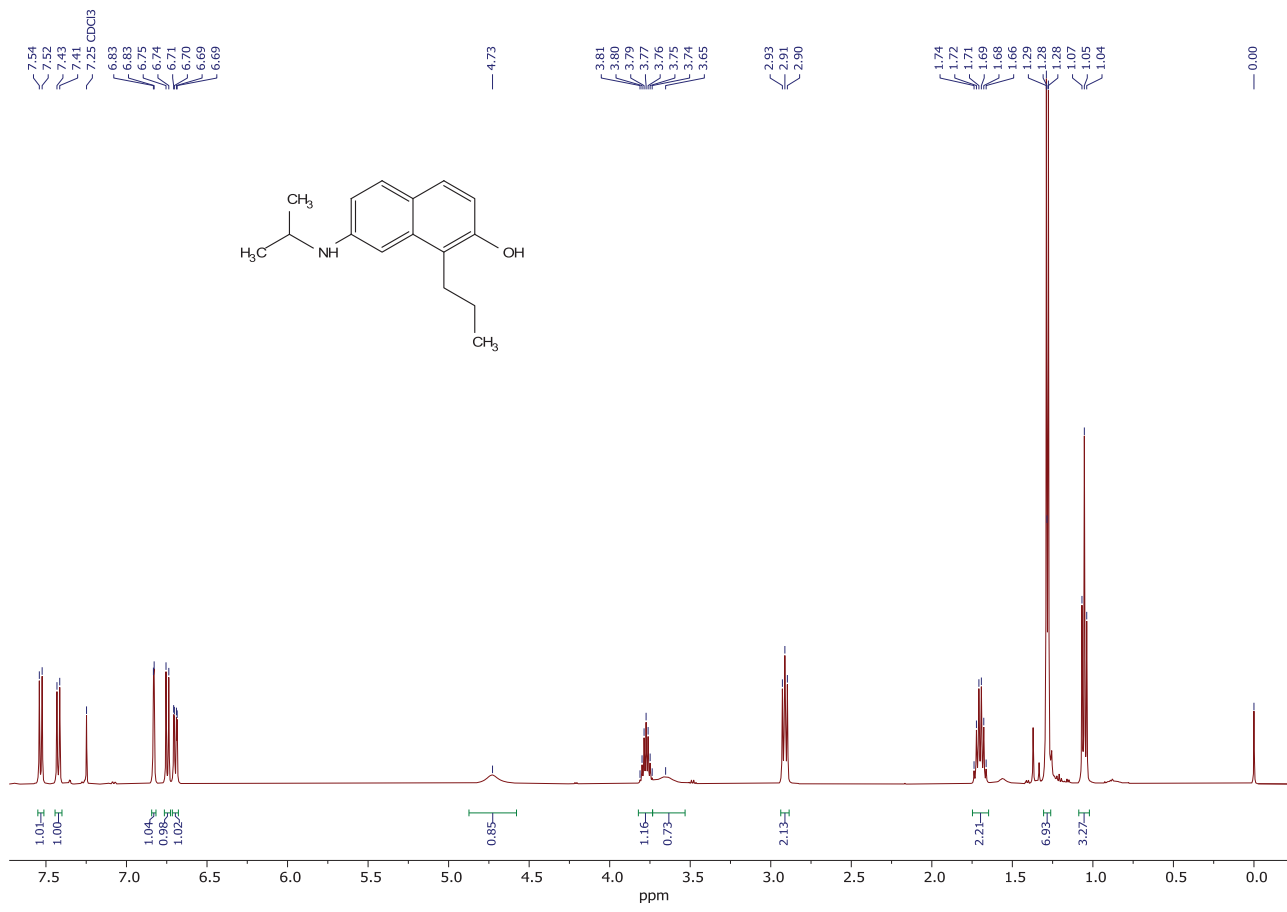
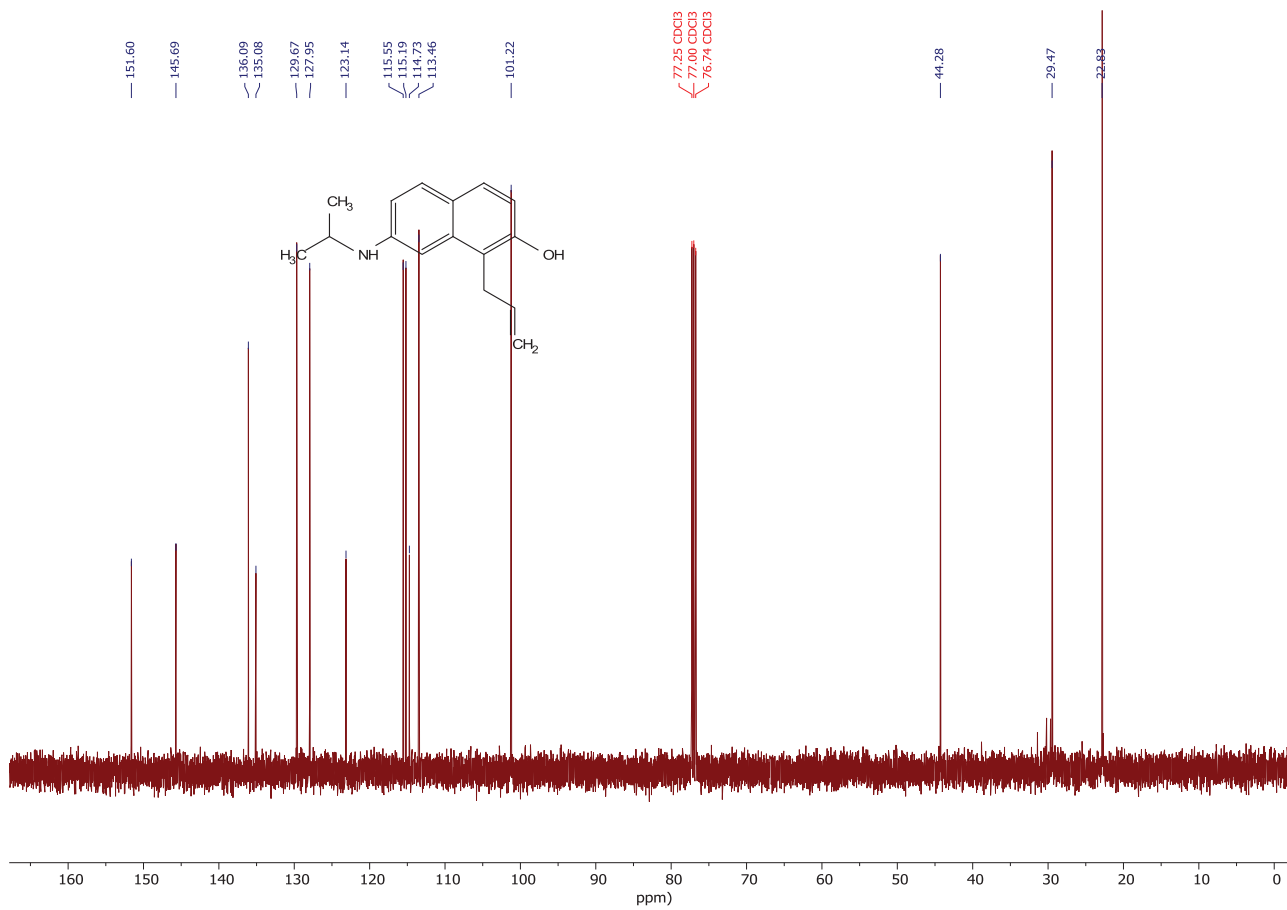


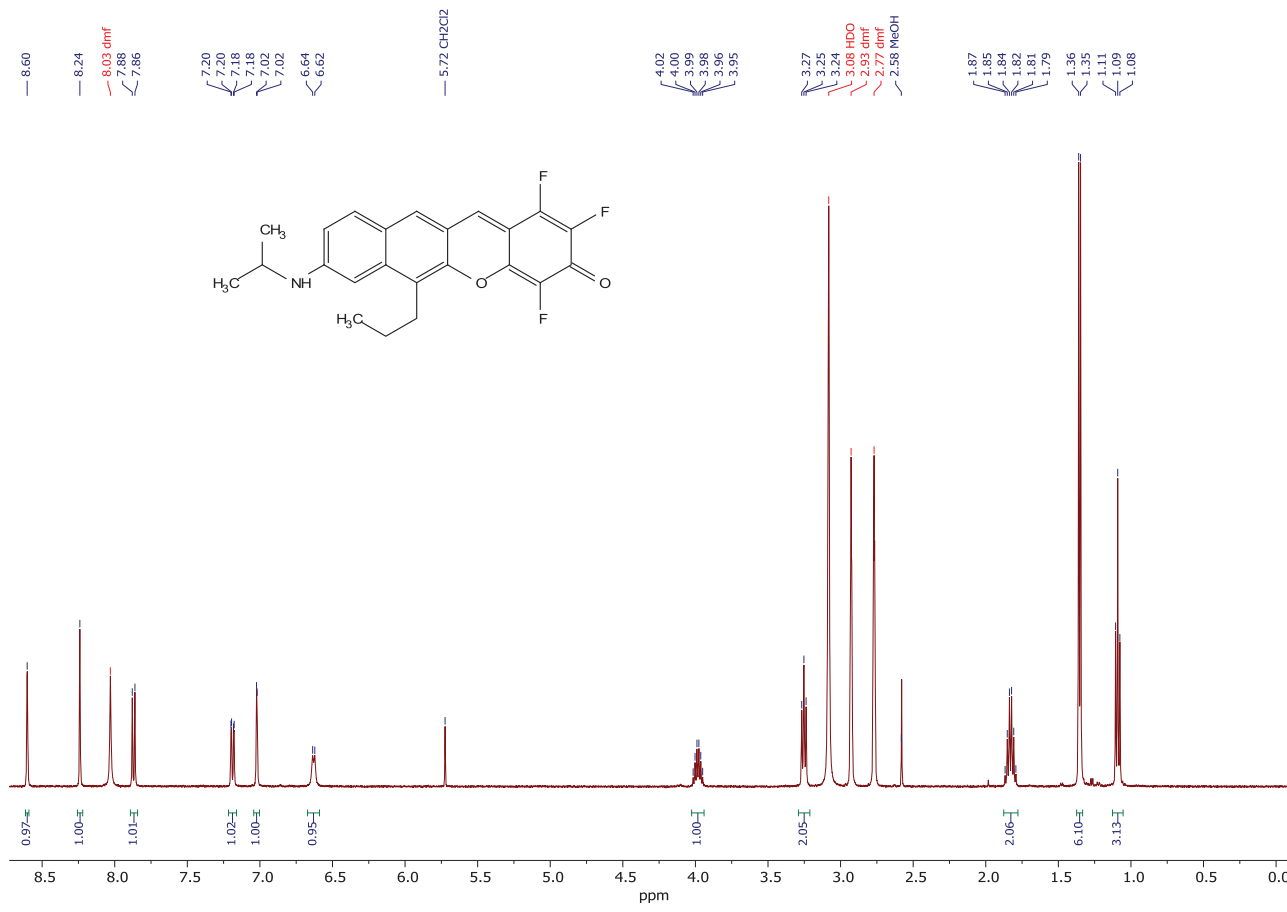
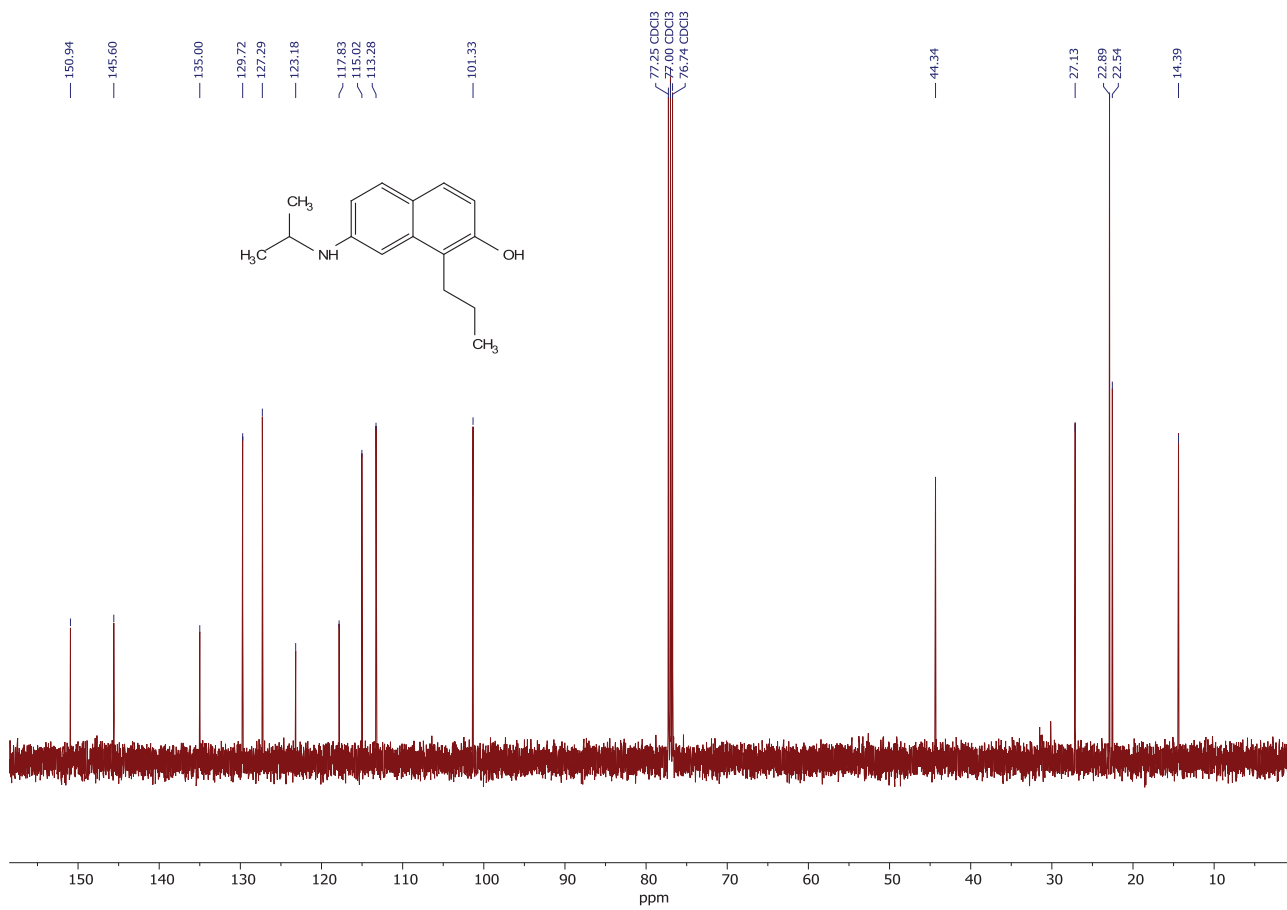


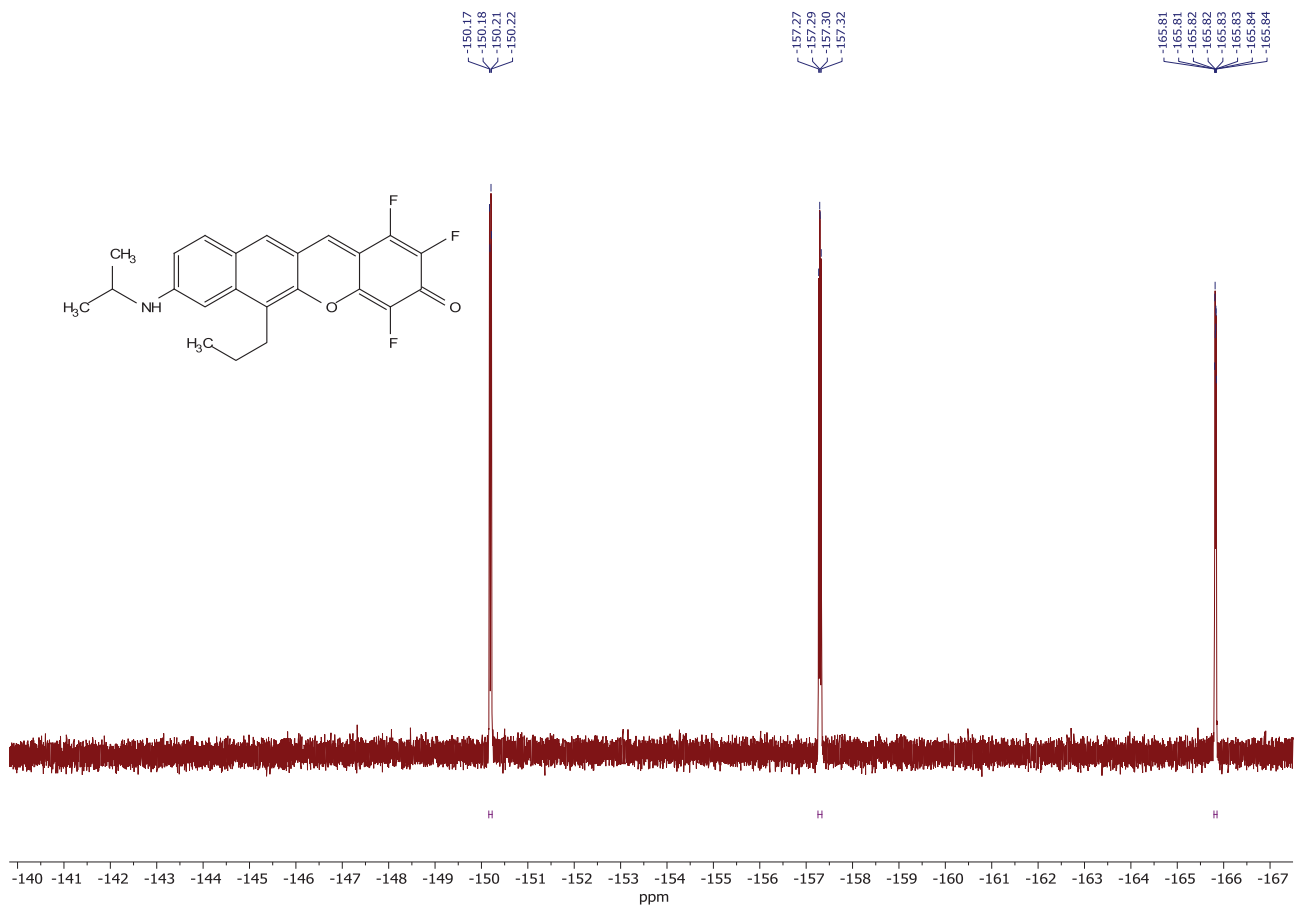
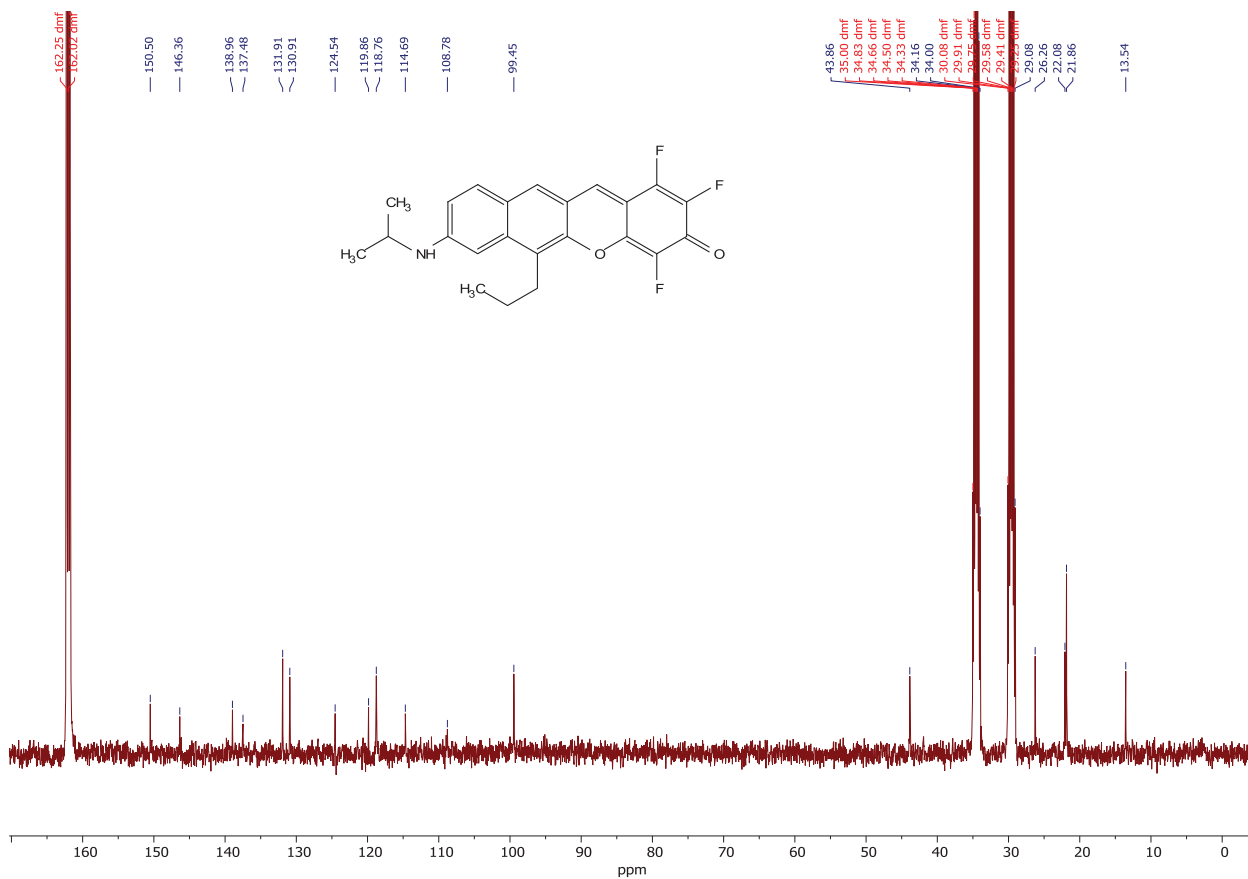




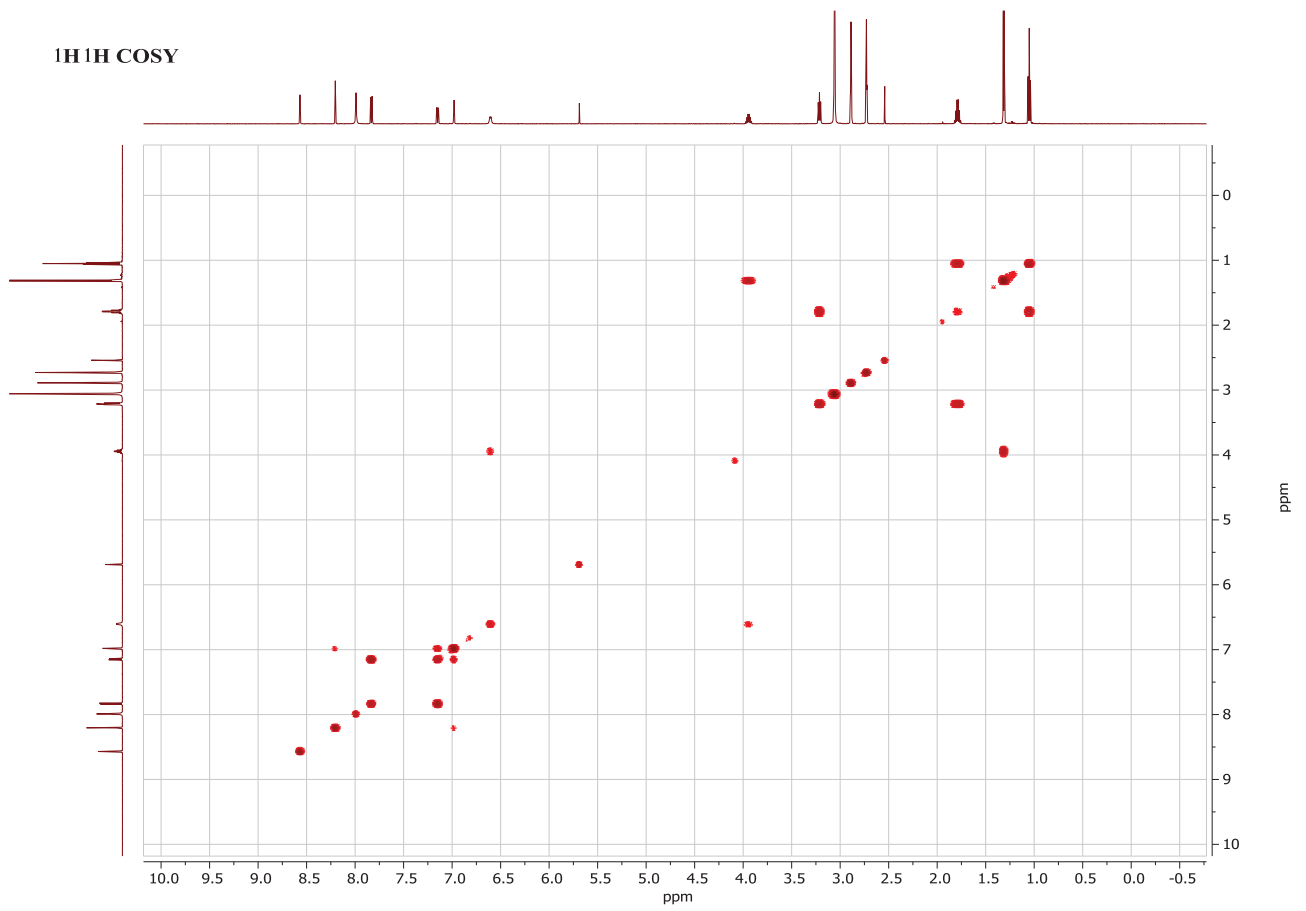




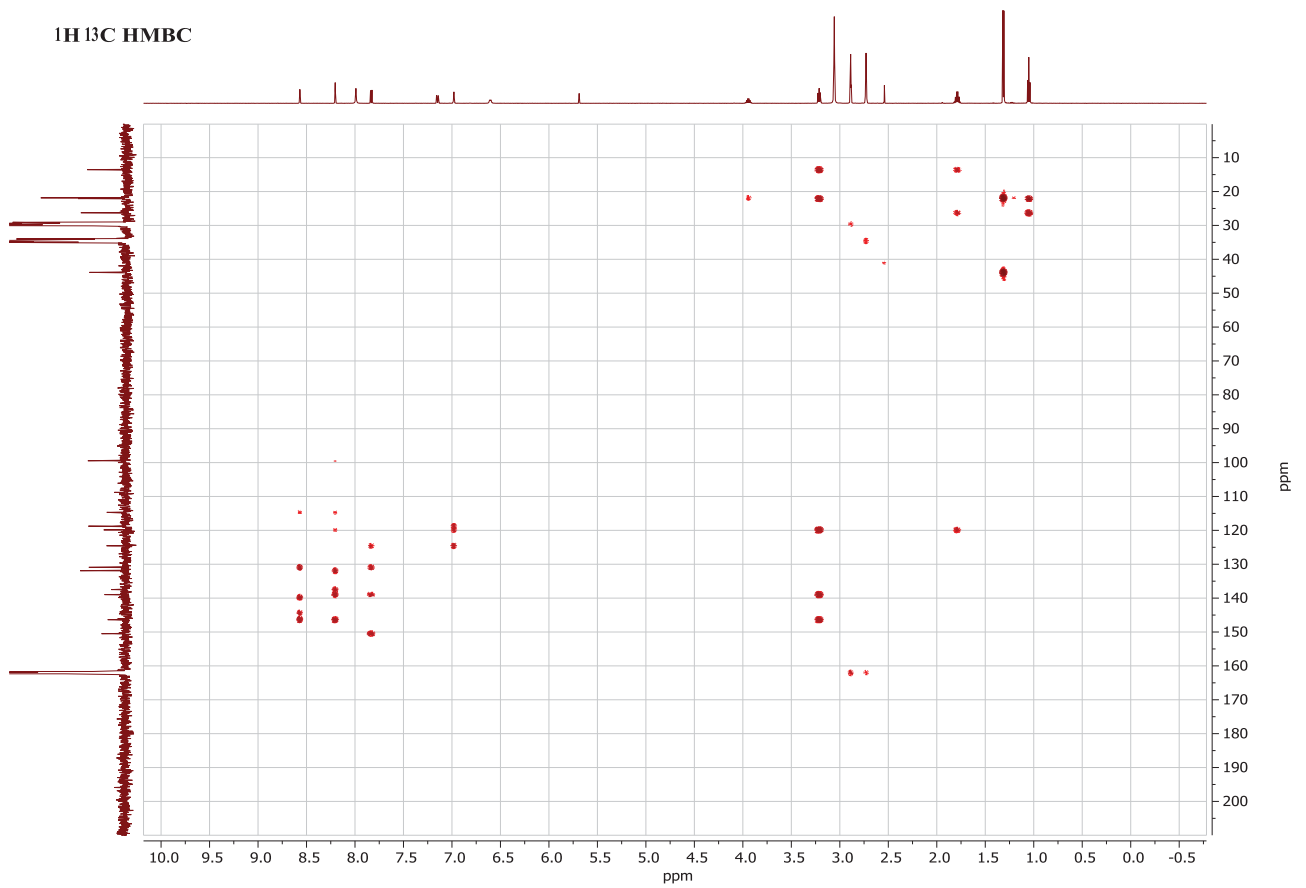


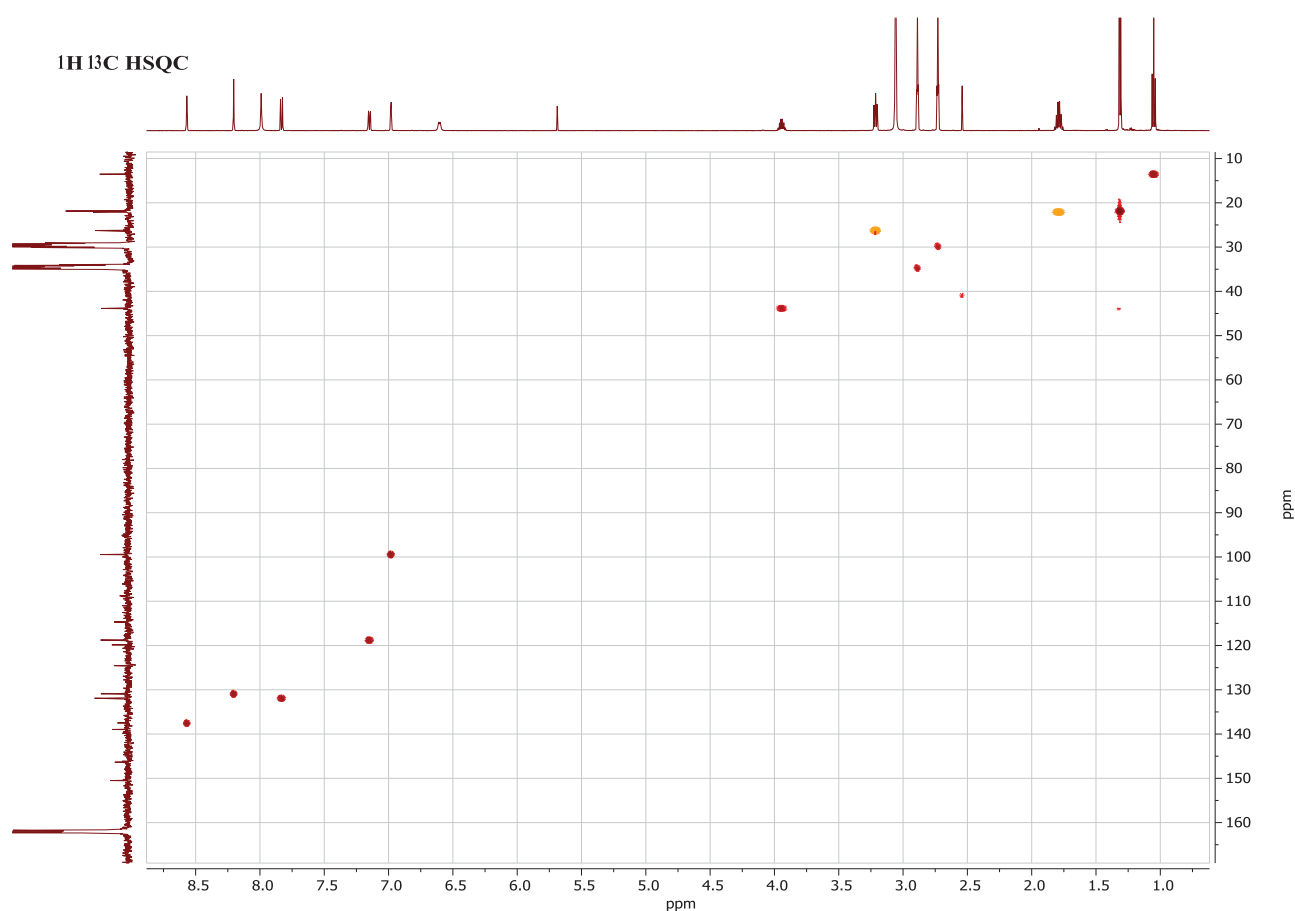


¹H ¹H COSY



¹H ¹³C HMBIC





1.1.3 X-Ray crystallography analysis of compound 16

The X-ray measurement of 16 was performed at 130.0(5) K on a Bruker D8 Venture PhotonII diffractometer equipped with a TRIUMPH monochromator and a MoK α fine focus sealed tube ($\lambda = 0.71073 \text{ \AA}$). A total of 2372 frames were collected with Bruker APEX3 program.⁴ The frames were integrated with the Bruker SAINT software package⁵ using a narrow-frame algorithm. The integration of the data using a triclinic unit cell yielded a total of 30681 reflections to a maximum θ angle of 27.00° (0.78 \AA resolution), of which 4078 were independent (average redundancy 7.524, completeness = 99.9%, $R_{\text{int}} = 3.11\%$, $R_{\text{sig}} = 1.74\%$) and 3236 (79.35%) were greater than $2\sigma(F_2)$. The final cell constants of $a = 8.2480(4) \text{ \AA}$, $b = 11.2545(5) \text{ \AA}$, $c = 11.6084(6) \text{ \AA}$, $\alpha = 66.730(2)^\circ$, $\beta = 71.581(2)^\circ$, $\gamma = 88.148(2)^\circ$, $V = 933.90(8) \text{ \AA}^3$, are based upon the refinement of the XYZ-centroids of 9896 reflections above $20 \sigma(I)$ with $5.458^\circ < 2\theta < 54.32^\circ$. Data were corrected for absorption effects using the Multi-Scan method (SADABS)⁶. The ratio of minimum to maximum apparent transmission was 0.971. The calculated minimum and maximum transmission coefficients (based on crystal size) are 0.978 and 0.994.

The structure was solved and refined using SHELXTL Software Package^{7,8} using the space group $P1$, with $Z = 2$ for the formula unit, $C_{23}H_{20}F_3NO_2$. The final anisotropic full-matrix least-squares refinement on F_2 with 269 variables converged at $R_1 = 3.98\%$, for the observed data and $wR_2 = 12.15\%$ for all data. The goodness-of-fit was 1.035. The largest peak in the final difference electron density synthesis was 0.327 e-/\AA^3 and the largest hole was -0.208 e-/\AA^3 with an RMS deviation of 0.046 e-/\AA^3 . On the basis of the final model, the

calculated density was 1.420 g/cm³ and F(000), 416 e⁻. The details concerning the crystal data and structural parameters of **16** are collected in Table S1.

The structure is fully ordered. All heavy atoms were refined anisotropically. All but one hydrogen atoms were placed in calculated positions and refined within the riding model, their temperature factors were not refined and were set to be 1.2 (Car-H atoms) or 1.5 (CH₃ atoms) times larger than U_{eq} of the corresponding heavy atom. The H atom of the amine group engaged in hydrogen bond was refined together with the isotropic ADP. The atomic scattering factors were taken from the International Tables.⁹ Molecular graphics was prepared using program Mercury 2020.2.0.¹⁰ Thermal ellipsoids parameters are presented at 20% probability level in Figure S1.

Table S1. Data collection and structure refinement parameters for **16**.

Formula	C ₂₃ H ₂₀ F ₃ NO
M_x/ g mol⁻¹	399.40
T/ K	130.5(5)
λ/ Å	0.71073
Crystal size	0.052×0.129×0.206mm
Space group	<i>P</i> $\bar{1}$
Unit cell dimensions	<i>a</i> = 8.2480(4) Å <i>α</i> = 66.730(2)° <i>b</i> = 11.2545(5) Å <i>β</i> = 71.581(2)° <i>c</i> = 11.6084(6) Å <i>γ</i> = 88.148(2)°
V/ Å³, Z	933.90(8), 2
D_x/ g cm⁻³	1.420
μ/ mm⁻¹	0.111
F(000)	416
θ_{min}, θ_{max}	2.62°, 27.00°
Index ranges	-10 ≤ <i>h</i> ≤ 10, -14 ≤ <i>k</i> ≤ 14, -14 ≤ <i>l</i> ≤ 14
Reflections collected/ independent	30681/ 4078 (<i>R</i> _{int} = 0.0311)
Completeness	99.9%
Absorption correction	Multi-Scan
T_{max}, T_{min}	0.994, 0.978
Refinement method	Full-matrix LSQ on <i>F</i> ²
Data / restraints / parameters	4078 / 0 / 269
GOF on <i>F</i>²	1.035
Final <i>R</i> indices	3236 data; <i>I</i> > 2σ(<i>I</i>) <i>R</i> 1 = 0.0398, <i>wR</i> 2 = 0.1112 all data <i>R</i> 1 = 0.0530, <i>wR</i> 2 = 0.1215
Δρ_{max}, Δρ_{min}	0.327 eÅ ⁻³ , -0.208 eÅ ⁻³

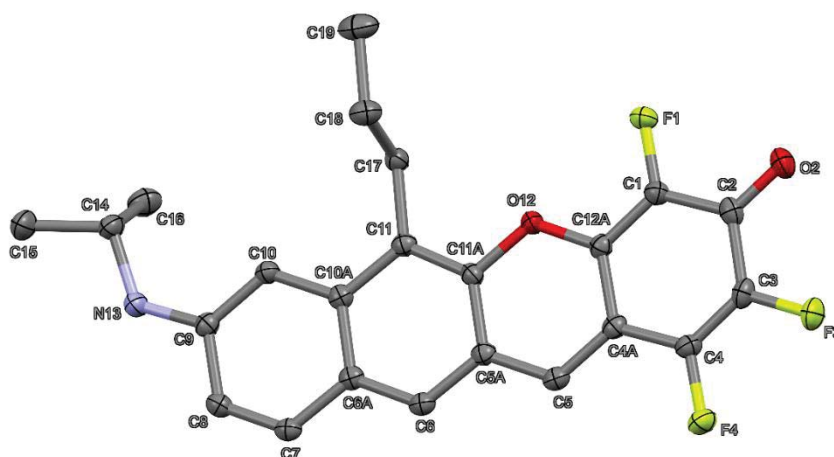


Figure S1. Thermal ellipsoid plot at 50% probability level together with numbering scheme of heavy atoms in the **16** structure, hydrogen atoms omitted for clarity.

A specimen of $C_{23}H_{20}F_3NO_2$, approximate dimensions 0.052 mm x 0.129 mm x 0.206 mm, was used for the X-ray crystallographic analysis. The X-ray intensity data were measured on a Bruker D8 VENTURE Bruker D8 VENTURE system equipped with a fine focus sealed tube ($MoK\alpha$, $\lambda = 0.71073 \text{ \AA}$) and a TRIUMPH monochromator.

Table S2. Data collection details for **16**.

Axis	dx/mm	$2\theta/^\circ$	$\omega/^\circ$	$\phi/^\circ$	$\chi/^\circ$	Width/ $^\circ$	Frames	Time/s	Wavelength/ \AA	Voltage/kV	Current/mA	Temperature/K
Phi	40.038	0.00	360.00	360.00	54.74	0.50	720	10.00	0.71076	50	30.0	130
Omega	40.037	3.00	357.00	0.00	-54.74	0.50	236	60.00	0.71076	50	30.0	130
Omega	40.037	3.00	357.00	90.00	-54.74	0.50	236	60.00	0.71076	50	30.0	130
Omega	40.037	3.00	357.00	180.00	-54.74	0.50	236	60.00	0.71076	50	30.0	130
Omega	40.037	3.00	357.00	270.00	-54.74	0.50	236	60.00	0.71076	50	30.0	130
Omega	40.037	3.00	251.00	360.00	54.74	0.50	236	60.00	0.71076	50	30.0	130
Omega	40.037	3.00	251.00	120.00	54.74	0.50	236	60.00	0.71076	50	30.0	130
Omega	40.037	3.00	251.00	240.00	54.74	0.50	236	60.00	0.71076	50	30.0	130

A total of 2372 frames were collected. The total exposure time was 29.53 hours. The frames were integrated with the Bruker SAINT software package using a narrow-frame algorithm. The integration of the data using a triclinic unit cell yielded a total of 30681 reflections to a maximum θ angle of 27.00° (0.78 \AA resolution), of which 4078 were independent (average redundancy 7.524, completeness = 99.9%, $R_{\text{int}} = 3.11\%$, $R_{\text{sig}} = 1.74\%$) and 3236 (79.35%) were greater than $2\sigma(F^2)$. The final cell constants of $a = 8.2480(4) \text{ \AA}$, $b = 11.2545(5) \text{ \AA}$, $c = 11.6084(6) \text{ \AA}$, $\alpha = 66.730(2)^\circ$, $\beta = 71.581(2)^\circ$, $\gamma = 88.148(2)^\circ$, volume = $933.90(8) \text{ \AA}^3$, are based upon the refinement of the XYZ-centroids of 9896 reflections above $20 \sigma(I)$ with $5.458^\circ < 2\theta < 54.32^\circ$. Data were corrected for absorption effects using the Multi-Scan method (SADABS). The ratio of minimum to maximum apparent transmission was 0.971. The calculated minimum and maximum transmission coefficients (based on crystal size) are 0.9780 and 0.9940.

The structure was solved and refined using the Bruker SHELXTL Software Package, using the space group P-1, with $Z = 2$ for the formula unit, $C_{23}H_{20}F_3NO_2$. The final anisotropic full-matrix least-squares refinement on F^2 with 269 variables converged at $R1 = 3.98\%$, for the observed data and $wR2 = 12.15\%$ for all data. The goodness-of-fit was 1.035. The largest peak in the final difference electron density synthesis was $0.327 e^-/\text{\AA}^3$ and the largest hole was $-0.208 e^-/\text{\AA}^3$ with an RMS deviation of $0.046 e^-/\text{\AA}^3$. On the basis of the final model, the calculated density was 1.420 g/cm^3 and $F(000)$, 416 e^- .

Table S3. Sample and crystal data for **16**.

Identification code	KVy_702	
Chemical formula	C ₂₃ H ₂₀ F ₃ NO ₂	
Formula weight	399.40 g/mol	
Temperature	130(0) K	
Wavelength	0.71073 Å	
Crystal size	0.052 x 0.129 x 0.206 mm	
Crystal system	triclinic	
Space group	P -1	
Unit cell dimensions	a = 8.2480(4) Å	α = 66.730(2)°
	b = 11.2545(5) Å	β = 71.581(2)°
	c = 11.6084(6) Å	γ = 88.148(2)°
Volume	933.90(8) Å ³	
Z	2	
Density (calculated)	1.420 g/cm ³	
Absorption coefficient	0.111 mm ⁻¹	
F(000)	416	

Table S4. Data collection and structure refinement for **16**.

Diffractometer	Bruker D8 VENTURE Bruker D8 VENTURE	
Radiation source	fine focus sealed tube (MoKα, λ = 0.71073 Å)	
Theta range for data collection	2.62 to 27.00°	
Index ranges	-10<=h<=10, -14<=k<=14, -14<=l<=14	
Reflections collected	30681	
Independent reflections	4078 [R(int) = 0.0311]	
Coverage of independent reflections	99.9%	
Absorption correction	Multi-Scan	
Max. and min. transmission	0.9940 and 0.9780	
Structure solution technique	direct methods	
Structure solution program	SHELXS-2013/1 (Sheldrick, 2015)	
Refinement method	Full-matrix least-squares on F ²	
Refinement program	SHELXL-2018/3 (Sheldrick, 2015)	
Function minimized	Σ w(F _o ² - F _c ²) ²	
Data / restraints / parameters	4078 / 0 / 269	
Goodness-of-fit on F ²	1.035	
Final R indices	3236 data; >2σ(I)	R1 = 0.0398, wR2 = 0.1112

	all data	R1 = 0.0530, wR2 = 0.1215
Weighting scheme	$w=1/[\sigma^2(F_o^2)+(0.0628P)^2+0.3780P]$ where $P=(F_o^2+2F_c^2)/3$	
Largest diff. peak and hole	0.327 and -0.208 eÅ ⁻³	
R.M.S. deviation from mean	0.046 eÅ ⁻³	

Table S5. Atomic coordinates and equivalent isotropic atomic displacement parameters (Å²) for **16**. U(eq) is defined as one third of the trace of the orthogonalized U_{ij} tensor.

	x/a	y/b	z/c	U(eq)
F1	0.59198(11)	0.87151(8)	0.74174(8)	0.0271(2)
O2	0.83840(14)	0.07770(10)	0.57891(11)	0.0297(3)
F3	0.94706(12)	0.15823(8)	0.31044(9)	0.0312(2)
F4	0.81335(11)	0.02886(9)	0.20159(8)	0.0286(2)
C1	0.64889(18)	0.90732(13)	0.60874(13)	0.0205(3)
C2	0.77691(18)	0.01719(14)	0.53072(14)	0.0221(3)
C3	0.82939(18)	0.05456(13)	0.38778(14)	0.0229(3)
C4	0.76315(18)	0.99031(13)	0.33468(13)	0.0209(3)
C4A	0.63781(17)	0.88022(13)	0.41367(13)	0.0191(3)
C5	0.57062(17)	0.80969(13)	0.36381(13)	0.0196(3)
C5A	0.44882(17)	0.70005(13)	0.44987(13)	0.0185(3)
C6	0.38022(17)	0.62316(13)	0.40407(13)	0.0190(3)
C6A	0.26282(16)	0.51527(13)	0.49094(13)	0.0176(3)
C7	0.19410(17)	0.43598(13)	0.44356(13)	0.0195(3)
C8	0.07893(17)	0.33121(13)	0.52662(13)	0.0199(3)
C9	0.02435(17)	0.29446(13)	0.66799(13)	0.0194(3)
C10	0.09064(17)	0.36895(13)	0.71781(13)	0.0190(3)
C10A	0.20845(16)	0.48068(13)	0.63245(13)	0.0180(3)
C11	0.27552(17)	0.56038(13)	0.68084(13)	0.0186(3)
C11A	0.39392(17)	0.66469(13)	0.58931(13)	0.0182(3)
O12	0.46228(12)	0.73813(9)	0.63823(9)	0.0197(2)
C12A	0.58274(17)	0.84114(13)	0.55527(13)	0.0180(3)
N13	0.91090(16)	0.18678(12)	0.74481(12)	0.0235(3)
C14	0.83755(19)	0.13330(14)	0.88939(14)	0.0241(3)
C15	0.7632(2)	0.99346(15)	0.93727(15)	0.0319(4)
C16	0.7019(2)	0.21457(16)	0.93665(15)	0.0320(4)
C17	0.22345(18)	0.53007(13)	0.82725(13)	0.0208(3)
C18	0.3317(2)	0.43334(15)	0.89773(14)	0.0273(3)
C19	0.2768(2)	0.40380(19)	0.04543(16)	0.0396(4)

Table S6. Bond lengths (Å) for **16**.

F1-C1	1.3524(15)	O2-C2	1.2397(17)
F3-C3	1.3432(16)	F4-C4	1.3507(15)
C1-C12A	1.3577(19)	C1-C2	1.4351(19)
C2-C3	1.457(2)	C3-C4	1.339(2)
C4-C4A	1.4251(19)	C4A-C5	1.366(2)
C4A-C12A	1.4393(18)	C5-C5A	1.4148(19)
C5-H5	0.95	C5A-C6	1.3916(19)
C5A-C11A	1.4223(18)	C6-C6A	1.3858(19)
C6-H6	0.95	C6A-C7	1.4275(19)
C6A-C10A	1.4463(18)	C7-C8	1.3482(19)
C7-H7	0.95	C8-C9	1.4407(18)
C8-H8	0.95	C9-N13	1.3534(18)
C9-C10	1.3960(19)	C10-C10A	1.4118(18)
C10-H10	0.95	C10A-C11	1.4327(19)
C11-C11A	1.3761(19)	C11-C17	1.5097(18)
C11A-O12	1.3882(16)	O12-C12A	1.3588(16)
N13-C14	1.4590(18)	N13-H13N	0.87(2)
C14-C15	1.522(2)	C14-C16	1.527(2)
C14-H14	1.0	C15-H15A	0.98
C15-H15B	0.98	C15-H15C	0.98
C16-H16A	0.98	C16-H16B	0.98
C16-H16C	0.98	C17-C18	1.532(2)
C17-H17A	0.99	C17-H17B	0.99
C18-C19	1.524(2)	C18-H18A	0.99
C18-H18B	0.99	C19-H19A	0.98
C19-H19B	0.98	C19-H19C	0.98

Table S7. Bond angles (°) for **16**.

F1-C1-C12A	119.83(12)	F1-C1-C2	116.86(12)
C12A-C1-C2	123.30(12)	O2-C2-C1	123.64(13)
O2-C2-C3	121.68(13)	C1-C2-C3	114.67(12)
C4-C3-F3	120.98(13)	C4-C3-C2	122.16(13)
F3-C3-C2	116.86(12)	C3-C4-F4	120.47(13)
C3-C4-C4A	122.48(13)	F4-C4-C4A	117.05(12)
C5-C4A-C4	124.36(12)	C5-C4A-C12A	118.91(12)
C4-C4A-C12A	116.71(12)	C4A-C5-C5A	120.59(12)
C4A-C5-H5	119.7	C5A-C5-H5	119.7
C6-C5A-C5	122.69(12)	C6-C5A-C11A	117.79(12)

C5-C5A-C11A	119.51(12)	C6A-C6-C5A	121.39(12)
C6A-C6-H6	119.3	C5A-C6-H6	119.3
C6-C6A-C7	121.18(12)	C6-C6A-C10A	120.08(12)
C7-C6A-C10A	118.74(12)	C8-C7-C6A	121.94(12)
C8-C7-H7	119.0	C6A-C7-H7	119.0
C7-C8-C9	120.16(12)	C7-C8-H8	119.9
C9-C8-H8	119.9	N13-C9-C10	124.02(12)
N13-C9-C8	116.58(12)	C10-C9-C8	119.39(12)
C9-C10-C10A	121.39(12)	C9-C10-H10	119.3
C10A-C10-H10	119.3	C10-C10A-C11	122.50(12)
C10-C10A-C6A	118.37(12)	C11-C10A-C6A	119.14(12)
C11A-C11-C10A	117.72(12)	C11A-C11-C17	120.45(12)
C10A-C11-C17	121.80(12)	C11-C11A-O12	117.00(12)
C11-C11A-C5A	123.84(12)	O12-C11A-C5A	119.16(12)
C12A-O12-C11A	121.00(10)	C1-C12A-O12	118.56(12)
C1-C12A-C4A	120.65(13)	O12-C12A-C4A	120.79(12)
C9-N13-C14	125.69(12)	C9-N13-H13N	113.7(14)
C14-N13-H13N	120.6(14)	N13-C14-C15	108.01(12)
N13-C14-C16	111.84(12)	C15-C14-C16	111.52(13)
N13-C14-H14	108.5	C15-C14-H14	108.5
C16-C14-H14	108.5	C14-C15-H15A	109.5
C14-C15-H15B	109.5	H15A-C15-H15B	109.5
C14-C15-H15C	109.5	H15A-C15-H15C	109.5
H15B-C15-H15C	109.5	C14-C16-H16A	109.5
C14-C16-H16B	109.5	H16A-C16-H16B	109.5
C14-C16-H16C	109.5	H16A-C16-H16C	109.5
H16B-C16-H16C	109.5	C11-C17-C18	113.20(11)
C11-C17-H17A	108.9	C18-C17-H17A	108.9
C11-C17-H17B	108.9	C18-C17-H17B	108.9
H17A-C17-H17B	107.8	C19-C18-C17	112.38(13)
C19-C18-H18A	109.1	C17-C18-H18A	109.1
C19-C18-H18B	109.1	C17-C18-H18B	109.1
H18A-C18-H18B	107.9	C18-C19-H19A	109.5
C18-C19-H19B	109.5	H19A-C19-H19B	109.5
C18-C19-H19C	109.5	H19A-C19-H19C	109.5
H19B-C19-H19C	109.5		

Table S8. Torsion angles (°) for **16**.

F1-C1-C2-O2	1.4(2)	C12A-C1-C2-O2	-179.67(14)
F1-C1-C2-C3	-177.94(11)	C12A-C1-C2-C3	1.0(2)
O2-C2-C3-C4	-179.64(14)	C1-C2-C3-C4	-0.3(2)
O2-C2-C3-F3	-0.3(2)	C1-C2-C3-F3	178.98(12)
F3-C3-C4-F4	-0.1(2)	C2-C3-C4-F4	179.14(12)
F3-C3-C4-C4A	-179.83(12)	C2-C3-C4-C4A	-0.6(2)
C3-C4-C4A-C5	-178.03(14)	F4-C4-C4A-C5	2.3(2)
C3-C4-C4A-C12A	0.8(2)	F4-C4-C4A-C12A	-178.94(11)
C4-C4A-C5-C5A	178.80(12)	C12A-C4A-C5-C5A	0.0(2)
C4A-C5-C5A-C6	-178.24(12)	C4A-C5-C5A-C11A	1.1(2)
C5-C5A-C6-C6A	179.11(12)	C11A-C5A-C6-C6A	-0.3(2)
C5A-C6-C6A-C7	-179.38(12)	C5A-C6-C6A-C10A	0.3(2)
C6-C6A-C7-C8	-179.55(13)	C10A-C6A-C7-C8	0.8(2)
C6A-C7-C8-C9	-1.4(2)	C7-C8-C9-N13	-178.82(12)
C7-C8-C9-C10	0.6(2)	N13-C9-C10-C10A	-179.82(13)
C8-C9-C10-C10A	0.9(2)	C9-C10-C10A-C11	178.61(12)
C9-C10-C10A-C6A	-1.4(2)	C6-C6A-C10A-C10	-179.06(12)
C7-C6A-C10A-C10	0.58(18)	C6-C6A-C10A-C11	0.93(19)
C7-C6A-C10A-C11	-179.42(11)	C10-C10A-C11-C11A	177.94(12)
C6A-C10A-C11-C11A	-2.06(19)	C10-C10A-C11-C17	-0.3(2)
C6A-C10A-C11-C17	179.72(12)	C10A-C11-C11A-O12	-177.72(11)
C17-C11-C11A-O12	0.52(19)	C10A-C11-C11A-C5A	2.1(2)
C17-C11-C11A-C5A	-179.62(12)	C6-C5A-C11A-C11	-1.0(2)
C5-C5A-C11A-C11	179.62(12)	C6-C5A-C11A-O12	178.88(11)
C5-C5A-C11A-O12	-0.52(19)	C11-C11A-O12-C12A	178.56(11)
C5A-C11A-O12-C12A	-1.31(18)	F1-C1-C12A-O12	-1.3(2)
C2-C1-C12A-O12	179.81(12)	F1-C1-C12A-C4A	178.09(11)
C2-C1-C12A-C4A	-0.8(2)	C11A-O12-C12A-C1	-178.13(12)
C11A-O12-C12A-C4A	2.52(18)	C5-C4A-C12A-C1	178.80(13)
C4-C4A-C12A-C1	-0.1(2)	C5-C4A-C12A-O12	-1.87(19)
C4-C4A-C12A-O12	179.26(11)	C10-C9-N13-C14	1.4(2)
C8-C9-N13-C14	-179.25(13)	C9-N13-C14-C15	-162.65(14)
C9-N13-C14-C16	74.27(18)	C11A-C11-C17-C18	-92.27(15)
C10A-C11-C17-C18	85.90(16)	C11-C17-C18-C19	-179.87(13)

Table S9. Anisotropic atomic displacement parameters (\AA^2) for **16**.The anisotropic atomic displacement factor exponent takes the form: $-2\pi^2[h^2 a^{*2} U_{11} + \dots + 2 h k a^* b^* U_{12}]$

	U_{11}	U_{22}	U_{33}	U_{23}	U_{13}	U_{12}
F1	0.0348(5)	0.0287(5)	0.0176(4)	-0.0108(3)	-0.0059(3)	-0.0040(4)
O2	0.0341(6)	0.0265(5)	0.0323(6)	-0.0152(5)	-0.0112(5)	-0.0039(4)
F3	0.0319(5)	0.0255(5)	0.0290(5)	-0.0068(4)	-0.0049(4)	-0.0111(4)
F4	0.0311(5)	0.0307(5)	0.0166(4)	-0.0048(3)	-0.0034(3)	-0.0077(4)
C1	0.0231(7)	0.0202(7)	0.0179(6)	-0.0083(5)	-0.0056(5)	0.0018(5)
C2	0.0217(7)	0.0195(7)	0.0282(7)	-0.0121(6)	-0.0091(6)	0.0031(5)
C3	0.0192(7)	0.0189(7)	0.0253(7)	-0.0054(6)	-0.0047(5)	-0.0017(5)
C4	0.0210(7)	0.0220(7)	0.0166(6)	-0.0059(5)	-0.0049(5)	0.0011(5)
C4A	0.0180(6)	0.0188(6)	0.0185(6)	-0.0059(5)	-0.0057(5)	0.0031(5)
C5	0.0202(7)	0.0210(7)	0.0158(6)	-0.0061(5)	-0.0056(5)	0.0032(5)
C5A	0.0189(6)	0.0187(6)	0.0175(6)	-0.0068(5)	-0.0063(5)	0.0032(5)
C6	0.0197(6)	0.0211(7)	0.0156(6)	-0.0071(5)	-0.0057(5)	0.0034(5)
C6A	0.0164(6)	0.0187(6)	0.0176(6)	-0.0075(5)	-0.0054(5)	0.0039(5)
C7	0.0204(6)	0.0222(7)	0.0169(6)	-0.0089(5)	-0.0064(5)	0.0041(5)
C8	0.0206(6)	0.0222(7)	0.0198(6)	-0.0110(5)	-0.0075(5)	0.0030(5)
C9	0.0182(6)	0.0195(6)	0.0187(6)	-0.0067(5)	-0.0053(5)	0.0017(5)
C10	0.0199(6)	0.0206(7)	0.0153(6)	-0.0070(5)	-0.0046(5)	0.0004(5)
C10A	0.0164(6)	0.0188(6)	0.0188(6)	-0.0078(5)	-0.0057(5)	0.0028(5)
C11	0.0181(6)	0.0198(6)	0.0171(6)	-0.0074(5)	-0.0052(5)	0.0032(5)
C11A	0.0200(6)	0.0179(6)	0.0194(6)	-0.0091(5)	-0.0078(5)	0.0023(5)
O12	0.0224(5)	0.0188(5)	0.0173(5)	-0.0079(4)	-0.0047(4)	-0.0026(4)
C12A	0.0179(6)	0.0166(6)	0.0186(6)	-0.0068(5)	-0.0052(5)	0.0024(5)
N13	0.0267(6)	0.0241(6)	0.0189(6)	-0.0087(5)	-0.0058(5)	-0.0054(5)
C14	0.0252(7)	0.0255(7)	0.0169(6)	-0.0050(5)	-0.0049(5)	-0.0049(6)
C15	0.0342(8)	0.0296(8)	0.0241(7)	-0.0060(6)	-0.0044(6)	-0.0108(6)
C16	0.0306(8)	0.0367(9)	0.0226(7)	-0.0099(6)	-0.0035(6)	0.0010(7)
C17	0.0222(7)	0.0216(7)	0.0184(6)	-0.0094(5)	-0.0045(5)	-0.0014(5)
C18	0.0294(8)	0.0318(8)	0.0195(7)	-0.0095(6)	-0.0078(6)	0.0035(6)
C19	0.0486(10)	0.0472(10)	0.0221(8)	-0.0115(7)	-0.0145(7)	0.0124(8)

Table S10. Hydrogen atomic coordinates and isotropic atomic displacement parameters (\AA^2) for **16**.

	x/a	y/b	z/c	U(eq)
H5	0.6060	0.8345	0.2705	0.024
H6	0.4146	0.6451	0.3113	0.023
H7	0.2306	0.4577	0.3508	0.023
H8	0.0337	0.2815	0.4919	0.024
H10	0.0557	0.3439	0.8111	0.023
H13N	-0.120(3)	0.151(2)	0.700(2)	0.045(6)
H14	-0.0679	0.1326	0.9263	0.029
H15A	-0.3252	-0.0080	0.8977	0.048
H15B	-0.2881	-0.0442	1.0343	0.048
H15C	-0.1450	-0.0574	0.9107	0.048
H16A	-0.2500	0.3059	0.8959	0.048
H16B	-0.3330	0.1829	1.0336	0.048
H16C	-0.3983	0.2071	0.9109	0.048
H17A	0.1012	0.4939	0.8701	0.025
H17B	0.2343	0.6119	0.8384	0.025
H18A	0.3210	0.3513	0.8868	0.033
H18B	0.4540	0.4695	0.8554	0.033
H19A	0.2811	0.4852	1.0569	0.059
H19B	0.3548	0.3469	1.0848	0.059
H19C	0.1593	0.3603	1.0895	0.059

Table S11. Hydrogen bond distances (\AA) and angles ($^\circ$) for **16**.

	Donor-H	Acceptor-H	Donor-Acceptor	Angle
N13-H13N \cdots O2#1	0.87(2)	2.00(2)	2.8664(16)	173.(2)

Symmetry transformations used to generate equivalent atoms:

#1 $x-1, y-1, z$

1.2. Spectroscopic characterization

Linear absorption and emission spectra were collected on freshly prepared solutions, under ambient conditions. Dilute solutions (optical density less than 0.1) were used to minimize inner filter effects and/or aggregation. Spectrophotometric grade solvents were used as received.

A Perkin-Elmer Lambda650 double beam spectrophotometer was used for linear absorption measurements, and an Edinburgh Instruments FLS1000 fluorometer for fluorescence spectroscopy. Fluorescence quantum yields were estimated using a dilute solution of fluorescein in NaOH 0.1 M as reference standard (QY = 90%, excitation wavelength: 490 nm). Emission decays were measured with the time-correlated single-photon counting (TCSPC) method, for excitation with a 60 ps pulsed laser diode (excitation wavelength: 405 nm). Fluorescence lifetimes were extracted from the reconvolution fit of experimental decay curves, and judged both by the chi-squared test and the visual inspection of residues.

Excitation anisotropies were collected with a Fluoromax-3 (Horiba Jobin-Yvon) fluorometer. The solvent (2-methyltetrahydrofuran) was stored over molecular sieves for 24h and filtered on PTFE syringe filters (0.22 μm pore size). Solutions were vitrified by rapid immersion in liquid nitrogen, using the Horiba FL-1013 liquid nitrogen dewar assembly.

Two-photon absorption spectra were collected with the two-photon-excited fluorescence (2PEF) technique,^{1,11,12} with a Nikon A1R MP+ Upright two-photon microscope. Freshly prepared solutions of the dyes were contained in 1 cm path length quartz cuvette and excited by a Coherent Chameleon Discovery femtosecond pulsed laser with tunable wavelength output (660-1320 nm) focused on the sample through a 25x water-dipping objective (NA=1.1). Fluorescence signal was collected in epifluorescence mode. Fluorescein in NaOH 0.1 M was used as standard for quantitative measurement of 2PA cross-sections,¹³ according to the procedure proposed by Albota et al.¹⁴

1.3. Photochemical stability

A freshly prepared air-equilibrated solution of each dye in chloroform (concentration $\approx 1\text{-}3 \times 10^{-5}$ mol L⁻¹) contained in a standard 1 cm \times 1 cm quartz cuvette was irradiated by a laser beam ($\lambda = 530.9$ nm) expanded with a lens to illuminate the entire volume of the sample. The absorbance of the solution was measured with a Perkin-Elmer Lambda650 spectrophotometer and monitored over time. The photodecomposition quantum yield ϕ_D was estimated according to the following expression:

$$\phi_D = \frac{(D(\lambda_{max},0) - D(\lambda_{max},T))N_A}{10^3 P \varepsilon(\lambda_{max}) \int_0^T (1 - 10^{-D(\lambda_{exc},t)}) dt} \quad (S1)$$

where $D(\lambda, t)$ is the optical density of the sample at wavelength λ and time t , T is the total irradiation time (in seconds), λ_{max} is the maximum of the absorption band (551 nm for **4**, 585 nm for **10**, 586 nm for **15**, 544 nm for **16** and 536 nm for **17**), N_A is the Avogadro's number, P is the irradiation intensity (in photons s⁻¹ cm⁻²), ε is the molar extinction coefficient (in M⁻¹ cm⁻¹) and λ_{exc} is the excitation wavelength.

2. Experimental data

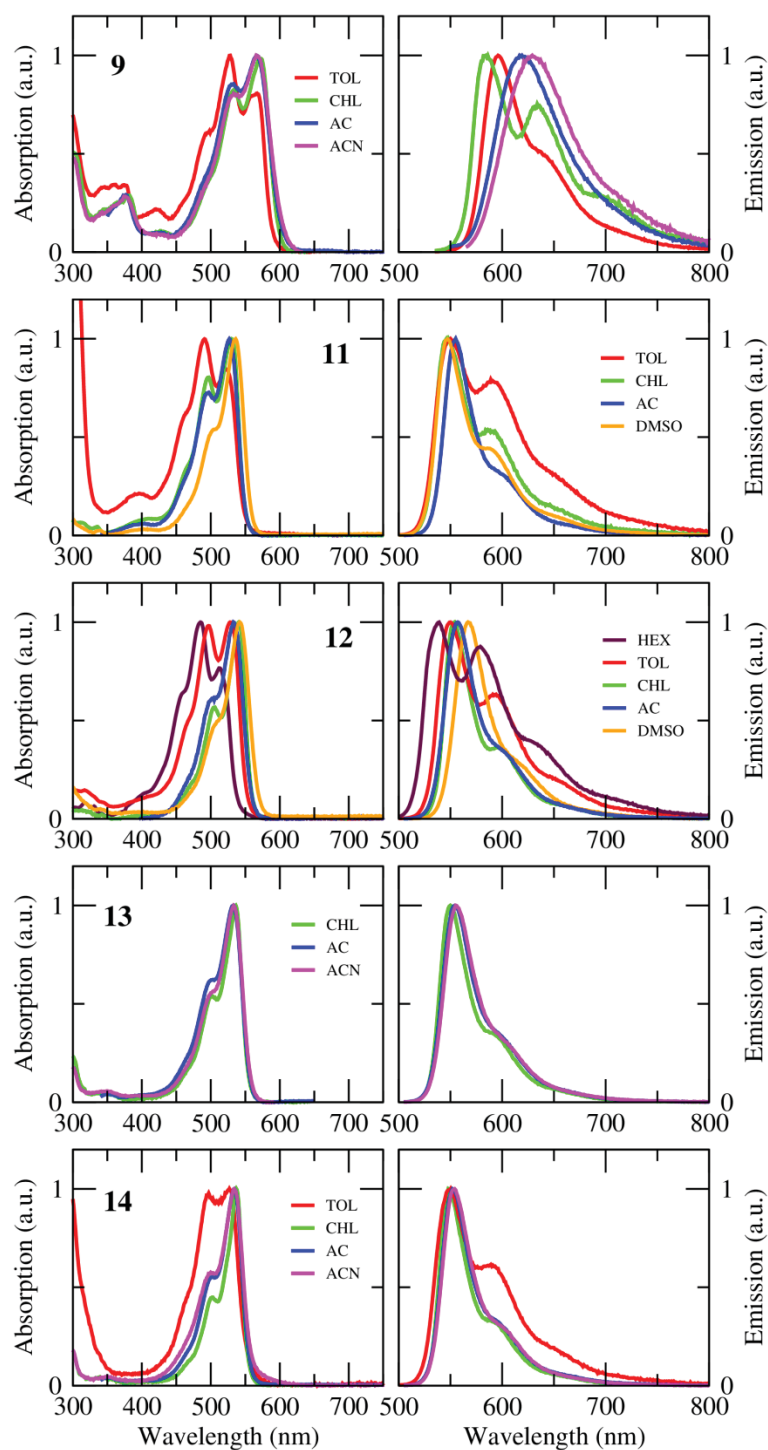


Figure S2. Normalized absorption (left) and emission (right) spectra of compounds **9** and **11-14** in solvents of different polarity (HEX: hexane, TOL: toluene, CHL: chloroform, AC: acetone, ACN: acetonitrile, DMSO: dimethyl sulfoxide).

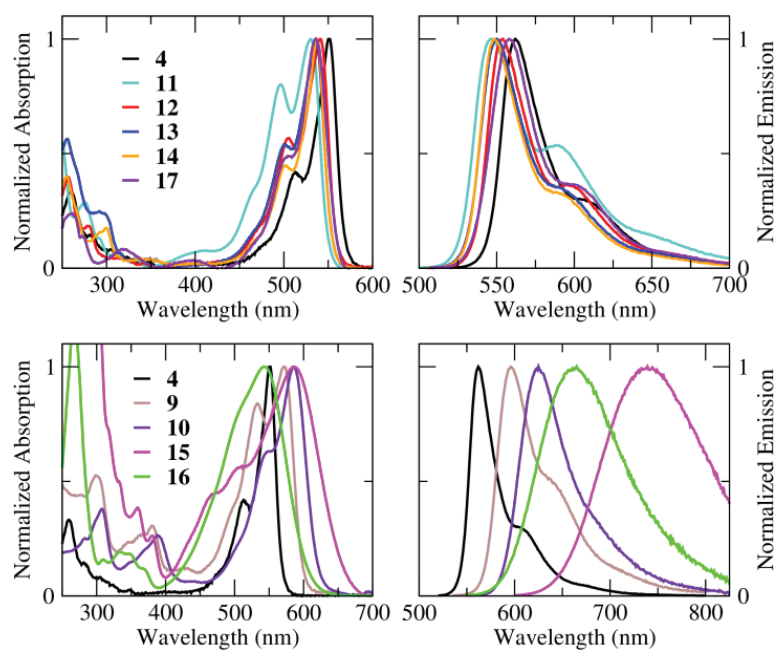


Figure S3. Normalized absorption (left) and emission (right) spectra of investigated compounds in chloroform: rhodols (top panels) and merocyanines (bottom panels; spectra of rhodol **4** are included for comparison).

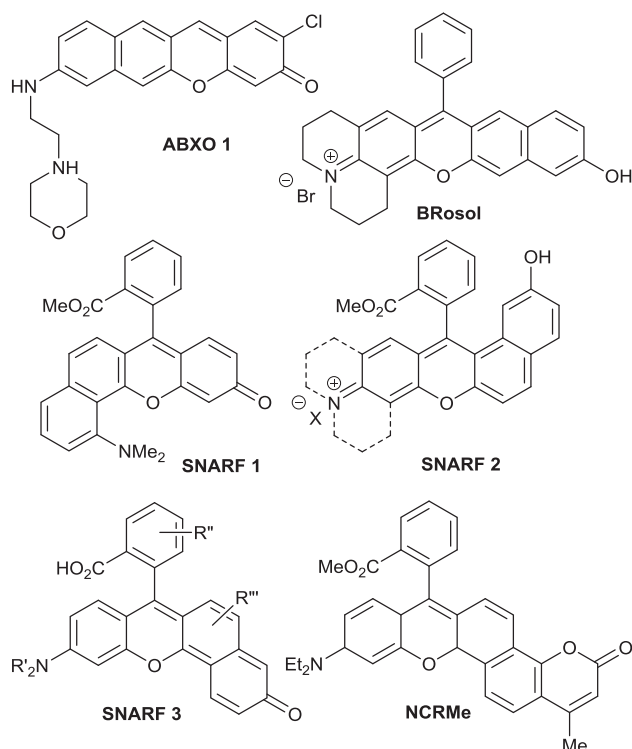


Figure S4. The structures of known π -expanded rhodols and merocyanines.

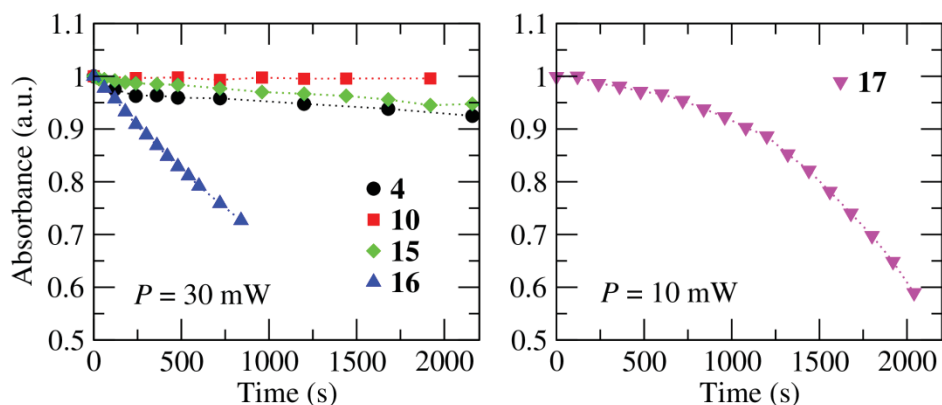


Figure S5. Temporal dependence of the absorbance at the maximum of the absorption band ($D(\lambda_{max})$) of **4**, **10**, **15**, **16** and **17** under continuous laser irradiation ($\lambda_{exc} = 530.9$ nm, laser power $P = 10$ or 30 mW). Dye **4**: $\lambda_{max} = 551$ nm; dye **10**: $\lambda_{max} = 585$ nm; dye **15**: $\lambda_{max} = 586$ nm; dye **16**: $\lambda_{max} = 544$ nm; dye **17**: $\lambda_{max} = 536$ nm. Solvent: chloroform.

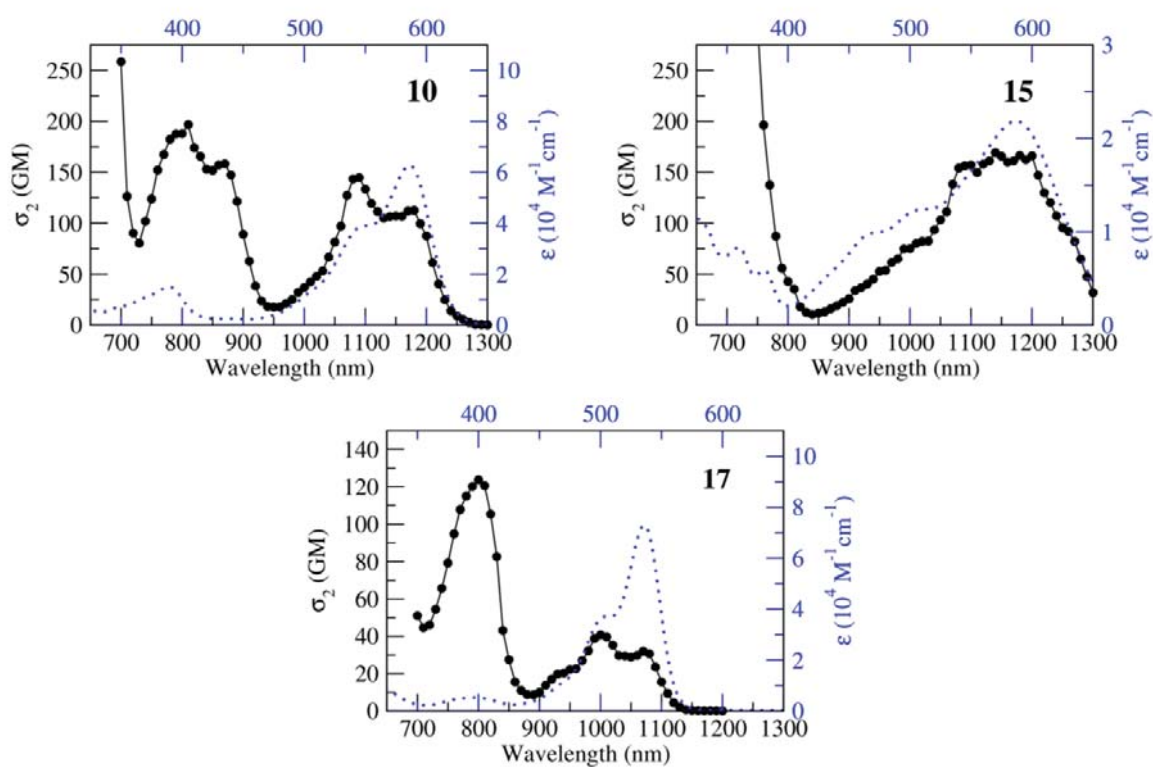


Figure S6. Two-photon absorption cross-section σ_2 (black dots) and molar extinction coefficient ϵ (blue dotted line) of **10**, **15** and **17** in chloroform ($1 \text{ GM} = 10^{-50} \text{ cm}^4 \text{ s photons}^{-1}$). The uncertainty on the cross-section is on the order of 20-25% for **15** and 10% for the other compounds.

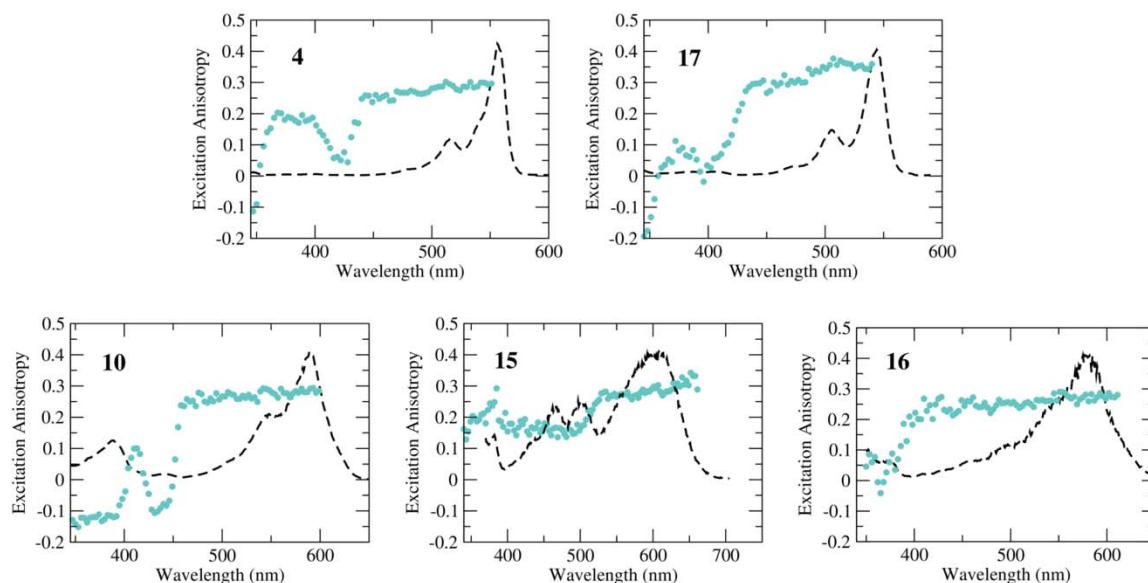


Figure S7. Excitation anisotropy (dots) of compounds **4**, **10**, **15**, **16** and **17** collected in glassy 2-methyltetrahydrofuran at 77 K. Excitation spectra collected under the same experimental conditions (dashed lines) are reported as a guide to the eye.

3. TDDFT results

3.1. Computational details

(TD)DFT calculations in the gas phase were performed with the Gaussian16 package.¹⁵ The long-range corrected hybrid functional M06-2X¹⁶ was used with the 6-31G(d) basis set. Stationary points located by geometry optimizations (ground state and excited state minima) were characterized by frequency analysis. The geometry of the first excited state was optimized in chloroform adopting the PCM model.^{17,18,19} TDDFT calculations on the optimized geometries included up to 15 singlet states.

3.2. Solvation model

We adopt the Onsager model,²⁰ where the solute is described as a point dipole located at the center of a spherical cavity inside the solvent, which, in turn, is treated as a continuum dielectric medium. The solvent generates at the solute location an electric field, called the reaction field F_r , proportional to the solute dipole moment.^{21,22,23} Two contributions to the solvent response can be recognized: an electronic component, F_{el} , due to the distortion of the electronic clouds of the solvent molecules, and an orientational component, F_{or} , due to the reorientation of polar solvent molecules around the solute.

Imposing the proportionality of both F_r components to the solute dipole moment, the total reaction field, $F_r = F_{el} + F_{or}$, experienced by the solvated dye is:

$$F_r = r_{el}\langle\hat{\mu}\rangle + r_{or}\langle\hat{\mu}\rangle \quad (S2)$$

where $\langle \hat{\mu} \rangle$ is the expectation value of the dipole moment operator of the solute in the state of interest, and the prefactors read:

$$r_{el} = \frac{2}{4\pi\epsilon_0 a^3} f(\epsilon_{opt}) \quad (S3)$$

$$r_{or} = \frac{2}{4\pi\epsilon_0 a^3} (f(\epsilon_{st}) - f(\epsilon_{opt})) \quad (S4)$$

where ϵ_0 is the vacuum permittivity, a is the radius of the cavity occupied by the solute, and $f(\epsilon) = \frac{\epsilon-1}{2\epsilon+1}$ with ϵ_{st} measuring the static dielectric constant and ϵ_{opt} is the squared refractive index at optical.

The electronic component of the reaction field, with typical frequencies in the UV, is treated in the antiadiabatic approximation, assuming its instantaneous response to charge fluctuations in the dye.²⁴ Conversely, the slow orientational motion of the solvent is treated in the adiabatic approximation, neglecting the associated kinetic energy.²⁵

With these approximations, the Hamiltonian describing a solvated molecule reads:

$$\hat{H}_{tot} = \hat{H}_g - \frac{r_{el}}{2} \hat{\mu}^2 - F_{or} \hat{\mu} + \frac{1}{2r_{or}} F_{or}^2 \quad (S5)$$

where H_g is the gas phase Hamiltonian and $\hat{\mu}$ is the dipole moment operator. The second term in the right hand side of Equation S5 includes the effects of fast solvation, while the last two terms account for the orientational contribution in polar solvents.

In our calculation, \hat{H}_{tot} is written on the basis of the eigenstates of the gas phase Hamiltonian as obtained from TDDFT calculations. In this work we considered 16 basis states, including the ground and the 15 lowest-energy excited states, which ensured convergence on calculated properties. The matrix elements of the dipole moment operator were calculated with Multiwfn software.²⁶ Only the x -component of the dipole moment was accounted for ($\hat{\mu} = \hat{\mu}_x$, where x identifies the direction connecting donor and acceptor moieties), since it is largely dominant over the other components. The parameter a entering the expressions for r_{el} and r_{or} (Equations S3-S4) was set to the Onsager radius calculated for the dyes (5.71 Å for **4**, 5.78 Å for **10**, 5.44 Å for **15** and **16**, 5.87 Å for **17**). The values of ϵ_{st} and ϵ_{opt} used for the different solvents are reported in Table S14.

To describe absorption, we used TDDFT results in the optimized ground-state geometry, while to describe emission we used the results obtained in the S_1 geometry optimized in chloroform within PCM formalism.²⁷

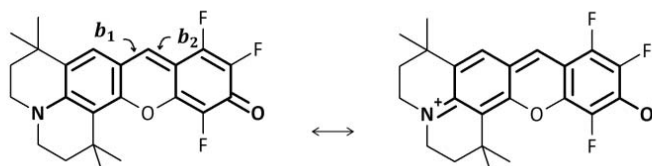


Figure S8. The two main resonance structures of rhodol **4**: neutral (left) and dipolar (right). The pi-conjugated skeleton of the rhodol is emphasized in bold.

Table S12. Length of bonds b_1 and b_2 (defined as in Figure S8) in the ground state equilibrium geometry and bond-length alternation (BLA = $b_2 - b_1$). The geometry was optimized in gas phase at M06-2X/6-31G(d) level.

	4	10	15	16	17
$b_1 / \text{\AA}$	1.424	1.422	1.434	1.435	1.434
$b_2 / \text{\AA}$	1.362	1.362	1.358	1.355	1.375
BLA / \AA	-0.062	-0.060	-0.076	-0.080	-0.059

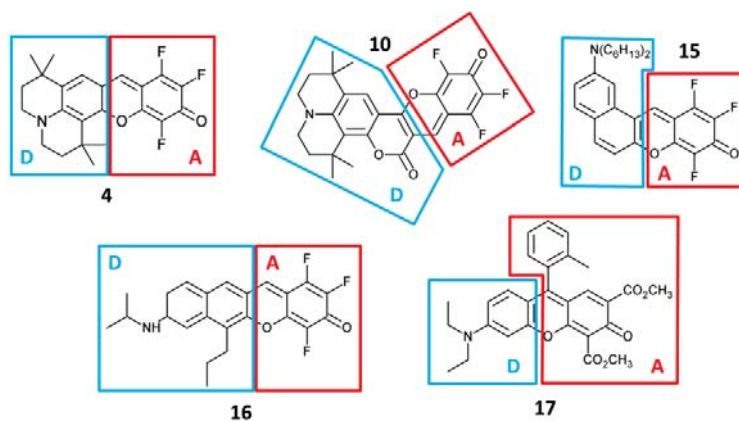


Figure S9. Colored polygons define the donor (D, blue) and acceptor (A, red) regions chosen for the calculation of the cumulative atomic charges reported in Table S13.

Table S13. Cumulative Hirshfeld atomic charges on the donor (D) and acceptor (A) groups calculated in the ground state and after vertical excitation to S_1 . Molecules have been partitioned as in Figure S9.

Compound	S_0		S_1		S_2	
	A	D	A	D	A	D
4	-0.2303	+0.2304	-0.3212	+0.3213	-(a)	-(a)
10	-0.1705	+0.1705	-0.2492	+0.2492	-(a)	-(a)
15	-0.2024	+0.2024	-0.2530	+0.2530	-0.4697	+0.4697
16	-0.1841	+0.1841	-0.3469	+0.3469	-(a)	-(a)
17	-0.2317	+0.2317	-0.3152	+0.3152	-(a)	-(a)

(a) not calculated.

Table S14. Dielectric properties of the solvents used in this work.

Solvent	ϵ_{opt}	ϵ_{st}
Hexane	1.89	1.88
Cyclohexane	2.03	2.03
Toluene	2.24	2.38
Chloroform	2.09	4.81
Acetone	1.85	20.7
Acetonitrile	1.81	37.5
Dimethyl sulfoxide	2.18	46.7

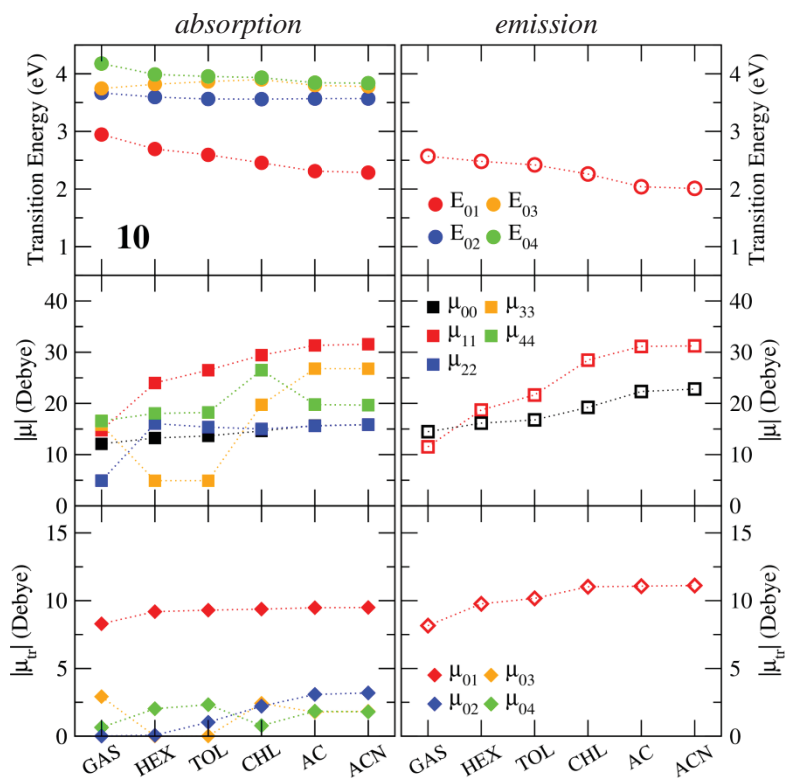


Figure S10. The same as in Figure 4 (main text) for dye 10.

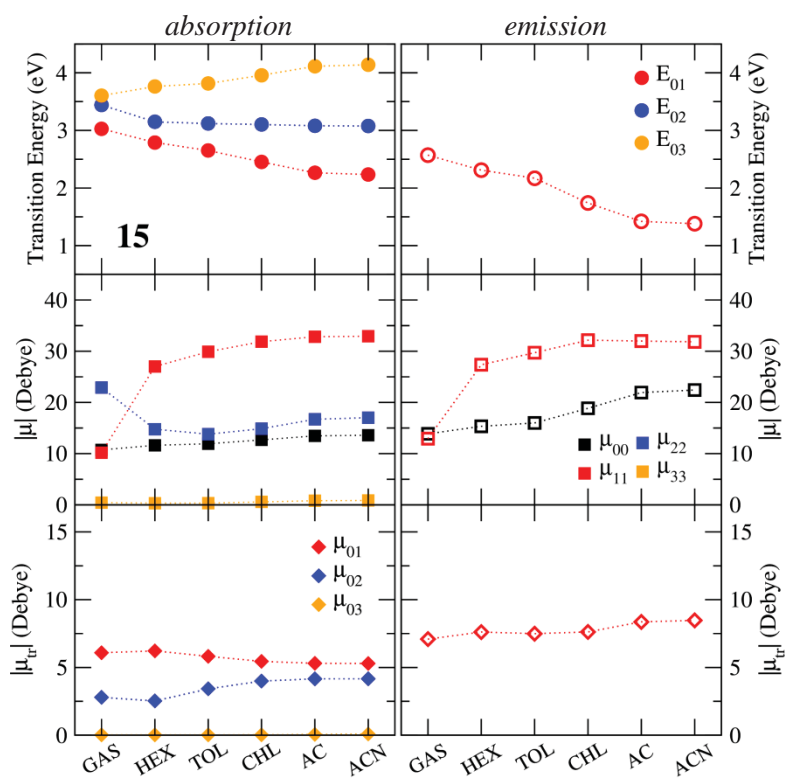


Figure S11. The same as in Figure 4 (main text) for dye 15.

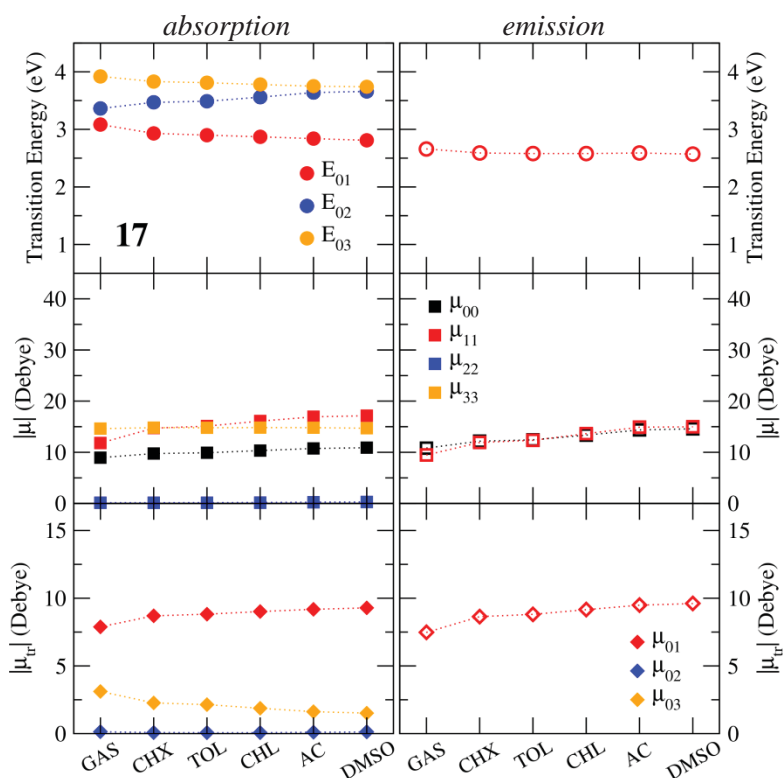


Figure S12. The same as in Figure 4 (main text) for dye 17.

4. Essential state models and the calculation of linear and nonlinear optical spectra in the essential state model

The two electronic basis states $D - \pi - A$ and $D^+ - \pi - A^-$ are separated by an energy gap $2z_0$ and are mixed by a matrix element $\sqrt{2}t$. A single effective vibrational coordinate accounts for the variation of the molecular geometry upon charge transfer, the strength of the coupling being measured by the vibrational relaxation energy, ε_v . Experimental spectra of **4** in nonpolar solvents point to a sizable anharmonicity. Accordingly, to reproduce the vibronic shape, the two basis states are assigned two harmonic potential energy surfaces with displaced minima, as to account for the different equilibrium geometries, and with different frequencies, ω_v and ω_t , for the neutral and zwitterionic state, respectively.

The Onsager model is again adopted to describe solvation.²⁸ The contribution of fast solvation (electronic solvation) is implicitly accounted for in the definition of the molecular Hamiltonian (and specifically in the definition of $2z_0$).²⁵ The orientational component of the solvent reaction field is instead treated within the adiabatic approximation, introducing the solvent relaxation energy ε_{or} , as an empirical parameter that increases with the solvent polarity.

The molecular model parameters, $2z_0$, $\sqrt{2}t$, μ_0 , ε_v , ω_v and ω_t , are adjusted to best reproduce experimental spectra and are all strictly solvent independent, so that the highly non-trivial dependence of optical spectra upon the solvent polarity is accounted for by just tuning ε_{or} .

The coupled electron-vibrational Hamiltonian is written on the non-adiabatic basis obtained as the direct product of the two electronic basis states times the vibrational eigenstates of the harmonic oscillator

associated to the vibrational coordinate. The vibrational basis is truncated to 10 states. The diagonalization of the Hamiltonian matrix yields the exact vibronic eigenstates of the system that enter the following expression for the calculation of optical spectra.

Specifically, the molar extinction coefficient $\varepsilon(\tilde{\nu})$, in units of $\text{M}^{-1} \text{cm}^{-1}$, was obtained from the following sum-over-states (SOS) expression:

$$\varepsilon(\tilde{\nu}) = \frac{10\pi N_A \tilde{\nu}}{3 \ln 10 \hbar c \varepsilon_0} \frac{1}{\sigma \sqrt{2\pi}} \sum_n \mu_{gn}^2 \exp\left[-\frac{1}{2} \left(\frac{\tilde{\nu}_{gn} - \tilde{\nu}}{\sigma}\right)^2\right] \quad (\text{S6})$$

where $\tilde{\nu}$ is the wavenumber (in cm^{-1}), N_A is the Avogadro number, c is the light speed, ε_0 is the vacuum dielectric constant, and σ is the width of the Gaussian bandshape assigned to each transition. The terms μ_{gn} and $\tilde{\nu}_{gn}$ are the transition dipole moment and wavenumber of the transition from the ground state (g) to the excited state n and the sum runs over all the excited states.

The fluorescence spectrum $I(\tilde{\nu})$ was calculated as:

$$I(\tilde{\nu}) \propto \frac{\tilde{\nu}^3}{\sigma \sqrt{2\pi}} \sum_n \mu_{fn}^2 \exp\left[-\frac{1}{2} \left(\frac{\tilde{\nu}_{fn} - \tilde{\nu}}{\sigma}\right)^2\right] \quad (\text{S7})$$

where f denotes the fluorescent state and the sum runs over all states having lower energy than f .

The 2PA cross-section (in GM units) was calculated according to the following expression:¹²

$$\sigma_2(\omega) = 10^{58} \frac{\hbar \omega^2}{4 \varepsilon_0^2 c^2} \text{Im}\langle \gamma(-\omega; \omega, \omega, -\omega) \rangle \quad (\text{S8})$$

where c is the speed of light and $\langle \gamma \rangle$ is the orientationally averaged second hyperpolarizability. The tensor elements of $\gamma(-\omega; \omega, \omega, -\omega)$ are obtained by the sum-over-states (SOS) expression, only including two-photon resonant terms:²⁹

$$\begin{aligned} \gamma_{ijkl}(-\omega; \omega, \omega, -\omega) = \frac{1}{\hbar^3} \sum_{lmn} & \left\{ \frac{\langle g|\mu_i|l\rangle \langle l|\bar{\mu}_j|m\rangle \langle m|\bar{\mu}_k|n\rangle \langle n|\mu_l|g\rangle}{(\Omega_{lg}-\omega)(\Omega_{mg}-2\omega)(\Omega_{ng}-\omega)} + \frac{\langle g|\mu_j|l\rangle \langle l|\bar{\mu}_i|m\rangle \langle m|\bar{\mu}_k|n\rangle \langle n|\mu_l|g\rangle}{(\Omega_{lg}^*-\omega)(\Omega_{mg}-2\omega)(\Omega_{ng}-\omega)} + \right. \\ & \left. \frac{\langle g|\mu_i|l\rangle \langle l|\bar{\mu}_j|m\rangle \langle m|\bar{\mu}_l|n\rangle \langle n|\mu_k|g\rangle}{(\Omega_{lg}-\omega)(\Omega_{mg}-2\omega)(\Omega_{ng}-\omega)} + \frac{\langle g|\mu_j|l\rangle \langle l|\bar{\mu}_i|m\rangle \langle m|\bar{\mu}_l|n\rangle \langle n|\mu_k|g\rangle}{(\Omega_{lg}^*-\omega)(\Omega_{mg}-2\omega)(\Omega_{ng}-\omega)} \right\} \quad (\text{S9}) \end{aligned}$$

In the SOS above, we set $\Omega_{lg} = \omega_{lg} - i\Gamma$ and $\bar{\mu} = \mu - \langle g|\hat{\mu}|g\rangle$, where the index g denotes the ground state, and the other indexes run over all excited states, both in the electronic ground and excited state manifold.

In this work, we considered only the x-component of the dipole moments, so that the only relevant tensor term is γ_{xxxx} . Accordingly, the orientationally averaged second hyperpolarizability reduces to $\langle \gamma \rangle = \frac{1}{3} \gamma_{xxxx}$.

In polar solvents, the Hamiltonian depends on the orientational component of the reaction field F_{or} : to account for the fluctuations of F_{or} around the equilibrium value, responsible for spectral broadening effects at finite temperature, the diagonalization of the molecular Hamiltonian and the calculation of the spectra is repeated on a grid of F_{or} values. The final spectra are finally calculated summing up the spectra calculated for different F_{or} values, weighting each spectrum for the relevant Boltzmann distribution (referred to the ground-state energy for absorption and to the Kasha's state for emission).

References

- ¹ H. Gopee, X. Kong, Z. He, I. Chambrier, D. L. Hughes, G. J. Tizzard, S. J. Coles and A. N. Cammidge, *J. Org. Chem.*, 2013, **78**, 9505-9511.
- ² M. Link, P. Kele, D. E. Achatz and O. S. Wolfbeis, *Bioorg. Med. Chem. Lett.*, 2011, **18**, 5538-5542.
- ³ M. Tian, M. Furuki, I. Iwasa, Y. Sato, L. S. Pu and S. Tatsuura, *J. Phys. Chem. B*, 2002, **106**, 4370-4376.
- ⁴ APEX3 V2019, Bruker Nano, Inc., 2019.
- ⁵ SAINT V8.40A, Bruker Nano, Inc., 2019.
- ⁶ SADABS V2016/2, Bruker Nano, Inc., 2019.
- ⁷ G. M. Sheldrick, *Acta Cryst.*, 2015, **A71**, 3-8.
- ⁸ G. M. Sheldrick, *Acta Cryst.*, 2015, **C71**, 3-8.
- ⁹ International Tables for Crystallography, Ed. A. J. C. Wilson, Kluwer: Dordrecht, 1992, Vol.C.
- ¹⁰ C. F. Macrae, I. Sovago, S. J. Cottrell, P. T. A. Galek, P. McCabe, E. Pidcock, M. Platings, G. P. Shields, J. S. Stevens, M. Towler and P. A. Wood, *J. Appl. Cryst.*, 2020, **53**, 226-235.
- ¹¹ C. Xu and W. W. Webb, *J. Opt. Soc. Am. B*, 1996, **13**, 481.
- ¹² F. Terenziani, C. Katan, E. Badaeva, S. Tretiak and M. Blanchard-Desce, *Adv. Mater.*, 2008, **20**, 4641-4678.
- ¹³ S. de Reguardati, J. Pahapill, A. Mikhailov, Y. Stepanenko and A. Rebane, *Opt. Express*, 2016, **24**, 9053.
- ¹⁴ M. A. Albota, C. Xu and W. W. Webb, *Appl. Opt.*, 1998, **37**, 7352.
- ¹⁵ M. J. Frisch, G. W. Trucks, H. B. Schlegel, G. E. Scuseria, M. A. Robb, J. R. Cheeseman, G. Scalmani, V. Barone, G. A. Petersson, H. Nakatsuji, X. Li, M. Caricato, A. V. Marenich, J. Bloino, B. G. Janesko, R. Gomperts, B. Mennucci, H. P. Hratchian, J. V. Ortiz, A. F. Izmaylov, J. L. Sonnenberg, D. Williams-Young, F. Ding, F. Lipparini, F. Egidi, J. Goings, B. Peng, A. Petrone, T. Henderson, D. Ranasinghe, V. G. Zakrzewski, J. Gao, N. Rega, G. Zheng, W. Liang, M. Hada, M. Ehara, K. Toyota, R. Fukuda, J. Hasegawa, M. Ishida, T. Nakajima, Y. Honda, O. Kitao, H. Nakai, T. Vreven, K. Throssell, J. E. Montgomery, J. A., Jr. Peralta, F. Ogliaro, M. J. Bearpark, J. J. Heyd, E. N. Brothers, K. N. Kudin, V. N. Staroverov, T. A. Keith, R. Kobayashi, K. Normand, J. Raghavachari, A. P. Rendell, J. C. Burant, S. S. Iyengar, J. Tomasi, M. Cossi, J. M. Millam, M. Klene, C. Adamo, R. Cammi, J. W. Ochterski, R. L. Martin, K. Morokuma, O. Farkas, J. B. Foresman and D. J. Fox, Gaussian16, revision B.01, Gaussian, Inc., Wallingford CT, 2016.
- ¹⁶ Y. Zhao and D. G. Truhlar, *Theor. Chem. Acc.*, 2008, **120**, 215-241.
- ¹⁷ M. Cossi, V. Barone, R. Cammi and J. Tomasi, *Chem. Phys. Lett.*, 1996, **255**, 327-335.
- ¹⁸ J. Tomasi, B. Mennucci and R. Cammi, *Chem. Rev.*, 2005, **8**, 2999-3094.
- ¹⁹ G. Scalmani and M. J. Frisch, *J. Chem. Phys.*, 2010, **132** (114110).
- ²⁰ L. Onsager, *J. Am. Chem. Soc.*, 1936, **58**, 1486-1493.
- ²¹ W. Liptay, *Angew. Chemie - Int. Ed.*, 1969, **8**, 177-188.
- ²² S. Di Bella, T. J. Marks and M. A. Ratner, *J. Am. Chem. Soc.*, 1994, **116**, 4440-4445.
- ²³ E. G. McRae, *J. Phys. Chem.*, 1957, **61**, 562-572.
- ²⁴ D. K. A. Phan Huu, R. Dhali, C. Pieroni, F. Di Maiolo, C. Sissa, F. Terenziani and A. Painelli, *Phys. Rev. Lett.*, 2020, **124**, 107401.
- ²⁵ A. Painelli, *Chem. Phys.*, 1999, **245**, 185-197.
- ²⁶ T. Lu and F. Chen, *J. Comput. Chem.*, 2012, **33**, 580-592.
- ²⁷ E. Cancès, B. Mennucci and J. Tomasi, *J. Chem. Phys.*, 1997, **107**, 3032-3041.
- ²⁸ A. Painelli and F. Terenziani, *Chem. Phys. Lett.*, 1999, **312**, 211-220.
- ²⁹ B. J. Orr and J. F. Ward, *Mol. Phys.*, 1971, **20**, 513-526.

9. DECLARATIONS OF THE AUTHORS OF PUBLICATIONS

mgr Kateryna Vygranenko
+48 794-375-755
kate.vygranenko@gmail.com

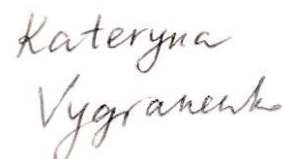
Instytut Chemii Organicznej PAN
ul. Kasprzaka 44/52
01-224 Warszawa
Polska

Warszawa, 23.05.2023

I declare that my contribution to the following publications consisted of:

1. Yevgen M. Poronik, **Kateryna V. Vygranenko**, Dorota Gryko and Daniel T. Gryko, *Chem. Soc. Rev.*, 2019, 48, 5242-5265. 'Rhodols – synthesis, photophysical properties and applications as fluorescent probes'.
Literature search and writing of the synthetic part of the manuscript, preparation of schemes, figures and tables.
2. **Kateryna V. Vygranenko**, Yevgen M. Poronik, Antoni Wrzosek, Adam Szewczyk and Daniel T. Gryko, *Chem. Comm.*, 2021, 57, 7782-7785. 'Red emissive sulfone-rhodols as mitochondrial imaging agents'.
Co-development of research concepts and interpretation of results. I have developed and carried out the synthesis of xanthone and transformed it into final rhodols under developed conditions. I participated in analysing the photophysical properties and preparation of the manuscript.
3. **Kateryna V. Vygranenko**, Yevgen M. Poronik, Manon H. E. Bousquet, Olena Vakuliuk, Denis Jacquemin and Daniel T. Gryko, *Chem. Comm.*, 2022, 58, 1542-1545. 'Direct transformation of coumarins into orange-red emitting rhodols'. Co-development of research concepts and interpretation of results.
I developed and carried out the preparation of the scope of formylcoumarins, transformed them into rhodols and optimized conditions of double Knoevenagel condensation. I took part in measurements of photophysical properties and interpretation of the obtained data.
4. Brunella Bardi, **Kateryna V. Vygranenko**, Beata Koszarna, Olena Vakuliuk, Łukasz Dobrzycki, Daniel T. Gryko, Francesca Terenziani, and Anna Painelli, *Chem.* 'A novel method for the programmed synthesis of merocyanines: new photophysical possibilities for a well-known class of fluorophores'. I took part in the optimization process, prepared all substrates, performed synthesis and participated in analyzing of the new merocyanine dyes.

Kateryna Vygranenko





Warsaw 24th May 2023.

I declare that my contribution to the following publications consisted of:

- › Yevgen M. Poronik, Kateryna V. Vygranenko, Dorota Gryko and Daniel T. Gryko, *Chem. Soc. Rev.*, 2019, 48, 5242-5265. 'Rhodols – synthesis, photophysical properties and applications as fluorescent probes'

Preparation and editing of the final version of the manuscript.

- › Kateryna V. Vygranenko, Yevgen M. Poronik, Antoni Wrzosek, Adam Szewczyk and Daniel T. Gryko, *Chem. Comm.*, 2021, 57, 7782-7785. 'Red emissive sulfone-rhodols as mitochondrial imaging agents'

Co-development of research concept, interpretation of results and preparation of the final version of the manuscript.

- › Kateryna V. Vygranenko, Yevgen M. Poronik, Manon H. E. Bousquet, Olena Vakuliuk, Denis Jacquemin and Daniel T. Gryko, *Chem. Comm.*, 2022, 58, 1542-1545. 'Direct transformation of coumarins into orange-red emitting rhodols'

Co-development of research concept, interpretation of results and preparation of the final version of the manuscript.

- › Brunella Bardi, Katerina V. Vygranenko, Beata Koszarna, Olena Vakuliuk, Łukasz Dobrzycki, Daniel T. Gryko, Francesca Terenziani, Anna Painelli, *Chem. Eur. J.*, 2023, <https://doi.org/10.1002/chem.202300979>. 'A novel method for the synthesis of merocyanines: new photophysical possibilities for a well-known class of fluorophores'

Co-development of research concept, interpretation of results and preparation of the final version of the manuscript.

Yours sincerely



Institute of Organic Chemistry
Polish Academy of Sciences

PhD Dorota Gryko
Professor of Chemistry

+48 22 343 20 51
dorota.gryko@icho.edu.pl

Warszawa 26 maja 2023 r.

I declare that my contribution to the following publication: Yevgen M. Poronik, **Kateryna V. Vygranenko**, Dorota Gryko and Daniel T. Gryko, *Chem. Soc. Rev.*, 2019, 48, 5242-5265. 'Rhodols – synthesis, photophysical properties and applications as fluorescent probes' consisted of correcting manuscript and discussing the its content

Digitally signed by
Dorota Gryko
Date: 2023.05.26
09:55:16 +02'00'

Dorota Gryko

Prof. Dorota Gryko



Warsaw 29th May 2023.

I declare that my contribution to the following publications consisted of:

- › Yevgen M. Poronik, Kateryna V. Vygranenko, Dorota Gryko and Daniel T. Gryko, *Chem. Soc. Rev.*, 2019, 48, 5242-5265. 'Rhodols – synthesis, photophysical properties and applications as fluorescent probes'

Co-development of research concept, writing a part of manuscript, editing the manuscript.

- › Kateryna V. Vygranenko, Yevgen M. Poronik, Antoni Wrzosek, Adam Szewczyk and Daniel T. Gryko, *Chem. Comm.*, 2021, 57, 7782-7785. 'Red emissive sulfone-rhodols as mitochondrial imaging agents'

A synthesis of one fluorescence probe, interpretation of results and preparation of the final version of the manuscript.

- › Kateryna V. Vygranenko, Yevgen M. Poronik, Manon H. E. Bousquet, Olena Vakuliuk, Denis Jacquemin and Daniel T. Gryko, *Chem. Comm.*, 2022, 58, 1542-1545. 'Direct transformation of coumarins into orange-red emitting rhodols'

Co-development of research concept, a synthesis of one fluorescence probe, interpretation of results and preparation of the final version of the manuscript.

Yours sincerely

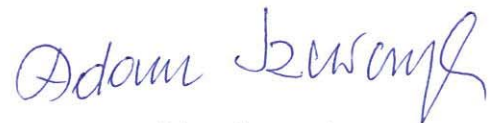
Prof. Dr hab. Adam Szewczyk
Pracownia Wewnątrzkomórkowych
Kanałów Jonowych
Instytut Biologii Doświadczalnej
im. Marcelego Nenckiego PAN
ul. Ludwika Pasteura 3, 02-093 Warszawa

Warszawa, 30.05.2023

Oświadczenie

Oświadczam, że mój wkład w powstanie poniższej publikacji polegał na redagowaniu manuskryptu, interpretacji i dyskusji wyników mikroskopii konfokalnej.

Kateryna V. Vygranenko, Yevgen M. Poronik, Antoni Wrzosek, Adam Szewczyk and Daniel T. Gryko,
Chem. Comm., 2021, 57, 7782-7785. 'Red emissive sulfone-rhodols as mitochondrial imaging agents'.



Adam Szewczyk

Dr Antoni Wrzosek

Laboratory of Intracellular Ion Channels

Nencki Institute of Experimental Biology PAS

3 Pasteur St., 02-093 Warsaw, Poland

Warsaw, 29.05.2023

Oświadczenie

Oświadczam, że mój wkład w powstanie poniższej publikacji polegał na wykonaniu pomiarów techniką mikroskopii konfokalnej i interpretacji otrzymanych wyników.

Kateryna V. Vygranenko, Yevgen M. Poronik, Antoni Wrzosek, Adam Szewczyk and Daniel T. Gryko, Chem. Comm., 2021, 57, 7782-7785. 'Red emissive sulfone-rhodols as mitochondrial imaging agents'.

Antoni Wrzosek
Antoni Wrzosek

Dr. Manon H. E. Bousquet
Manon.Bousquet@univ-nantes.fr

Ref. **Contribution Letter**

Nantes, 29/05/2023

To whom it may concern,

I hereby declare that my contribution to the publication below:

1. Kateryna V. Vygranenko, Yevgen M. Poronik, Manon H. E. Bousquet, Olena Vakuliuk, Denis Jacquemin and Daniel T. Gryko, *Chem. Comm.*, 2022, **58**, 1542-1545

I co-development of the research concept for theory, performed simulations and interpreted their results and prepare the the final version of the manuscript.

With best regards

Dr. Manon Bousquet

Prof. Denis Jacquemin
Denis.Jacquemin@univ-nantes.fr

Ref. **Contribution Letter**

Nantes, 23/05/2023

To whom it may concern,

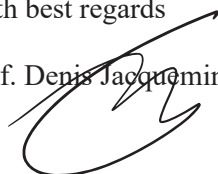
I hereby declare that my contribution to the publication below:

1. Kateryna V. Vygranenko, Yevgen M. Poronik, Manon H. E. Bousquet, Olena Vakuliuk, Denis Jacquemin and Daniel T. Gryko, *Chem. Comm.*, 2022, **58**, 1542-1545

I supervised the theoretical parts of this work and wrote the theoretical section of the manuscript. I was involved in the proof checking of the full manuscript.

With best regards

Prof. Denis Jacquemin





**UNIVERSITÀ
DI PARMA**

**DIPARTIMENTO DI SCIENZE
CHIMICHE, DELLA VITA E DELLA
SOSTENIBILITÀ AMBIENTALE**

Parma, 23/05/2023

I declare that my contribution to the publication

B. Bardi, K. V. Vygranenko, B. Koszarna, O. Vakuliuk, Ł. Dobrzycki, D. T. Gryko, F. Terenziani, A. Painelli, *Chem. Eur. J.*, 2023, DOI: 10.1002/chem.202300979 “A novel method for the synthesis of merocyanines: new photophysical possibilities for a well-known class of fluorophores”

Consisted of the spectroscopic characterization (absorption, fluorescence, fluorescence anisotropy, two-photon absorption), conduction of photostability measurements, execution of the theoretical calculations, participation to the discussion of the results, and writing of part of the original draft.

Yours sincerely,

Dr. Brunella Bardi
brunella.bardi@unipr.it



Institute of Organic Chemistry
Polish Academy of Sciences

Dr Olena Vakuliuk

+48 22 343 20 20
olena.vakuliuk@icho.edu.pl

Institute of Organic Chemistry
Polish Academy of Sciences
Kasprzaka 44/52
01-224 Warsaw
Poland

Warsaw 24th of May 2023 r.

Hereby I declare that my contribution to the following publications:

- > **Kateryna V. Vygranenko**, Yevgen M. Poronik, Manon H. E. Bousquet, Olena Vakuliuk, Denis Jacquemin and Daniel T. Gryko, *Chem. Comm.*, 2022, 58, 1542-1545. 'Direct transformation of coumarins into orange-red emitting rhodols';
- > Brunella Bardi, **Kateryna V. Vygranenko**, Beata Koszarna, Olena Vakuliuk, Łukasz Dobrzycki, Daniel T. Gryko, Francesca Terenziani, and Anna Painelli, *Chem. Eur. J.* 2023, doi.org/10.1002/chem.202300979 'A novel method for the synthesis of merocyanines: new photophysical possibilities for a well-known class of fluorophores'.

consisted of final amending of the Electronic Supporting Information.

Olena Vakuliuk



Institute of Organic Chemistry
Polish Academy of Sciences

dr Beata Koszarna

+48 22 343 20 37

beata.koszarna@icho.edu.pl

Warsaw 24th May 2023

I declare that my contribution to the publication is as follows:

Brunella Bardi, **Kateryna V. Vygranenko**, Beata Koszarna, Olena Vakuliuk, Łukasz Dobrzycki, Daniel T. Gryko, Francesca Terenziani, and Anna Painelli, Chem. Eur. J. 2023, doi.org/10.1002/chem.202300979
'A novel method for the synthesis of merocyanines: new photophysical possibilities for a well-known class of fluorophores'

I participated in the absorption and fluorescence measurements.

Yours sincerely



UNIVERSITY
OF WARSAW
Faculty of Chemistry



dr hab. Łukasz Dobrzycki
e-mail: dobrzyc@chem.uw.edu.pl
University of Warsaw, Faculty of Chemistry
Pasteur 1 str., 02-093 Warsaw

Warsaw, 24.05.2023

Hereby I declare that in the following publication:

Bardi, Brunella, Vygranenko, Katerina V., Koszarna, Beata, Vakuliuk, Olena, Dobrzycki, Łukasz, Gryko, Daniel T., Terenziani, Francesca, Painelli, Anna „A Novel Method for the Synthesis of Merocyanines: New Photophysical Possibilities for a Well-Known Class of Fluorophores”, *Chem. Eur. J.* **2023**, e202300979, DOI: 10.1002/chem.202300979

my contribution was limited to single crystal X-ray diffraction measurement, structure solution and refinement of the crystal of the compound **16** and preparation of the experimental section located in the appropriate part of the Supplementary.

Łukasz Dobrzycki



**UNIVERSITÀ
DI PARMA**

DEPARTMENT OF CHEMISTRY,
LIFE SCIENCES AND
ENVIRONMENTAL SUSTAINABILITY

Parma, May 23, 2023

To whom it may concern,

I declare that my contribution to the following publication:

B. Bardi, K. V. Vygranenko, B. Koszarna, O. Vakuliuk, Ł. Dobrzycki, D. T. Gryko, F. Terenziani, A. Painelli
A Novel Method for the Synthesis of Merocyanines: New Photophysical Possibilities for a Well-Known Class of Fluorophores
Chemistry-A European Journal, <http://dx.doi.org/10.1002/chem.202300979>

consisted of: conceptualization and supervision of the spectroscopic characterization part and interpretation of the results, co-supervision of the computational part, co-writing of the relevant parts of the manuscript, preparation of the final version of the manuscript and of the accompanying letter, submission of the paper and publication duties.

Sincerely,

Prof. Francesca Terenziani

Tel: +39 0521 905453

Fax: +39 0521 905556

E-mail: francesca.terenziani@unipr.it



**UNIVERSITÀ
DI PARMA**

**DIPARTIMENTO DI SCIENZE
CHIMICHE, DELLA VITA E DELLA
SOSTENIBILITÀ AMBIENTALE**

Anna Painelli
Professor of Physical Chemistry
anna.painelli@unipr.it

Parma, May 24, 2023

To whom it may concern

I hereby declare that my contribution to the paper

A Novel Method for the Synthesis of Merocyanines: New Photophysical Possibilities for a Well-Known Class of Fluorophores

Authors: Brunella Bardi, Katerina V. Vygranenko, Beata Koszarna, Olena Vakuliuk, Łukasz Dobrzycki, Daniel T. Gryko, Francesca Terenziani, and Anna Painelli

Chem. Eur. J. 2023, e202300979

was mainly devoted to the supervision of the theoretical work aimed at the interpretation of optical spectra. I also contributed to the manuscript preparation.

With best regards

Anna Painelli